Design, Synthesis and Delivery of Peptide-Based Systems

A Thesis presented for the degree of Doctor of Philosophy

Alexandra Webster

Supervised by Dr Steven Cobb

Department of Chemistry, Durham University

March 2018

Supervised by Dr Steven L. Cobb

Dr Steven Cobb

Department of Chemistry, University Science Laboratories, South Road, Durham, DH1 3LE.

+44 (0) 191 3342086

s.l.cobb@durham.ac.uk

Abstract

Peptide-based therapeutics have been an active area of research for a number of years. They have been found applications as drug-delivery agents, anticancer therapies and as antibiotics, the latter of which is particularly notable when set against a present-day backdrop of the increasing problem of antibiotic resistance. However, the use of peptides is still limited as they suffer from poor bioavailability as a result of their vulnerability to proteolytic degradation. Peptoids are a class of peptidomimetics which represent a potential proteolytically stable alternative to peptides. Chapter 1 introduces peptoids, common methods of their synthesis and their potential therapeutic applications. The challenges associated with controlling peptoid secondary structure are also discussed, along with commonly seen methods of imposing conformational rigidity. Chapter 2 details our attempts to address this problem by synthesising a library of biaryl-containing cyclic peptoids which represent novel peptoid scaffolds. In Chapter 3, we synthesise the active domain (p15) of the known anticancer peptide CIGB-300 along with three stapled analogues on which binding assays can be carried out. In Chapter 4, we synthesise six cell-penetrating peptoids (CPPos) which have previously been reported to localise in mitochondria. Onto these peptoids we conjugated the known anticancer peptide D-KLA and show the ability of these peptoids to increase proapoptotic activity. Flow cytometry and confocal microscopy is then used to demonstrate mitochondrial localisation of the most active peptide-peptoid hybrid, KLA-CPPo6. Having shown the ability of CPPos to transport biologically active cargo, we then conjugate the p15 peptide, previously introduced in Chapter 3, to the six CPPos in preparation for the evaluation of their anticancer activity.

Acknowledgements

Thanks first and foremost go to my supervisor, Dr Steven Cobb. His support and guidance throughout my time at Durham University have been invaluable. Thanks also go to the Cobb group, past and present, all of whom have helped me in one way or another in my time here. In particular, thanks go to Diana Gimenez for her help with hexafluorobenzene stapling, Caitlin Mooney for her advice on peptide synthesis and Dr Hannah Bolt for sharing her expertise in peptoid synthesis.

I would also like to thank Dr Jackie Mosely, Dr Dave Parker and Peter Stokes of the mass spectrometry service in the Department of Chemistry, and Dr Juan Aguilar Malavia and the rest of the NMR service staff in the Department of Chemistry for their patience and advice regarding the characterisation of my compounds. Thanks also go to Ian Edwards for his assistance in crystal screening. Further thanks go to Dr Ehmke Pohle for his advice on crystallisation and general enthusiasm.

I am also grateful for the assistance of people from a number of other research groups in the department: Dr Gary Sharples and Marikka Beecroft for their help with antibacterial screening, Alice Harnden of the Parker group for help with hydrogenation reactions and the members of Professor Graham Sandford's research group for loans of various chemicals and the use of their carousel.

I would like to highlight the contributions of Dr Jingyi Zong who synthesised the KLA peptides and Dr Ka-Leung Wong and his group, particularly Lijun Jiang who carried out anti-cancer screenings on the KLA-peptoids. Collaboration with Dr Ga-Lai Law on peptide-peptoid hybrids is also ongoing.

Finally, I would like to thank my family and friends who have helped and supported me throughout my research, particularly during the times when things haven't been going to plan and I have struggled. Without their support I wouldn't have got this far. Thank you.

Abbreviations

Ac Acetyl

Acm Acetamidomethyl

AIDS Acquired immune deficiency syndrome

ALCL Anaplastic large-cell lymphoma

ALK Anaplastic lymphoma receptor tyrosine kinase

AML Acute myeloid leukemia

AMP Antimicrobial peptide

APL Acute promyelocytic leukemia

Ar Aryl

AZT 2',3'-Dideoxy-3'-azidothymidine

B23 Nucleophosmin

BLI Bio-layer interferometry

Boc *tert*-Butyloxycarbonyl

Bu Butyl

CK2 Casein kinase 2

CD Circular dichroism

CF 5(6)-Carboxyfluorescein

CPP Cell-penetrating peptide

CPPo Cell-penetrating peptoid

CuAAC Copper-catalysed alkyne azide cycloaddition

DCE 1,2-Dichloroethane

DCM Dichloromethane

DIC *N,N'*-diisopropylcarbodiimide

DIPEA *N*,*N'*-diisopropylethylamine

DMF *N*,*N'*-dimethylformamide

DMSO Dimethyl sulphoxide

DNA Deoxyribonucleic acid

ED_{50} Median effective dose

EDC 1-Ethyl-3-(3-dimethylaminopropyl)carbodiimide

EDT 1,2-Ethanedithiol

ESI LCMS Electrospray ionisation liquid chromatography mass spectrometry

EtOH Ethanol

FDA Food and Drug Administration

Fmoc 9-Fluorenylmethyl carbamate

FSH Follicle stimulating hormone

h Hour

HATU 1-[Bis(dimethylamino)methylene]-1H-1,2,3-triazolo[4,5-*b*]pyridinium 3-oxid hexafluorophosphate

HDI Histone deacetylase inhibitor

HFIP 1,1,1,3,3,3-Hexafluoro-2-propanol

HIV Human immunodeficiency virus

HOAt Hydroxy-7-azabenzotriazole

HOBt 1-Hydroxybenzotriazole

HOMO Highest occupied molecular orbital

HPLC High pressure liquid chromatography

HRMS High resolution mass spectrometry

Hyx 5-Hexynoic acid

IC_{50} Half maximal inhibitory concentration

LCMS Liquid chromatography mass spectrometry

LUMO Lowest unoccupied molecular orbital

MALDI Matrix assisted laser desorption ionisiation mass spectrometry

MCR Multi-component reaction

MeCN Acetonitrile

MeOH Methanol

MIC Minimum inhibitory concentration

MIDA *N*-methyliminodiacetic acid

min Minutes

MRI Magnetic resonance imaging

MRSA Methicillin-resistant *Staphylococcus aureus*

MS Mass spectrometry

MW Molecular weight

m/z Mass to charge ratio

NES Nuclear export signal

NLS Nuclear localisation signal

NMR Nuclear magnetic resonance

NOE Nuclear Overhauser effect

NoLS Nucleolar localisation signal

NPM1 Nucleophosmin

NPM1c+ Cytoplasm-positive nucelophosmin

Pbf 2,2,4,6,7-Pentamethyldihydrobenzofuran-5-sulfonyl

PPI/PPII Polyproline type I/type II

PyBOP® Benzotriazol-1-yl-oxytripyrrolidinophosphonium hexafluorophosphate

QToF Quadrupole time of flight

RARα Retinoic acid receptor α

RCM Ring closing metathesis

rDNA Ribosomal deoxyribonucleic acid

Rhod Rhodamine B

RNA Ribonucleic acid

RP-HPLC Reverse-phase high performance liquid chromatography

rpm Revolutions per minute

RT Room temperature

SPhos 2-Dicyclohexylphosphino-2',6'-dimethoxybiphenyl

SPPS Solid phase peptide/peptoid synthesis

TBTA Tris(benzyltriazolylmethyl)amine

TEA Trimethylamine

TFA Trifluoroacetic acid

THF Tetrahydrofuran

TMSCl Trimethylsilyl chloride

TIPS Triisopropylsilane

TQD Triple quadrupole

ToF Time of flight

Trt Trityl

U-4CR Ugi 4-component reaction

UPLC Ultra-high performance liquid chromatography

UV-Vis Ultraviolet-Visible

v/v Volume concentration

WHO World Health Organisation

Contents

Chapter 1

Introduction

1.1 Peptoids vs Peptides

N-Substituted glycines, or peptoids are a class of peptidomimetic where the side chain is located on the nitrogen of the amide bond rather than the α-carbon (**Figure 1.1**).[1]

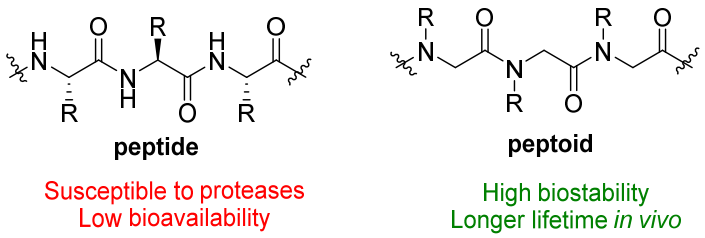

Figure 1.1 Comparison of the structure of peptides and peptoids.

As with peptides, peptoids are oligomeric and contain side chains which may comprise a variety of functional groups. However, the presence of the side-chain on the nitrogen precludes the backbone hydrogen bonding which is responsible for the secondary structures seen in peptides.[2] The result of this is a number of differences in the physical and biological properties of peptides and peptoids. For instance, peptoids are highly resistant to enzymatic degradation; a significant problem in the application of peptide therapeutics.[3, 4] However, the lack of inherent defined secondary structure in peptoids results in a lack of conformational rigidity with *cis*/*trans* isomerism of the amide bonds (**Figure 1.2**) a particular challenge to control.[5-9]

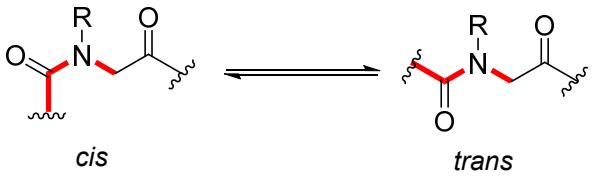

Figure 1.2 *Cis*/*trans* isomerism around the peptoid backbone amide bonds.

1.2 Synthesis of Peptoids

The first peptoids were synthesised using standard peptide coupling methods via Fmoc-protected *N*-substituted glycine monomers (**Scheme 1.1**). This monomer method of peptoid synthesis requires prior synthesis of *N*-substituted glycine monomers which is both labour-intensive and time consuming.

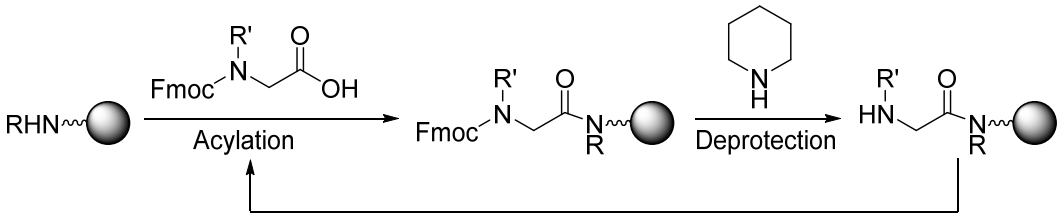

Scheme 1.1 Solid phase peptoid synthesis using *N*-substituted glycine monomers.

In 1992 the synthesis of peptoids via the sub-monomer method was reported (**Scheme 1.2**).[10] Synthesis is carried out on resin and involves two steps: acylation with a haloacetic acid followed displacement of the halogen by an amine.

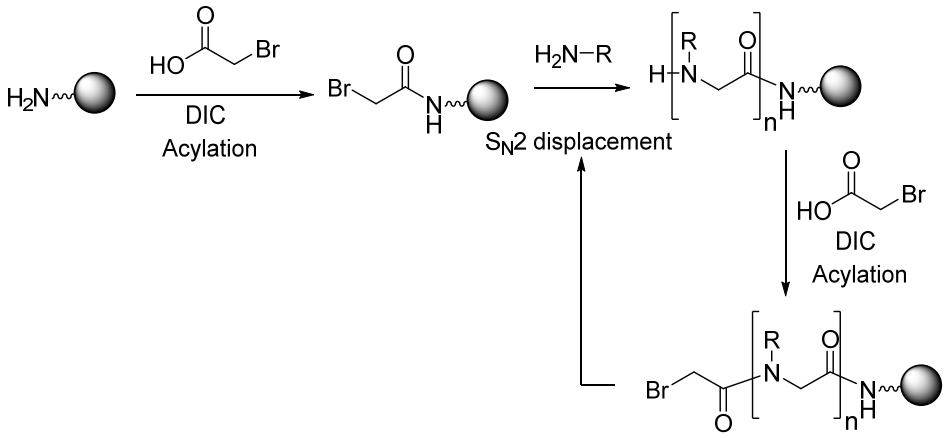

Scheme 1.2 The sub-monomer method of peptoid synthesis.

The sub-monomer method allows for the incorporation of many different functional groups on the side chain via >300 commercially available primary amines, as well as various novel sub-monomers that can be synthesised. This method also does not require the use of protecting groups, other than on the side chains, and, as with solid phase peptide synthesis, enables easy purification as excess reagents may be washed away after each addition. Once cleaved from the resin, the crude peptoid may then undergo final purification via HPLC. Finally, this method is automatable on commercially available synthesisers, making synthesis facile. The sub-monomer method remains the most frequently used method of peptoid synthesis.

There are also several methods of making peptoids in solution. The bromoacetyl bromide method is a sub-monomeric method where bromoacetyl bromide is added to a secondary amine in a solution-phase acylation. Following filtration and evaporation, a primary amine is then added in a solution-phase substitution and the resulting peptoid is purified by flash column chromatography before the next acylation and substitution cycle (**Scheme 1.3**).[11] The need for purification between each cycle means that this method is far more time-consuming than the solid-phase sub-monomer method.

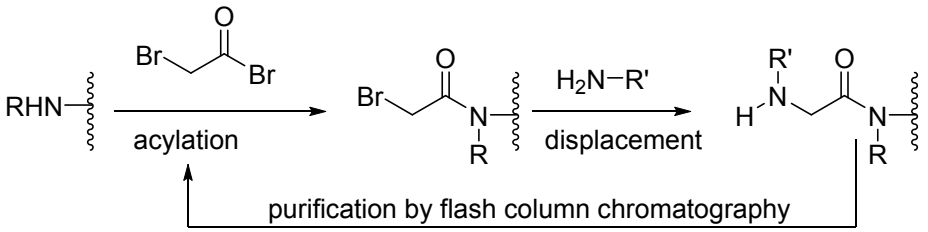

Scheme 1.3 Solution phase peptoid synthesis using the bromoacetylbromide method.

An efficient method of synthesising a dipeptoid backbone is the Ugi four-component reaction (Ugi-4CR, **Scheme 1.4**). This process is a one-pot solution phase reaction between a primary amine, an oxo compound, a carboxylic acid and an isocyanide.[12]

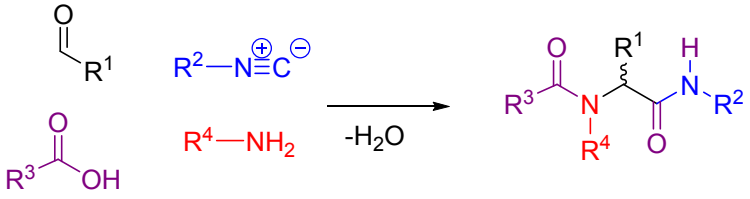

Scheme 1.4 Synthesis of a dipeptoid by Ugi-4CR.

The Ugi-4CR is a useful reaction that has previously been used to form peptoid macrocycles, cryptands and cages[13, 14] and will be further discussed as a method of forming cyclic peptoids.

1.3 Potential Therapeutic applications of peptoids

Over the past decade, developing medical applications for peptides has, and continues to be a highly active area of research. At present there are over 60 peptide-based drugs on the market which have been approved by the US Food and Drug Administration and more than 140 in clinical trials.[15] This interest in peptide-based therapeutics arises from their biocompatibility and ability to form defined secondary and tertiary structures, resulting in high selectivity. However, there are significant difficulties in the development of peptide-based therapeutics; namely that they are readily metabolised *in vivo*, resulting in short half-lives. As previously mentioned, the movement of the side chain from the α-carbon to the backbone amide nitrogen in peptoids confers resistance to enzymatic degradation and thus peptoids are seen as attractive candidates for therapeutics.[3,4]

1.3.1 Cell-penetrating peptoids

A major barrier to using many promising drugs and imaging probes is their inability to pass through eukaryotic cell membranes, resulting in poor bioavailability. The side chain functionality of peptides, however, enables various cargo (such as biologically active molecules) to be attached. Cell-penetrating peptides (CPPs) are characteristically no longer than 30 amino acids in length, amphiphilic[16, 17] and have an overall positive charge at physiological pH.[18-21] They enter the cell by mechanisms that require no energy and may or may not be receptor mediated.

CPPs have previously been synthesised and successfully internalised in a variety of cells *in vitro*, for example rat brain and spinal cord,[22] calf aorta,[23] porcine and human umbilical vein endothelium,[16] in osteoclast culture[24] as well as a variety of cell lines, such as HeLa.[25-27]

More recently, CPPs have been internalised in cancerous cells such as acute myeloid leukaemia.[28] Such studies have utilised cell-penetrating peptides to transport cytotoxic or imaging moieties.[29-31]

Although some CPPs are now being used for *in vivo* experiments (**Table 1.1**),[31, 32] there remain inherent problems. The aforementioned fragility of short peptides in biological systems where they are rapidly metabolised means that the CPP would have to be injected very close to the site of interest which may not be feasible. Failure to do this could lead to early release of the cargo being carried, negating selectivity with potentially disastrous consequences if the cargo is toxic. Whilst various solutions to this fundamental problem are under investigation,[33-36] peptoids offer a potential solution.[37]

Table 1.1 Commonly used CPPs for *in vivo* experiments.

Name	Sequence	Origin	References
TAT (48 – 60)	GRKKRRQRRRPPQ	Human immunodeficiency virus 1 (HIV 1)	38-41
Polyarginine	R_n (n = 6-9)		42-44
Transportan/TP10	GWTLNS/AGYLLGKINLKALAALAKKIL	galanin-Lys-mastoparan	45
pVec	LLIILRRRIRKQAHAHSK	VE-cadherin	46, 47
Pep-1	KETWWETWWTEWSQPKKKRKV	NLS from Simian Virus 40 large T antigen and reverse transcriptase of HIV-1	48-50
Penetratin	RQIKIWFQNRRMKWKK	Drosophila Antennapedia homeodomain	38, 41, 51

Various cell-penetrating peptoids (CPPos) have been synthesised and investigated. As with cell-penetrating peptides, CPPos are short (~12 residues) and amphiphilic. Furthermore, a study showed that peptoids are anywhere between 3 – 30 times more permeable than the analogous peptide.[52] In this study, the compounds were conjugated to a dexamethasone derivative. This triggered the activation of the Gal4-responsive luciferase upon entry into living cells and the level of luciferase expression was used as a measure of the cell permeability of the compound. It is thought that the reason for the increased permeability of peptoids relative to peptides is due to the lack of backbone-NH protons in peptoids resulting in greater lipophilicity.

CPPos are still in the early stages of research, but even so, several have already been synthesised that show promising cell permeability and, in some cases, the ability to localise in different organelle.[53-56] CPPos will be discussed in more detail in **Chapter 4**.

1.3.2 Bioactive Peptoids

Antimicrobial peptides (AMPs) have been an active area of research for decades; many such peptides will kill bacteria whilst showing low cytotoxicity to mammalian cells. This is explained by the difference between cell membranes of bacteria and mammalian cells. Similar to the motifs found in cell-penetrating peptides and peptoids, AMPs feature segregated cationic and hyrdrophobic regions. The cationic regions bind to anionic bacterial cell membranes and the hydrophobic regions cause permeabilisation leading to leakage and eventually death.[57] Because mammalian cell membranes are largely zwitterionic, the effect of AMPs is different and gives some selectivity. The exact mechanism for the action of AMPs on bacterial cell membranes is not well defined with several possibilities such as the carpet,[57] barrel-stave pore,[57] torroidal pore[58] and aggregate models.[59] In addition to this, some AMPs have also shown activity against a broad spectrum of cancers.[60-64] The reason for selectivity between cancerous cells and non-cancerous cells is not known, although it has been hypothesised that membranes of cancerous cells are in some way different to those of healthy cell, perhaps more negatively charged or with higher transmembrane potentials.[60-64] Furthermore, AMPs appear to be able to overcome multidrug resistance seen in some cancer cells.[65-67] However, in spite of promising results against bacteria and, in one case, comparable results to doxorubicin in mouse ovarian cancer, AMPs have yet to be involved in widespread trials; they suffer from the same problems as cell-penetrating peptides, notably lack of stability *in vivo* resulting in poor bioavailability.

As is the case for cell-penetrating peptides, peptoids are seen as a potential alternative to peptides in the field of drug discovery. Peptoids may be used as selective delivery agents for biologically active molecules, or the cell-penetrating peptoids themselves may be biologically active. For instance, some of the peptoids investigated have also demonstrated some antimicrobial and anti-cancer activity.[55, 68] In fact, it has been found that anti-microbial peptoids are analogous to AMPs in many ways, for instance in the relationship between structure and function. X-ray reflectivity studies showed that peptoid **1**, which also shows anti-microbial activity (see **Section 1.3.2.1**), is membrane active and forms a stable membrane-bound orientation, similar to that of AMPs

pexiganan and LL-37. This shows that the similarity to behaviour of AMPs extends to the molecular level.[69]

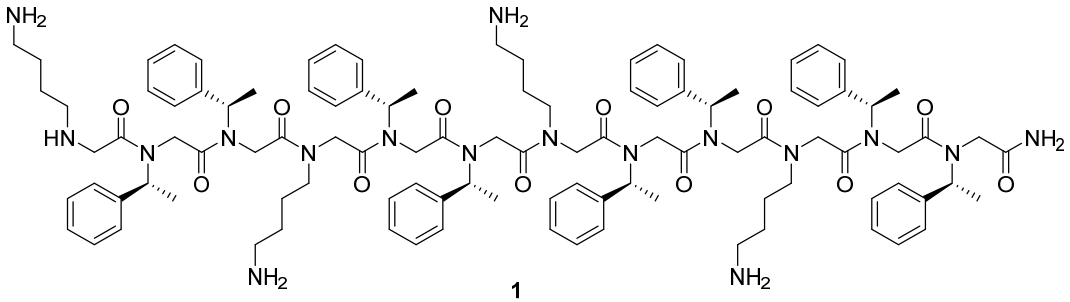

1

1.3.2.1 Antimicrobial peptoids

As is the case with AMPs, antimicrobial peptoids appear to work primarily by membrane permeabilisation and disruption.[70, 71] Peptoids active against a range of bacteria, such as *Escherichia coli*,[72] *Bacillus subtilis*,[69] *Pseudomonas aeruginosa* biofilms[73] and *Mycobacterium tuberculosis*[74] have been synthesised. In 2008 the Barron group investigated the structure-activity relationship of helical peptoids designed to mimic the α-helical structure of AMP magainin-2.[69] Amongst the peptoids investigated was one with the sequence H-(*N*Lys-*N*spe-*N*spe)$_4$-NH$_2$ (**1**). Peptoid helices have a periodicity of three residues per turn, so the peptoid structure comprised two *N*spe residues, which are both hydrophobic and helix-inducing, with *N*Lys incoroporated every third residue to provide a cationic face.

Peptoid **1** was found to have low micromolar MICs for both *E. coli* and *B. subtilis* (3.5 μM and 0.88 μM respectively) and a selectivity ratio of 6.0 between the *E. coli* and human erythrocytes (measured by the quotient of the 10% haemolytic dose and the MIC against *E. coli*). To compare, the selectivity ratio of pexiganan, a peptide considered to have low cytotoxicity, is 24. However, an analogue of **1** where the *N*spe residue in position six is replaced by L-proline (sequence H-*N*Lys-*N*spe-*N*spe-*N*Lys-*N*-spe-L-Pro-(*N*Lys-*N*spe-*N*spe)$_2$-NH$_2$, **2**) was also tested and found to retain the helical structure of **1** whilst having similar MICs, but with a selectivity ratio of 20.

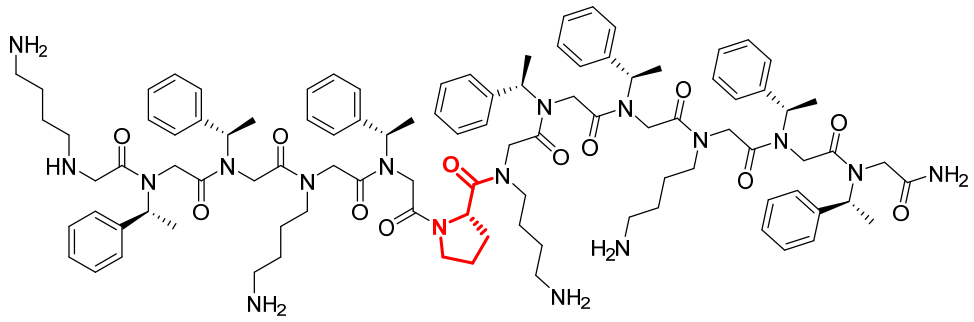

2

Peptoids have also been shown to be active against other pathogens. Work within this group has demonstrated the activity of peptoids against the parasite *Leishmania mexicana*.[75, 76] Leishmaniasis is a neglected tropical disease with an estimated 12 million people currently infected and more than 350 million more at risk of infection.[77] There is no vaccine available and current treatments are expensive, require parenteral administration and carry the risk of severe side-effects.[78, 79]

A library of over 30 peptoids was synthesised and their activity against both the promastigote and amastigote forms of the *L. mexicana* parasite, the causative agent of cutaneous leishmaniasis was investigated.[80] Peptoids synthesised followed four motifs: $N_xN_yN_y$, where N_x is a lysine type side chain of varying chain lengths and N_y is an uncharged, hydrophobic aromatic or aliphatic side chain; $N_xN_yN_z$ where N_z is a different uncharged, hydrophobic aromatic or aliphatic side chain; $(N_xN_yN_y)(N_xN_zN_z)$-type co-block sequence; and sequences where one or two of the *N*Lys side chains is replaced by the uncharged *N*amy side chain (**Figure 1.3**).

The group found that peptoids with fluorinated or chlorinated side chains showed increased activity against axenic amastigotes (whilst maintaining activity against promastigotes) when compared to peptoids with only non-chlorinated or fluorinated side chains, but that the most active analogues contained both the *N*pfb and *N*spe side chains. The presence of aromatic side chains also appeared necessary with peptoids containing the aliphatic side chains showing very little activity against either form of the parasite. Finally, hydrophobicity increased biological activity and replacement of one or two of the *N*Lys side chains with *N*amy greatly increasing activity against amastigotes and having micromolar ED_{50} values.

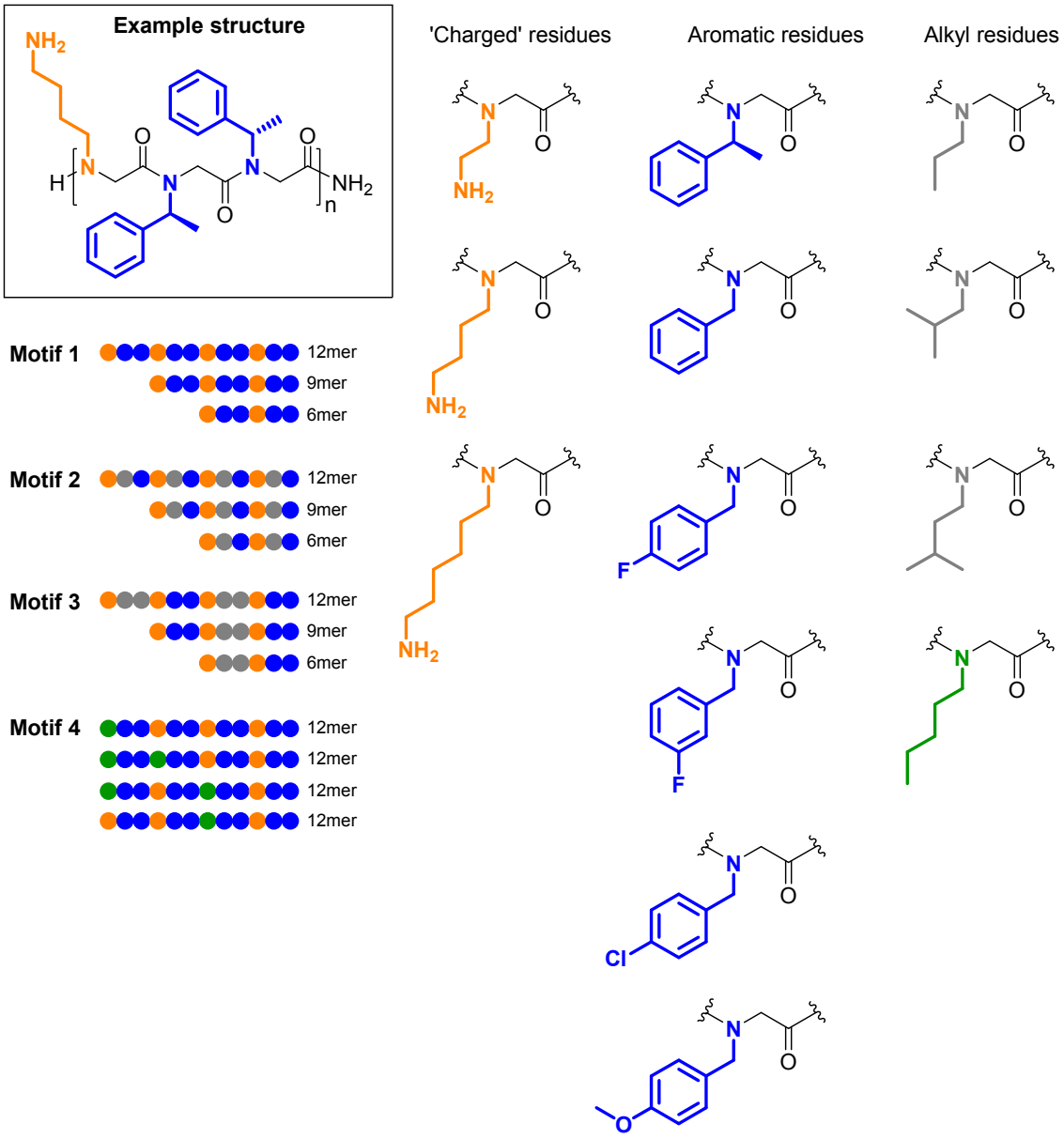

Figure 1.3 The structure of the anti-leishmanial peptoids investigated and the side chains used.

Following testing against axenic amastigotes, four peptoids (**Figure 1.4**), three 'hit' compounds (**3**, **4** and **5**) and a negative control (**6**), were chosen for testing against the clinically relevant *L. mexicana* infected murine macrophages. It was found that activity against axenic amastigotes did not necessarily indicate activity against intra-macrophage amastigotes. Furthermore, all three peptoids which showed activity against intra-macrophage amastigotes were equivalently (**5**) or more cytotoxic (**3** and **4**) to host macrophages. This is consistent with earlier work[76] and shows that the balance between biological activity and cytotoxicity must be finely tuned.

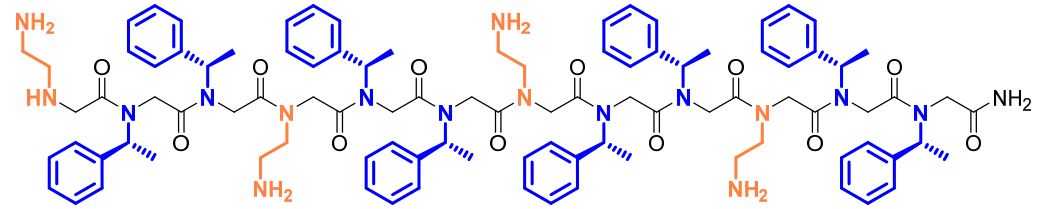

3, ED_{50} = >5 μM against intracellular amastigotes

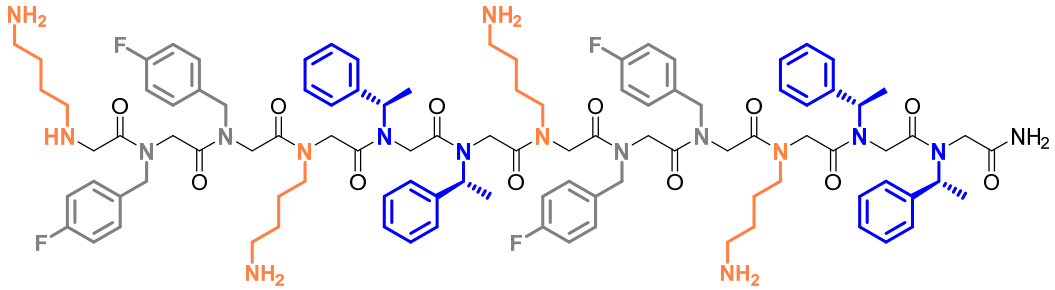

4, ED_{50} = >5 μM against intracellular amastigotes

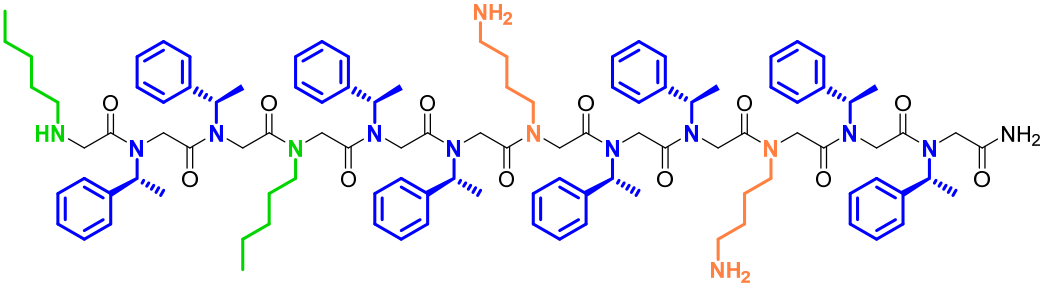

5, ED_{50} = >1.6 μM against intracellular amastigotes

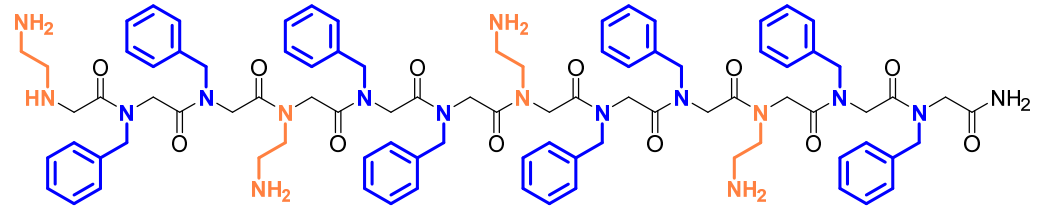

6, ED_{50} = >5 μM against intracellular amastigotes

Figure 1.4 The structure of the anti-leishmanial peptoids tested against *L. mexicana* infected murine macrophages. Peptoid **6** is the negative control and showed no activity against amastigotes. The structures are colour-coded according to the motifs shown in **Figure 1.3**. Amphotericin B was used as a positive control (ED_{50} = 0.195 μM against intracellular amastigotes).

The anti-fungal activity of peptoids has also been tested in a 2016 paper by Luo *et al.* where their efficacy against *Candida albicans* biofilms was investigated.[81] Biofilm formation is thought to be linked to antimicrobial resistance, in part due to their polymicrobial nature and propensity for metabolic inactivity.[82] Further, *C. albicans*-containing biofilms are associated with infections of both biotic and abiotic surfaces, including surgical implants.[83, 84] In 2016 Luo *et al.* published work in which 18 peptoids were tested against single species biofilms of *C. albicans, E. coli*, and *Staphylococcus aureus.*[81] The three most effective peptoids (**Figure 1.5**) were then tested against mixed species biofilms containing *C. albicans* and either *E. coli* or *S. aureus*.

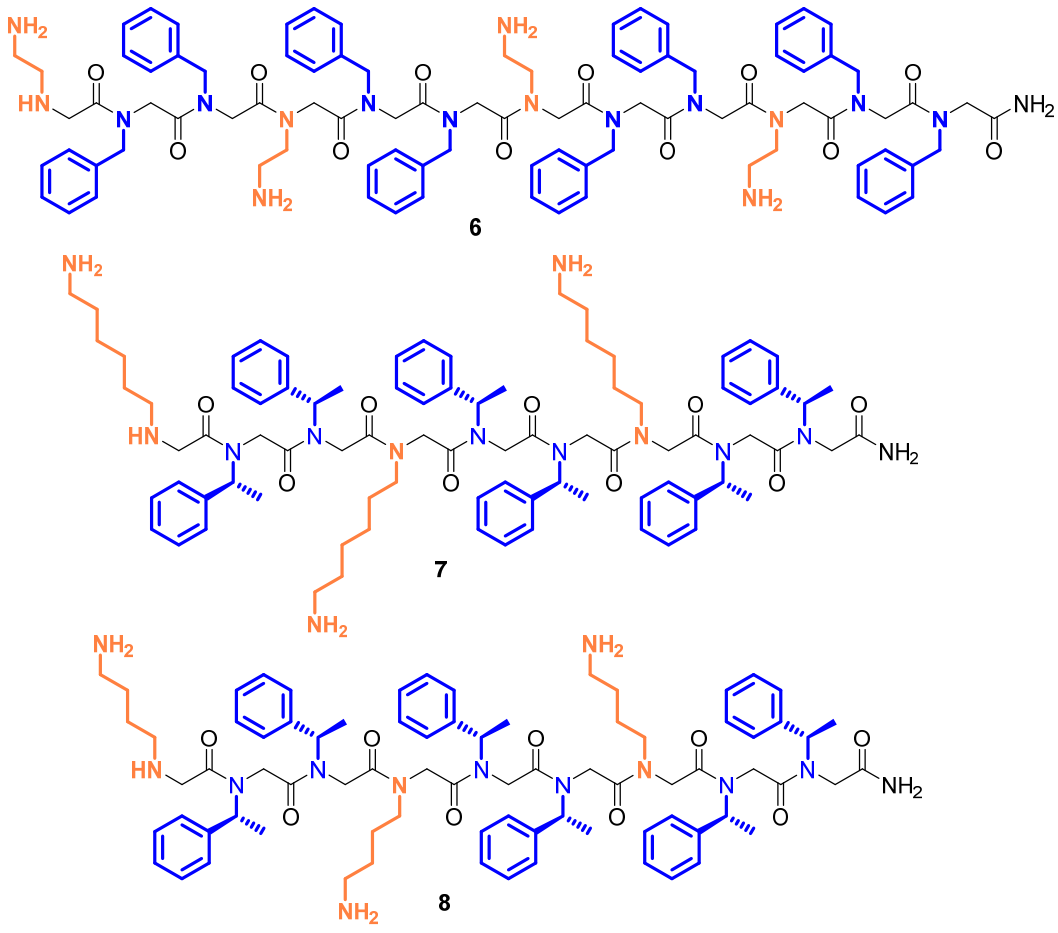

Figure 1.5 The structure of the three most effective peptoids tested against *C. albicans* biofilms. All three follow the $N_xN_yN_y$ motif (motif 1 in **Figure 1.3**). Positively charged side-chains are coloured orange and the hydrophobic side chains are coloured blue.

All peptoids tested were of the motif $N_xN_yN_y$ where N_x is a positively charged side chain of either *N*Lys, *N*ae or *N*ah and N_y is either the achiral aromatic *N*phe or the chiral aromatic *N*spe side chain. For each combination, the sequence was repeated two,

three or four times to test the effect of peptoid length on activity. Generally, it was found that the twelve-residue peptoids were the most active, except against single species biofilms of *S. aureus* where the nine-residue peptoids were most active. Against single species biofilms of *E. coli* the twelve-residue peptoids were the most active unless N_x was Nah, in which case the nine-residue peptoids were most active. In all cases, the six-residue peptoids were mostly inactive.

For sequences of the same length, *N*ae-containing peptoids (ie peptoids containing the shortest cationic side-chain length) were more active than peptoids containing the longer cationic side-chains (*N*Lys and *N*ah). For the most part, *N*ah-containing peptoids tended to be less active than peptoids containing *N*Lys or *N*ae, with the exception of the sequence (*N*ah*N*spe*N*spe)$_3$ (**7**). The authors of the paper speculated that the reason for the reduced activity of *N*ah*N*y*N*y peptoids is due to greater flexibility arising from the longer aminohexane side chain. Finally, chirality made a difference to the activity in peptoids containing *N*Lys or *N*ah with *N*spe-containing peptoids being more active than *N*phe-containing peptoids. In the case of *N*ae-containing peptoids, the presence of chiral side chains made little difference. Three of the 18 peptoids, considered the most active across all three single-species biofilms (**Figure 1.5**), were taken forward for testing against polymicrobial biofilms (**Figure 1.6**): (*N*Lys*N*spe*N*spe)$_3$ (**8**) , (*N*ae*N*phe*N*phe)$_4$ (**6**) and (*N*ah*N*spe*N*spe)$_3$ (**7**). Against mixed-species biofilms of *C. albicans* and *E. coli* peptoid **7** was the most active, but against mixed-species biofilms of *C. albicans* and *S. aureus* peptoid **8** showed the most reduction in *S. aureus*, whilst peptoid **6** showed the most reduction in *C. albicans*. The presence of *S. aureus* in the biofilm appeared to make *C. albicans* less susceptible to peptoid **7**. The primary mode of action of these peptoids against all three species is thought to be via cell-membrane permeabilisation, which is consistent with results of assays carried out by Luo *et al,* although possible secondary intracellular targets were not investigated.[81] This proposed mode of action is similar to that of antimicrobial peptides, i.e. disruption of prokaryotic cell membranes.[57]

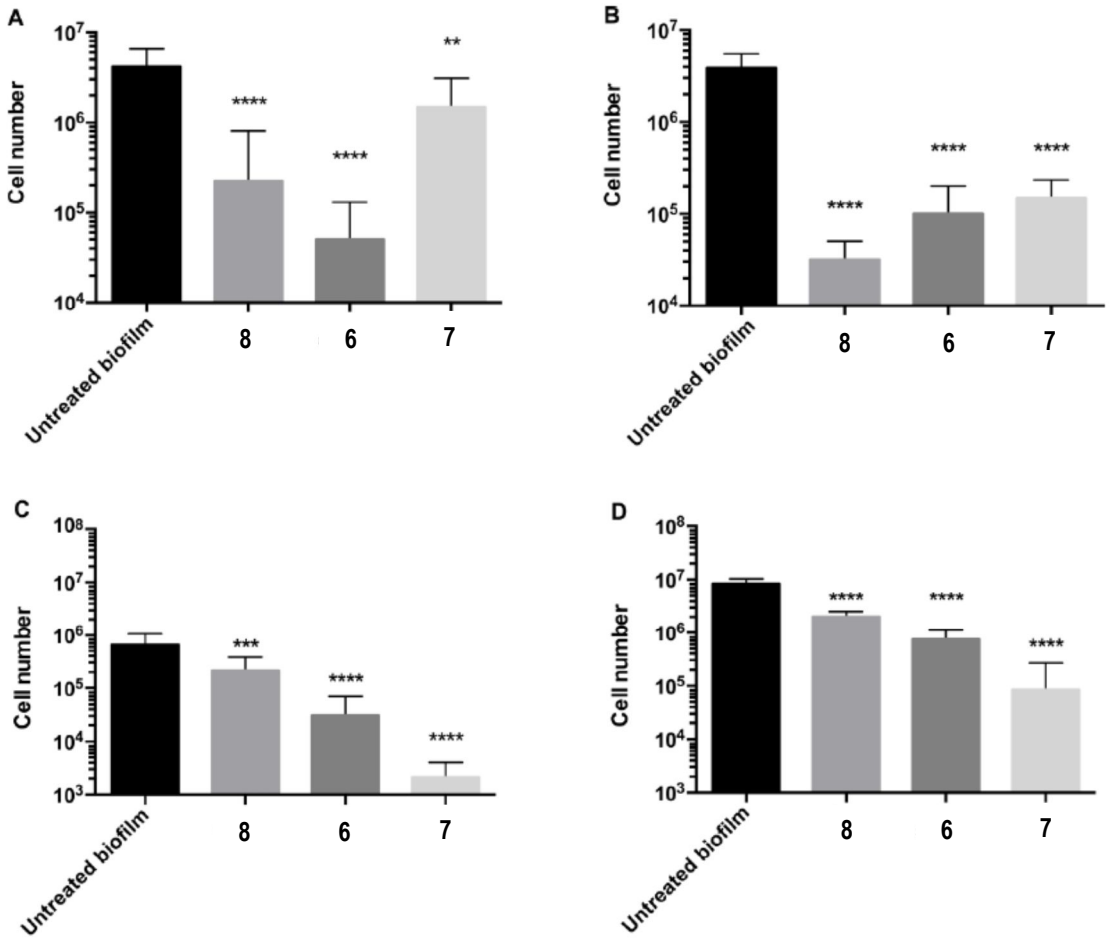

Figure 1.6 PMA-qPCR quantification of cell numbers following treatment by 100 μm peptoid treatment of polymicrobial biofilms of *C. albicans* with either *S. aureus* or *E. coli*: Cell numbers of A) *C. albicans* and B) *S. aureus* within the same biofilm following treatment with peptoids, and C) *C. albicans* and D) *E. coli* within the same biofilm following treatment with peptoids (**p<0.01, ****p<0.0001; mean_SD, n=3).

1.3.2.2 Anticancer Peptoids

Like AMPs, some antimicrobial peptoids have also proven to be active against cancer and also like AMPs, the peptoids do not show decreased toxicity to multidrug resistant lines of cancer cells in comparison to the non-resistant lines.[55, 68] This appears to be because the main cytotoxic activity towards cancer cells involves damaging the cell membrane; peptoids translocate into the cells and upon translocation appear to damage the cell membrane causing lysis. It is also possible that the peptoids also have targets within the cell since increased cell death was also observed after longer incubation with the peptoids in some concentration ranges. It was observed that at low

concentrations, peptoids are able to cross cell membranes with no or reparable damage to the membrane, but may then target organelle.[68] At high concentrations, the peptoids interact with membranes in such a way that they are damaged irreparably. However, the main issue with peptoids as anti-cancer agents is selectivity between healthy cells and cancer cells with some of the peptoids tested reporting haemolysis at high concentrations.[55] In fact, some peptoids showed little or no selectivity between cancerous cells and healthy cells.

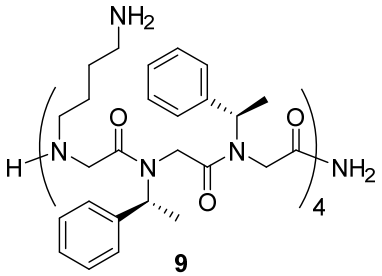

9

However the amphipathic cell penetrating peptoid, H-(*N*lys-*N*spe-*N*spe)$_4$-NH$_2$ (**9**), was tested on a mouse with implanted human breast cancer cells and it was found that this peptoid significantly inhibited tumour growth whilst causing no other observable toxicity at the therapeutic dose.[68] It should, however, be emphasised that this *in vivo* experiment was only a preliminary study and toxicity of these compounds needs to be thoroughly investigated in conjunction with any possible biological application.

More recently, a library of triazine-bridged cyclic peptoids was synthesised with the aim of targeting the Skp2/p300 interaction.[85] The Skp2 receptor has been shown to be overexpressed in many cancers and downregulates tumour suppressor proteins, thereby promoting tumour progression and metastasis.[86-89] p300 acetylates p53, an important protein involved in tumour suppression and sometimes referred to as “guardian of the genome” due to its role in preventing genome mutation. Acetylation of p53 is necessary for its stability and activation, so by binding p300, Skp2 inhibits the function of p53 by blocking acetylation.[90, 91]

In 2016, Oh *et al*. synthesised a library of peptoid macrocycles with the aim of targeting the Skp2/p300 interaction.[85] The features and methods of synthesising cyclic peptoids will be covered more extensively further on, but in this study, peptoid macrocycles were used as larger molecules capable of covering large protein interfaces. The peptoid library was generated by split-mix synthesis using eleven different amines for the displacement steps until a series of pentameric linear peptoids was produced. The peptoids were then capped with cyanuric chloride (**10**) and cyclisation was achieved by

deprotection of a cysteine incorporated as the first residue on each peptoid followed by subsequent base-mediated substitution. Finally, to remove the final chloride, the peptoid was treated with methoxyethylamine (**Scheme 1.5**). This produced a library of triazine-bridged cyclic peptoids with theoretical diversity of 161,051. The library of peptoids was subjected to an affinity-based on-bead screen to identify peptoids which bound to the target protein. From this peptoid **11** was identified and the binding affinity determined by fluorescence anisotropy. Peptoid **11** was then used to treat both HeLa cells and WS-1 normal human fibroblast cells at various concentrations and apoptotic activity tested. It was found that peptoid **11** triggered apoptosis in the HeLa cells but had no effect on the WS-1 cells, indicating possible selectivity between healthy and malignant cells.

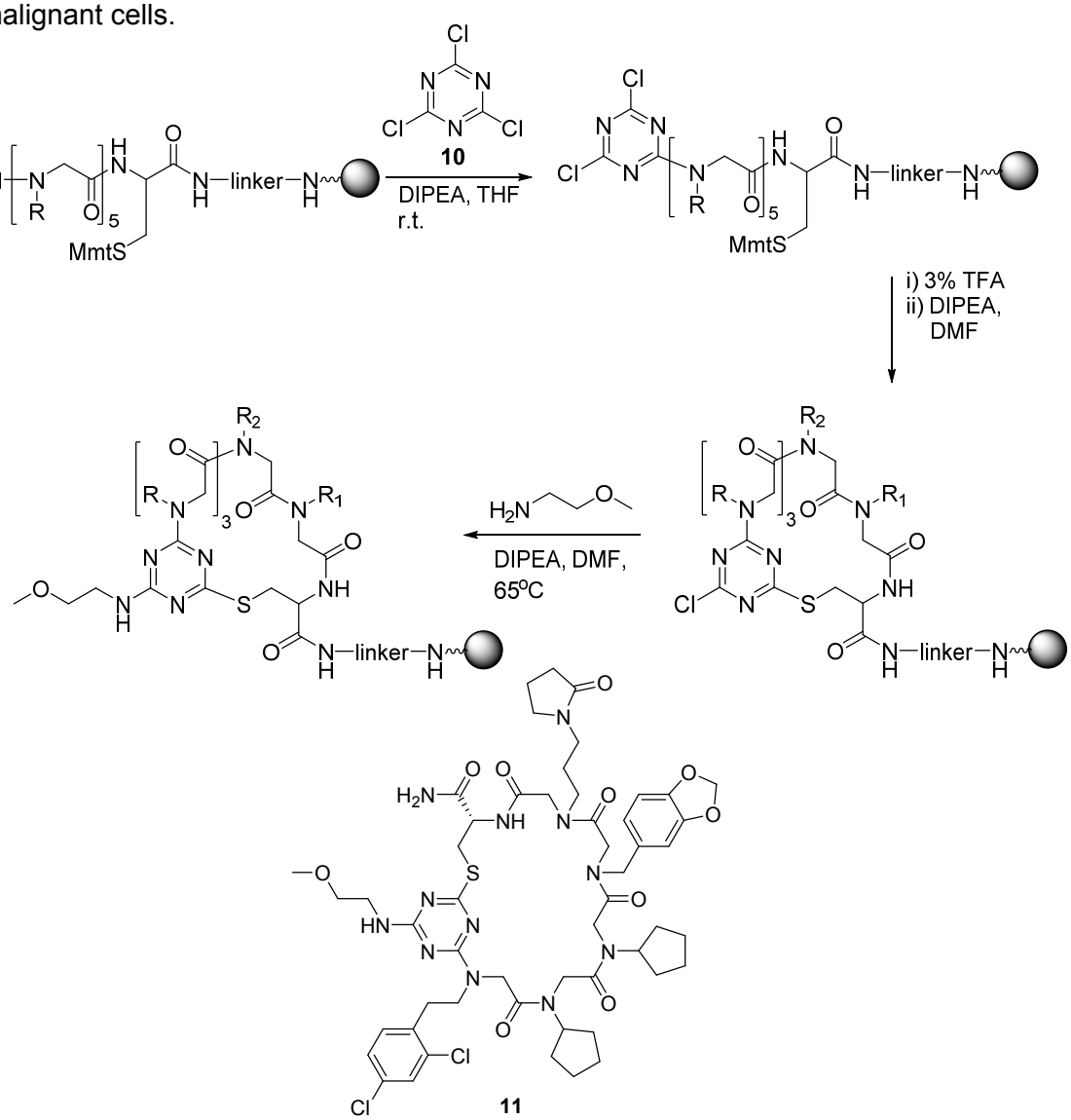

Scheme 1.5 Synthesis of peptoid macrocycles for targeting the Skp2/p300 interaction and the structure of the key peptoid isolated.

1.4 Obstacles to the use of peptoids as therapeutics: *cis/trans* isomerism and a lack of defined secondary structure

Whilst peptoids appear to show a lot of promise as therapeutic agents, there are still some significant obstacles to their use. One of the biggest challenges is to overcome a lack of defined secondary structure. In order to design drugs that interact with a specific target, conformational rigidity can be important. As well as increasing the affinity of the compound to the target,[92] conformational rigidity reduces the likelihood and severity of off-target effects due to lack of specificity.[93] Limiting off-target effects is particularly difficult whilst treating certain diseases; the side-effects that commonly occur during current cancer treatments are well documented.[94]

In peptides inter- and intra-chain hydrogen bonding involving the amide proton enables formation stable secondary structures. Peptide secondary structures can broadly be split into three main conformations: α-helices, β-sheets and random coil. The α-helix conformation in naturally occurring peptides is a right handed coil with 3.6 residues per turn (**Figure 1.7a**). Hydrogen bonding between the oxygen carbonyl of residue *i* and the backbone amide hydrogen of residue *i* + *4* stabilises the α-helix conformation. Peptide α-helices are directional with backbone carbonyls pointing towards the C-terminal end of the peptide (**Figure 1.7b**).[95]

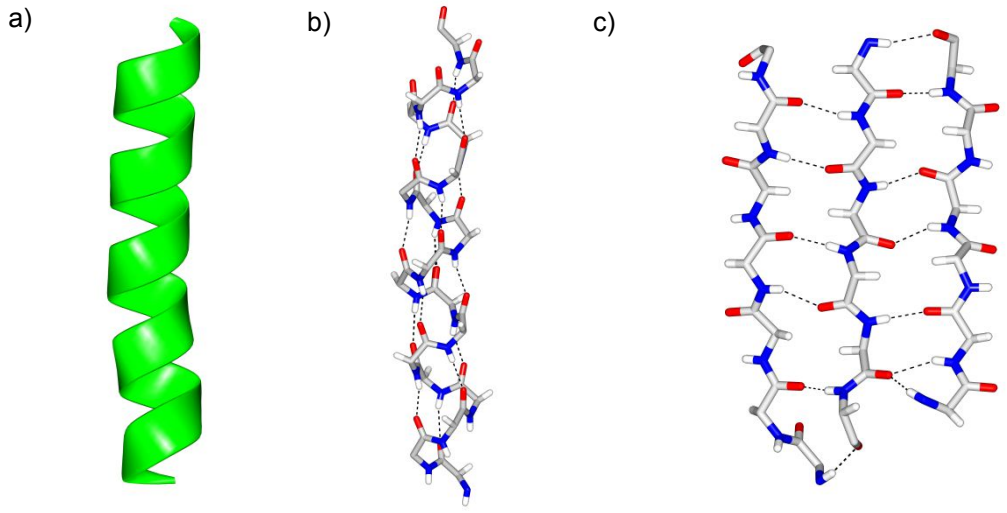

Figure 1.7 Peptide secondary structures with side-chains omitted for clarity: a) Ribbon drawing of an α-helix; b) The α-helix backbone showing hydrogen bonding between carbonyl oxygens and amide hydrogens; c) Peptide backbone showing an antiparallel β-sheet conformation with inter-chain hydrogen bonding.

The β-sheet conformation comprises peptide strands which are lined up in either a parallel or antiparallel fashion and stabilised by backbone hydrogen bonding between neighbouring strands (**Figure 1.7c)**.[96]

Peptide secondary structures can be defined by the allowed dihedral angles (*φ* and *ψ*, **Figure 1.8**) of the constituent amino acids.

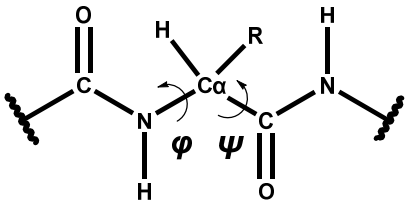

Figure 1.8 The dihedral angles of amino acids in a peptide backbone. The angle between N and Cα is *φ* and the angle between Cα and the carbonyl carbon is *ψ*.

The allowed combination of *φ* and *ψ* can be plotted on a Ramachandran plot (**Figure 1.9**). The allowed regions are characteristic of particular secondary structures.[97, 98]

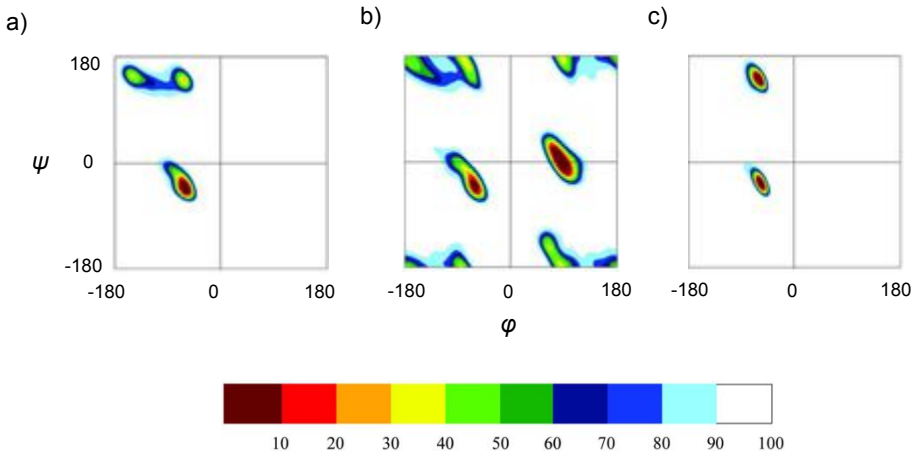

Figure 1.9 Experimentally observed Ramachandran plots of allowed dihedral angles (*φ* and *ψ*). The plot is colour coded according to the percentage of total amino acids in each area, i.e 10% of all amino acids are in the dark red areas, which make them the most densly populated. The white area typically takes up about 80 – 90% of the total area but only contains 10% of all amino acids: a) Observed regions for alanine. The region in the lower left quadrant is characteristic of the α-helical conformation. The region in the upper left quadrant contains two maxima and is the β-sheet region; b) Observed regions for glycine. Glycine has more allowed regions as a result of its lack of side-chain. This results in fewer steric clashes with neighbouring groups and hence can adopt a wider range of conformations; c) Observed regions for proline. Proline is a five membered ring about the backbone amide which restricts *φ* to about -65° resulting in fewer favourable conformations. Ramachandran plots obtained from Hovmöller *et al*., *Acta Cryst. D.*, (2002), **58**, 768-776. Reproduced with permission of the International Union of Crystallography, https://journals.iucr.org

In peptoids, the side-chain is moved from the α-carbon to the nitrogen in the amide bond, forming a tertiary amide. The movement of the side-chains and subsequent lack of amide proton means that the backbones of peptoids are more flexible than their peptide counterparts. The amide backbones of peptoids are able to adopt *cis*- or *trans*-conformations (**Figure 1.2**) and they are able to occpy regions of Ramachandran plots that are typically disallowed for peptides.[99] Furthermore, whilst peptide secondary structure is controlled by backbone hydrogen bonding, this is absent in peptoids meaning that any secondary structure is purely due to steric and electronic interactions.[10, 100]

1.4.1 Peptoid secondary structures: helices

The most studied peptoid secondary structure is the peptoid helix with such well-established chemistry that the rational synthesis of such structures is possible.[69, 101, 102] Peptoid helices commonly adopt a polyproline type one (PP1) structure with all-*cis* stereochemistry along the backbone (**Figure 1.10**). Peptoid helices contain three residues per turn with a pitch of about 6 Å. Whilst the peptoid backbone is intrinsically flexible and achiral, the incorporation of bulky side chains in the N_α positions can significantly restrict movement, and if the side chain is also chiral, this can induce chiral helices (**Figure 1.11** shows some commonly used bulky, chiral groups).[103-105]

Helical peptoids are studied using circular dichroism (CD) spectroscopy. In CD spectroscopy, the sample is exposed to circularly polarised light at different wavelengths and the absorption measured. Typically, peptoids adopting a helical secondary structure have a characteristic double minimum at 202 nm and 218 nm, similar to peptide helices, suggesting a structure similar to PP1 helices. Helical handedness is controlled by the chirality of the α-chiral side-chain and peptoids with side-chains of opposite chirality will give mirror image CD spectra. Inclusion of bulky, chiral side-chains adjacent to the backbone nitrogens can induce helicity in peptoids as short as five residues. However, in general, shorter peptoids are more likely to show interconversion between *cis* and *trans* conformations and therefore less defined secondary structure.[103] CD spectra of peptoids will show greater helicity if there is an aromatic side-chain at *i* and *i* + 3, however, stable peptoid helices can be formed if at least 50% of the monomers are chiral.[106] Helical peptoids have been synthesised that are stable to 75 °C and 8 M urea. The stability of helical peptoids, especially to heat, is consistent with the dominant role of steric interactions in structural stabilisation.[107]

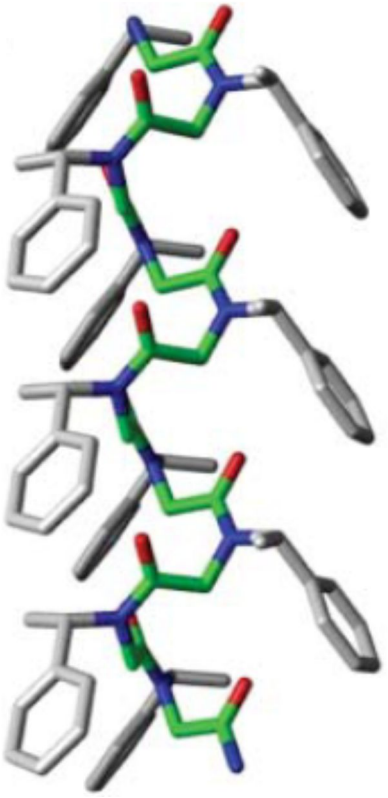

Figure 1.10 Polyproline type 1 peptoid helix. The structure was generated using molecular mechanics. Image reproduced in part from Fowler and Blackwell, *Org. Biomol. Chem*., (2009), with permission from The Royal Society of Chemistry.[100]

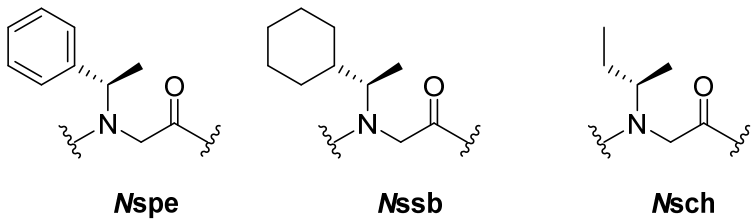

Figure 1.11 Bulky, chiral side-chains commonly used to induce helicity in peptoids.

More recently, polyproline type 2 (PP2) peptoid helices where the amide bonds are all *trans* have also been synthesised using multiple *N*-aryl glycine monomers[108] (**Figure 1.12**). *Cis*/*trans* isomerism in peptoids is influenced by electronic effects due to n → π* interactions between backbone carbonyls and side-chains, favouring *cis* conformations, or between carbonyl groups, favouring the *trans* configuration. Inclusion of electron deficient side chains lowers the HOMO - (n) LUMO (π*) gap between backbone

carbonyl and side-chain groups, favouring *cis* configurations. Conversely, electron rich side-chains destabilise this interaction in relation to the n → π* between adjacent backbone carbonyl groups (**Figure 1.13**).[7, 109] Therefore, whilst *N*-aryl glycine monomers favour *trans* configuration, a highly electron deficient polyfluorobenzyl side chain (**Figure 1.12**) favours a *cis* conformation.[6]

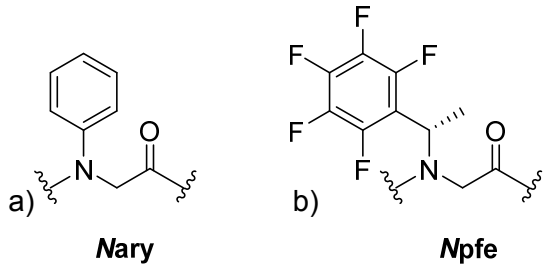

Figure 1.12 *N*-aryl glycine (*N*ary) side chain and pentafluorobenzyl (*N*pfe) side chain.

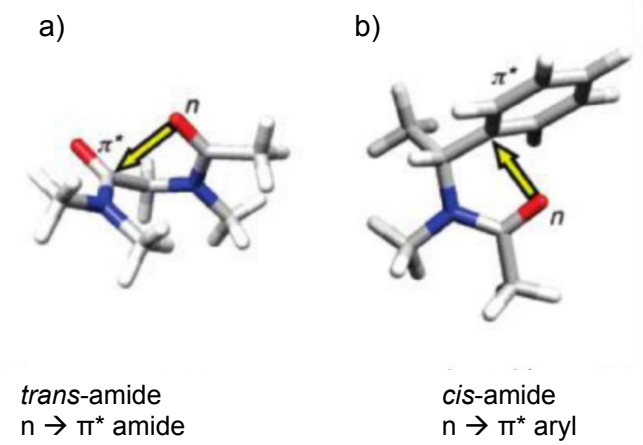

Figure 1.13 n → π* interactions between a) backbone amide carbonyls stabilising the *trans* conformation and b) backbone amide carbonyl and side chain stabilising the *cis* conformation. Oxygen is shown in red and nitrogen is blue. Adapted with permission from B. C. Gorske, B. L. Bastian, G. D. Geske and H. E. Blackwell, *J. Am. Chem. Soc.*, 2007, **129**, 8928-8929. Copyright 2007 American Chemical Society.[6]

1.4.2 Other peptoid secondary structures: turn structures and nanosheets

Other peptoid secondary structures have also been achieved, although the chemistry for these is in its infancy compared to that of helical secondary structures.

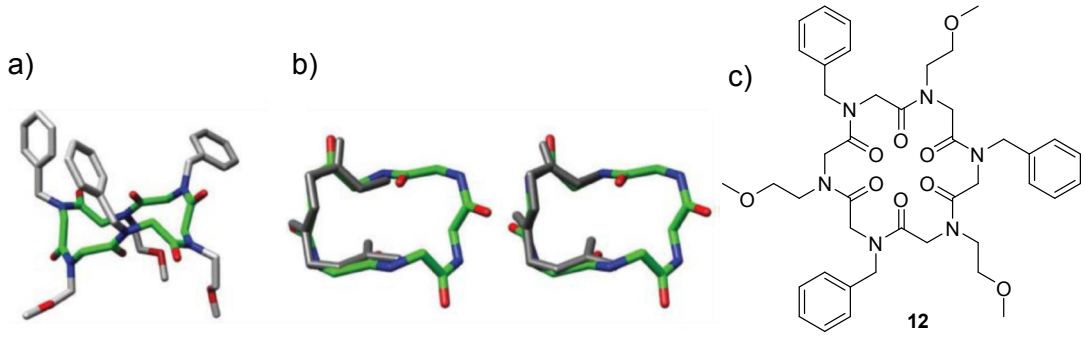

Figure 1.14 a) The x-ray crystal structure of an example macrocyclic peptoid hexamer with a turn structure b) the peptoid backbone with type I (left) and type III (right) peptide, both in grey c) chemical structure of macrocyclic peptoid hexamer (**12**). Image reproduced from Fowler and Blackwell, *Org. Biomol. Chem*., (2009), with permission from The Royal Society of Chemistry.[100]

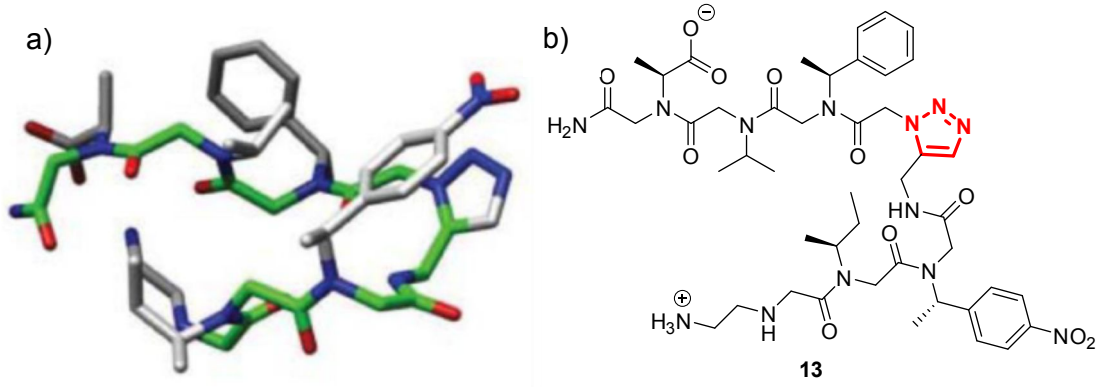

Figure 1.15 a) The NMR structure of the turn induced by an included triazole group with the backbone in green b) the structure of the example peptoid with the triazole highlighted in red. Image reproduced Fowler and Blackwell, *Org. Biomol. Chem*., (2009), with permission from The Royal Society of Chemistry.[100]

Peptoid turns have so far been induced by two methods: macrocyclisation[110] (which is discussed in greater detail in **Section 1.6**) and by the inclusion of heterocyclic monomers whose geometry mimics that of a turn.[111-113] Head-to-tail macrocyclisation (further discussed in **Section 1.6.1**) of linear peptoids containing alternating aromatic and alkyl side-chains form amphiphilic structures whereby hydrophobic residues are on one face and hydrophilic residues are on another. For hexamers (e.g. peptoid **12**) and octamers of this type, the structure resembles type I and type III β-turns with two amide

bonds in the turn region adopting a *cis* configuration while the rest of the amide bonds are *trans*[100, 110, 114] (**Figure 1.14**).

Alternatively, a monomer may be incorporated which mimics the turn structure. An example of this is the triazole monomer (**13**, **Figure 1.15** as an example). The triazole is a conformationally rigid structure that forms a tight turn. Inclusion of bulky α-chiral groups next to the triazole further stabilise this structure.[111]

Recently, peptoids have been designed that self-assemble into nanosheets: flat, 2D, planar bilayers of only 2.7 nm thickness, but that extend for many tens of microns in width and length[115] (**Figure 1.16**). Peptoid nanosheets are considered mimics of peptide β-sheets, however, unlike peptide β-sheets which have an inherent twist arising from the backbone chirality of peptides, peptoid nanosheets are completely flat. The first reported synthesis of a peptoid nanosheet was by the Zuckermann group in 2010 and consisted of two 36 residue peptoids of opposing charge: (*N*ae*N*pe)$_{18}$ (**14**) and (*N*ce*N*pe)$_{18}$ (**15**).

Nanosheet self-assembly was dependent on the constituent peptoids having alternating polar and non-polar, aromatic monomers and was dependent on periodicity: repeating units of two sub-monomers were necessary and having repeating units of three or four monomers did not result in nanosheet formation. The peptoids dissolved in concentrations of >50% acetonitrile but were stable to a range of pHs and temperatures.[115, 116]

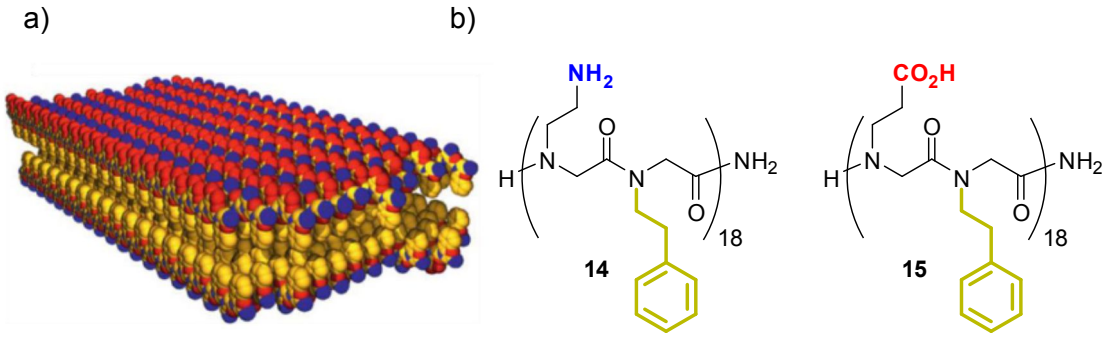

Figure 1.16 a) Peptoid nanosheet structure as obtained via molecular modelling. Oxygen is red, nitrogen is blue and carbon is yellow; b) Structures of positively charged peptoid (*N*ae*N*pe)$_{18}$ (**14**) and negatively charged peptoid (*N*ce*N*pe)$_{18}$ (**15**). Image reprinted with permission from Springer Nature, *Nat. Mater.,* "Free-floating ultrathin two-dimensional crystals from sequence-specific peptoid polymers," Nam *et al.*, copyright 2010 Nature Publishing Group.[115]

Later work by the Zuckermann group reported the synthesis of single peptoids capable of nanosheet self-assembly. Two peptoids were made using the same design principles from the two peptoid nanosheet, i.e. containing positively and negatively charged monomers with two-fold periodicity of alternating polar and non-polar aromatic residues. The first peptoid had a block charge copolymer-type structure of $(Nae Npe)_9(Nce Npe)_9$ and the second alternated positively and negatively charged monomers, $(Nae Npe Nce Npe)_{18}$. Both formed nanosheets, but the block copolymer structure was the most stable towards changes in pH and temperature.[117]

1.5 Attempts to rigidify peptoid secondary structure: cyclisation

In nature, one of the ways in which conformational rigidity is achieved is by forming covalent bonds that effectively 'staple' the three dimensional structure in place. For instance, small cyclic peptides exhibit strong antibacterial properties[118-121] and di-sulphide bridges are common in cysteine-containing peptides to constrain side chains.[122-124] In novel synthetic peptides, cyclisation can also lead to resistance to proteolysis and greater cell penetration.[110, 125, 126]

As with peptides, cyclic peptoids have been shown in several cases to improve cell penetration and also to enhance antimicrobial activity when compared to their linear precursors.[127] Cyclisation of linear peptoids restricts the movement of the peptoid, increasing rigidity and reducing the number of possible conformations.

1.6 Methods of cyclising peptoids

(Note: Parts of the below content can also be found in the minireview 'Recent Advances in the Synthesis of Peptoid Macrocycles' in Chemistry- A European Journal.[128] Reproduced with permission).

Recent cyclisation methods have been split into three broad techniques: head-to-tail, side chain- to-side chain and side chain-to-tail cyclisation and these will be discussed in the context of their possible applications.

1.6.1 Head-to-tail cyclisation

In 2007 the Kirschenbaum group reported the synthesis of peptoid macrocycles.[110] The technique used was head-to-tail cyclisation, carried out in the solution phase as a condensation reaction between the N-terminus and the carboxylic acid terminus (yielded by cleavage from 2-chlorotrityl resin, **Scheme 1.6**).

We have already briefly seen a cyclic peptoid hexamer (**12**) as an example of a peptoid turn structure (**Figure 1.14**). This peptoid was synthesised *via* efficient head to tail cyclisation from the linear precursor (**16**, **Scheme 1.6**).

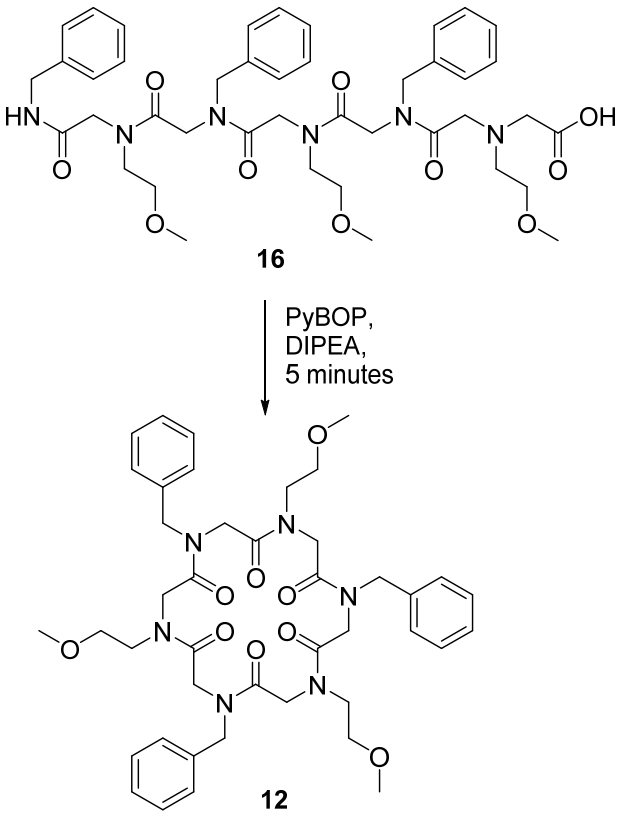

Scheme 1.6 Head to tail cyclisation of a linear peptoid (**16**) hexamer to form a cyclohexamer (**12**).

This methodology was more widely applied and chains up to 20-mer lengths underwent rapid room temperature cyclisations giving up to 90% yields after 5 minutes at room temperature at moderate dilutions (0.6 – 3.0 mM). Cyclisation of the peptoid octamer was also found to proceed with little accumulation of the intermolecular reaction products at concentrations ranging from 0.3 to 78 mM. Conversely, ring strain meant that the tetramer only cyclised with a 12% yield after 5 minutes. Notably, Shin *et al.*

managed to crystallise the cyclic hexamer (**12**) and the resulting crystal structure showed the hydrophobic phenyl side chains oriented on one face and the hydrophilic methoxy ethyl side chains oriented on the other face. This has implications for the future design of peptoid oligomers; it may be possible to design more complex peptoids which cyclise to form an ordered, amphiphilic structure.[110]

This method of head-to-tail cyclisation was more recently used to make a cyclic peptoid octamer (**17**, **Scheme 1.7**) which assembles to form a nanotubular structure (**Figure 1.17**), capable of reversibly sequestering water.[129]

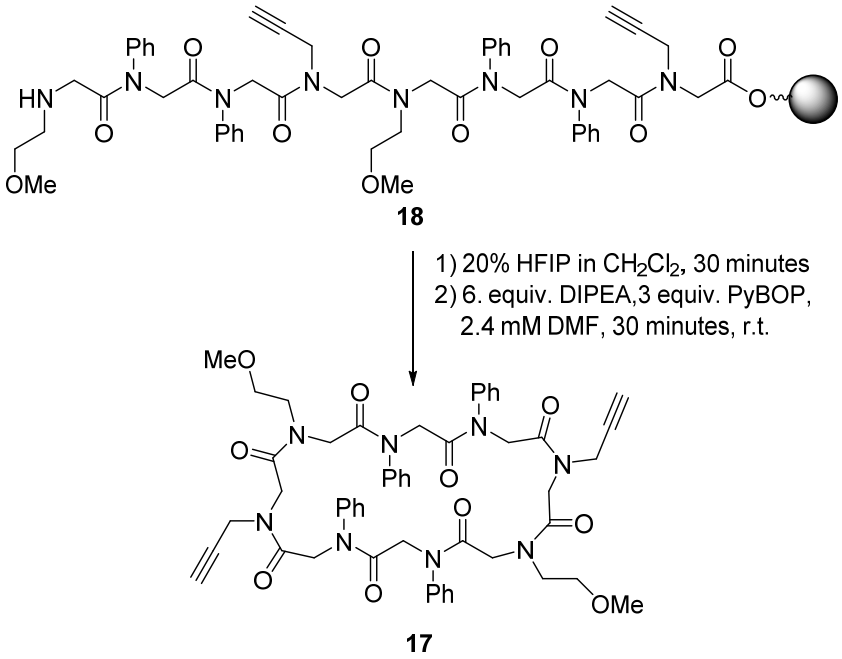

Scheme 1.7 Formation of a cyclic peptoid (**17**) from linear peptoid (**18**) which assembles into a nanotubular structure and is capable of reversibly sequestering water.

The linear parent peptoid (**18**) was designed to incorporate side chains that would impose a sequence of *cis* (*c*) and *trans* (*t*) amide bond configurations that corresponds to *ccttcctt*; a sequence observed in many peptoid macrocycles.[110] *N*-aryl glycine monomer units (**Figure 1.12**) have been shown to exhibit a strong preference for a *trans* conformation, as described previously in **Section 1.4.1**, whilst some *N*-alkyl monomer units show a preference for *cis* conformation.[108] This principle was used to select the side chains in the synthesis of the linear parent peptoid (**18**); the aryl groups enforced the *trans* conformation about the amide bonds whilst the methoxy groups were included to improve water solubility and the propargyl groups allow for possible further modification. The resulting macrocyle conformation was as predicted with the

alkyl groups allowing a *cis*-conformation of associated amide bonds and the aryl groups enforcing *trans*-conformations.

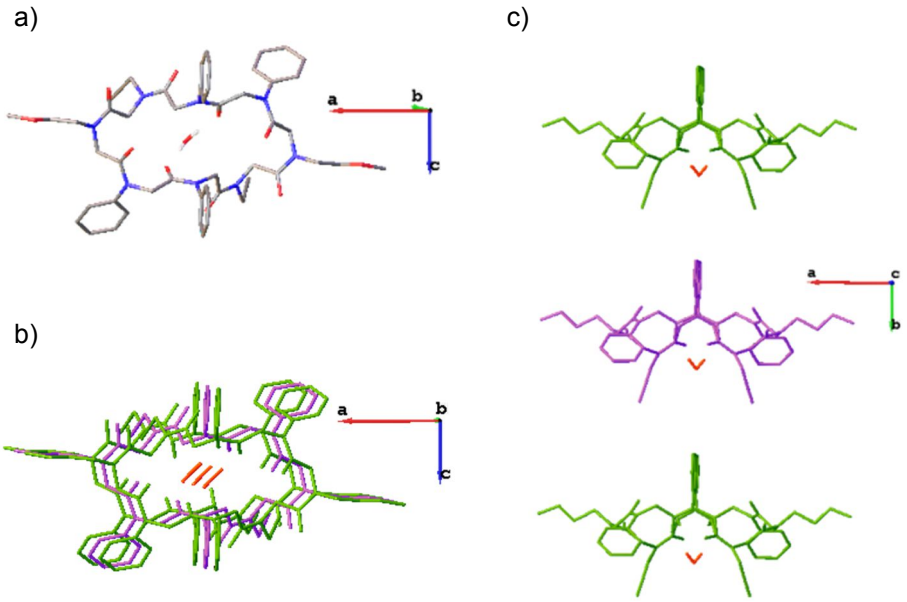

Figure 1.17 Crystal structure of water-sequestering peptoid macrocycle: (**17**), a) crystal structure of single molecule with oxygen in red and, nitrogen in blue and hydrogen in white; b) top view of three stacked peptoid macrocycles showing the cavity in which water (red) is sequestered; c) side view of three stacked peptoid macrocycles. Hydrogen is omitted (except for the water molecules) for clarity.

1.6.1.2 Small head-to-tail macrocyclic alpha peptoids

Since 2007, efforts have been made to synthesise smaller (3- to 5- mer) cyclic peptoids, but until recently, the yields obtained were often relatively low , particularly for the trimers (< 20%) or conditions were not optimised.[130-133] They are desirable targets since small cyclic tetrapeptides may act as histone deacetylase inhibitors (HDIs).[134, 135] HDIs have long been used as mood stabilisers and anti-epileptics, but are now also attracting interest as possible treatments for inflammatory[136] and parasitic diseases,[137] as well as cancers.[138] In 2012, Olsen *et al*. reported the synthesis of cyclotetrameric peptoid-peptide hybrids which inhibited class 1 histone deacetylases.[139] Hoping to provide the tools to eventually make entirely peptoid-based HDIs, in 2014, Culf *et al.* successfully synthesised cyclic tri-, tetra- and pentapeptoids in high yield (**Scheme 1.8**).[140]

The reactions were carried out in solution using a variety of activators and bases and found that a mixture of 1-Ethyl-3-(3-dimethylaminopropyl)carbodiimide (EDC), 1-

Hydroxy-7-azabenzotriazole (HOAt) and triethylamine (TEA) resulted in the best yields. When n = 1 or 3 the reported yields after overnight, room temperature incubation were 90% and 97% respectively. Under the same conditions, when n = 2, the reported yield was 38%, but when EDC and TEA were replaced with 1-[Bis(dimethylamino)methylene]-1H-1,2,3-triazolo[4,5-b]pyridinium 3-oxid hexafluorophosphate (HATU) and diisopropyl ethylamine (DIPEA), and the reaction was carried out at 50 °C overnight, the reported yield rose to 80%.

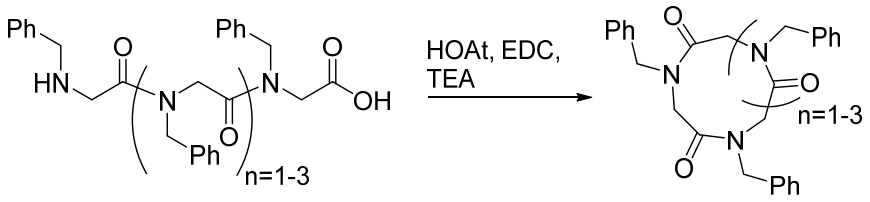

Scheme 1.8 Head-to-tail synthesis of short cyclic peptoids.

The authors did not elaborate on why the cyclisation of n = 2 was such a challenge, however they speculated that an increase in temperature improved the yield because of an increased rate of *cis-trans* isomerisation about the amide bonds.

1.6.1.3 Macrocyclic arylopeptoids

An interesting variation of head-to-tail cyclisation was reported in 2014 by Hjelmgaard *et al.* where arylopeptoids are cyclised and form nanotubular structures.[141]

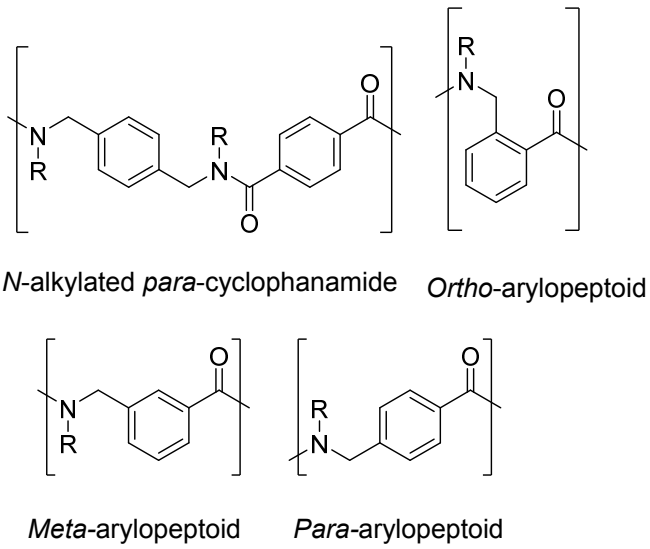

N-alkylated *para*-cyclophanamide *Ortho*-arylopeptoid

Meta-arylopeptoid *Para*-arylopeptoid

Figure 1.18 Comparison of the repeating units of *N*-alkylated *para*-cyclophanamides and arylopeptoids.

Arylopeptoids, which are considered a subclass of peptoids whereby the backbone is extended by a phenyl ring at each residue, are closely related to *N*-alkylated *para*-cyclophanamides (**Figure 1.18**). Macrocyclic *N*-alkylated *para*-cyclophanamides, if the R group is a long, hydrophobic chain, form a hydrophobic cavity and thus, these compounds show potential as selective hosts and artificial enzymes. Arylopeptoids can be efficiently synthesised, based on the sub-monomer method, and can readily undergo head-to-tail macrocyclisation (**Scheme 1.9**) to form rigid, well-defined structures, similar to *N*-alkylated *para*-cyclophanamides.

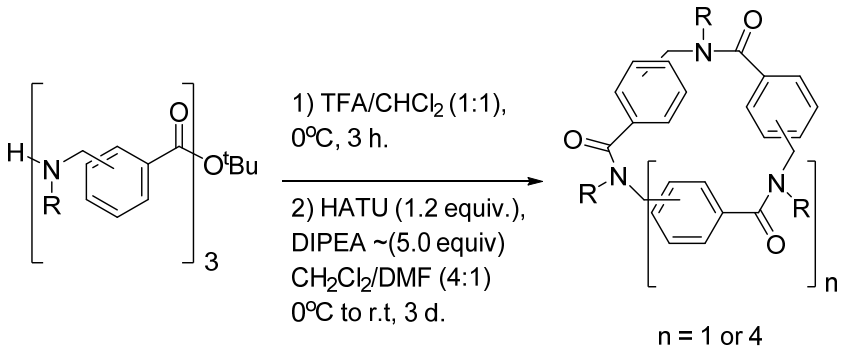

Scheme 1.9 Head-to-tail macrocyclisation of arylopeptoids.

The reactions in **Scheme 1.9** were carried out on *ortho*-, *meta*- and *para*-arylopeptoids. *Para*-arylopeptoids have a rigid backbone which means that head-to-tail cyclisation is challenging. Thus the resulting macrocycles were cyclohexamers (n=4, e.g. **19**) rather than cyclotrimers (n=1). Formation of the cyclotrimer (**20**) or cyclohexamer (**21**) from the *ortho*-arylopeptoid is dependent on the side chain; the substituents around the ring are more hindered, so a bulky side chain will favour formation of the cyclohexamer. Conversely, the *meta*-arylopeptoid favours the cyclotrimer (e.g. **22**), even with a bulky isopropyl side chain.

Crystal structures of some of the macrocycles showed the formation of tubular structures. In the case of the *ortho*-arylopeptoid the cyclohexamer (**21**) formed when the side chain is an isopropyl group contains one acetonitrile molecule (from the crystallisation solvent) in an interior cavity (**Figure 1.19**). These cyclohexamers stack to form a tubular array, even in the absence of any hydrogen bonding. It is speculated that a water molecule which bridges two consecutive rings may further stabilise the supramolecular assembly. Importantly, the presence of the acetonitrile molecule indicates that the interior cavity of this tubular array is large enough to accommodate a molecule, and thus the system has potential to be a selective host.

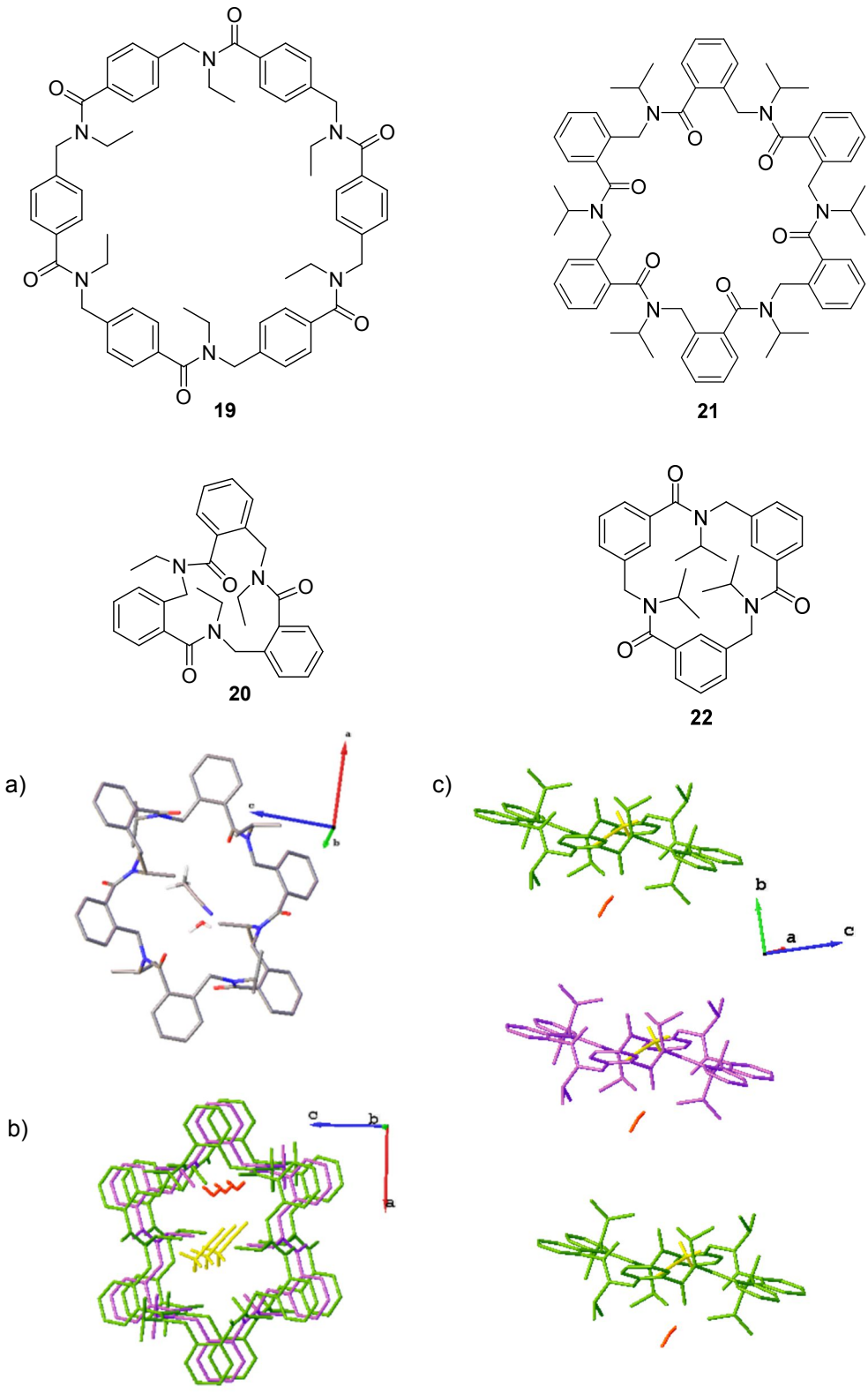

Figure 1.19 Crystal structure of orthoarylopeptoid cyclohexamer (**21**): a) crystal structure of single molecule with oxygen in red and, nitrogen in blue and hydrogen in white; b) top view of three stacked arylopeptoid macrocycles showing the cavity containing water (red) and acetonitrile (yellow); c) side view of three stacked peptoid macrocycles. Hydrogen is omitted (except for the water and acetonitrile molecules) for clarity.

1.6.1.4 Consecutive Ugi reactions

The Ugi 4-component reaction (U-4CR) is a multi-component reaction (MCR) which involves a ketone or aldehyde, an isocyanide and a carboxylic acid (**Scheme 1.10**).[142]

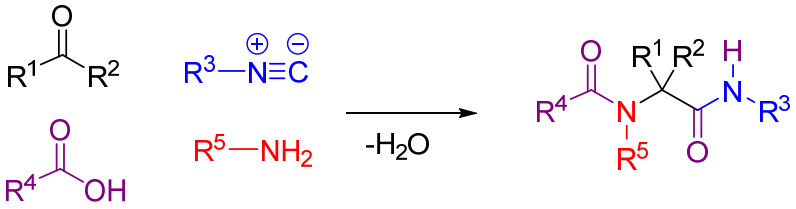

Scheme 1.10 General example of the Ugi 4-component reaction.

The U-4CR is used to synthesise large libraries of compounds, thanks to the ready availability of a wide range of suitable building blocks. Whilst there are many reports of U-4CRs being used to make peptoids and peptoid hybrids,[13, 143-146] U-4CRs have also been used to make and cyclise peptoids. In 2008, Vercillo *et al.* reported the syntheses of peptoid macrocycles using consecutive U-4CRs as a way to generate peptoid-RGD motifs.[14] The peptide-RGD is the tripeptide L-arginine-glycine-L-aspartate and peptoid-RGD is the corresponding peptoid sequence (i.e. with the side chains moved from the α-carbons to the backbone amide nitrogens). RGD is common to many peptides involved in cellular recognition[147] and the RGD loop is recognised by nearly half of all known integrins. Integrins are a family of cell-adhesion molecules and have key roles in various processes, including thrombosis, metastasis and osteoporosis.[147] Hence, integrins are attractive therapeutic targets and Vercillo *et al*. hoped that their peptoid-RGD-containing macrocycles could be used in this way. In order to achieve this, three consecutive Ugi reactions were carried out; the first two, U-4CRs, yielded the acyclic parent peptoid (**28**) and the third, an Ugi three-component 4-centre reaction, cyclised the parent peptoid to form peptoid-RGD-containing macrocycle **29** (**Scheme 1.11**).[14] Many RGD peptide macrocycles and nonpeptidic mimics have been shown to be highly active antagonists for a range of integrins.[148-151] These RGD peptide macrocycles and nonpeptidic mimics are also selective for particular integrins, due to the conformational rigidity imposed by cyclisation. However, studies of the activity and selectivity of **29** in comparison with the macrocyclic peptide analogue are not yet available.

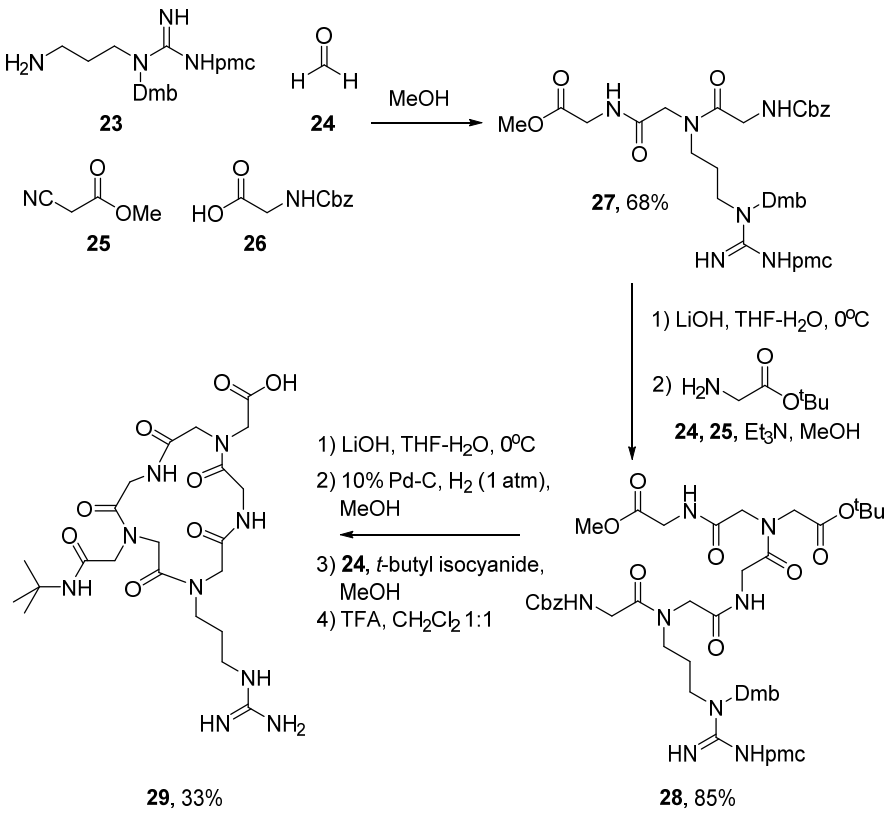

Scheme 1.11 Synthesis of peptoid-RGD-containing macrocycle (**29**) by consecutive Ugi reactions.

1.6.2 Side chain cyclisation

1.6.2.1 Grubbs' Ring-Closing metathesis

Olefin metathesis is a widely applied method of carbon-carbon bond formation using ruthenium alkylidene catalysts. Ring-closing metathesis (RCM, **Figure 1.20**) can be used to form large macrocycles.[152]

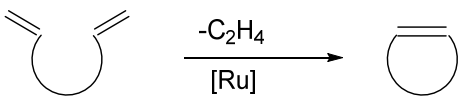

Figure 1.20 Representative Ring-Closing Metathesis (RCM).

RCM has many features that make it attractive for use in the formation of cyclic peptoids; the catalysts are tolerant of a wide variety of functional groups, allowing variation in the side chain groups. The catalysts are easily handled, not requiring the

use of glove boxes, and the reaction is clean, producing few by-products, making purification straightforward. RCM is usually carried out in solution phase, and, as seen above, cyclisation of peptoids can also be carried out in solution. However, particularly when transition metal catalysts are used, solid phase synthesis is preferred; carrying out the reaction with the peptoid on resin allows removal of any non-resin-bound by-products and unreacted starting materials by simply washing the resin. This also simplifies recovery of the catalyst. The solid phase synthesis of cyclic peptoids by RCM (**Scheme 1.12**) was reported by Khan *et al.* in 2011.[153]

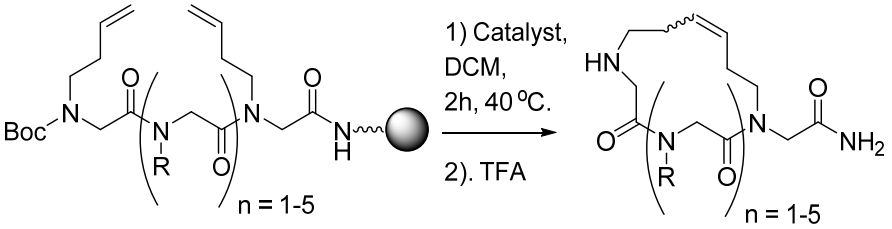

Scheme 1.12 Grubbs Ring Closing Metathesis reaction on resin to form cyclic peptoids as reported by Khan *et al*.

Initially, the double bonds in the side chain were included by the use of allylamine for the substitution step of peptoid synthesis, but this produced the corresponding cyclic peptoids in very low yields (10 – 20%). The parent peptoid structure was subsequently altered to extend the length of the alkene-containing side chain by swapping allylamine for 3-buten-1-amine in the corresponding substitution step.

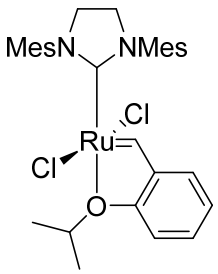

30

Various catalysts were tested, but the most effective one was phosphine free (**30**), giving a yield of 80% compared to 20% of the next best catalyst when reacted with a model peptoid. The reaction was carried out both under microwave conditions and at 40 °C on a shaker, with the latter conditions being slightly more efficient, particularly in minimising formation of dimers.

1.6.2.2 Thiol-ene

The thiol-ene reaction (**Scheme 1.13**) is considered a type of 'click chemistry' due to high yields, stereoselectivity and rates.[154, 155] There are two mechanisms by which the thiol-ene reaction may proceed; either by radical addition or Michael addition, catalysed by either a base or a nucleophile.

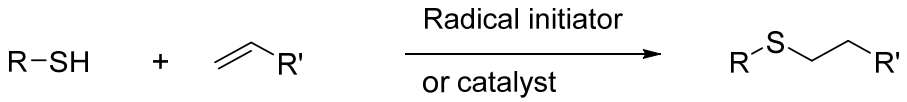

Scheme 1.13 The thiol-ene reaction.

The thiol-ene reaction has been used to cyclise peptides, using a maleimide (**31**) as the source of the double bond.[156] Non-protected maleimides can only be incorporated at the end of the chain since they are labile to the nucleophilic bases that are used in peptide/peptoid synthesis. 2,5-Dimethylfuran (**32**) can be used to protect maleimides (**Scheme 1.14**); 2,5-dimethylfuran (**32**) reacts with the maleimide (**31**) by Diels-Alder cycloaddition. The protected maleimide (**33**) can be deprotected by heating.

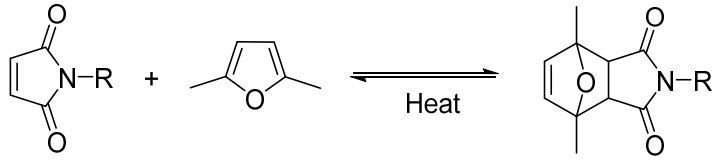

31 **32** **33**

Scheme 1.14 Protection of maleimides by Diels-Alder reaction with 2,5-dimethylfuran.

In principle, protection of the maleimide in this way allows it to be incorporated at any place in a peptide/peptoid chain; however, in the paper, maleimido group inclusion was at the *N*-terminus only (**34**). After cleavage from the resin, the maleimide was deprotected and cyclisation occurred in the same step to give cyclic peptoid **35** (**Scheme 1.15**).

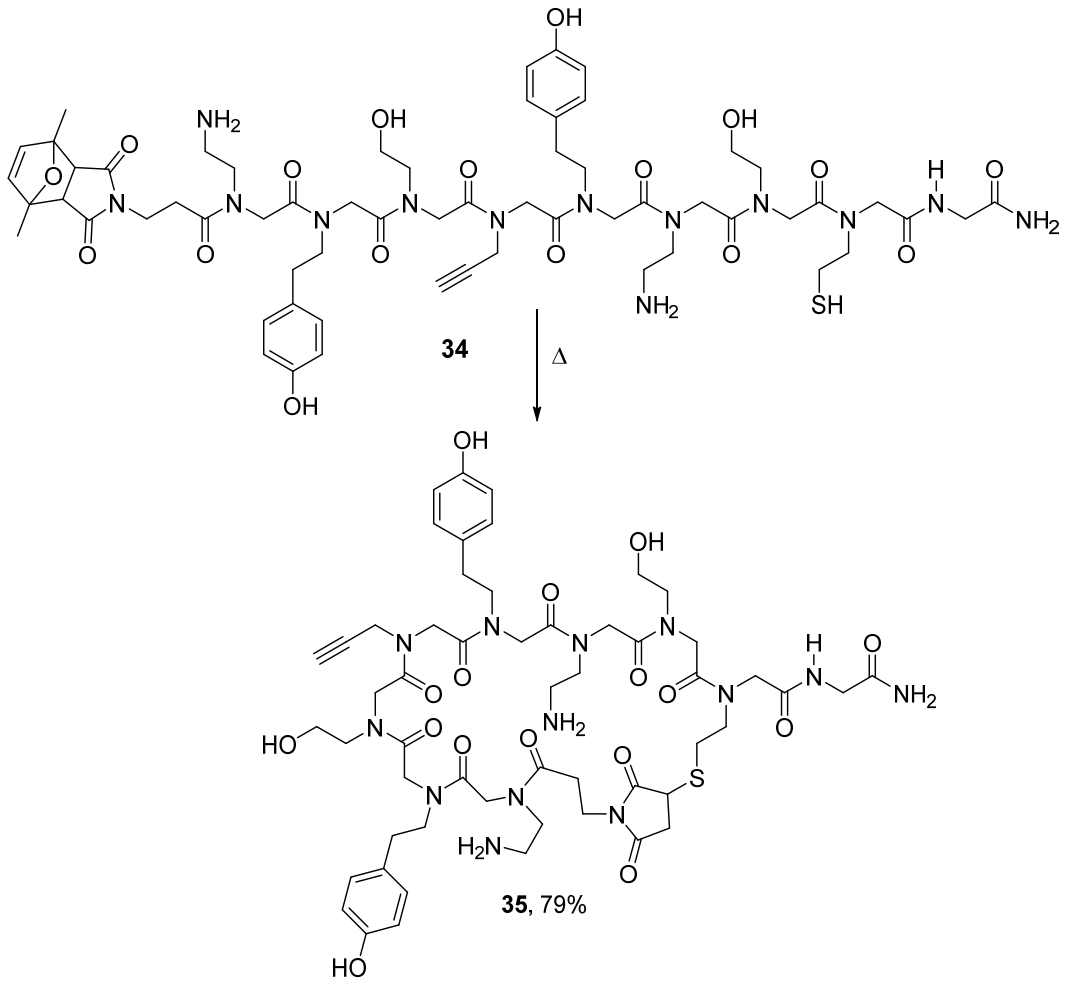

Scheme 1.15 Peptoid cyclisation by a thiol-ene reaction.

In the paper by Elduque *et al.* the cyclised peptoid (**35**) was then used to attach a nucleoside, 2',3'-dideoxy-3'-azidothymidine (AZT, **36**), via Huisgen reaction to form peptoid-AZT conjugate **37** (**Scheme 1.16**).[156]

AZT (**36**) is an anti-retroviral drug used to treat HIV/AIDS.[157] At high doses, AZT is associated with side effects such as anaemia, neutropenia, hepatotoxicity, cardiomyopathy and myopathy. This limits the dose that can be given to patients, and this means that some HIV replication still occurs. This allows resistance to develop so that, ultimately, the progression of the disease is only slowed.[158] Development of resistance is slowed by combining AZT with other anti-retroviral medicines. Conjugation of AZT to cyclic peptoids is of interest to see whether cell uptake and subsequent interaction with components of the cell is improved, or different.

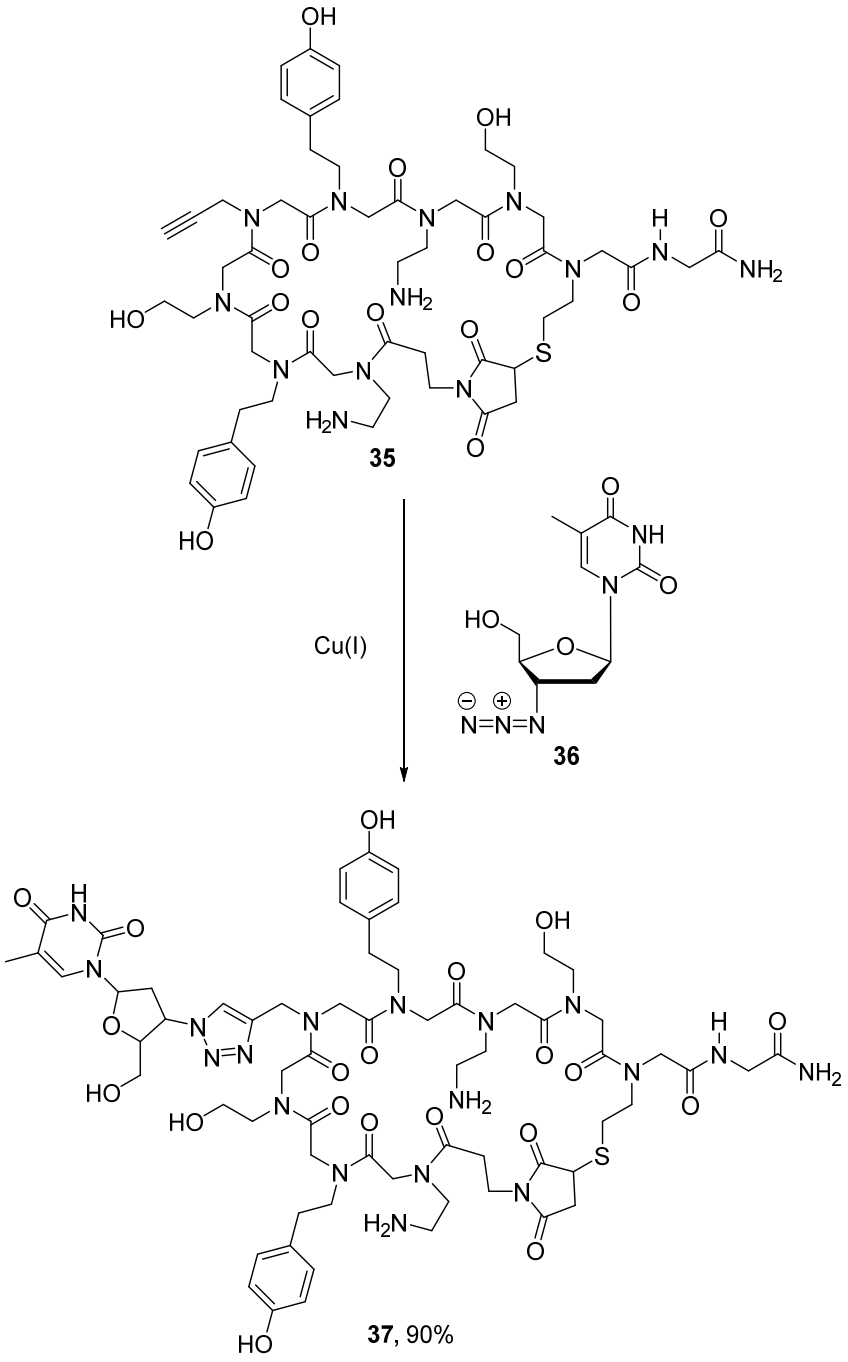

Scheme 1.16 Conjugation of a nucleoside to a cyclic peptoid by Huisgen condensation to form and AZT-containing cyclic peptoid (**37**).

1.6.2.3 Copper(I)-Catalysed Azide-Alkyne Cycloaddition (CuAAC)

Copper(I)-catalysed azide-alkyne cycloaddition (CuAAC) refers to a 1,3 dipolar cycloaddition between an azide and an alkyne to give a 1,2,3-triazole (**Scheme 1.17**). CuAAC is considered a 'click' reaction, and is catalysed by a Cu(I) compound in the

presence of a non-nucleophilic base.[159] It is a high yielding and versatile reaction since the required functional groups are easily incorporated into a variety of compounds.

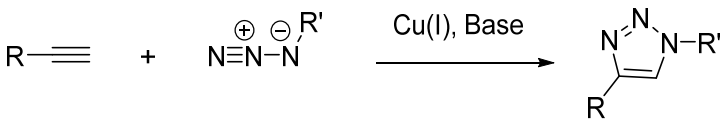

Scheme 1.17 Copper(I)-catalysed azide-alkyne cycloaddition (CuAAC).

CuAAC as a method to cyclise peptoids was first reported in 2007 by the Kirshenbaum group (**Scheme 1.18**).[160] This on-resin reaction was used as a way to 'staple' helical peptoid chains in order to rigidify the structure.

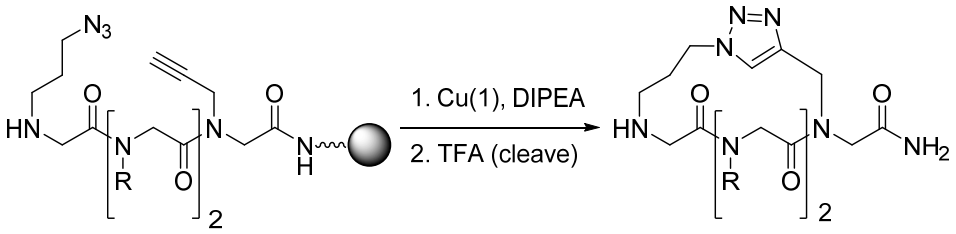

Scheme 1.18 CuAAC to form a cyclic peptoid.

In 2012, the Kirshenbaum group used CuAAC in the solution phase to form a bicyclic peptoid (**Scheme 1.19**).[161] A linear peptoid containing both an azide and an alkyne group side chain (**38**) was first synthesised, cleaved from the resin and then cyclised by head to tail condensation between the N-terminus and the carboxylic acid-terminus to form the a monocyclic peptoid (**39**). Bicyclic peptoid **40** was then formed by CuAAC between the side chain alkyne and azide groups. This intramolecular reaction was the major reaction pathway under dilute conditions, giving a yield of 27% but formation of the homodimeric, doubly crosslinked peptoid (**41**) with a yield of 4% was also observed. Crystal structures of **40** and **41** were obtained (**Figure 1.21**). Whilst **40** appeared to exist in only one configuration, bicyclic peptoid **41** was found to be a mixture of two backbone conformations and further investigation determined the conformation of the monocyclic peptoid to be the main factor contributing to the conformation of the resulting bicyclic peptoid. The formation of bicyclic peptoids by the use of the efficient and versatile CuAAC has the potential to unlock more complex, constrained peptoid conformations.

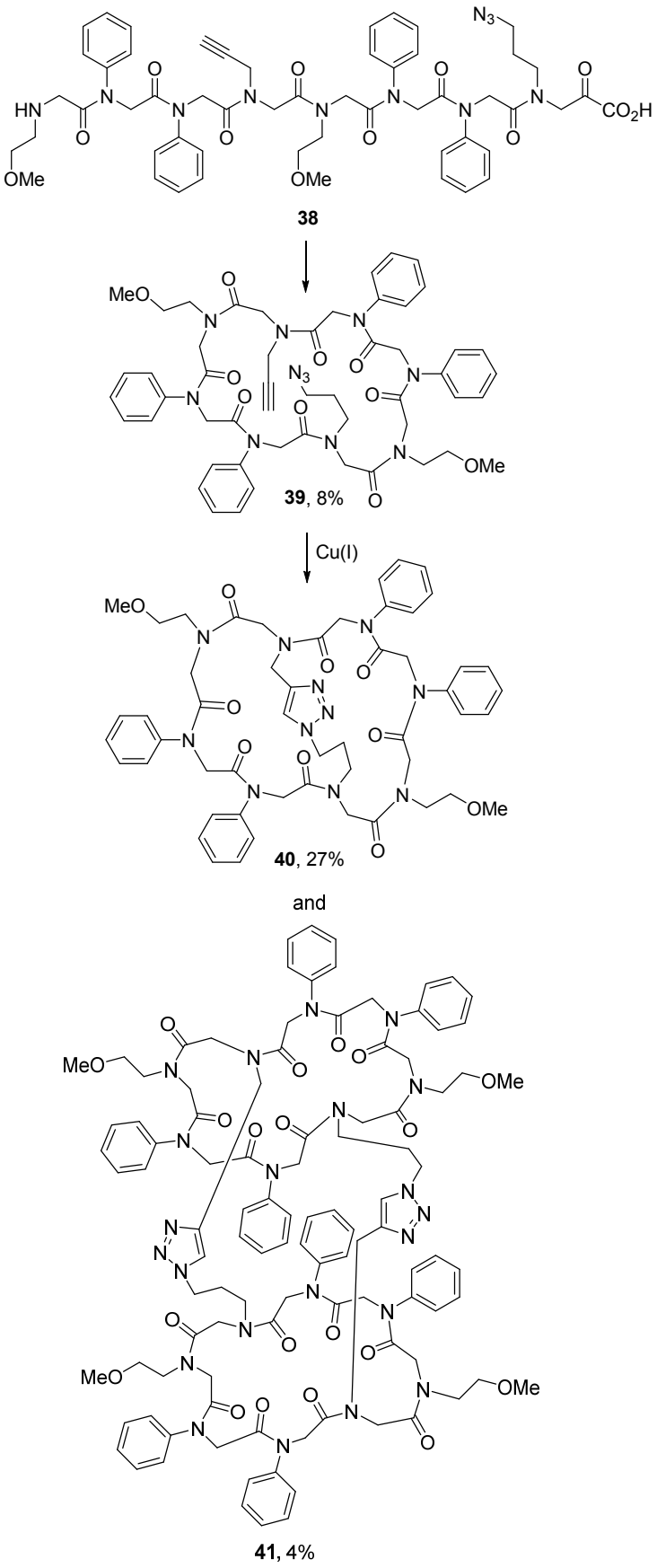

Scheme 1.19 Formation of a bicyclic peptoid (**40**, major product) using CuAAC, and the homodimeric, doubly crosslinked peptoid (**41**, minor product).

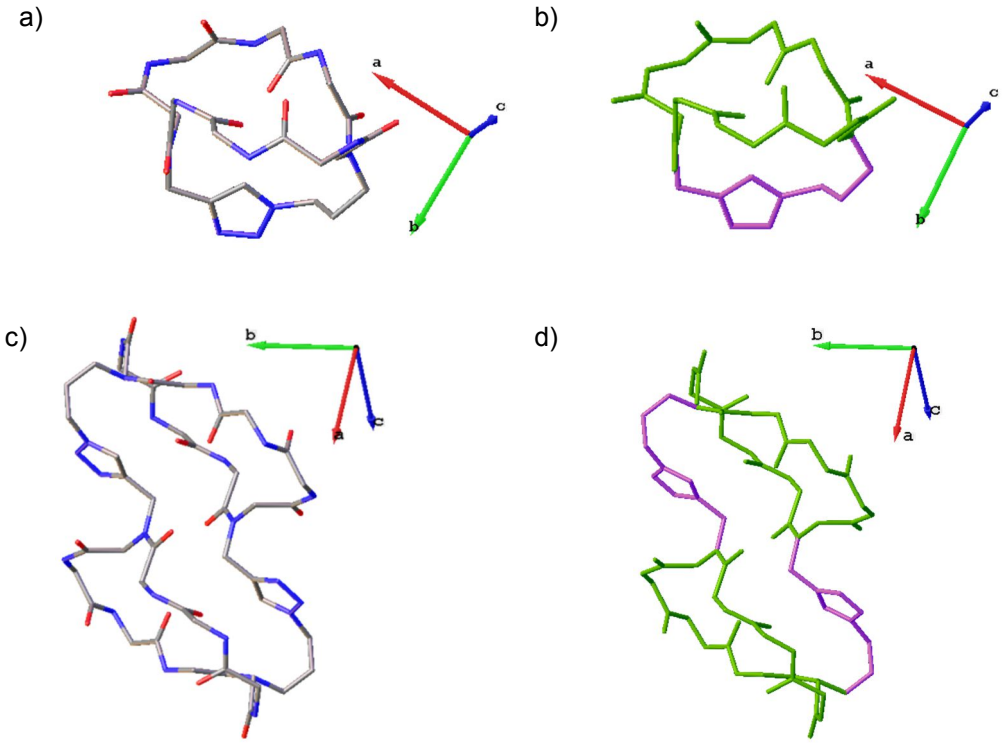

Figure 1.21. Crystal structures of bicyclic peptoid cyclooctamer (**40**) and the homodimeric, doubly crosslinked peptoid (**41**): a) crystal structure of cyclooctamer (**40**) with oxygen in red and, nitrogen in blue and hydrogen in white; b) crystal structure of **40** highlighting the triazole and bridging side-chains (purple) and the original cyclic peptoid structure obtained via head-to-tail macrocyclisation (green); c) crystal structure of the homodimeric, doubly crosslinked peptoid (**41**) with oxygen in red and, nitrogen in blue and hydrogen in white; b) crystal structure of **41** highlighting the triazole and bridging side-chains (purple) and the original cyclic peptoid structures obtained via head-to-tail macrocyclisation (green). Non-bridging side-chains and all hydrogen atoms are omitted for clarity.

1.6.3 Side chain-to-tail cyclisation

1.6.3.1 Nucleophilic substitution

In 2015, Kaniraj and Maayan reported a high yielding side-chain-to-tail method of cyclic peptoid synthesis. The linear parent peptoid includes a chloride side chain that reacts with a secondary amine at the terminus of the peptoid chain by substitution under basic conditions (**Scheme 1.20**).[162] The cyclisation reaction was carried out whilst the peptoid was still on resin, meaning that protecting groups on any side chain functional groups could be removed at the same time as the peptoid was cleaved from the resin. This allowed for the inclusion of a wide range of functional groups in the peptoid chain.

Cyclisation occured with the propyl chloride side chain in various positions on the peptoid chain to form ring sizes as small as 4 and as large as 19.

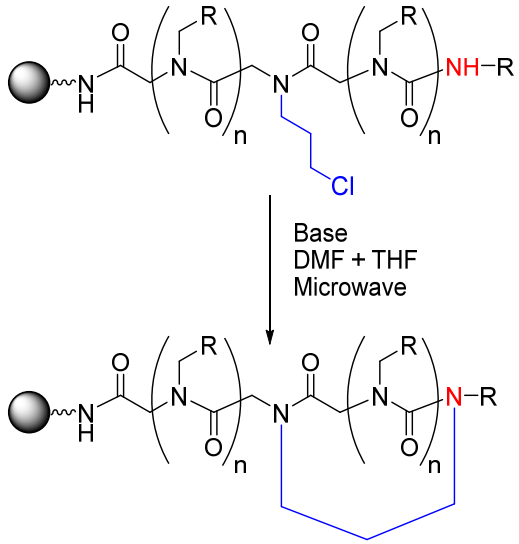

Scheme 1.20 Side chain to tail formation of a cyclic peptoid by halide substitution.

We have already seen head-to-tail macrolactamisation but macrolactamisation can also be used in a side chain-to-tail cyclisation (**Scheme 1.21**).[163] However, unlike in the head-to-tail method, the side chain-to-tail method is carried out whilst the peptoid is still on resin.

The sequences chosen for the peptoids were based on linear and cyclic sequences seen to inhibit the interaction between apolipoprotein E and amyloid-β; a cause of Alzheimer's disease, though whether the cyclic peptoids actually interacted with either compound was not confirmed.

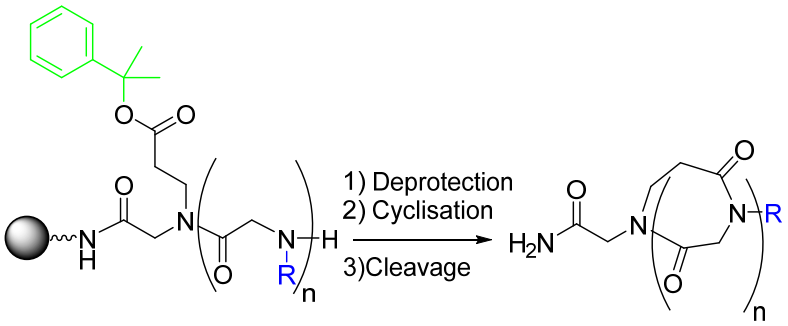

Scheme 1.21 Side chain to tail macrolactamisation.

The sequencing of peptoids is problematic; something that is a major barrier to their utility. In 2014, the successful sequencing of peptoids was achieved by first cyclising a modified linear peptoid on resin (**Scheme 1.22**).

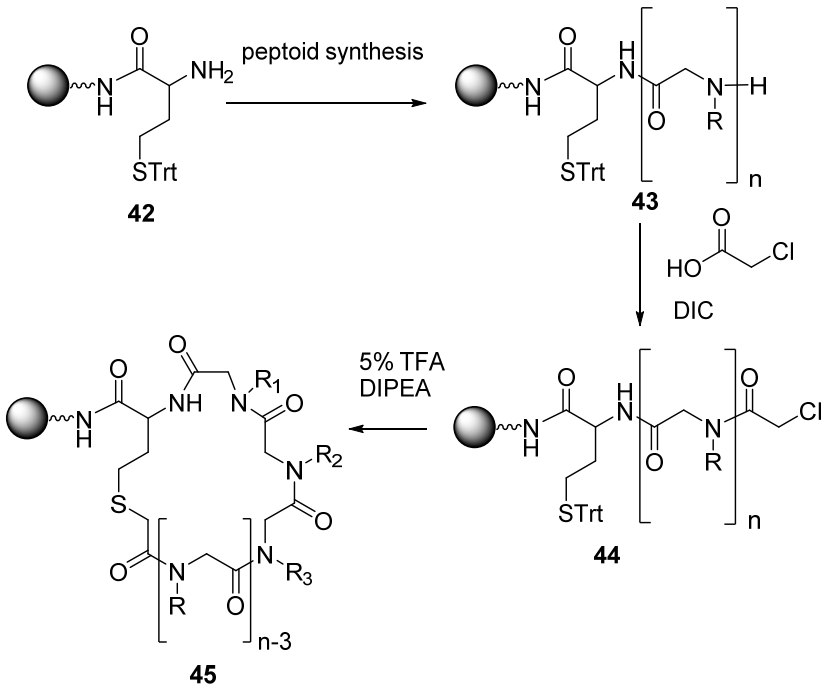

Scheme 1.22 Synthesis of a cyclic peptoid precursor (**45**) to a sequenceable linear peptoid.

A homocysteine residue was incorporated into the sequence as the first residue giving **42**. The peptoid (**43**) is then synthesised by the sub-monomer method and the N-terminus is chloroacetylated (**44**). Subsequent deprotection of the homocysteine sulfur and base-mediated cyclisation gave a cyclic peptoid (**45**) which, when cleaved from the resin, gave a linear peptoid that was tagged at each end. The incorporation of two different end groups enabled sequencing by tandem mass spec. The thioether could be oxidised by mCPBA to yield the linear peptoid. However, due the strong oxidising ability of mCPBA, other functional groups in the peptoid were affected. In order to prevent side reactions with other functional groups, the peptoid is synthesised on Tentagel S NH_2 resin and CNBr can be used to cleave the peptoid and open the ring (**Scheme 1.23**), giving the tagged linear peptoid (**46**).[164]

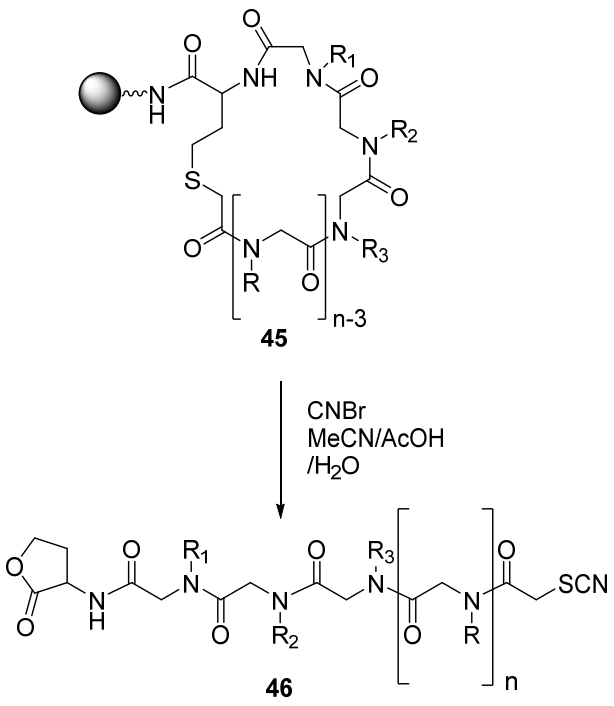

45

46

Scheme 1.23 Cleavage of cyclic peptoid (**45**) to give the tagged linear peptoid (**46**).

1.7 Conclusions and Project Overview

Numerous studies have shown that peptoids have huge potential as novel therapeutic agents, with their resistance to proteolytic degradation of particular interest. Their potential applications are wide ranging, from anti-infective agents, to anticancer drugs, to imaging probes, to transporters for other therapeutic agents. However, peptoid therapeutics are not without their own drawbacks, mainly arising from *cis/trans* isomerism of the amide bonds and the lack of backbone hydrogen bonding resulting in poorly defined secondary structures. A lack of conformational rigidity presents a serious problem for certain therapeutic applications, as this is often linked to good selectivity and binding affinity for a specific target. Poor selectivity and binding affinity can result in reduced effectiveness of the drug and increase the chance of off-target effects

Chapter 2 looks at boronic acid-containing peptoids. The first part of Chapter 2 details attempts to make a novel protected boronic-acid building block that may be incorporated anywhere in a peptoid sequence. Boronic acids are synthetically and therapeutically useful functionalities but their application in peptoids is thus far limited. The ability to incorporate boronic acids at any point in a peptoid chain using the sub-

monomer method is therefore beneficial. The second part of Chapter 2 looks to synthesise a library of novel cyclic peptoids via Suzuki-Miyaura cross-coupling (**Scheme 1.24**). In doing so, we hope to report novel peptoid scaffolds that impose conformational rigidity. A further feature of these peptoids the presence of the biaryl group which is a motif seen in many therapeutics and which is discussed further in **Chapter 2**.

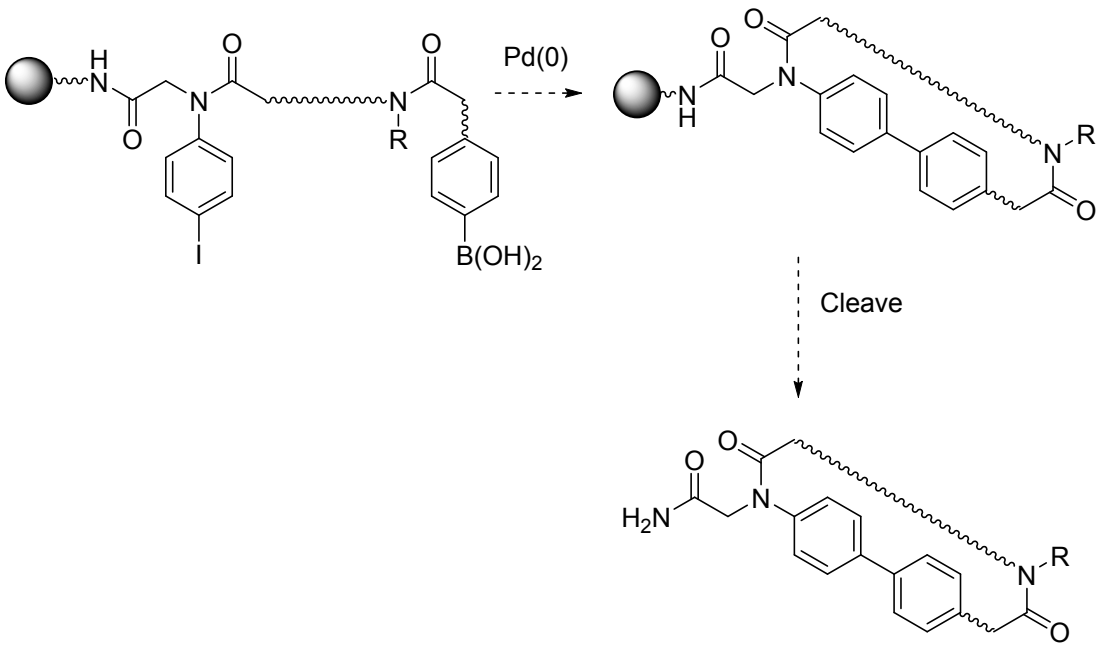

Scheme 1.24 Proposed Suzuki-Miyaura cross-coupling to form a cyclic peptoid.

Chapter 3 reports the synthesis of the nucleophosmin-binding segment of the anticancer peptide CIGB300 and three stapled analogues in order to carry out binding assays. The ultimate aim is making a more stable analogue of the whole peptide. This is done in two ways, summarised in **Figure 1.22**. The first way is by making minor alterations to the structure of the active peptide via different stapling methods, for example by replacing the existing disulphide bridge with a C-C linked bridge. The second way to stabilise the peptide is, by replacing the attached peptidic transporting unit with a series of short cell-penetrating peptoids, and this is the theme of **Chapter 4**.

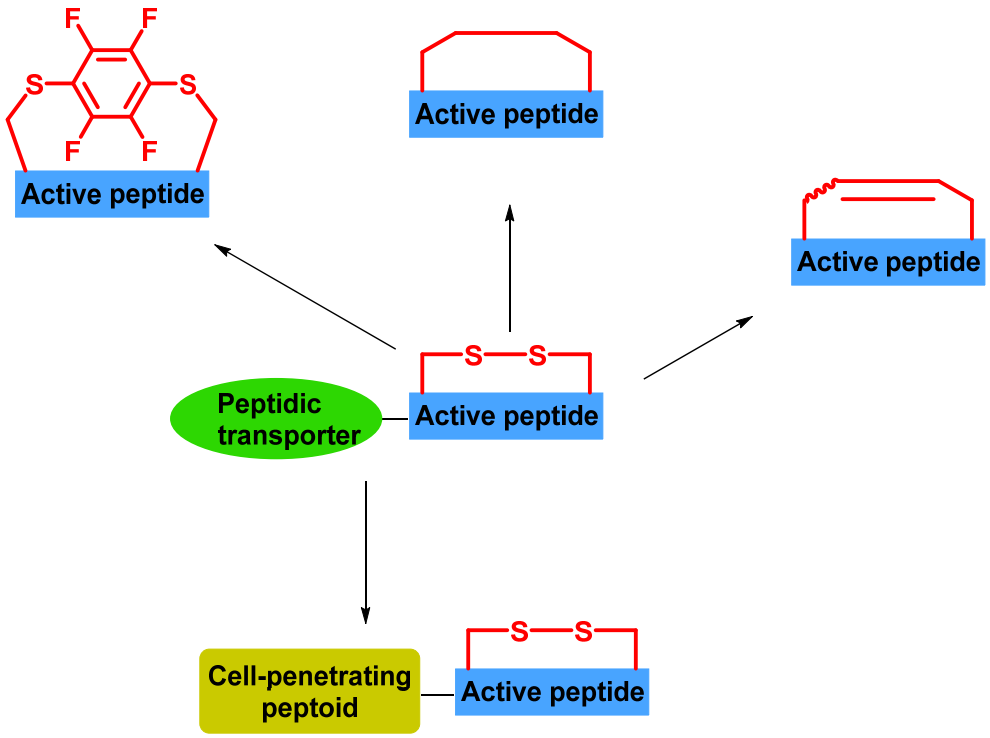

Figure 1.22 Strategy for stabilising an existing anticancer peptide

Chapter 4 describes the use of a series of short cell-penetrating peptoids to deliver bioactive peptides to their targets. The first peptide sequence this is applied to is the anticancer KLA peptide sequence (D-(KLAKKLAK)$_2$). The resulting peptoid-KLA peptide hybrids are shown to be toxic to HeLa cells whilst the unmodified KLA peptide shows little toxicity. The second peptide sequence is the nucleophosmin-binding part of CIGB-300, synthesised in **Chapter 3**. The resulting chimeras will then be conjugated to a luminescent probe.

1.8 References

1. R. J. Simon, R. S. Kania, R. N. Zuckermann, V. D. Huebner, D. A. Jewell, S. Banville, S. Ng, L. Wang, S. Rosenberg and C. K. Marlowe, *Proc. Natl. Acad. Sci.*, 1992, **89**, 9367-9371.
2. J. Seo, B. C. Lee and R. N. Zuckermann, in *Comprehensive Biomaterials*, ed. P. Ducheyne, Elsevier, Oxford, 2011, vol. 2, pp. 53-76.
3. S. M. Miller, R. J. Simon, S. Ng, R. N. Zuckermann, J. M. Kerr and W. H. Moos, *Bioorganic Med. Chem. Lett.*, 1994, **4**, 2657-2662.
4. S. M. Miller, R. J. Simon, S. Ng, R. N. Zuckermann, J. M. Kerr and W. H. Moos, *Drug Dev. Res.*, 1995, **35**, 20-32.
5. Q. Sui, D. Borchardt and D. L. Rabenstein, *J. Am. Chem. Soc.*, 2007, **129**, 12042-12048.
6. B. C. Gorske, B. L. Bastian, G. D. Geske and H. E. Blackwell, *J. Am. Chem. Soc.*, 2007, **129**, 8928-8929.

7. B. C. Gorske, J. R. Stringer, B. L. Bastian, S. A. Fowler and H. E. Blackwell, *J. Am. Chem. Soc.*, 2009, **131**, 16555-16567.
8. C. Caumes, O. Roy, S. Faure and C. Taillefumier, *J. Am. Chem. Soc.*, 2012, **134**, 9553-9556.
9. J. S. Laursen, J. Engel-Andreasen, P. Fristrup, P. Harris and C. A. Olsen, *J. Am. Chem. Soc.*, 2013, **135**, 2835-2844.
10. R. N. Zuckermann, J. M. Kerr, S. B. H. Kent and W. H. Moos, *J. Am. Chem. Soc.*, 1992, **114**, 10646-10647.
11. T. Hjelmgaard, S. Faure, C. Caumes, E. De Santis, A. A. Edwards and C. Taillefumier, *Org. Lett.*, 2009, **11**, 4100-4103.
12. A. d. F. S. Barreto, O. E. Vercillo, M. A. Birkett, J. C. Caulfield, L. A. Wessjohann and C. K. Z. Andrade, *Org. Biomol. Chem.*, 2011, **9**, 5024-5027.
13. D. G. Rivera and L. A. Wessjohann, *J. Am. Chem. Soc.*, 2006, **128**, 7122-7123.
14. O. E. Vercillo, C. K. Z. Andrade and L. A. Wessjohann, *Org. Lett.*, 2008, **10**, 205-208.
15. K. Fosgerau and T. Hoffmann, *Drug Discov. Today*, 2015, **20**, 122-128.
16. J. Oehlke, A. Scheller, B. Wiesner, E. Krause, M. Beyermann, E. Klauschenz, M. Melzig and M. Bienert, *Biochim. Biophys. Acta, Biomembr.*, 1998, **1414**, 127-139.
17. M. Pooga, M. Hällbrink, M. Zorko, U. Langel and lo, *FASEB J.*, 1998, **12**, 67-77.
18. L. Maler, *Adv. Drug Delivery Rev.*, 2013, **65**, 1002-1011.
19. E. Eiríksdottir, H. Myrberg, M. Hansen and U. Langel, *Drug. Des. Rev. Online*, 2004, **1**, 161-173.
20. M. Zorko and Ü. Langel, *Adv. Drug Delivery Rev.*, 2005, **57**, 529-545.
21. D. J. Mitchell, L. Steinman, D. T. Kim, C. G. Fathman and J. B. Rothbard, *J. Pept. Res.*, 2000, **56**, 318-325.
22. D. Derossi, A. H. Joliot, G. Chassaing and A. Prochiantz, *J. Biol. Chem.*, 1994, **269**, 10444-10450.
23. A. Scheller, J. Oehlke, B. Wiesner, M. Dathe, E. Krause, M. Beyermann, M. Melzig and M. Bienert, *J. Pept. Sci.*, 1999, **5**, 185-194.
24. M. A. Chellaiah, N. Soga, S. Swanson, S. McAllister, U. Alvarez, D. Wang, S. F. Dowdy and K. A. Hruska, *J. Biol. Chem.*, 2000, **275**, 11993-12002.
25. E. Vivès, P. Brodin and B. Lebleu, *J. Biol. Chem.*, 1997, **272**, 16010-16017.
26. A. Eguchi, T. Akuta, H. Okuyama, T. Senda, H. Yokoi, H. Inokuchi, S. Fujita, T. Hayakawa, K. Takeda, M. Hasegawa and M. Nakanishi, *J. Biol. Chem.*, 2001, **276**, 26204-26210.
27. S. Violini, V. Sharma, J. L. Prior, M. Dyszlewski and D. Piwnica-Worms, *Biochemistry*, 2002, **41**, 12652-12661.
28. K. Li, X.-X. Lv, F. Hua, H. Lin, W. Sun, W.-B. Cao, X.-M. Fu, J. Xie, J.-J. Yu, Z. Li, H. Liu, M.-Z. Han and Z.-W. Hu, *Int. J. Cancer*, 2014, **134**, 692-702.
29. Y. Yang, Y. Yang, X. Xie, X. Cai, H. Zhang, W. Gong, Z. Wang and X. Mei, *Biomaterials*, 2014, **35**, 4368-4381.
30. L. Fei, L.-P. Yap, P. S. Conti, W.-C. Shen and J. L. Zaro, *Biomaterials*, 2014, **35**, 4082-4087.
31. D. M. Copolovici, K. Langel, E. Eriste and U. Langel, *ACS Nano*, 2014, **8**, 1972-1994.
32. S. Stalmans, E. Wynendaele, N. Bracke, D. Knappe, R. Hoffmann, K. Peremans, I. Polis, C. Burvenich and B. De Spiegeleer, *Protein Pept. Lett.*, 2014, **21**, 399-406.
33. D. S. Youngblood, S. A. Hatlevig, J. N. Hassinger, P. L. Iversen and H. M. Moulton, *Bioconjug. Chem.*, 2006, **18**, 50-60.
34. E. L. Snyder, B. R. Meade, C. C. Saenz and S. F. Dowdy, *PLoS Biol*, 2004, **2**, e36.
35. V. Parthsarathy, P. L. McClean, C. Hölscher, M. Taylor, C. Tinker, G. Jones, O. Kolosov, E. Salvati, M. Gregori, M. Masserini and D. Allsop, *PLoS One*, 2013, **8**, e54769.
36. N. Umezawa, M. A. Gelman, M. C. Haigis, R. T. Raines and S. H. Gellman, *J. Am. Chem. Soc.*, 2001, **124**, 368-369.
37. A. M. Czyzewski and A. E. Barron, *AIChE J.*, 2008, **54**, 2-8.
38. Y.-L. Tseng, J.-J. Liu and R.-L. Hong, *Mol. Pharmacol.*, 2002, **62**, 864-872.
39. H. Brooks, B. Lebleu and E. Vivès, *Adv. Drug Delivery Rev.*, 2005, **57**, 559-577.
40. V. P. Torchilin, *Adv. Drug Delivery Rev.*, 2008, **60**, 548-558.
41. P. Järver, I. Mäger and Ü. Langel, *Trends Pharmacol. Sci.*, **31**, 528-535.
42. M. S. Sarac, A. Cameron and I. Lindberg, *Infect. Immun.*, 2002, **70**, 7136-7139.

43. M. S. Sarac, J. R. Peinado, S. H. Leppla and I. Lindberg, *Infect. Immun.*, 2004, **72**, 602-605.
44. Z. Niu, E. Tedesco, F. Benetti, A. Mabondzo, I. M. Montagner, I. Marigo, D. Gonzalez-Touceda, S. Tovar, C. Diéguez, M. J. Santander-Ortega and M. J. Alonso, *J. Control. Release*, 2017, **263**, 4-17.
45. S. Stalmans, N. Bracke, E. Wynendaele, B. Gevaert, K. Peremans, C. Burvenich, I. Polis and B. De Spiegeleer, *PLoS One*, 2015, **10**, e0139652.
46. H. Myrberg, L. Zhang, M. Mäe and Ü. Langel, *Bioconjug. Chem.*, 2008, **19**, 70-75.
47. A. Elmquist, M. Lindgren, T. Bartfai and Ü. Langel, *Exp. Cell Res.*, 2001, **269**, 237-244.
48. Z. You-en, W. Jia-ning, T. Jun-ming, G. Ling-yun, Y. Jian-ye, H. Yong-zhang, T. Yan, F. Shou-zhi, K. Xia and Z. Fei, *Mol. Cells*, 2009, **27**, 159-166.
49. M. C. Morris, J. Depollier, J. Mery, F. Heitz and G. Divita, *Nat. Biotechnol.*, 2001, **19**, 1173.
50. E. Gros, S. Deshayes, M. C. Morris, G. Aldrian-Herrada, J. Depollier, F. Heitz and G. Divita, *Biochim. Biophys. Acta, Biomembr.*, 2006, **1758**, 384-393.
51. W. B. Bowne, J. Michl, M. H. Bluth, M. E. Zenilman and M. R. Pincus, *Cancer Ther.*, 2007, **5B**, 331-344.
52. N. C. Tan, P. Yu, Y.-U. Kwon and T. Kodadek, *Bioorganic Med. Chem.*, 2008, **16**, 5853-5861.
53. D. K. Kölmel, A. Hörner, F. Rönicke, M. Nieger, U. Schepers and S. Bräse, *Eur. J. Med. Chem.*, 2014, **79**, 231-243.
54. P. A. Wender, D. J. Mitchell, K. Pattabiraman, E. T. Pelkey, L. Steinman and J. B. Rothbard, *Proc. Natl. Acad. Sci.*, 2000, **97**, 13003-13008.
55. W. Huang, J. Seo, J. S. Lin and A. E. Barron, *Mol. Biosyst.*, 2012, **8**, 2626-2628.
56. S. B. L. Vollrath, D. Furniss, U. Schepers and S. Brase, *Org. Biomol. Chem.*, 2013, **11**, 8197-8201.
57. Y. Shai, *Pept. Sci.*, 2002, **66**, 236-248.
58. K. Matsuzaki, *Biochim. Biophys. Acta, Rev. Biomembr.*, 1998, **1376**, 391-400.
59. M. Wu, E. Maier, R. Benz and R. E. W. Hancock, *Biochemistry*, 1999, **38**, 7235-7242.
60. S. K. Bhutia and T. K. Maiti, *Trends Biotechnol.*, 2008, **26**, 210-217.
61. D. W. Hoskin and A. Ramamoorthy, *Biochim. Biophys. Acta, Biomembr.*, 2008, **1778**, 357-375.
62. C. Leuschner and W. Hansel, *Curr. Pharm. Des.*, 2004, **10**, 2299-2310.
63. S. R. Dennison, M. Whittaker, F. Harris and D. A. Phoenix, *Curr. Protein Pept. Sci.*, 2006, **7**, 487-499.
64. N. Papo and Y. Shai, *Cell Mol. Life Sci.*, 2005, **62**, 784-790.
65. M. A. Baker, W. L. Maloy, M. Zasloff and L. S. Jacob, *Cancer Res.*, 1993, **53**, 3052-3057.
66. C. B. Park, H. S. Kim and S. C. Kim, *Biochem. Biophys. Res. Commun.*, 1998, **244**, 253-257.
67. C. B. Park, K.-S. Yi, K. Matsuzaki, M. S. Kim and S. C. Kim, *Proc. Natl. Acad. Sci.*, 2000, **97**, 8245-8250.
68. W. Huang, J. Seo, S. B. Willingham, A. M. Czyzewski, M. L. Gonzalgo, I. L. Weissman and A. E. Barron, *PLoS One*, 2014, **9**, e90397.
69. N. P. Chongsiriwatana, J. A. Patch, A. M. Czyzewski, M. T. Dohm, A. Ivankin, D. Gidalevitz, R. N. Zuckermann and A. E. Barron, *Proc. Natl. Acad. Sci.*, 2008, **105**, 2794-2799.
70. A. M. Czyzewski, H. Jenssen, C. D. Fjell, M. Waldbrook, N. P. Chongsiriwatana, E. Yuen, R. E. W. Hancock and A. E. Barron, *PLoS One*, 2016, **11**, e0135961.
71. N. P. Chongsiriwatana, M. Wetzler and A. E. Barron, *Antimicrob. Agents Chemother.*, 2011, **55**, 5399-5402.
72. B. Mojsoska, G. Carretero, S. Larsen, R. V. Mateiu and H. Jenssen, 2017, **7**, 42332.
73. R. Kapoor, M. W. Wadman, M. T. Dohm, A. M. Czyzewski, A. M. Spormann and A. E. Barron, *Antimicrob. Agents Chemother.*, 2011, **55**, 3054-3057.
74. R. Kapoor, P. R. Eimerman, J. W. Hardy, J. D. Cirillo, C. H. Contag and A. E. Barron, *Antimicrob. Agents Chemother.*, 2011, **55**, 3058-3062.
75. H. L. Bolt, G. A. Eggimann, P. W. Denny and S. L. Cobb, *Med. Chem. Commun.*, 2016, **7**, 799-805.
76. G. A. Eggimann, H. L. Bolt, P. W. Denny and S. L. Cobb, *ChemMedChem*, 2015, **10**, 233-237.

77. J. Alvar, I. D. Vélez, C. Bern, M. Herrero, P. Desjeux, J. Cano, J. Jannin, M. d. Boer and W. H. O. L. C. T. the, *PLoS One*, 2012, **7**, e35671.
78. L. Kedzierski, *J. Glob. Infect. Dis.*, 2010, **2**, 177-185.
79. N. Singh, M. Kumar and R. K. Singh, *Asian. Pac. Trop. Biomed.*, 2012, **5**, 485-497.
80. H. L. Bolt, G. A. Eggimann, P. W. Denny and S. L. Cobb, *MedChemComm*, 2016, **7**, 799-805.
81. Y. Luo, H. L. Bolt, G. A. Eggimann, D. F. Mc Auley, R. Mc Mullan, T. Curran, M. Zhou, C. A. B. Jahoda, S. L. Cobb and F. T. Lundy, *ChemBioChem*, 2016, DOI: 10.1002/cbic.201600381, n/a-n/a.
82. N. Høiby, T. Bjarnsholt, M. Givskov, S. Molin and O. Ciofu, *Int. J. Antimicrob. Agents*, 2010, **35**, 322-332.
83. S. Cairns, J. G. Thomas, S. J. Hooper, M. P. Wise, P. J. Frost, M. J. Wilson, M. A. O. Lewis and D. W. Williams, *PLoS One*, 2011, **6**, e14759.
84. M. M. Harriott and M. C. Noverr, *Trends Microbiol.*, **19**, 557-563.
85. M. Oh, J. H. Lee, H. Moon, Y.-J. Hyun and H.-S. Lim, *Angew. Chem., Int. Ed.*, 2016, **55**, 602-606.
86. J. R. Skaar, J. K. Pagan and M. Pagano, *Nat. Rev. Drug Discovery*, 2014, **13**, 889-903.
87. K. Nakayama, H. Nagahama, Y. A. Minamishima, S. Miyake, N. Ishida, S. Hatakeyama, M. Kitagawa, S.-i. Iemura, T. Natsume and K. I. Nakayama, *Dev. Cell*, **6**, 661-672.
88. D. D. Hershko, *Cancer*, 2008, **112**, 1415-1424.
89. Z. Wang, P. Liu, H. Inuzuka and W. Wei, *Nat. Rev. Cancer*, 2014, **14**, 233-247.
90. S. I. Reed, *Cancer Cell*, 2008, **13**, 88-89.
91. M. Kitagawa, S. H. Lee and F. McCormick, *Mol. Cell*, **29**, 217-231.
92. A. Ivankin, A. Antipova, I. Radzishevsky, A. Mor, G. A. Caputo, W. F. DeGrado and D. Gidalevitz, *Biophys. J.*, 2010, **98**, 85a.
93. K. Strebhardt, *Nat. Rev. Drug Discovery*, 2010, **9**, 643-660.
94. B. A. Chabner and T. G. Roberts, *Nat. Rev. Cancer*, 2005, **5**, 65-72.
95. L. Pauling, R. B. Corey and H. R. Branson, *Proc. Natl. Acad. Sci.*, 1951, **37**, 205-211.
96. B. K. Ho and P. M. G. Curmi, *J. Mol. Biol.*, 2002, **317**, 291-308.
97. S. Hovmoller, T. Zhou and T. Ohlson, *Acta. Crystallogr. Sect. D*, 2002, **58**, 768-776.
98. G. N. Ramachandran, C. Ramakrishnan and V. Sasisekharan, *J. Mol. Biol.*, 1963, **7**, 95-99.
99. R. V. Mannige, *PeerJ*, 2017, **5**, e3327.
100. S. A. Fowler and H. E. Blackwell, *Org. Biomol. Chem.*, 2009, **7**, 1508-1524.
101. M. Baskin and G. Maayan, *Chem. Sci.*, 2016, **7**, 2809-2820.
102. B. Kang, W. Yang, S. Lee, S. Mukherjee, J. Forstater, H. Kim, B. Goh, T.-Y. Kim, V. A. Voelz, Y. Pang and J. Seo, *Sci. Rep.*, 2017, **7**, 4786.
103. P. Armand, K. Kirshenbaum, R. A. Goldsmith, S. Farr-Jones, A. E. Barron, K. T. V. Truong, K. A. Dill, D. F. Mierke, F. E. Cohen, R. N. Zuckermann and E. K. Bradley, *Proc. Natl. Acad. Sci.*, 1998, **95**, 4309-4314.
104. K. Kirshenbaum, A. E. Barron, R. A. Goldsmith, P. Armand, E. K. Bradley, K. T. V. Truong, K. A. Dill, F. E. Cohen and R. N. Zuckermann, *Proc. Natl. Acad. Sci.*, 1998, **95**, 4303-4308.
105. M. Wetzler and A. E. Barron, *Pept. Sci.*, 2011, **96**, 556-560.
106. C. W. Wu, T. J. Sanborn, K. Huang, R. N. Zuckermann and A. E. Barron, *J. Am. Chem. Soc.*, 2001, **123**, 6778-6784.
107. T. J. Sanborn, C. W. Wu, R. N. Zuckermann and A. E. Barron, *Biopolymers*, 2002, **63**, 12-20.
108. N. H. Shah, G. L. Butterfoss, K. Nguyen, B. Yoo, R. Bonneau, D. L. Rabenstein and K. Kirshenbaum, *J. Am. Chem. Soc.*, 2008, **130**, 16622-16632.
109. B. C. Gorske, R. C. Nelson, Z. S. Bowden, T. A. Kufe and A. M. Childs, *J. Org. Chem.*, 2013, **78**, 11172-11183.
110. S. B. Y. Shin, B. Yoo, L. J. Todaro and K. Kirshenbaum, *J. Am. Chem. Soc.*, 2007, **129**, 3218-3225.
111. J. K. Pokorski, L. M. Miller Jenkins, H. Feng, S. R. Durell, Y. Bai and D. H. Appella, *Org. Lett.*, 2007, **9**, 2381-2383.
112. J. R. Stringer, J. A. Crapster, I. A. Guzei and H. E. Blackwell, *J. Org. Chem.*, 2010, **75**, 6068-6078.
113. M. Rainaldi, V. Moretto, M. Crisma, E. Peggion, S. Mammi, C. Toniolo and G. Cavicchioni, *J. Pept. Sci.*, 2002, **8**, 241-252.

114. B. Yoo and K. Kirshenbaum, *Curr. Opin. Chem. Biol.*, 2008, **12**, 714-721.
115. K. T. Nam, S. A. Shelby, P. H. Choi, A. B. Marciel, R. Chen, L. Tan, T. K. Chu, R. A. Mesch, B.-C. Lee, M. D. Connolly, C. Kisielowski and R. N. Zuckermann, *Nat. Mater.*, 2010, **9**, 454.
116. R. Kudirka, H. Tran, B. Sanii, K. T. Nam, P. H. Choi, N. Venkateswaran, R. Chen, S. Whitelam and R. N. Zuckermann, *Pept. Sci.*, 2011, **96**, 586-595.
117. R. V. Mannige, T. K. Haxton, C. Proulx, E. J. Robertson, A. Battigelli, G. L. Butterfoss, R. N. Zuckermann and S. Whitelam, *Nature*, 2015, **526**, 415-420.
118. J. A. Robinson, S. C. Shankaramma, P. Jetter, U. Kienzl, R. A. Schwendener, J. W. Vrijbloed and D. Obrecht, *Bioorganic Med. Chem.*, 2005, **13**, 2055-2064.
119. S. Finger, A. Kerth, M. Dathe and A. Blume, *Biochim. Biophys. Acta, Biomembr.*, 2015, **1848**, 2998-3006.
120. A. Kling, P. Lukat, D. V. Almeida, A. Bauer, E. Fontaine, S. Sordello, N. Zaburannyi, J. Herrmann, S. C. Wenzel, C. König, N. C. Ammerman, M. B. Barrio, K. Borchers, F. Bordon-Pallier, M. Brönstrup, G. Courtemanche, M. Gerlitz, M. Geslin, P. Hammann, D. W. Heinz, H. Hoffmann, S. Klieber, M. Kohlmann, M. Kurz, C. Lair, H. Matter, E. Nuermberger, S. Tyagi, L. Fraisse, J. H. Grosset, S. Lagrange and R. Müller, *Science*, 2015, **348**, 1106-1112.
121. N. Bionda, R. M. Fleeman, C. de la Fuente-Núñez, M. C. Rodriguez, F. Reffuveille, L. N. Shaw, I. Pastar, S. C. Davis, R. E. W. Hancock and P. Cudic, *Eur. J. Med. Chem.*, 2016, **108**, 354-363.
122. D. J. Craik, N. L. Daly and C. Waine, *Toxicon*, 2001, **39**, 43-60.
123. M. R. Vippila, P. K. Ly and G. D. Cuny, *J. Nat. Prod.*, 2015, **78**, 2398-2404.
124. A. S. Ravipati, S. T. Henriques, A. G. Poth, Q. Kaas, C. K. Wang, M. L. Colgrave and D. J. Craik, *ACS Chem. Biol.*, 2015, **10**, 2491-2500.
125. K. Bańkowski, E. Witkowska, O. M. Michalak, K. Sidoryk, E. Szymanek, B. Antkowiak, M. Paluch, K. E. Filip, M. Cebrat, B. Setner, Z. Szewczuk, P. Stefanowicz, P. Cmoch and J. Izdebski, *Eur. J. Med. Chem.*, 2013, **63**, 457-467.
126. N. Nischan, H. D. Herce, F. Natale, N. Bohlke, N. Budisa, M. C. Cardoso and C. P. R. Hackenberger, *Angew. Chem., Int. Ed.*, 2015, **54**, 1950-1953.
127. M. L. Huang, S. B. Y. Shin, M. A. Benson, V. J. Torres and K. Kirshenbaum, *ChemMedChem*, 2012, **7**, 114-122.
128. A. M. Webster and S. L. Cobb, *Chem. Eur. J.*, DOI: 10.1002/chem.201705340, n/a-n/a.
129. S. B. L. Vollrath, C. Hu, S. Brase and K. Kirshenbaum, *Chem. Commun.*, 2013, **49**, 2317-2319.
130. M. L. Huang, M. A. Benson, S. B. Y. Shin, V. J. Torres and K. Kirshenbaum, *Eur. J. Org. Chem.*, 2013, **2013**, 3560-3566.
131. S. A. Fowler, D. M. Stacy and H. E. Blackwell, *Org. Lett.*, 2008, **10**, 2329-2332.
132. N. Maulucci, I. Izzo, G. Bifulco, A. Aliberti, C. De Cola, D. Comegna, C. Gaeta, A. Napolitano, C. Pizza, C. Tedesco, D. Flot and F. De Riccardis, *Chem. Commun.*, 2008, DOI: 10.1039/B806508J, 3927-3929.
133. O. Roy, S. Faure, V. Thery, C. Didierjean and C. Taillefumier, *Org. Lett.*, 2008, **10**, 921-924.
134. C. M. Sandra, P. Vishal, G. William and K. O. Adegboyega, *Curr. Top. Med. Chem.*, 2010, **10**, 1423-1440.
135. T. A. Miller, D. J. Witter and S. Belvedere, *J. Med. Chem.*, 2003, **46**, 5097-5116.
136. F. Blanchard and C. Chipoy, *Drug Discov. Today*, 2005, **10**, 197-204.
137. V. Patil, W. Guerrant, P. C. Chen, B. Gryder, D. B. Benicewicz, S. I. Khan, B. L. Tekwani and A. K. Oyelere, *Bioorganic Med. Chem.*, 2010, **18**, 415-425.
138. M. Dokmanovic, C. Clarke and P. A. Marks, *Mol. Cancer Res.*, 2007, **5**, 981-989.
139. C. A. Olsen, A. Montero, L. J. Leman and M. R. Ghadiri, *ACS Med. Chem. Lett.*, 2012, **3**, 749-753.
140. A. S. Culf, M. Čuperlović-Culf, D. A. Léger and A. Decken, *Org. Lett.*, 2014, **16**, 2780-2783.
141. T. Hjelmgaard, O. Roy, L. Nauton, M. El-Ghozzi, D. Avignant, C. Didierjean, C. Taillefumier and S. Faure, *Chem. Commun.*, 2014, **50**, 3564-3567.
142. A. Dömling and I. Ugi, *Angew. Chem., Int. Ed.*, 2000, **39**, 3168-3210.
143. M. C. N. Brauer, R. A. W. Neves Filho, B. Westermann, R. Heinke and L. A. Wessjohann, *Beilstein J. Org. Chem.*, 2015, **11**, 25-30.

144. S.-H. Chung, T.-J. Lin, Q.-Y. Hu, C.-H. Tsai and P.-S. Pan, *Molecules*, 2013, **18**, 12346-12367.
145. L. A. Wessjohann and E. Ruijter, *Mol. Diversity*, 2005, **9**, 159-169.
146. L. A. Wessjohann, B. Voigt and D. G. Rivera, *Angew. Chem., Int. Ed.*, 2005, **44**, 4785-4790.
147. E. Ruoslahti and M. Pierschbacher, *Science*, 1987, **238**, 491-497.
148. R. Haubner, W. Schmitt, G. Hölzemann, S. L. Goodman, A. Jonczyk and H. Kessler, *J. Am. Chem. Soc.*, 1996, **118**, 7881-7891.
149. J. Wermuth, S. L. Goodman, A. Jonczyk and H. Kessler, *J. Am. Chem. Soc.*, 1997, **119**, 1328-1335.
150. D. Arosio, L. Manzoni, E. M. V. Araldi and C. Scolastico, *Bioconjug. Chem.*, 2011, **22**, 664-672.
151. H. Vilaça, P. M. T. Ferreira and N. M. Micaelo, *Tetrahedron*, 2014, **70**, 5420-5427.
152. R. H. Grubbs, *Tetrahedron*, 2004, **60**, 7117-7140.
153. S. N. Khan, A. Kim, R. H. Grubbs and Y.-U. Kwon, *Org. Lett.*, 2011, **13**, 1582-1585.
154. C. Nilsson, N. Simpson, M. Malkoch, M. Johansson and E. Malmström, *J. Polym. Sci., Part A: Polym. Chem.*, 2008, **46**, 1339-1348.
155. C. E. Hoyle and C. N. Bowman, *Angew. Chem., Int. Ed.*, 2010, **49**, 1540-1573.
156. X. Elduque, E. Pedroso and A. Grandas, *J. Org. Chem.*, 2014, **79**, 2843-2853.
157. B. Argante, D. A. Gabriele and B. Fabrizia, *Curr. Clin. Pharmacol.*, 2008, **3**, 20-37.
158. P. R. Meyer, S. E. Matsuura, A. M. Mian, A. G. So and W. A. Scott, *Mol. Cell*, 1999, **4**, 35-43.
159. V. V. Rostovtsev, L. G. Green, V. V. Fokin and K. B. Sharpless, *Angew. Chem., Int. Ed.*, 2002, **41**, 2596-2599.
160. J. M. Holub, H. Jang and K. Kirshenbaum, *Org. Lett.*, 2007, **9**, 3275-3278.
161. S. B. L. Vollrath, S. Brase and K. Kirshenbaum, *Chem. Sci.*, 2012, **3**, 2726-2731.
162. P. J. Kaniraj and G. Maayan, *Org. Lett.*, 2015, **17**, 2110-2113.
163. S. Park and Y.-U. Kwon, *ACS Comb. Sci.*, 2015, **17**, 196-201.
164. K. J. Lee and H.-S. Lim, *Org. Lett.*, 2014, **16**, 5710-5713.

Chapter 2

Boronic Acid-Containing Peptoids

2.1 Background

2.1.1 Boronic acids as synthetic building blocks

Boronic acids are synthetically useful building blocks, providing access to many novel compounds. They can undergo functional group conversion to generate halides[1-4] (**Scheme 2.1**), alcohols[5] (**Scheme 2.2**), esters[6] (**Scheme 2.3**) and various amino groups[7-11] (**Figure 2.1**). Boronic acids are also useful for generating carbon-heteroatom bonds[12-14] (**Figure 2.2**). However, our main interests in the inclusion of boronic acids in peptoids are firstly, their use in the formation of carbon-carbon bonds, specifically the synthesis of biaryl groups via Suzuki-Miyaura cross-coupling[15] (**Scheme 2.4**).

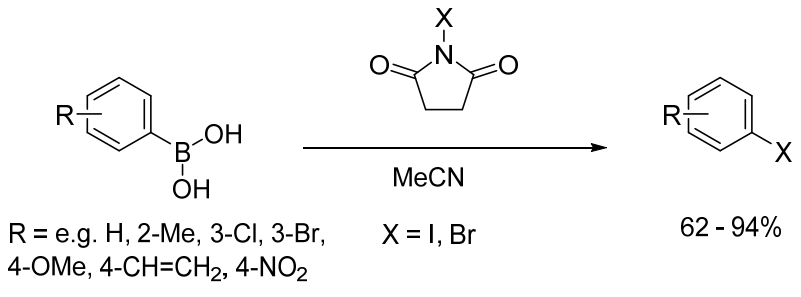

Scheme 2.1 Example of stereoselective halodeboronation of alkenylboronic acids.[4]

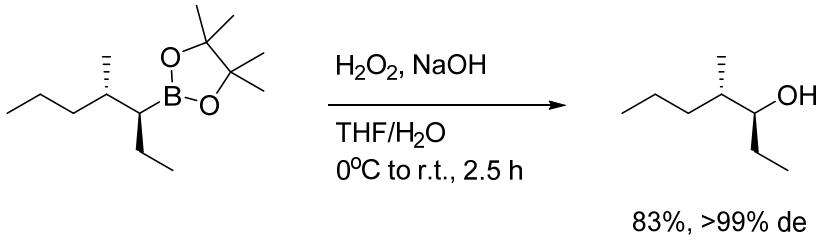

Scheme 2.2 Stereospecific oxygenation of boronic esters to generate an alcohol.[5]

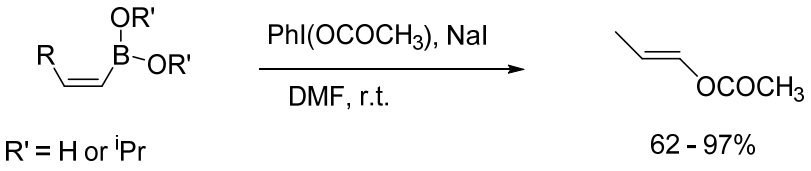

Scheme 2.3 Stereoselective oxygenation of boronic esters to generate an ester.[6]

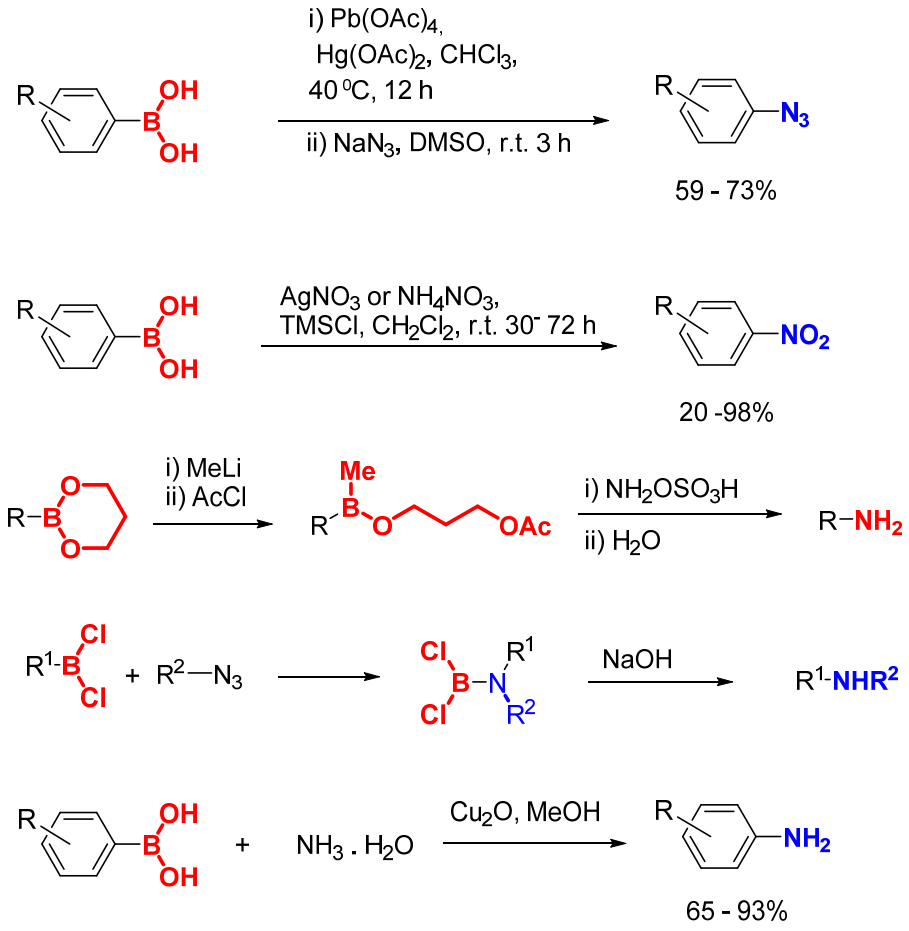

Figure 2.1 Examples of amination reactions starting from boronic acids and esters.

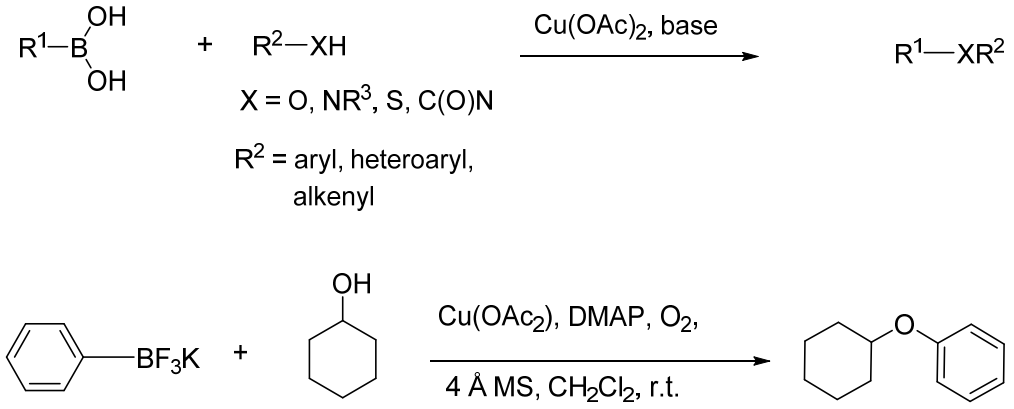

Figure 2.2 Generating carbon-heteroatom bonds from boronate-containing compounds (via Chan-Lam coupling reactions).

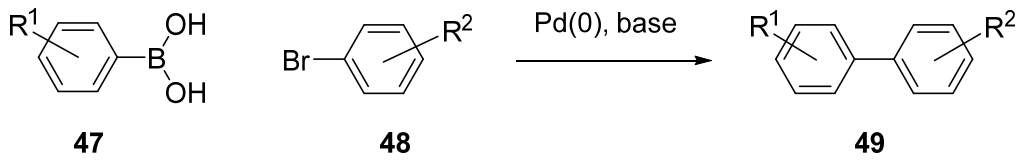

47 **48** **49**

Scheme 2.4 General example of a Suzuki-Miyaura cross- coupling reaction.

2.1.2 Carbon-carbon bond formation

C-C bond formation reactions using boronic acid building blocks are particularly useful and this was recognised in 2010 when Suzuki was one of the recipients of the Nobel Prize for Chemistry for his eponymous coupling reactions involving boronic acid building blocks (**Scheme 2.4**).[15] The Suzuki-Miyaura coupling reaction reacts a boronic acid, **47**, with a halide, **48** using Pd(0) as a catalyst and a base to form a new C-C bond, forming a biaryl group, **49**. These reactions are of particular interest in peptoid chemistry as they provide a potential route towards cyclic and stapled peptoids. Cyclic peptoids are a desirable target because they may show greater activity against pathogens and may be more specific for certain targets[16] and has been discussed in detail in **Chapter 1**. Various attempts have already been made towards stapling and cyclising peptoids (see **Chapter 1**), but boron cross-coupling reactions have so far not been attempted as a way to achieve this.

Whilst the example in **Scheme 2.4** shows an aromatic boronic acid, **47**, Suzuki-Miyaura coupling also extends to heteroaromatic and alkenyl boronic acids. It should also be noted that there are many other similar cross-coupling reactions and insertions (including Heck-type and Sonagashira-type coupling reactions) and using other metal catalysts, such as iridium,[17] nickel[18] and rhodium[19, 20] but Suzuki-Miyaura coupling is the most relevant to this project and the other reactions will not be discussed here.

2.1.2.1 The biaryl group

The biaryl group, for example, **49**, **Scheme 2.4**, is of particular interest for peptides and peptoids. Not only do they provide a route to cyclic peptides[21-28] and peptoids, but the biaryl group has attracted interest from the pharmaceutical industry as it shows activity across a wide range of therapeutic classes, including anti-inflammatory, anti-fungal, anti-tumour, anti-hypertensive and anti-rheumatic agents[29, 30] (two examples are shown in **Figure 2.3**). Furthermore, it is also possibly useful as an infertility treatment since it is an agonist for follicle stimulating hormone (FSH) receptors.[31]

Biaryls interact with hydrophobic aromatic residues in peptides and proteins, but also show favourable interactions with the more polar amide and hydroxide groups and positively charged moieties. This means that the biaryl group can potentially interact with a wide range of receptors.[32] In fact, statistical analysis of NMR-derived binding data performed on 11 protein targets showed that compounds containing biphenyl substructures bound preferentially to the proteins with a high level of specificity (>250 fold).[32]

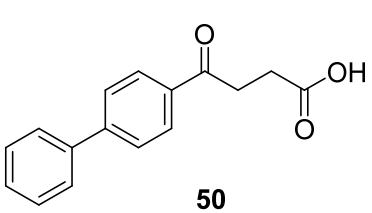

50

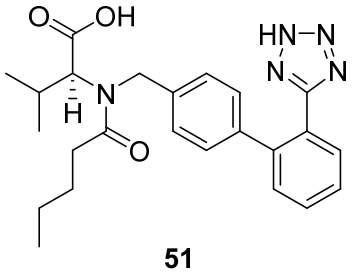

51

Figure 2.3 Biaryl containing drugs: **50**, Fenbufen, is used to treat arthritis,[33] **51**, Valsartan is an antihypertensive drug.[34]

Biaryl scaffolds are considered privileged structures by the pharmaceutical industry.[30, 32] Privileged structures are used to describe molecular frameworks that are capable of binding to a diverse array of receptors. So ubiquitous is the biaryl motif, that in a 2003 review, it was stated that 4.3% of all known drugs contained a biphenyl.[30, 32]

2.1.2.2 Biaryls in antibacterial compounds

Some biaryl-containing compounds show anti-bacterial activity against both Gram-positive and Gram-negative bacteria.[35, 36] A notable study by Jefferson *et al*. in 2004 carried out lead optimisation of a compound (**52**, **Figure 2.4**) that had been shown to bind to bacterial 23S RNA and inhibit bacterial protein synthesis in a cell-free system (IC_{50} = 14 μM) but lacked antibacterial activity in MIC assays with *E. coli* and *S. aureus*.[36]

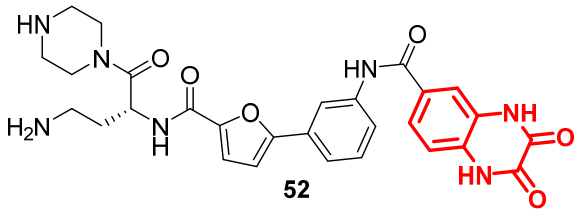

52

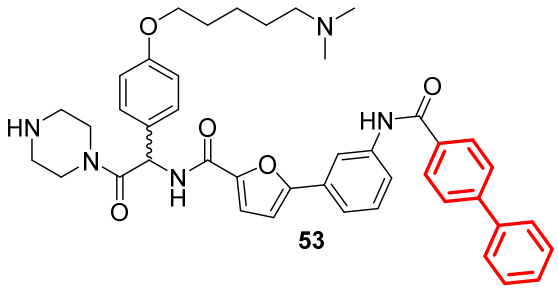

53

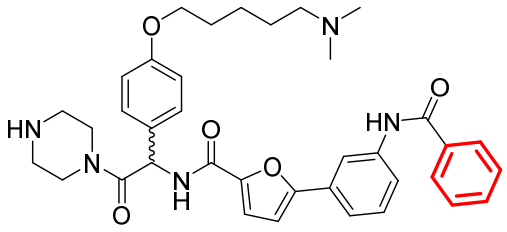

54

Figure 2.4 Structure of and comparison of activities of three compounds investigated in lead optimisation studies by Jefferson *et al.* Substituted substructures are in red. Compound **52** is the original hit compound which inhibits bacterial protein synthesis (IC_{50} = 14 μM) but showed no activity against *E. coli* or *S. aureus*. Compound **53** contained the biaryl group and was most effective against *E. coli* and *S. aureus* (MICs = 6 – 13 μM and 3 – 6 μM respectively, IC_{50} in the cell-free system = 9 μM). Compound **54** is the phenyl substituted compound which was inactive against *E. coli* and *S. aureus* (IC_{50} in the cell-free system = 40 μM).

The authors suggested that this lack of activity was down to poor cell penetration and/or the action of efflux pumps, resulting in inadequate compound availability inside the cell. Their most effective compound (**53**, **Figure 2.4**) contained a biphenyl group and was active against *E. coli* and *S. aureus* (MICs were 6 – 13 μM and 3 – 6 μM respectively) as well as against multi-drug resistant *S. aureus* (MIC 13 – 25 μM). Furthermore, compound **53** was found to have a 4-fold greater *in vitro* activity compared to the phenyl substituted compound, **54** (IC_{50} = 9 μM and 40 μM respectively) which showed no activity up to 100 μM in assays against *S. aureus* and *E. coli*. This suggests that the biphenyl group is critical for antibacterial activity, at least in the compounds investigated.

The biaryl motif is also found in various biologically active peptides, for example vancomycin (**55**, **Figure 2.5**) which is widely used as an intravenous antibiotic and is used to treat conditions such as meningitis caused by methicillin-resistant *S. aureus.*[37, 38] The biphenomycins are a family of tripeptide macrocycles linked by a biaryl group.[27] Biphenomycin A (**56**, **Figure 2.7**) and biphenomycin B (**57**, **Figure 2.7**) have both been the target of total synthesis projects due to their observed activity against Gram-positive and β-lactamase resistant bacteria.[24, 27, 39-41] Furthermore, biphenomycin A (**10**) was found to be effective against bacterial infections in mice, even exceeding expectations from the *in vitro* studies.[42]

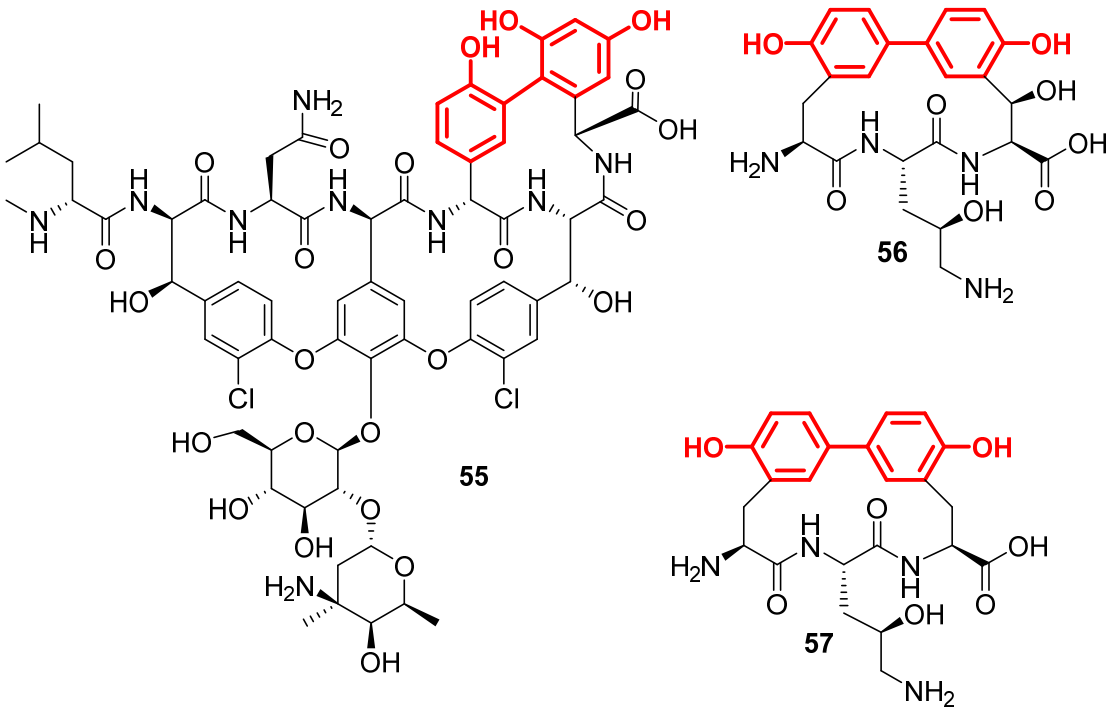

Figure 2.5 Antibacterial cyclic peptides containing biaryl linkages. **55** is vancomycin, **56** is biphenomycin A, **57** is biphenomycin B. The biaryl motifs are highlighted in red.

2.1.2.3 Other biologically active biaryl-containing compounds

RP 66453 (**58**, **Figure 2.6**) binds selectively to the neurotensin receptor in guinea pigs (IC_{50} = 30 μg/mL).[23, 43, 44] Neurotensin is a 13-amino acid peptide which is found throughout the central nervous system as well as in enteroendocrine cells in the small intestine where it is involved in smooth muscle contraction.[45] Neurotensin is implicated in many biological pathways: it appears to be involved with dopamine signalling,[46] is a mitogen for pancreatic and colorectal cancers[47-49] and neurotensin-deficient mice are less prone to obesity.[50] Structural modifications of RP 66453 (leaving the biaryl linkage intact) have produced neurotensin antagonists that are claimed to be useful in the treatment of various illnesses, such as depression, anxiety disorders, irritable bowel syndrome and pancreatitis.[51]

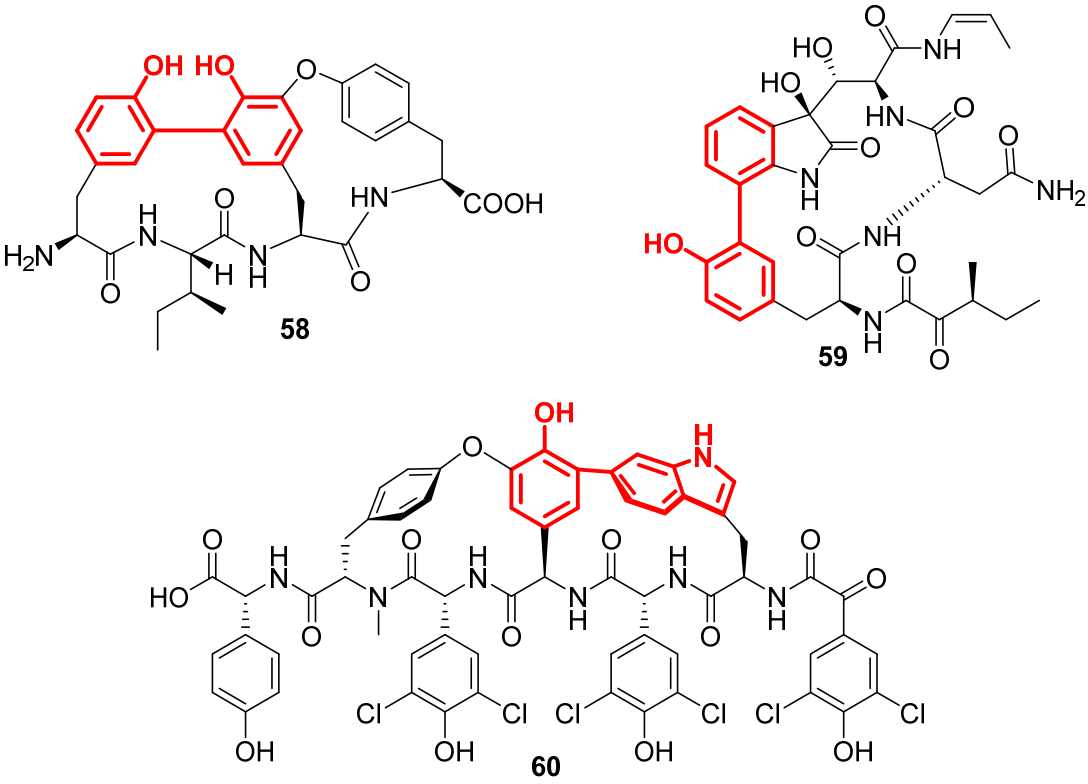

Figure 2.6 Biologically active cyclic peptides containing biaryl linkages. Compound **58** is RP66453, a neurotensin antagonist. Compound **59** is TMC-95A which shows anti-tumour activity. Compound **60** is complestatin (of chloropeptin II) which inhibits HIV-1 induced cytopathicity.

TMC-95A (**59**, **Figure 2.6**) is another tripeptide, cyclised by a biaryl linkage, similar to the biphenomycins. It was isolated from the fermentation broth of *Apiospora montagnei* and shows reversible, non-covalent 20S proteasome inhibition.[52, 53] Proteasomal

degradation of a variety of cellular proteins is essential for many intracellular processes, including cell-cycle progression, apoptosis and regulation of metabolic pathways.[54] Hence, proteasome inhibitors attract interest as potential drug targets.[55] TMC-95A showed activity against HCT-116 human colon carcinoma cells (IC_{50} = 4.4 μM) and HC-60 human promyelocytic leukaemia cells (IC_{50} = 9.8 μM).[53] More recently, TMC-95A was shown to promote neurite outgrowth in PC12 rat pheochromocytoma cells, activity that may be applicable to repairing damaged neurons and hence are of interest in the development of drugs to treat conditions such as Parknson's disease.[56]

Finally, complestatin (**60**, **Figure 2.6**) is a cyclic peptide containing a biaryl linkage isolated from *Streptomyces lavendulae* and inhibits HIV cytopathicity and HIV-1 antigen expression in MT-4 cells with no observable toxicity to the cells up to 400 μM concentrations.[28, 57] When the MT-4 cells were pretreated with complestatin prior to exposure to HIV-1, HIV-1 induced cytopathicity was inhibited. However, pretreatment of the HIV-1 with complestatin had no effect. This indicates that complestatin's primary mode of action is via interaction with the cells, inhibiting viral adsorption to the cell surface.[37]

2.1.3 Previously synthesised boron-containing peptoids

In spite of the obvious synthetic utility of boronic acids, there are at present few literature examples of boronic acids being incorporated into peptoids. Furthermore, the methods in the literature have limitations.

The first method involved the synthesis of a boronic acid pinacol ester-containing amine, **61** via functional group conversion of an alcohol, **62**, (**Scheme 2.5**). This was then made into a short peptoid, **64** (generic structure **63**), via a 4-component Ugi reaction (**Scheme 2.6**).[58]

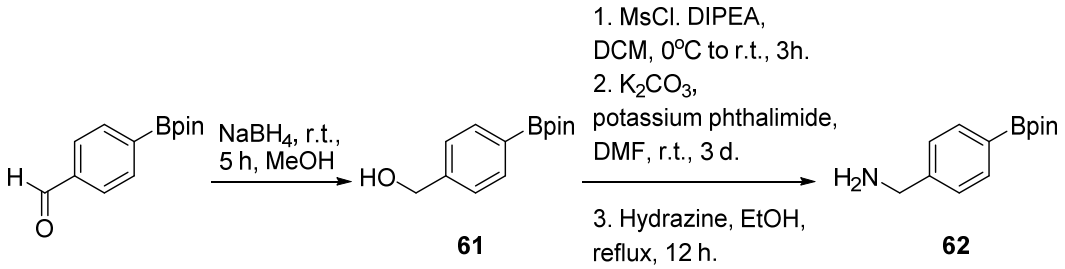

Scheme 2.5 Synthesis of the amine building block **62**.

Following synthesis, the peptoid was reacted further in a Suzuk-Miyaura cross-coupling reaction (example in **Scheme 2.7**).[58]

Whilst this set of reactions gives moderate yields, it is limited in scope. For the synthesis of longer peptoids, the submonomer method is superior; it is less time consuming and purification between additions is more straightforward. However, no attempt was made to use boronic acid pinacol ester building block in a submonomer synthesis.

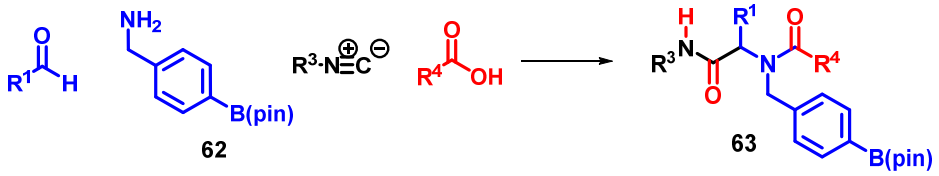

Scheme 2.6 4-component Ugi reaction for the formation of a boronic acid-containing peptoid, **63** from a boronic acid pinacol ester, **62**.

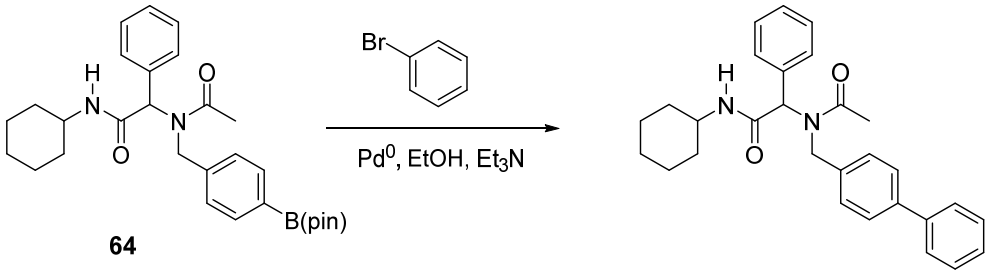

Scheme 2.7 A Suzuki-Miyaura cross-coupling reaction on a short peptoid, **64**.

The second method uses a copper mediated 1,3-cycloaddition reaction to incorporate a boronic acid at the end of a longer peptoid chain to form boronic acid-containing peptoid **65** (**Scheme 2.8**). Boronic acid-containing peptoid **65** was then cyclised by coupling with a hexose at the other end of the chain to form cyclic peptoid **66** (**Scheme 2.9**).[59] The obvious downside to this method is the necessity of the formation of the triazole in the reaction. It has already been seen that such peptoids may still penetrate cells, but whilst the triazole is an amide bond mimic, it would be useful to be able to include boronic acids without the need to also include a triazole.

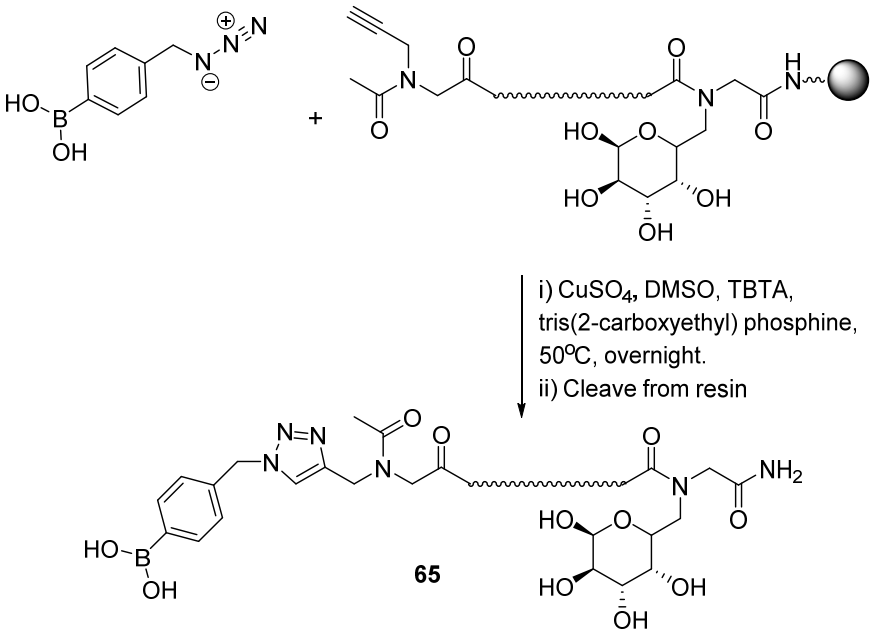

Scheme 2.8 Incorporation of a boronic acid into a peptoid using a copper-mediated 1, 3 cycloaddition.

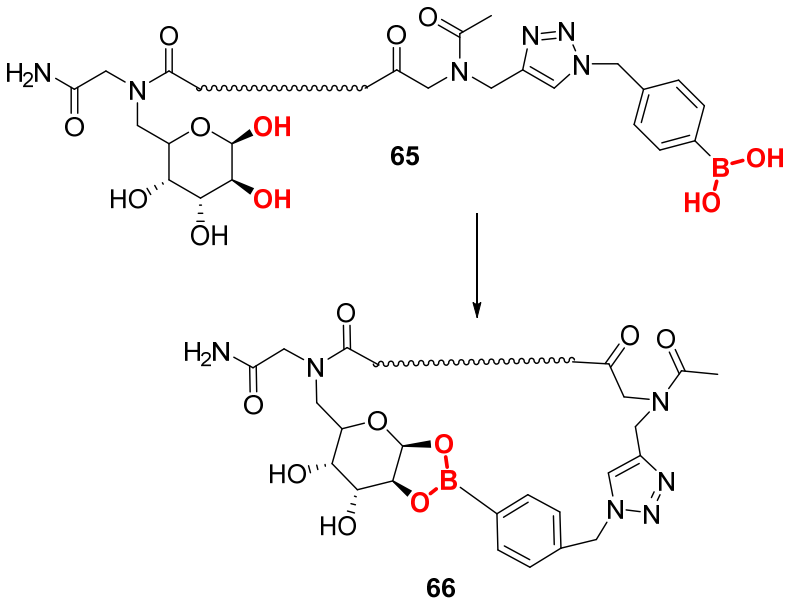

Scheme 2.9 Cyclisation of a boronic acid-containing peptoid, **65**, via coupling of a boronic acid with a hexose side chain to form cyclic peptoid **66**.

2.1.4 Aims

Boronic acids are undoubtedly highly useful synthetic building blocks in various fields of organic chemistry but with regards to peptoids they have been considerably under used. Part of this is due to the difficulty in incorporating boronic acids into peptoids. Boronic acids have so far only been incorporated onto the end of peptoids,[58,59] although the CuAAC method[59] (**Scheme 2.8**) could feasibly be used to incorporate boronic acids elsewhere in the peptoid chain via post-translational modification. However, this is a lengthy process involving overnight reaction times. Additionally, the azidomethyl phenylboronic acids need to be synthesised. Ideally, we would like to be able to incorporate boronic acids directly via the submonomer method. 3- and 4-(aminomethyl)phenylboronic acid pinacol esters (**67** and **68**) are commercially available and could be used in the submonomer method. However, direct conversion from the pinacol ester to the boronic acid frequently results in partial deprotection, even after using harsh conditions, long reaction times. It can also be difficult to separate the boronic acid from the free diol without reforming the ester.[60-62] An alternative protecting group is the MIDA group. MIDA boronates (e.g. **69**) are benchtop stable and deprotection is much more straightforward than for pinacol esters.[63,64] The boronic acid is protected by *N*-methyliminodiacetic acid (**70**, MIDA) which can be removed under aqueous basic conditions. MIDA-protected boronic acids were chosen because they are air stable and compatible with a wide variety of synthetic conditions. Additionally, previous work within the group had demonstrated their stability toward amide coupling conditions.[65] However, there are no commercially available MIDA boronates which can be used directly in submonomer peptoid synthesis without capping the peptoid.

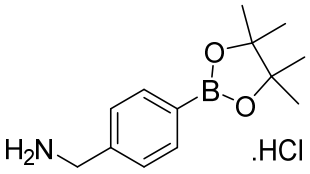

67

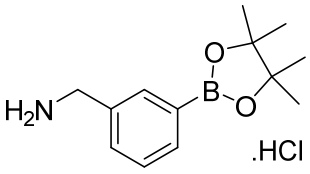

68

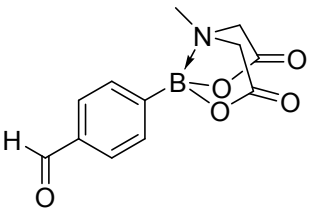

69

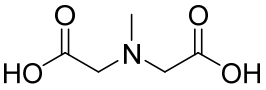

70

The first aim was therefore to synthesis a MIDA boronate-containing builing block compatible with the submonomer method of peptoid synthesis that could be used to incorporate a boronic acid anywhere in a peptoid (**Scheme 2.10**).

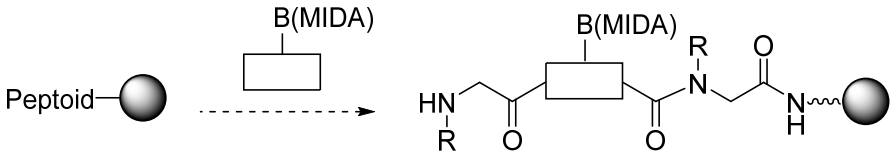

Scheme 2.10 Aim one: Incorporation of a MIDA boronate into a peptoid via the sub-monomer

Achieving this goal would open up access to a range of peptoids that could be used to target specific carbohydrates and thus enable selective delivery of therapeutics and imaging agents.

The second aim in this chapter was to make and cyclise a boronic-acid containing peptoid and in the process, form a biaryl group (**Scheme 2.11**). Linear biaryl-containing peptoids have already been synthesised, however we wanted to explore the use of Suzuki-Miyaura cross-coupling as a route to cyclic peptoids, the utility of which have already been discussed in **Chapter 1**. It was envisaged that cyclic peptoids containing a biaryl motif could be useful as therapeutics to target protein-protein interactions in a similar manner to biaryl-containing peptides such as those in the biphenomycin family and, accordingly, the activity of these novel peptoid scaffolds against *E. coli* and *S. aureus* was then investigated.

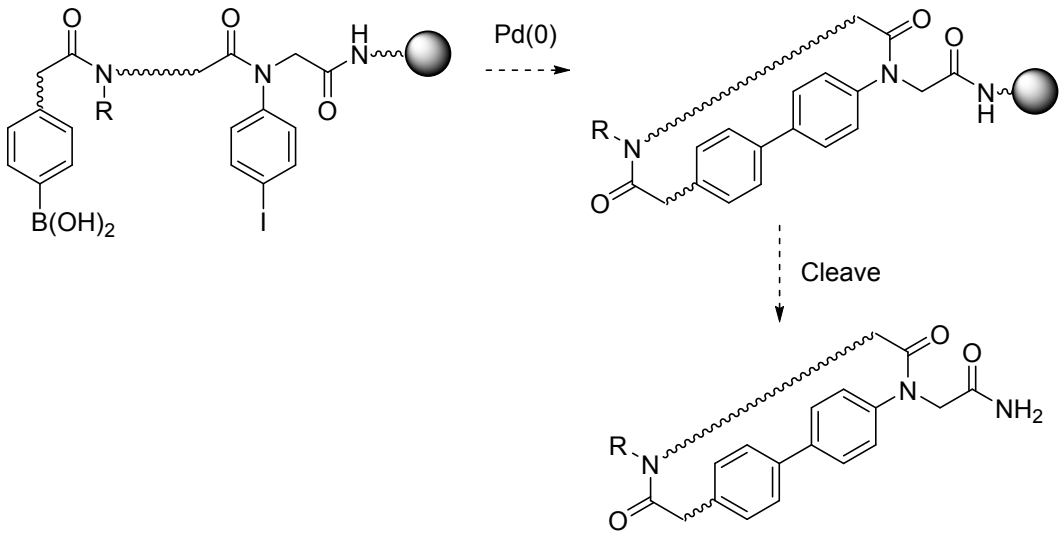

Scheme 2.11 Proposed Suzuki-Miyaura cross-coupling to form a cyclic peptoid and incorporate a biaryl group.

2.2 Making a boronic acid-containing building block with two potential coupling groups

At present, primary amines containing a pinacol boronate esters (e.g. **67** and **69**) are commercially available, as are MIDA boronates containing aldehyde and acid functionalities (e.g. **69** and **71**).

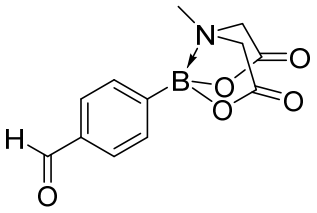

69

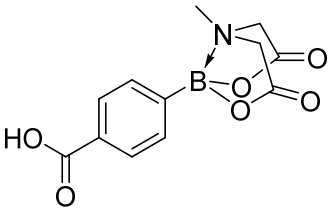

71

However, these cannot be incorporated directly into the middle of a peptoid via the submonomer method. The acid-functionalised MIDA boronate, **71** can be incorporated at the *N*-terminus of the peptoid, however, this will cap the peptoid meaning that the peptoid chain cannot be further extended. The ability to incorporate the boronic acid anywhere in a peptoid chain is desirable since this would give access to novel functionalities anywhere in the peptoid sequence via post-translational conversion of the boronic acids. Incorporation of a boronic acid without capping the peptoid also allows coupling of other groups, such as lanthanide probes for the investigation of cell-penetrating ability, or chelators for MRI contrast agents so the peptoid can be used for imaging applications.

Reductive amination is the reaction of an aldehyde with a primary amine to make a secondary amine (**Scheme 2.12**). A secondary amine used in the displacement step of the sub-monomer method of peptoid synthesis would cap the peptoid. However, if the amine used in the reductive amination reaction is a glycine, the resulting compound will have two reactive groups: a carboxylic acid and a secondary amine, effectively making a peptoid monomer (e.g. **72**). This can be incorporated into a peptoid using standard solid phase peptide coupling conditions (e.g. PyBOP and DIPEA). Following this, peptoid synthesis can continue via the submonomer method. A suitable MIDA boronate which contains an aldehyde functional group, 4-formylphenylboronic acid MIDA ester is commercially available (**69**, 5g is £95.00 from Sigma Aldrich).

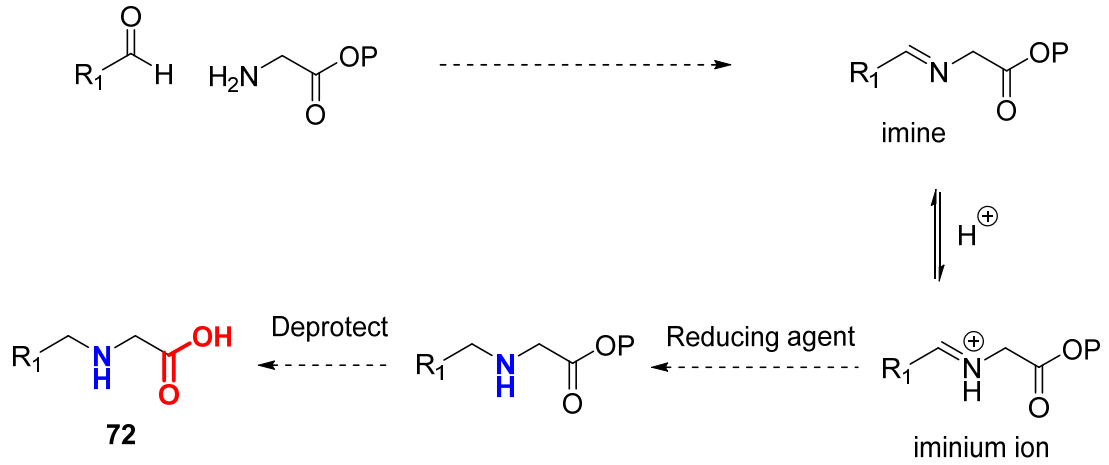

Scheme 2.12 Proposed formation of a secondary amine by reductive amination, followed by removal of the acid protecting group to give a peptoid monomer with two reactive sites (**72**). The carboxylic acid is in red and the secondary amine is in blue. P is a generic protecting group.

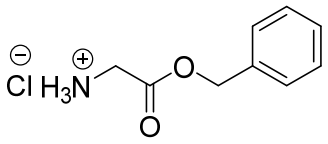

73

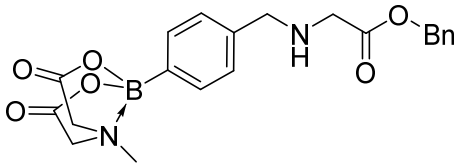

74

Glycine benzyl ester (**73**) was chosen as the amino acid as this most closely replicates the flexibility of the peptoid backbone and the benzyl ester is stable to acidic and basic conditions. Reaction of 4-formylphenyl boronic acid MIDA ester (**69**) with glycine benzyl ester (**73**) via reductive amination should give the monomer **74**.

The first attempted synthesis of the target molecule **74** was a one-pot reaction whereby MIDA boronate **69** and glycine benzyl ester (**73**) were added an hour before the reducing agent, sodium cyanoborohydride (**Scheme 2.13**). The first set of conditions used sodium cyanoborohydride as the reducing agent and acetonitrile as the solvent. Although ethanol tends to be the preferred solvent for reductive aminations, initial tests showed that MIDA boronate **69** was stable for several days in acetonitrile, whereas new spots were visible on the thin-layer chromatography (TLC) plates in less than an hour in ethanol. Glycine benzyl ester, **73**, was added in a 1.1-fold excess in an attempt to reduce formation of the tertiary amine, **75**.

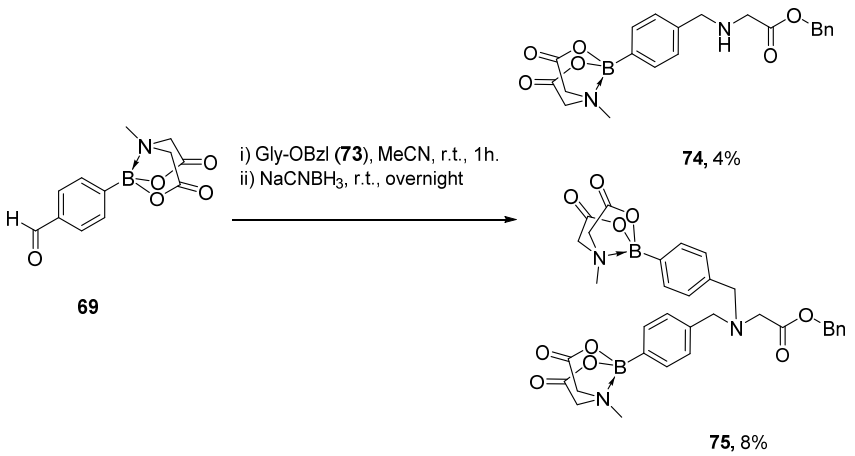

Scheme 2.13 The first set of reductive amination conditions for the attempted synthesis of target compound **74**.

Whilst target molecule **74** was successfully synthesised, by the time it had been purified and isolated by column chromatography, the best yield obtained was 4%. Furthermore, the tertiary amine **75** was also isolated in an 8% yield after purification. We also suspected some deprotection of the MIDA ester because of the presence of multiple additional spots on the TLC and several peaks in the ^{11}B NMR spectrum of the crude reaction mixture; however these additional compounds were not isolated. Indeed, it proved challenging to isolate all of these compounds as, in spite of apparently good separation on the TLC plates, these compounds appear to pull each other through the silica in the column, resulting in a significant overlap of fractions, leading to a reduction in yield.

Alternatively, for reductive aminations, including those in the literature using compounds containing a boronic acid MIDA ester, sodium triacetoxyborohydride (**30**) is the reducing agent of choice.[63] Whilst sodium cyanoborohydride is considered a mild reducing agent, sodium triacetoxyborohydride is even milder and has the added benefit of producing no toxic side products, unlike sodium cyanoborohydride which can generate hydrogen cyanide. The downside of using sodium triacetoxyborohydride is that it is water sensitive and as such, all reactions have to be carried out in dry conditions and under an inert atmosphere. Sodium triacetoxyborohydride should improve the efficiency of the reaction in two ways: first, as a milder reducing agent it would not remove the MIDA group, and second, it might also reduce the amount of tertiary amine, **75**, produced. Both of these effects would not only directly improve the yield of target molecule **74**, but by reducing the amount of, or not forming the side

products purification by column chromatography would be easier. This reaction was carried out slightly differently from the one described by **Scheme 2.13**; all reagents were added together and the best yield of **74** (34% after purification) was obtained using 1.5 molar equivalents of glycine benzyl ester (**73**) in relation to aldehyde **69** (**Scheme 2.14**).

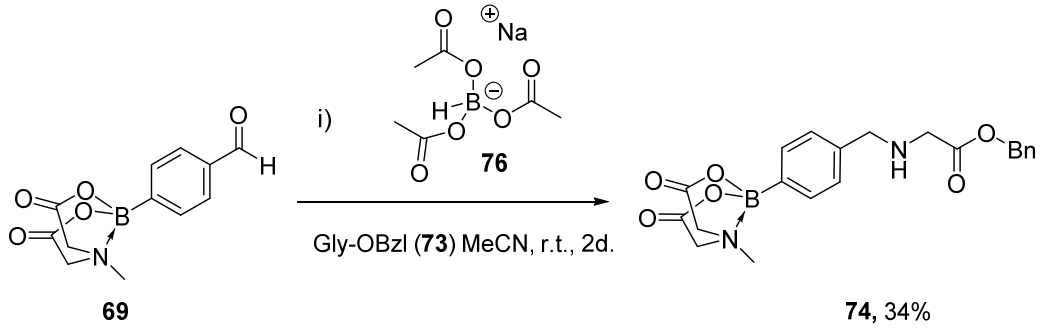

Scheme 2.14: Reductive amination using sodium triacetoxyborohydride (**30**) as the reducing agent to give target peptoid monomer **74**.

It was found that this set of conditions was an improvement on the initial set of conditions in **Scheme 2.13**. TLC analysis showed only two spots: one corresponding to the starting aldehyde (**69**) and one new spot which was found after purification of the crude reaction mixture to be target compound **74**. There was no evidence of any deprotection of the MIDA boronate group. The reaction was stopped after two days because LC mass spec. analysis indicated that tertiary amine **75** was starting to form, although this was evidently not present in a large amount as none was isolated from column chromatography of the crude reaction mixture. As a result of all of this, purification was much simpler and the isolated yield of monomer **74** was improved to a workable 34%. A further 14% can be attributed to unreacted aldehyde, **69**. However, this still leaves around 50% of the yield unaccounted for. Monomer **74** was isolated as a colourless, sticky solid which, once out of solution proved very difficult to re-dissolve. Initial purification involved extracting monomer **74** into ethyl acetate and washing with aqueous sodium bicarbonate and water. However, after ethyl acetate had been removed, the crude reaction mixture would only re-dissolve in ethyl acetate when heated. It is therefore possible that some monomer **74** was left in the aqueous washings, contributing to the poor yield.

The presence of starting aldehyde **69** clearly showed that the reductive amination reaction did not go to completion and this would be an obvious area to look at in order to improve the yield. The fact that it was the aldehyde, **69**, that was present showed

that the problem was in imine formation rather than its subsequent reduction and therefore a possible route to improving the yield would be the addition of an acid catalyst. However, this could also lead to formation of the tertiary amine, **75**.

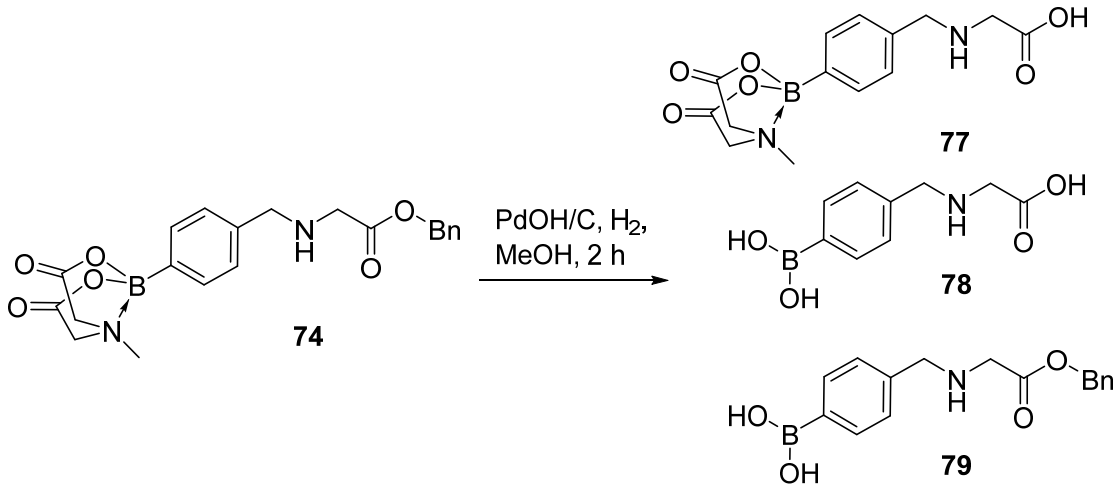

Scheme 2.15 Deprotection of the benzyl ester of monomer **74** and the compounds identified in the ESI LCMS of the crude reaction mixture (**77** – **79**, **Figure 2.7**).

Deprotection of the benzyl ester was attempted next. Solubility of monomer **74** was problematic; it was completely insoluble in most solvents, including ethyl acetate, acetonitrile and isopropanol, and only sparingly soluble in methanol. This is unhelpful as MIDA boronates are known to decompose in solutions containing alcohols if left for more than an hour.[66] This is consistent with the earlier TLC experiments which showed the appearance of new spots when 4-formylphenylboronic acid MIDA ester (**69**) was dissolved and left to stand in ethanol. Nevertheless, we proceeded with the hydrogenation using PdOH/C under argon (**Scheme 2.15**). The reaction was left for two hours at room temperature and ESI LCMS was used to determine that the reaction had finished. Unfortunately, the ESI LCMS (**Figure 2.7**) showed multiple compounds were present, including the target compound, **77**, and its analogue with the free boronic acid, **78**. The third major fraction in the ESI LCMS corresponded to the starting material with the boronic acid deprotected and benzyl ester intact, **79**. Even though the benzyl ester had not been fully removed, the reaction was stopped since MIDA boronate decomposition was clearly already happening. ^{11}B NMR of the crude product mixture (**Figure 2.8**) showed two peaks, including one at δ = 29.14 ppm which is characteristic of free boronic acids, providing further evidence of MIDA ester deprotection. Previous purifications of mixtures containing free and MIDA protected boronic acids were inefficient and extremely time-consuming, so no purification attempts were carried out.

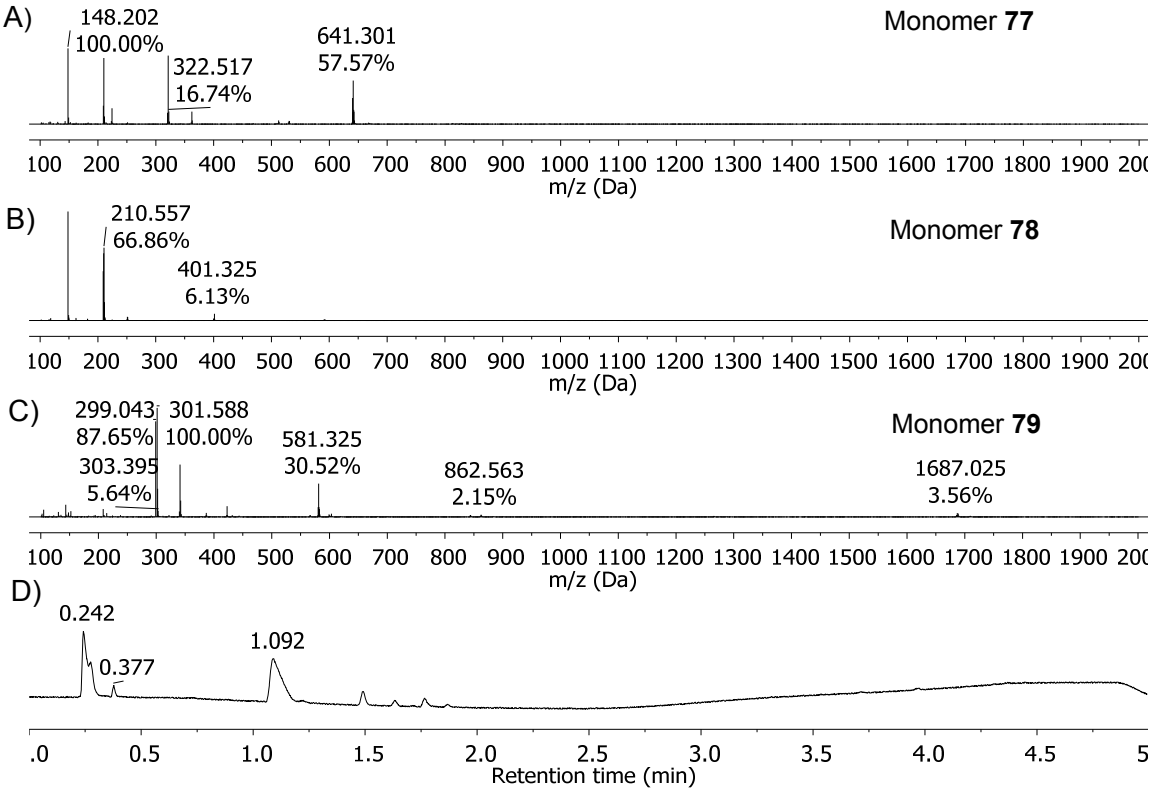

Figure 2.7 Electrospray LCMS and chromatogram of the crude reaction mixture following attempted deprotection of the benzyl ester of monomer **74** (**Scheme 2.15**). A) Mass spectrum fraction containing peaks corresponding to target compound **77**, $[M + H]^+$ = 322, corresponding to 0.38 minutes in the chromatogram. B) Mass spectrum fraction containing peaks corresponding to the compound with a free carboxylic acid and free boronic acid, **78**, $[M + H]^+$ = 211, corresponding to 0.24 minutes in the chromatogram. C) Mass spectrum fraction containing peaks corresponding to the starting material with free boronic acid, **79**, $[M + H]^+$ = 300, corresponding to 1.09 minutes in the chromatogram. D) The chromatogram of the reaction mixture (detection at 220 nm).

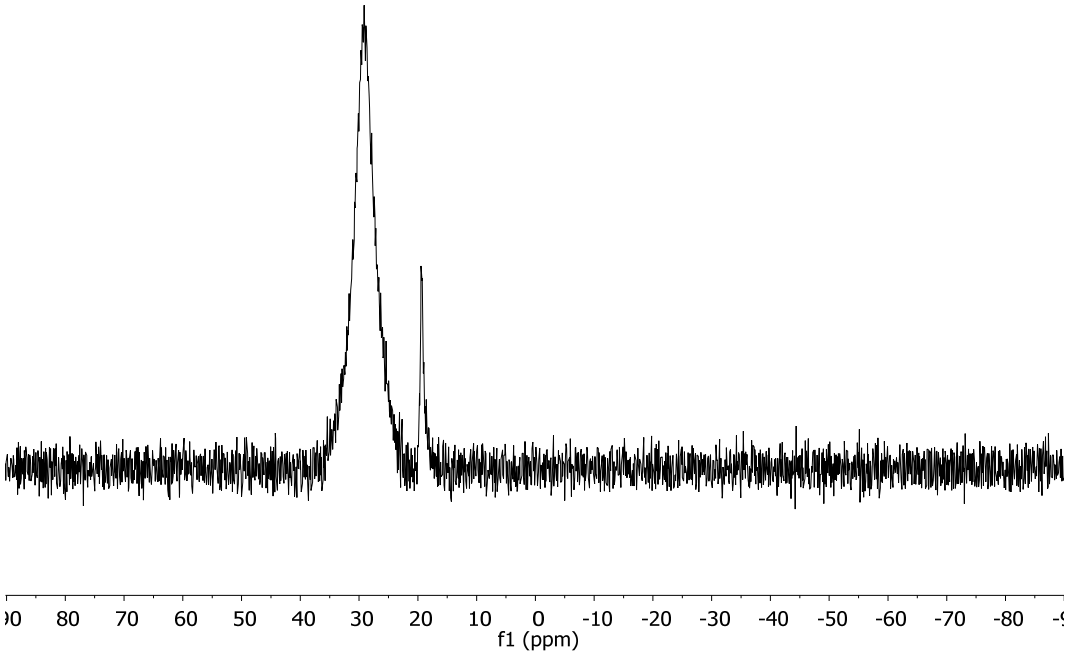

Figure 2.8 ^{11}B NMR of the crude reaction mixture following attempted deprotection of the benzyl ester of **74**, using conditions shown in **Scheme 2.15**.

2.3 Synthesis of Biaryl-Containing Cyclic Peptoids

2.3.1 Synthetic Strategy

Our chosen method of biaryl group formation was via Suzuki-Miyaura cross-coupling (**Scheme 2.4**). We wanted to carry out the cross-coupling reaction on resin. By keeping the linear parent peptoid on resin, the need for cleavage and purification prior to cyclisation is precluded. Solid phase reactions also simplify the final purification steps since unreacted materials and other side products can be washed off the resin prior to cleavage and subsequent HPLC purification. We also hoped that carrying out the cross-coupling reaction on resin would remove competition from intermolecular cross-coupling, essentially generating pseudo-high dilution conditions.

2.3.2 Incorporation of the reactive groups

In order to carry out a cyclisation via Suzuki-Miyaura cross-coupling, the resin-bound linear parent peptoid must contain both an aromatic iodide and an aromatic boronic acid. 3-Iodobenzylamine (**80**) and 4-iodoaniline (**81**) are commercially available and

can be incorporated into the peptoid at any position via the submonomer method of synthesis (**Scheme 2.16**).

Both the 3- and 4-carboxyphenyl boronic acid MIDA esters (**82** and **71**) were, at the time the reactions were carried out, commercially available from Sigma Aldrich (4-carboxyphenyl boronic acid MIDA ester (**71**) has since been discontinued).

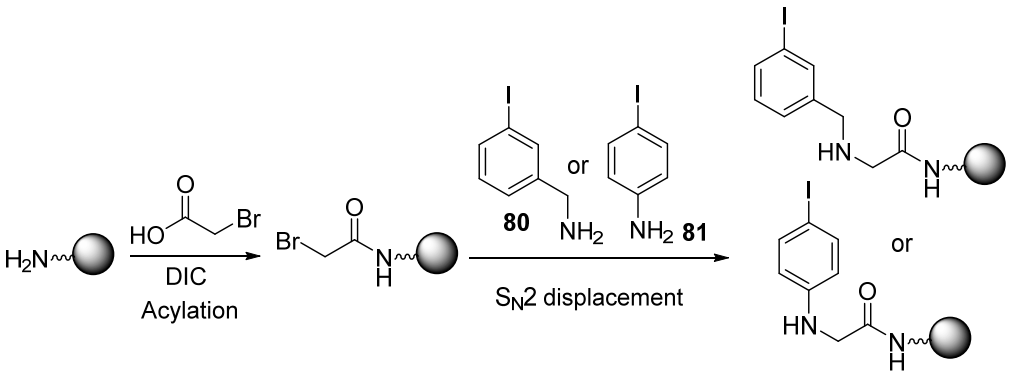

Scheme 2.16: Incorporation of an aromatic iodide via the submonomer method of peptoid synthesis using 3-iodobenzylamine (**80**) or 4-iodoaniline (**81**).

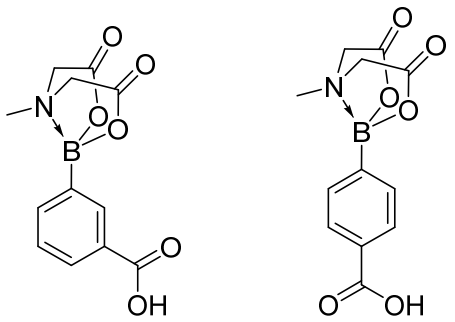

82 **71**

4-Carboxyphenyl boronic acid was used to test coupling conditions for suitability. A linear resin-bound peptoid containing iodoaniline (**83**) was first synthesised and confirmed by ESI LCMS on a portion of cleaved peptoid (**84**, **Scheme 2.17**).

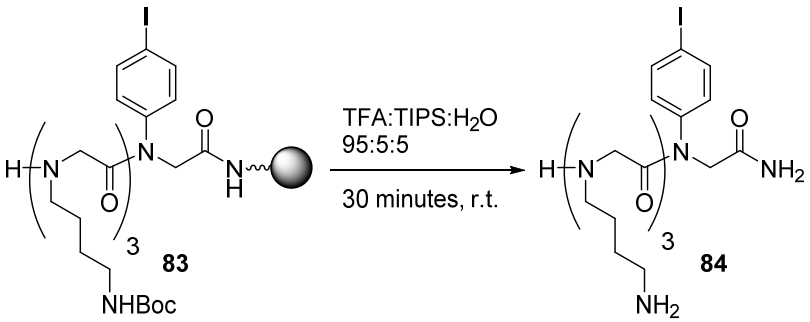

Scheme 2.17 Iodoaniline-containing peptoid (resin-bound peptoid **83** and free peptoid **84**).

Couplings were then carried out on resin-bound peptoid **83** in the presence of DIC (**Scheme 2.18**) at room temperature for one hour and at 50°C for 30 minutes and 15 minutes. Following coupling of the MIDA boronate, a portion of the peptoid (**85**) was cleaved from the resin (**Scheme 2.19**) and the free peptoid (**86**) was analysed by electrospray LCMS (**Figures 2.9 – 2.11**).

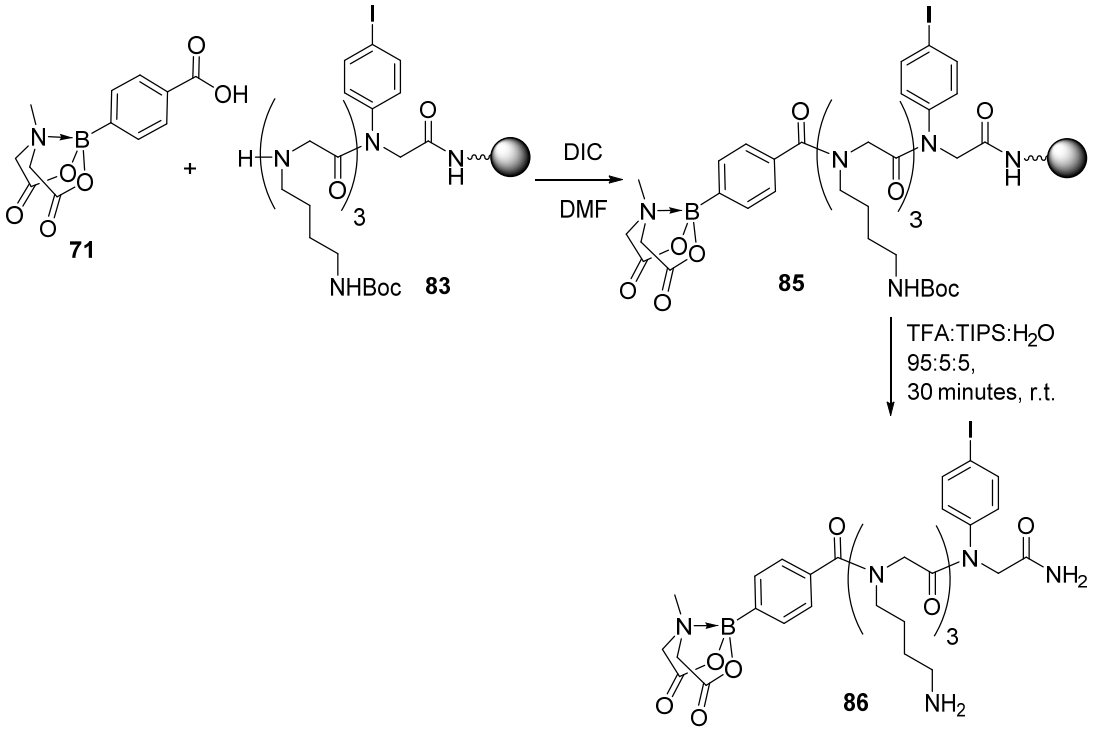

Scheme 2.18 Incorporation of 4-carboxyphenyl boronic acid MIDA ester (**71**) into a peptoid to followed by cleavage from the resin for ESI LCMS analysis.

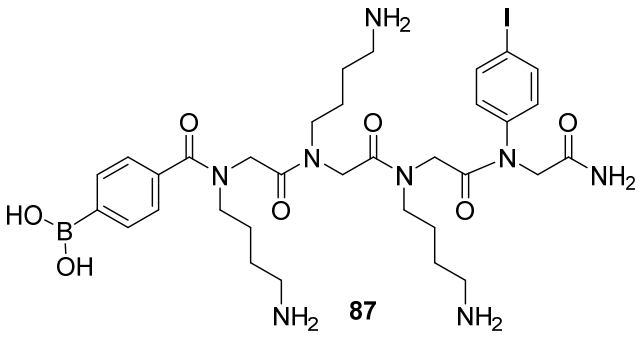

In all three reactions, coupling of the MIDA boronate was incomplete. Peaks with *m/z* 660 were seen in the LCMS of all three reactions. This corresponds to peptoid **84**. The best level of conversion was seen in the reaction at room temperature for one hour.

However, the LCMS of each reaction mixture also showed evidence of deprotection of the MIDA group with peaks at *m/z* 809 and 405. The level of deprotection is unclear as the retention time is the same as that of the MIDA boronate. No further reactions at 50°C were carried out as prolonged heating is likely to increase the rate of deprotection. All coupling reactions with MIDA boronates were subsequently carried out for one hour at room temperature.

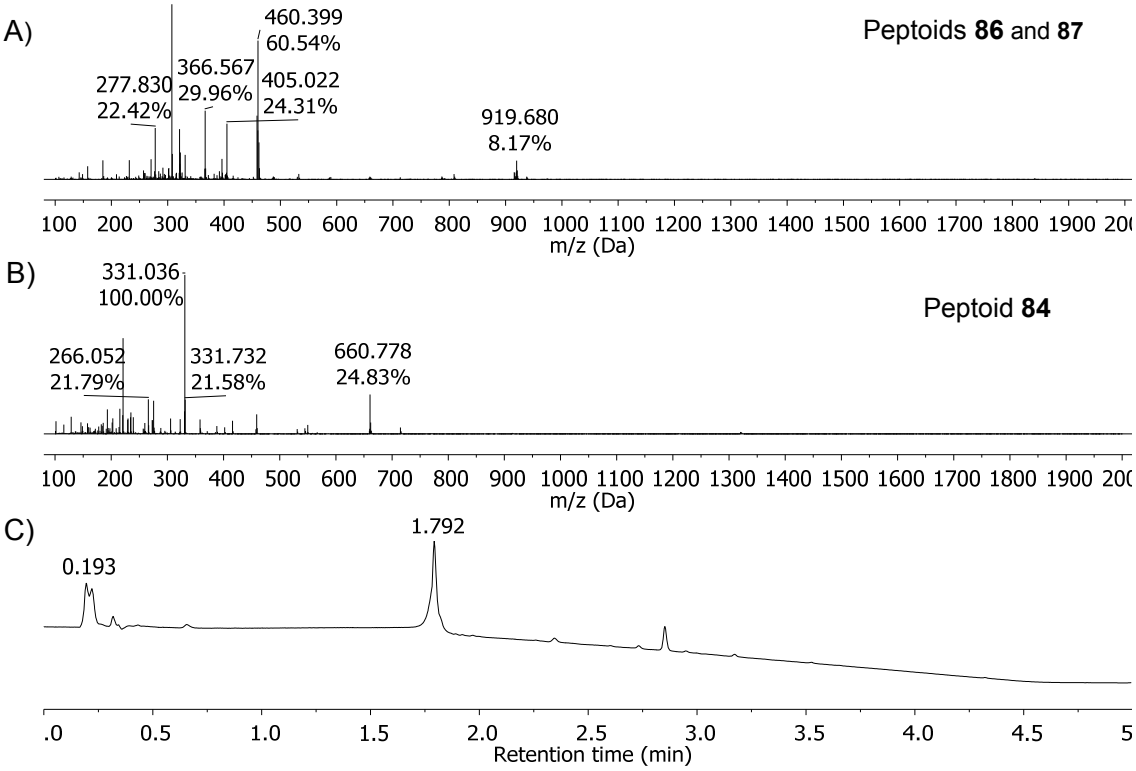

Figure 2.9 Electrospray LCMS and chromatogram following coupling of 4-carboxyphenylboronic acid MIDA ester (**71**) onto resin-bound peptoid **83** (**Scheme 2.18**). Coupling was carried out at room temperature for 1 hour. Test cleavage conditions are also shown in **Scheme 2.18**. A) Mass spectrum fraction containing peaks corresponding to linear peptoid **86**, $[M + H]^+$ = 919, corresponding to 1.79 minutes in the chromatogram. Also present are peaks corresponding to peptoid boronic acid **87**, $[M + H]^+$ = 809. B) Mass spectrum fraction containing peaks corresponding to unreacted linear peptoid **84**, i.e. with no MIDA boronate, $[M + H]^+$ = 660, corresponding to 0.19 minutes in the chromatogram. C) The chromatogram of the test-cleave mixture (detection at 220 nm).

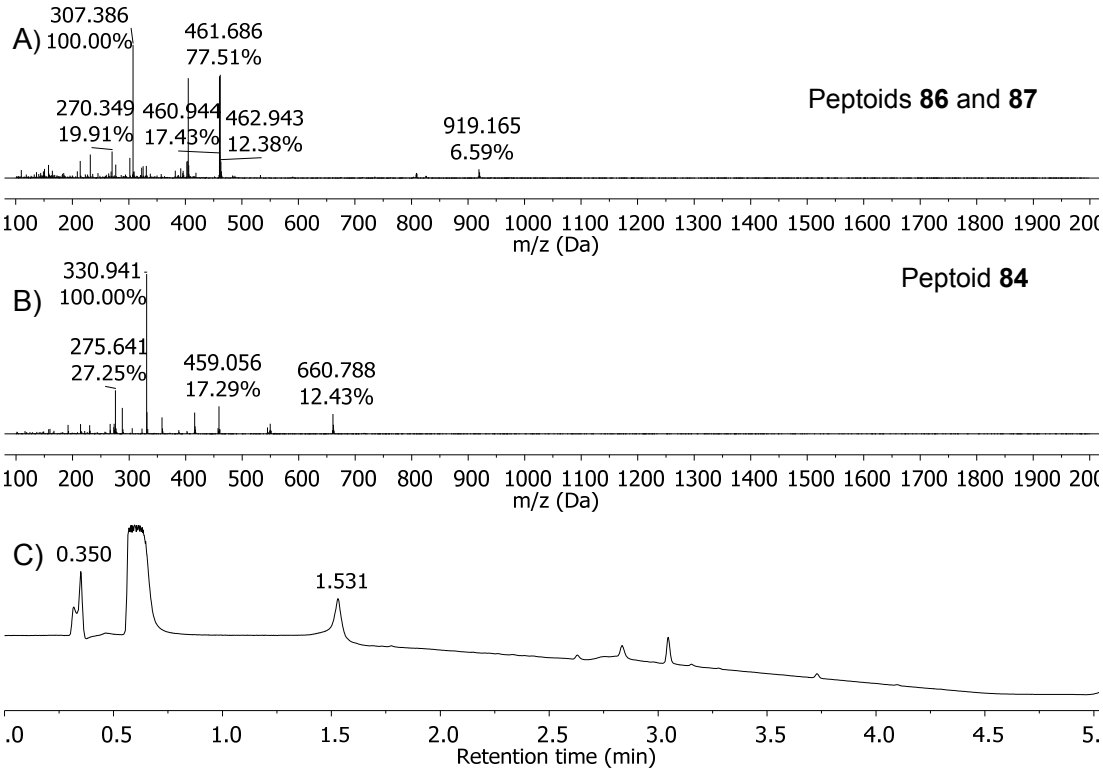

Figure 2.10 Electrospray LCMS and chromatogram following coupling of 4-carboxyphenylboronic acid MIDA ester (**71**) onto resin-bound peptoid **83** (**Scheme 2.18**). Coupling was carried out at 50°C for 15 minutes. Test cleavage conditions are also shown in **Scheme 2.18**. A) Mass spectrum fraction containing peaks corresponding to linear peptoid **86**, $[M + H]^+$ = 919, corresponding to 1.53 minutes in the chromatogram. Also present are peaks corresponding to peptoid boronic acid **87**, $[M + H]^+$ = 809. B) Mass spectrum fraction containing peaks corresponding to unreacted linear peptoid **84**, i.e. with no MIDA boronate, $[M + H]^+$ = 660, corresponding to 0.35 minutes in the chromatogram. C) The chromatogram of the test-cleave mixture (detection at 220 nm).

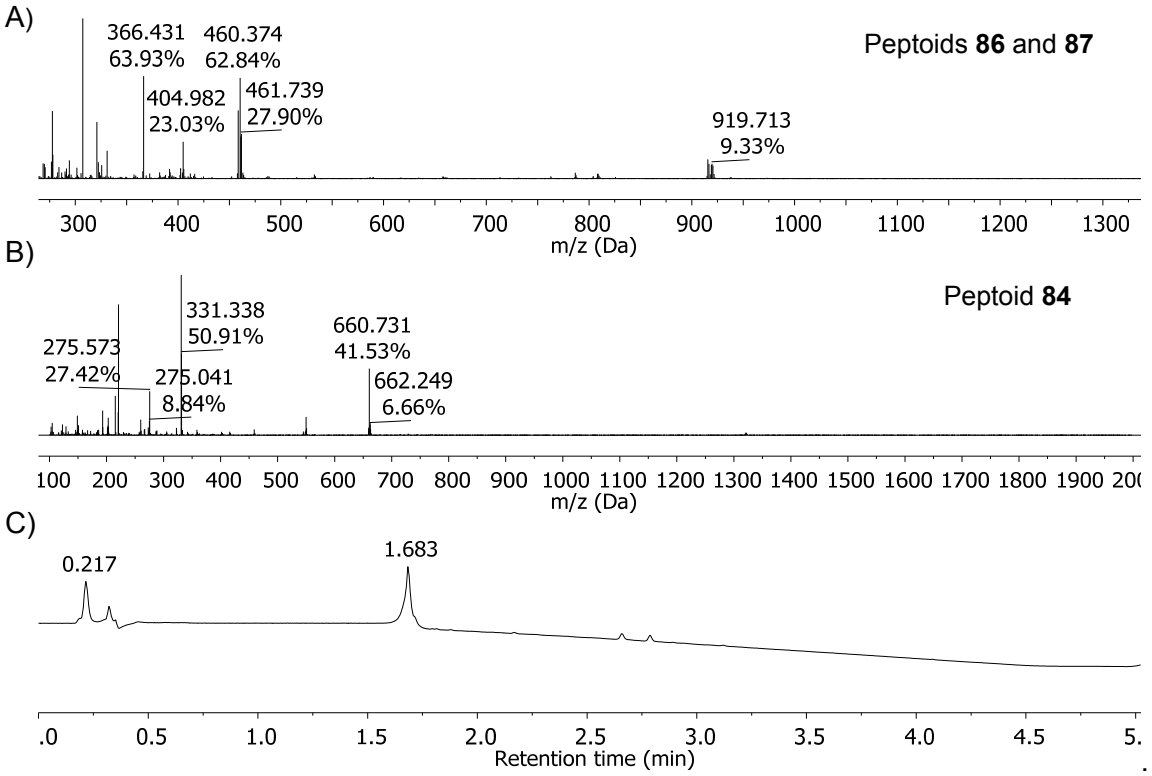

Figure 2.11 Electrospray LCMS and following coupling of 4-carboxyphenylboronic acid MIDA ester (**71**) onto resin-bound peptoid **83** (**Scheme 2.18**). Coupling was carried out at 50°C for 30 minutes. Test cleavage conditions are also shown in **Scheme 2.18**. A) Mass spectrum fraction containing peaks corresponding to linear peptoid **86**, $[M + H]^+$ = 919, corresponding to 1.68 minutes in the chromatogram. Also present are peaks corresponding to peptoid boronic acid **87**, $[M + H]^+$ = 809. B) Mass spectrum fraction containing peaks corresponding to unreacted linear peptoid **84**, ie with no MIDA boronate, $[M + H]^+$ = 660, corresponding to 0.22 minutes in the chromatogram. C) The chromatogram of the test-cleave mixture (detection at 220 nm).

2.3.3 Synthesis of linear biaryl peptoids

As previously mentioned, we wanted to carry out the cyclisation reaction whilst the peptoid was still on resin. The first set of conditions under which Suzuki cross-coupling was attempted used tetrakis palladium as the catalyst, with 2M Na_2CO_3 as a base in 9:1 ethanol:toluene, heated at 95°C for 24 hours. These conditions were obtained from a 2005 paper by Fernàndez *et al*. in which they carried out Suzuki cross-coupling reactions onto Rink Amide resin-bound 5-bromonicotinic acid (**88**, **Scheme 2.19**).[67]

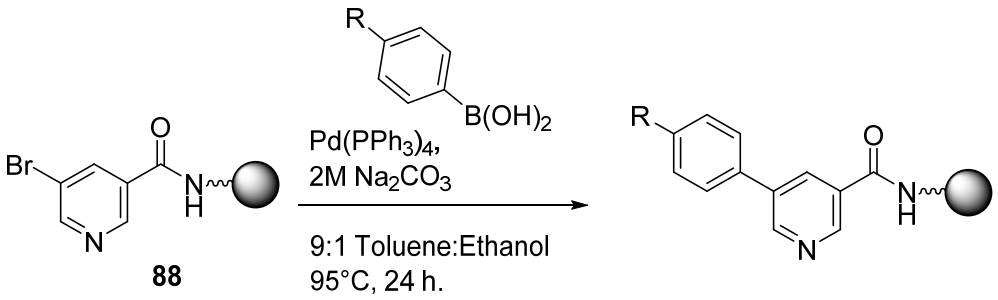

Scheme 2.19 Suzuki cross-coupling reaction carried out on resin-bound 5-nicotinic acid (**88**).[67]

Before attempting to use these conditions to synthesise a cyclic peptoid, we first attempted Suzuki cross-coupling reactions on a series of linear peptoids (**89** – **91**, **Figure 2.12**).

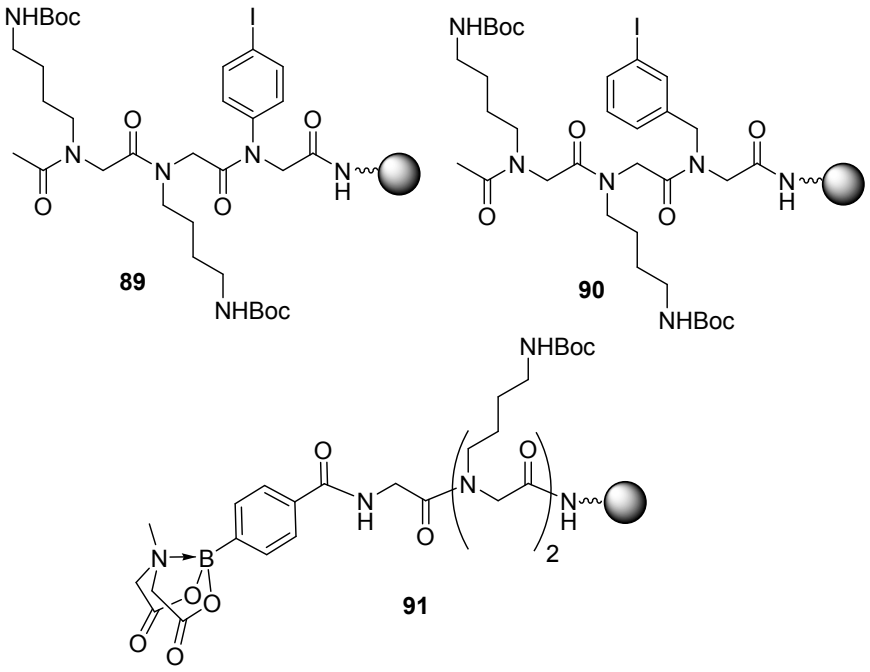

Figure 2.12 The three resin-bound linear peptoids synthesised for test Suzuki-Miyaura cross-coupling reactions.

Two peptoids, **89** and **90**, contained as the first residue, aromatic iodine functionalities from 4-iodoaniline, **81**, and from 3-iodobenzylamine, **80** respectively. The aromatic iodide residues were incorporated as the first residue to investigate whether steric hindrance as a result of proximity to the resin would prevent the cross-coupling reaction from taking place. If the cross-coupling reaction failed to work for an intermolecular reaction, it would be unlikely to work for the intramolecular reaction. The peptoids were capped with an acyl group to prevent side-reactions with a free terminal amine. The

ESI LCMS of the test cleave mixture of the peptoid containing 4-iodoaniline (**Figure 2.13**) showed two major components were present: the desired iodine-containing peptoid, **92**, and a peptoid with deletion of the iodoaniline residue, **93**, (**Scheme 2.20**) even after a nearly three hour reaction time.

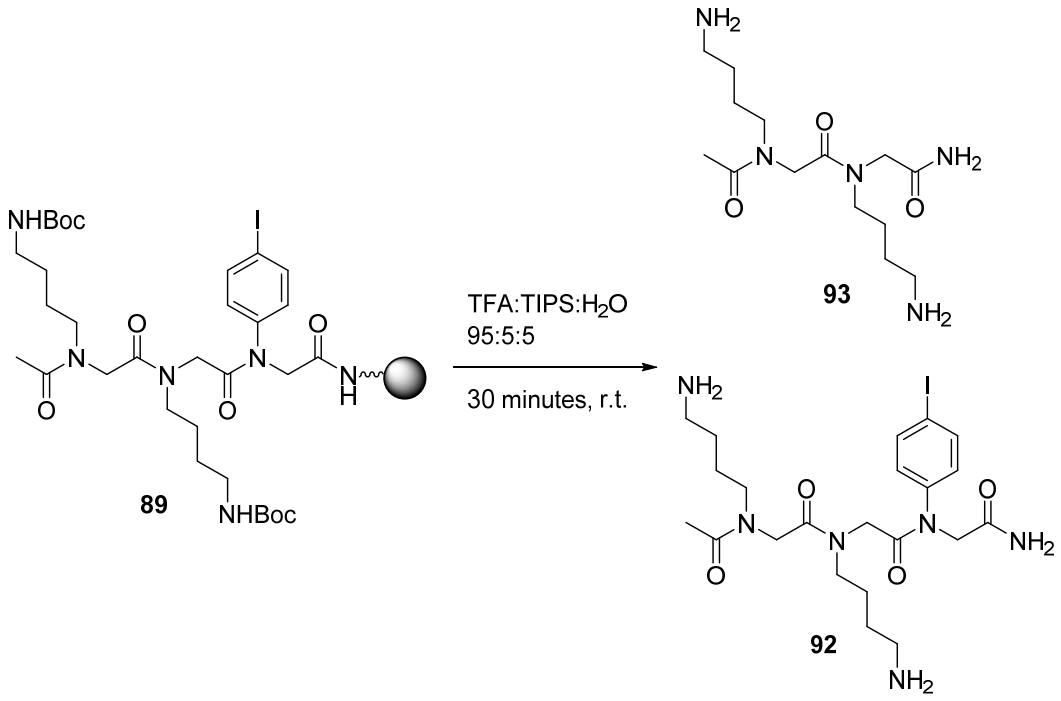

Scheme 2.20 Cleavage of a peptoid containing an iodoaniline functionality (**89**) from Rink Amide resin.

The presence of the deletion side-product is not surprising. Aniline is known to be a difficult submonomer to incorporate into peptoids due to its low nucleophilicity. Using silver salts in the displacement step has been reported to accelerate the reaction up to 76-fold.[68] However, no further modifications to the reaction conditions were attempted. For the peptoid containing the 3-iodobenzylamine monomer, **90**, the ESI LCMS of the test cleave mixture (**Figure 2.14**) showed only the desired peptoid, **94**, (**Scheme 2.21**) with no detectable signals corresponding to a deletion.

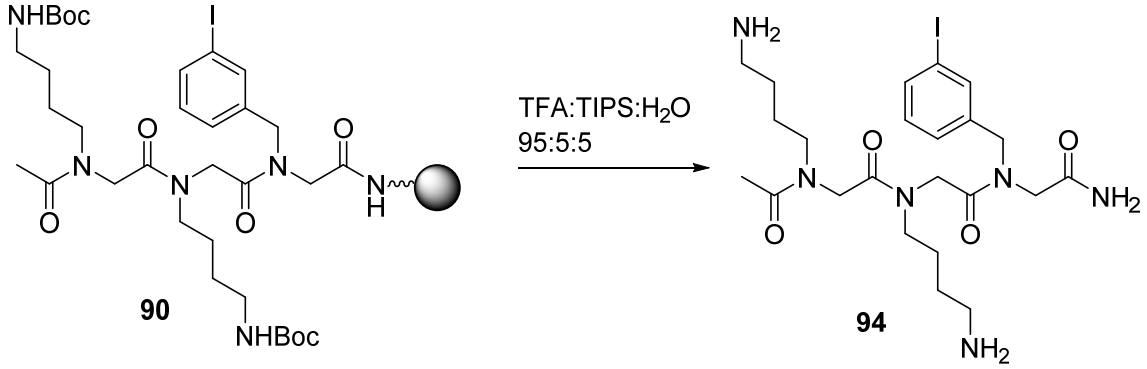

Scheme 2.21 Cleavage of a peptoid containing a 3-iodobenzylamine functionality (**90**) from Rink Amide resin.

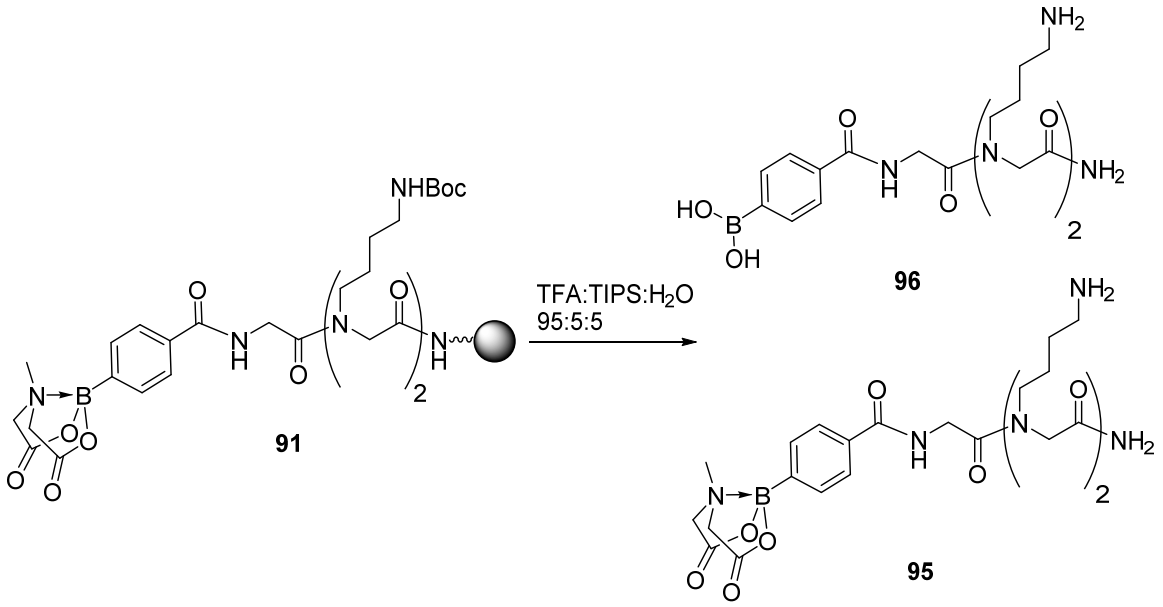

Scheme 2.22 Test cleave reaction of a peptoid containing a terminal boronic acid MIDA ester (**91**) from Rink Amide resin

The third linear peptoid made, **91**, contained a terminal aromatic boronic acid MIDA ester. The ESI LCMS of the test cleave mixture (**Figure 2.15**) showed three major peaks in the chromatogram: one at 0.65 minutes, one at 0.82 minutes and one at 1.71 minutes. The peak at 0.65 minutes corresponded to the free boronic acid-containing peptoid, **96** and the peak at 0.82 minutes corresponded to the MIDA boronate-containing peptoid, **95**. The peak at 1.71 minutes corresponded to a compound with a mass of 586 or 293. However, no reasonable reaction by-products or side products (e.g. deletions, partially deprotected species, starting material or reagents) correspond to either mass, so we proceeded on the assumption that this peak was not significant

and ignored it. Two things were notable: first that there were no peaks corresponding to deletion of the boronate building block, indicating that coupling of 4-carboxyphenylboronic acid had gone to completion, unlike in the previous test reactions. Second, that there was a separate peak in the LCMS chromatogram corresponding to the free boronic acid; in the test reactions (**Scheme 2.18** and **Figures 2.9** – **2.11**), masses corresponding to the free boronic acid were seen in the same peak in the chromatogram as the MIDA boronate. This indicates that MIDA deprotection occured in either the coupling reaction or in the test cleave reaction. However, since the next step is carrying out the Suzuki-Miyaura cross-coupling reaction, protection of the boronic acid is not critical.

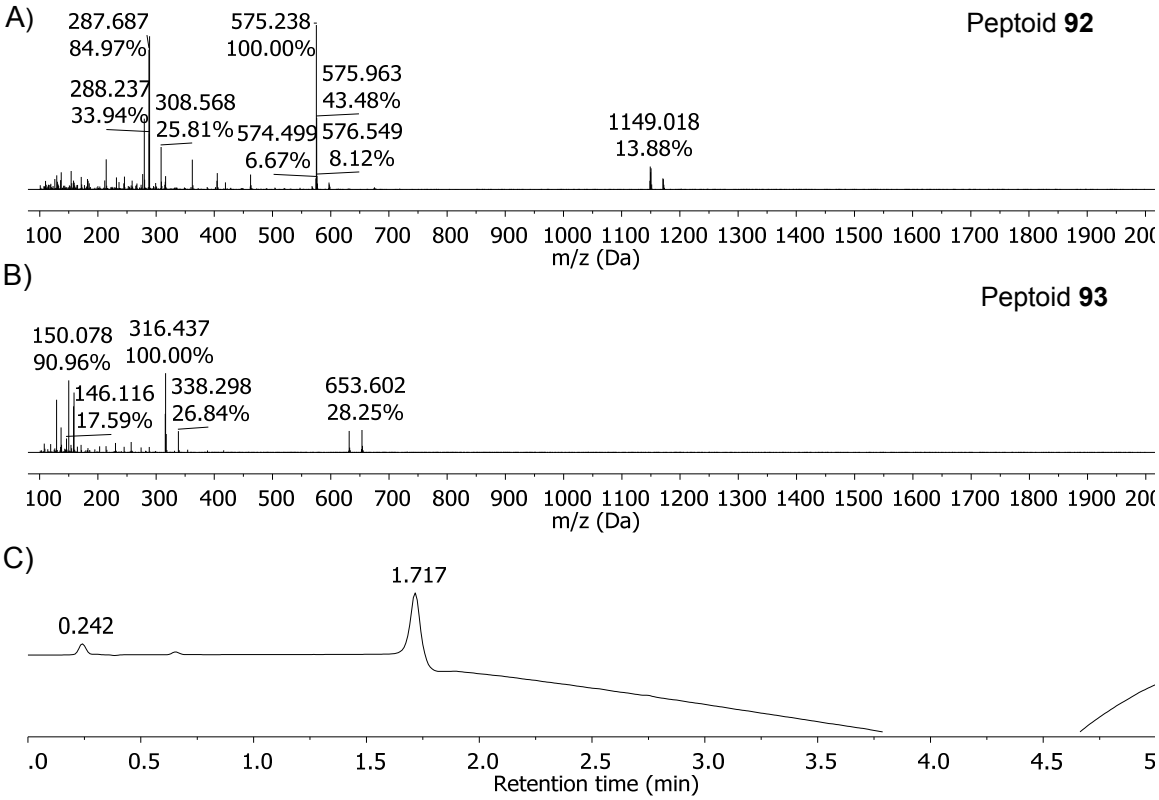

Figure 2.13 Electrospray LCMS and chromatogram of the crude reaction mixture following synthesis of iodoaniline-containing linear peptoid **89.** Test cleave conditions are shown in **Scheme 2.20**. A) Mass spectrum fraction containing peaks corresponding to iodine-containing linear peptoid **92**, $[M + H]^+$ = 575, corresponding to 1.71 minutes in the chromatogram. B) Mass spectrum fraction containing peaks corresponding to peptoid with aromatic iodide deletion, **93**, $[M + H]^+$ = 316, $[M + Na]^+$ = 338, corresponding to 0.24 minutes in the chromatogram. C) The chromatogram of the test cleave mixture (detection at 220 nm).

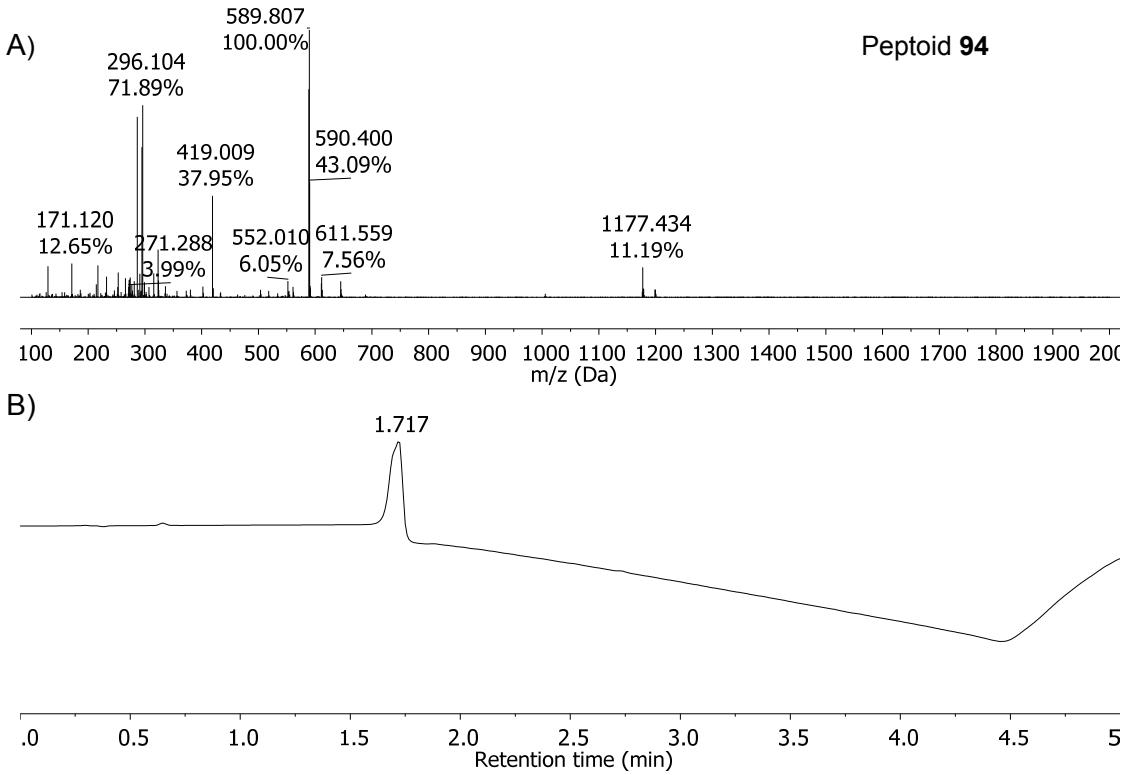

Figure 2.14 Electrospray LCMS and chromatogram of the crude reaction mixture following synthesis of 3-iodobenzylamine-containing linear peptoid **90**. Test cleave conditions are shown in **Scheme 2.21**. A) Mass spectrum fraction containing peaks corresponding to iodine-containing linear peptoid **94**, $[M + H]^+$ = 589, corresponding to 1.71 minutes in the chromatogram. B) The chromatogram of the test cleave mixture (detection at 220 nm).

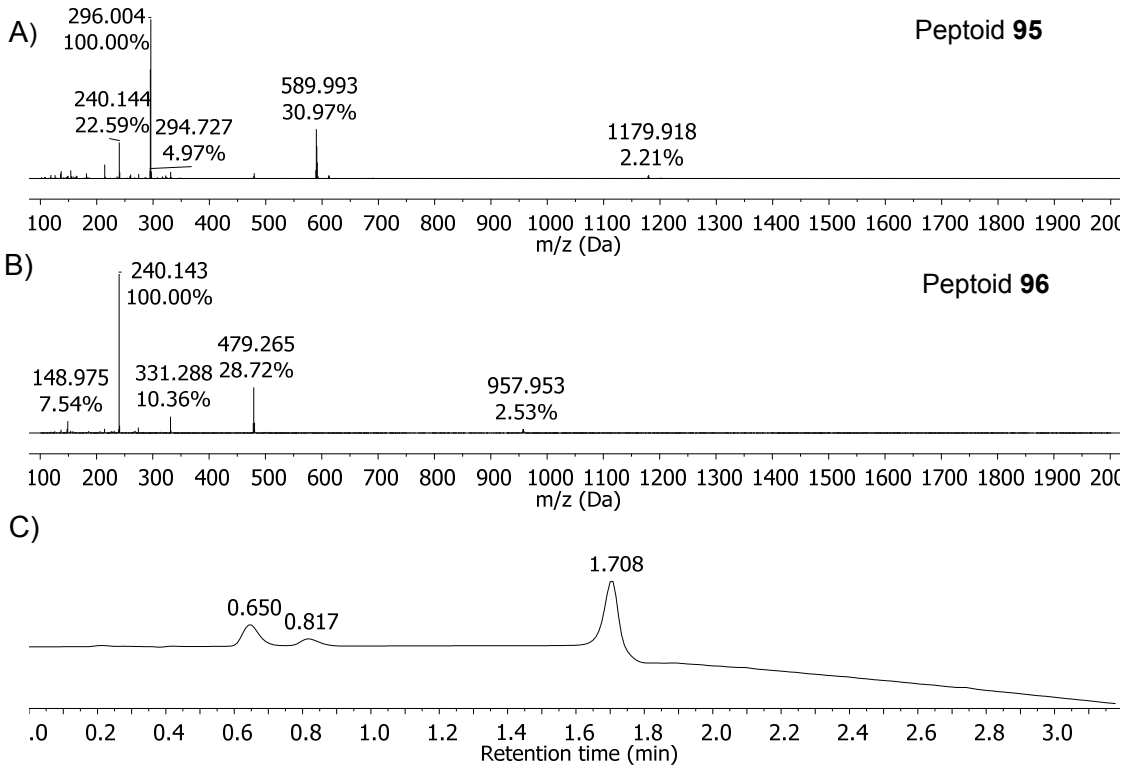

Figure 2.15 Electrospray LCMS and chromatogram of the crude reaction mixture following synthesis of MIDA boronate-containing linear peptoid **91**. Test cleave conditions are shown in **Scheme 2.22**. A) Mass spectrum fraction containing peaks corresponding to MIDA boronate-containing linear peptoid **95**, $[M + H]^+$ = 589, corresponding to 0.82 minutes in the chromatogram. B) Mass spectrum fraction containing peaks corresponding to free boronic acid-containing peptoid, **96**, $[M + H]^+$ = 479, corresponding to 0.65 minutes in the chromatogram. C) The chromatogram of the test cleave mixture (detection at 220 nm).

Having successfully synthesised the linear peptoids **89** – **91**, on resin Suzuki-Miyaura cross-coupling was attempted. Resin-bound peptoids **89** and **90** were both reacted with phenylboronic acid (**97**) using the ethanolic toluene conditions (**Schemes 2.23** and **2.24**). Following the reaction, the peptoid was cleaved from the resin and analysed by ESI LCMS. In both cases, biaryl-containing linear peptoids (**98** and **99**) were found in the ESI LCMS of the crude peptoids (**Figures 2.16** and **2.17**). These were, however,

not isolated. Whilst other peaks were visible in the respective ESI LCMS chromatograms, the masses of the compounds present could not be assigned to any peptoid-related byproduct. Notably, in the reaction with the iodoaniline-containing linear peptoid, **89**, no mass peaks corresponding to unreacted peptoid were present, but in the reaction with the iodobenzylamine-containing linear peptoid, **94**, unreacted peptoid appeared in the mass spec under the same peak in the chromatogram (1.63 minutes) as the biaryl-containing peptoid, **99**.

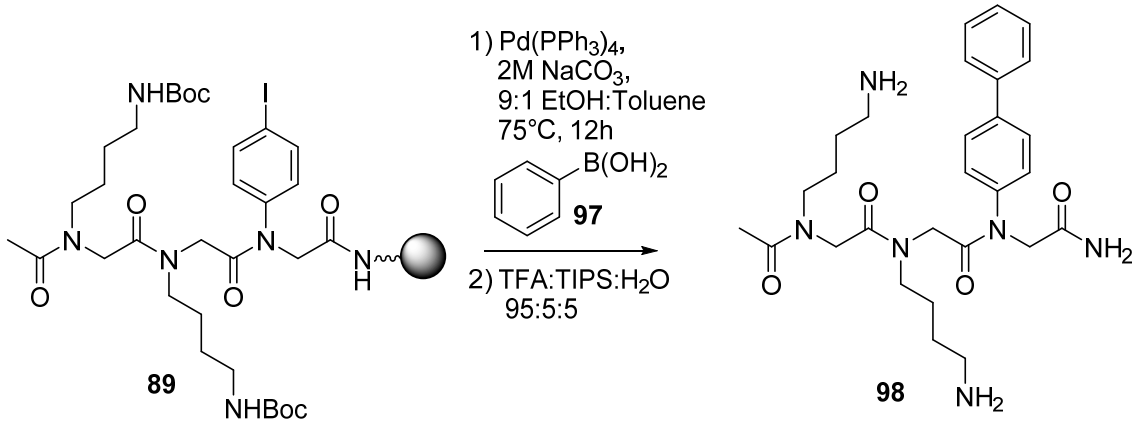

Scheme 2.23 Intermolecular Suzuki cross-coupling reaction carried out on aromatic iodide containing peptoid (**89**).

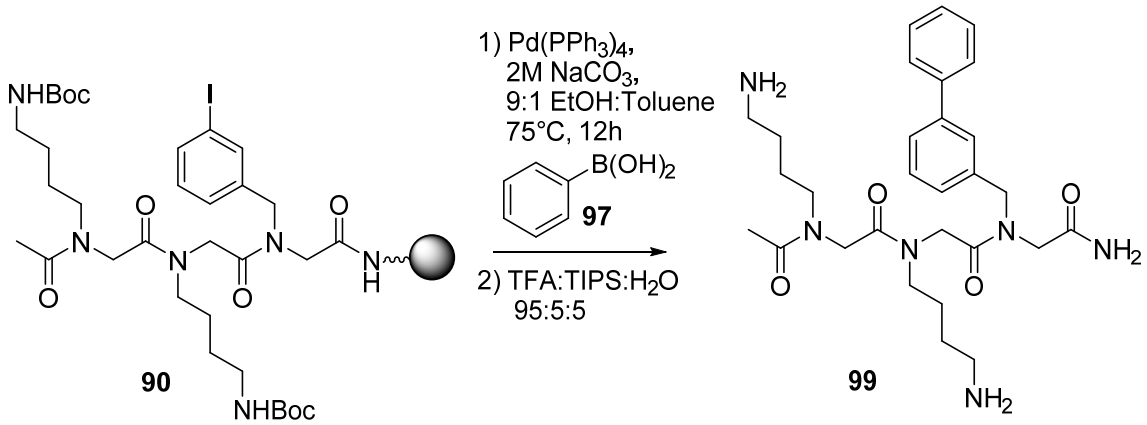

Scheme 2.24 Intermolecular Suzuki cross-coupling reaction carried out on aromatic iodide containing peptoid (**90**).

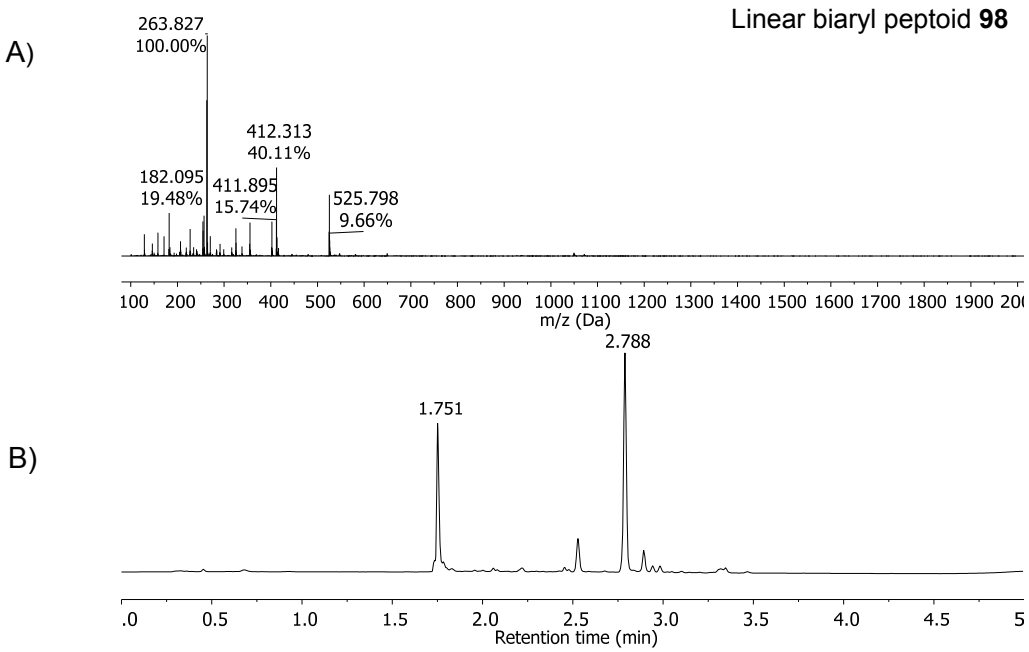

Figure 2.16 Electrospray LCMS and chromatogram of the crude reaction mixture following the Suzuki cross-coupling reaction between iodoaniniline containing peptoid (**89**) and phenylboronic acid (**97**), **Scheme 2.23**. A) Mass spectrum fraction containing peaks corresponding to biaryl-containing peptoid **98**, $[M + H]^+$ = 525, corresponding to 1.75 minutes in the chromatogram. B) The chromatogram of the test-cleave mixture (detection at 280 nm).

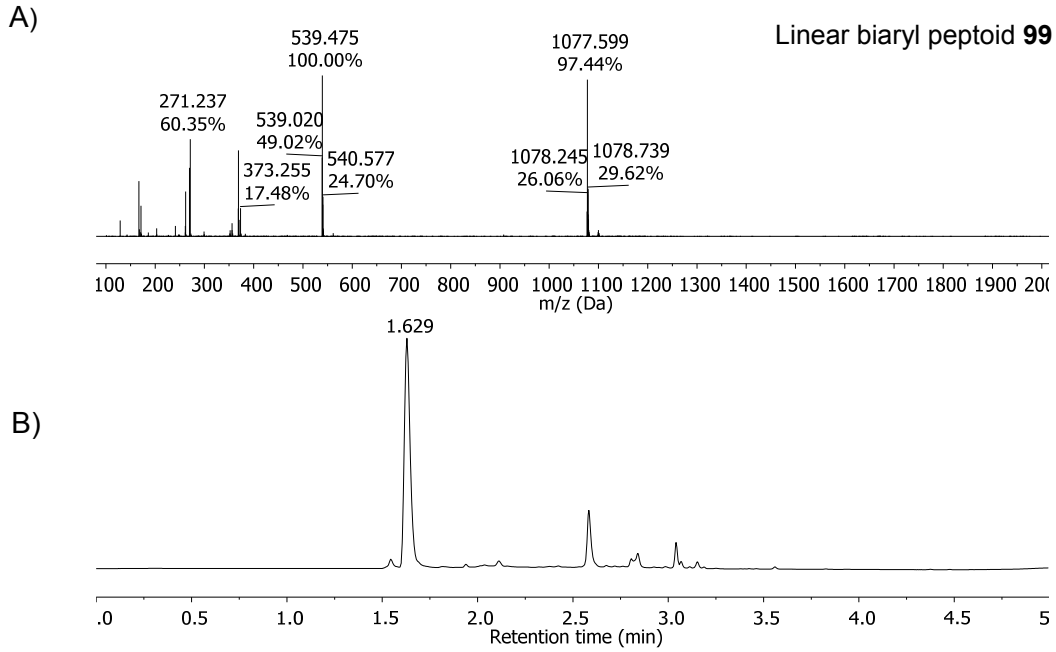

Figure 2.17 Electrospray LCMS and chromatogram of the crude reaction mixture following the Suzuki cross-coupling reaction between iodobenzylamine-containing peptoid **90** with phenyl boronic acid (**97**), **Scheme 2.24**. A) Mass spectrum fraction containing peaks corresponding to biaryl-containing peptoid **99**, $[M + H]^+$ = 539, corresponding to 1.63 minutes in the chromatogram. B) The chromatogram of the test cleave mixture (detection at 280 nm).

The linear aromatic iodide-containing peptoids (**89** and **90**) were then reacted with phenylboronic acid MIDA ester (**100**, **Schemes 2.27** and **2.28**). The aim of these reactions was to see whether the cross-coupling reaction could be done without prior deprotection of the MIDA ester. Since MIDA boronates are deprotected in the presence of aqueous base we hoped that the sodium carbonate used for the cross-coupling reaction would also deprotect the MIDA ester. The reaction conditions remained the same and, again, following the reaction, the peptoid was cleaved from the resin and analysed by ESI LCMS. In both cases, linear biaryl-containing peptoids **98** and **99** were seen (**Figures 2.18** and **2.19**), though, again, neither was isolated. As with the reactions of the linear peptoids with phenylboronic acid, **97**, unexplained peaks were present in the chromatogram, and unreacted linear iodobenzylamine-containing peptoid, **94**, appeared in the ESI LCMS under the same chromatogram peak as the biaryl-containing peptoid, **99**.

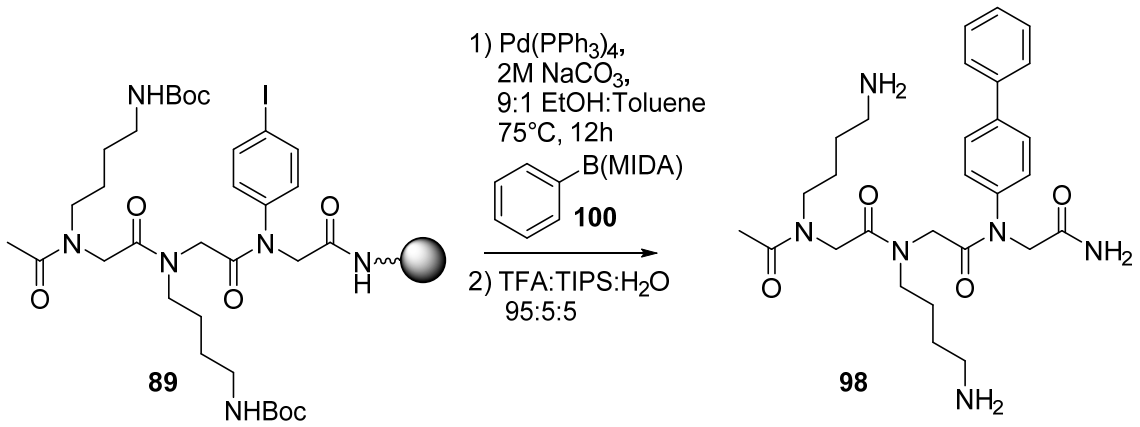

Scheme 2.25 Intermolecular Suzuki cross-coupling reaction carried out on aromatic iodide containing peptoid (**89**).

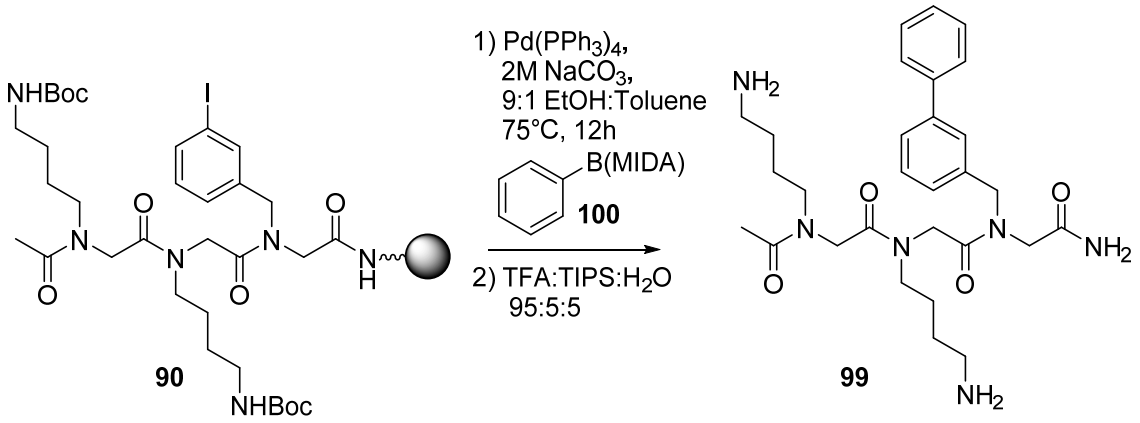

Scheme 2.26 Intermolecular Suzuki cross-coupling reaction carried out on aromatic iodide containing peptoid (**90**).

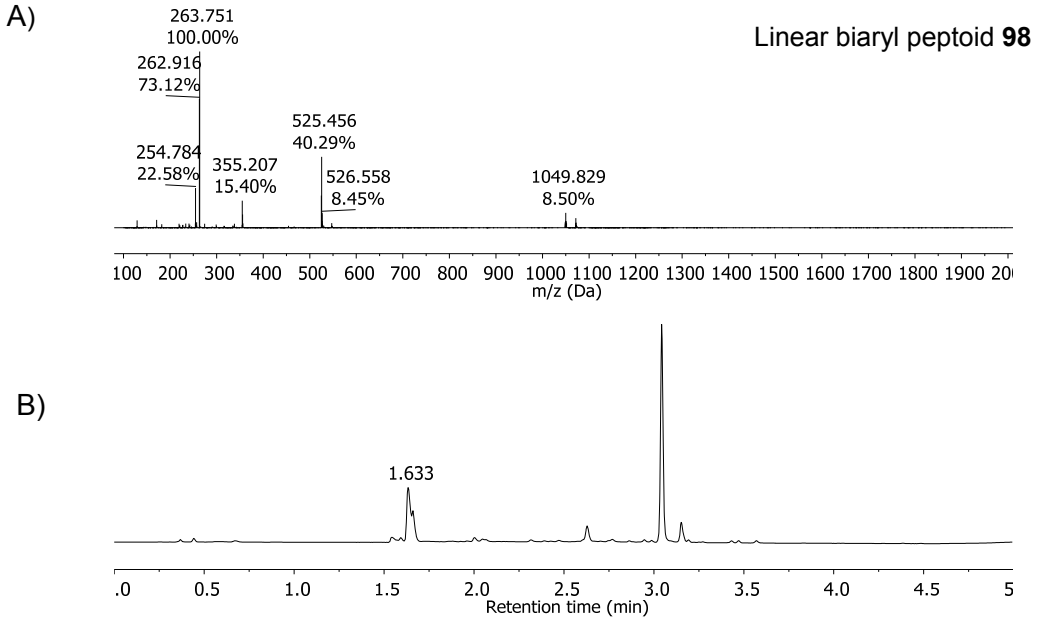

Figure 2.18 Electrospray LCMS and chromatogram of the crude reaction mixture following the Suzuki cross-coupling reaction between iodoaniline-containing linear peptoid **89** with phenyl boronic acid MIDA ester (**100**), **Scheme 2.25**. A) Mass spectrum fraction containing peaks corresponding to biaryl-containing peptoid **98**, $[M + H]^+$ = 525 corresponding to 1.63 minutes in the chromatogram. B) The chromatogram of the test cleave mixture (detection at 280 nm).

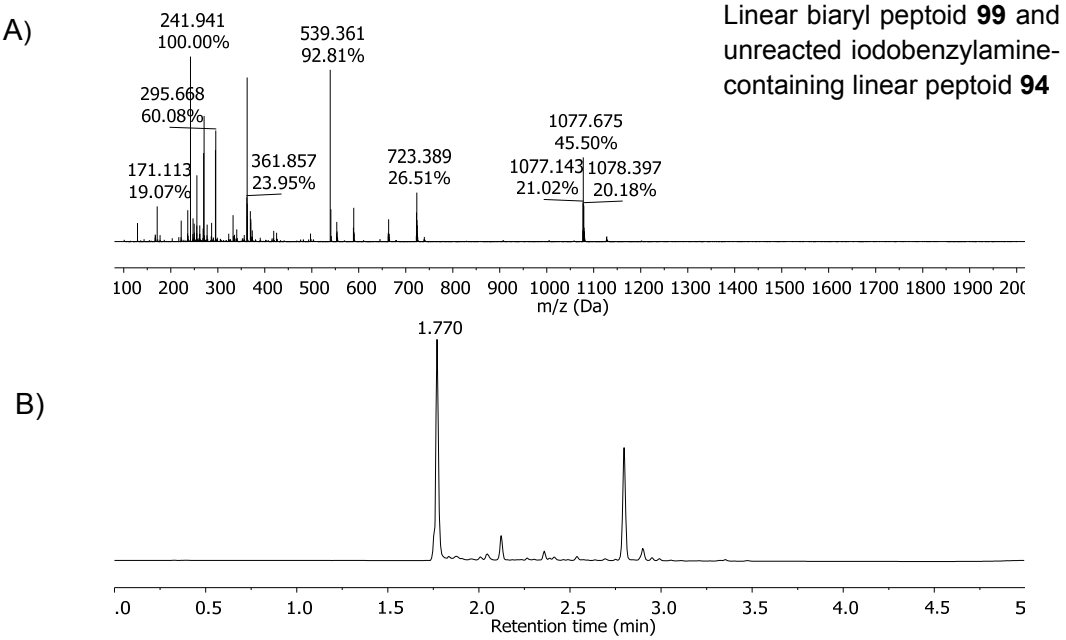

Figure 2.19 Electrospray LCMS and chromatogram of the crude reaction mixture following the Suzuki cross-coupling reaction between iodobenzylamine-containing linear peptoid **90** with phenyl boronic acid MIDA ester (**100**), **Scheme 2.26**. A) Mass spectrum fraction containing peaks corresponding to biaryl-containing peptoid **99**, $[M + H]^+$ = 539, and unreacted peptoid **94**, $[M+H]^+$ = 589.2 corresponding to 1.77 minutes in the chromatogram. B) The chromatogram of the test cleave mixture (detection at 280 nm).

Next, the Suzuki-Miyaura cross-coupling reaction was carried out on the MIDA boronate-containing linear peptoid, **91**. Resin-bound peptoid **91** was then reacted with iodobenzene (**101**) under ethanolic toluene conditions (**Scheme 2.27**), cleaved from the resin and the crude peptoid (**102**) analysed by ESI LCMS (**Figure 2.20**). Unlike the reactions on the iodine-containing linear peptoids (**89** and **90**), there was only one major peak in the chromatogram, corresponding to the biaryl-containing peptoid, **102**. No peaks corresponding to the unreacted linear peptoid, **95**, were seen.

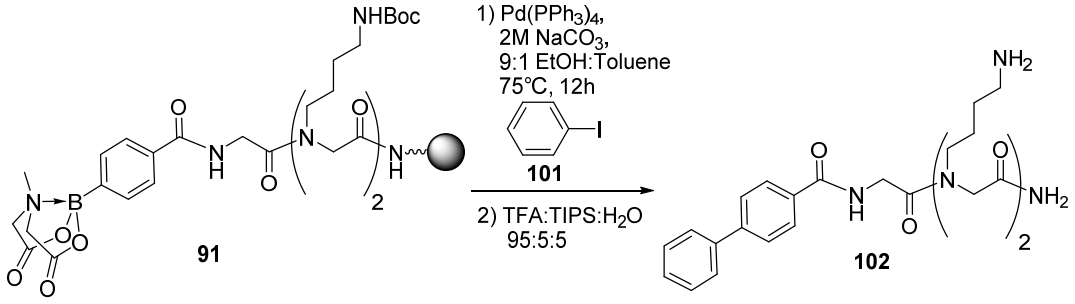

Scheme 2.27 Intermolecular Suzuki cross-coupling reaction carried out on a MIDA boronate-containing short peptoid (**91**).

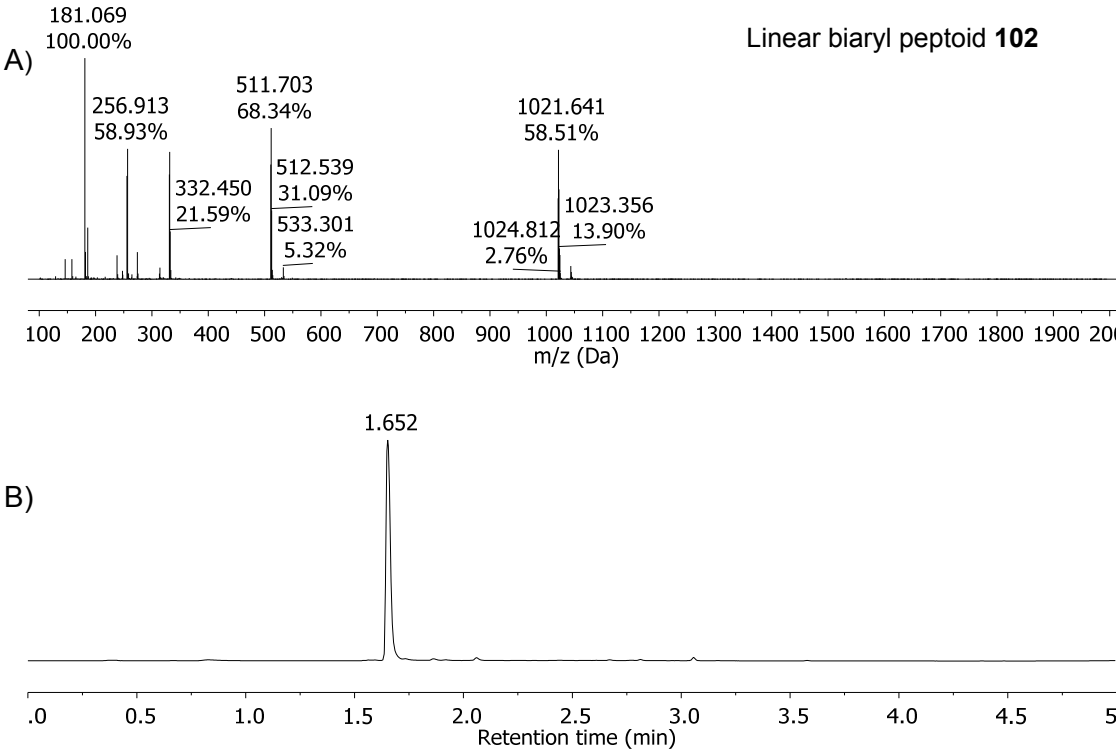

Figure 2.20 Electrospray LCMS and chromatogram of the crude reaction mixture following the Suzuki cross-coupling reaction between MIDA boronate-containing linear peptoid **91** with iodobenzylamine (**101**), **Scheme 2.27**. A) Mass spectrum fraction containing peaks corresponding to biaryl-containing peptoid **102**, $[M + H]^+$ = 511, corresponding to 1.65 minutes in the chromatogram. B) The chromatogram of the test cleave mixture (detection at 280 nm).

2.3.4 Cyclisation

Having successfully carried out cross-coupling reactions on a series of linear peptoids, we then attempted cyclisation via an intramolecular Suzuki cross-coupling reaction. The previous ethanolic toluene conditions were applied to a resin-bound short linear peptoid containing both an aromatic iodide and an aromatic MIDA boronate (**103**, **Scheme 2.28**) which was synthesised using conditions previously described in **Section 2.3.2**. The coupling time was extended to 48 hours to account for the increased difficulty in bringing the reactive groups together. The peptoid was then cleaved from the resin and purified by HPLC. However, in spite of seeing peaks in the ESI LCMS corresponding to the cyclic peptoid (**104**, **Figure 2.21**), we were unable to isolate it. Having failed to isolate the cyclic peptoid on several occasions, we therefore looked to adjust our reaction conditions.

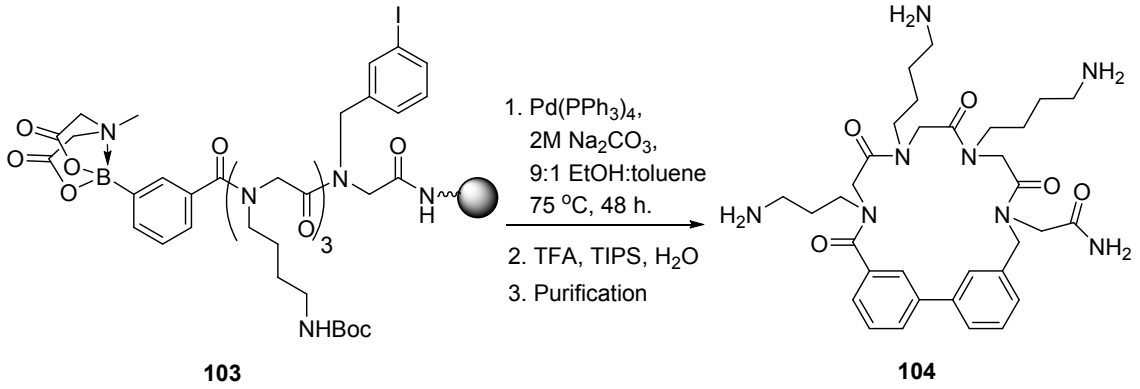

Scheme 2.28 Intramolecular Suzuki cross-coupling to synthesise a biaryl-containing cyclic peptoid (**104**).

In 2016 Nam and Seo screened different reaction conditions and reported Suzuki-Miyaura cross-couplings on resin-bound peptoids.[69] Unlike the ethanolic toluene conditions previously attempted, the reaction conditions screened in this study were carried out on a series on linear peptoids. Since their peptoids were more similar to our compounds than anything seen in previous work, we looked to adapt these optimised reaction conditions. To test these conditions we first looked to carry out intermolecular Suzuki-Miyaura cross couplings once more on linear peptoids. The intermolecular reactions were carried out on aromatic iodide-containing peptoids **89** and **90** (with phenylboronic acid MIDA ester, **100**) as well as MIDA boronate-containing peptoid **105** (with iodobenzene, **101**, **Scheme 2.29**).

Following purification by HPLC and subsequent ESI LCMS analysis of the fractions, we found that, surprisingly, the reaction had been unsuccessful with iodine-containing

peptoids (**89** and **90**), but had been successful on the peptoid containing the MIDA boronate (**105**) and the biaryl-containg linear peptoid, **106** was isolated as a white powder (8%).

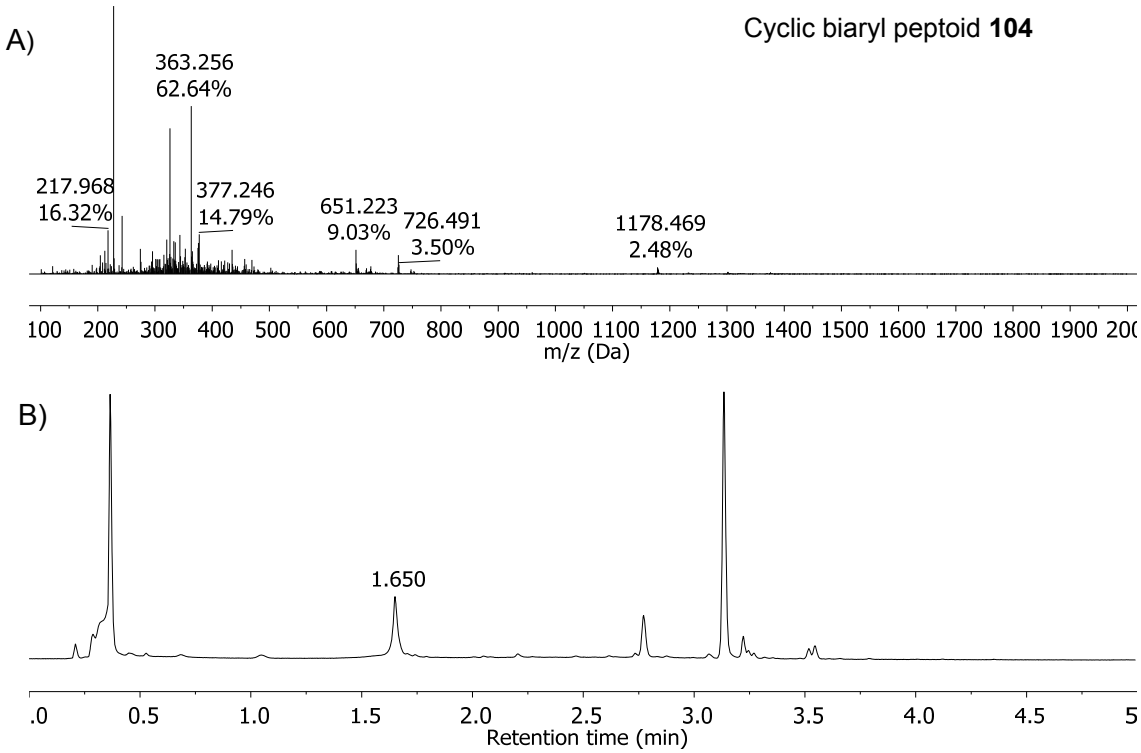

Figure 2.21 Electrospray LCMS and chromatogram of the crude reaction mixture following attempted cyclisation *via* Suzuki cross-coupling reaction of linear resin-bound linear peptoid **103**, under conditions described in **Scheme 2.28**. A) Mass spectrum fraction containing peaks corresponding to biaryl-containing cyclic peptoid **104**, $[M + H]^+$ = 651, corresponding to 1.65 minutes in the chromatogram. B) The chromatogram of the test cleave mixture (detection at 280 nm).

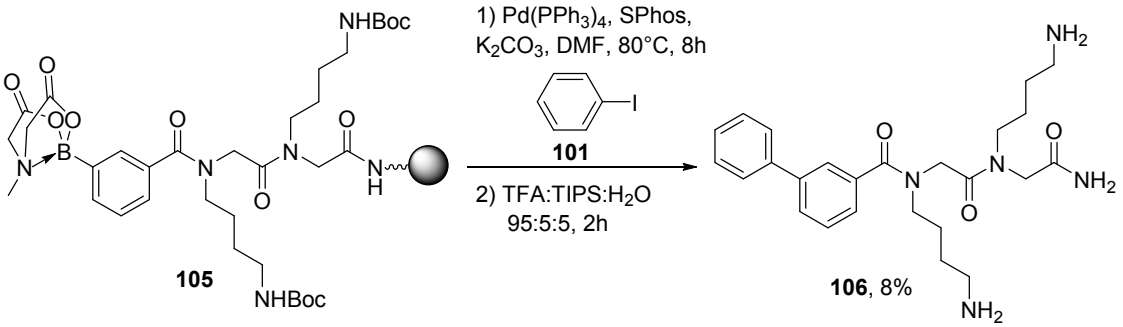

Scheme 2.29 Intermolecular Suzuki-Miyarua cross coupling to synthesise linear biaryl-containing peptoid (**106**).

In spite of the reaction failing for two of the linear peptoids and an 8% yield from the third, we decided to try carrying out a cyclisation reaction on the short linear peptoid **103** (**Scheme 2.30**). Following HPLC purification, cyclic peptoid **104** was isolated as a white solid and confirmed by accurate mass analysis and analytical HPLC. Whilst biaryl-containing cyclic peptoid **104** was the only compound isolated, the elimination product (**107**) was seen in the ESI LCMS of some HPLC fractions. Another reaction byproduct seen in the ESI LCMS of the crude product (**Figure 2.22**) mixture and in some HPLC fractions arises from the elimination of iodine and deprotection of the MIDA boronate to give compound **108**.

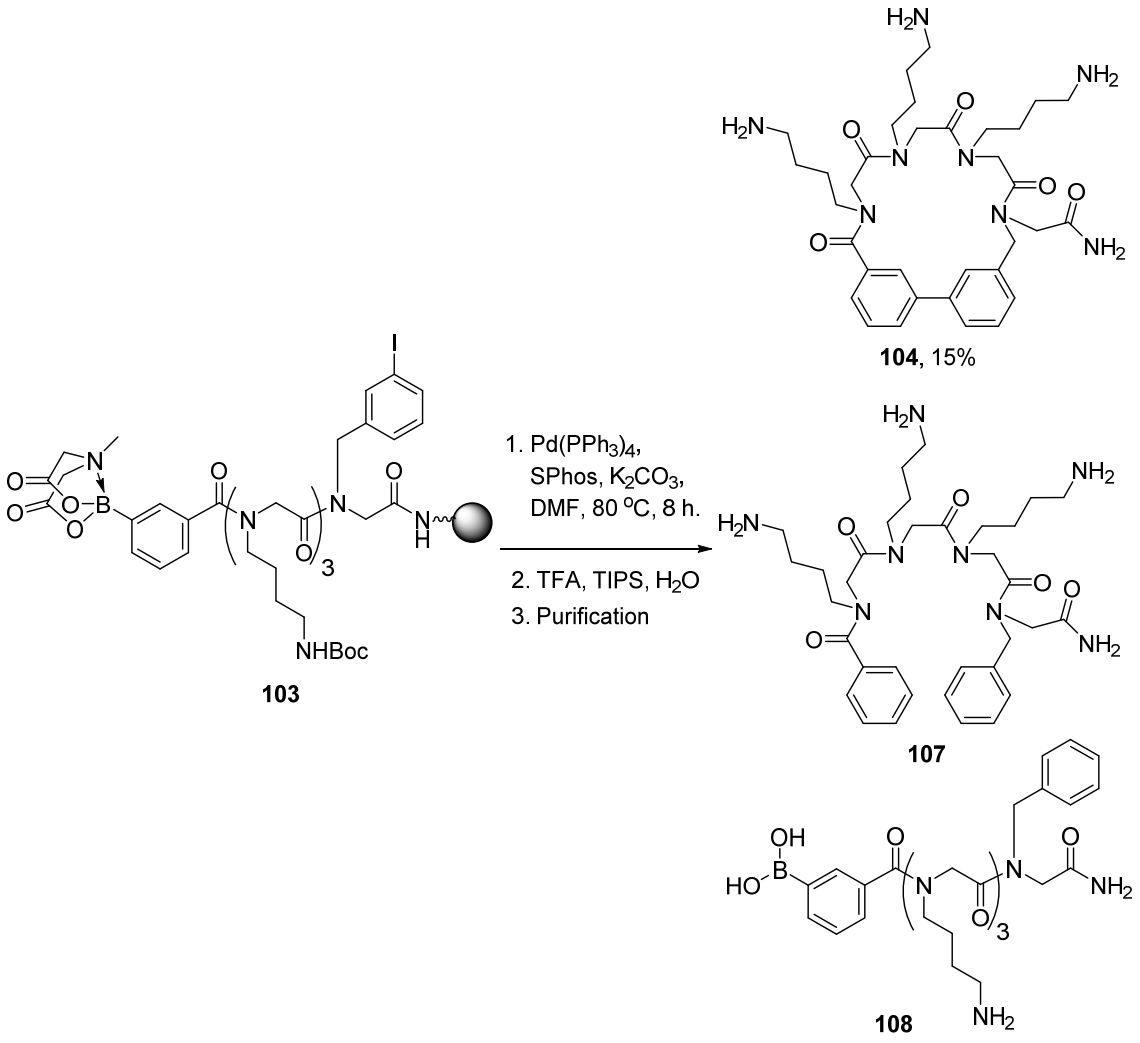

Scheme 2.30 Solid phase cyclisation of parent linear peptoid (**103**) into resin bound cyclic peptoid (**104**) via Suzuki cross-coupling.

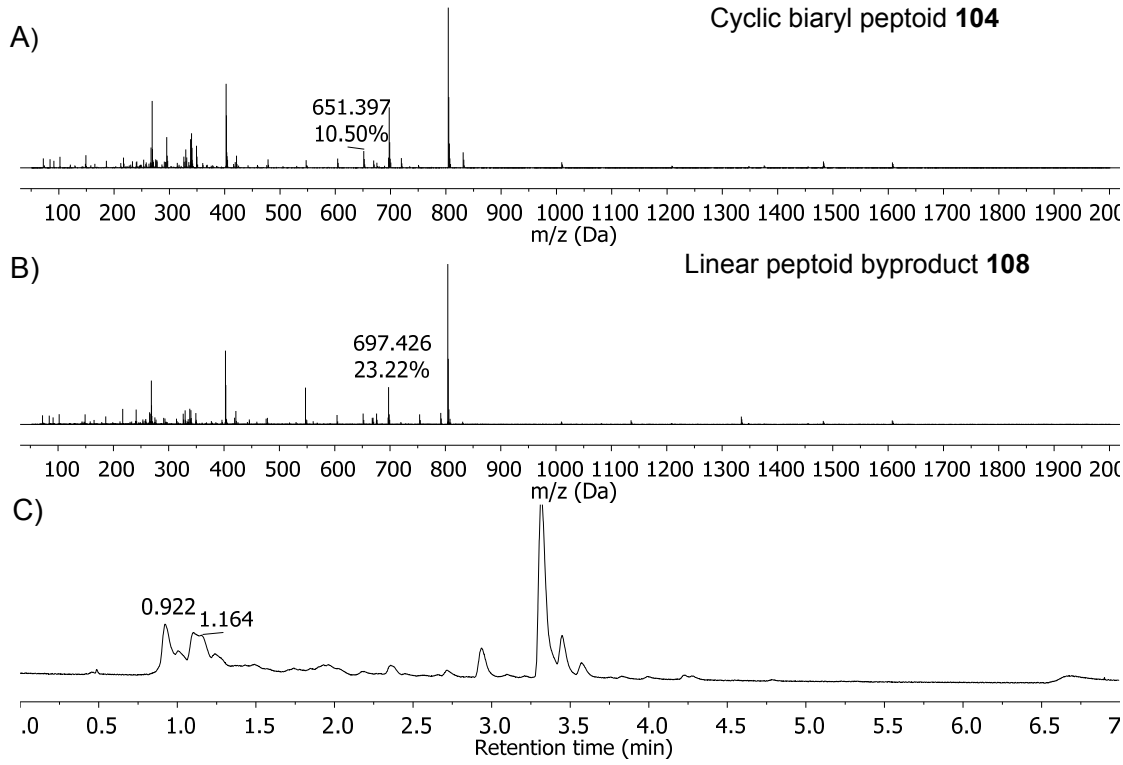

Figure 2.22 Electrospray LCMS and chromatogram of crude reaction mixture following attempted cyclisation *via* Suzuki-Miyaura cross-coupling of linear resin-bound peptoid **103** under conditions described in **Scheme 2.30**. A) Mass spectrum fraction containing peaks corresponding to biaryl-linked cyclic peptoid **104**, $[M + H]^+ = 651$, corresponding to 0.92 minutes in the chromatogram. B) Mass spectrum fraction containing peaks corresponding to free boronic acid-containing peptoid byproduct, **108**, $[M + H]^+ = 697$, corresponding to 1.16 minutes in the chromatogram. C) The chromatogram of the test cleave mixture (detection at 280 nm).

Having shown that it is possible to carry out on resin cyclisation by Suzuki-Miyaura cross-coupling of linear peptoid, we wanted to investigate whether flexibility of the chain made a difference. To test this, we made peptoid **109**, an analogue of peptoid **103** where the third *N*Lys residue was replaced by a glycine residue, essentially removing the side chain of the third residue, and carried out the cross-coupling reaction (**Scheme 2.31**). Again, the cyclic peptoid (**110**) was isolated as a white solid and confirmed by accurate mass analysis and analytical HPLC, and again, the elimination product, **111**, whilst not isolated, was seen in the ESI LCMS of some HPLC fractions. As with the reaction on linear peptoid **103**, the free boronic acid iodine elimination byproduct, **112**, was also seen in the ESI LCMS of the crude reaction mixture (**Figure 2.23**).

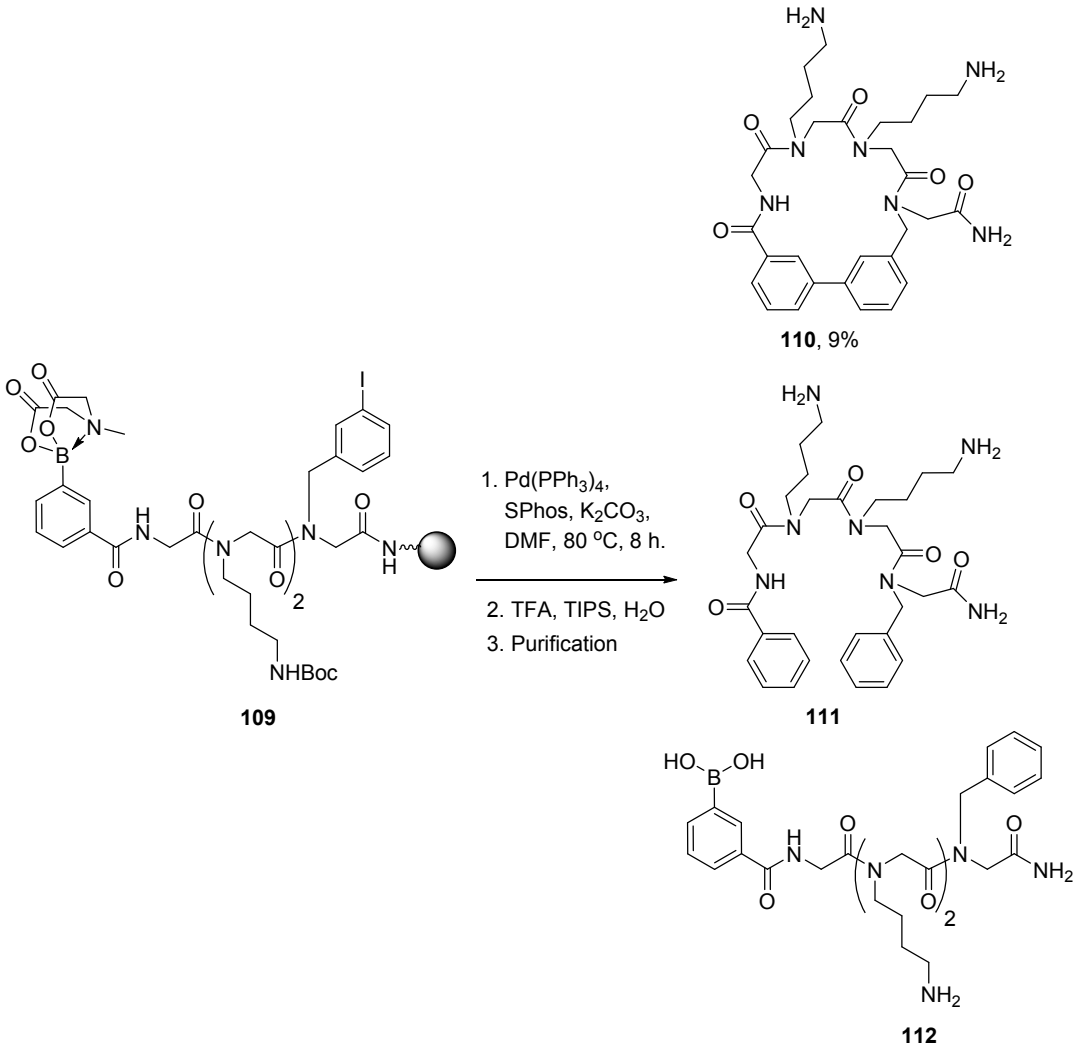

Scheme 2.31 Solid phase cyclisation of parent linear peptoid (**109**) into resin bound cyclic peptoid (**110**) via Suzuki cross-coupling.

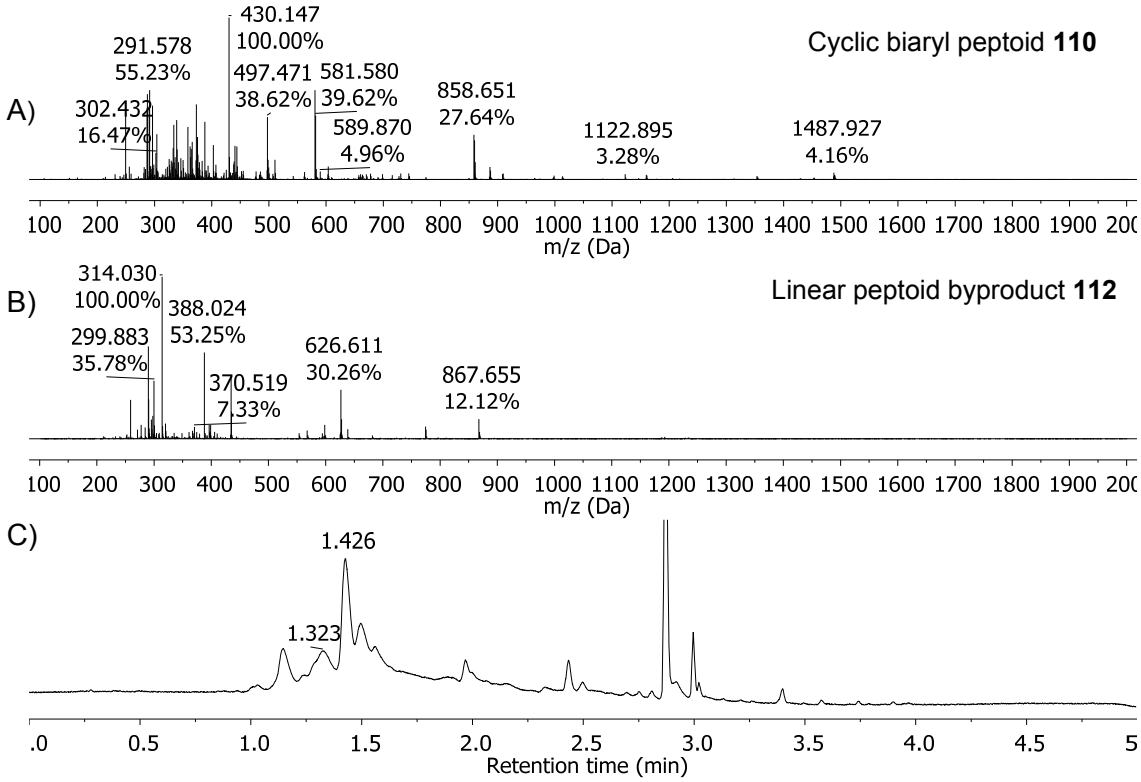

Figure 2.23 Electrospray LCMS and chromatogram of crude reaction mixture following attempted cyclisation *via* Suzuki-Miyaura cross-coupling of linear peptoid **109** under conditions described in **Scheme 2.31**. A) Mass spectrum fraction containing peaks corresponding to biaryl-linked cyclic peptoid **110**, $[M + H]^+ = 581$, corresponding to 1.43 minutes in the chromatogram. B) Mass spectrum fraction containing peaks corresponding to free boronic acid-containing peptoid byproduct, **112**, $[M + H]^+ = 626$, corresponding to 1.32 minutes in the chromatogram. C) The chromatogram of the test cleave mixture (detection at 280 nm).

2.3.5 Synthesis of a peptoid library

Next, we wanted to probe the effects of chain length and regio-isomerism of the MIDA boronate. Therefore, we synthesised a library of eight linear peptoids (**103**, **109** and **113** – **118**) on which cyclisation *via* intramolecular Suzuki-Miyaura cross-coupling was carried out to give eight cyclic biaryl-containing peptoids (**104**, **110** and **119** – **124**, **Table 2.1**).

Table 2.1 The library of biaryl-linked cyclic peptoids and their linear parent peptoids

Linear peptoid	Cyclic peptoid[a]	Yield (%)[b]
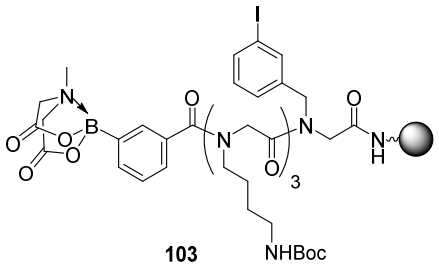 **103**	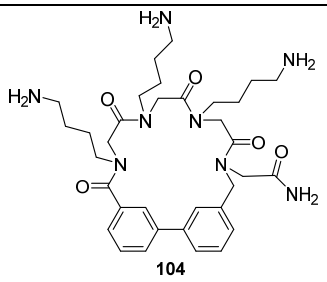 **104**	15
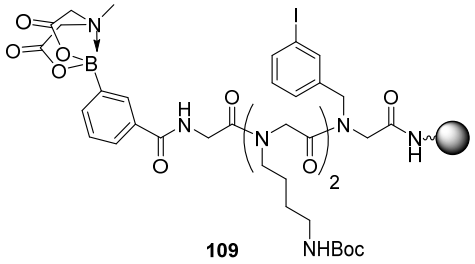 **109**	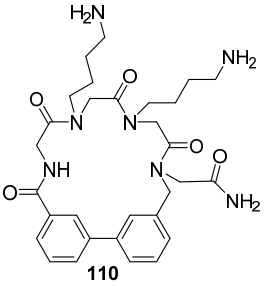 **110**	9
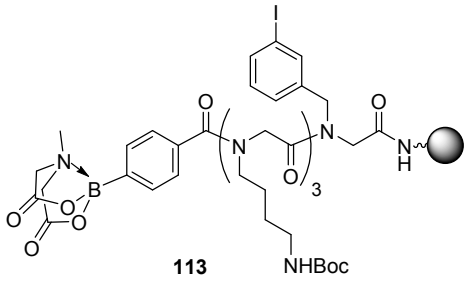 **113**	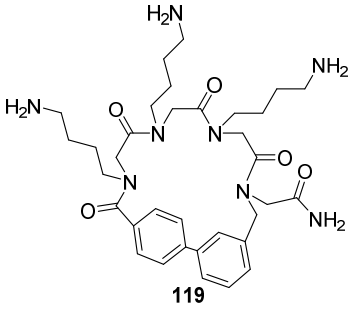 **119**	23
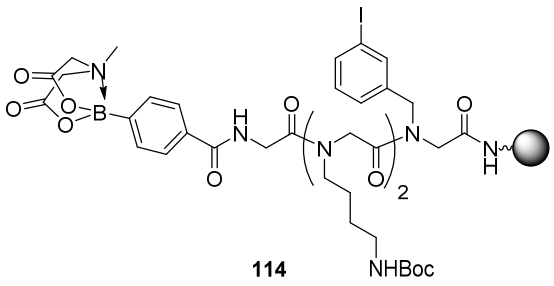 **114**	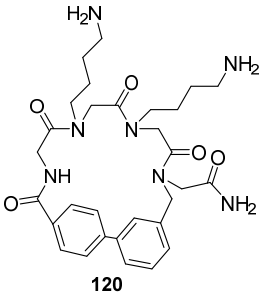 **120**	22

Linear peptoid	Cyclic peptoid[a]	Yield (%)[b]
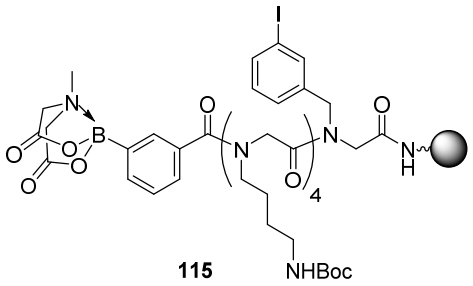 **115**	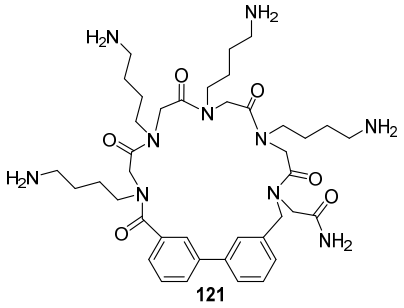 **121**	14
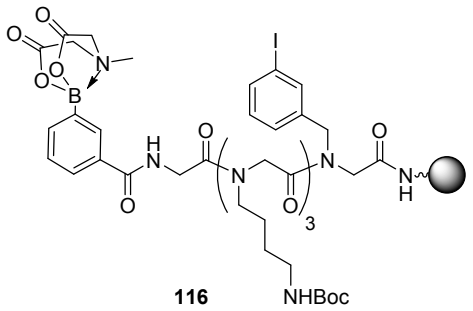 **116**	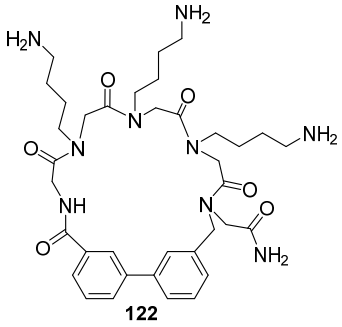 **122**	13
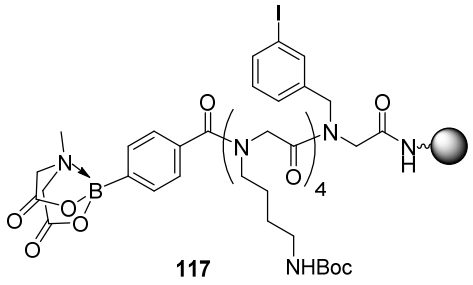 **117**	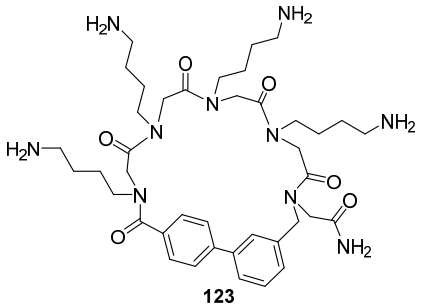 **123**	3
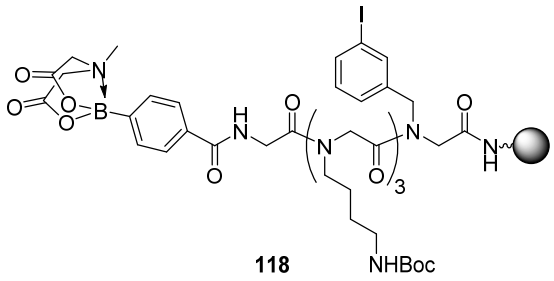 **118**	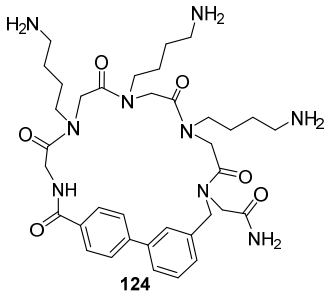 **124**	17

[a] Cyclic peptoids synthesized from linear parent peptoids under conditions shown in Scheme 2.6 and Scheme 2.7

[b] Isolated yields are calculated assuming that parent linear peptoids were synthesized with full conversion (e.g. 100% yield).

Biaryl-containing cyclic peptoids were isolated from all of the linear sequences investigated but the isolated yields did vary. Perhaps predictably, the longer sequences (**115** – **118**) appeared to be more difficult to cyclise, presumably due to a larger entropic penalty associated with constraining more flexible chains. With the exception of cyclic peptoids **110** and **122**, in each case, the yield of the cyclic peptoid recovered was lower as the sequence increased in length. For the shorter linear peptoids containing the 3-MIDA boronate building block (i.e. compare **103** and **109**) incorporation of a less hindered glycine monomer into the sequence (**109**) reduced the yield of the cyclic peptoid obtained (i.e. compare **104** and **110**). This may indicate that the *N*lys monomer confers some level of secondary structure in the linear peptoid (**103**) that makes the cross-coupling cyclisation reaction more favorable, whereas the extra flexibility conferred by the glycine monomer in **109** results in a greater entropic penalty having to be paid. Interestingly, the opposite is seen for the longer peptoids (i.e. **117** and **118**) with the glycine-containing linear peptoid (**118**) cyclising more readily than the *N*lys-containing counterpart (**117**). For the shorter linear peptoids containing the 4-MIDA boronate building block (**113** and **114**), the presence of the *N*lys side chain versus the glycine monomer appeared to make little difference to the efficiency of cyclisation, however, both resulting cyclic peptoids (**119** and **120**) were isolated in higher yields than the cyclic peptoids (**104** and **110**) formed from the corresponding shorter 3-MIDA boronate containing linear peptoids (**103** and **109**). This perhaps suggests that the formation of 3,4-biaryl-linked cyclic peptoids (**119** and **120**) is favored over the formation of the corresponding 3,3-biaryl-linked cyclic peptoids (**104** and **110**). The same trend is also seen as peptoid sequence length is increased, i.e. 3,4-biaryl-linked cyclic peptoid **124** was isolated in a higher yield than the corresponding 3,3-biaryl-linked cyclic peptoid **122.** However, given that the isolated yields in all of the aforementioned cases were not significantly different, it is difficult to draw any definitive conclusions from the data obtained. To gain more accurate information would require the linear peptoids to be cleaved and purified prior to Suzuki cross-coupling, but as discussed earlier the on-resin cyclisation confers many advantages in the overall synthetic strategy.

2.3.5 Biological Testing against *E. coli* and *S. aureus*

Five of the biaryl-containing peptoids were tested against Gram positive (*S. aureus*) and Gram negative (*E. coli*) bacteria: the linear biaryl peptoid, **106**, and the four shorter biaryl-linked cyclic peptoids, **104**, **110**, **119** and **120**. Peptoids were dissolved first in

water and then diluted further with Isosensitest broth. 50 µL of the resulting peptoid solution and 50 µL of bacteria were added to each test well to give the final peptoid concentrations listed in **Table 2.2**. Concentrations were deliberately high (i.e. in the mM ranges rather than µM ranges) in order to see if the peptoids showed any anti-bacterial activity, before any attempt to determine the minimum inhibitory concentration (MIC) ranges. Each compound was tested in triplicate, and positive (bacteria and medium with no peptoid) and negative (medium with no bacteria or peptoid) controls were also included. After incubation at 37°C for 16 hours with shaking the A_{650} readings were taken and the results are shown in **Figure 2.24**. Unfortunately, none of the peptoids tested showed activity against either *S. aureus* or *E. coli* and any differences in A650 readings between peptoids and the control were within error. The concentrations tested were deliberately high (i.e. on a mmol scale) and so the lack of anti-bacterial activity is a potential indicator of difficulty in permeabilising the bacterial cell membranes.

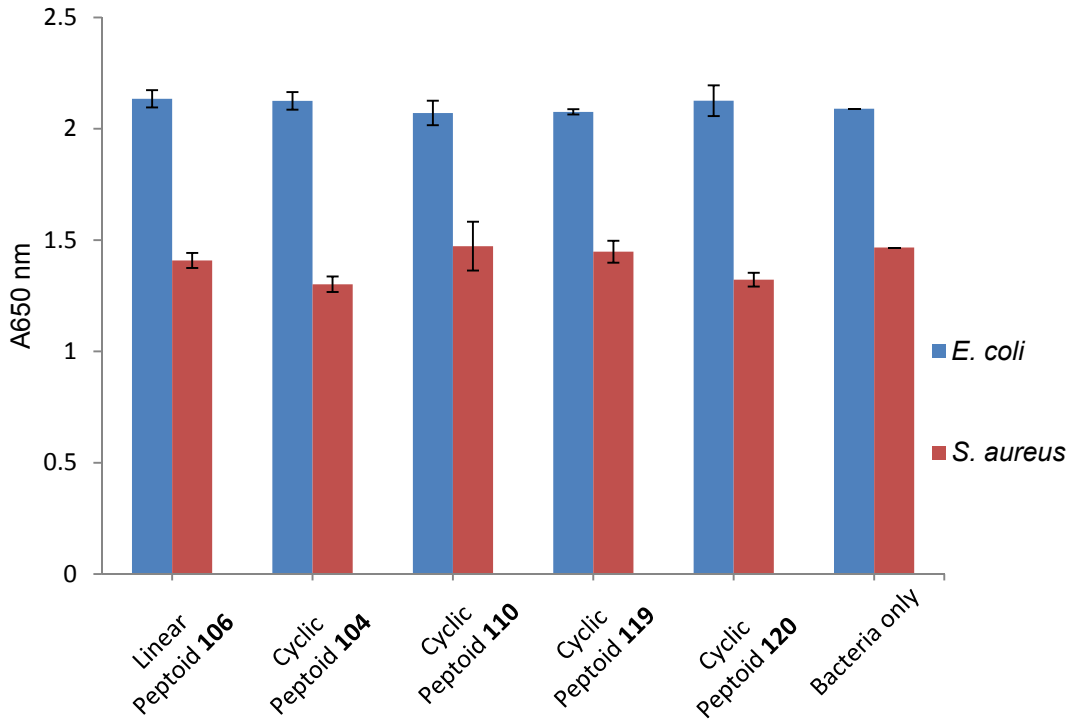

Figure 2.24 Results of bacterial testing of biaryl-containing peptoids against *S. aureus* and *E. coli*. Comparison of absorbance at 650 nm readings of peptoid-bacteria cultures and the positive control (i.e. bacteria only) following incubation at 37°C for 16 hours.

Table 2.2 Peptoids tested against *S. aureus* and *E. coli* and their concentrations

Compound number	Concentration/ mM
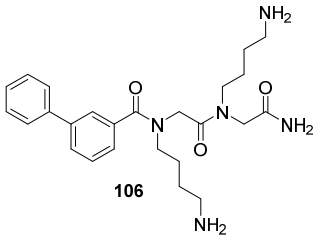 **106**	1.4
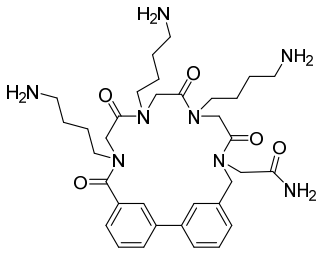 **104**	4.4
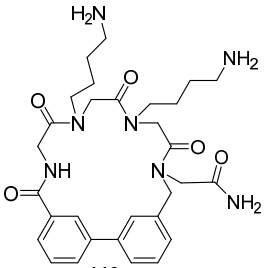 **110**	4.0
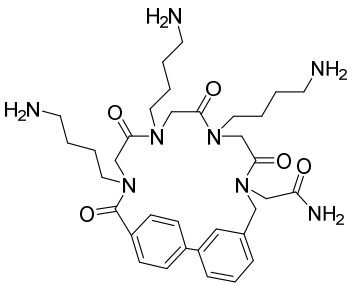 **119**	5.3
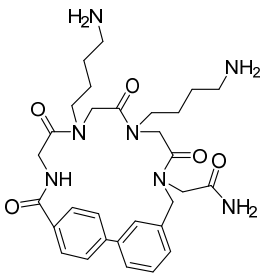 **120**	4.3

2.4 Conclusions

2.4.1 Synthesis of the boronic acid-containing peptoid monomer

A benzyl-protected MIDA boronate-containing peptoid monomer was successfully synthesised *via* a reductive amination reaction between 4-formylphenylboronic acid MIDA ester (**69**) and glycine benzyl ester (**73**).

The first attempts at the reaction used sodium cyanoborohydride as the reducing agent. However, whilst the reaction afforded the benzyl-protected target monomer (**74**), the isolated yield was low as these conditions also produced the tertiary amine (**75**) and was suspected of causing partial loss of the MIDA group. This resulted in a crude reaction mixture that was difficult to purify. All of these factors contributed to a poor isolated yield of the target monomer (**74**) of only 4%. The use of sodium triacetoxyborohydride (**76**) as an alternative, milder reducing agent proved more effective; no tertiary amine was seen, nor any suspected deprotection of the MIDA boronate and after a much more straightforward purification, the target monomer was isolated in a 34% yield in the most effective reaction conditions used (**Scheme 2.14**).

Unfortunately, the target monomer (**74**) turned out to be a sticky, resinous solid which was insoluble in non-alcoholic solvents, and only poorly soluble in ethanol and methanol. This meant that subsequent attempted deprotection of the benzyl ester resulted in partial deprotection of the MIDA boronate before complete removal of the benzyl ester.

2.4.2 Synthesis of biaryl-linked cyclic peptoids

Linear peptoids containing terminal MIDA-protected boronic acids were successfully synthesised using the peptoid submonomer method and standard solid phase peptoid coupling conditions (**Scheme 2.18**). 3- or 4-carboxyphenyl boronic acid (**82** and **71** respectively) were used as the MIDA boronate-containing monomer and treated as an amino acid. The MIDA ester remained intact following the coupling conditions used (DIC at room temperature for an hour) and following cleavage using 95% TFA.

Aromatic iodine-containing linear peptoids were also made by using 3-iodobenzylamine (**80**) and 4-iodoanline (**81**) as amines in the displacement step of submonomer peptoid synthesis (**Scheme 2.16**), although use of 4-iodoaniline (**81**) resulted in the observation of a deletion product as a result of the low nucleophilicity of the aniline submonomer.

On-resin intermolecular Suzuki-Miyaura cross-coupling using tetrakis palladium in ethanolic toluene conditions (**Schemes 2.23 – 2.27**) was attempted on the linear

peptoids and resulting LCMS analysis of the crude reaction mixtures showed that this had been successful, although none of the linear biaryl-containing peptoids were isolated at this stage.

In spite of the apparent success of the intermolecular Suzuki-Miyaura cross-coupling reaction using ethanolic toluene conditions, when used to attempt the intramolecular cyclisation reaction on a peptoid containing both an aromatic iodide residue and a boronic acid-containing residue (**103**), the reaction was unsuccessful and we were unable to isolate the cyclic product (**104**). We therefore attempted the cross-coupling reactions using conditions described by Nam and Seo in a 2016 paper.[69] Under these conditions we isolated linear biaryl peptoid **106** in an 8% yield (**Scheme 2.29**). When used in the intramolecular Suzuki-Miyaura cross-coupling reaction, we were able to isolate the cyclic biaryl-containing peptoid **104** in a 15% yield. (**Scheme 2.30**) However, we also observed in the LCMS of the HPLC fractions the presence of the linear elimination product (**107**) and the linear peptoid where the iodine has been removed and the MIDA boronate deprotected (**108**).

We then synthesised a library of eight cyclic biaryl-containing peptoids (**104**, **110** and **119** to **124**) to test whether these conditions were applicable to peptoids of different chain lengths, chain flexibilities and in the case of regio-isomerism around the biaryl group. All peptoids were successfully synthesised in yields of 3 – 23% (**Table 2.1**).

Finally, five of the biaryl-containing peptoids (one linear peptoid, **106**, and four cyclic peptoids, **104**, **110**, **119** and **120**) were screened against *S. aureus* and *E. coli* in high concentrations (1.4 – 5.3 mM, **Table 2.2**). Unfortunately, however, none showed any activity against either bacterial species at the concentrations tested. In spite of this, the methodology will develop to be more widely applicable to different peptoid structures to create a novel class of cyclic peptoids. Some of the future directions for this work are described in **Chapter 5**.

2.5 References

1. H. C. Brown, T. Hamaoka and N. Ravindran, *J. Am. Chem. Soc.*, 1973, **95**, 6456-6457.
2. J. M. Murphy, X. Liao and J. F. Hartwig, *J. Am. Chem. Soc.*, 2007, **129**, 15434-15435.
3. A. D. Ainley and F. Challenger, *J. Chem. Soc.*, 1930, **0**, 2171-2180.
4. C. Thiebes, C. Thiebes, G. K. S. Prakash, N. A. Petasis and G. A. Olah, *Synlett*, 1998, **1998**, 141-142.
5. P. B. Tripathy and D. S. Matteson, *Synthesis*, 1990, **1990**, 200-206.
6. M. Murata, K. Satoh, S. Watanabe and Y. Masuda, *J. Chem. Soc., Perkin Trans. 1*, 1998, DOI: 10.1039/A801469H, 1465-1466.

7. G. K. S. Prakash, C. Panja, T. Mathew, V. Surampudi, N. A. Petasis and G. A. Olah, *Org. Lett.*, 2004, **6**, 2205-2207.
8. M.-L. Huber and J. T. Pinhey, *J. Chem. Soc., Perkin Trans. 1*, 1990, **0**, 721-722.
9. H. C. Brown, K. W. Kim, T. E. Cole and B. Singaram, *J. Am. Chem. Soc.*, 1986, **108**, 6761-6764.
10. H. C. Brown, A. M. Salunkhe and B. Singaram, *J. Org. Chem.*, 1991, **56**, 1170-1175.
11. Y. Yu, J. Srogl and L. S. Liebeskind, *Org. Lett.*, 2004, **6**, 2631-2634.
12. D. M. T. Chan, K. L. Monaco, R.-P. Wang and M. P. Winters, *Tetrahedron Lett.*, 1998, **39**, 2933-2936.
13. P. Y. S. Lam, C. G. Clark, S. Saubern, J. Adams, M. P. Winters, D. M. T. Chan and A. Combs, *Tetrahedron Lett.*, 1998, **39**, 2941-2944.
14. T. D. Quach and R. A. Batey, *Org. Lett.*, 2003, **5**, 4397-4400.
15. N. Miyaura and A. Suzuki, *J. Chem. Soc., Chem. Commun.*, 1979, **0**, 866-867.
16. S. B. Y. Shin, B. Yoo, L. J. Todaro and K. Kirshenbaum, *J. Am. Chem. Soc.*, 2007, **129**, 3218-3225.
17. T. Koike, X. Du, T. Sanada, Y. Danda and A. Mori, *Angew. Chem., Int. Ed.*, 2003, **42**, 89-92.
18. J. Bouffard and K. Itami, *Org. Lett.*, 2009, **11**, 4410-4413.
19. K. Ukai, M. Aoki, J. Takaya and N. Iwasawa, *J. Am. Chem. Soc.*, 2006, **128**, 8706-8707.
20. T. Miura and M. Murakami, *Chem. Commun.*, 2007, **0**, 217-224.
21. A. Afonso, L. Feliu and M. Planas, *Tetrahedron*, 2011, **67**, 2238-2245.
22. A.-C. Carbonnelle and J. Zhu, *Org. Lett.*, 2000, **2**, 3477-3480.
23. M. Bois-Choussy, P. Cristau and J. Zhu, *Angew. Chem., Int. Ed.*, 2003, **42**, 4238-4241.
24. R. Lépine and J. Zhu, *Org. Lett.*, 2005, **7**, 2981-2984.
25. T. C. Roberts, P. A. Smith, R. T. Cirz and F. E. Romesberg, *J. Am. Chem. Soc.*, 2007, **129**, 15830-15838.
26. J. Dufour, L. Neuville and J. Zhu, *Synlett*, 2008, **2008**, 2355-2359.
27. H. Waldmann, Y.-P. He, H. Tan, L. Arve and H.-D. Arndt, *Chem. Commun.*, 2008, **0**, 5562-5564.
28. Z. Wang, M. Bois-Choussy, Y. Jia and J. Zhu, *Angew. Chem., Int. Ed.*, 2010, **49**, 2018-2022.
29. G. W. Bemis and M. A. Murcko, *J. Med. Chem.*, 1996, **39**, 2887-2893.
30. D. A. Horton, G. T. Bourne and M. L. Smythe, *Chem. Rev.*, 2003, **103**, 893-930.
31. T. Guo, A. E. P. Adang, R. E. Dolle, G. Dong, D. Fitzpatrick, P. Geng, K.-K. Ho, S. G. Kultgen, R. Liu, E. McDonald, B. F. McGuinness, K. W. Saionz, K. J. Valenzano, N. C. R. van Straten, D. Xie and M. L. Webb, *Bioorganic Med. Chem. Lett.*, 2004, **14**, 1713-1716.
32. P. J. Hajduk, M. Bures, J. Praestgaard and S. W. Fesik, *J. Med. Chem.*, 2000, **43**, 3443-3447.
33. J. Bernstein, *Am. J. Med.*, 1983, **75**, 70-74.
34. N.-C. Li, A. Lee, R. A. Whitmer, M. Kivipelto, E. Lawler, L. E. Kazis and B. Wolozin, *BMJ*, 2010, **340**.
35. G. C. Look, C. Vacin, T. M. Dias, S. Ho, T. H. Tran, L. L. Lee, C. Wiesner, F. Fang, A. Marra, D. Westmacott, A. E. Hromockyj, M. M. Murphy and J. R. Schullek, *Bioorganic Med. Chem. Lett.*, 2004, **14**, 1423-1426.
36. E. A. Jefferson, P. P. Seth, D. E. Robinson, D. K. Winter, A. Miyaji, L. M. Risen, S. A. Osgood, M. Bertrand and E. E. Swayze, *Bioorganic Med. Chem. Lett.*, 2004, **14**, 5257-5261.
37. M. N. Preobrazhenskaya and E. N. Olsufyeva, *Antiviral Res.*, 2006, **71**, 227-236.
38. C. Liu, A. Bayer, S. E. Cosgrove, R. S. Daum, S. K. Fridkin, R. J. Gorwitz, S. L. Kaplan, A. W. Karchmer, D. P. Levine, B. E. Murray, M. J. Rybak, D. A. Talan and H. F. Chambers, *Clin. Infect. Dis.*, 2011, **52**, 285-292.
39. U. Schmidt, V. Leitenberger, R. Meyer and H. Griesser, *J. Chem. Soc., Chem. Commun.*, 1992, **0**, 951-953.
40. Y.-P. He, H. Tan, L. Arve, S. Baumann, H. Waldmann and H.-D. Arndt, *Chem. Asian J.*, 2011, **6**, 1546-1556.
41. X. Yu and D. Sun, *Molecules*, 2013, **18**, 6230.
42. M. Ezaki, M. Iwami, M. Yamashita, S. Hashimoto, T. Komori, K. Umehara, Y. Mine, M. Kohsaka, H. Aoki and H. Imanaka, *J. Antibiot.*, 1985, **38**, 1453 - 1461.
43. G. Helynck, C. Dubertret, D. Frechet and J. Leboul, *J. Antibiot.*, 1998, **51**, 512 - 514.

44. S. Boisnard, A.-C. Carbonnelle and J. Zhu, *Org. Lett.*, 2001, **3**, 2061-2064.
45. C. Friry, S. Feliciangeli, F. Richard, P. Kitabgi and C. Rovere, *Biochem. Biophys. Res. Commun.*, 2002, **290**, 1161-1168.
46. P. R. Dobner, J. Fadel, N. Deitemeyer, R. E. Carraway and A. Y. Deutch, *Proc. Natl. Acad. Sci.*, 2001, **98**, 8048-8053.
47. X. Wang, Q. Wang, K. L. Ives and B. M. Evers, *Clin. Cancer Res.*, 2006, **12**, 5346-5355.
48. J.-J. Maoret, Y. Anini, C. Rouyer-Fessard, D. Gully and M. Laburthe, *Int. J. Cancer*, 1999, **80**, 448-454.
49. K. Iwase, B. M. Evers, M. R. Hellmich, H. J. Kim, S. Higashide, D. Gully, J. C. Thompson and C. M. Townsend, *Cancer*, 1997, **79**, 1787-1793.
50. J. Li, J. Song, Y. Y. Zaytseva, Y. Liu, P. Rychahou, K. Jiang, M. E. Starr, J. T. Kim, J. W. Harris, F. B. Yiannikouris, W. S. Katz, P. M. Nilsson, M. Orho-Melander, J. Chen, H. Zhu, T. Fahrenholz, R. M. Higashi, T. Gao, A. J. Morris, L. A. Cassis, T. W. M. Fan, H. L. Weiss, P. R. Dobner, O. Melander, J. Jia and B. M. Evers, *Nature*, 2016, **533**, 411.
51. F. F. Clerc, M. C. Dubroeucq, G. Helynck, J. Leboul and J. P. Martin, US Pat., 5 840 682, 1998.
52. B. K. Albrecht and R. M. Williams, *Proc. Natl. Acad. Sci.*, 2004, **101**, 11949-11954.
53. Y. Koguchi, J. Kohno, M. Nishio, K. Takahashi, T. Okuda, T. Ohnuki and S. Komatsubara, *J. Antibiot.*, 2000, **53**, 105 - 109.
54. A. L. Goldberg, R. Stein and J. Adams, *Chem. Biol.*, 1995, **2**, 503-508.
55. J. Kohno, Y. Koguchi, M. Nishio, K. Nakao, M. Kuroda, R. Shimizu, T. Ohnuki and S. Komatsubara, *J. Org. Chem.*, 2000, **65**, 990-995.
56. M. Inoue, H. Zhai, H. Sakazaki, H. Furuyama, Y. Fukuyama and M. Hirama, *Bioorganic Med. Chem. Lett.*, 2004, **14**, 663-665.
57. J. Garfunkle, F. S. Kimball, J. D. Trzupek, S. Takizawa, H. Shimamura, M. Tomishima and D. L. Boger, *J. Am. Chem. Soc.*, 2009, **131**, 16036-16038.
58. S.-H. Chung, T.-J. Lin, Q.-Y. Hu, C.-H. Tsai and P.-S. Pan, *Molecules*, 2013, **18**, 12346-12367.
59. S. Chirayil and K. J. Luebke, *Tetrahedron Lett.*, 2012, **53**, 726-729.
60. S. R. Inglis, E. C. Y. Woon, A. L. Thompson and C. J. Schofield, *J. Org. Chem.*, 2010, **75**, 468-471.
61. A. J. J. Lennox and G. C. Lloyd-Jones, *Chem. Soc. Rev.*, 2014, **43**, 412-443.
62. A. K. L. Yuen and C. A. Hutton, *Tetrahedron Lett.*, 2005, **46**, 7899-7903.
63. E. P. Gillis and M. D. Burke, *J. Am. Chem. Soc.*, 2008, **130**, 14084-14085.
64. D. M. Knapp, E. P. Gillis and M. D. Burke, *J. Am. Chem. Soc.*, 2009, **131**, 6961-6963.
65. N. Colgin, T. Flinn and S. L. Cobb, *Org. Biomol. Chem.*, 2011, **9**, 1864-1870.
66. E. P. Gillis and M. D. Burke, *Aldrichimica acta*, 2009, **42**, 17-27.
67. J.-C. Fernàndez, L. Solé-Feu, D. Fernández-Forner, N. de la Figuera, P. Forns and F. Albericio, *Tetrahedron Lett.*, 2005, **46**, 581-585.
68. C. Proulx, S. Yoo, M. D. Connolly and R. N. Zuckermann, *J. Org. Chem.*, 2015, **80**, 10490-10497.
69. H. Y. Nam and J. Seo, *Pept. Sci.*, 2016, **106**, 82-88.

Chapter 3

Nucleophosmin-Targeting Peptides and Analogues

3.1 Nucleophosmin (NPM1)

Nucleophosmin (NPM1) is part of the nucelophosmin/nucleoplasmin family of histone chaperones found in all animals.[1] It is a phosphoprotein found in all tissues and primarily located in the nucleolus, but able to shuttle between nucleoli, the nucleoplasm and cytoplasm. It exists in three different isoforms (NPM1.1, NPM1.2 and NPM1.3). Both NPM1.2 and NPM1.3 are shorter than NPM1.1, with NPM1.2 missing an internal segment, whilst NPM1.3 is missing the final 35 amino acids at the 3' end, with respect to NPM1.1 (**Figure 3.1**).[2, 3] NPM1.1 is the most abundant isoform and is localised in the nucleolus.[4] It is this isoform that is the primary target for anticancer drugs, and will be referred to as NPM1 from hereon in. NPM1 has multiple functions, including in ribosome biogenesis[5] and transport,[6-8] histone chaperoning,[9-11] centrosome duplication during the cell cycle,[12, 13] RNA expression[14, 15] and DNA replication and repair.[16, 17] There is much interest in the numerous roles and mechanisms of action of NPM1, particularly since its implication in the pathogenesis of acute myeloid leukemia,[18] and as such there are multiple reviews covering its various functions.[1, 4, 19-22] For the purposes of our work, we are most interested in its oncogenic and tumour suppressing properties.

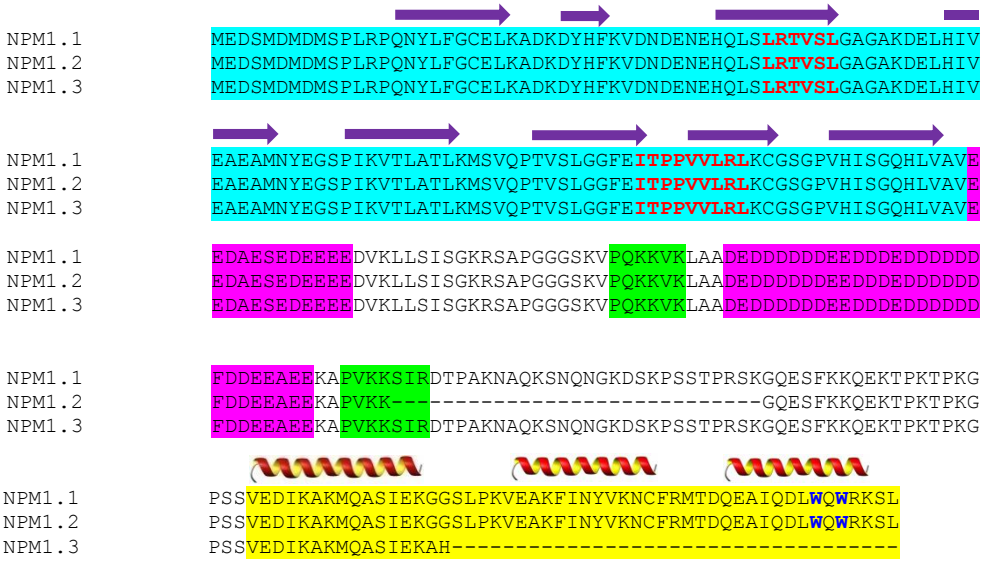

Figure 3.1 Comparison of the sequences of NPM1.1, 1.2 and 1.3. The N-terminal core domain is highlighted in cyan. Nuclear export signals (NES) in the N-terminal domain are in bolded red text. Acidic-rich regions in the central domain are highlighted in magenta, while the bipartite nuclear localization signal (NLS) is highlighted in green. The C-terminal nucleic acid binding domain is highlighted in yellow. Trp288 and Trp290, which form the nucleolar localization signal (NoLS) are in bolded blue text. The β-strand structures in the N-terminal core domain are indicated by the purple arrows above the sequence, whilst the three alpha helices of the C-terminal domain are also indicated above the sequence. The aligned sequences were generated using the Clustal W software.[23]

3.1.2 The structure of Nucleophosmin

NPM1 is a modular protein consisting of three domains: the N-terminal, or core domain which is responsible for chaperone activity and oligomerisation, a central domain involved in ribonuclease activity, and the C-terminal domain associated with nucleic acid binding (**Figure 3.2**).[2, 24, 25] The N-terminal is highly conserved throughout the nucleoplasmin family, and is considered the core domain. X-Ray crystallography shows the structure of the core domain to be a jelly roll barrel formed by the organisation of eight anti-parallel β strands. Five NPM1 monomers associate to form a crown-shaped pentamer. Two pentamers come together in a head-to-head fashion whereby each monomer from one ring only associates with one monomer from the second ring.[26] Charge distribution of the oligomer is asymmetric with negatively charged residues clustered on one face (**Figure 3.3**).

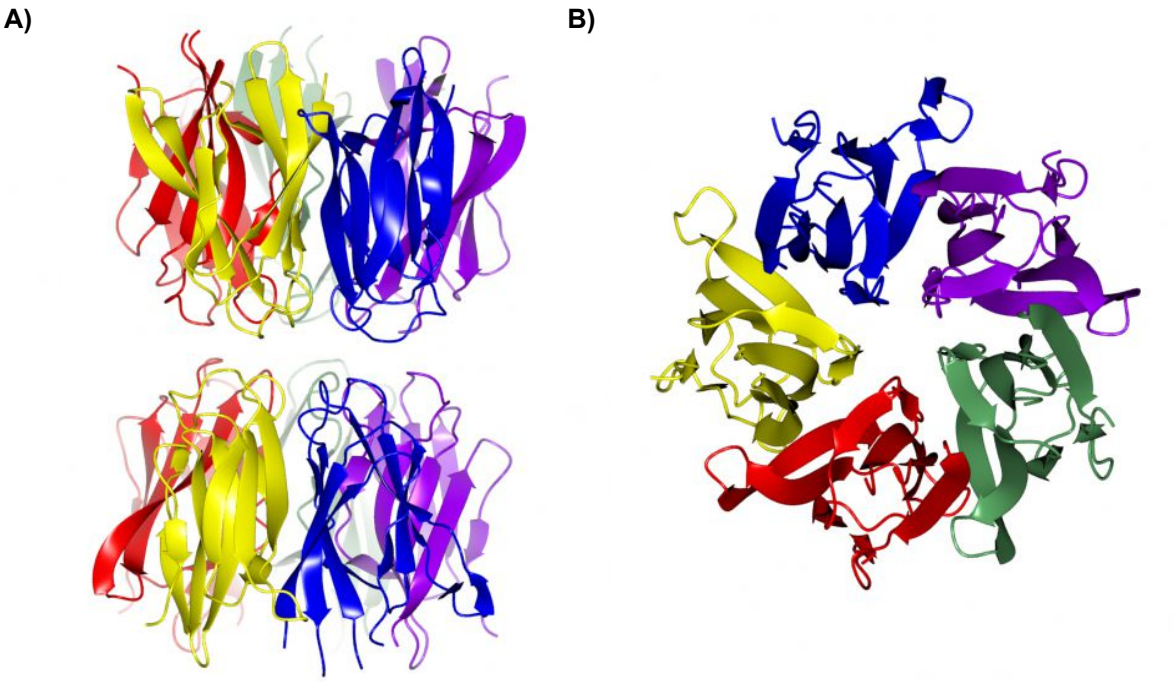

Figure 3.2 Crystal structure of the N-terminal core domain of NPM1. A) Five monomers associate to form a pentamer, two of which interact in a head-to-head fashion to form a decamer; B) The crown-shaped pentamer showing a channel through the middle forming the 'jelly roll barrel' shape. Structures were obtained from the Protein Data Bank (4N8M, Mitrea *et al.*[27]) and generated using CCP4 software.[28]

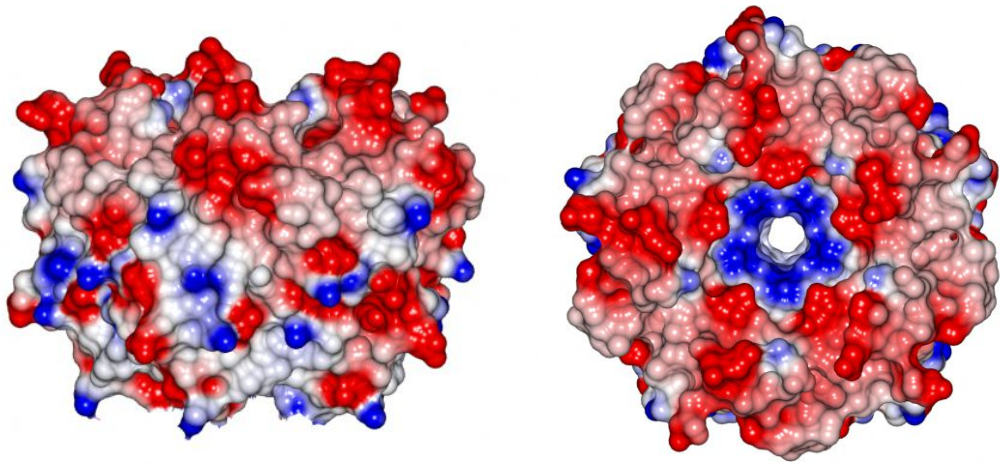

Figure 3.3 Electrostatic potential map of an NPM1 pentamer; negatively charged residues (red) are clustered on one face away from the neutral (white) and positive (blue) areas. Positively charged residues are clustered around the central pore. Structures were obtained from the Protein Data Bank (4N8M, Mitrea *et al.*[27]) and generated using CCP4 software.[28]

It is thought that the state of oligomerisation is related to a particular function of NPM1.[29] For example, the oligomeric form of NPM1 is stabilised by hydrogen bonding and hydrophobic interactions indicating a level of chemical and thermal stability associated with chaperones.[30] Further, the oligomeric form of NPM1 has been linked to nucleolar localisation and its role in cell proliferation.[13,27,31,32] Conversely, the monomeric form of NPM1 is thought to be associated with induction of apoptosis and DNA repair.[33] Destabilisation of the pentameric NPM1 appears to proceed via sequential phosphorylation of serine and threonine residues mediated by different kinases.[27]

The central domain appears to be largely unstructured and contains two acidic stretches (residues 120-132 and 161-188) as a result of consecutive aspartate or glutamate residues. These residues result in areas of negative charge which are involved in binding to histones, possibly in conjunction with the N-terminal domain and perhaps by mimicking the charges of DNA and RNA.[34,35] At either end of this acidic stretch is a bipartite nuclear localisation signal (NLS).

The C-terminal domain is involved in binding to DNA and RNA, and is a three-helix bundle stabilised by two phenylalanine and two tryptophan residues which form a small, but well defined hydrophobic core (**Figure 3.4**). The aromatic region is part of an atypical nucleolar localisation signal (NoLS), possibly unique to NPM1. Mutations in this region, particularly of the Trp residues results in unfolding of the helices and loss of nucleolar localisation and is characteristic of patients with acute myeloid leukemia.[36,37]

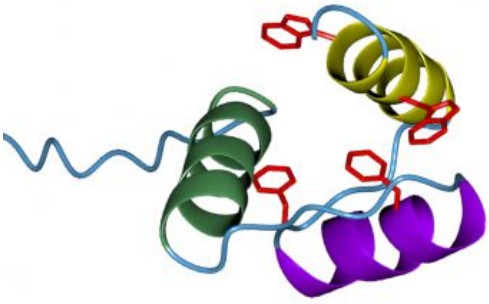

Figure 3.4 A solution-phase NMR structure of the three-helix bundle of the C-terminal domain. The two phenylalanine and tryptophan residues are also shown and form a hydrophobic core. Structures were obtained from the Protein Data Bank (2LLH, Gallo *et al.*[38]) and generated using CCP4 software.[28]

3.1.3 Nucleophosmin and cancer

NPM1 shows both oncogenic and tumour supressing behaviour. It is overexpressed in many solid tumours, including pancreas,[39] liver,[40] prostate,[41] thyroid,[42] glioma[43] and glioblastoma[44] and colon.[45] Overexpression of NPM1 correlates with metastatisation and a higher mitotic index, and as such is thought to be an indicator of a poor prognosis.[46, 47] The exact mechanisms by which NPM1 influence tumorigenesis are not yet known, however several possible factors may contribute. First, NPM1 is involved in ribosome biogenesis and protein synthesis, both of which are increased in tumour cells.[48] Second, NPM1 is involved in DNA repair and hence inhibits senescence and apoptotic responses.[49,50]

NPM1 has a function in cell apoptosis via regulation of the ARF-p53 tumour suppressor pathway.[51-54] The p53 protein prevents tumour formation and is sometimes called 'the guardian of the genome.'[55] Its anticancer role is carried out via several different pathways. p53 can activate DNA repair proteins where DNA has been damaged, thus preventing replication of damaged DNA. p53 can also stop cell growth by stopping the cell cycle at the G1/S phase whilst damaged DNA is repaired. In cases where DNA is damaged beyond repair, p53 will then trigger apoptosis. One of the proteins responsible for regulating p53 is MDM2. MDM2 binds to p53, transporting it from the nucleus to the cytoplasm, where it is ubiquinated and marked for degradation.[56] One of the inhibitors of MDM2 is p14ARF. Free p14ARF complexes to the MDM2 protein, preventing the MDM2 protein from binding to p53 and marking it for degradation, thus allowing p53 to trigger DNA repair/cell apoptosis. In healthy, unstressed cells, NPM1 binds to p14ARF in the nucleolus; in fact NPM1 is a major p14ARF reservoir.[52] This means that MDM2 is able to down-regulate p53. However, when the cell is subject to stress, such as DNA damage, NPM1 releases p14 ARF which then binds to MDM2, preventing degradation of p53.[53] In addition, NPM1 interacts directly with MDM2, protecting p53 from proteolysis. Therefore, depletion of NPM1 has been shown to increase cell apoptosis due to an increase in free p14ARF. Conversely, up-regulation of NPM1 increases nucleolar retention of p14ARF.[51]

However, at low levels NPM1 acts as a tumour suppressor by interacting with unduplicated centrosomes. Phosphorylation of NPM1 triggers its release from the centrosomes, allowing duplication to occur. During mitosis, NPM1 re-associates with the centrosomes and controls duplication. NPM1 inactivation allows unrestricted duplication of centrosomes, increasing the risk of cellular transformation, thereby promoting genomic instability.[57]

It is notable that, in some cancers, reduced levels of NPM1 have been observed and are associated with poor outcomes, for example in breast cancers in which there is evidence that it has a suppressive role.[58,59]

3.1.3.1 Nuclophosmin and leukemia

In blood cancers, mutations in NPM1 as well as chromosomal translocations are frequently seen. In acute myeloid leukemia (AML), the NPM1 gene is the most frequently mutated, seen 35% of all AML patients.[60] Consequently, The World Health Organisation recognises AML with mutations in the NPM1 gene as a distinct category in its classifications.[61] There are over 30 different identified mutations, but all occur at the C-terminus.[59] One, but usually both tryptophan residues (Trp288 and Trp290) are replaced, destabilising the helical secondary structure of the C-terminal domain and disrupting the nucleolar localisation signal (NoLS). Furthermore, a new nuclear export signal (NES) is generated, reinforcing the two already present on the N-terminal domain, causing localisation of the mutant NPM1 in the cytosol.[36] For this reason mutated NPM1 seen in AML is referred to NPM1c+, i.e. cytoplasm positive, and is a hallmark of AML. In addition, NPM1c+ oligomerises with wild-type NPM1, causing localisation of wild-type NPM1 into the cytoplasm, resulting in very little nucleolar localisation of NPM1.[62] Moreover, NPM1 mutation in knock-in mice models resulted in AML initiation.[63,64]

The exact mechanism by which NPM1c+ initiates AML is not fully understood, but it is thought that mutation of the NPM1 gene hinders several tumour suppression pathways. For example, the N-terminus is unaltered in NPM1c+, and so binding to p14ARF still occurs, and as a result p14ARF is transported into the cytoplasm and proteolytically degraded.[65] NPM1c+ also binds to Fbw7γ- responsible for degrading several proto-oncogenes- and transports it into the cytoplasm, resulting in degradation. Thus, in addition to weakening a tumour suppressing pathway, NPM1c+ also results in oncogene stabilisation.[66] Finally, the mutated, unfolded C-terminal domain has also been shown to contain amyloidogenic sections, possibly resulting in the gain of cytosolic functions of NPM1c+.[67]

As well as mutation of the C-terminus, NPM1 promotes oncogenesis by forming chimeric proteins in several other haematological malignancies. For example, in anaplastic large-cell lymphoma (ALCL) fusion of the 5’ end of the NPM1 gene with the 3’ end of the anaplastic lymphoma receptor tyrosine kinase (ALK) gene is seen in 85%

of ALK+ patients, accounting for 30% of all ALCL cases.[68] The resulting chimera is a protein where the N-terminal domain of NPM1 is fused to the kinase domain of ALK. The NPM-ALK protein dimer shows aberrant localisation in the cytoplasm, and further, the chimeric NPM-ALK may dimerise with wild-type NPM1, causing NPM1 dislocation into the nucleus. The chimeric NPM-ALK protein is a major driver of tumourigenesis in ALCL. It is thought that the role of NPM is to enable oligomerisation, which is a requirement for the autophosphorylation of tyrosine and, therefore, the activation of ALK. When active, ALK triggers a number of cell signalling pathways which result in increased cell proliferation and resistance to apoptosis.[69]

In rare cases of acute promyelocytic leukemia (APL), a gene translocation causes the N-terminus of NPM1 to fuse with the DNA-binding domain of retinoic acid receptor α (RARα).[70] As with the NPM-ALK chimera, the role of NPM is to facilitate dimerization. In doing so, this interferes with the transcriptional ability of RARα, stopping myeloid differentiation. Uniquely among leukemias, this arrest of differentiation in APL is reversible by treatment with all-*trans* retinoic acid.[71]

3.1.4 Nucleophosmin as a target for anticancer compounds

Due to its role in DNA repair and regulation of apoptopic pathways, as well as the association of mutations and translocations of the NPM1 gene, NPM1 has been widely investigated as a target for anticancer drugs. Various approaches have been explored; targeting the N-terminal domain in order to disrupt oligomerisation or to inhibit its interaction with other proteins,[72-74] targeting the C-terminal domain nucleic acid interactions to cause nucleolar stress[75] or to promote refolding and relocalisation in the nucleolus,[76] selective targeting of NPM1c+ mutants in AML,[77,78] and targeting sites of NPM1 post-translational modification.[79] These strategies have been detailed in the context of several promising NPM1-targeting compounds in a recent review[4] and will not be discussed here. In our work, one particular compound is of interest: P15-Tat, or CIGB-300.

3.1.4.1 P15-Tat or CIGB-300 and nucleophosmin

CIGB-300, **125**, **Figure 3.5**, is a cyclic peptide (P15) attached to a cell-penetrating peptide (Tat, derived from the HIV-Tat protein), sequence (GRKKRRQRRRPPQ-β-ala-CWMSPRHLGTC).[80] CIGB-300 (**125**) was identified by screening a random cyclic

peptide phage library against the human papillomavirus (HPV-16)E7 acidic domain. CIGB-300 was designed to target casein kinase 2 (CK2), a protein that phosphorylates threonine and serine. CK2 is implicated in tumourigenesis and elevated levels are associated with aggressive malignancies.[81,82] CIGB-300 does not interact directly with CK2, but with its phosphorylation targets, specifically inhibiting phosphorylation of Ser125 on NPM1.[79] Blocking phosphorylation of Ser125 appears to trigger nucleolar disassembly on tumour cells, which can be seen via confocal analysis on CIGB-300 treated and untreated cell cultures (**Figure 3.6**).

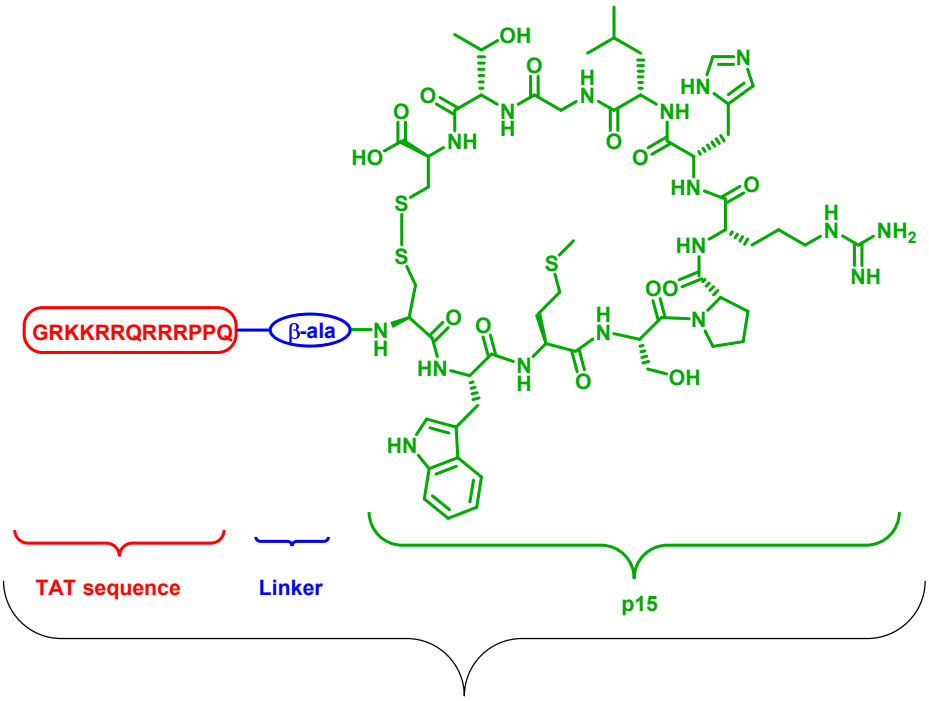

CIGB300, **125**

Figure 3.5 Structure of anticancer peptide CIGB-300 (**125**). The active, cyclic peptide, p15, is highlighted in green. The active peptide is attached to cell-penetrating peptide derived from the HIV-Tat protein, highlighted in red, with a β-alanine linker, highlighted in blue.

Following treatment with CIGB-300 (**125**), there appears to be initial concentration of NPM1/B23 and fibrillarin in the nucleolus (**Figure 3.6**, arrow two), followed by subsequent loss of nucleolar structure (**Figure 3.6**, arrows 3 and 4). Further, treatment of cells with CIGB-300 leads to apoptosis in several tumour cell lines, including breast, cervical, lung and laryngeal. It is unclear how nucleolar disassembly leads to apoptosis, though the nucleolus is considered a cellular stress sensor, it is possible that breakdown of the nucleolus triggers a proapoptotic response. Additionally, inhibition of

CK2 has been shown to trigger nucleolar breakdown and interfere with ribosome biogenesis. Mutation of Ser125 on NPM1, the target of CIGB-300, resulted in similar observations, suggesting CK2 regulation of ribogenesis operates through NPM1.[4] Finally, phosphorylation of NPM1 via CK2 regulates chaperone activity, interference with which may prevent proper folding of ribosomal proteins and also with histone assembly at nucleolar rDNA.[83] Interestingly, work by Perera *et al.* in 2014 demonstrated a synergistic effect in nude mice xenografted with human cervical tumours when treated with a combination of CIGB-300 (**125**) and a number of existing cancer treatments, most notably cisplatin and paclitaxel.[84]

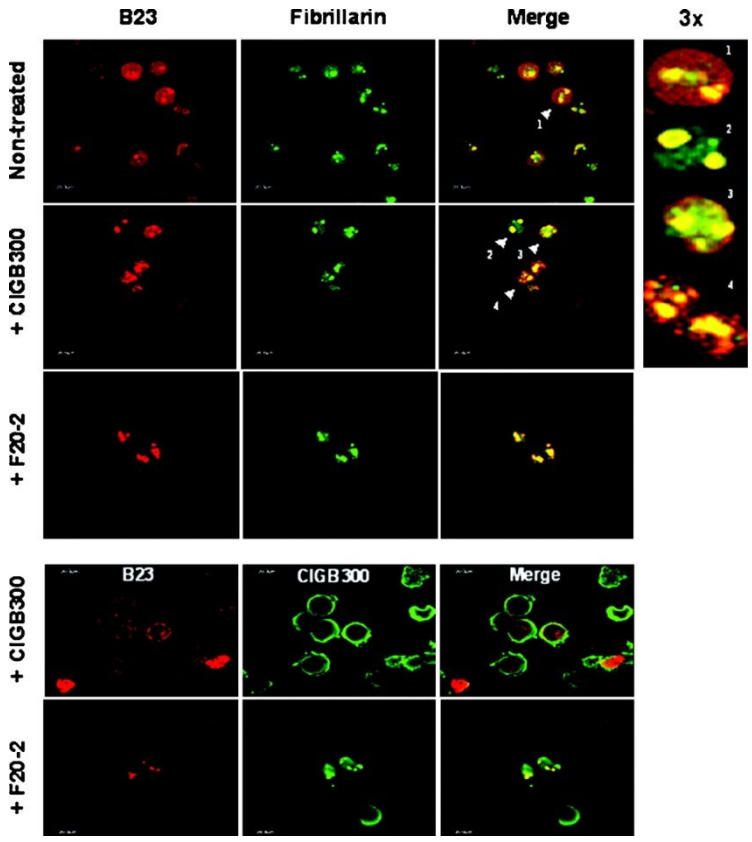

Figure 3.6 Confocal microscopy of CIGB-300 treated and untreated cell cultures showing nucleolar disassembly. Fibrillarin is a protein localised in the nucleolus, so changes in the distribution of both fibrillarin and NPM1 (labelled B23) indicated nucleolar dysfunction. F20-2 is a control peptide. Figure adapted from Perera *et al*., 2009.[79]

CIGB-300 has attracted such interest as a novel anticancer drug that it has entered phase I clinical trials for locally advanced cervical cancer[85,86] and phase II clinical trials for squamous cell carcinoma (ClinicalTrials.gov, identifier NCT01639625). Clinical trials in human patients with locally advanced cervical cancer found that administration of

CIGB-300 by injection into cervical malignancies was well tolerated and showed some benefits. In 75% of patients there was significant lesion reduction whilst 19% showed full histological regression, and no maximum-tolerated dose of dose-limiting toxicity was achieved.

3.1.5 Aims

CIGB-300 (**125**) is a novel anticancer peptide chimera which has been intensely investigated and has even entered clinical trials.[86] However, cyclisation occurs via the formation of a disulphide bridge which is reversible.

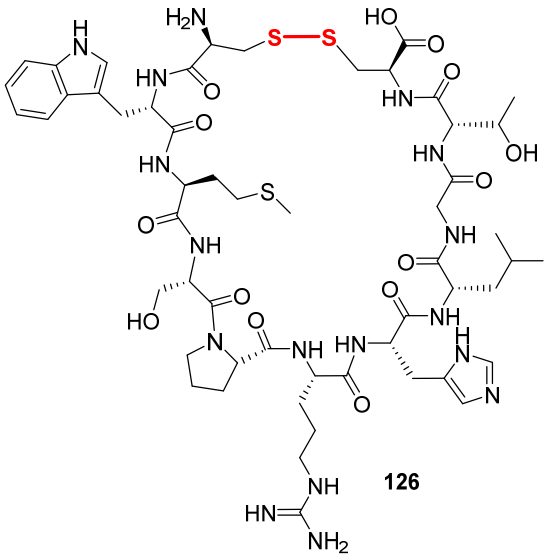

126

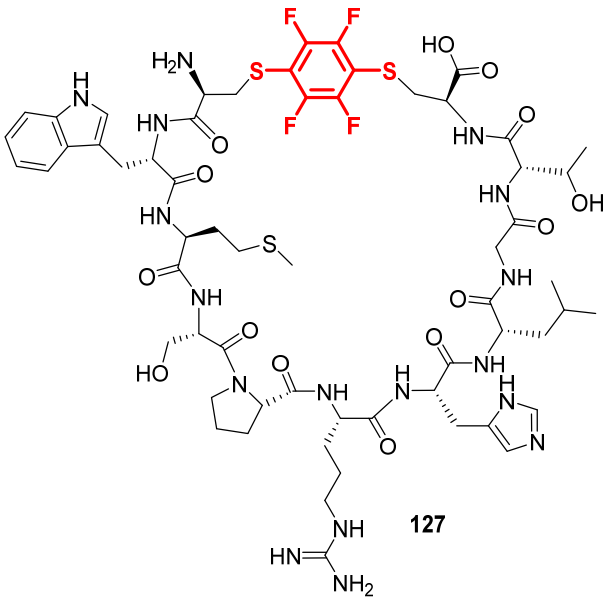

127

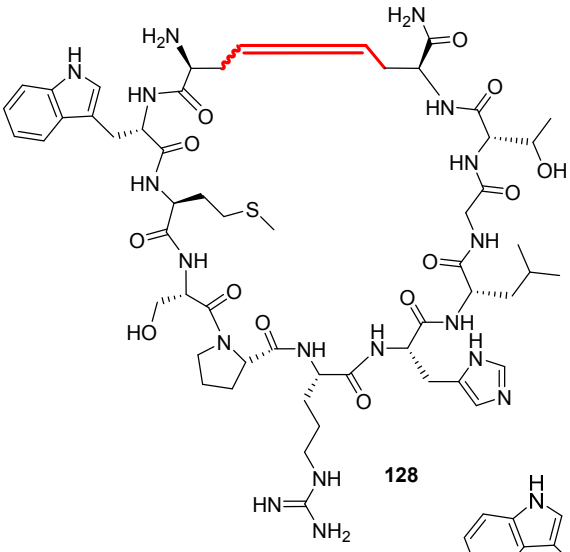

128

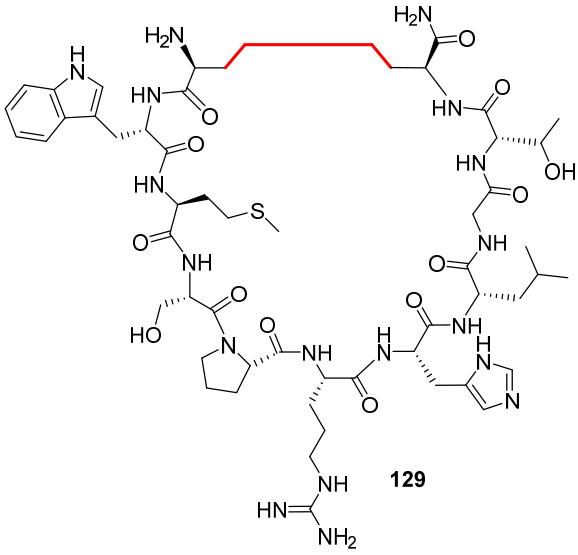

129

Hence *in vivo* stability of the active peptide (p15, **126**, the disulphide bridge is highlighted in red) may be compromised and may limit its versatility, for example by requiring local injection to solid tumour masses. We are interested in synthesising analogues of the active peptide, p15, with the aim of improving stability of the peptide whilst maintaining its binding affinity for NPM1. Our strategy for improving the stability of p15 is via alternative methods of cyclisation. The group has previously published work demonstrating the stapling of peptides via reaction of hexafluorobenzene with cysteine side chains.[87] This is the first proposed analogue (F-p15, **127**). Second, Grubbs ring-closing metathesis (RCM) is a well-established method of stapling peptides and thus stabilising secondary structures.[88-90] A C=C stapled analogue of p15 (C=C-p15) is the second analogue (**128**). A further analogue can then be accessed by hydrogenation of the double bond to obtain a C-C stapled analogue (**129**).

3.2 Synthesis of p15 peptide (126)

Our strategy for the synthesis of the p15 peptide (1**26**, **Figure 3.7**) was to use solid-phase peptide synthesis (SPPS) with Fmoc-protected amino acids.

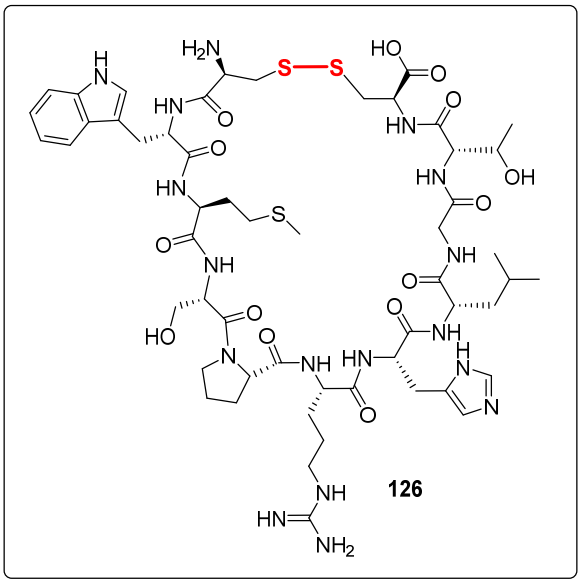

Figure 3.7 Target compound p15 (**126**).

Scheme 3.1 shows the generic method of SPPS in which the peptide is built onto a solid support, or resin, which can be washed after each amino acid coupling or deprotection step. Purification is then carried out by HPLC after cleavage of the peptide from the resin.

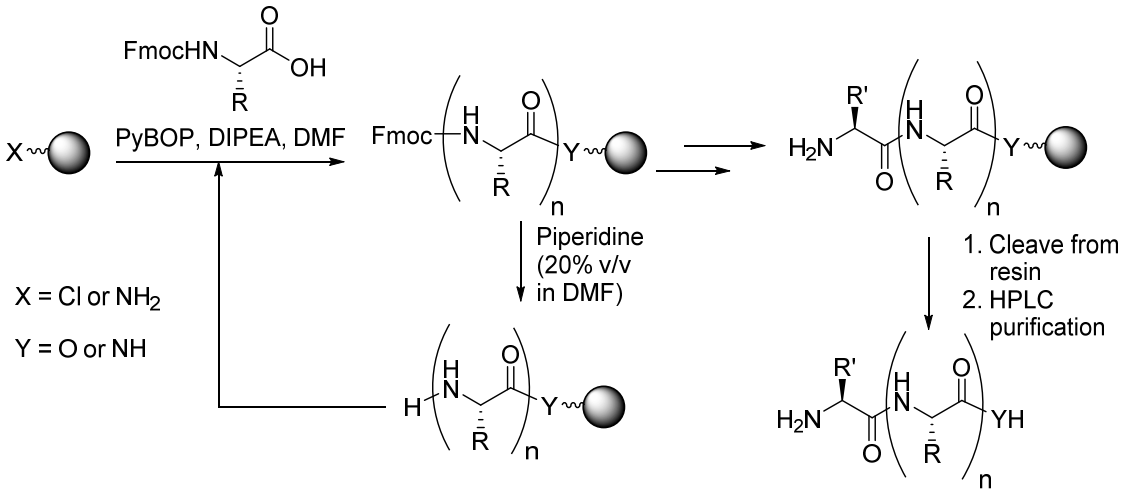

Scheme 3.1 Generic method for solid phase peptide synthesis (SPPS). Other activating agents and additives may be used.

3.2.1 Problematic amino acids

SPPS is the standard method of peptide synthesis and, since its introduction by Merrifield in 1963,[91] has seen many advances in the resins and coupling reagents to improve reaction times and prevent side reactions including racemisation. Protection of reactive side chains, such as those containing amine, acid and thiol functionalities is vital, however, some amino acids remain problematic. In the p15 peptide (**126**) the amino acids that require attention are cysteine (**130**), histidine (**131**), methionine (**132**), and the combination of tryptophan (**133**), and arginine (**134**), **Figure 3.8**.

Cysteine (**130**) is problematic for two reasons. When it is located at the C-terminus of a peptide, anchoring as an ester to the resin, elimination of the sulfhydryl group and subsequent addition of piperidine (**135**) may occur during any Fmoc deprotection step (**Scheme 3.2**).[92] This happens regardless of the protecting group used, including two of the most widely used: trityl (Trt) and acetamidomethyl (Acm, both shown in **Scheme 3.2**). Of the two, β-elimination happens more readily from the Acm group. Furthermore, the propensity for cysteine to undergo β-elimination is exacerbated if threonine (or serine) is adjacent to it. To reduce the occurrence of this side-reaction, trityl resins are used (e.g. 2-chlorotrityl chloride). The bulk around the C-terminal cysteine shields the α-proton from attack by base (**Scheme 3.3**), although β-elimination cannot be fully prevented.

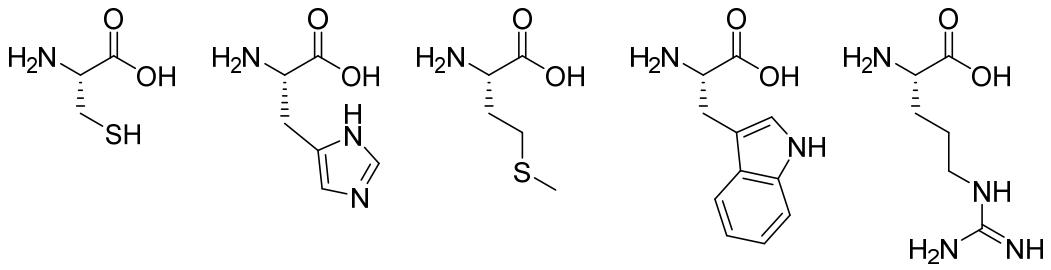

130 **131** **132** **133** **134**

Figure 3.8 Amino acids in the p15 peptide that are prone to side-reactions (including racemisation) during synthesis or cleavage: cysteine (**130**), histidine (**131**), methionine (**132**), tryptophan (**133**) and arginine (**134**).

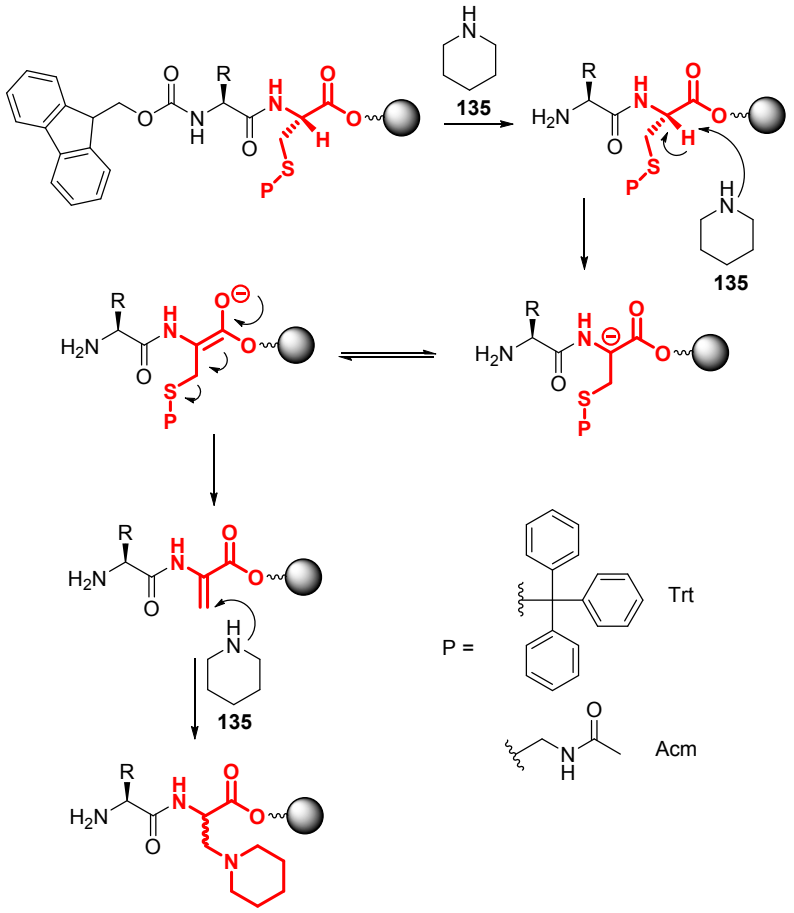

Scheme 3.2 Base-induced β-elimination followed by addition of piperidine (**135**) at C-terminal cysteine anchored at the resin by an ester. Cysteine and its subsequent modifications are highlighted in red.

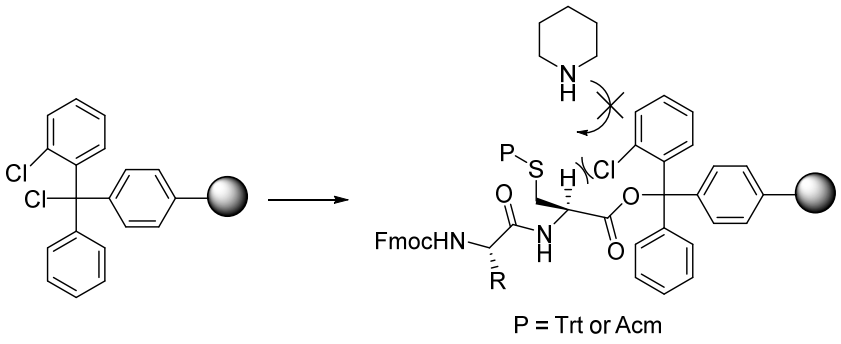

Scheme 3.3 Use of 2-chlorotrityl chloride resin to block base-induced β-elimination of the sulfhydryl group

The second way in which cysteine (**130**) may be problematic is via racemisation, with trityl-protected cysteine (Cys(Trt)) particularly prone to this.[93] Racemisation is base-induced and may occur when cysteine is located at any position in the peptide and proceeds via the activated amino acid (**Scheme 3.4**). However, once a further coupling

to the cysteine at the N-terminus has been carried out, there seems to be little risk of racemisation.

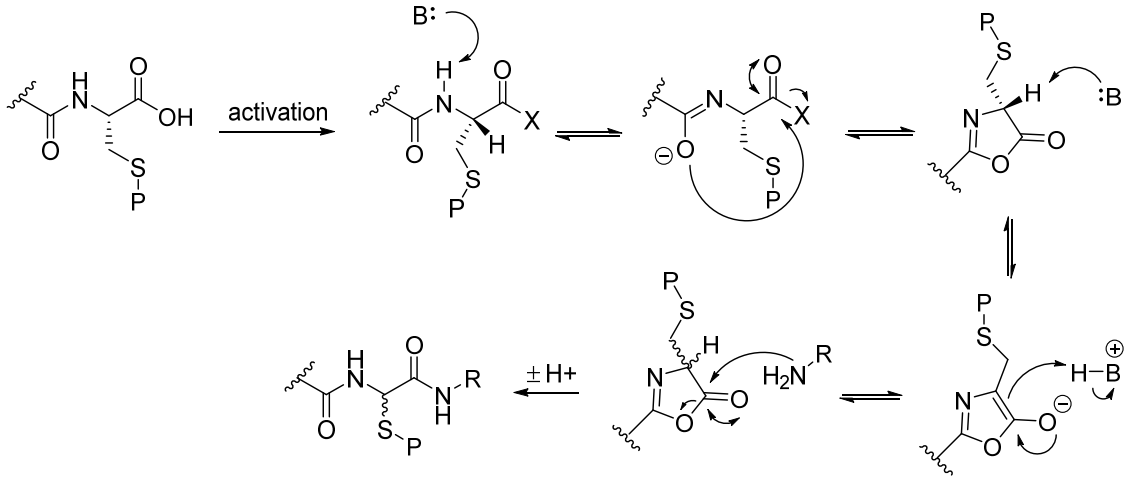

Scheme 3.4 Base-induced racemisation of cysteine proceeding via formation of an oxazolone ring followed by abstraction of the α-hydrogen.

All amino acids have the potential for racemisation, but the activating agents used increase the rate of the coupling reaction enough that for most amino acids, racemisation is negligible. However, the sulfhydryl side chain increases the acidity of the α-hydrogen, making racemisation prior to coupling more likely. Cysteine racemisation happens with both Trt and Acm protection of the thiol. Common practice in SPPS is 'preactivation' of the amino acid to be coupled to the peptide; i.e. incubation of the amino acid, activating agent and base for five minutes prior to addition to the peptide. Removal of the preactivation step has been found to significantly reduce cysteine racemisation.[93,94]

Histidine (**131**) is another amino acid that is particularly prone to racemisation. The mechanism is the same as for cysteine (**Scheme 3.4**), except that, unlike cysteine, the α-hydrogen is not abstracted by an added base, but by the side chain via the π-nitrogen (**Scheme 3.5**).[95] Protection of the π-nitrogen can shield the α-hydrogen,[96, 97] but these amino acids tend to be expensive. Fortunately, a study of amino acid racemisation in microwave assisted SPPS showed that racemisation of histidine only became significant (>5% D-histidine observed) at elevated temperatures; at conventional room temperature, the presence of D-histidine was only found at 0.65% (compared to 1.09% D-cysteine).[95]

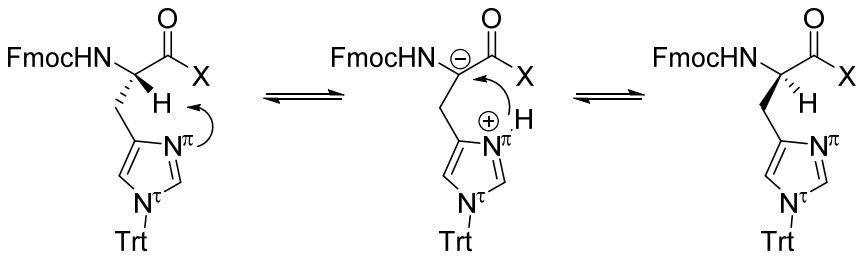

Scheme 3.5. Abstraction of the α-hydrogen of histidine by the π-nitrogen of the side chain.

Methonine (**132**) is prone to acid-catalysed oxidation to the sulfoxide (oxidation to the sulfone requires strong oxidants). This can happen during cleavage from resin when TFA is used (**Scheme 3.6**).[98] Methionine sulfoxide can be reduced back to the thioester by treatment with Me_4I/Me_2S in neat TFA (**Scheme 3.7**).[99] Oxidation can be suppressed by using scavengers such as dimethyl sulfide, 1,2-ethanedithiol (EDT) or thioanisole[100] (although thioanisole has been shown to partially remove Acm protecting groups from cysteine).[101]

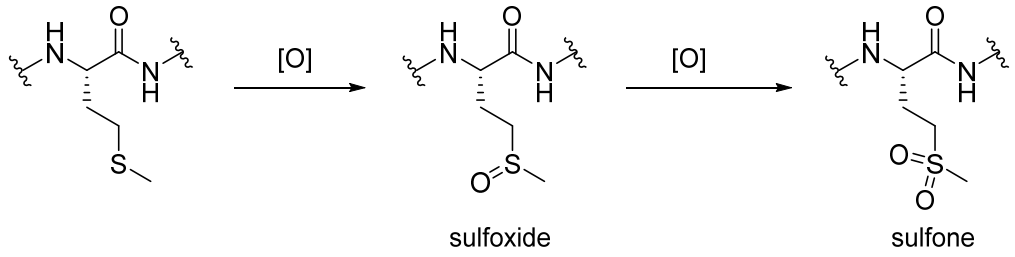

Scheme 3.6 Oxidation of methionine to methionine sulfoxide. Further oxidation to methionine sulfone only occurs in the presence of strong oxidising agents.

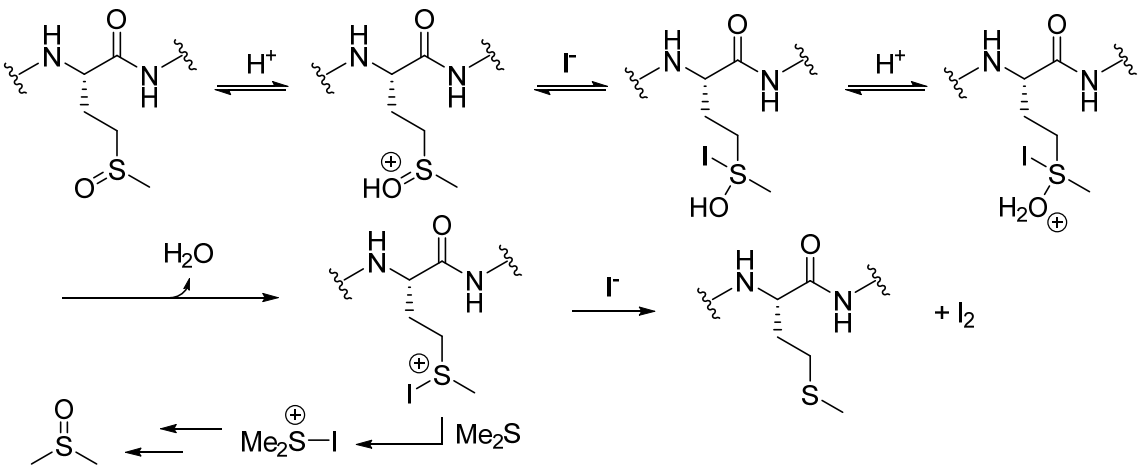

Scheme 3.7 Reduction of methionine sulfoxide to methionine in the presence of Me_4I/Me_2S.

Tryptophan (**133**) can sometimes be used in SPPS without protection of the indole group on the side chain. However, in peptides that also contain arginine (**134**) residues, modification of the indole can occur during cleavage via generation of sulfonyl moieties from arginine protecting groups such as Pmc and Pbf (**Scheme 3.8**).[102 103] This can be almost completely prevented by Boc protection of the indole nitrogen.[104]

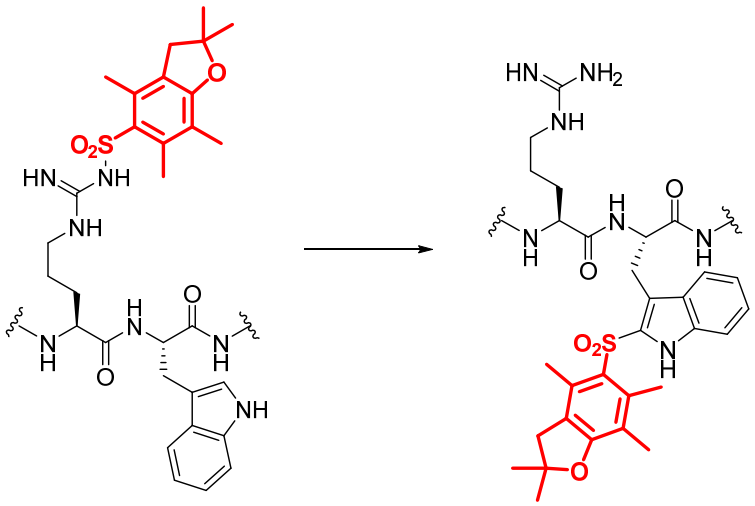

Scheme 3.8 Side chain modification of tryptophan by transfer of the Pbf protecting group (highlighted in red) from arginine.

3.2.2 Synthesis of the linear p15 peptide (136)

To minimise and prevent these side reactions described in **Section 3.2.1**, the following steps were taken: peptide synthesis was carried out on 2-chlorotrityl chloride resin to minimise base-induced β-elimination of the C-terminal cysteine, synthesis was carried out manually and at room temperature with no preactivation step to minimise cysteine and histidine racemisation and Fmoc-Trp(Boc)-OH was used to prevent Pbf transfer from the arginine. No extra precautions were initially taken to prevent methionine oxidation since the extent of this side reaction cannot be predicted and we hoped that it would not be significant enough to require specialist scavengers which are often stench hazards, toxic and difficult to handle.

Cysteine was Acm-protected as removal of the Acm group can be achieved without removing the peptide from the resin and occurs with simultaneous disulphide formation. Accordingly, linear resin-bound p15 peptide (**136**, the Acm protecting groups are highlighted in red), was made (**Scheme 3.9**).

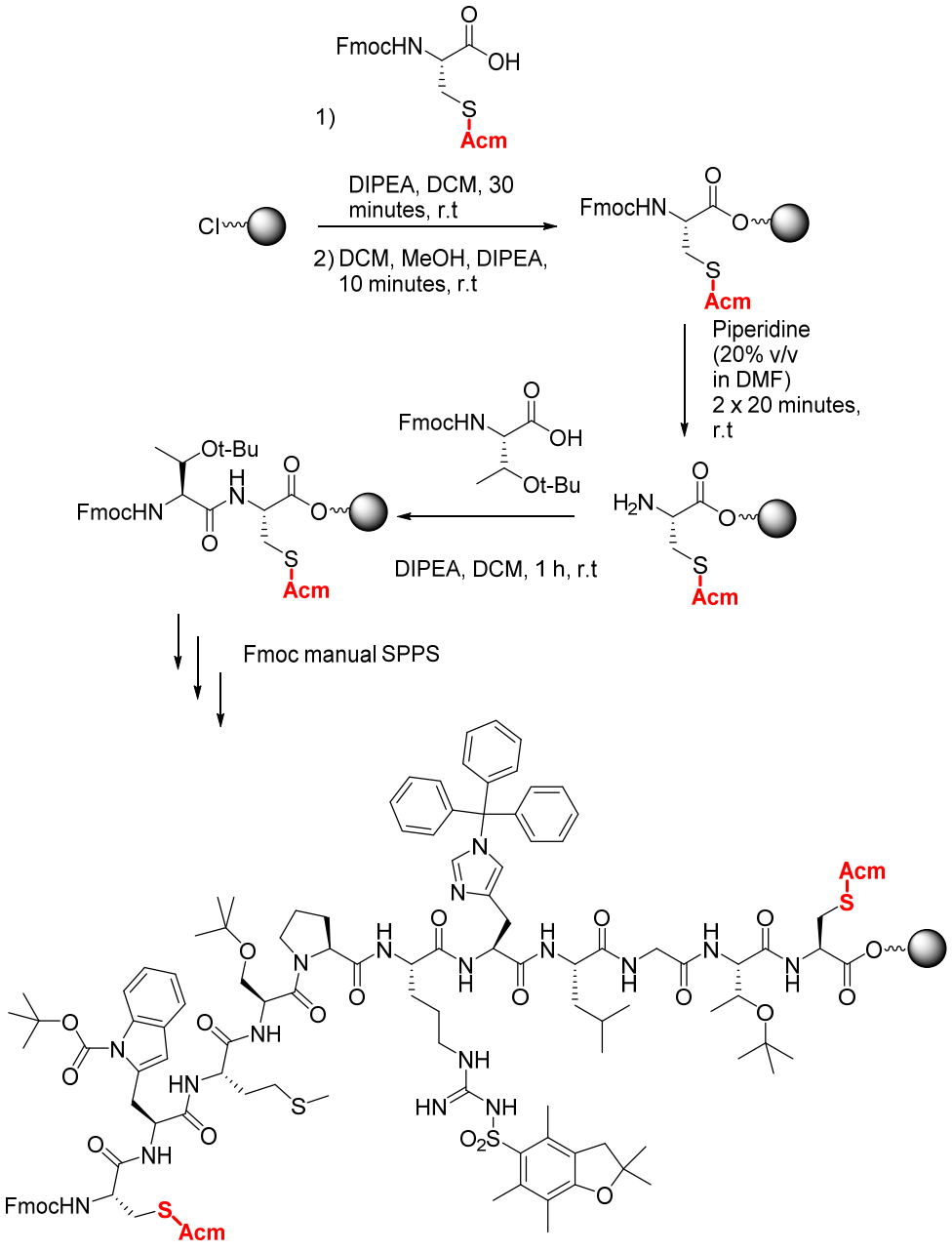

136

Scheme 3.9 Manual SPPS of linear, resin-bound p15 peptide with Acm-protected cysteine (**136**) on 2-chlorotrityl chloride resin. Fmoc manual SPPS conditions, amino acids used in order of addition: Fmoc-Cys(Acm)-OH, Fmoc-Thr(tBu)-OH, Fmoc-Gly-OH, Fmoc-Leu-OH, Fmoc-His(Trt)-OH, Fmoc-Arg(Pbf)-OH, Fmoc-Pro-OH, Fmoc-Ser(tBu)-OH, Fmoc-Met-OH, Fmoc-Trp(Boc)-OH, Fmoc-Cys(Acm)-OH. Coupling conditions: Amino acid, PyBOP, DIPEA, DMF, r.t., 1h. Fmoc-Ser(tBu)-OH and the second Fmoc-Cys(Acm)-OH underwent double coupling. Fmoc deprotection of amino acids: Piperidine (20% v/v in DMF), r.t. 2 x 20 minutes.

3.2.2.1 Optimisation of cleavage conditions

After synthesis of linear resin-bound p15 (**136**) several test cleaves under different conditions were carried out. Three cleaves using trifluoroacetic acid (TFA) were carried out to investigate the extent of methionine oxidation (**Scheme 3.10**, compare **137** and **138**).

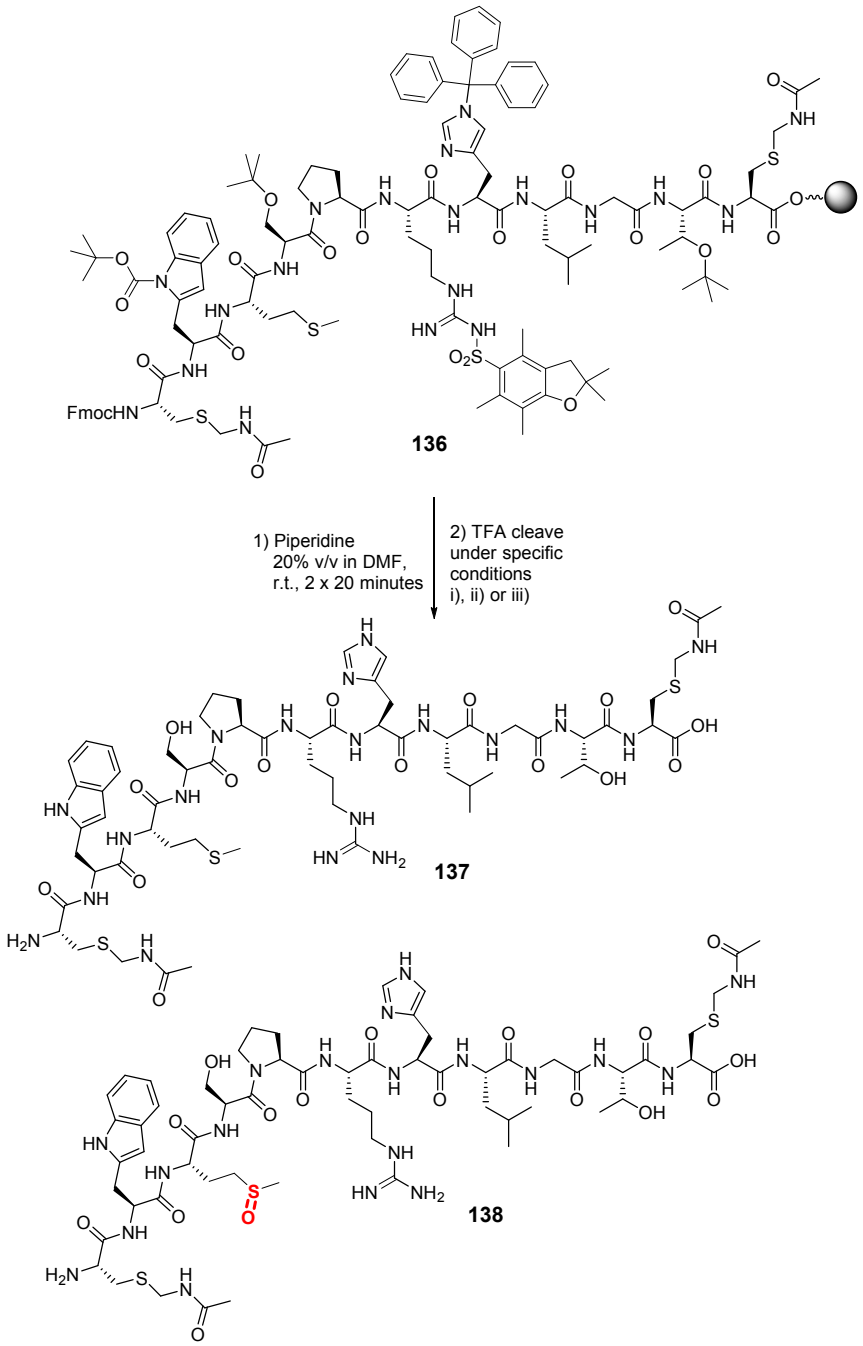

Scheme 3.10 TFA cleavage of linear resin-bound p15 peptide (**136**) to give target peptide **137**. The methionine oxidised analogue is **138** with the oxidised methionine highlighted in red. Reagents and conditions: i) TFA:TIPS:water, 95:2.5:2.5 r.t. 4 h; ii) TFA:TIPS:water, 95:2.5:2.5, r.t. 2 h; iii) TFA: EDT: water:TIPS, 94:2.5:2.5:1, r.t. 4h.

A further cleave using 1,1,1,3,3,3-hexafluoro-2-propanol (HFIP) in dichloromethane, was carried out to yield the fully protected peptide (**139**, **Scheme 3.11**). Cleavage with TFA:TIPS:water resulted in complete removal of all acid-labile protecting groups after four hours. However, there appeared to be a significant amount of methionine oxidation and both the target peptide (**137**) and the methionine-oxidised analogue (**138**) were seen in the LCMS (**Figure 3.9**). Cleavage with the same cocktail but for 2 hours was carried out to see if this reduced methionine oxidation. The LCMS and chromatogram of the cleavage mixture are shown in **Figure 3.10**. The LCMS of the peptide obtained from the shortened cleavage not only showed only partial deprotection of the peptide with residual Pbf protection of arginine evident (see **140** and **141**), but also that methionine oxidation was still significant.

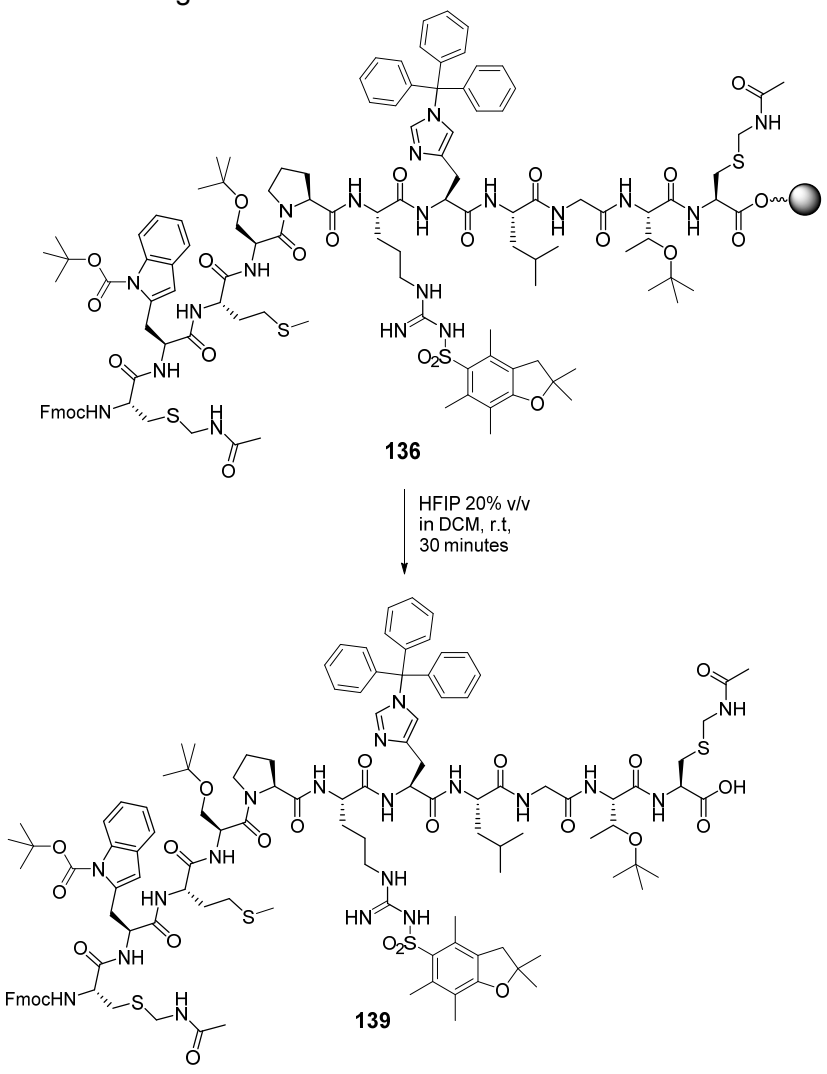

Scheme 3.11 Cleavage of linear resin-bound p15, 13, using 20% HFIP in DCM to yield the fully protected peptide (**139**).

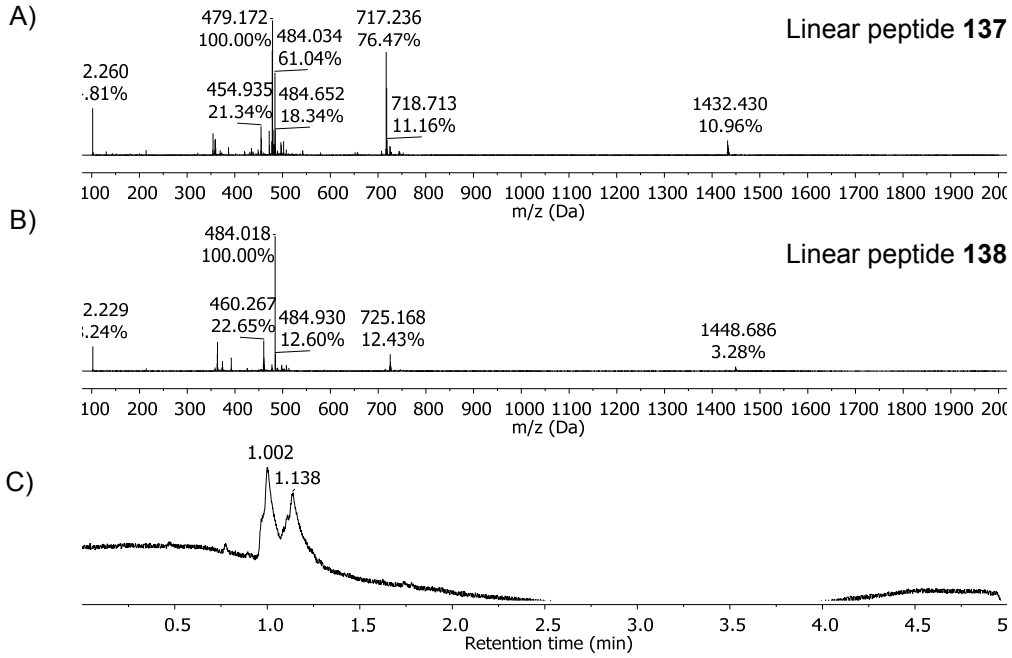

Figure 3.9 LCMS following cleavage of p15 peptide from resin (TFA:TIPS:water, 95:2.5:2.5 for four hours). A) Mass spectrum of cleaved target peptide (**137**), ($[M+H]^+$ = 1432) corresponding to the peak at 1.14 minutes in the chromatogram. B) Mass spectrum of the deprotected peptide with oxidised methionine (**138**), ($[M+H]^+$ = 1448) corresponding to the peak at 1.00 minutes in the chromatogram. C) The chromatogram of the cleaved peptide mixture (detection at 280nm).

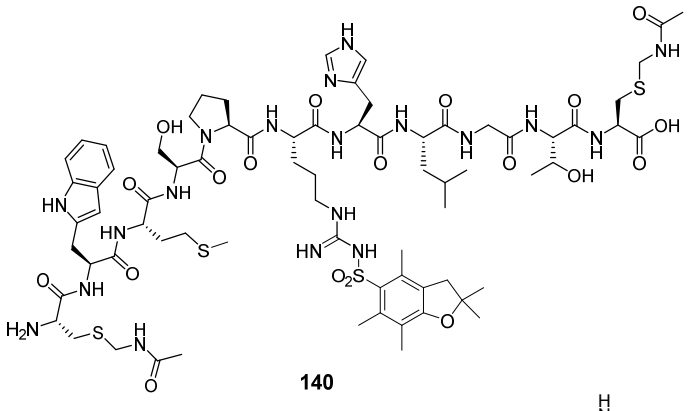

140

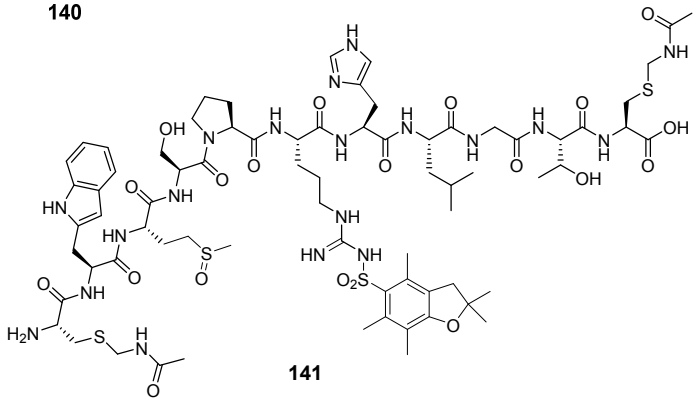

141

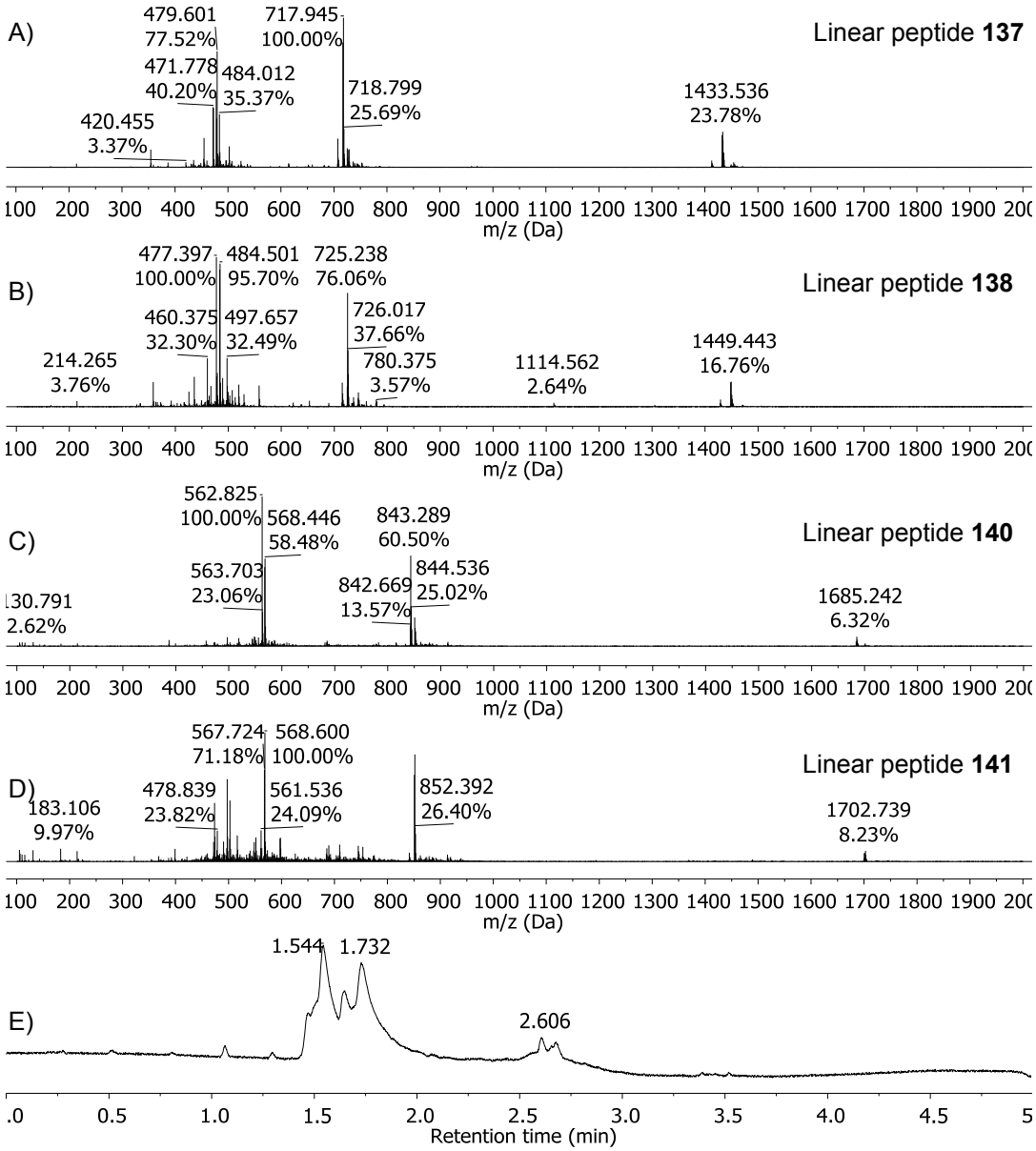

Figure 3.10 LCMS following cleavage of p15 peptide from resin (TFA:TIPS:water, 95:2.5:2.5 for two hours). A) Mass spectrum of the parent linear peptide (**137**), ($[M+H]^+$ = 1432) corresponding to the peak at 1.73 minutes in the chromatogram. B) Mass spectrum of the linear parent peptide with oxidised methionine (**138**), ($[M+H]^+$ = 1448) corresponding to the peak at 1.54 minutes in the chromatogram. C) Mass spectrum of peptide with residual Pbf protecting groups (**140**), ($[M+H]^+$ = 1685) corresponding to the peak at 2.68 in the chromatogram. D) Mass spectrum of peptide with residual Pbf protecting groups and methionine oxidation (**141**), ($[M+H]^+$ = 1702) corresponding to the peak at 2.61 in the chromatogram. E) The chromatogram of the cleaved peptide mixture (detection at 280nm).

Next, deprotection with the addition of EDT as a scavenger was attempted. The cleavage cocktail used was TFA:EDT:water:TIPS, 94:2.5:2.5:1, and the deprotection was for four hours. The LCMS and chromatogram are shown in **Figure 3.11**. Analysis of the LCMS and chromatogram showed only one major peak, corresponding to the deprotected peptide (**137**) with no evidence of methionine oxidation. However, EDT is toxic and very smelly; even on a test cleave scale all glassware had to be thoroughly cleaned with bleach. Work up of the peptide required use of the rotary evaporator which also had to be cleaned with bleach after use. As a result, it was decided to avoid the use of EDT for full cleaves, unless its use was necessary to obtain enough peptide for subsequent use.

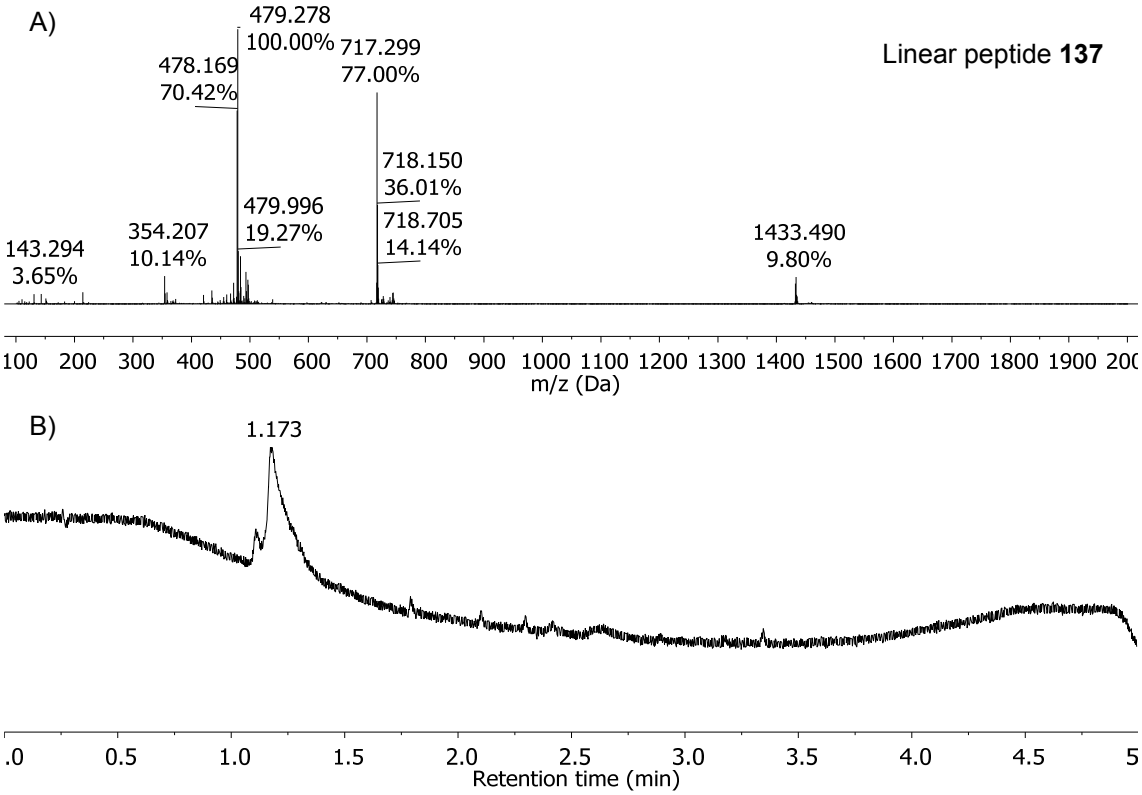

Figure 3.11 LCMS following cleavage of p15 peptide from resin (TFA:EDT:water:TIPS, 94:2.5:2.5:1 for four hours). A) Mass spectrum of the target linear peptide (**137**), ($[M+H]^+$ = 1433) corresponding to the peak at 1.17 minutes in the chromatogram. B) The chromatogram of the cleaved peptide mixture (detection at 280nm).

Cleavage conditions to yield the fully protected peptide (**139**) were also investigated. Access to the fully protected peptide is desirable as this enables solution phase reactions to be carried out whilst minimising the risk of unwanted side-reactions. The cleavage conditions used were 20% HFIP in DCM and the LCMS and chromatogram are shown in **Figure 3.12**. The LCMS chromatogram shows two major peaks: one at 3.38 minutes and one at 3.81 minutes. The peak at 3.81 minutes is the fully protected peptide ($[M+2H]^{2+}/2$ = 1181), and the peak at 3.38 minutes is the fully protected peptide with a loss of the trityl protecting group on the histidine residue (**142**), ($[M+2H]^{2+/}2$ = 1061). Deprotection of the histidine is potentially problematic since the basic properties of the histidine nitrogen may interfere in subsequent reactions.

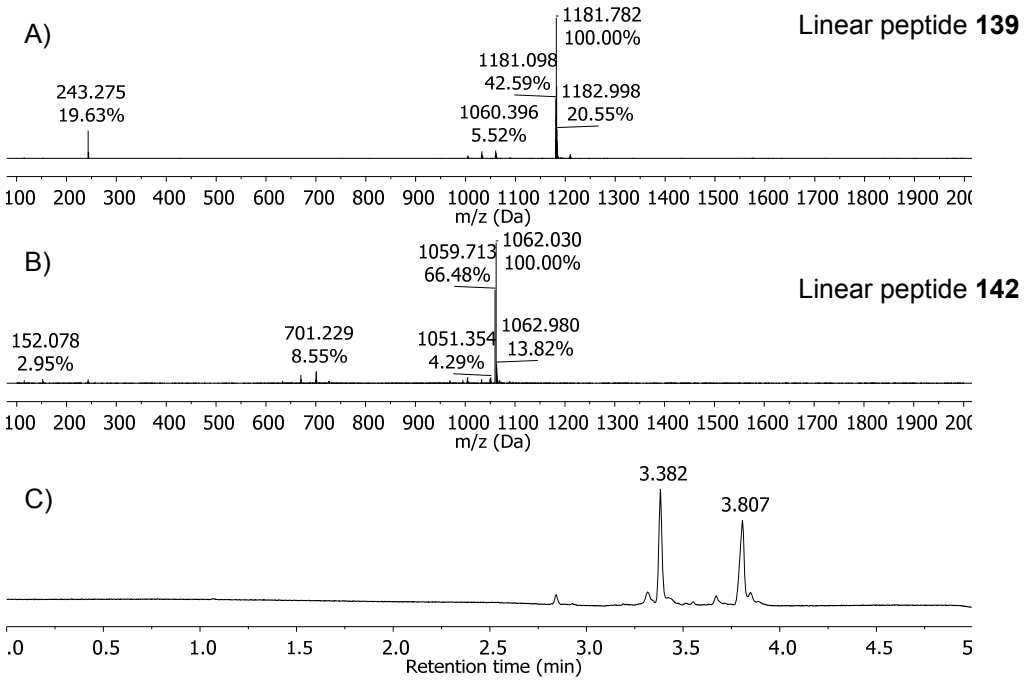

Figure 3.12 LCMS following cleavage of p15 peptide from resin (20% HFIP in DCM for 30 minutes). A) Mass spectrum of the protected peptide (**139**), ($[M+2H]^{2+}/2$ = 1181) corresponding to the peak at 3.81 minutes in the chromatogram. B) Mass spectrum of the peptide with a free histidine (**142**), ($[M+2H]^{2+}/2$ = 1061) corresponding to the peak at 3.38 minutes in the chromatogram. C) The chromatogram of the cleaved peptide mixture (detection at 280nm).

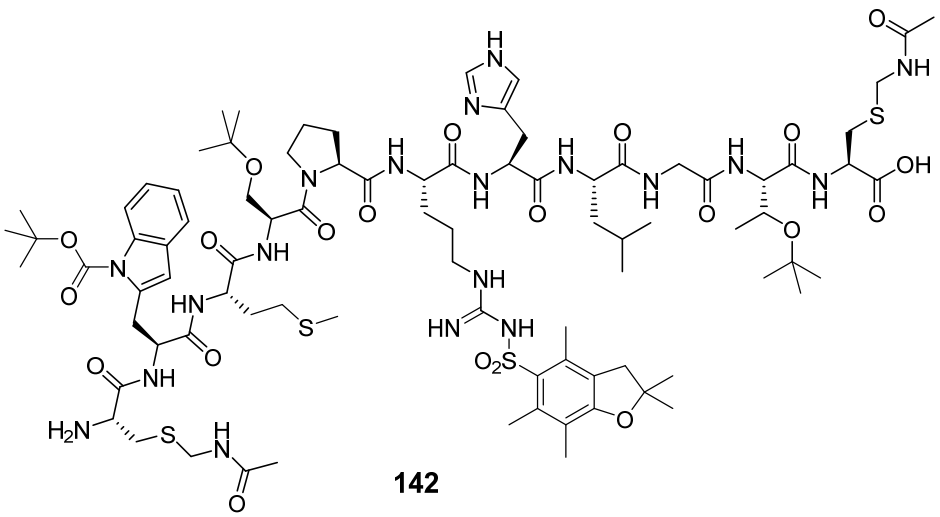

142

3.2.3 Formation of the disulphide bridge

Disulphide bridges are found in naturally occurring peptides and proteins and provide a method of stabilising their biologically active forms.[105-107] Disulphide formation is reversible and is generated by oxidative folding of cysteine-containing peptides. Synthetically, many methods of disulphide formation have been reported.[108-112] Disulphide formation may be carried out on the peptide in solution or whilst the peptide is still attached to the resin (solid-phase). The method of cysteine oxidation depends on the protecting group strategy employed. If trityl-protected cysteine is used, cleavage from the resin yields the linear peptide which is then cyclised by air oxidation in a buffer solution at pH 7.5 – 8 (**Scheme 3.12**).

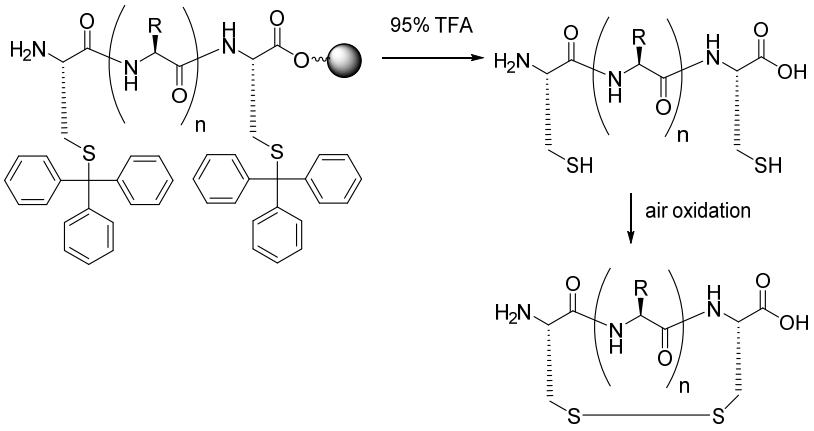

Scheme 3.12 Standard air oxidation approach for disulphide formation from trityl-protected cysteine.

Progress of the reaction is usually followed by HPLC and additives such as DMSO or H_2O_2 may be used to speed up the reaction. However, it should be noted that such additives, particularly H_2O_2, would also oxidise the methionine residue in the p15 peptide and their use would therefore be inappropriate here.

When Acm-protected cysteine is used, cyclisation is concomitant with removal of the Acm group (**Scheme 3.13**). Removal of the Acm group is carried out in the presence of iodine which also oxidises the cysteine to form the disulphide. This may be carried out in solution using iodine in 40% acetic acid followed by quenching of the solution by 1M ascorbic acid. Since cleavage of the peptide from the resin using TFA will leave the Acm groups intact, this method enables purification of the linear peptide prior to oxidation. Conversely, treatment of the resin-bound peptide with iodine will remove the Acm groups and form the disulphide, leaving the protecting groups on other residues intact. The iodine can then be washed off the resin, and the fully deprotected cyclic peptide obtained by cleavage with 95% TFA. Carrying out the cyclisation on the resin-bound peptide has several advantages over solution-phase methods. In solution-phase, oxidation has to be carried out in high dilution in order to favour intramolecular reaction over intermolecular reaction. Further, work up of the solution-phase reaction requires high volumes of ascorbic acid solution to destroy the iodine and prevent side reactions. This results in a high volume of peptide solution to purify, making this method very time consuming. Carrying out the reaction on resin results in pseudo-high dilution conditions, and the iodine can be simply washed off the resin after the reaction, making purification less tedious. This was, therefore, the method of choice.

The disadvantage of the iodine oxidation method (**Scheme 3.13**) is that it is inherently inefficient; removal of the Acm groups can be slow, but extended reaction times are likely to result in side reactions, including over-oxidation of the cysteine to cysteic acid.[113-115] The crude peptide will therefore contain a mixture of the cyclic peptide with residual mono- and bis- Acm-protected cysteine-containing peptide. However, the aim is to obtain enough cyclised peptide to carry out binding assays and attempt to get a crystal structure, so maximising the yield was not considered of primary importance.

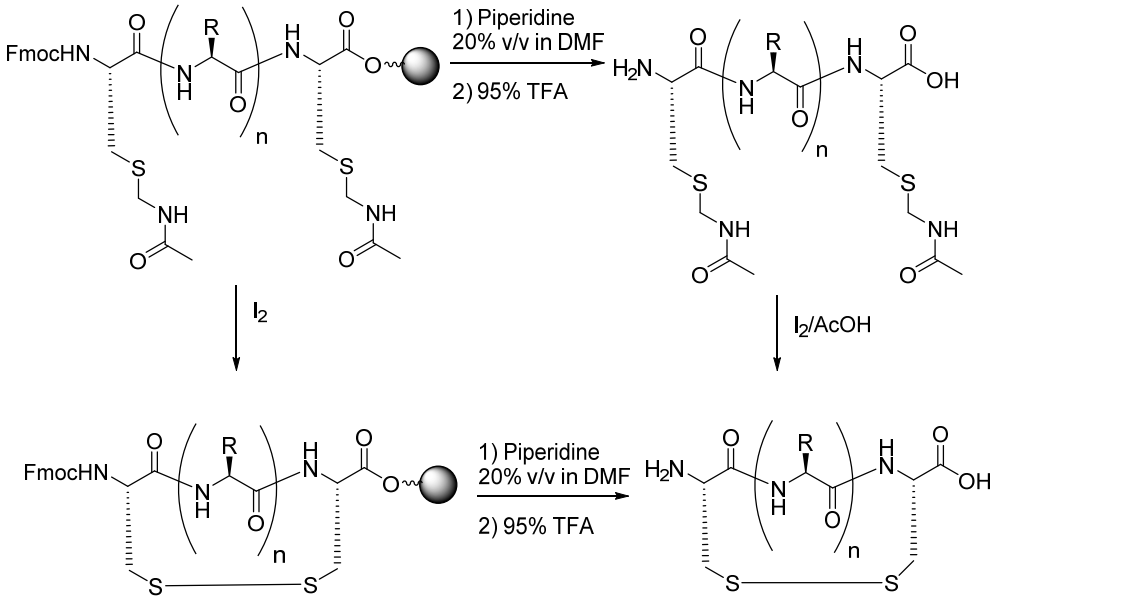

Scheme 3.13 Standard approaches for disulphide formation from Acm-protected cysteine.

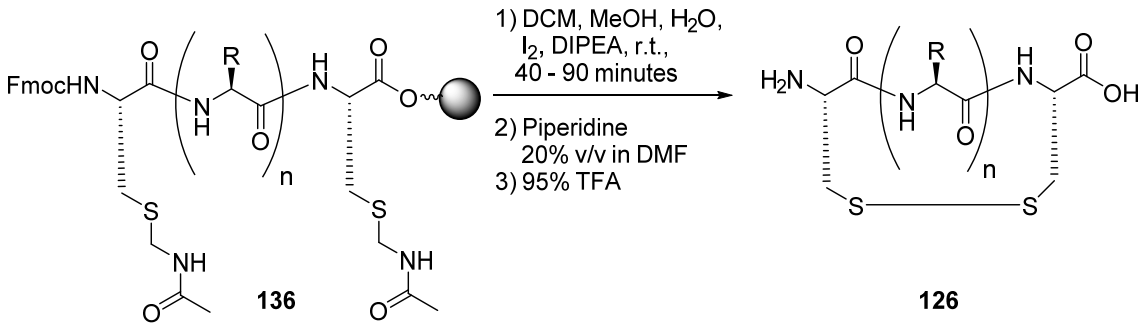

Scheme 3.14 On-resin disulphide formation from Acm-protected cysteine following the Bachem procedure.

The first set of conditions attempted was adapted from a procedure used by Bachem to form a single disulphide bridge from Acm-protected cysteine in a peptide on SASRIN resin (**Scheme 3.14**). This procedure involved swelling the resin in a mixture of DCM:MeOH:water (60:25:4 v/v/v) and then adding eight equivalents of iodine (relative to the resin-bound peptide) in DCM and 8 equivalents of DIPEA to neutralise the hydrogen iodide that is evolved as a by-product of the reaction. The peptide was put on a shaker for forty minutes initially, although reaction for 90 minutes was later attempted.

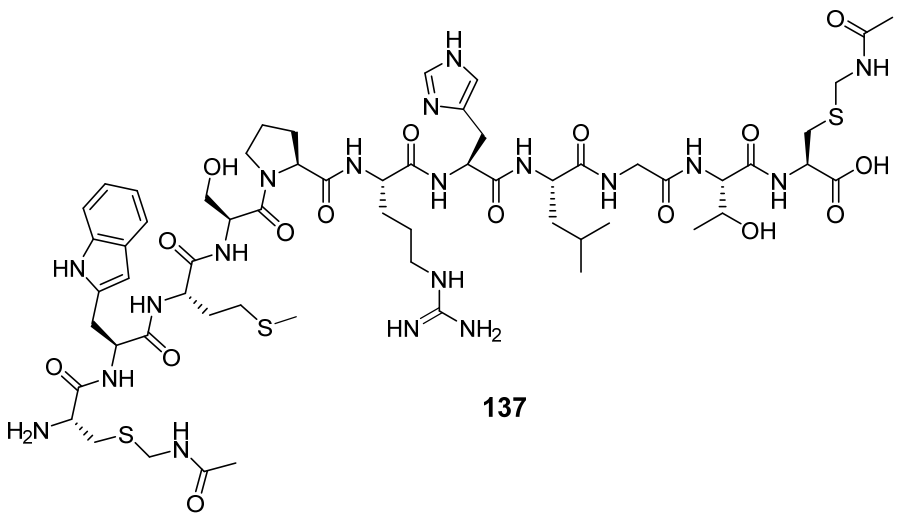

137

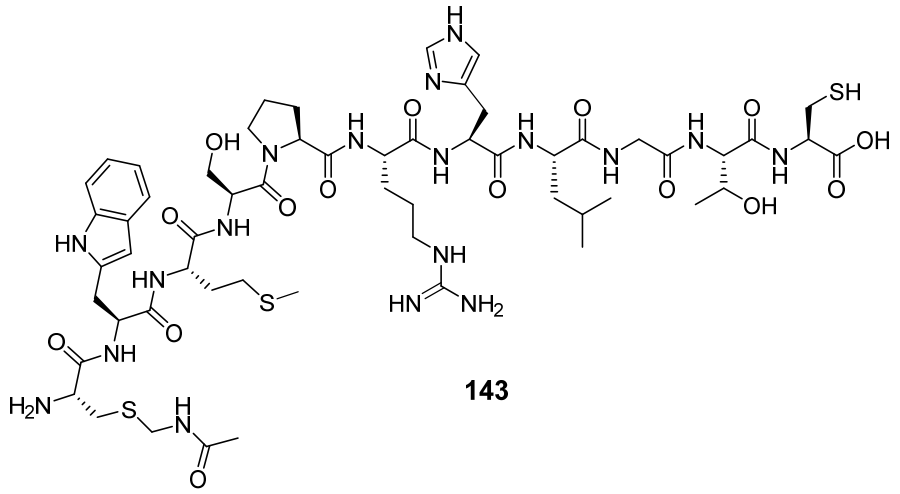

143

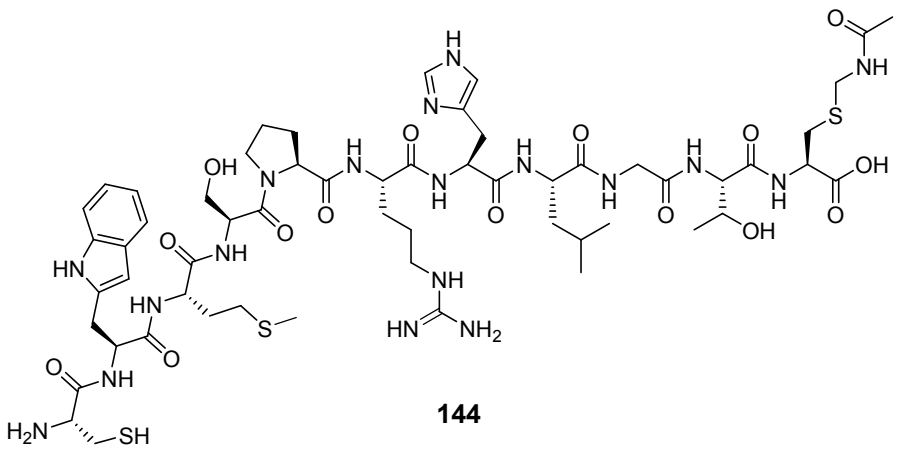

144

For the forty minute reaction, the results were as predicted; a mixture of bis- Acm protected (**137**), mono- Acm protected (**143** and/or **144**) and cyclised peptide (**126**) were obtained (**Figure 3.13** shows the LCMS of a HPLC fraction containing all three

compounds). The bis-Acm protected peptide (**137**) appeared to be the primary product, appearing in the majority of HPLC fractions, whilst the cyclised p15 peptide (**126**) was not isolated. Increasing the reaction time to 90 minutes resulted in a greater level of deprotection with the mono-Acm protected peptide (**143** and/or **144**) appearing in more HPLC fractions and the bis-Acm protected peptide (**137**) appearing in fewer. Further, the cyclised p15 peptide (**126**) could be isolated, although yield was poor (0.8%).

The poor yield was not only because of the inefficiency of the reaction. Cyclisation reactions were carried out on a 0.1 mmol scale, but the masses of crude peptide obtained following cleavage from the resin were smaller than expected; 6 mg – 16 mg of crude peptide was obtained from each reaction, whilst in a hypothetical scenario where the yield of cyclised p15 peptide (**126**) is 100%, this would require 128 mg of peptide. There are several possible reasons for such poor crude peptide yields. First, loading of the resin is poor; 2-chlorotrityl chloride resin is very moisture sensitive and contact with water either through prolonged exposure to atmospheric water, or poor handling during coupling of the first amino acid will result in a reduction of available loading sites. Second, peptide could be lost in the cleavage procedure, for example through inefficient filtration. Third, peptide could be cleaved in the course of the cyclisation reaction itself, for example through exposure to acid generated as a byproduct of the reaction (although DIPEA was used in order to neutralise any acidic byproducts). To find out which of the above possibilities was the reason for the poor yield, 0.1 mmol of bis-Acm protected linear peptide was cleaved from the resin using the same cleavage cocktail as the one used following the cyclisation reactions (TFA:TIPS:H_2O, 95:2.5:2.5). The mass of crude peptide obtained from a 0.1 mmol reaction was 73 mg showing that, whilst there appear to be some problems with resin loading and/or cleavage of the peptide, large amounts of peptide are being cleaved in the cyclisation reaction itself. Since the presence of DIPEA should neutralise any acidic byproducts, we suspected the solvents used were responsible for the loss of peptide, and attempted the reaction in DCM only (**Scheme 3.15**).

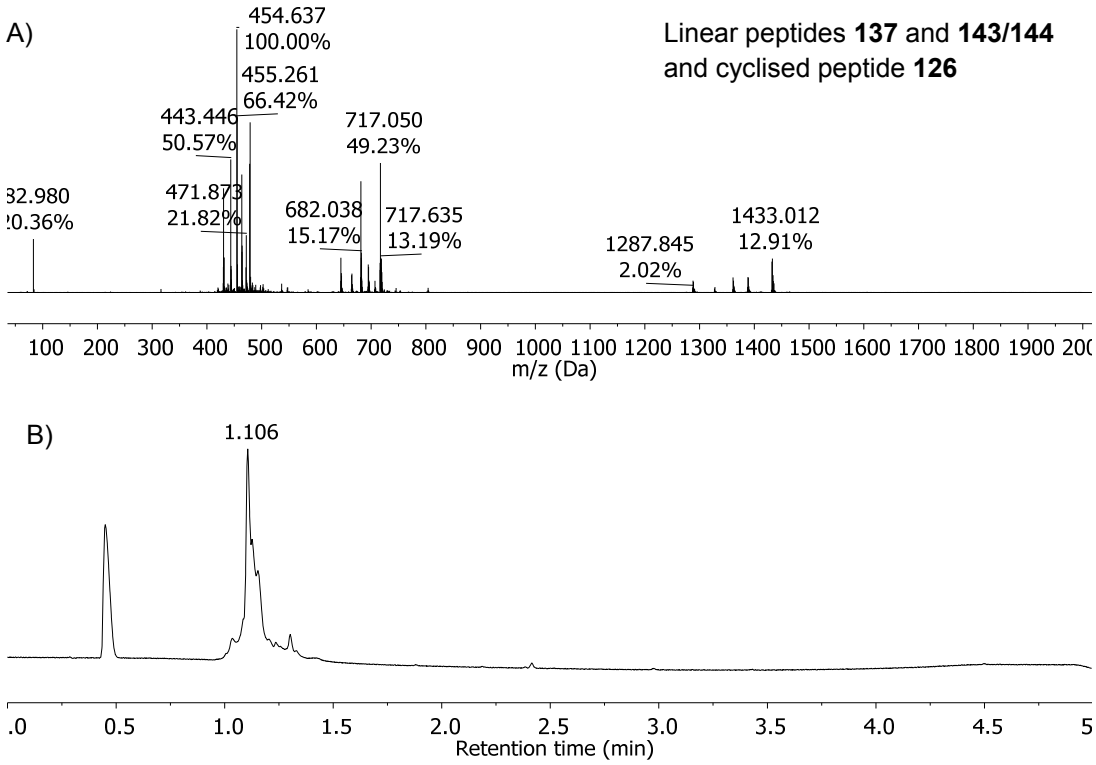

Figure 3.13 LCMS of a HPLC fraction following attempted on-resin disulphide formation (**Scheme 3.14**, 40 minutes). A) Peaks corresponding to the bis-Acm protected peptide (**137**), $[M+ H]^+$ =1433, the mono-Acm protected peptide (**143** and/or **144**), $[M + H]^+$ = 1361 and cyclised p15 peptide (**126**), $[M + H]^+$ = 1288, retention time 1.16 minutes; B) The chromatogram of the peptide mixture (detection at 280 nm).

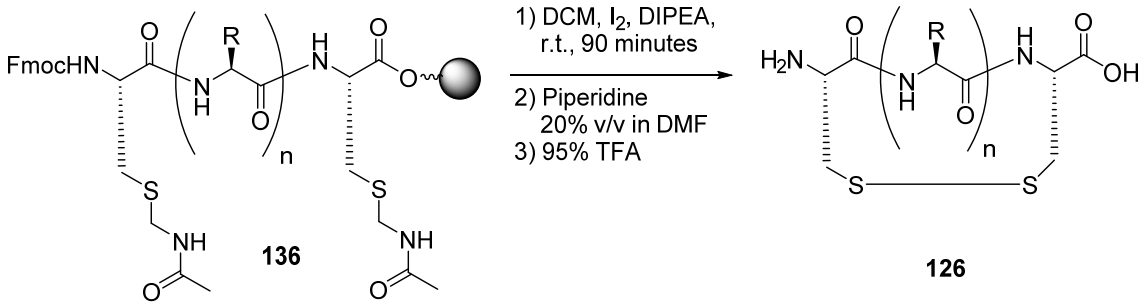

Scheme 3.15 On-resin disulphide formation from Acm-protected cysteine using DCM as the only solvent.

Cyclisation in DCM generated 67 mg of crude peptide, indicating that the presence of methanol and/or water, even in small volumes encourages cleavage of the peptide from the resin. Whilst, once again, a mixture of bis-Acm protected (**137**), mono-Acm protected (**143** and/or **144**) and cyclic p15 (**126**) could be seen in the mass spectra of the crude peptide and the HPLC fractions, the cyclised p15 peptide was isolated in a 19% overall yield (**Figure 3.14** shows the analytical HPLC trace of purified p15 peptide, **126**).

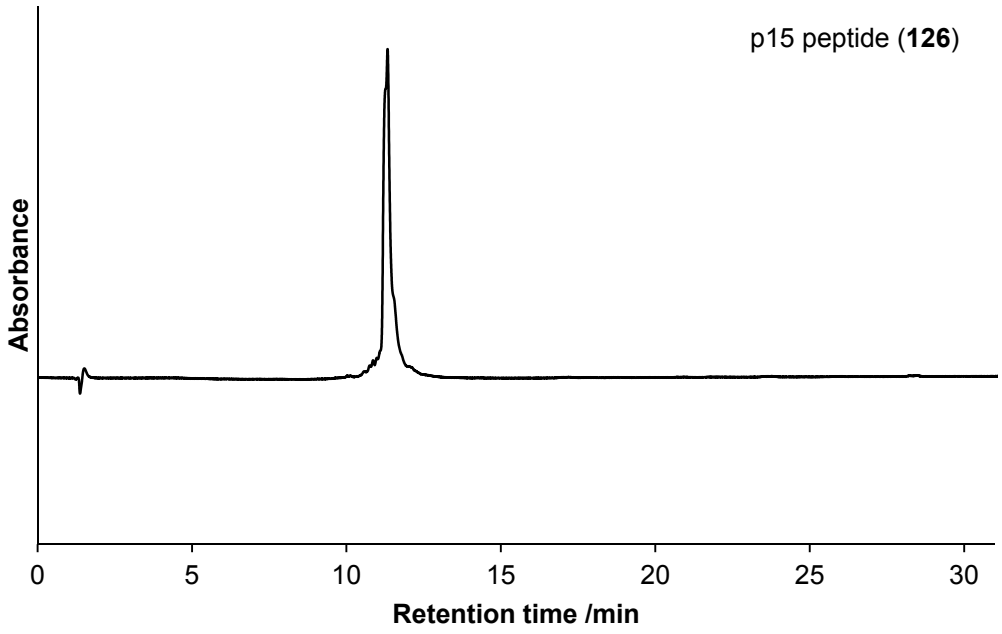

Figure 3.14 Analytical HPLC trace of purified p15 peptide (**126**), λ = 280 nm.

3.3 Synthesis of the tetrafluoro-stapled p15 peptide (F-p15, 127)

Previous work within the group has investigated the stapling of peptides using hexafluorobenzene (**145**), **Scheme 3.16**.[87] We wanted to apply this methodology to create a tetrafluoro-stapled p15 analogue (F-p15, **3**, **Figure 3.15**).

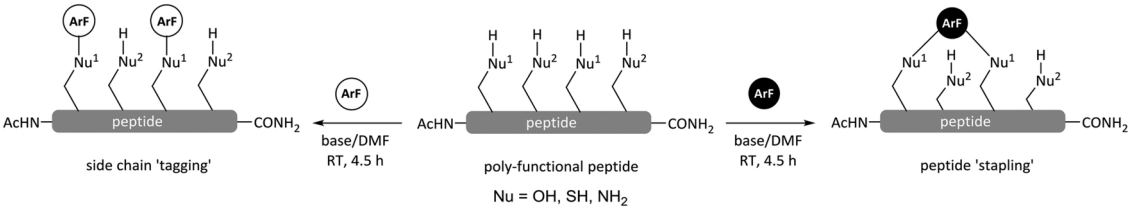

Scheme 3.16 Tagging and stapling of peptides using hexafluorobenzene (**145**).

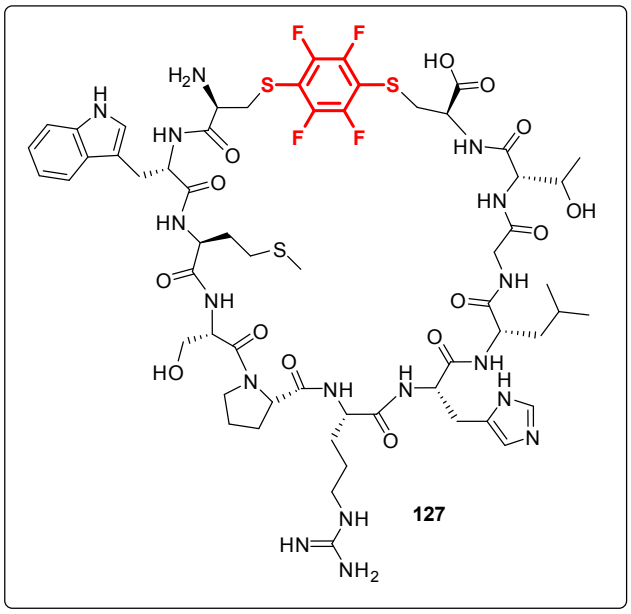

Figure 3.15 Target compound tetrafluoro-stapled p15 peptide (F-p15, **127**).

Two linear peptides were first synthesised using SPPS methods described in **Section 3.2**, **Scheme 3.9**. The first was linear resin-bound p15 (**136**), i.e. with Acm-protected cysteine, and the second was the Trt-protected analogue (**146**), which was cleaved from the resin to give the fully deprotected p15 peptide (**147**, **Scheme 3.17**) which was used in the solution-phase reaction (**Scheme 3.17**). The LCMS of the crude linear peptide (**Figure 3.16**) was deemed clean enough to attempt the stapling reaction without prior purification of linear peptide **147**.

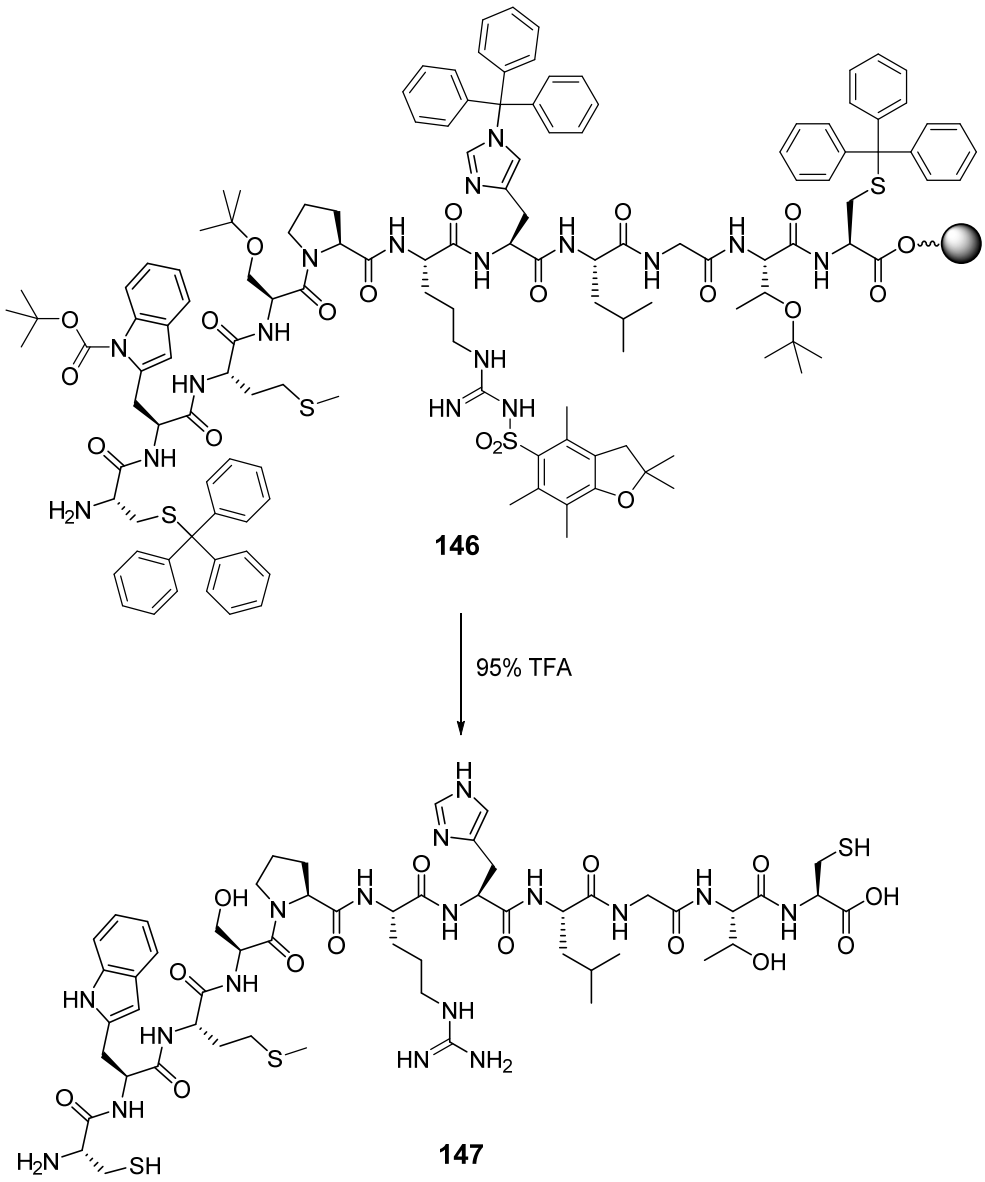

Scheme 3.17 Cleavage of Cys(Trt) linear resin-bound p15 (**146**) to give the fully deprotected linear p15 peptide (**147**).

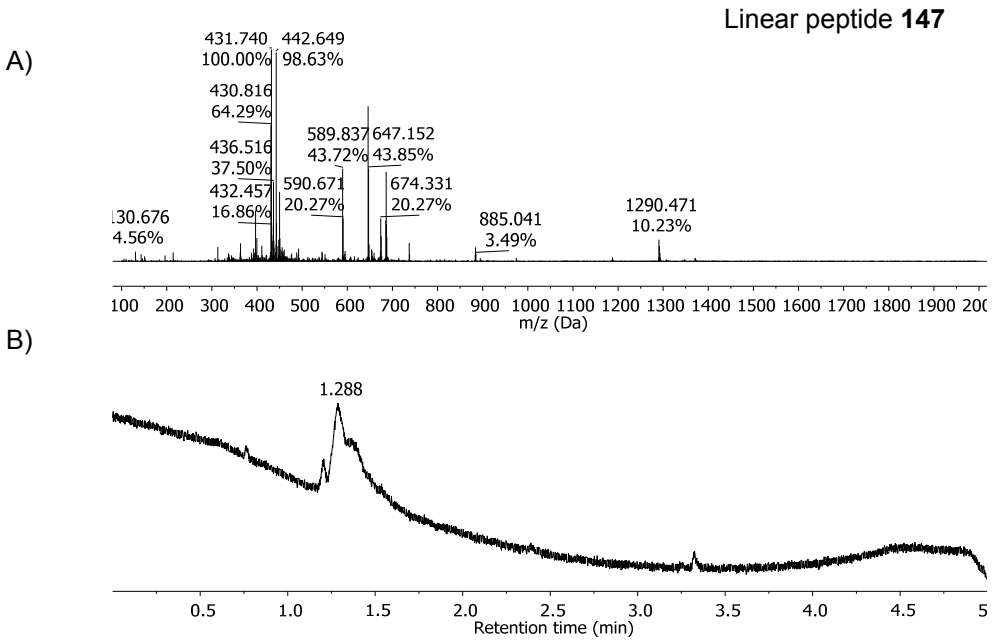

Figure 3.16 LCMS following cleavage of Cys(Trt) linear resin-bound p15 peptide (**146**, TFA:EDT:water:TIPS, 94:2.5:2.5:1 for four hours). A) Mass spectrum of the fully deprotected linear peptide (**147**), ($[M+H]^+$ = 1290) corresponding to the peak at 1.29 minutes in the chromatogram. B) The chromatogram of the cleaved peptide mixture (detection at 280nm).

Having synthesised the two linear peptides, **136** and **147**, we proceeded to attempt the stapling reactions. Cyclisation was first attempted on the resin bound peptide (**136**, **Scheme 3.18**). Conditions were similar to those used for disulphide bond formation in **Section 3.2.3** except with the addition of hexafluorobenzene which we hoped would intercept disulphide formation to give the target tetrafluorobenzene-stapled peptide (F-p15, **3**). However, the on-resin reaction of peptide **136** with hexafluorobenzene (**145**) suffered from the same problem as the disulphide formation reactions; only 3 mg crude peptide was generated from a 0.05 mmol scale reaction which corresponds to a maximum possible yield of 4%. Further, the reaction failed, producing a mixture of bis-Acm protected peptide (**137**), mono-Acm protected peptide, (**143** and/or **144**) and cyclised (disulphide-containing) p15 (**126**). We therefore attempted the reactionon the linear peptide in solution.

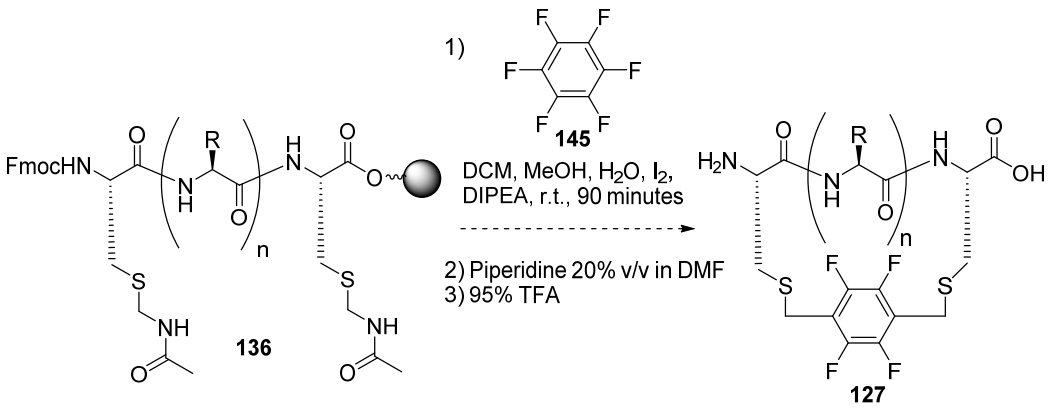

Scheme 3.18. Attempted on-resin stapling of p15 with hexafluorobenzene (**145**).

For the solution-phase reaction of peptide **147** with hexafluorobenzene (**145**), five equivalents of hexafluorobenzene (**145**) were added to a solution of linear peptide **147** in 50 mM DIPEA in DMF and shaken at room temperature for four hours (**Scheme 3.19**). The LCMS of the crude reaction mixture (**Figure 3.17**) showed the tetrafluoro-stapled peptide to be the main component, but some of the mono-adduct (**148** and/or **149**- the specific regio-isomer cannot be distinguished here) was also seen, as well as some uncyclised linear parent peptide, **147**.

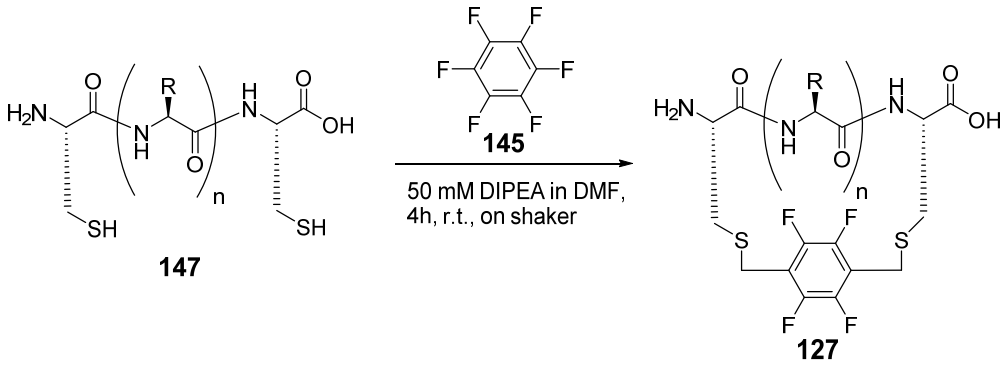

Scheme 3.19 Attempted solution-phase stapling of p15 with hexafluorobenzene (**145**).

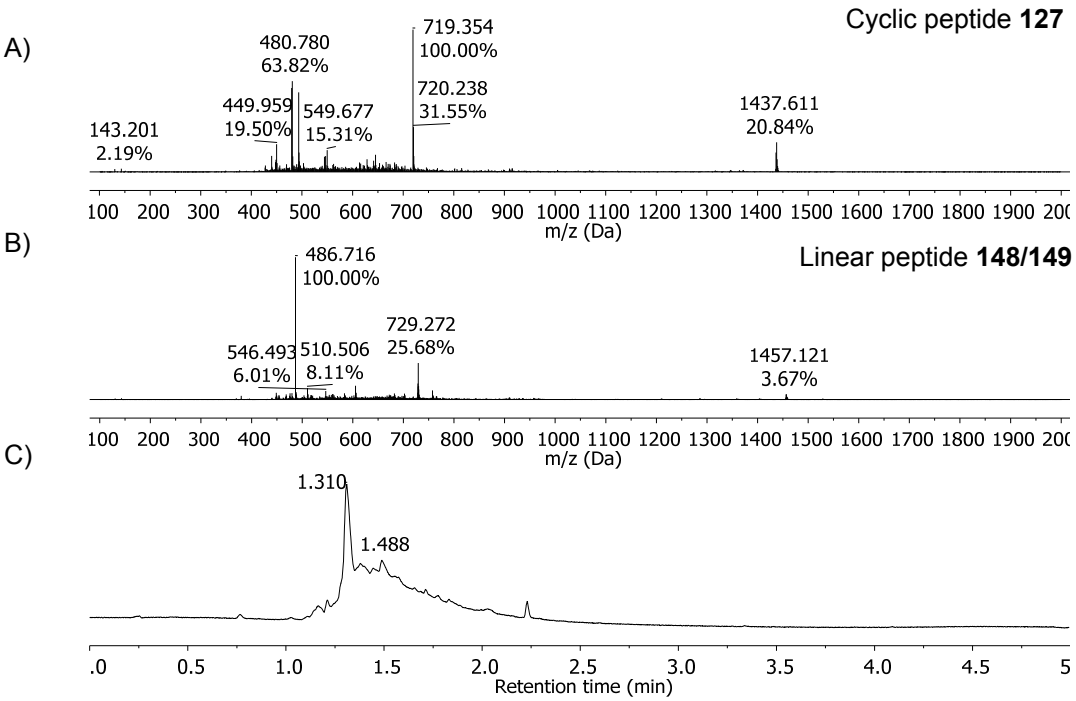

Figure 3.17 LCMS of the crude reaction mixture after reaction with hexafluorobenzene (**145**) following conditions described in **Scheme 3.18**. A) Mass spectrum of F-p15 (**127**) corresponding to the peak at 1.31 minutes in the chromatogram, $[M + H]^+$ = 1437. B) Mass spectrum of the mono-adduct (**148** and/or **149**) corresponding to the peak at 1.49 minutes in the chromatogram, $[M + H]^+$ = 1457 C) The chromatogram of the peptide mixture (detection at 280 nm).

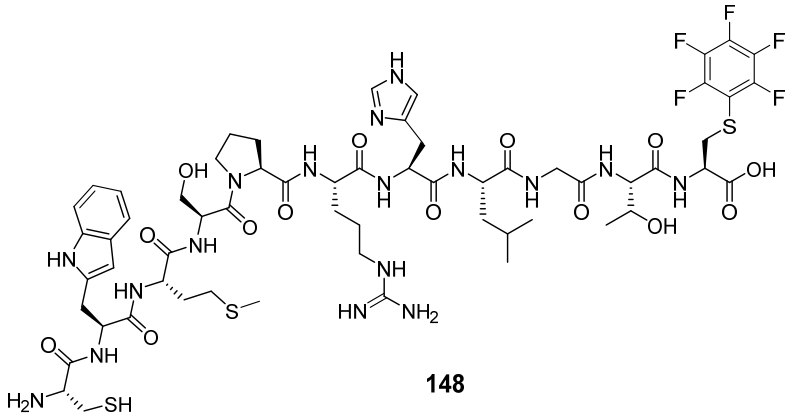

148

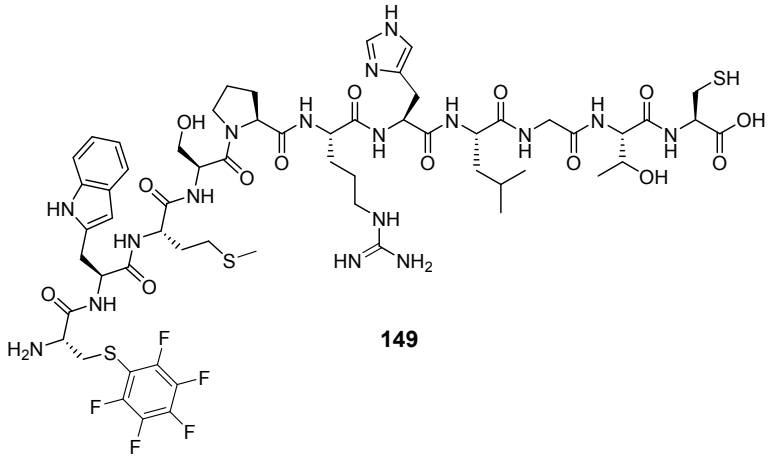

149

Subsequent purification of the crude reaction mixture gave F-p15 (**127**) in 32% yield (**Figure 3.18** shows the analytical HPLC trace of the purified F-p15 peptide, **127**). This was sufficient for use in binding assays and crystallisation studies so no further reactions were deemed necessary. ^{19}F NMR was also carried out (δ_F(376 MHz, D_2O)) and the spectra showed two peaks: one corresponding to TFA (m, -76.5), leaving one peak corresponding to aromatic fluorines (m, -133.36 – -134.27). This is consistent with all four fluorine atoms being in very similar environments.

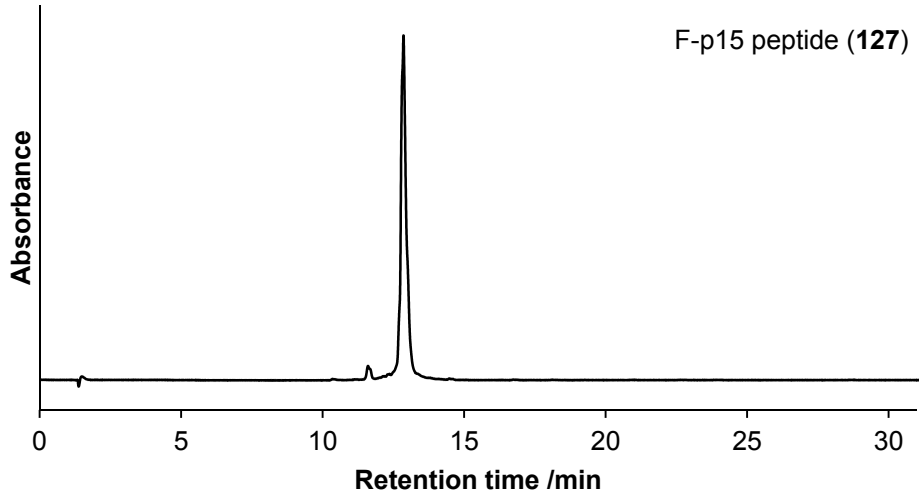

Figure 3.18 Analytical HPLC trace of purified F-p15 peptide (**127**), λ = 280 nm.

3.4 Synthesis of C=C stapled p15 (128)

Grubbs' ring-closing metathesis (RCM) is a well-established method of stapling peptides, both as a replacement for disulphide bridges and as a way of stabilising existing secondary structures such as alpha helices.[88, 89] Grubbs' RCM on peptides is usually carried out whilst the peptide is still attached to the resin; the resin-bound peptide will be fully protected, precluding side-reactions with reactive side chains, and attachment of the peptide to a solid support generates pseudo-high dilution conditions, thus reducing cross-methathesis reactions. We therefore used Grubbs' RCM to synthesise a C=C stapled p15 peptide analogue (**128**, **Figure 3.19**).

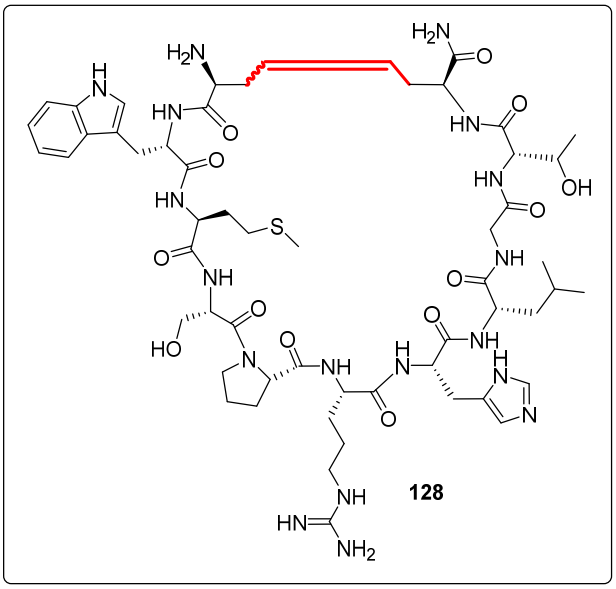

Figure 3.19 Target compound C=C stapled p15 peptide (**128**).

We first synthesised a linear p15 peptide on the cysteine residues were replaced with allyl glycine residues (**150**, **Scheme 3.20**). The peptide was synthesised on Rink Amide resin as this is easier to handle than 2-chlorotrityl resin. LCMS analysis following a test cleave of the linear allyl glycine peptide (**150**) showed that synthesis had been successful by the appearance of linear peptide **151** in the spectrum (**Figure 3.20**).

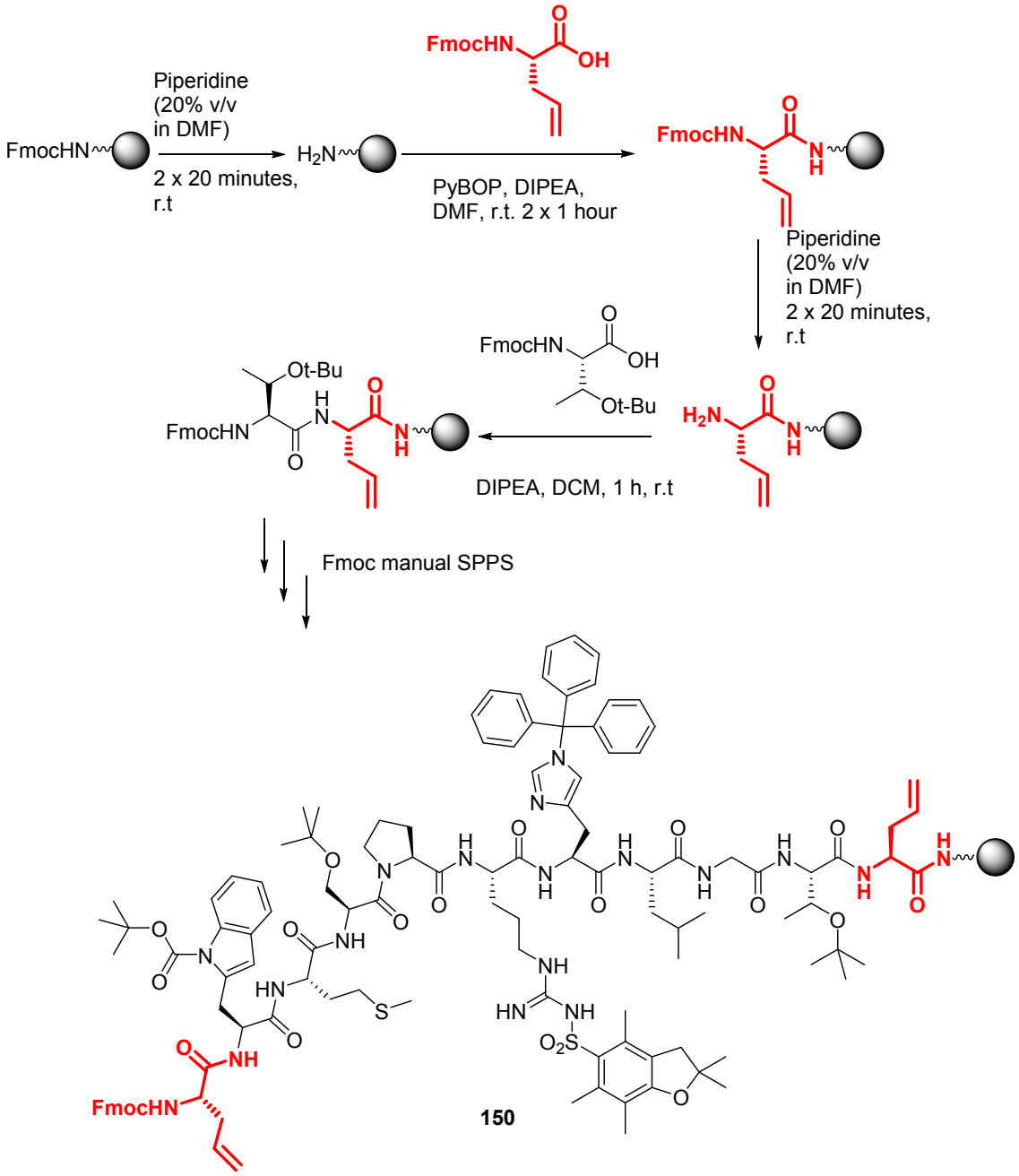

Scheme 3.20 Manual SPPS of linear, resin-bound fully protected linear allylglycine p15 peptide analogue (**150**) on Rink amide resin. Fmoc manual SPPS conditions, amino acids used in order of addition: Fmoc-allylglycine-OH, Fmoc-Thr(tBu)-OH, Fmoc-Gly-OH, Fmoc-Leu-OH, Fmoc-His(Trt)-OH, Fmoc-Arg(Pbf)-OH, Fmoc-Pro-OH, Fmoc-Ser(tBu)-OH, Fmoc-Met-OH, Fmoc-Trp(Boc)-OH, Fmoc-allylglycine-OH. Coupling conditions: Amino acid, PyBOP, DIPEA, DMF, r.t., 1h. Fmoc-Ser(tBu)-OH and the Fmoc-allylglycine-OH underwent double coupling. Fmoc deprotection of amino acids: Piperidine (20% v/v in DMF), r.t. 2 x 20 minutes.

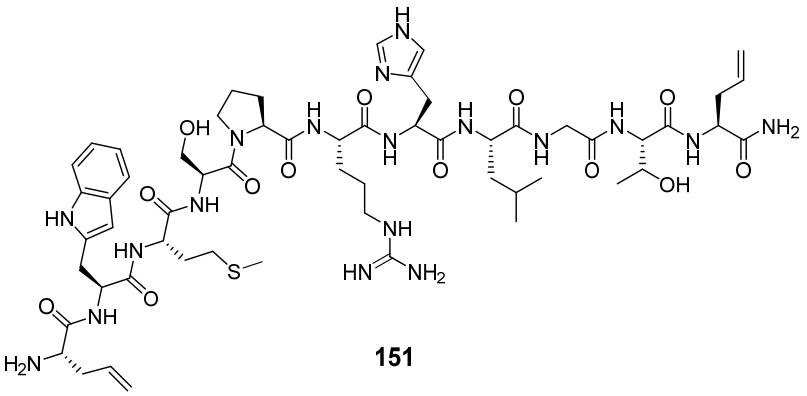

151

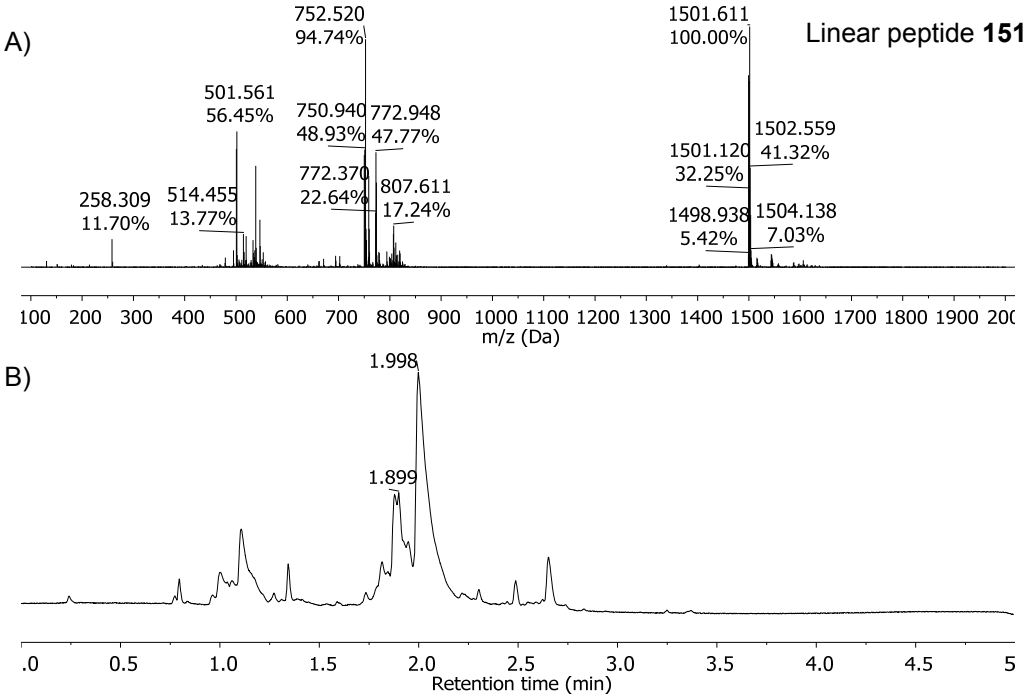

Figure 3.20 LCMS of test cleave mixture of linear allyl glycine peptide (**27**). A) Mass spectrum of linear peptide **151**, corresponding to the peak at 2.00 minutes in the chromatogram, $[M+ H]^+$ = 1501. B) The chromatogram of the crude reaction mixture (detection at 280 nm).

Having successfully synthesised the linear resin-bound parent peptide (**150**) we attempted cyclisation by Grubbs' RCM (**Scheme 3.21**).[116] The reaction conditions and their results are summarised in **Table 3.1**.

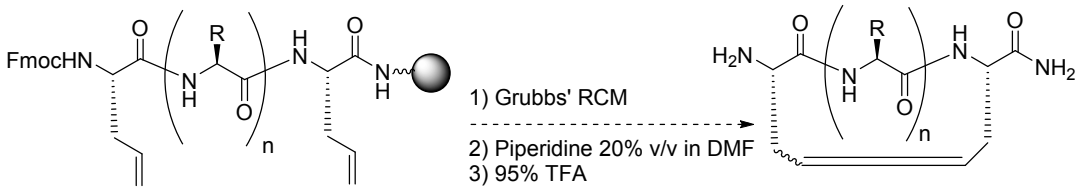

Scheme 3.21 Formation of C=C-p15 (**128**) by Grubbs' RCM, stapling a resin-bound allyl glycine-containing parent peptide (**150**).

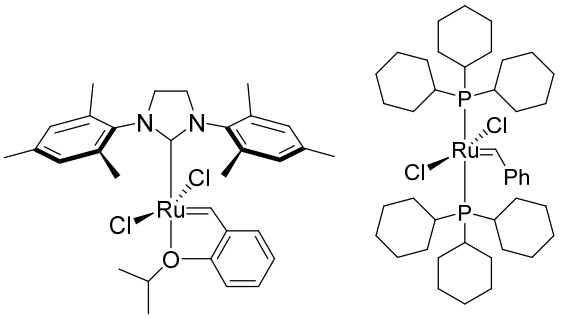

Figure 3.21 Grubbs' RCM catalysts used in RCM reactions attempted: 2nd Generation Hoveyda-Grubbs catalyst (**152**)[117] and 1st Generation Grubbs catalyst (**153**).[118]

Table 3.1 Summary of RCM reaction conditions attempted on linear parent peptide **150**.

Reaction number	Catalyst	Solvent	LiCl (0.4 M in DMF)	Temperature	Reaction time	Cyclic peptide 128
1	**152**	DCM	No	r.t	2 h	Not seen in crude LCMS
2	**152**	DCE	No	r.t	2 h x 2	Not seen in crude LCMS
3	**152**	DCM	Yes	reflux	18 h	Crude LCMS inconclusive
4	**153**	DCE	No	r.t	2 h x 2	Not seen in crude LCMS
5	**153**	DCE	Yes	r.t	2 h x 2	Not seen in crude LCMS
6	**152**	DCE	Yes	80°C	18 h	5% isolated yield (0.1 mmol scale)
7*	**152**	DCE	Yes	80°C	24 h x 2	11% isolated yield (0.1 mmol scale)

*EDT used in cleavage step

The first set of reaction conditions attempted used the 2nd Generation Hoveyda Grubbs' catalyst (**152**, **Figure 3.21**) in DCM which was added to the resin-bound peptide (**150**). The reaction mixture was then refluxed for two hours under nitrogen (Reaction number 1, **Table 3.1**). Following work-up, the LCMS of the crude peptide showed only one peak corresponding to the uncyclised peptide, **151**, (**Figure 3.22**).

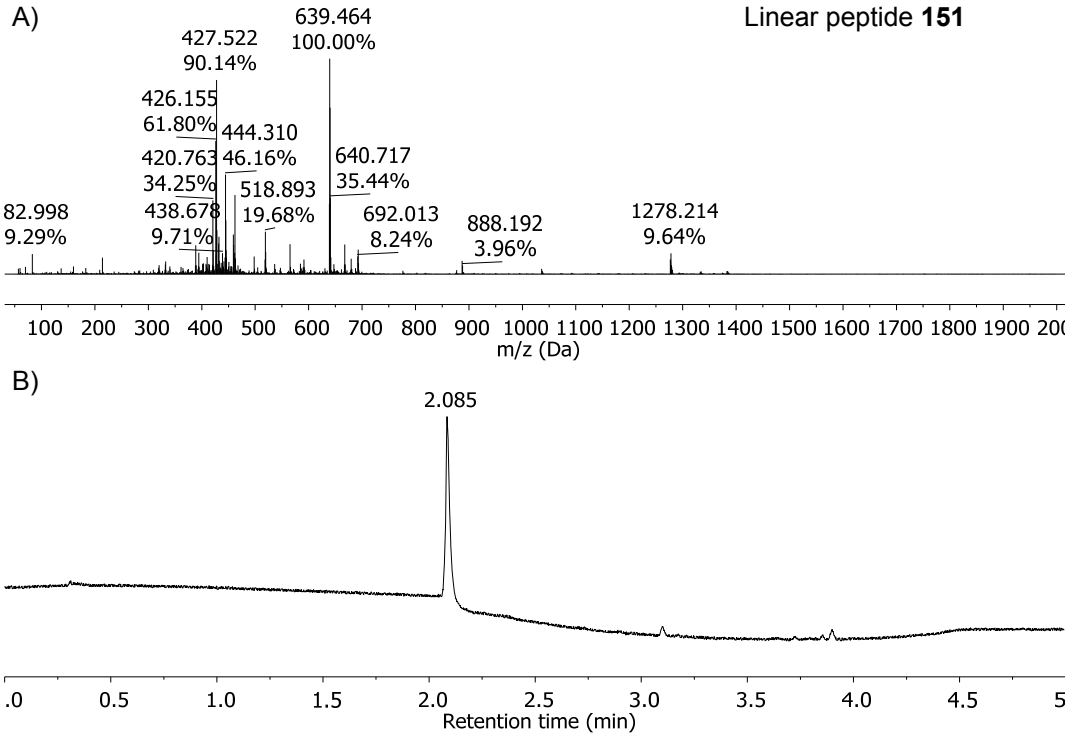

Figure 3.22 LCMS of the crude reaction mixture after Grubbs' RCM using 2nd generation Hoveyda Grubbs' catalyst in DCM, refluxed for 2 hours A) Mass spectrum of linear peptide **151** corresponding to the peak at 2.09 minutes in the chromatogram, $[M+ H]^+$ = 1278. B) The chromatogram of the crude reaction mixture (detection at 280 nm).

Following this, the reaction was repeated replacing DCM with 1,2-dichloroethane (DCE) as the solvent. This time the reaction was carried out at room temperature, and after the first two hours, a second portion of catalyst (20 mol% in DCE) was added and the reaction left for a further two hours (Reaction number 2, **Table 3.1**). However, the result was the same with only uncyclised peptide **151** obtained.

The third set of conditions attempted used DCM as a solvent once again, and 20 mol% of 2nd generation Hoveyda-Grubbs catalyst (**152**, **Figure 3.21**). However, 1 mL of a stock solution of DCM containing 10% lithium chloride (0.4M) in DMF was added to the reaction mixture to prevent any aggregation of the resin-bound peptide.[119] The reaction mixture was refluxed for 18 hours (Reaction number 3, **Table 3.1**). The LCMS of the crude reaction mixture showed mostly the uncyclised peptide (**27**), but following HPLC purification, a peak possibly corresponding to cyclised C=C stapled peptide (**128**) was seen in one of the fractions, as a mixture with the uncyclised peptide (**151**, **Figure 3.23**).

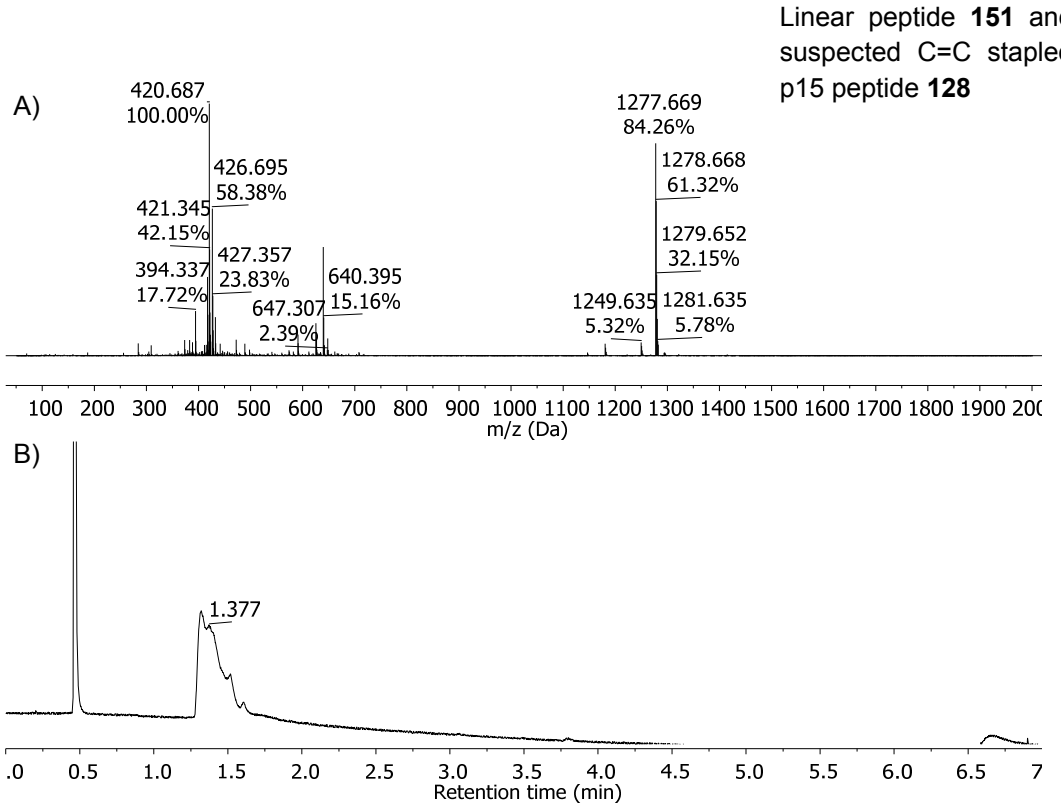

Figure 3.23 LCMS of the a HPLC fraction from reaction of allyl glycine-containing linear peptide (**150**) with Grubbs' RCM using 2nd generation Hoveyda Grubbs' catalyst, **152**, in DCM with lithium chloride as an additive, refluxed for 18 hours A) Mass spectrum of the HPLC fraction containing a peak corresponding to the uncyclised peptide (**151**), $[M + H]^+$ = 1278, and possible C=C stapled peptide (**128**), $[M + H]^+$ = 1250, corresponding to the peak at 1.38 minutes in the chromatogram. B) The chromatogram of the crude reaction mixture (detection at 280 nm).

The 2nd generation Hoveyda-Grubbs catalyst (**152**) is often preferred over 1st and 2nd Generation Grubbs catalysts because, although it is more expensive, it is also much less air and moisture sensitive.[120] However, the trade-off for this is a lower reactivity.[121] To find out if this was the reason for the failure of the reaction, several reactions were carried out: two using the 1st generation Grubbs catalyst (**153**, Reaction numbers 4 and 5, **Table 3.1**) and one using the 2nd generation Hoveyda-Grubbs catalyst (**152**) heated in DCE for 18 hours (Reaction number 6, **Table 3.1**). The conditions used for the reactions with the 1st generation catalysts were based on those described by Kim *et al*. in Nature Protocols.[89] The first reaction used 20 mol% 1st generation Grubbs catalyst in DCE and the reaction mixture was stirred at room temperature under nitrogen for two hours before a second addition of catalyst (20 mol% in DCE) and the reaction mixture stirred for a further two hours under nitrogen (Reaction number 4, **Table 3.1**). The second reaction followed the same steps except with an addition of 1 mL DCE containing 10% lithium chloride (0.4M) in DMF (Reaction number 5, **Table 3.1**). The LCMS of the resulting crude reaction mixtures showed, once again, only the linear peptide (**151**). The final reaction of this set used the 2nd generation Hoveyda-Grubbs catalyst (**152**) 20 mol% in DCE, the lithium chloride additive and was heated at 80 °C for 18 hours (Reaction number 6, **Table 3.1**). This set of conditions was chosen because DCE has a higher boiling point than DCM and so the reaction can be heated at a higher temperature, and this might be enough to force a reaction. The LCMS of the crude reaction mixture showed both the C=C stapled peptide, (**128**), and the uncyclised peptide (**151**, **Figure 3.24**).

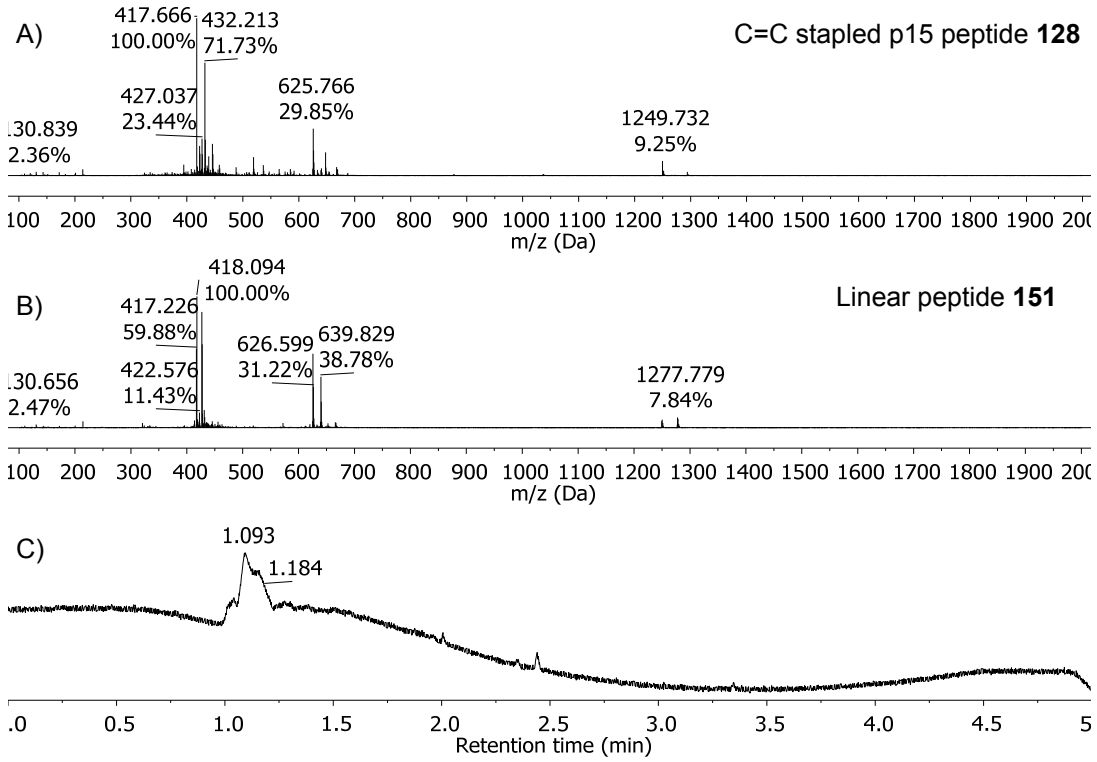

Figure 3.24 LCMS of the crude reaction mixture after reaction of allyl glycine-containing linear peptide (**150**) with Grubbs' RCM using 2nd generation Hoveyda Grubbs' catalyst (**152**) in DCE with lithium chloride as an additive, refluxed for 18 hours A) Mass spectrum fraction containing a peak corresponding to C=C stapled peptide (**128**), $[M + H]^+$ = 1250, corresponding to the peak at 1.09 minutes in the chromatogram. B) Mass spectrum fraction containing a peak corresponding to the uncyclised peptide (**151**), $[M + H]^+$ = 1278, corresponding to the peak at 1.18 minutes in the chromatogram. C) The chromatogram of the crude reaction mixture (detection at 280 nm).

Subsequent purification of the crude reaction mixture gave the C=C stapled peptide (**128**) in 12% yield. However, the reaction was only carried out on a 0.02 mmol scale, so further material was needed in order for binding assays and crystallisation studies to be carried out, and for further reaction to obtain the C-C stapled p15 peptide (**129**). The reaction was therefore repeated on a 0.1 mmol scale. However, this time yield of the C=C stapled peptide was only 5%. LCMS of the crude reaction mixture (**Figure 3.25**) and of HPLC fractions from the subsequent purification showed peaks in the mass spec of mass 1265 and 1293. These correspond to the C=C stapled and linear peptides with oxidised methionine (**154** and **155**). The methionine is likely to be oxidised in the cleavage by TFA. This can be reduced by the use of EDT as an additive during the cleave, as described in **Section 3.2.2**. The reaction was therefore carried out again using the same conditions, except with a second addition of catalyst solution after 24 hours of heating, followed by a further 24 hours of stirring at 80 °C.

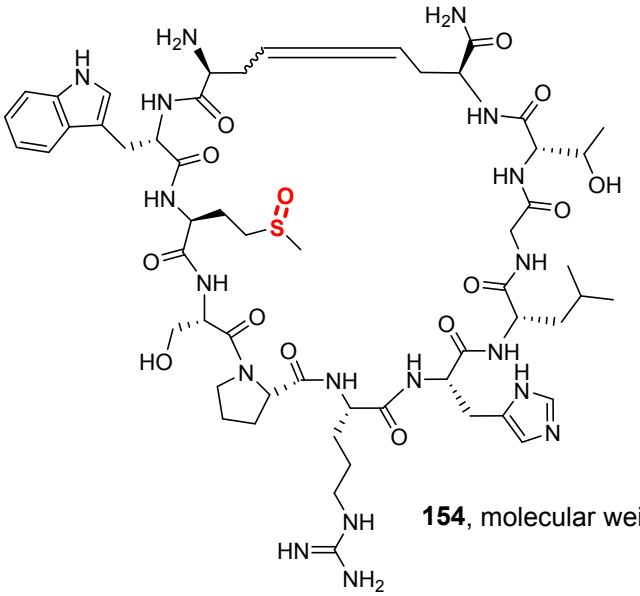

154, molecular weight: 1265.5

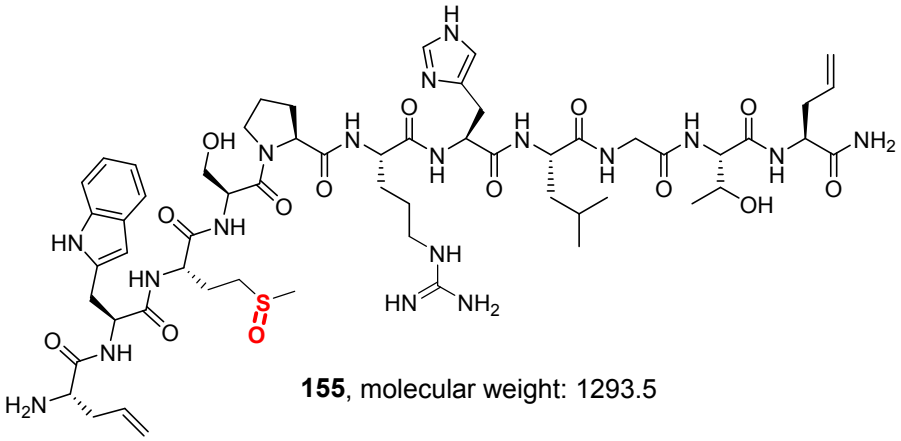

155, molecular weight: 1293.5

The peptide was cleaved from the resin using TFA:EDT:water:TIPS 94:2.5:2.5:1 and purified by HPLC. This time, no masses relating to methionine-oxidised side-products (**154** and **155**) were seen in the LCMS of any HPLC fractions. Furthermore, the yield was an improved 11%. The analytical HPLC trace of the purified C=C stapled p15 peptide is shown in **Figure 3.26**.

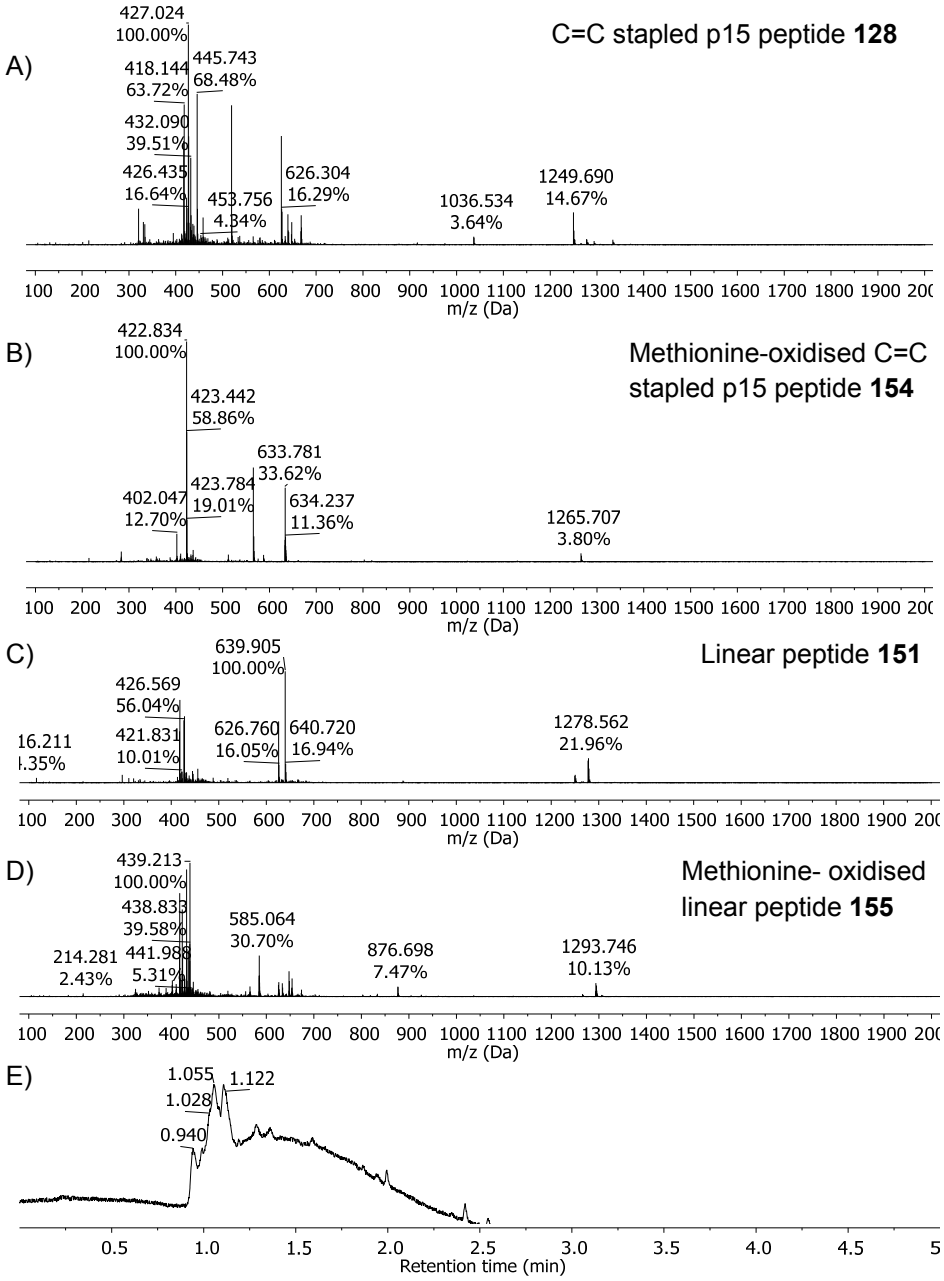

Figure 3.25 LCMS of the crude reaction mixture (0.1 mmol) after Grubbs' RCM using 2nd generation Hoveyda Grubbs' catalyst (**152**) in DCE with lithium chloride as an additive, refluxed for 18 hours. A) Mass spectrum fraction containing a peak corresponding to C=C stapled peptide **128**, $[M + H]^+$ = 1250, corresponding to the peak at 1.06 minutes in the chromatogram. B) Mass spectrum fraction containing a peak corresponding to the C=C stapled peptide with oxidised methionine **154**, $[M + H]^+$ = 1265, corresponding to the peak at 0.94 minutes in the chromatogram. C) Mass spectrum fraction containing a peak corresponding to uncyclised peptide **151**, $[M + H]^+$ = 1278, corresponding to the peak at 1.12 minutes in the chromatogram. D) Mass spectrum fraction containing a peak corresponding to the uncyclised peptide with oxidised methionine **155**, $[M + H]^+$ = 1293, corresponding to the peak at 1.03 minutes in the chromatogram. D) The chromatogram of the crude reaction mixture (detection at 280 nm).

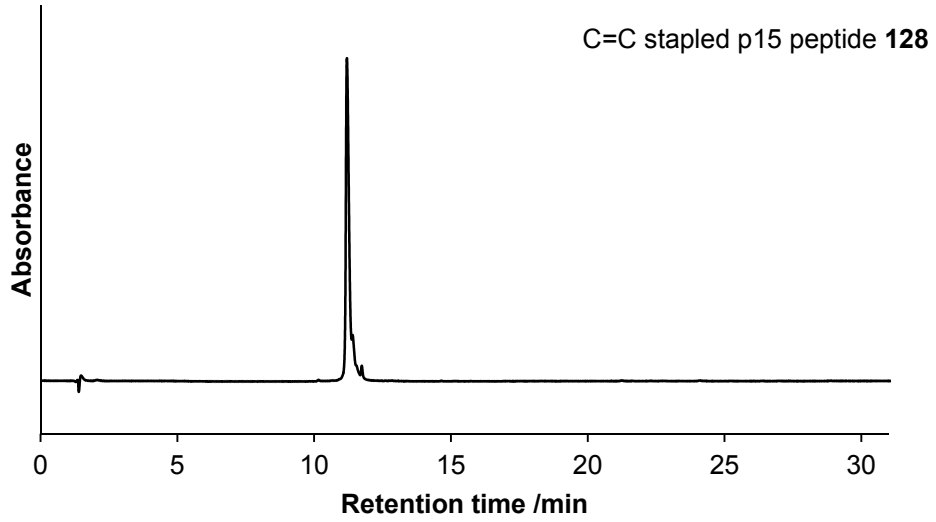

Figure 3.26 Analytical HPLC trace of purified C=C stapled p15 peptide (**128**), λ =280 nm.

3.6 Synthesis of the C-C stapled p15 peptide (129)

Having isolated the C=C stapled p15 peptide (**128**), the C-C stapled p15 peptide (**129**, **Figure 3.27**) was made.

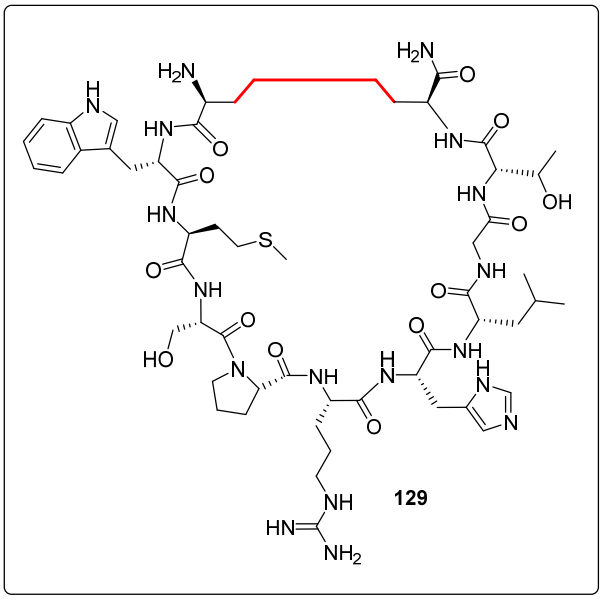

Figure 3.27 Target compound C-C stapled p15 peptide (**129**).

To a solution of 2 mg of the C=C stapled p15 peptide (**128**) in ethanol, palladium on carbon was added (**Scheme 3.22**). The mixture was stirred under a hydrogen atmosphere for two hours, after which LCMS analysis (**Figure 3.28**) showed complete hydrogenation of the double bond to give peptide **129** in a 50% yield without further purification.

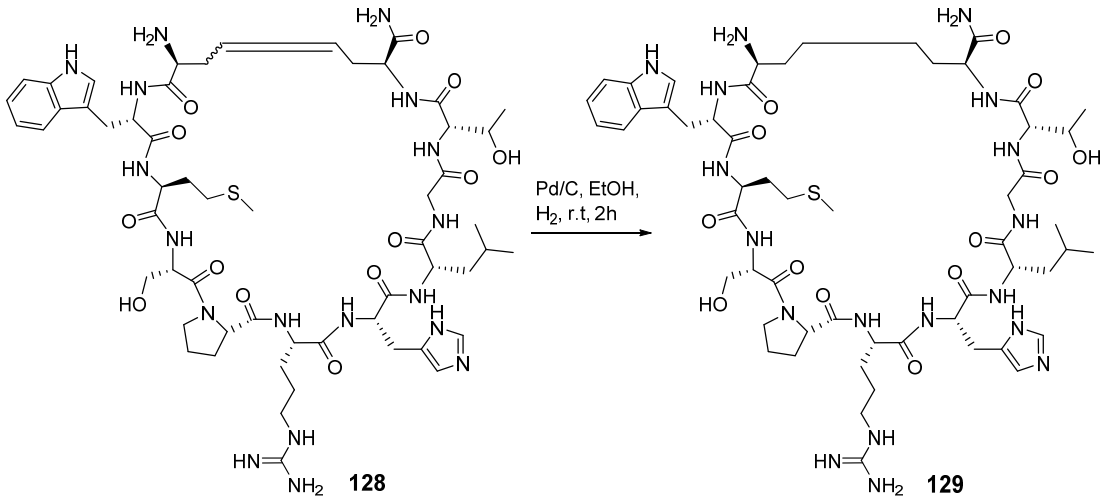

Scheme 3.22 Formation of C-C-p15 (**129**) by palladium-catalysed hydrogenation of C=C-p15, (**128**, 2mg).

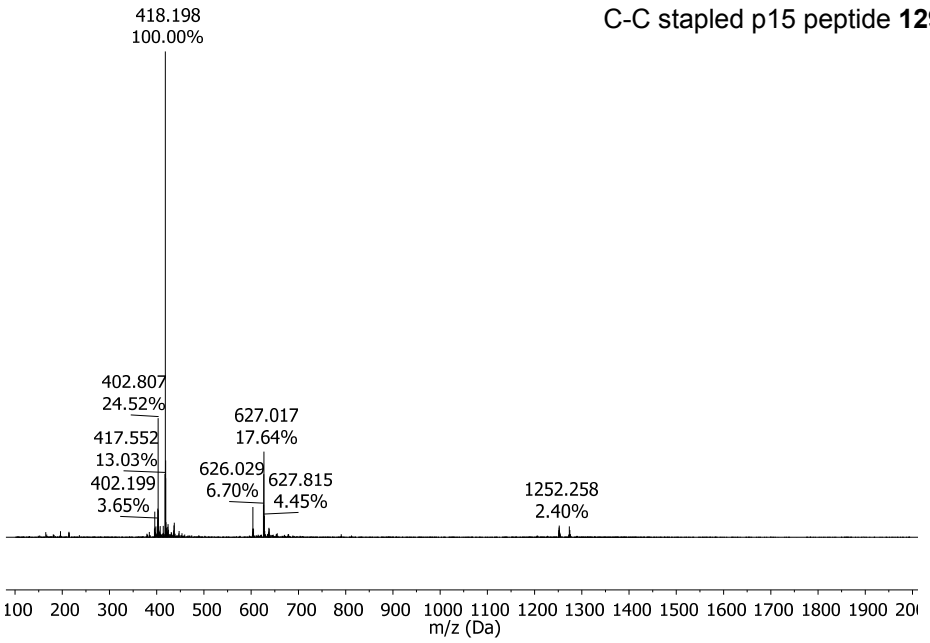

Figure 3.28 LCMS following hydrogenation of C=C-p15 (**128**) to form C-C-p15 (**5**) using conditions described in **Scheme 3.21**. Mass spectrum of C-C-p15 (**129**), $[M+H]^+$ = 1252.

An analytical HPLC trace of C-C stapled peptide (**Figure 3.29**) was obtained, and based on this, no further purification was carried out.

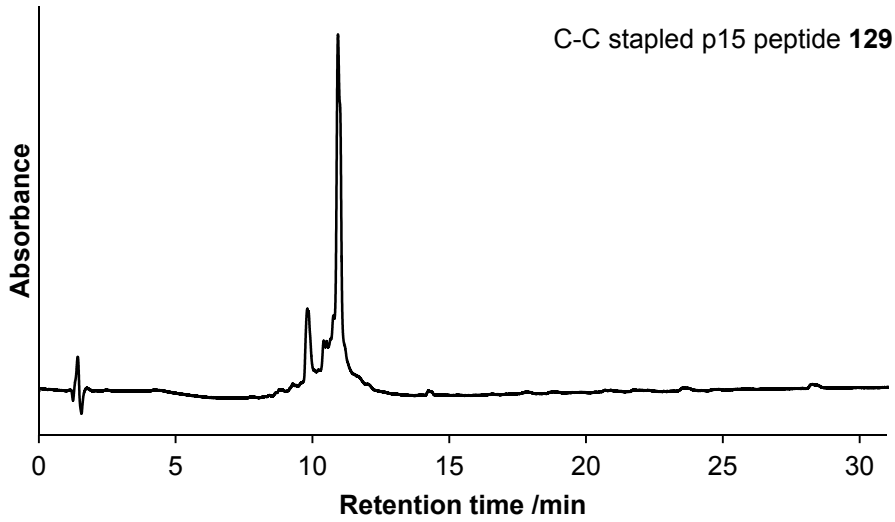

Figure 3.29 Analytical HPLC trace of C-C stapled p15 peptide (**129**), λ = 280 nm.

3.6 Binding assays

Having synthesised p15 (**126**) and three analogues, F-p15 (**127**), C=C-p15 (**128**) and C-C-p15 (**129**), we wanted to see whether the structural alterations affected the ability of the peptides to bind to the target protein, NPM1. Binding assays are being carried out by the Law group at The Hong Kong Polytechnic University and this work is still in progress. However, preliminary results from bio-layer interferometry (BLI) binding assays are shown in **Figure 3.30**. These results indicate that p15 (**126**) and C-C p15 (**129**) bind more strongly with NPM1 than F-p15 (**127**) and C=C p15 (**128**). This is as expected; C-C p15 (**129**) is the most structurally similar to p15 (**126**) of all the analogues we made, and so we would expect to see similar binding affinities. Work is ongoing in the Law lab to gain further information, such as dissociation constants for p15 (**126**) and each of the analogues made (**127** – **129**).

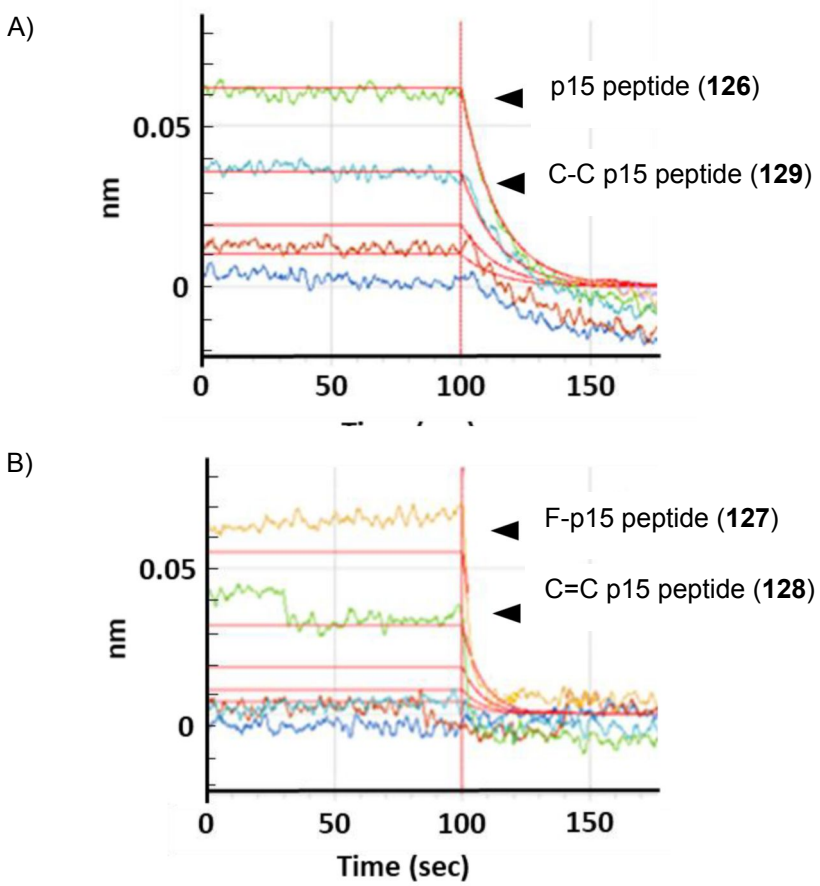

Figure 3.30 Results from BLI assays showing binding interactions between p15 and analogues and NPM1. A) Association (0 -100 seconds) followed by dissociation (from 100 seconds) observed between p15 (**126**) and NPM1 and C-C p15 (**129**) and NPM1. B) Association (0 -100 seconds) followed by dissociation (from 100 seconds) observed between F-p15 (**127**) and NPM1 and C-C p15 (**128**) and NPM1.

3.7 Crystallisation studies

Crystallisation of the four p15 analogues, p15 (**126**), F-p15 (**127**), C=C-p15 (**128**) and C-C-p15 (**129**) was attempted via screening of peptide solutions in water at concentrations shown in **Table 3.2**. Crystallisation was carried out on each peptide in isolation. Vapour diffusion conditions in the hanging drop format were set up manually using 2 μL of peptide solution per well in addition to 2μL of pre-prepared solutions for each set of conditions for the JCSG+ screen.[122] At the time of writing, no crystal structures had been obtained.

Table 3.2 Concentrations of peptides used in crystallisation studies

Peptide	Concentration/ mg/mL
p15 (**126**)	12
F-p15 (**127**)	10
C=C-p15 (**128**)	5
C-C-p15 (**129**)	0.4

3.8 Conclusions

The synthetic p15 peptide (**126**) and three analogues: F-p15 (**127**), C=C-p15 (**128**) and C-C-p15 (**129**) were successfully made and BLI binding assays were carried out by the Law lab at The Hong Kong Polytechnic University.

Where the first residue was cysteine (p15 and F-p15), linear peptides were synthesised on 2-chlorotrityl chloride to suppress base-induced elimination of the first cysteine residue (**Scheme 3.9**). For C=C p15 and C-C p15, the linear parent peptide had allylglycine as its first residue and Rink Amide resin was used since this is easier to handle than 2-chlorotrityl resin and base-induced elimination was not a problem for this peptide (**Scheme 3.20**).

Investigations into peptide cleavage conditions found that methionine was readily oxidised under standard 95% TFA conditions. However, methionine oxidation could be suppressed by the addition of EDT to the cleavage cocktail.

We used solid-phase cyclisation conditions to obtain p15 (**126**) and C=C-p15 (**128**), and solution-phase cyclisation conditions to obtain F-p15 (**3**). C-C-p15 (**129**) was obtained by hydrogenation of C=C-p15 (**128**). Solid-phase iodine oxidation conditions on Acm-protected cysteine were used to obtain cyclic p15 (**126**, **Scheme 3.15**) because reaction times are necessarily short (30 minutes – 2 hours, compared to 72 hours for air oxidation, **Scheme 3.13**, according to literature procedures).[80] However, iodine oxidation is inherently inefficient with a limited maximum achievable yield due to the propensity of side-reactions as a result of over oxidation. Accordingly the best isolated yield obtained was 19%.

Cyclisation of F-p15 (**127**) was carried out in solution on the fully deprotected peptide using a procedure based on methodology developed by previous work within the group (**Scheme 3.19**).[87] The best isolated yield achieved was 32%, however mono-substituted, uncyclised peptide (**148** and/or **149**), as well as the uncyclised parent peptide (**147**) could be seen in the LCMS suggesting that the low yield was a result of the reaction not going to completion.

Grubb's RCM was used to make C=C p15 (**128**) from the resin-bound allylglycine-containing linear parent peptide (**150**). Various reaction conditions were attempted including the use of Grubb's 1st Generation Catalyst (**153**) and Hoveyda-Grubb's 2nd Generation Catalyst (**152**), use of DCM and DCE as solvents, different reaction times and temperatures and the use of LiCl as an additive to prevent aggregation (**Table 3.1**). The most effective conditions were found to use the Hoveyda-Grubb's 2nd Generation Catalyst (**152**) in DCE with10% LiCl (0.4 M in DMF) for 48 hours at 80°C with a second addition of catalyst solution after 24 hours (**Scheme 3.21, Table 3.1**, Reaction number 7). This gave the purified C=C p15 peptide in 11% yield when EDT was used in the cleavage cocktail to suppress methionine oxidation.

Hydrogenation of C=C p15 (**128**) using Pd/C under a hydrogen atmosphere (**Scheme 3.22**) gave C-C p15 (**129**) in a 50% yield with no further purification after work up. Since only a small quantity of C=C p15 (**128**) was taken forward for the hydrogenation reaction, small losses of peptide in the work up translated into a large loss of yield.

Overall yields for each peptide were low with the best being 32% for F-p15 (**127**). However, little time was spent optimising the synthesis of any peptide since the main objective was to get sufficient amounts to use in binding assays and initial crystallisation screens. In this respect, we were successful for p15 (**126**), F-p15 (**127**) and C=C-p15 (**128**), having prepared enough to send to our collaborators to carry out

binding assays and also to run full crystallisation screens for each in the hanging drop format at recommended concentrations (between 5 and 40 mg/mL). However, the maximum concentration solution of C-C-p15 (**129**) we were able to make and use to carry out a full screen was very low and so failure to crystallise may be a result of this.

Preliminary results from BLI binding assays carried out by the Law lab at The Hong Kong Polytechnic University (**Figure 3.30**) showed that p15 (**126**) and C-C p15 (**129**) bound more strongly to NPM1 than F-p15 (**127**) and C=C p15 (**128**). Work is ongoing to obtain more information, such as dissociation constants, however, these results indicate that C-C p15 (**129**) has binding activity with NPM1 that is comparable to the anticancer peptide p15 (**126**) and therefore has the potential to be a more stable alternative.

3.9 References

1. J. K. Box, N. Paquet, M. N. Adams, D. Boucher, E. Bolderson, K. J. O'Byrne and D. J. Richard, *BMC Mol. Biol.*, 2016, **17**, 19.
2. H. Umekawa, J. H. Chang, J. J. Correia, D. Wang, P. T. Wingfield and M. O. Olson, *Cell Mol. Biol. Res.*, 1993, **39**.
3. M. J. Lim and X. W. Wang, *Cancer Detect. Prev.*, 2006, **30**.
4. A. Di Matteo, M. Franceschini, S. Chiarella, S. Rocchio, C. Travaglini-Allocatelli and L. Federici, *Oncotarget*, 2016, **7**, 44821-44840.
5. N. Huang, S. Negi, A. Szebeni and M. O. J. Olson, *J. Biol. Chem.*, 2005, **280**, 5496-5502.
6. J. Y. Ahn, X. Liu, D. Cheng, J. Peng, P. K. Chan, P. A. Wade and K. Ye, *Mol. Cell*, 2005, **18**.
7. R. S. Savkur and M. O. Olson, *Nuc. Acids Res.*, 1998, **26**, 4508-4515.
8. L. B. Maggi, Jr., M. Kuchenruether, D. Y. Dadey, R. M. Schwope, S. Grisendi, R. R. Townsend, P. P. Pandolfi and J. D. Weber, *Mol. Cell. Biol.*, 2008, **28**, 7050-7065.
9. A. Szebeni and M. O. J. Olson, *Protein Sci.*, 1999, **8**, 905-912.
10. M. Okuwaki, K. Matsumoto, M. Tsujimoto and K. Nagata, *FEBS Lett.*, 2001, **506**, 272-276.
11. M. Eitoku, L. Sato, T. Senda and M. Horikoshi, *Cell Mol. Life Sci.*, 2008, **65**, 414-444.
12. M. Okuda, *Oncogene*, 2002, **21**, 6170.
13. W. Wang, A. Budhu, M. Forgues and X. W. Wang, *Nat. Cell. Biol.*, 2005, **7**, 823.
14. J. E. Herrera, R. Savkur and M. O. Olson, *Nuc. Acids Res.*, 1995, **23**, 3974-3979.
15. K. Murano, M. Okuwaki, M. Hisaoka and K. Nagata, *Mol. Cell Biol.*, 2008, **28**, 3114-3126.
16. M. Poletto, L. Lirussi, D. M. Wilson and G. Tell, *Mol. Biol. Cell*, 2014, **25**, 1641-1652.
17. O. Ziv, A. Zeisel, N. Mirlas-Neisberg, U. Swain, R. Nevo, N. Ben-Chetrit, M. P. Martelli, R. Rossi, S. Schiesser, C. E. Canman, T. Carell, N. E. Geacintov, B. Falini, E. Domany and Z. Livneh, *Nat. Commun.*, 2014, **5**, 5437.
18. L. Federici and B. Falini, *Protein Sci.*, 2013, **22**, 545-556.
19. S. Grisendi, C. Mecucci, B. Falini and P. P. Pandolfi, *Nat. Rev. Cancer*, 2006, **6**, 493.
20. L. J. Frehlick, J. M. Eirín-López and J. Ausió, *BioEssays*, 2007, **29**, 49-59.
21. N. Meani and M. Alcalay, *Expert Rev. Anticancer Ther.*, 2009, **9**, 1283-1294.
22. T. Naoe, T. Suzuki, H. Kiyoi and T. Urano, *Cancer Sci.*, 2006, **97**, 963-969.

23. M. A. Larkin, G. Blackshields, N. P. Brown, R. Chenna, P. A. McGettigan, H. McWilliam, F. Valentin, I. M. Wallace, A. Wilm, R. Lopez, J. D. Thompson, T. J. Gibson and D. G. Higgins, *Bioinformatics*, 2007, **23**, 2947-2948.
24. K. Hingorani, A. Szebeni and M. O. Olson, *J. Biol. Chem.*, 2000, **275**.
25. M. Okuwaki, *J. Biochem.*, 2008, **143**.
26. H. H. Lee, H. S. Kim, J. Y. Kang, B. I. Lee, J. Y. Ha, H. J. Yoon, S. O. Lim, G. Jung and S. W. Suh, *Proteins*, 2007, **69**, 672-678.
27. D. M. Mitrea, C. R. Grace, M. Buljan, M.-K. Yun, N. J. Pytel, J. Satumba, A. Nourse, C.-G. Park, M. Madan Babu, S. W. White and R. W. Kriwacki, *Proc. Natl. Acad. Sci.*, 2014, **111**, 4466-4471.
28. M. D. Winn, C. C. Ballard, K. D. Cowtan, E. J. Dodson, P. Emsley, P. R. Evans, R. M. Keegan, E. B. Krissinel, A. G. W. Leslie, A. McCoy, S. J. McNicholas, G. N. Murshudov, N. S. Pannu, E. A. Potterton, H. R. Powell, R. J. Read, A. Vagin and K. S. Wilson, *Acta. Crystallogr. Sect. D*, 2011, **67**, 235-242.
29. E. Colombo, J. C. Marine, D. Danovi, B. Falini and P. G. Pelicci, *Nat. Cell Biol.*, 2002, **4**.
30. D. Marasco, A. Ruggiero, C. Vascotto, M. Poletto, P. L. Scognamiglio, G. Tell and L. Vitagliano, *Biochem. Biophys. Res. Commun.*, 2013, **430**, 523-528.
31. S. S. Negi and M. O. J. Olson, *J. Cell Sci.*, 2006, **119**, 3676-3685.
32. A. Koike, H. Nishikawa, W. Wu, Y. Okada, A. R. Venkitaraman and T. Ohta, *Cancer Res.*, 2010, **70**, 6746-6756.
33. A. Koike, H. Nishikawa, W. Wu, Y. Okada, A. R. Venkitaraman and T. Ohta, *Cancer Res.*, 2010, **70**.
34. S. S. Gadad, P. Senapati, S. H. Syed, R. E. Rajan, J. Shandilya, V. Swaminathan, S. Chatterjee, E. Colombo, S. Dimitrov, P. G. Pelicci, U. Ranga and T. K. Kundu, *Biochemistry*, 2011, **50**, 2780-2789.
35. M. W. Adkins and J. K. Tyler, *J. Biol. Chem.*, 2004, **279**, 52069-52074.
36. C. G. Grummitt, F. M. Townsley, C. M. Johnson, A. J. Warren and M. Bycroft, *J. Biol. Chem.*, 2008, **283**, 23326-23332.
37. B. Falini, N. Bolli, J. Shan, M. P. Martelli, A. Liso, A. Pucciarini, B. Bigerna, L. Pasqualucci, R. Mannucci, R. Rosati, P. Gorello, D. Diverio, G. Roti, E. Tiacci, G. Cazzaniga, A. Biondi, S. Schnittger, T. Haferlach, W. Hiddemann, M. F. Martelli, W. Gu, C. Mecucci and I. Nicoletti, *Blood*, 2006, **107**, 4514-4523.
38. A. Gallo, C. Lo Sterzo, M. Mori, A. Di Matteo, I. Bertini, L. Banci, M. Brunori and L. Federici, *J. Biol. Chem.*, 2012, **287**, 26539-26548.
39. Y. Zhu, M. Shi, H. Chen, J. Gu, J. Zhang, B. Shen, X. Deng, J. Xie, X. Zhan and C. Peng, *Oncotarget*, 2015, **6**, 21443-21451.
40. J. P. Yun, J. Miao, G. G. Chen, Q. H. Tian, C. Q. Zhang, J. Xiang, J. Fu and P. B. S. Lai, *Br. J. Cancer*, 2007, **96**, 477.
41. L. Léotoing, L. Meunier, M. Manin, C. Mauduit, M. Decaussin, G. Verrijdt, F. Claessens, M. Benahmed, G. Veyssière, L. Morel and C. Beaudoin, *Oncogene*, 2007, **27**, 2858.
42. A. Pianta, C. Puppin, A. Franzoni, D. Fabbro, C. Di Loreto, S. Bulotta, M. Deganuto, I. Paron, G. Tell, E. Puxeddu, S. Filetti, D. Russo and G. Damante, *Biochem. Biophys. Res. Commun.*, 2010, **397**, 499-504.
43. J. Chen, J. Sun, L. Yang, Y. Yan, W. Shi, J. Shi, Q. Huang, J. Chen and Q. Lan, *Biochem. Biophys. Res. Commun.*, 2015, **466**, 124-130.
44. K. Holmberg Olausson, T. Elsir, K. Moazemi Goudarzi, M. Nistér and M. S. Lindström, *Sci. Rep.*, 2015, **5**, 16495.
45. Y. Nozawa, N. Van Belzen, A. C. J. Van Der Made, W. N. M. Dinjens and F. T. Bosman, *J. Pathol.*, 1996, **178**, 48-52.
46. B. Y. Yung, *Chang Gung Med. J.*, 2007, **30**, 285-293.
47. E. Colombo, M. Alcalay and P. G. Pelicci, *Oncogene*, 2011, **30**, 2595.
48. P. Roussel and D. Hernandez-Verdun, *Exp. Cell Res.*, 1994, **214**, 465-472.
49. M. Poletto, M. C. Malfatti, D. Dorjsuren, P. L. Scognamiglio, D. Marasco, C. Vascotto, A. Jadhav, D. J. Maloney, D. M. Wilson, A. Simeonov and G. Tell, *Mol. Carcinog.*, 2016, **55**, 688-704.
50. M. S. Lindström, *Biochem. Res. Int.*, 2011, **2011**, 195209.
51. C. Korgaonkar, J. Hagen, V. Tompkins, A. A. Frazier, C. Allamargot, F. W. Quelle and D. E. Quelle, *Mol. Cell. Biol.*, 2005, **25**.
52. K. Itahana, K. P. Bhat, A. Jin, Y. Itahana, D. Hawke, R. Kobayashi and Y. Zhang, *Mol. Cell*, 2003, **12**, 1151-1164.

53. F. X. Qin, H. Y. Shao, X. C. Chen, S. Tan, H. J. Zhang, Z. Y. Miao, L. Wang, C. Hui and L. Zhang, *Int. J. Med. Sci.*, 2011, **8**, 287-294.
54. E. Colombo, P. Martinelli, R. Zamponi, D. C. Shing, P. Bonetti, L. Luzi, S. Volorio, L. Bernard, G. Pruneri and M. Alcalay, *Cancer Res.*, 2006, **66**.
55. A. Efeyan and M. Serrano, *Cell Cycle*, 2007, **6**, 1006-1010.
56. P. Chène, *Nat. Rev. Cancer*, 2003, **3**, 102.
57. M. J. Lim and X. W. Wang, *Cancer Detect. Prev.*, 2006, **30**, 481-490.
58. P. R. Karhemo, A. Rivinoja, J. Lundin, M. Hyvonen, A. Chernenko, J. Lammi, H. Sihto, M. Lundin, P. Heikkila, H. Joensuu, P. Bono and P. Laakkonen, *Am. J. Pathol.*, 2011, **179**, 1004-1014.
59. E. M. Heath, S. M. Chan, M. D. Minden, T. Murphy, L. I. Shlush and A. D. Schimmer, *Leukemia*, 2017, **31**, 798.
60. B. Falini, C. Mecucci, E. Tiacci, M. Alcalay, R. Rosati, L. Pasqualucci, R. Starza, D. Diverio, E. Colombo and A. Santucci, *N. Engl. J. Med.*, 2005, **352**.
61. J. W. Vardiman, J. Thiele, D. A. Arber, R. D. Brunning, M. J. Borowitz, A. Porwit, N. L. Harris, M. M. Beau, E. Hellstrom-Lindberg and A. Tefferi, *Blood*, 2009, **114**.
62. A. De Cola, L. Pietrangelo, F. Forlì, D. Barcaroli, M. C. Budani, V. Graziano, F. Protasi, C. Di Ilio, V. De Laurenzi and L. Federici, *Cell Death Dis.*, 2014, **5**, e1427.
63. K. Cheng, P. Sportoletti, K. Ito, J. G. Clohessy, J. Teruya-Feldstein, J. L. Kutok and P. P. Pandolfi, *Blood*, 2010, **115**.
64. G. S. Vassiliou, J. L. Cooper, R. Rad, J. Li, S. Rice, A. Uren, L. Rad, P. Ellis, R. Andrews and R. Banerjee, *Nat. Genet.*, 2011, **43**.
65. E. Colombo, P. Martinelli, R. Zamponi, D. C. Shing, P. Bonetti, L. Luzi, S. Volorio, L. Bernard, G. Pruneri, M. Alcalay and P. G. Pelicci, *Cancer Res.*, 2006, **66**, 3044-3050.
66. P. Bonetti, T. Davoli, C. Sironi, B. Amati, P. G. Pelicci and E. Colombo, *J. Cell Biol.*, 2008, **182**, 19-26.
67. C. Di Natale, P. L. Scognamiglio, R. Cascella, C. Cecchi, A. Russo, M. Leone, A. Penco, A. Relini, L. Federici, A. Di Matteo, F. Chiti, L. Vitagliano and D. Marasco, *FASEB J.*, 2015, **29**, 3689-3701.
68. S. Morris, M. Kirstein, M. Valentine, K. Dittmer, D. Shapiro, D. Saltman and A. Look, *Science*, 1994, **263**, 1281-1284.
69. J. Duyster, R. Y. Bai and S. W. Morris, *Oncogene*, 2001, **20**.
70. R. L. Redner, E. A. Rush, S. Faas, W. A. Rudert and S. J. Corey, *Blood*, 1996, **87**.
71. K. Okazuka, M. Masuko, Y. Seki, H. Hama, N. Honma, T. Furukawa, K. Toba, K. Kishi and Y. Aizawa, *Int. J. Hematol.*, 2007, **86**, 246-249.
72. W. Qi, K. Shakalya, A. Stejskal, A. Goldman, S. Beeck, L. Cooke and D. Mahadevan, *Oncogene*, 2008, **27**, 4210.
73. H. J. Chan, J. J. Weng and B. Y. Yung, *Biochem. Biophys. Res. Commun.*, 2005, **333**, 396-403.
74. A. Szebeni, J. E. Herrera and M. O. Olson, *Biochemistry*, 1995, **34**, 8037-8042.
75. S. Chiarella, A. De Cola, G. L. Scaglione, E. Carletti, V. Graziano, D. Barcaroli, C. Lo Sterzo, A. Di Matteo, C. Di Ilio, B. Falini, A. Arcovito, V. De Laurenzi and L. Federici, *Nuc. Acids Res.*, 2013, **41**, 3228-3239.
76. H. Mukherjee, K.-P. Chan, V. Andresen, M. L. Hanley, B. T. Gjertsen and A. G. Myers, *ACS Chem. Biol.*, 2015, **10**, 855-863.
77. S. Yi, L. Wen, J. He, Y. Wang, F. Zhao, J. Zhao, Z. Zhao, G. Cui and Y. Chen, *Ann. Hematol.*, 2015, **94**, 201-210.
78. H. T. Chi, B. T. Ly, H. A. Vu, Y. Sato, P. C. Dung and P. T. Xinh, *Asian Pac. J. Trop. Biomed.*, 2014, **4**, 570-574.
79. Y. Perera, H. G. Farina, J. Gil, A. Rodriguez, F. Benavent, L. Castellanos, R. E. Gómez, B. E. Acevedo, D. F. Alonso and S. E. Perea, *Mol. Cancer Ther.*, 2009, **8**, 1189-1196.
80. S. E. Perea, O. Reyes, Y. Puchades, O. Mendoza, N. S. Vispo, I. Torrens, A. Santos, R. Silva, B. Acevedo, E. López, V. Falcón and D. F. Alonso, *Cancer Res.*, 2004, **64**, 7127-7129.
81. J. H. Trembley, G. Wang, G. Unger, J. Slaton and K. Ahmed, *Cell Mol. Life Sci.*, 2009, **66**, 1858-1867.
82. M. Ruzzene and L. A. Pinna, *Biochim. Biophys. Acta*, 2010, **1804**, 499-504.
83. A. Szebeni, K. Hingorani, S. Negi and M. O. J. Olson, *J. Biol. Chem.*, 2003, **278**, 9107-9115.

84. Y. Perera, N. D. Toro, L. Gorovaya, J. Fernandez-De-Cossio, H. G. Farina and S. E. Perea, *Molecular and clinical oncology*, 2014, **2**, 935-944.
85. A. M. Solares, A. Santana, I. Baladrón, C. Valenzuela, C. A. González, A. Díaz, D. Castillo, T. Ramos, R. Gómez, D. F. Alonso, L. Herrera, H. Sigman, S. E. Perea, B. E. Acevedo and P. López-Saura, *BMC cancer*, 2009, **9**, 146.
86. M. R. Sarduy, I. García, M. A. Coca, A. Perera, L. A. Torres, C. M. Valenzuela, I. Baladrón, M. Solares, V. Reyes, I. Hernández, Y. Perera, Y. M. Martínez, L. Molina, Y. M. González, J. A. Ancízar, A. Prats, L. González, C. A. Casacó, B. E. Acevedo, P. A. López-Saura, D. F. Alonso, R. Gómez and S. E. Perea-Rodríguez, *Br. J. Cancer*, 2015, **112**, 1636.
87. D. Gimenez, C. A. Mooney, A. Dose, G. Sandford, C. R. Coxon and S. L. Cobb, *Org. Biomol. Chem.*, 2017, **15**, 4086-4095.
88. H. E. Blackwell, J. D. Sadowsky, R. J. Howard, J. N. Sampson, J. A. Chao, W. E. Steinmetz, D. J. O'Leary and R. H. Grubbs, *J. Org. Chem.*, 2001, **66**, 5291-5302.
89. Y.-W. Kim, T. N. Grossmann and G. L. Verdine, *Nat. Protoc.*, 2011, **6**, 761.
90. Y. H. Lau, P. de Andrade, Y. Wu and D. R. Spring, *Chem. Soc. Rev.*, 2015, **44**, 91-102.
91. R. B. Merrifield, *J. Am. Chem. Soc.*, 1963, **85**, 2149-2154.
92. J. Lukszo, D. Patterson, F. Albericio and S. A. Kates, *Lett. Pept. Sci.*, 1996, **3**, 157-166.
93. Y. Han, F. Albericio and G. Barany, *J. Org. Chem.*, 1997, **62**, 4307-4312.
94. Y. M. Angell, J. Alsina, G. Barany and F. Albericio, *J. Pept. Res.*, 2002, **60**, 292-299.
95. S. A. Palasek, Z. J. Cox and J. M. Collins, *J. Pept. Sci.*, 2007, **13**, 143-148.
96. H. Hibino and Y. Nishiuchi, *Tetrahedron Lett.*, 2011, **52**, 4947-4949.
97. M. Mergler, F. Dick, B. Sax, J. Schwindling and T. Vorherr, *J. Pept. Sci.*, 2001, **7**, 502-510.
98. H. Huang and D. L. Rabenstein, *J. Pept. Res.*, 1999, **53**, 548-553.
99. C. P. R. Hackenberger, *Org. Biomol. Chem.*, 2006, **4**, 2291-2295.
100. D. S. King, C. G. Fields and G. B. Fields, *Int. J. Pept. Protein. Res.*, 1990, **36**, 255-266.
101. E. Atherton, R. C. Sheppard and P. Ward, *J. Chem. Soc., Perkin Trans. 1*, 1985, DOI: 10.1039/P19850002065, 2065-2073.
102. A. StierandovÁ, N. F. Sepetov, G. V. Nikiforovich and M. Lebl, *Int. J. Pept. Protein. Res.*, 1994, **43**, 31-38.
103. C. G. Fields and G. B. Fields, *Tetrahedron Lett.*, 1993, **34**, 6661-6664.
104. A. Isidro-Llobet, M. Álvarez and F. Albericio, *Chem. Rev.*, 2009, **109**, 2455-2504.
105. S. F. Betz, *Protein Sci.*, 1993, **2**, 1551-1558.
106. N. Darby and T. E. Creighton, in *Protein Stability and Folding: Theory and Practice*, ed. B. A. Shirley, Humana Press, Totowa, NJ, 1995, DOI: 10.1385/0-89603-301-5:219, pp. 219-252.
107. V. T. Maulik, S. L. Jennifer and J. S. Teruna, *Curr. Protein Pept. Sci.*, 2009, **10**, 614-625.
108. T. M. Postma and F. Albericio, *Eur. J. Org. Chem.*, 2014, **2014**, 3519-3530.
109. L. Chen, I. Annis and G. Barany, in *Current Protocols in Protein Science*, John Wiley & Sons, Inc., 2001, DOI: 10.1002/0471140864.ps1806s23.
110. Y. Yang, W. V. Sweeney, K. Schneider, B. T. Chait and J. P. Tam, *Protein Sci.*, 1994, **3**, 1267-1275.
111. E. Calce, R. M. Vitale, A. Scaloni, P. Amodeo and S. De Luca, *Amino Acids*, 2015, **47**, 1507-1515.
112. T. M. Postma and F. Albericio, *Org. Lett.*, 2013, **15**, 616-619.
113. P. Sieber, B. Kamber, B. Riniker and W. Rittel, *Helv. Chim. Acta*, 1980, **63**, 2358-2363.
114. H. Lamthanh, C. Roumestand, C. Deprun and A. MÉNez, *Int. J. Pept. Protein. Res.*, 1993, **41**, 85-95.
115. D. G. Simonsen, *J. Biol. Chem.*, 1933, **101**, 35-42.
116. O. M. Ogba, N. C. Warner, D. J. O'Leary and R. H. Grubbs, *Chem. Soc. Rev.*, 2018, Advance Article.
117. S. B. Garber, J. S. Kingsbury, B. L. Gray and A. H. Hoveyda, *J. Am.Chem.Soc.,* 2000, **122**, 8168-8179.
118. P. Schwab, M. B. France, J. W. Ziller and R. H. Grubbs, *Angew. Chem. Int. Ed. Engl.*, 1995, **34**, 2039-2041.
119. A. N. Whelan, J. Elaridi, R. J. Mulder, A. J. Robinson and W. R. Jackson, *Can. J. Chem.*, 2005, **83**, 875-881.

120. S. H. Hong, A. G. Wenzel, T. T. Salguero, M. W. Day and R. H. Grubbs, *J. Am. Chem. Soc.*, 2007, **129**, 7961-7968.
121. K. Jarzembska, S. Seal, K. Woźniak, A. Szadkowska, M. Bieniek and K. Grela, *ChemCatChem*, 2009, **1**, 144-151.
122. J. Newman, D. Egan, T. S. Walter, R. Meged, I. Berry, M. Ben Jelloul, J. L. Sussman, D. I. Stuart and A. Perrakis, *Acta. Crystallogr. Sect. D*, 2005, **61**, 1426-1431.

Chapter 4

Peptide-Peptoid hybrids

4.1 Cell-penetrating peptoids

In **Chapter 1**, **Section 1.2.1** we briefly described the features of cell-penetrating peptoids: similar to cell-penetrating peptides, they are short (~12 residues) and amphiphilic. Whilst many cell-penetrating peptides have been reported and used as transporters for therapeutics, such as in CIGB-300 (**125**, see **Chapter 3**), research into cell-penetrating peptoids is still in its infancy and there are no reports on their use in the transport of biologically active cargo.

Several peptoids have already been synthesised that show promising cell permeability and, in some cases, the ability to localise in different organelle. Kölmel et al synthesised a library of short peptoids (4 residues, **156** – **161**) containing cationic lysine side chains. Each peptoid was tagged with Rhodamine B, which fluoresces red, in order to visualise the location of the peptoids within the cell.[1]

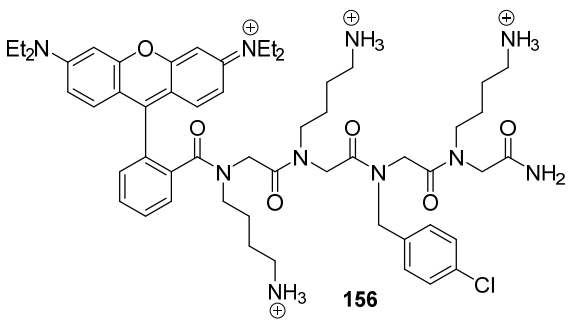

156

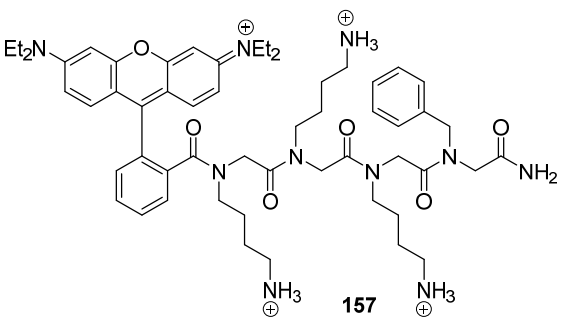

157

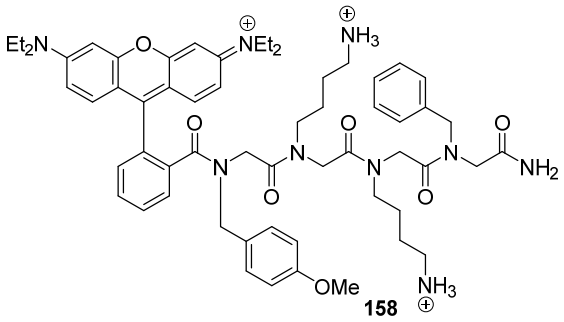

158

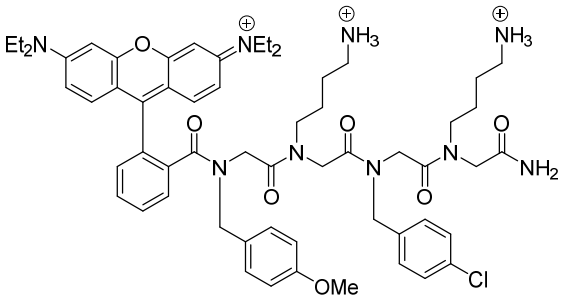

159

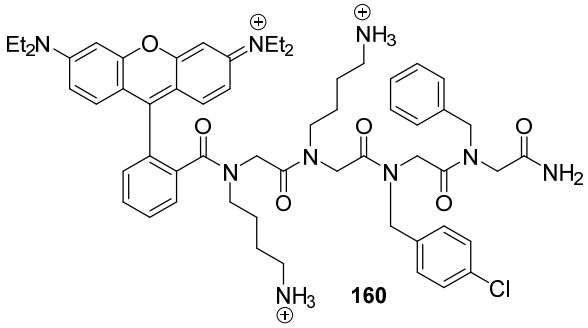

160

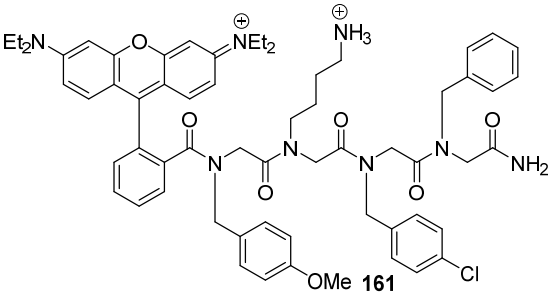

161

The peptoids were then incubated with HeLa cells at 37°C for 24 hours. The nucleus and mitochondria were co-stained with dyes that fluoresce at different wavelengths (the nucleus was stained with Hoechst 33342 which fluoresced blue and the mitochondria stained with 100 nM Mitochondria Green™ which fluoresced green). When all three dyes were excited together, it was possible to see whether the peptoids had entered the nucleus or the mitochondria. All peptoids, to some degree, showed up in the nucleus, but of particular interest were the peptoids that also entered the mitochondria, two examples of which (**159** and **161**) are shown in **Figure 4.1**. Mitochondria are involved in many metabolic and pathological processes and thus are attractive therapeutic targets.[2-4]

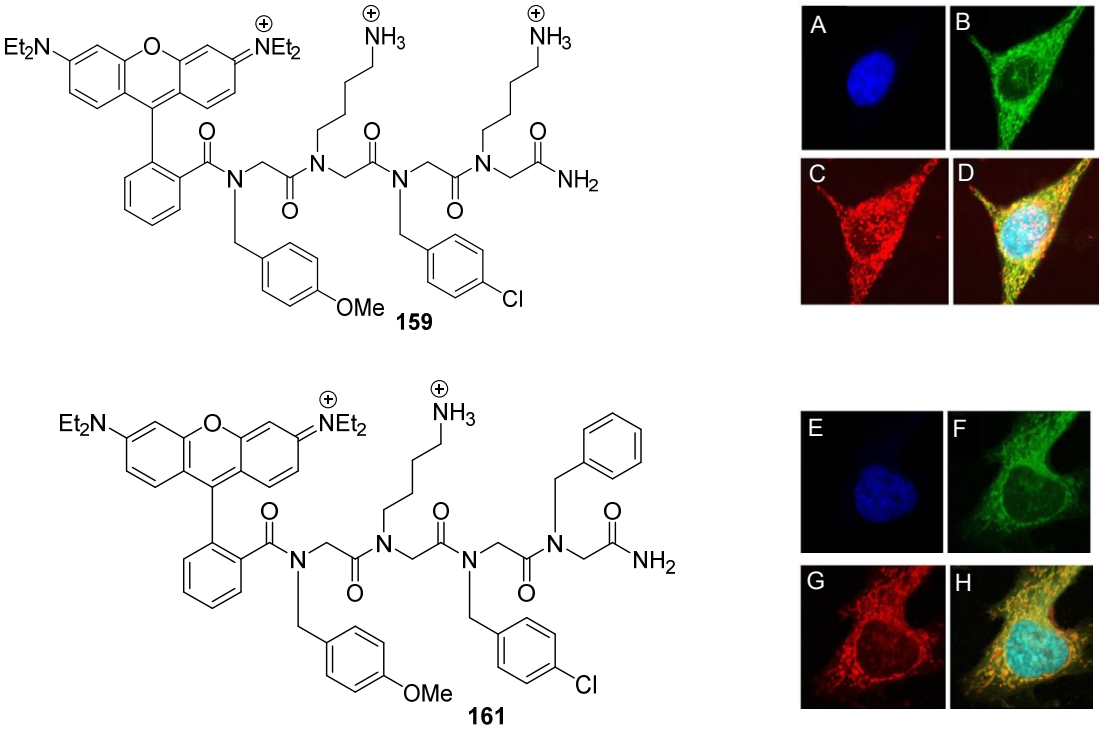

Figure 4.1 Peptoids **159** and **161** were able to enter mitochondria of HeLa cells. The nuclei are stained blue with Hoechst 33342 (A and E), mitochondria are stained green with 100 nm Mitochondria Green (B and F), peptoids are red as are result of the Rhodamine B tag (C and G). D and H are merges of the respective emission channels to highlight co-localisation of the peptoids in the mitochondria or nuclei. Microscopy images adapted from Kölmel *et al*., *Pharmaceuticals*, 2012.[1]

This was followed up with the synthesis of further cell penetrating peptoids. The peptoids were, again, short (6 residues). However, in this paper, they incorporated side chain functionality by copper-catalysed alkyne azide cycloaddition (CuAAC, **Scheme 4.1**).[5]

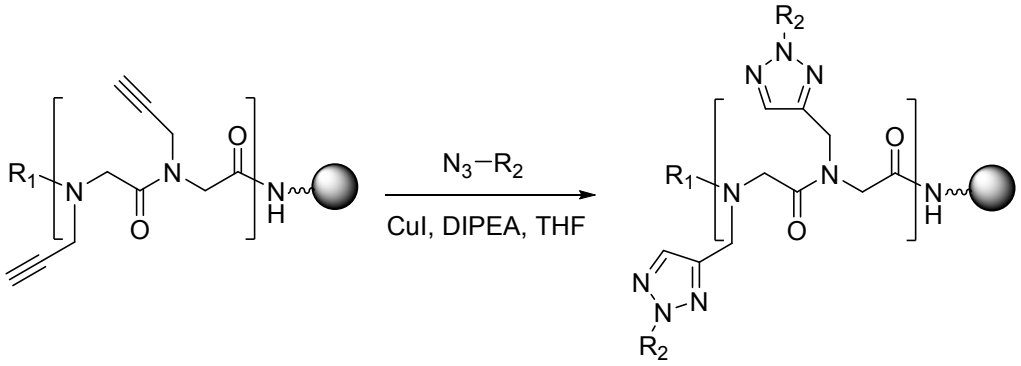

Scheme 4.1 Copper catalysed alkyne azide cycloaddition as a way of incorporating different functionalities into peptoids.

In this method, the peptoid backbone chain is synthesised using the sub-monomer method, but the amine used contains an alkyne. Once the peptoid chain has been made to the desired length, the alkyne group or groups can be reacted, still on resin, with an azide via click chemistry.

Two different R groups may be incorporated if one of the alkyne building blocks is protected by TIPS. The group made four peptoids; two of which had hydrophilic side chains, **162** and **163** and two of which were amphiphilic, **164** and **165** (**Figure 4.2**). Uptake was investigated once again by confocal microscopy. The hydrophilic peptoids showed internalisation in HeLa cell nuclei, followed by accumulation in the endosomal compartments and release into the cytosol over 24 hours.

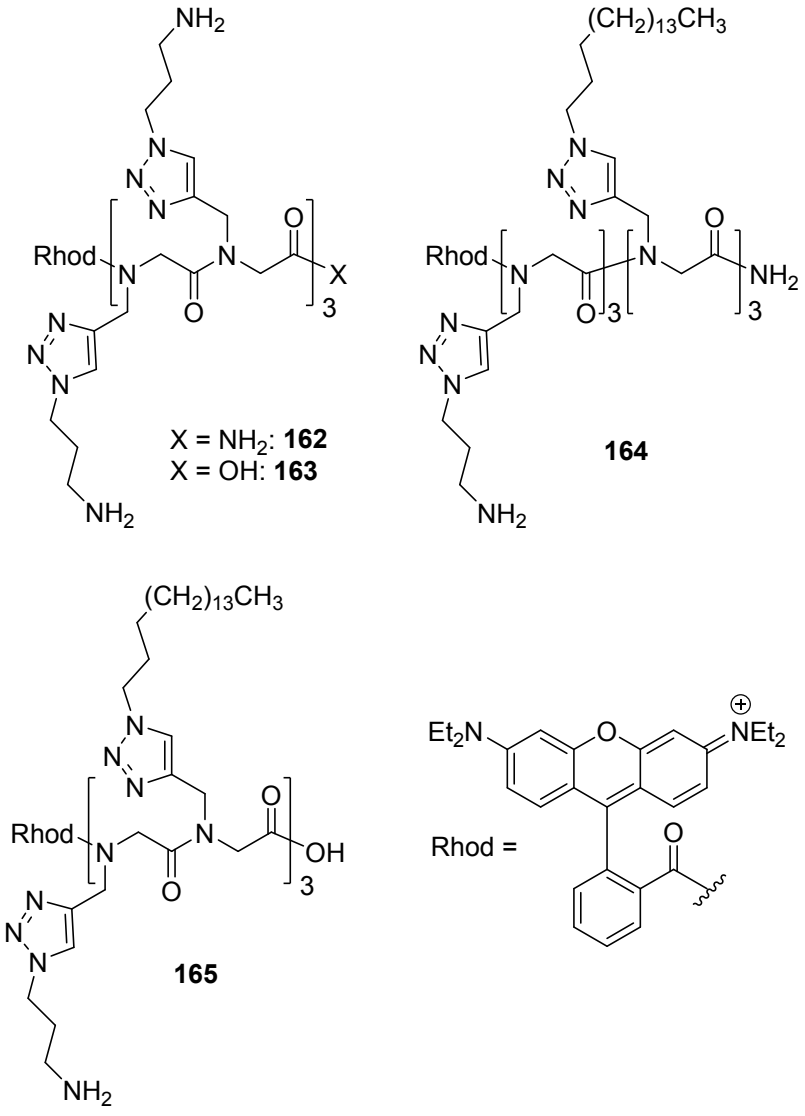

Figure 4.2 Structures of cell-penetrating peptoids made using CuAAC by S. B. L. Vollrath *et al.*

The amphiphilic peptoids, **164** and **165** showed an increase in cellular uptake and intracellular distribution when cellular fluorescence from the confocal images was quantified using Leica LASAF software. These results showed that, first, the triazole group did not hinder the cell penetrating ability of the peptoids, second that whether the terminal group was an amide or an acid made little difference, and third, that an overall lower net positive charge allowed for effective internalisation. The reason for this has not yet been established, though it could be due to an amphiphilic structural motif. Studies seem to indicate that a helical conformation with an overall positive charge is necessary for internalisation of some cell-penetrating peptoids,[6] so it is possible that amphiphilic peptoids more readily adopt the favoured helical conformation.

CuAAC was also used in a study in 2014 to incorporate novel cationic side chains into hexameric peptoids (**166** – **170**) and these peptoids were found to localise either in endosomal compartments or, in one case, the cytosol itself.[7]

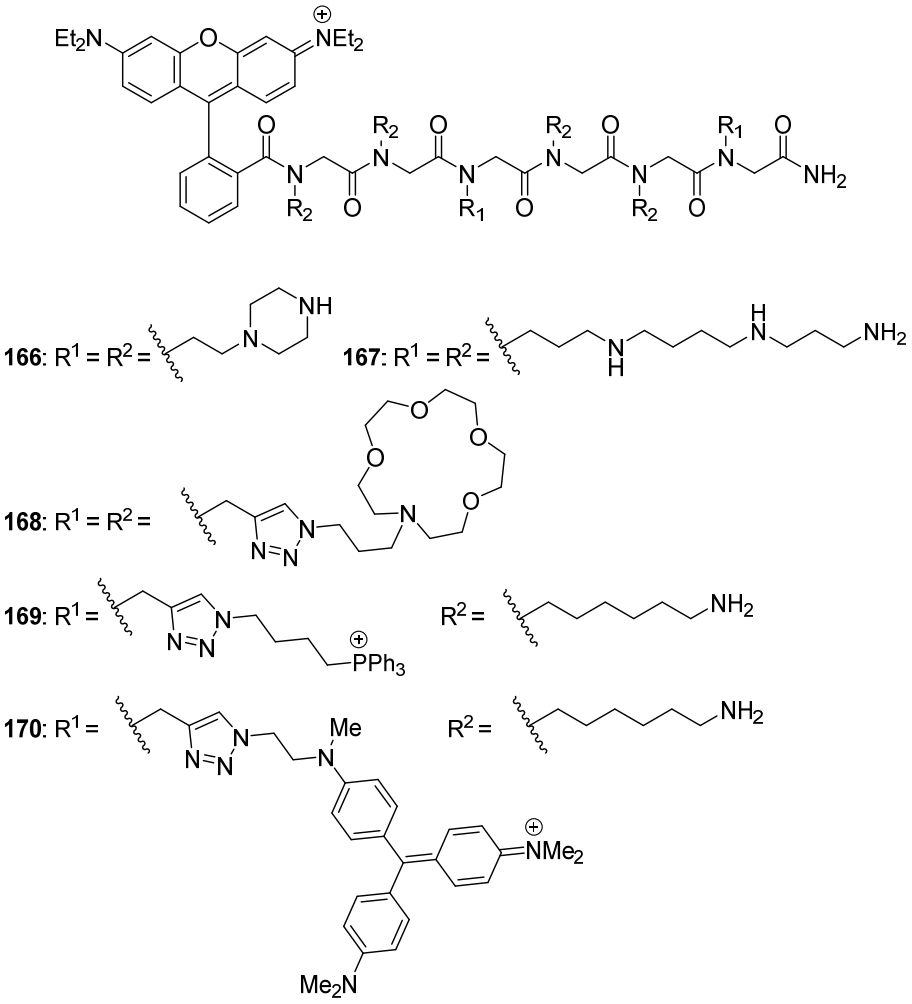

Figure 4.3 Structure of cell penetrating peptoids containing novel cationic side chains.

The cationic side chains incorporated were chosen for their high charge density, containing multiple amino functionalities, a quaternary ammonium salt or a triphenylphosphonium salt (**Figure 4.3**). As in the 2012 study, the peptoids were incubated with HeLa cells at 37°C for 24 hours and subsequently subjected to confocal microscopy. It was found that peptoid **167** accumulated in the cytosol of the HeLa cells whilst peptoids **166** and **168** – **170** accumulated exclusively in vesicles, thought to be endosomal in nature. It is suspected that the reason for peptoid **167** localising in the cytosol is due to the presence of the multiple amine groups in the side chains, resulting in greater positive charge density, enabling peptoid **167** to overcome endosomal entrapment. This is supported by the observation that monomeric to tetrameric analogues of peptoid **167** also accumulated in vesicles.

Huang *et al.* also synthesised a library of cell penetrating peptoids to investigate their cell permeability. The peptoids synthesised were amphipathic and contained either an *N*-lysine or *N*-guanidine side chain as the source of positive charge with 5(6)-carboxyfluorescein (CF) tagged on the end. CF-$(Arg)_8$-NH_2 and a polyguanide peptoid CF-$(Nbtg)_8$-NH_2 (see **Figure 4.4** for key to abbreviations) were included as comparators. Four peptoids consisted of repeating units of three residues to form one 9-mer and eight 12-mers and two more peptoids were 12-mers consisting of four hydrophobic residues and eight *N*Lys residues (**Table 4.1**).[8]

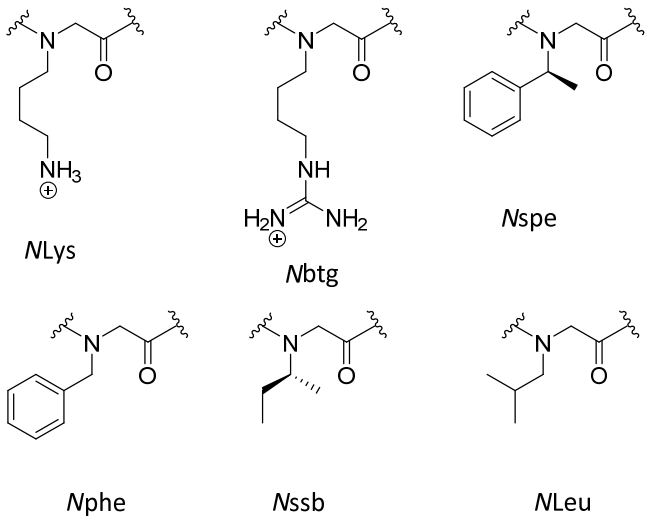

Figure 4.4 Peptoid monomer side-chain structures and abbreviations

Table 4.1 Library of polyguanidine cell penetrating peptoids.[8]

Group	Compound number	Sequence
Polyguanidine comparators	**171**	CF-$(Arg)_8$-NH_2
	172	CF-$(N\text{btg})_8$-NH_2
*N*Lys(1/3) variants	**173**	CF-$(N\text{Lys}\text{-}N\text{spe}\text{-}N\text{spe})_3$-$NH_2$
	174	CF-$(N\text{Lys}\text{-}N\text{spe}\text{-}N\text{spe})_4$-$NH_2$
	175	CF-$(N\text{Lys}\text{-}N\text{phe}\text{-}N\text{phe})_4$-$NH_2$
	176	CF-$(N\text{Lys}\text{-}N\text{ssb}\text{-}N\text{ssb})_4$-$NH_2$
*N*Lys(2/3) variants	**177**	CF-$(N\text{Lys}\text{-}N\text{Lys}\text{-}N\text{spe})_4$-$NH_2$
	178	CF-$(N\text{Lys})_8$-$(N\text{spe})_4$-NH_2
	179	CF-$(N\text{Lys})_8$-$(N\text{Leu})_4$-NH_2
Guanidylated variants	**180**	CF-$(N\text{btg}\text{-}N\text{spe}\text{-}N\text{spe})_4$-$NH_2$
	181	CF-$(N\text{btg}\text{-}N\text{btg}\text{-}N\text{spe})_4$-$NH_2$

Cell uptake was measured by mean fluorescence arising from the 5(6)-carboxyfluorescein. Important results from this study were that cellular uptake and cytotoxicity of peptoid chains containing the non-aromatic residues *N*ssb and *N*Leu (**176** and **179**) was much lower compared to peptoid chains containing aromatic residues *N*pm and *N*spe (**173**, **174**, **178**, **179**, **180** and **181**). Additionally, the cellular uptake and cytotoxicity of the 9-mer was considerably decreased compared to the analogous 12-mer. The chiral *N*spe group also displayed better cellular uptake and higher cytotoxicity compared to the non-chiral *N*pm group.

It is also important to control the ratio of hydrophobic residues to cationic residues with the best results coming from peptoids with two hydrophobic residues to every one cationic residue. Finally, guanidylation had no effect on cell penetration where there was only one cationic side chain to two hydrophobic side chains (compare **19** and **25**) but where there were two cationic side chains to one hydrophobic side chain (compare **177** and **181**) guanidylation dramatically increased cell uptake and cytotoxicity, i.e **181** showed increased cell penetration compared to **177**. The two peptoids that showed the

most efficient cell penetration were **174** and **181** with **181** being slightly less cytotoxic (**Figure 4.5**).

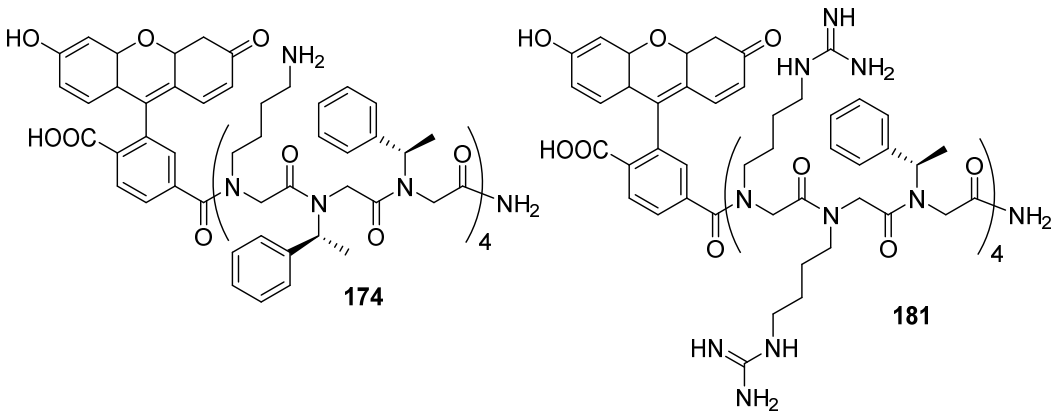

Figure 4.5 Structures of the two peptoids which showed the best cell-penetration (**174** and **181**) according to the 2012 Huang *et al.* study.

These findings can be rationalised; the *N*btg group gives more penetrating peptoids due to stronger membrane interactions by the guanidinium heads[9] whilst the chiral aromatic hydrophobic groups induce formation of an alpha helix, further favouring membrane interactions and promoting internalisation. In terms of the intracellular distribution of the peptoids, the comparators CF-$(Arg)_8$-NH_2 and CF-$(N\text{btg})_8$-NH_2 (**171** and **172**) showed distinctly different behaviour in comparison to two of the peptoids with the best cellular uptake (**174** and **181**). For all three peptoids looked at, cellular uptake gradually increased with incubation time whilst for CF-$(Arg)_8$-NH_2 (**171**) the maximum uptake was reached at around four hours after which there was a marked decrease in uptake. This is consistent with degradation of the peptide contributing further evidence of the comparatively superior stability of peptoids. However, both comparators (**171** and **172**) had a much more diffuse distribution compared to the other two peptoids; the comparators showed a much more uniform distribution and were found throughout the cells whereas the other two peptoids were found mainly or solely in the cytosol.

The mechanism of peptoid internalisation is not currently known, however it is widely believed that both energy-dependent endocytosis and energy-independent direct translocation are involved.[10] As a final part of the above study, the incubation temperature was lowered to 4°C and the effect on peptoid internalisation was investigated. The uptake of **174** was greatly reduced as was the uptake of **181**, although the latter still showed considerable uptake, indicating that the mechanism of internalisation was either energy-dependent or very sensitive to membrane fluidity. To

compare, CF-$(Arg)_8$-NH_2 (**171**) and CF-$(N\text{btg})_8$-NH_2 (**172**) showed markedly different behaviour; uptake was not reduced at 4°C, in fact the uptake of CF-$(Arg)_8$-NH_2 (**171**) was even higher at 4°C, indicating a different mechanism of uptake compared to the other two peptoids.[8] Finally, it should be noted that with all of these studies, the fluorescent labels are small. The results described in these papers therefore give no indication of the level of uptake or the distribution of cell-penetrating peptoids conjugated to larger cargo.

In 2017, Marouseau *et al*. designed a guanidine rich peptoid motif (**182**) and the cell-penetrating ability of these peptoids investigated by flow cytometry. The cell-penetrating ability of these novel peptoid scaffolds was compared to polyaminated peptoids (**183**), benzyl peptoids (**184**) and polyguanidine comparators (**185**, **Figure 4.6**).[11]

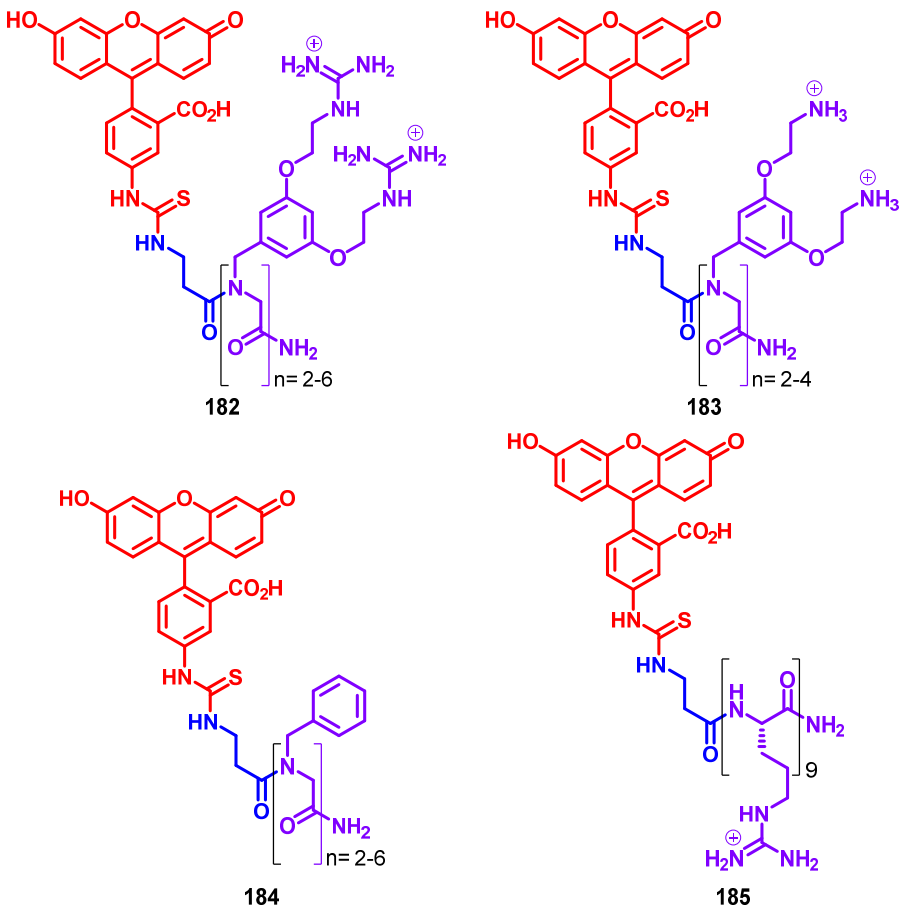

Figure 4.6 Structures of the guanidine-rich peptoids (**182**), polyaminated peptoids (**183**), benzyl peptoids (**184**) and polyguanidine comparators (**185**) whose cell-penetrating ability was investigated by flow cytometry. Each set of compounds has a modular structure consisting of a fluorophore (red), β-alanine spacer (blue) and peptoid or peptide chain (purple).

It was found that the polyaminated peptoids (**183**) up to n = 4 and benzyl peptoids (**184**) up to n = 6 showed no significant cell penetration when compared to a blank control. However, the guanidine-rich peptoids (**182**) reached a maximal uptake when n = 4 of 80% of the polyguanidine comparator (**185**). This showed that the backbone and fluorophore were not responsible for cell uptake, but that the presence of the guanidine groups was key to cell-penetration for these peptoid motifs.

4.1.2 Aims

In this chapter, we describe the synthesis of a series of peptide-peptoid chimeras using a selection of the short cell-penetrating peptoids described by Kölmel *et al*.[1] as transporters for biologically active peptides. The first peptide we will use is the anticancer KLA peptide (**186**, **Figure 4.7**) which induces apoptosis by targeting mitochondrial membranes.[12, 13] As previously discussed, Kölmel *et al*. synthesised a series of short, cell-penetrating peptoids which were shown to localise in mitochondria. It is envisaged that conjugation of the KLA peptide onto these cell-penetrating peptoids will result in an effective anticancer agent.

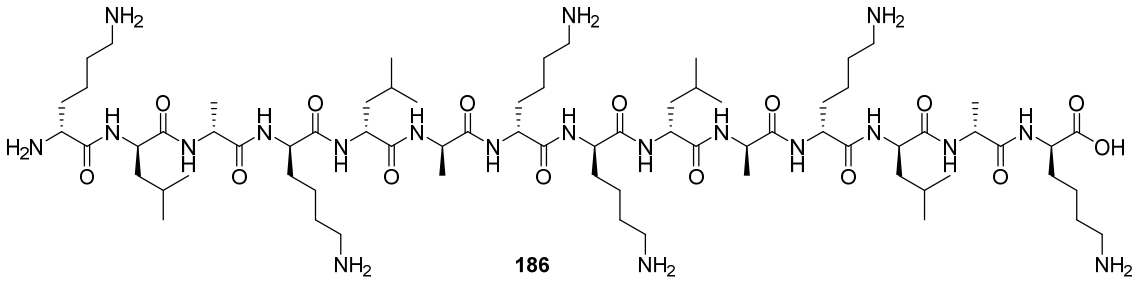

186

Figure 4.7 Structure of the anticancer KLA peptide (**186**).

The second peptide we will use is the p15 peptide (**126**, **Figure 4.8**), which we discussed in **Chapter 3**.

As previously discussed in **Chapter 3**, the p15 peptide (**126**) is the active domain of the anticancer peptide CIGB-300 (**Figure 4.8**). It targets NPM1 which is localised in the nucleolus.[14] However, the active p15 peptide is not cell-penetrating and therefore, on its own, will show no anticancer activity. For this reason, the p15 peptide is conjugated to a TAT sequence (hence p15-TAT).[15] TAT is a cell-penetrating peptide derived from HIV with a sequence GRKKRRQRRRPPQ and the sequence of p15-TAT, or CIGB-300 is GRKKRRQRRRPPQ-β-ala-CWMSPRHLGTC.[16] The TAT sequence can be taken up by cells and localised in the nucleus. The mechanism of cell-uptake is disputed and appears at least partly dependent on the properties of the attached cargo, for example,

its size, the linkage between peptide and cargo and orientation of the peptide relative to the cargo.[17]

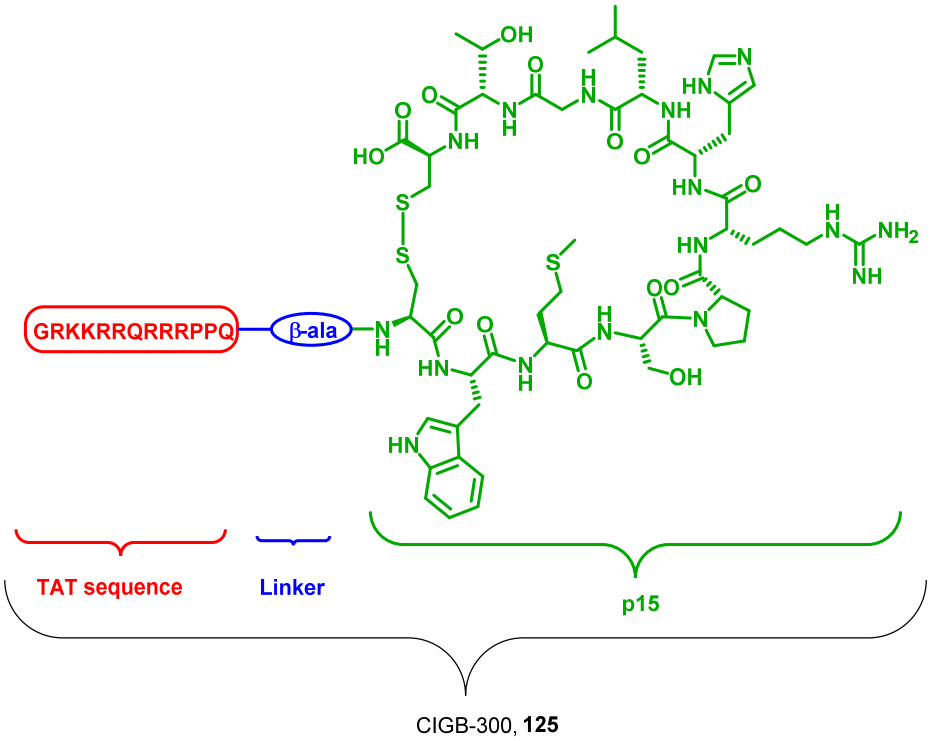

Figure 4.8 Structure of anticancer peptide CIGB-300 (**125**). The active, cyclic peptide, p15, is highlighted in green. The active peptide is attached to cell-penetrating peptide derived from the HIV-Tat protein, highlighted in red, with a β-alanine linker, highlighted in blue.

Whilst the TAT sequence is clearly successful at delivering the active p15 peptide to cancerous cells, as demonstrated by success in clinical trials in human patients with cervical cancer, it will encounter the same problems *in vivo* as any other peptide as a result of susceptibility to proteolytic degradation. Administration of CIGB-300 in all clinical trials has been by injection directly into cervical malignancies.[18, 19] **Chapter 3** detailed our attempts to improve the stability of the active p15 peptide via replacement of the disulphide bridge with different linkages. In this chapter, we will investigate more proteolytically stable alternatives to TAT. Improving the stability of both the active peptide and its cell-penetrating domain could allow it to be used to treat forms of cancer where the tumours are less accessible and local injection unfeasible. Peptoids may offer a proteolyitically stable alternative to the TAT sequence. The short, cell-penetrating peptoids synthesised by Kölmel *et al*. were shown to localise in the nucleus to various extents, although nucleolar localisation was not investigated. We will,

therefore synthesise a series of p15-peptoid hybrids to investigate their anticancer properties.

4.2 Synthesis of the peptide-peptoid hybrids

The peptide-peptoid hybrids we will make will have a modular design consisting of the cell-penetrating peptoid, active peptide (KLA, **186** or p15, **126**) and luminescent probe, with spacers between the peptoid, peptide and, for the p15 hybrids, the probe as well (**Figure 4.9**). The spacer between the peptoid and peptide is two glycine residues and the spacer between the peptide and probe is derived from 5-hexynoic acid. Our compounds are configured in this way because we wanted to have the luminescent probe at an end of the sequence but attached to the active peptide. If the conjugate was configured as follows: peptide-peptoid-probe, presence of the probe would only show localisation of the cell penetrating peptoid whilst the active peptide could have degraded or detached from the peptoid. The colours of the different components in **Figure 4.9** will also be used to represent the different components of our structures, i.e. the cell-penetrating peptoid will be purple, spacers will be blue, the active peptide will be green and the imaging component will be red.

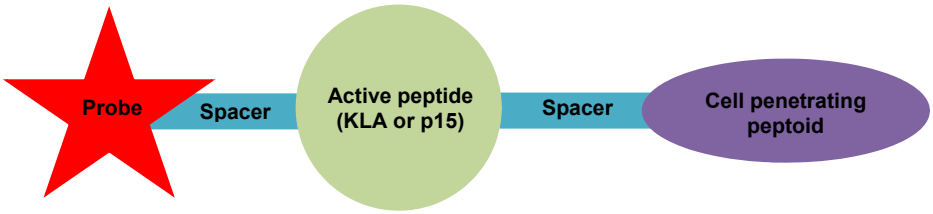

Figure 4.9 Structure of our peptide-peptoid conjugates.

4.3 KLA peptide-peptoids

4.3.1 The KLA sequence as an anti-cancer peptide

The KLA peptide (**186**) has been widely studied for its anticancer properties. It was initially designed as an antimicrobial peptide and subsequently found to induce apoptosis by targeting mitochondrial membranes.[20, 21] The KLA peptide has a sequence of $_{D}$(KLAKKLAK)$_2$, **186**.

The KLA peptide (**186**) has a cationic α-helical amphipathic structure, and it is this that enables interaction with the mitochondrial membranes[22] and induces subsequent permeation and mitochondrial swelling. This triggers the release of cytochrome c and cell apoptosis.[23, 24]

As with the p15 peptide (**126**), KLA suffers from poor cell-penetrating ability and thus has been conjugated to various targeting moieties in an attempt to deliver the peptide into cells more efficiently.[22] Examples of such delivery vehicles include cell-penetrating peptides,[12, 13, 23, 25, 26] nanoparticles[27-29] and cyclic peptides.[30] Whilst conjugation of KLA with these compounds improves drug delivery, there are downsides such as the ease of conjugation and stability of the targeting moiety. Cell-penetrating peptoids provide a more proteolytically stable alternative. Kölmel *et al*. synthesised a library of short cell-penetrating peptoids, some of which localised in the mitochondria.[1] These peptoids are therefore suitable candidates for the delivery of the KLA peptide. Furthermore, since KLA consists of D-amino acids, it is far more stable to proteolytic degradation than peptides made of naturally occurring L-amino acids. Therefore, a KLA-peptoid conjugate is expected to be proteolytically stable than a KLA-peptide conjugate.

4.3.2 The KLA peptide-peptoids

(*Note: Peptide synthesis and purification was carried out by Jingyi Zong at Durham University*)

Initially, six cell-penetrating peptoids with two terminal glycine residues as spacers (**187** – **192**) were made. This glycine 'spacer' was included to minimise steric interactions between the peptoid and the peptide and to prevent interference of the peptoid in the KLA peptide's anticancer activity.

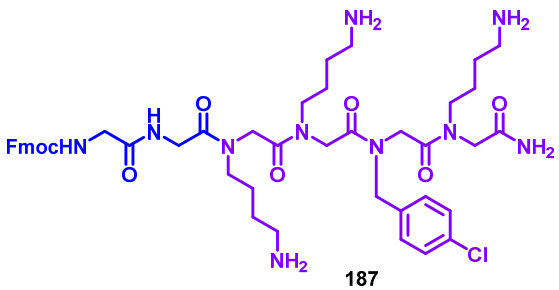

187

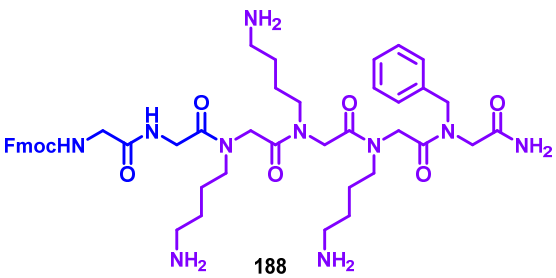

188

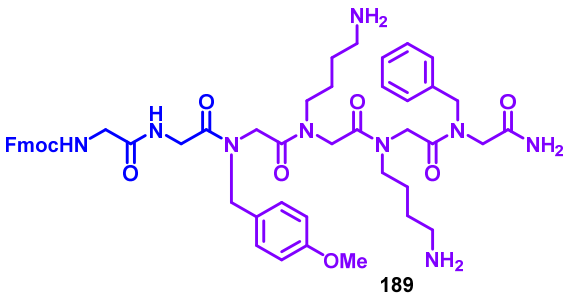

189

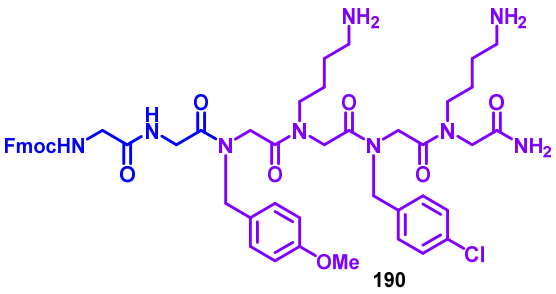

190

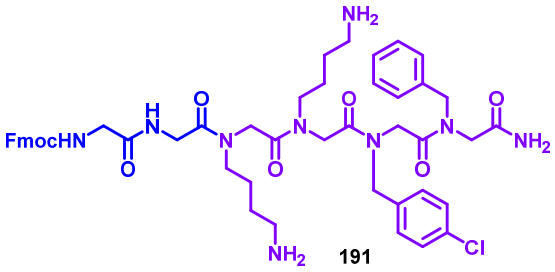

191

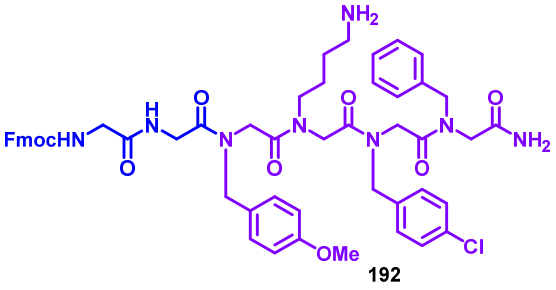

192

On to these peptoids, the KLA sequence was built to give six KLA-peptoid hybrids (**193** – **198**). The D-KLA-amide (**199**) was also made for use as a reference to which the activity of the KLA-peptoid hybrids could be compared.

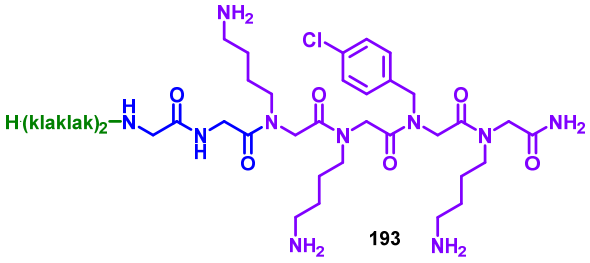

193

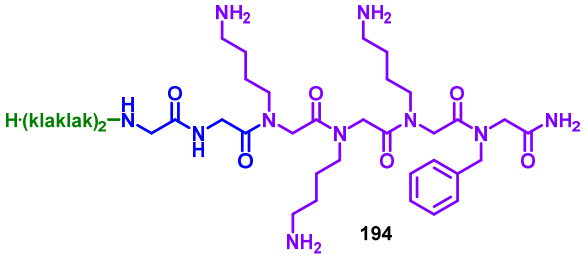

194

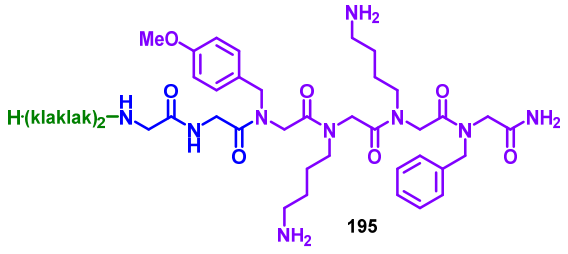

195

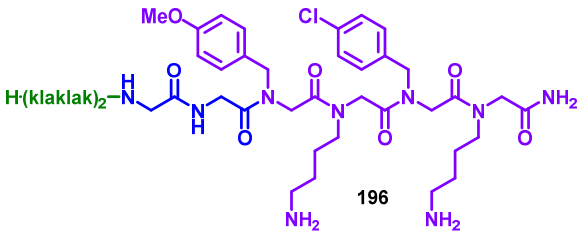

196

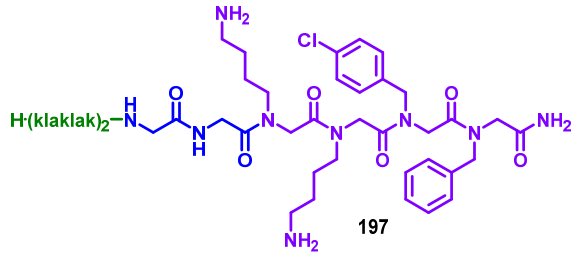

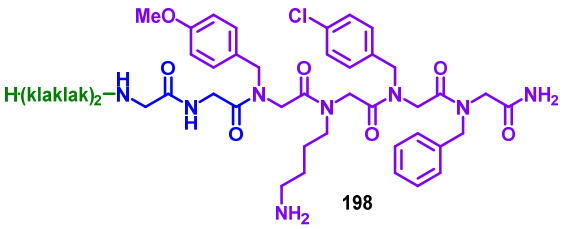

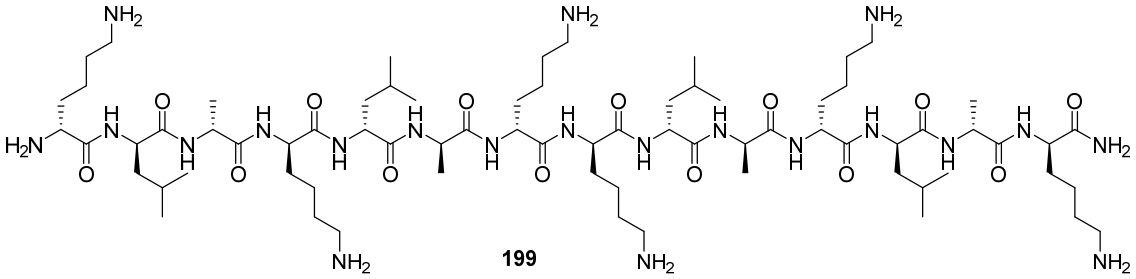

The KLA-peptoid hybrids were made by first synthesising the cell penetrating peptoids onto Rink Amide resin *via* the sub-monomer method (**Scheme 4.2**. Then a spacer consisting of two glycine units was attached to the end via solid-phase peptide synthesis (SPPS) conditions (see **Table 4.2** for a summary of the peptoids made). At this point a test cleave was carried out in order to confirm successful peptoid synthesis by LCMS analysis (**Figure 4.10** shows the LCMS and chromatogram of peptoid-GG **33**). Finally, the KLA sequence was built onto the resin-bound peptoid-spacer using SPPS conditions (**Scheme 4.2**). The peptide-peptoid hybrids were then cleaved from the resin using 95% TFA (**Scheme 4.2**) and analysed by ESI LCMS, MALDI, accurate mass and analytical HPLC. **Table 4.3** shows the peptoid-peptide hybrids made and their MALDI data. Following purification by HPLC, the cytotoxicity of the peptide-peptoid hybrids (**193** – **198**), as well as the free D-KLA amide (**199**), was tested against HeLa cells.

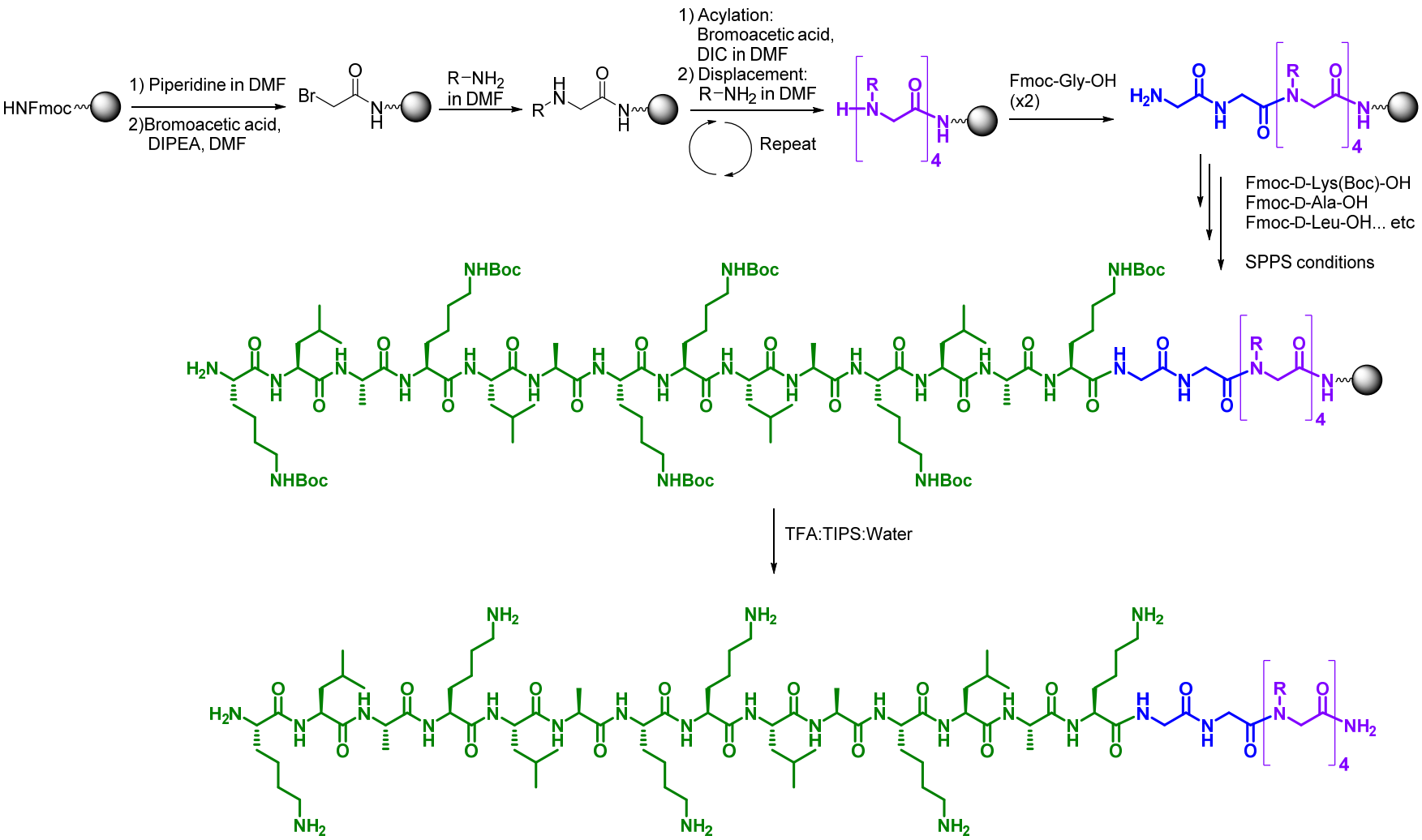

Scheme 4.2 Approach to building linear KLA-peptide hybrids

Table 4.2 List of cell-penetrating peptoids with glycine spacers synthesised

Name	Sequence	Molecular weight	Observed mass
CPPo1 (**187**)	Fmoc-GG-*N*lys*N*lys*N*pcb*N*lys-NH_2	919.52	920.8 = $[M+H]^+$
CPPo2 (**188**)	Fmoc-GG-*N*lys*N*lys*N*lys*N*phe-NH_2	885.08	886.0 = $[M + H]^+$
CPPo3 (**189**)	Fmoc-GG-*N*pmb*N*lys*N*lys*N*phe-NH_2	934.11	935.0 = $[M + H]^+$
CPPo4 (**190**)	Fmoc- GG-*N*pmb*N*lys*N*pcb*N*lys-NH_2	968.55	969.5 = $[M + H]^+$
CPPo5 (**191**)	Fmoc- GG-*N*lys*N*lys*N*pcb*N*phe-NH_2	938.52	939.9 = $[M + H]^+$
CPPo6 (**192**)	Fmoc- GG-*N*pmb*N*lys*N*pcb*N*phe-NH_2	987.55	988.3 = $[M + H]^+$

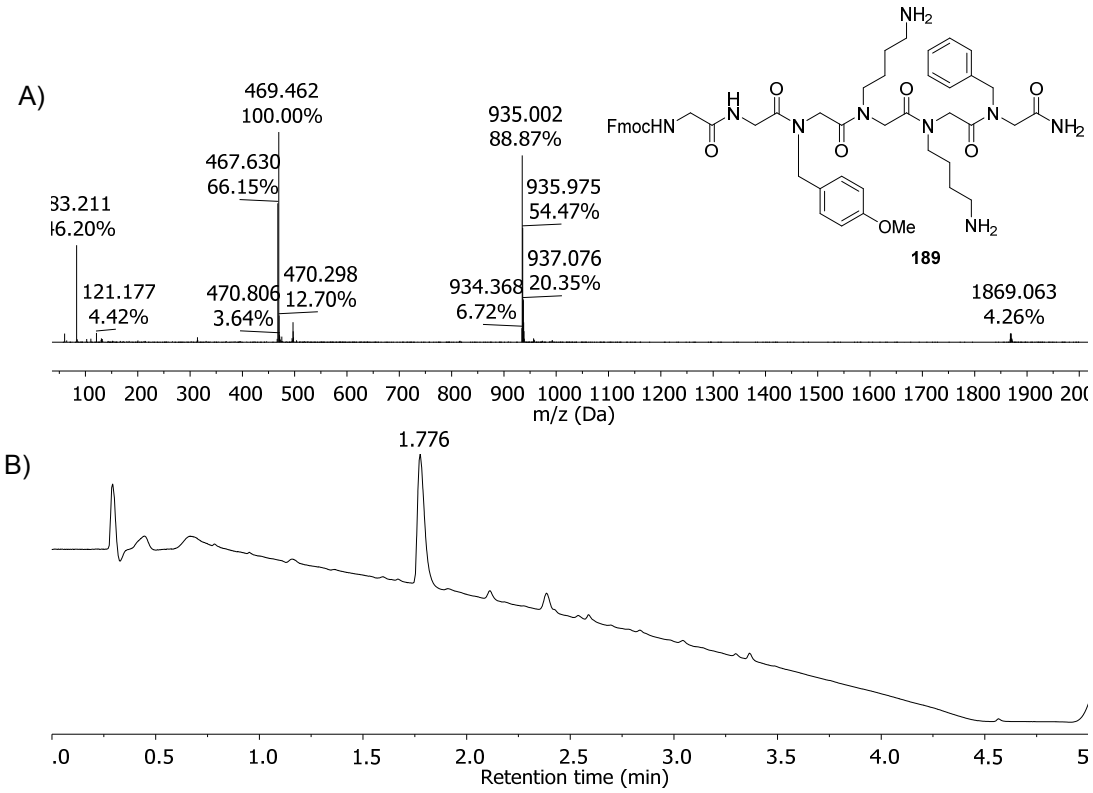

Figure 4.10 LCMS of the test cleave mixture of peptoid-GG **189**. A) Mass spectrum of the fraction containing peptoid-GG **189**, $[M+H]^+$ = 935, retention time 1.78 minutes; B) The chromatogram of the test cleave mixture (detection at 220 nm).

Table 4.3 List of peptoid-peptide hybrids made and their MALDI-ToF data

Name	Sequence	Molecular weight	Observed mass
KLA-CPPo1 (**193**)	H-(KLAKKLAK)$_2$-GG-*N*lys*N*lys*N*pcb*N*lys-NH_2	2200.5	2203.5 = $[M+H]^+$
KLA-CPPo2 (**194**)	H-(KLAKKLAK)$_2$ -GG-*N*lys*N*lys*N*lys*N*phe-NH_2	2167.4	2191.5 = $[M+Na]^+$
KLA-CPPo3 (**195**)	H-(KLAKKLAK)$_2$-GG-*N*pmb*N*lys*N*lys*N*phe-NH_2	2216.4	2240.5 = $[M + Na]^+$
KLA-CPPo4 (**196**)	H-(KLAKKLAK)$_2$- GG-*N*pmb*N*lys*N*pcb*N*lys-NH_2	2250.4	2252.9 = $[M + H]^+$
KLA-CPPo5 (**197**)	H-(KLAKKLAK)$_2$- GG-*N*lys*N*lys*N*pcb*N*phe-NH_2	2220.4	2244.4 = $[M + H]^+$
KLA-CPPo6 (**198**)	H-(KLAKKLAK)$_2$- GG-*N*pmb*N*lys*N*pcb*N*phe-NH_2	2269.3	2293.2 = $[M + Na]^+$

4.3.3 Cytoxicity of KLA and KLA-CPPos

(Note: MTT experiments were carried out by Lijun Jiang at Hong Kong Baptist University).

The cytotoxicity assays showed that the D-KLA peptide amide (**199**) was not very toxic against HeLa cells; there was very little activity at concentrations below 200 μM, and even at 500 μM, 60% of the HeLa cells survived (**Figure 4.11**). Conversely, at the highest concentration measured (100 μM), all bar one (**194**) of the six peptoid-KLA hybrids were more toxic to the HeLa cells than D-KLA. Hybrids **193** – **195** whilst either as effective as or better at killing the HeLA cells than the D-KLA, were still not very toxic against the HeLa cells. This suggests that the three peptoids were able to carry the KLA peptide into the cells, but perhaps do not localise in the mitochondria. This is supported by the much stronger toxicity seen for KLA-peptoids **196** – **198**. Peptoid-KLA hybrid **198** was the most effective- it was as effective at 10 μM as D-KLA was at 200 μM (**Figure 4.12**). This was as expected since in the original study, the corresponding cell-penetrating peptoid (**161**) was most effective at localising in the mitochondria.

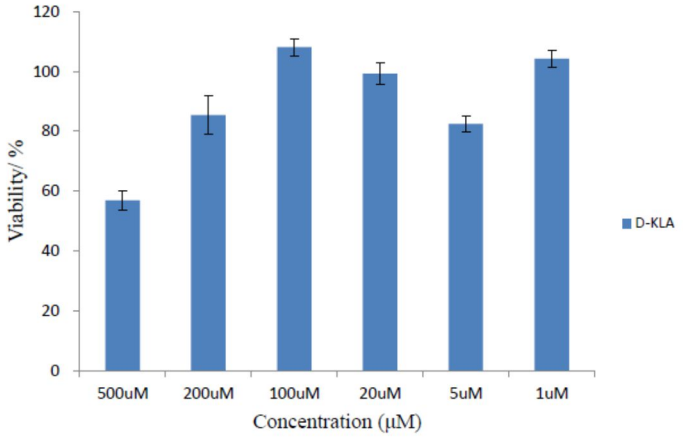

Figure 4.11 MTT assay determined cell viability of HeLa cell line after incubation with D-KLA (**199**) for 24 hours at 37°C.

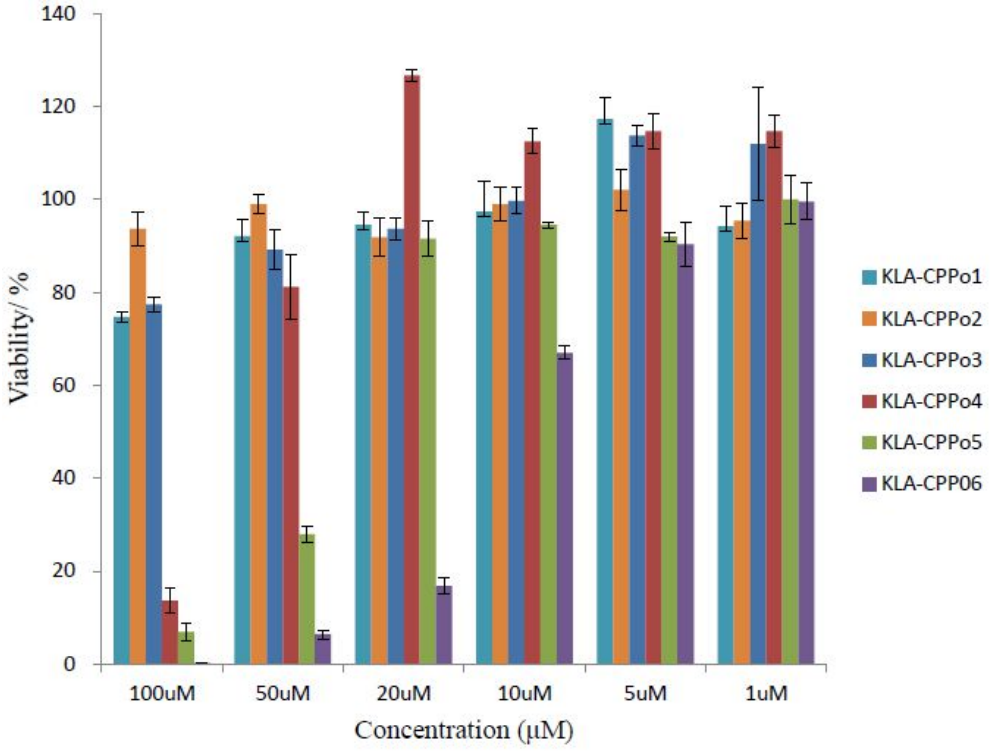

Figure 4.12 Cell viability inhibitory activities of the KLA-peptoid hybrids (**193-198**) on HeLa cells.

Because there was such a large increase in cell viability between 20 µM (~20%) and 10 µM (~70%) of KLA-CPPo6 (**198**), further MTT assays were carried out between 5 µM and 20 µM to define an IC_{50} value (**Figure 4.13**). It was found that at 8 µM, viability of the HeLA cells was 37.97 % ± 0.5%, but at 5 µM, HeLa cell viability jumps to over 100%.

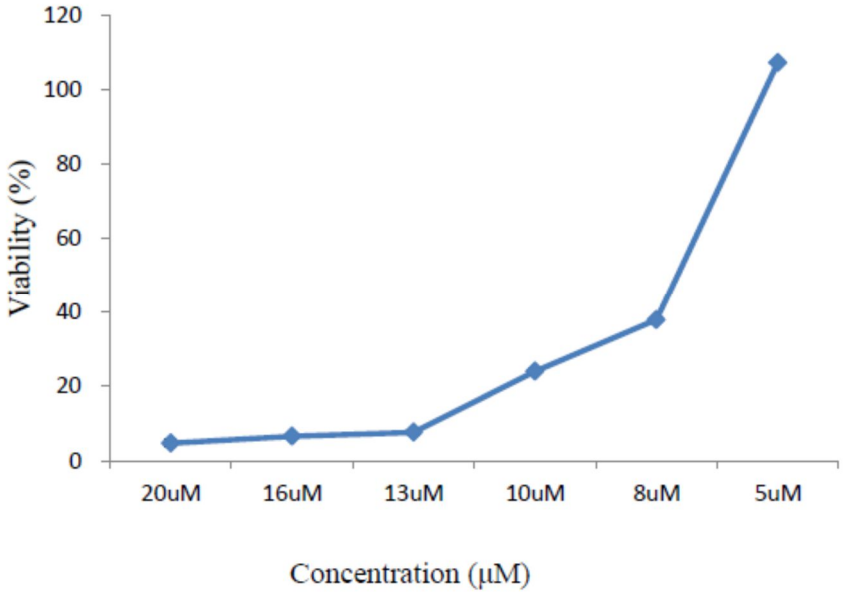

Figure 4.13 MTT assay determined cell viability of HeLA cell line after incubation with KLA-CPPo6 (**198**) for 24 hours at 37°C.

4.3.4 Cellular uptake and *in vitro* imaging

(Note: Rhodamine B conjugation was carried out by Jingyi Zong at Durham University. Flow cytometry and confocal microscopy was carried out by the Wong group at Hong Kong Baptist University).

To confirm that peptoid-KLA hybrid **198** was localising in the mitochondria the peptoid-KLA hybrid was synthesised once more, except this time, before cleavage, Rhodamine B (**200**) was conjugated to the end using DIC and HOBt as coupling agents to give Rhod-KLA-CPPo6 (**201**, **Scheme 4.3**). The crude peptoid was purified by HPLC and analysed by LCMS, MALDI-ToF and analytical HPLC (see experimental section, **Chapter 6**). The analytical HPLC trace showed two peaks in the pure product (**Figure 4.14**). Rhodamine is known to form an equilibrium between a 'non-fluorescent' closed spirolactam form and a 'fluorescent' form with an open structure. This is proton-mediated (**Scheme 4.4**). Previous work by Birtalan *et al*.,[31] showed that the 'non-fluorescent' form has a shorter retention time than the 'fluorescent form. Therefore the first peak should represent the 'non-fluorescent' form (**202**) and the second peak should represent the 'fluorescent' form (**203**). Addition of a few drops of 1% TFA in water results in an increase in absorbance of the second peak relative to the first, providing evidence that the second peak is indeed the 'fluorescent' form (**203**).

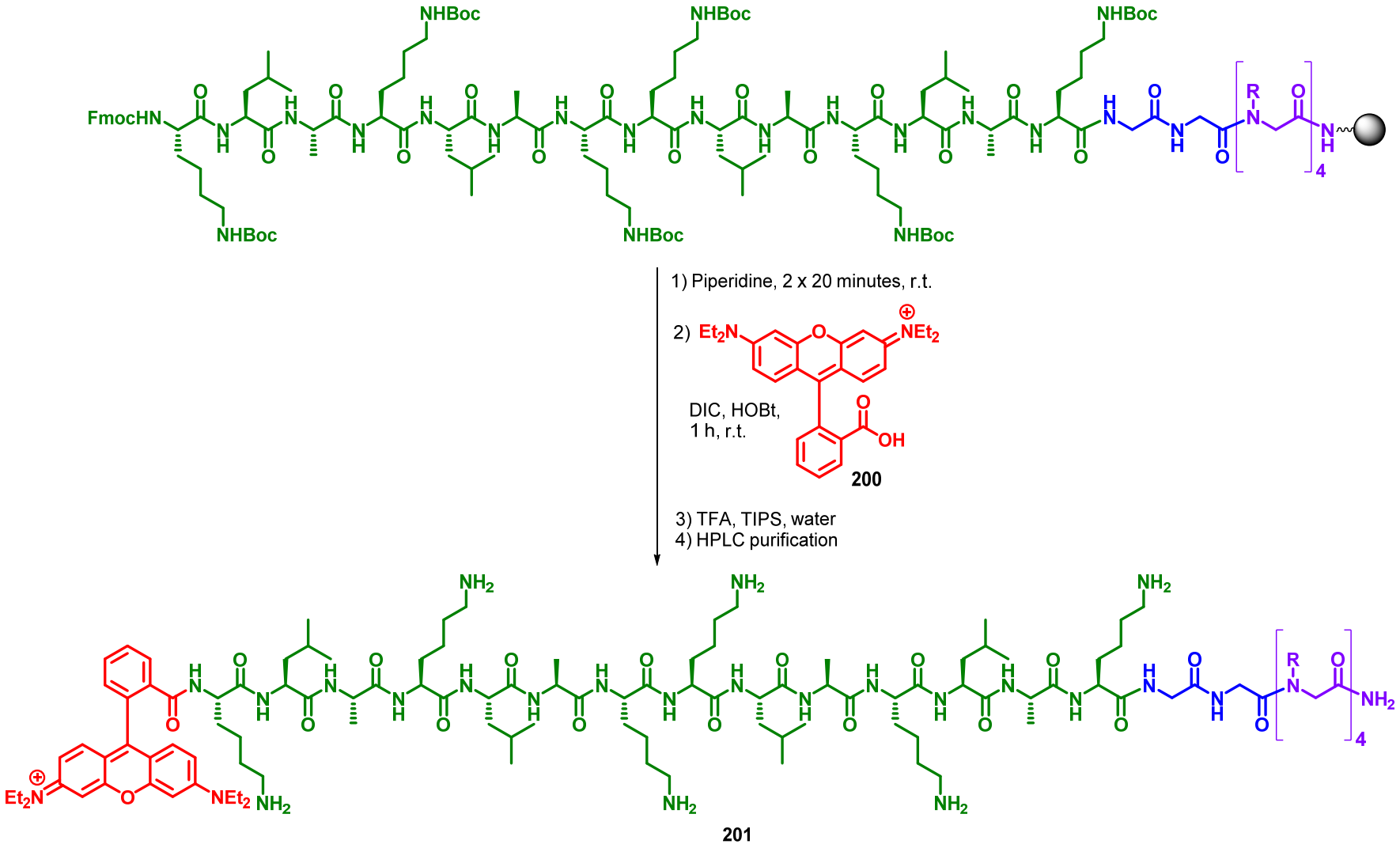

Scheme 4.3 Conjugation of rhodamine B (**200**) onto the resin-bound KLA-CPPo6 to make Rhod-KLA-CPPo6 (**201**).

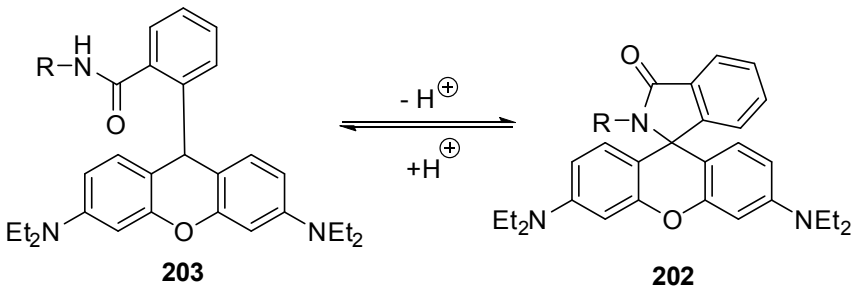

Scheme 4.4 Interconversion of the rhodamine B moiety of Rhod-KLA-CPPo6 (**201**).

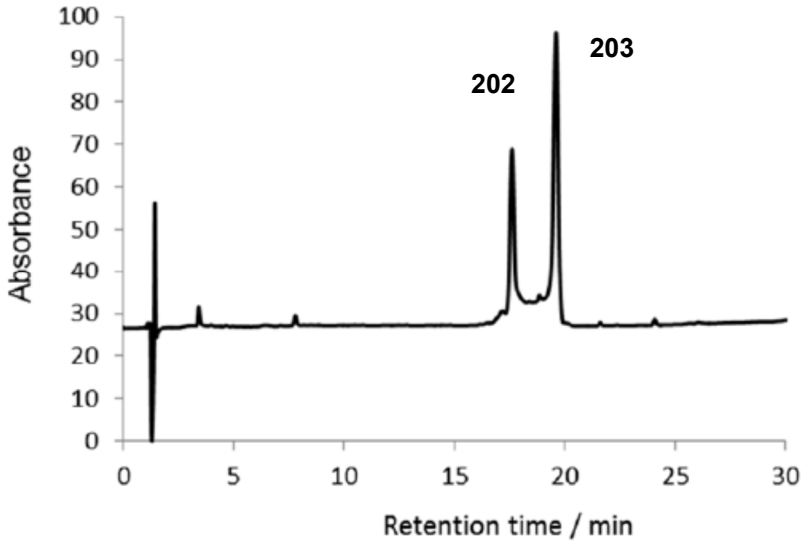

Figure 4.14 Analytical HPLC trace of pure Rhod-KLA-CPPo6 (**201**) showing two peaks: one corresponding to the closed, 'non-fluorescent' form (**202**) and the second corresponding to the open, 'fluorescent' form (**203**).

The uptake of Rhod-KLA-CPPo6 (**201**) was analysed by flow cytometry. Rhod-KLA-CPPo6 (**201**) was incubated with HeLa cells for 12 hours and its uptake was compared to a blank sample (**Figure 4.15**). The uptake of Rhod-KLA-CPPo6 (**201**) could be seen clearly.

Having shown the ability of Rhod-KLA-CPPo6 (**201**) to enter the HeLa cells, confocal microscopy experiments were carried out to investigate localisation within the cells. Rhod-KLA-CPPo6 (**201**) was incubated with HeLa cells for 24 hours and examined by laser confocal microscopy. Mito-tracker was used to locate the mitochondria within the cells and the merge of the images of Rhod-KLA-CPPo6 (**201**) and Mito-tracker showed clear co-localisation (**Figure 4.16**). This confirmed that CPPo6 delivers the KLA into the mitochondria of HeLa cells, thus resulting in a significant improvement in anticancer activity.

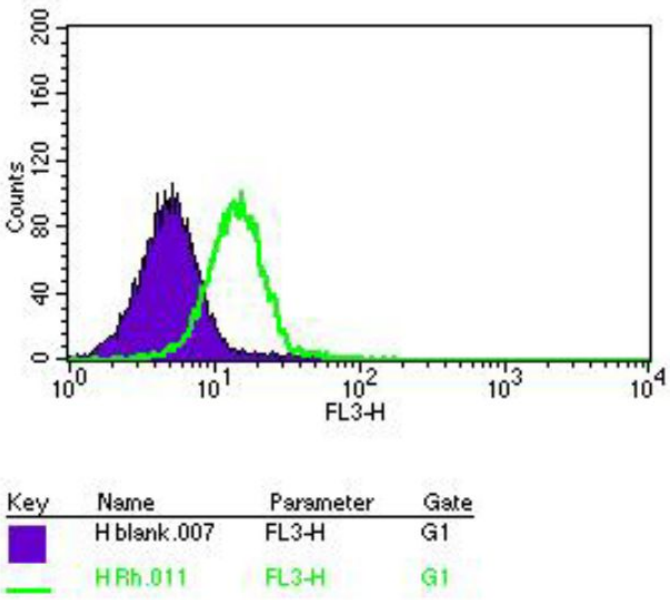

Figure 4.15 Cellular uptake of Rhod-KLA-CPPo6 (**201**) by flow cytometry in HeLa cells.

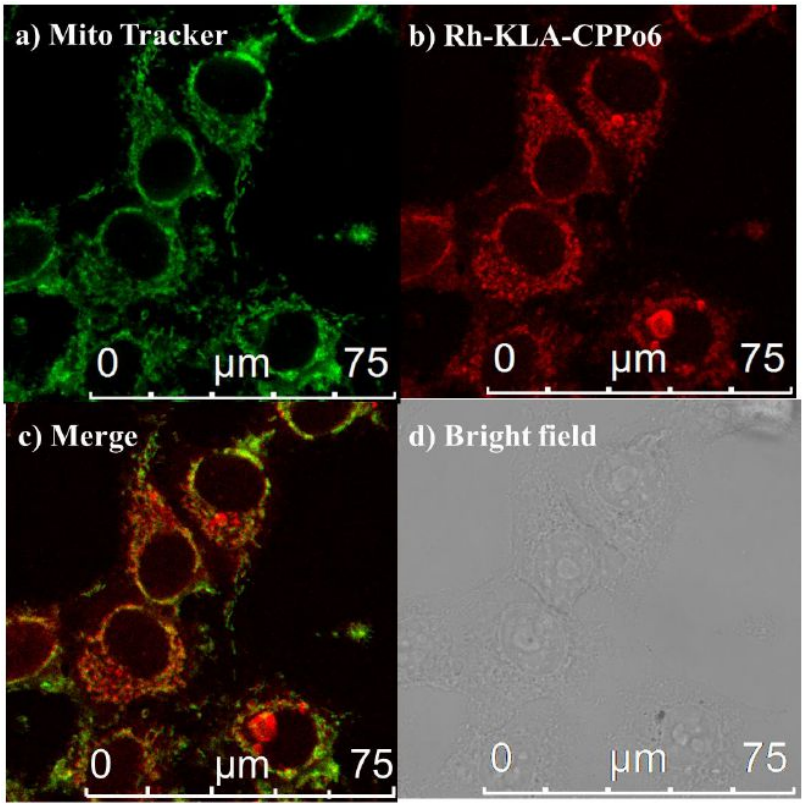

Figure 4.16 Confocal microscopy images of Rhod-KLA-CPPo6 (**201**) in HeLa cells. Concentration = 10 μM, incubation time= 24 hours.

4.4 Delivery of the p15 peptide

Having demonstrated the ability of the short cell-penetrating peptoids synthesised by Kölmel *et al*. (**156** – **161**) to deliver biologically active cargo into cells and induce anticancer activity, we aim to make a series of p15-peptoid conjugates (**204** – **209**). A luminescent probe will be attached to the N-terminus of the peptide-peptoid to give a modular probe, as described in **Figure 4.9**. Each conjugate will then be used to monitor inhibition of cell proliferation in several different cell lines in work that will be carried out by the Law lab at The Hong Kong Polytechnic University.

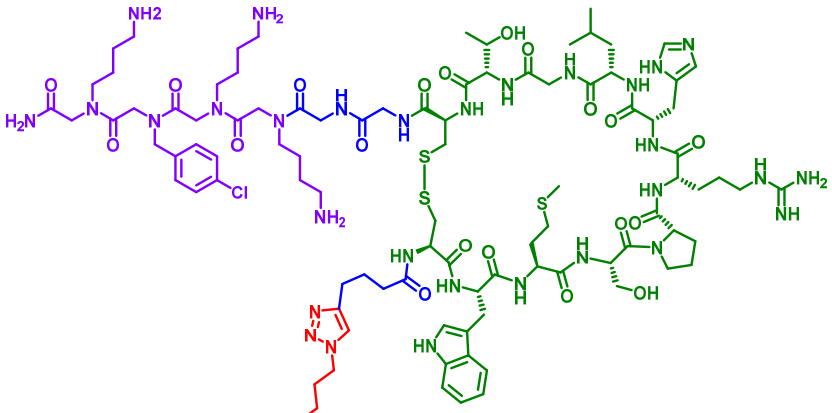

204

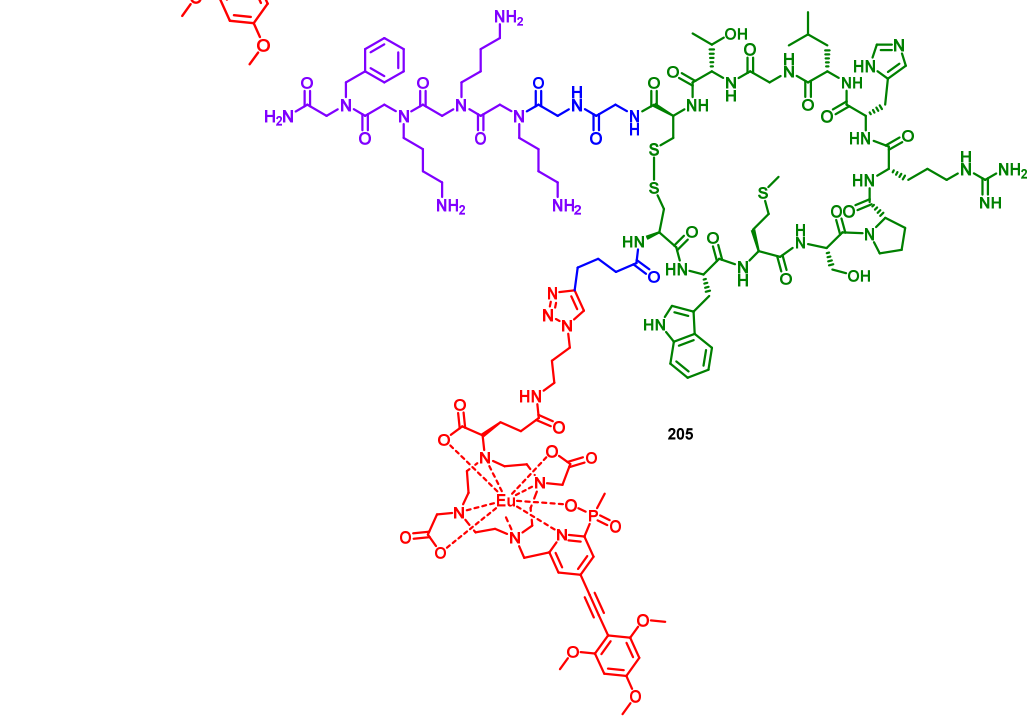

205

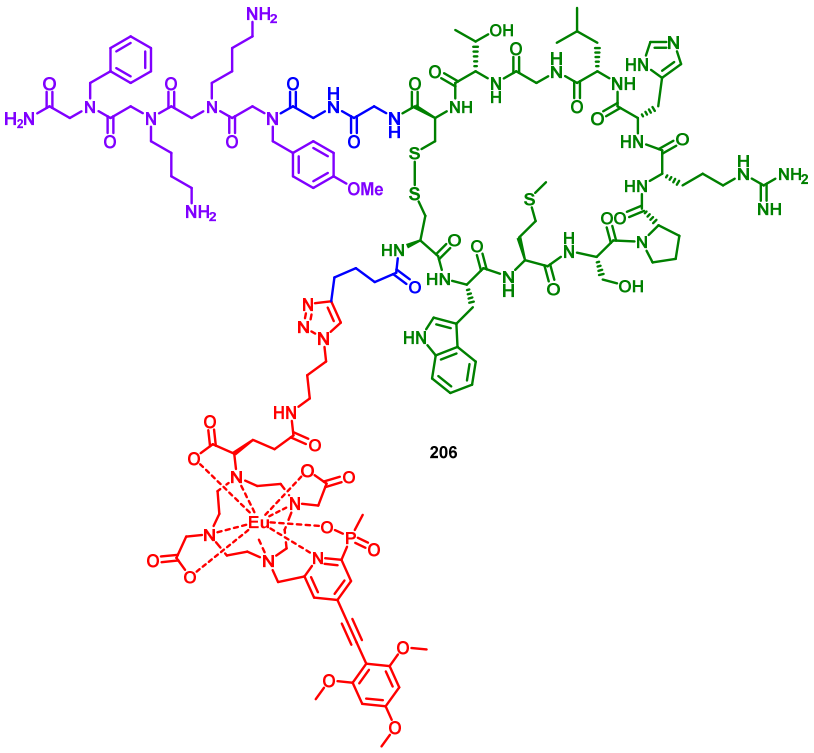

206

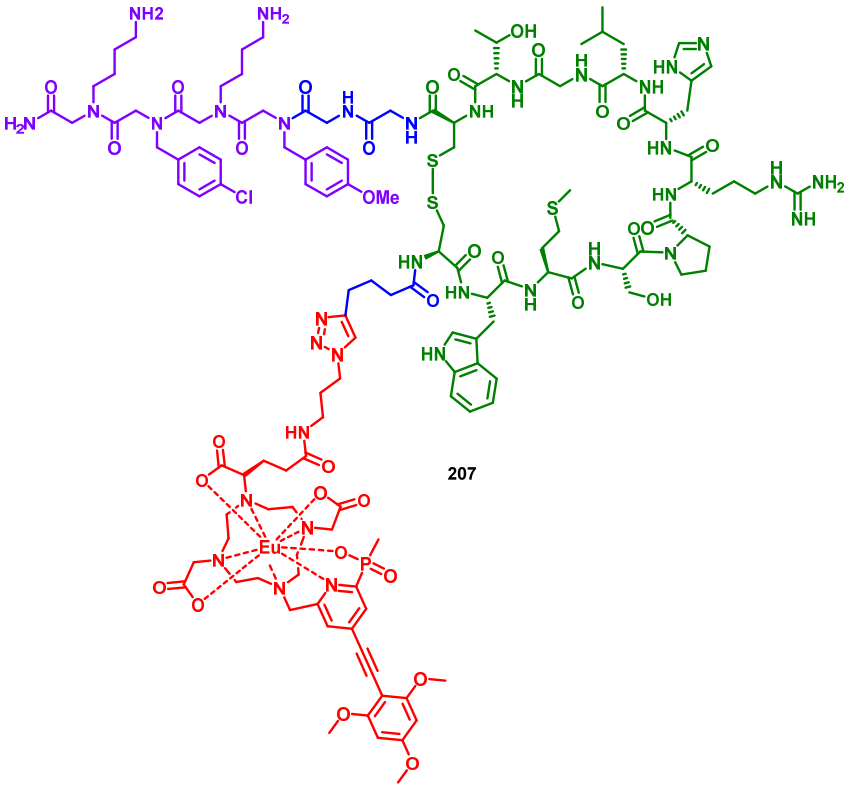

207

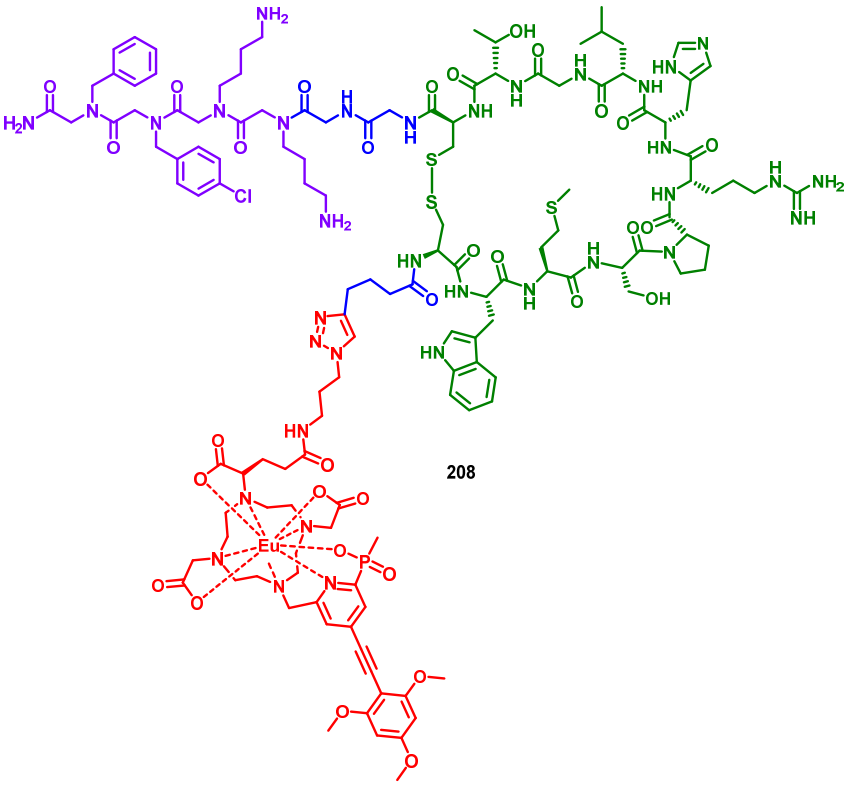

208

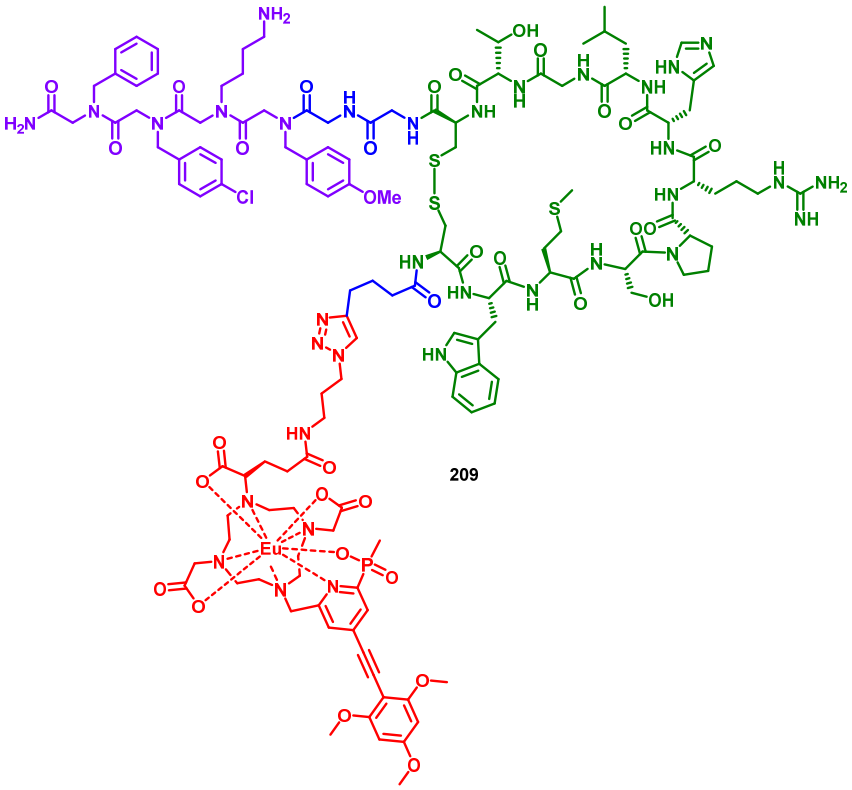

209

4.4.1 Synthesis of the peptoid-peptide hybrids

Synthesis of the peptoid-peptide hybrids is summarised in **Scheme 4.5**. The cell-penetrating peptoids (**210** – **215**) were manually synthesised on 2-chlorotrityl chloride resin using the sub-monomer method. The resin was swollen in DCM for 40 minutes before addition of bromoacetic acid. After our initial attempts to synthesise peptoids **201** – **215**, we struggled to obtain enough peptoid for even LCMS analysis. This is because when 2-chlorotrityl chloride resin is used, in the loading step, acidic by-products are released that can cause premature cleavage of the peptoid from the resin. This can be prevented by the addition of neat DIPEA in the loading step to neutralise any acidic by-products. The loading step of our second attempt at peptoid synthesis therefore used bromoacetic acid and DIPEA, and the resin was left on the shaker at room temperature for 40 minutes. Following the loading step, sub-monomer synthesis proceeded as usual with amine displacements for 1 hour at room temperature and subsequent bromoacetic couplings in the presence of DIC for 20 minutes at room temperature. Bromoacetylation and amine displacement steps were repeated until the final submonomer was added. At this point test cleaves (using 20% 1,1,1,3,3,3-hexafluoroisopropanol (HFIP) in DCM for half an hour at room temperature) were carried out to confirm successful peptoid synthesis (**Figure 4.17** shows the LCMS and chromatogram of peptoid **59**). The Boc-*N*Lys protected peptoids, **210** – **215** were obtained from this cleavage cocktail (see **Table 4.3** for a summary of the peptoids synthesised and their LCMS data).

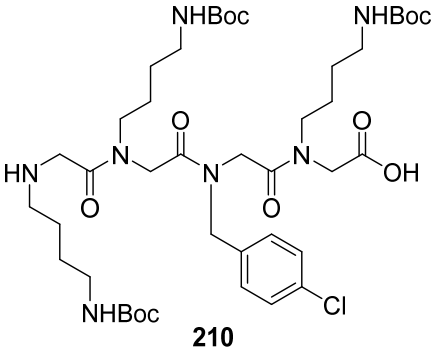

210

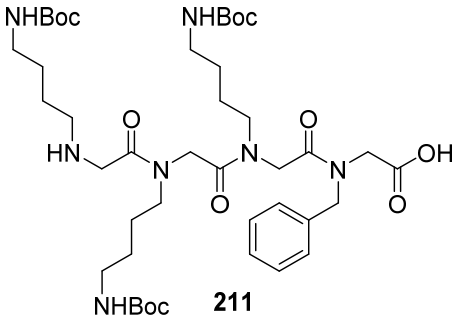

211

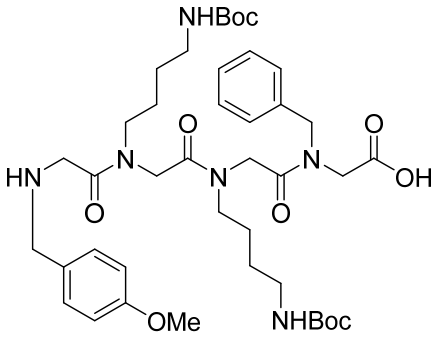

212

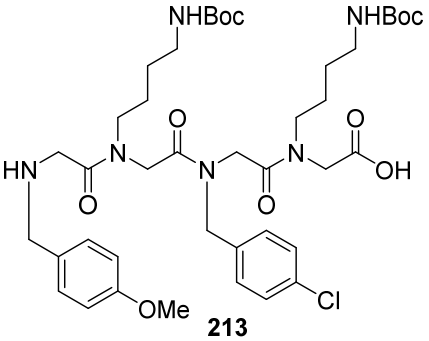

213

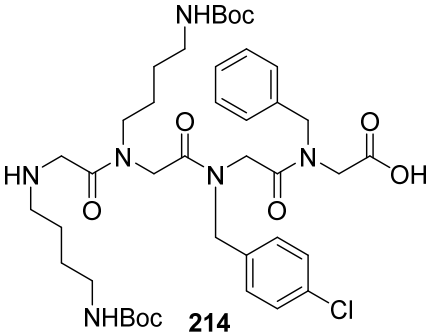

214

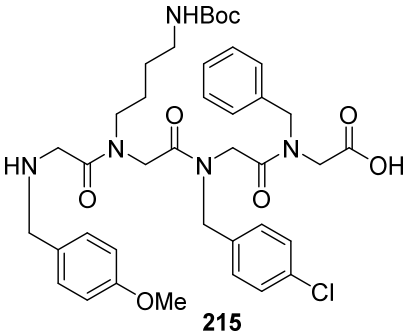

215

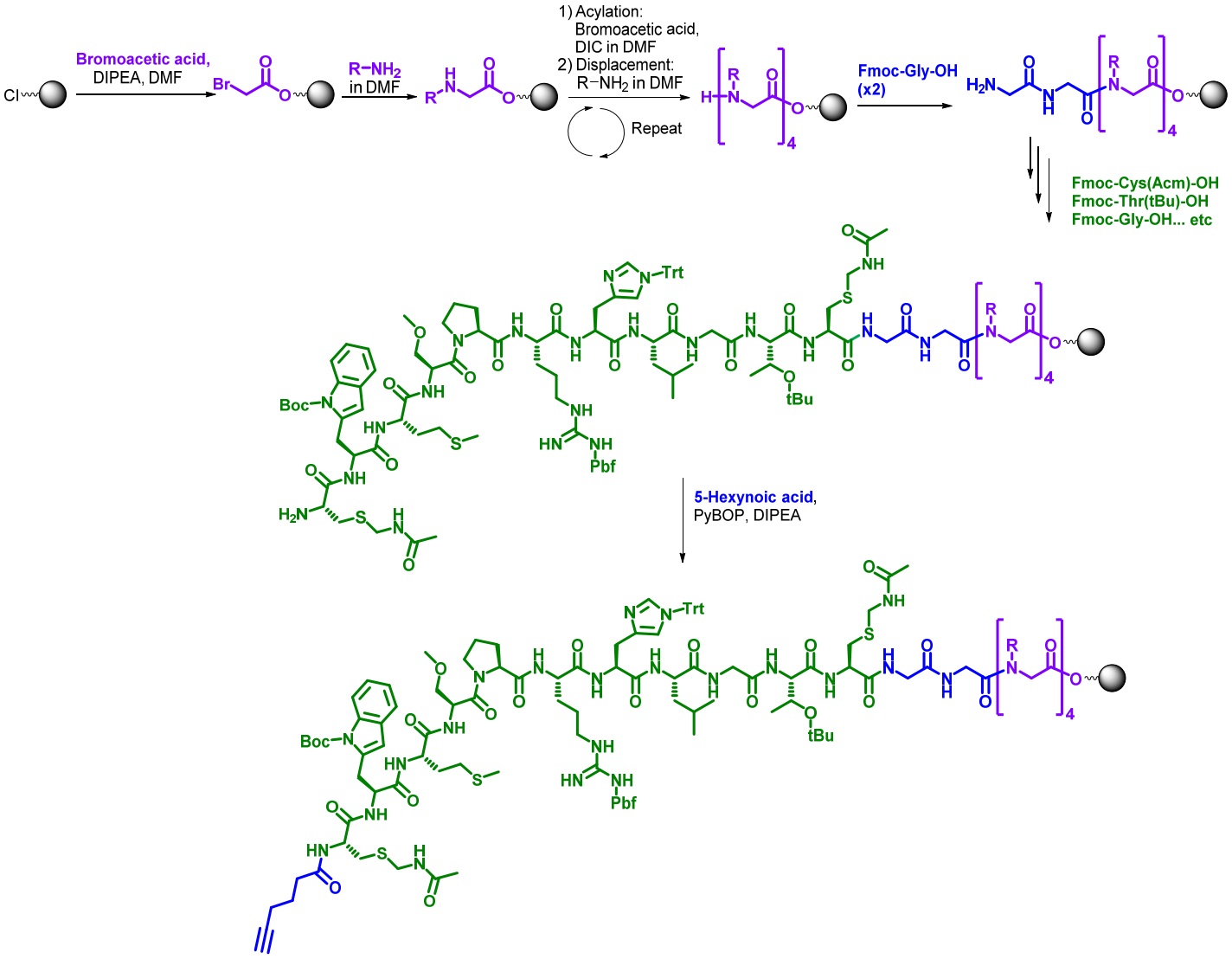

Scheme 4.5 Approach to building linear peptoid-p15 hybrids

Table 4.4 List of Boc-protected cell-penetrating peptoid acids made and their LCMS data

Name	Sequence	Molecular weight	Observed mass
CPPo7 (**210**)	Boc*N*lysBoc*N*lys*N*pcbBoc*N*lys-OH	884.51	885.5 = $[M+H]^+$
CPPo8 (**211**)	Boc*N*lysBoc*N*lysBoc*N*lys*N*phe-OH	850.07	851.5 = $[M + H]^+$
CPPo9 (**212**)	*N*pmbBoc*N*lysBoc*N*lys*N*phe-OH	798.98	800.5 = $[M + H]^+$
CPPo10 (**213**)	*N*pmbBoc*N*lys*N*pcbBoc*N*lys-OH	833.42	834.4 = $[M + H]^+$
CPPo11 (**214**)	Boc*N*lysBoc*N*lys*N*pcb*N*phe-OH	803.40	804.4 = $[M + H]^+$
CPPo12 (**215**)	*N*pmbBoc*N*lys*N*pcb*N*phe-OH	752.31	753.4 = $[M + H]^+$

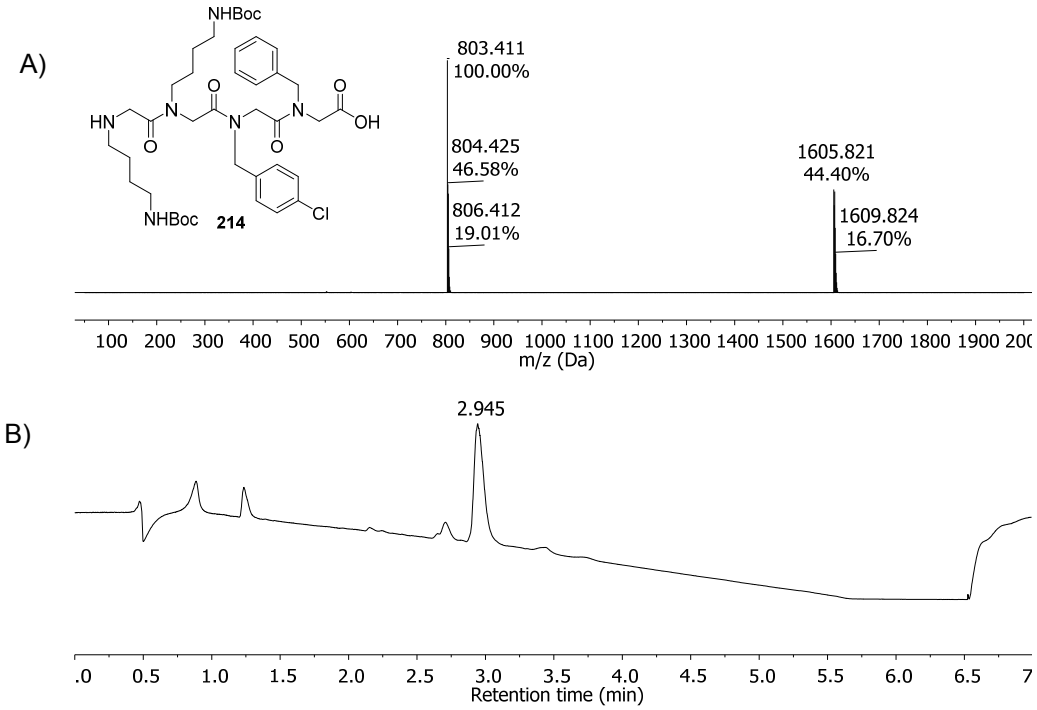

Figure 4.17 LCMS of the test cleave mixture of Boc-protected peptoid acid **214**. A) Mass spectrum of the fraction containing peptoid **214**, $[M+H]^+$ = 804, retention time 2.95 minutes; B) The chromatogram of the test cleave mixture (detection at 220 nm).

To the peptoid was then added two glycine residues by standard solid-phase Fmoc synthesis using PyBOP and DIPEA for the coupling steps and 20% piperidine v/v in DMF for the Fmoc deprotections. From here, the p15 peptide was built onto the peptoid via the glycine spacers using standard solid-phase Fmoc synthesis, and as described in **Chapter 3**, **Scheme 3.8**. Synthesis was carried out manually and at room temperature with no preactivation step to minimise cysteine and histidine racemisation and Fmoc-Trp(Boc)-OH was used to prevent Pbf transfer from the arginine. To confirm successful synthesis of the peptide-peptoid hybrid, a test cleave using TFA:TIPS:water

was carried out and the resulting crude peptide-peptoid analysed by ESI LCMS and MALD-ToF. **Table 4.5** summarises the MALDI-ToF data for the peptide-peptoid hybrids made at this stage (**216** – **221**). Finally, 5-hexynoic acid (Hyx) was added to the N-terminus of the peptide whilst still on resin using PyBOP and DIPEA and left for 1 hour on the shaker at room temperature (**Scheme 4.5**). At this point a final test cleave was carried out (using TFA:TIPS:water) and the resulting crude peptoid-peptide hybrids were analysed by LCMS and MALDI-ToF to confirm successful synthesis of the hexynoic acid-peptoid-peptide hybrid. **Table 4.6** summarises the peptoid-peptide hybrids made (**222** – **227**) and their MALDI-ToF data. The six resin-bound Hyx-p15-CPPos (**228** – **233**) were sent to the Law lab at The Hong Kong Polytechnic University.

Table 4.5 List of p15-peptoid hybrids made and their MALDI-ToF data

Name	Sequence	Molecular weight	Observed mass
p15-CPPo7 (**216**)	Fmoc-p15-GG-*N*lys*N*lys*N*pcb*N*lys-OH	2335.2	2336.6 = $[M+H]^+$
p15-CPPo8 (**217**)	Fmoc-p15 -GG-*N*lys*N*lys*N*lys*N*phe-OH	2300.8	2301.5 = $[M+H]^+$
p15-CPPo9 (**218**)	Fmoc-p15-GG-*N*pmb*N*lys*N*lys*N*phe-OH	2349.8	2350.3 = $[M+H]^+$
p15-CPPo9 (**219**)	Fmoc-p15- GG-*N*pmb*N*lys*N*pcb*N*lys-OH	2384.2	2384.9 = $[M+H]^+$
p15-CPPo10 (**220**)	Fmoc-p15- GG-*N*lys*N*lys*N*pcb*N*phe-OH	2354.2	2355.0 = $[M+H]^+$
p15-CPPo11(**221**)	Fmoc-p15- GG-*N*pmb*N*lys*N*pcb*N*phe-OH	2403.2	2404.0 = $[M+H]^+$

Table 4.6 List of Hyx-p15-peptoid hybrids made and their MALDI-ToF data

Name	Sequence	Molecular weight	Observed mass
Hyx-p15-CPPo7 (**222**)	Hyx-p15-GG-*N*lys*N*lys*N*pcb*N*lys-OH	2207.1	2208.5 = $[M+H]^+$
Hyx-p15-CPPo8 (**223**)	Hyx-p15 -GG-*N*lys*N*lys*N*lys*N*phe-OH	2172.6	2173.4 = $[M+H]^+$
Hyx-p15-CPPo9 (**224**)	Hyx-p15-GG-*N*pmb*N*lys*N*lys*N*phe-OH	2221.7	2222.7 = $[M+H]^+$
Hyx-p15-CPPo9 (**225**)	Hyx-p15- GG-*N*pmb*N*lys*N*pcb*N*lys-OH	2256.1	2257.3 = $[M+H]^+$
Hyx-p15-CPPo10 (**226**)	Hyx-p15- GG-*N*lys*N*lys*N*pcb*N*phe-OH	2226.1	2227.1 = $[M+H]^+$
Hyx-p15-CPPo11(**227**)	Hyx-p15- GG-*N*pmb*N*lys*N*pcb*N*phe-OH	2275.1	2276.1 = $[M+H]^+$

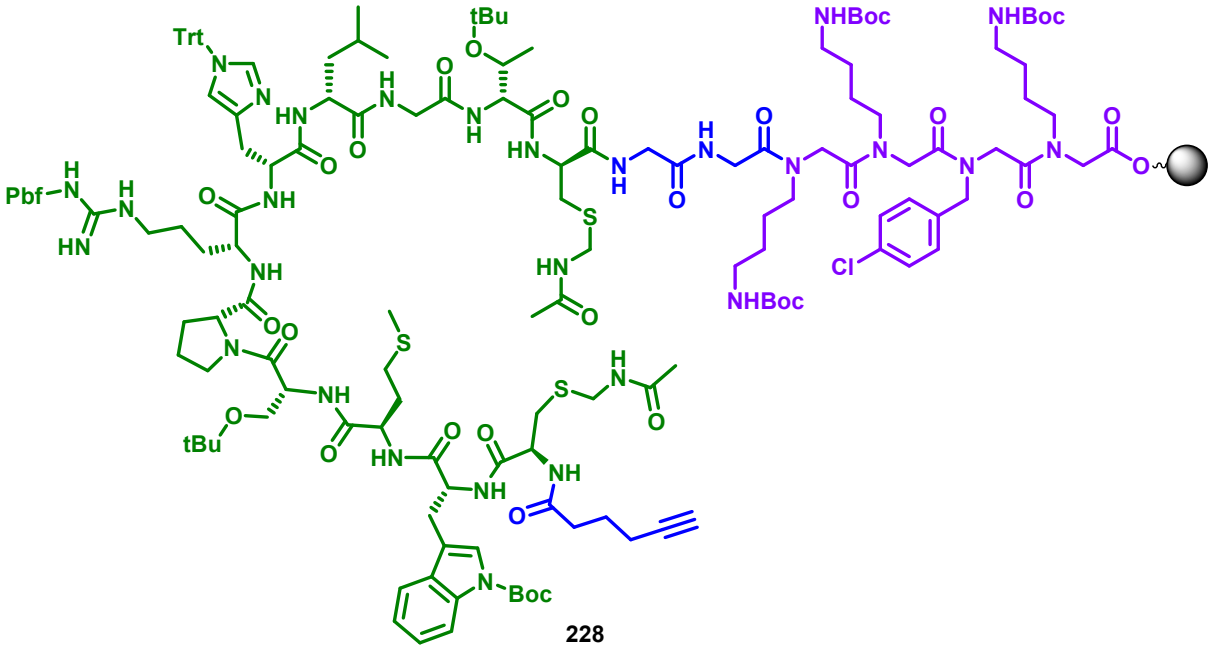
Trt
tBu
NHBoc
NHBoc
Pbf
Cl
NHBoc
tBu
Boc

228

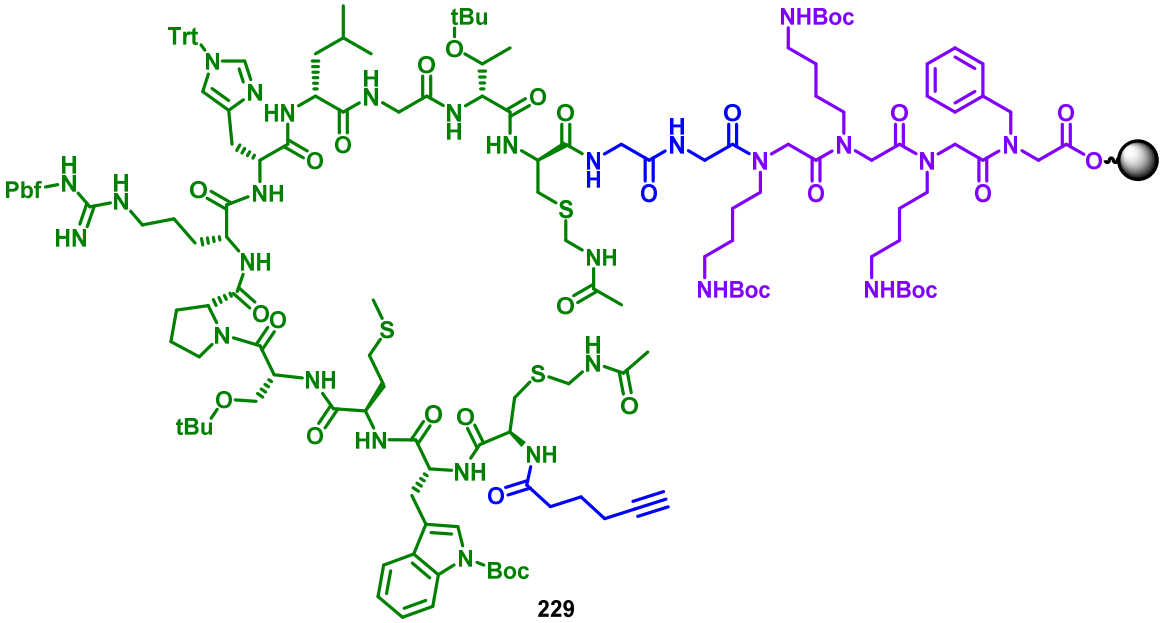
Trt
tBu
NHBoc
Pbf
NHBoc
NHBoc
tBu
Boc

229

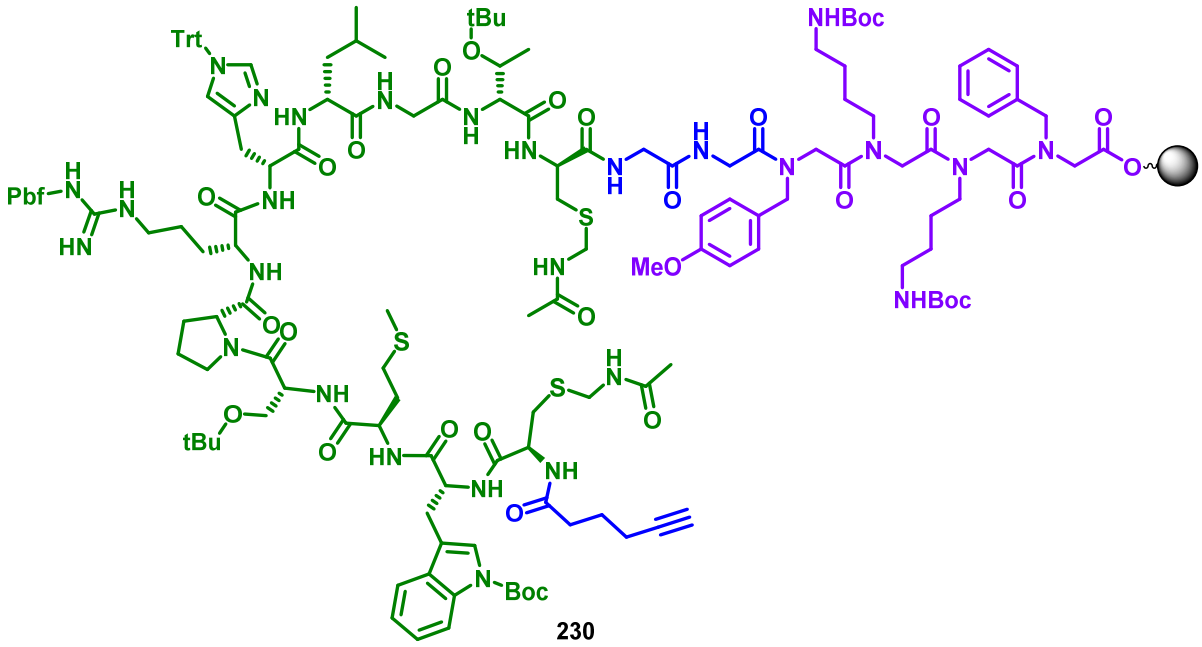
Trt
tBu
NHBoc
Pbf
MeO
NHBoc
tBu
Boc

230

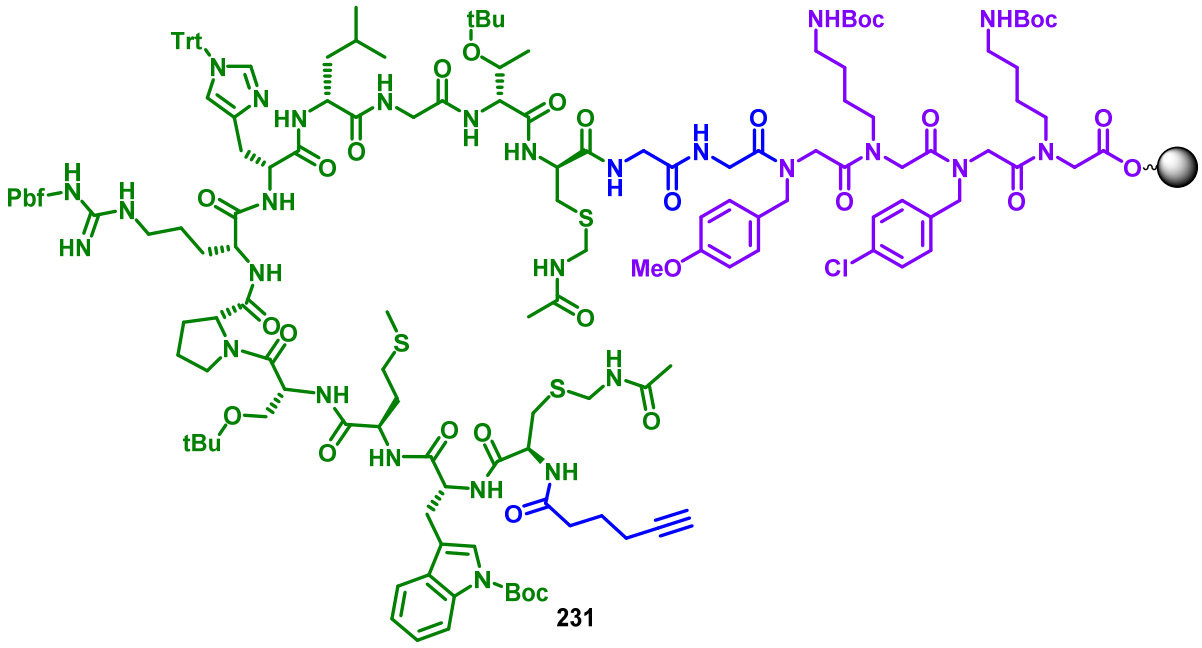
Trt
tBu
NHBoc
NHBoc
Pbf
MeO
Cl
tBu
Boc

231

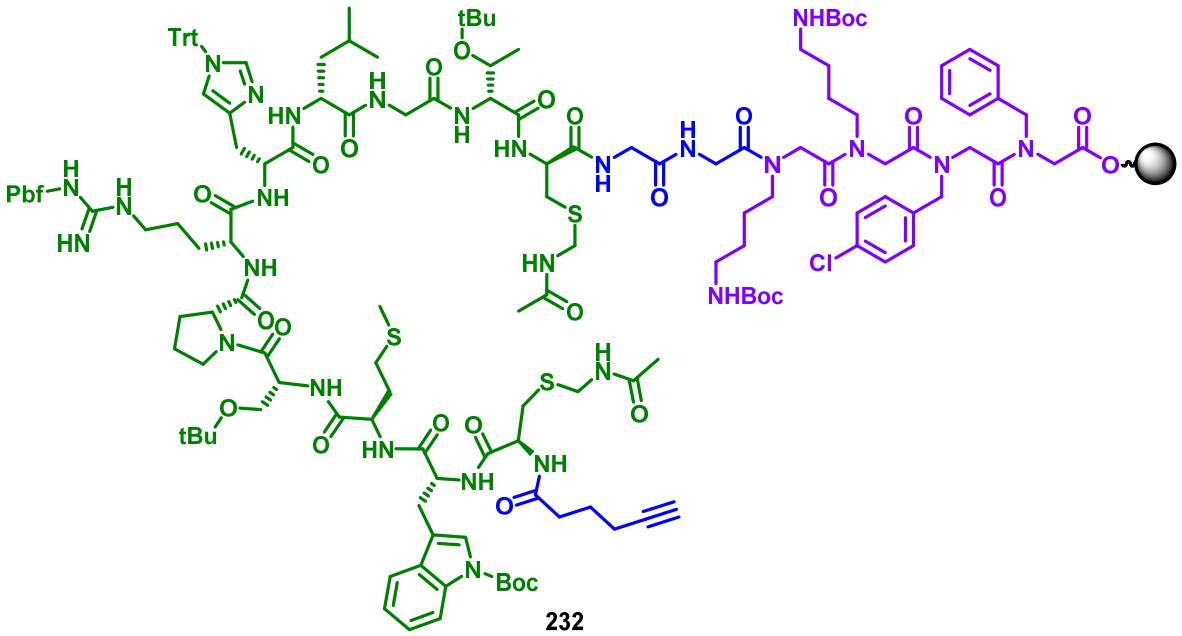

232

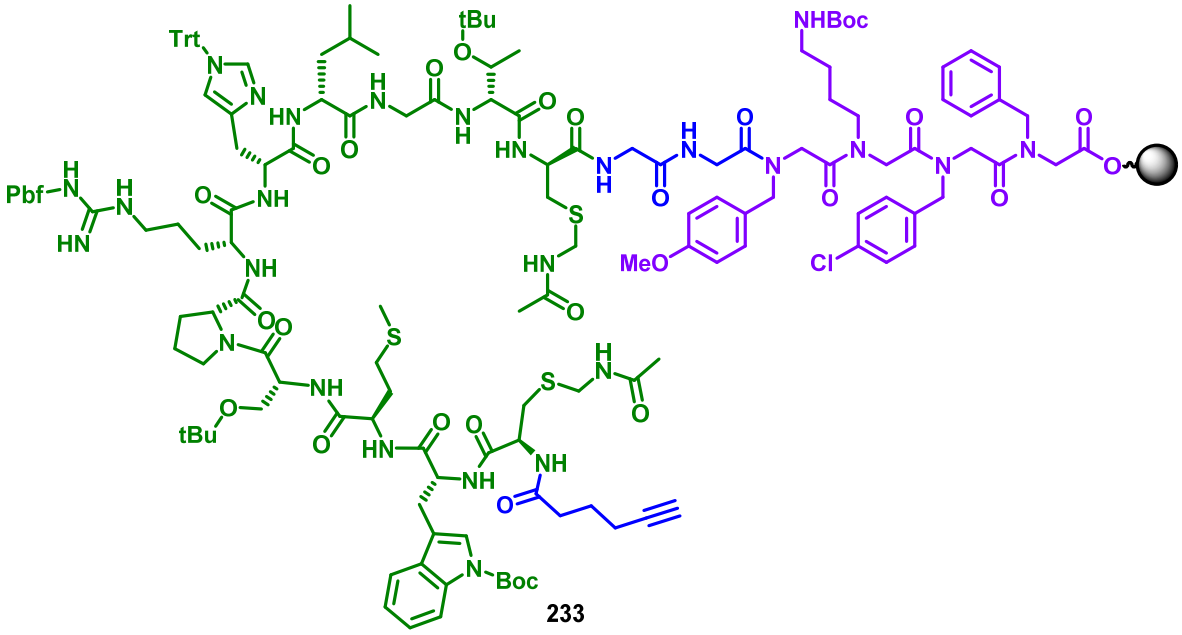

233

The peptide can then be cyclised whilst still on resin using iodine and DIPEA in DMF or DCM, as discussed in **Chapter 3**. The peptoid-peptide hybrid can be simultaneously deprotected and cleaved from the resin using TFA:EDT:water:TIPS 94:2.5:2.5:1 for four hours (**Scheme 4.6**). Finally, the 5-hexynoic acid provides a handle through which the probe can be connected to the peptoid-peptide hybrid via a copper-catalysed azide-alkyne cycloaddition (CuAAC) (**Scheme 4.7**).

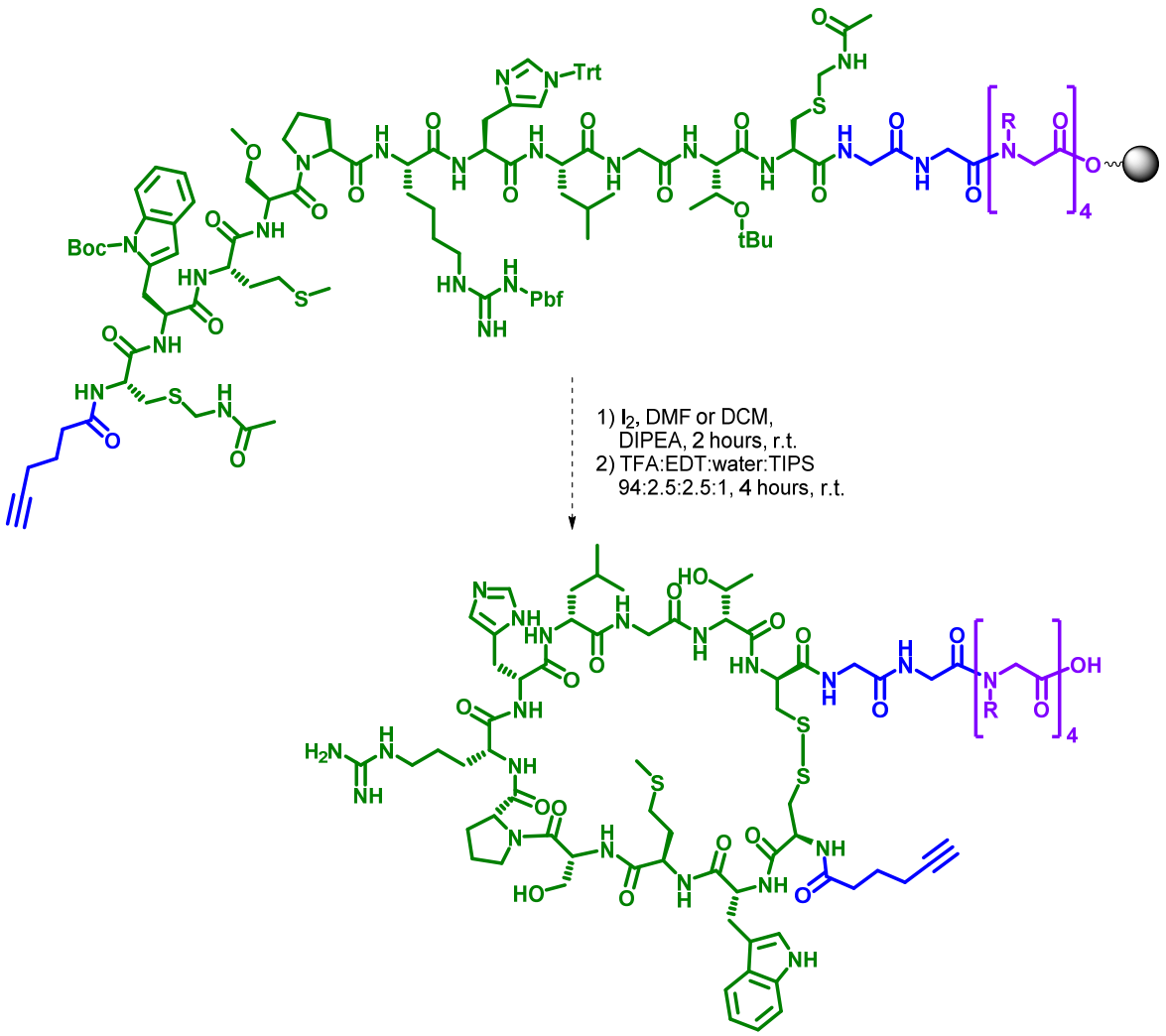

Scheme 4.6 Proposed cyclisation of the linear p15-peptoid hybrids.

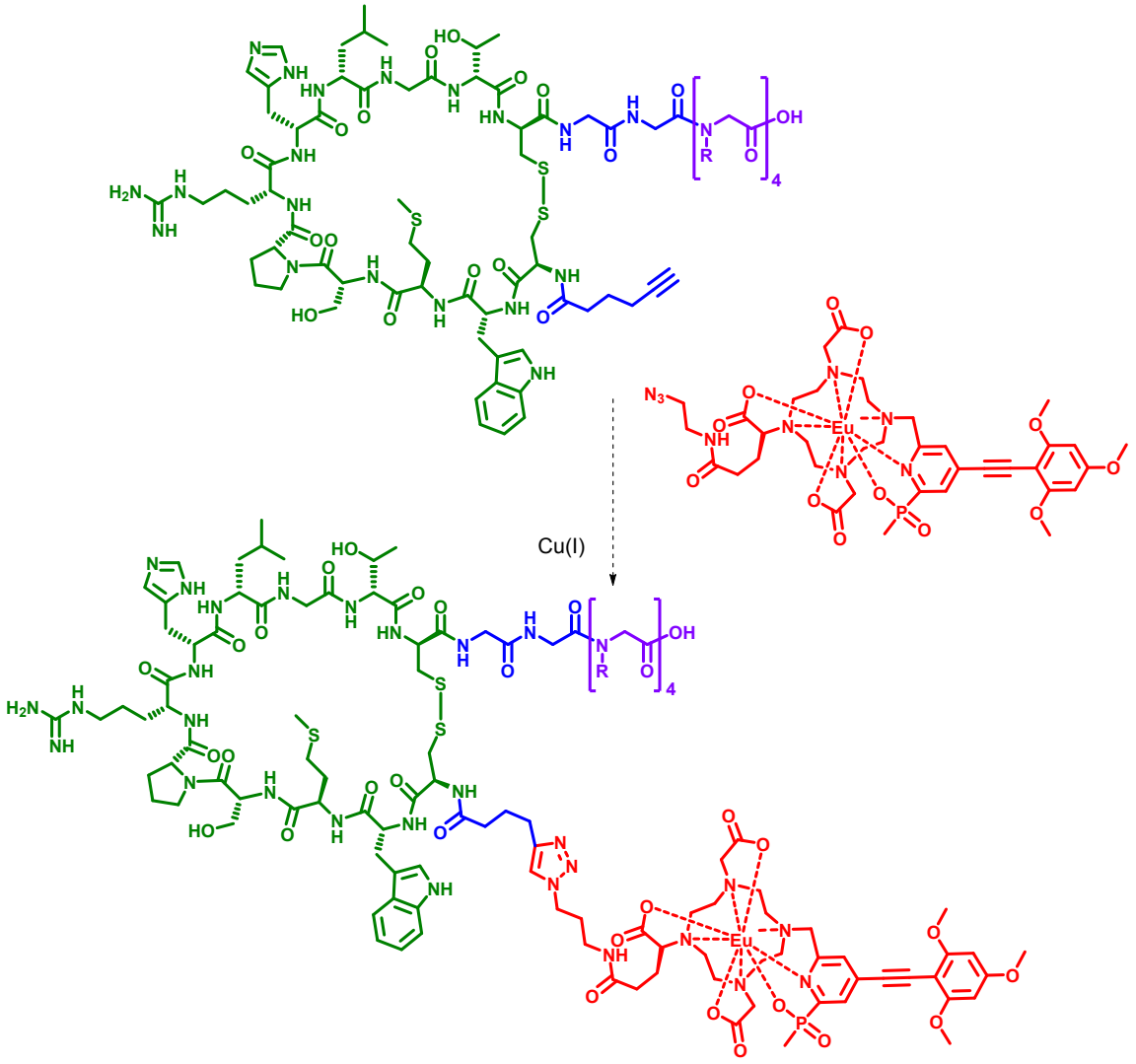

Scheme 4.7 Proposed conjugation of the imaging agent to the peptoid-peptide hybrids

4.5 Conclusions

Cell-penetrating peptides have been well researched as a means of internalising biologically active cargo within cells. Cell-penetrating peptoids can be considered a proteolytically stable alternative to cell-penetrating peptides. In this Chapter we synthesised a series of six cell-penetrating peptoids (**187** – **192**) whose sequences were first reported by Kölmel *et al*. in 2012. Onto these peptoids were built the known anticancer peptide sequence D-(KLAKKLAK)$_2$ (**186**) to make six KLA-CPPos (**193** - **198**, **Scheme 4.2**). The KLA peptide targets mitochondrial membranes, but is unable to enter the cell on its own. Conjugation of the KLA peptide to a transporter which can localise the peptide in the mitochondria should therefore enhance anticancer activity. The six KLA-peptoid hybrids (**193** – **198**) were used in cell-proliferation assays against HeLa cells and their activity compared to the D-KLA peptide amide (**199**, **Figures 4.11** and **4.12**). Of the six KLA-peptide hybrids, KLA-CPPo6 (**198**) was the most effective with an IC_{50} of ~8μM (**Figure 4.13**) and over 60 times lower than the D-KLA amide. This was as predicted since the cell-penetrating peptoid CPPo6 (**198**) was derived from the cell-penetrating peptoid (**161**) which showed the best mitochondrial localisation in the work by Kölmel *et al*.

To prove that KLA-CPPo6 localises in the mitochondria, Rhodamine B was conjugated to the end of KLA-CPPo6 to form Rhod-KLA-CPPo6 (**201**, **Scheme 4.3**). The uptake of the chimera could then be studied by flow cytometry and localisation within the cell seen with confocal microscopy. Uptake of Rhod-KLA-CPPo6 could clearly be seen from flow cytometry (**Figure 4.15**) and the confocal microscopy showed that Rhod-KLA-CPPo6 was able to localise in the mitochondria (**Figure 4.16**).

Having shown the ability of cell-penetrating peptoids to transport the KLA peptide and enhance its anticancer activity, we investigated whether the peptoids could also be effective transporters for the p15 peptide. We have previously discussed the p15 peptide in **Chapter 3**; it is the active domain of the known anticancer peptide CIGB-300 (**125**). In CIGB-300, the p15 peptide is conjugated to the cell-penetrating TAT peptide. We wanted to find out whether replacing the TAT sequence with a cell-penetrating peptoid would make a more proteolytically stable compound whilst retaining or improving the overall anticancer activity. To this end, we synthesised the six cell-penetrating peptoids we used in the KLA studies on 2-chlorotrityl chloride resin, and onto these built the linear p15 sequence (**Scheme 4.5**). Finally, onto the end of the p15-CPPos we conjugated 5-hexynoic acid (**Scheme 4.5**) to give resin-bound Hyx-p15-CPPos (**228** – **233**). The 5-hexynoic acid moiety acts as a spacer and a handle onto which the imaging probe can be attached *via* CuAAC. The resin-bound Hyx-p15-

CPPos (**228** – **233**) were sent to collaborators in Hong Kong, where their activity will be investigated by the Law lab at The Hong Kong Polytechnic University. We are currently awaiting the results of these studies.

4.6 References

1. D. K. Kolmel, D. Furniss, S. Susanto, A. Lauer, C. Grabher, S. Brase and U. Schepers, *Pharmaceuticals*, 2012, **5**, 1265-1281.
2. D. C. Wallace, *Science*, 1999, **283**, 1482-1488.
3. D. C. Wallace, *Annu. Rev. Genet.*, 2005, **39**, 359-407.
4. M. Millard, J. D. Gallagher, B. Z. Olenyuk and N. Neamati, *J. Med. Chem.*, 2013, **56**, 9170-9179.
5. S. B. L. Vollrath, D. Furniss, U. Schepers and S. Brase, *Org. Biomol. Chem.*, 2013, **11**, 8197-8201.
6. J. S. Bahnsen, H. Franzyk, A. Sandberg-Schaal and H. M. Nielsen, *Biochim. Biophys. Acta, Biomembr.*, 2013, **1828**, 223-232.
7. D. K. Kölmel, A. Hörner, F. Rönicke, M. Nieger, U. Schepers and S. Bräse, *Eur. J. Med. Chem.*, 2014, **79**, 231-243.
8. W. Huang, J. Seo, J. S. Lin and A. E. Barron, *Mol. Biosyst.*, 2012, **8**, 2626-2628.
9. X. N. Jing, M. J. Yang, M. R. Kasimova, M. Malmsten, H. Franzyk, L. Jorgensen, C. Foged and H. M. Nielsen, *Biochim. Biophys. Acta, Biomembr.*, 2012, **1818**, 2660-2668.
10. K. M. Stewart, K. L. Horton and S. O. Kelley, *Org. Biomol. Chem.*, 2008, **6**, 2242-2255.
11. E. Marouseau, A. Neckebroeck, H. Larkin, A. Le Roux, L. Volkov, C. L. Lavoie and E. Marsault, *RSC Adv.*, 2017, **7**, 6059-6063.
12. H. Y. Kim, S. Kim, H. Youn, J.-K. Chung, D. H. Shin and K. Lee, *Biomaterials*, 2011, **32**, 5262-5268.
13. V. V. Lemeshko, *Arch. Biochem. Biophys.*, 2010, **493**, 213-220.
14. Y. Perera, H. G. Farina, J. Gil, A. Rodriguez, F. Benavent, L. Castellanos, R. E. Gómez, B. E. Acevedo, D. F. Alonso and S. E. Perea, *Mol. Cancer Ther.*, 2009, **8**, 1189-1196.
15. S. E. Perea, O. Reyes, Y. Puchades, O. Mendoza, N. S. Vispo, I. Torrens, A. Santos, R. Silva, B. Acevedo, E. López, V. Falcón and D. F. Alonso, *Cancer Res.*, 2004, **64**, 7127-7129.
16. A. Di Matteo, M. Franceschini, S. Chiarella, S. Rocchio, C. Travaglini-Allocatelli and L. Federici, *Oncotarget*, 2016, **7**, 44821-44840.
17. F. Madani, S. Lindberg, Langel, #220, lo, S. Futaki, Gr, #228 and A. slund, *J. Biophys*, 2011, **2011**.
18. A. M. Solares, A. Santana, I. Baladrón, C. Valenzuela, C. A. González, A. Díaz, D. Castillo, T. Ramos, R. Gómez, D. F. Alonso, L. Herrera, H. Sigman, S. E. Perea, B. E. Acevedo and P. López-Saura, *BMC cancer*, 2009, **9**, 146.
19. M. R. Sarduy, I. Garcia, M. A. Coca, A. Perera, L. A. Torres, C. M. Valenzuela, I. Baladron, M. Solares, V. Reyes, I. Hernandez, Y. Perera, Y. M. Martinez, L. Molina, Y. M. Gonzalez, J. A. Ancizar, A. Prats, L. Gonzalez, C. A. Casaco, B. E. Acevedo, P. A. Lopez-Saura, D. F. Alonso, R. Gomez, S. E. Perea-Rodriguez and C.-I. S. Grp, *Br. J. Cancer*, 2015, **112**, 1636-1643.
20. H. M. Ellerby, S. J. Martin, L. M. Ellerby, S. S. Naiem, S. Rabizadeh, G. S. Salvesen, C. A. Casiano, N. R. Cashman, D. R. Green and D. E. Bredesen, *J. Neurosci.*, 1997, **17**, 6165-6178.
21. D. W. Hoskin and A. Ramamoorthy, *Biochim. Biophys. Acta, Biomembr.*, 2008, **1778**, 357-375.
22. H. M. Ellerby, W. Arap, L. M. Ellerby, R. Kain, R. Andrusiak, G. D. Rio, S. Krajewski, C. R. Lombardo, R. Rao, E. Ruoslahti, D. E. Bredesen and R. Pasqualini, *Nat. Med.*, 1999, **5**, 1032.
23. J. C. Mai, Z. Mi, S.-H. Kim, B. Ng and P. D. Robbins, *Cancer Res.*, 2001, **61**, 7709-7712.
24. H. Li, S. K. Kolluri, J. Gu, M. I. Dawson, X. Cao, P. D. Hobbs, B. Lin, G.-q. Chen, J.-s. Lu, F. Lin, Z. Xie, J. A. Fontana, J. C. Reed and X.-k. Zhang, *Science*, 2000, **289**, 1159-1164.

25. I. D. Alves, M. Carré, M.-P. Montero, S. Castano, S. Lecomte, R. Marquant, P. Lecorché, F. Burlina, C. Schatz, S. Sagan, G. Chassaing, D. Braguer and S. Lavielle, *Biochim. Biophys. Acta, Biomembr.*, 2014, **1838**, 2087-2098.
26. B. Law, L. Quinti, Y. Choi, R. Weissleder and C.-H. Tung, *Mol. Cancer Ther.*, 2006, **5**, 1944-1949.
27. W.-H. Chen, J.-X. Chen, H. Cheng, C.-S. Chen, J. Yang, X.-D. Xu, Y. Wang, R.-X. Zhuo and X.-Z. Zhang, *Chem. Commun.*, 2013, **49**, 6403-6405.
28. X. Ma, X. Wang, M. Zhou and H. Fei, *Adv. Healthc. Mater.*, 2013, **2**, 1638-1643.
29. L. Agemy, D. Friedmann-Morvinski, V. R. Kotamraju, L. Roth, K. N. Sugahara, O. M. Girard, R. F. Mattrey, I. M. Verma and E. Ruoslahti, *Proc. Natl. Acad. Sci.*, 2011, **108**, 17450-17455.
30. H. M. Ellerby, D. E. Bredesen, S. Fujimura and V. John, *J. Med. Chem.*, 2008, **51**, 5887-5892.
31. E. Birtalan, B. Rudat, D. K. Kölmel, D. Fritz, S. B. L. Vollrath, U. Schepers and S. Bräse, *Pept. Sci.*, 2011, **96**, 694-701.

Chapter 5

Conclusions and Future Work

The aims of this project were two-fold: first we aimed to widen the diversity of peptoid architecture by the synthesis of peptoids containing synthetically useful building blocks and novel motifs. This work was described in **Chapter 2**. The second aim was to stabilise a known cyclic anticancer peptide by synthesising stapled analogues of the active peptide and by using cell-penetrating peptoids as transporters. This work is described in **Chapter 3** and **Chapter 4.**

5.1 Novel peptoid architecture

In **Chapter 2** we successfully synthesised a peptoid monomer which contained a MIDA-protected boronic acid as the side chain (**74**). This was achieved *via* a reductive amination reaction between glycine benzyl ester (**73**) and 4-formylphenyl boronic acid MIDA ester (**69**).

The benzyl ester protected peptoid monomer was successfully synthesised in a 34% yield by using sodium triacetoxyborohydride as a reducing agent and acetonitrile as the reaction solvent. However, subsequent deprotection had to be carried out in methanol and as a result, removal of the MIDA ester from the boronic acid was seen within two hours. Attempts to optimise the reductive amination step were not carried out, but these could include use of acid catalysts to improve the efficiency of imine formation. However, there is little point carrying out optimisation if the end product is going to decompose on deprotection of the benzyl ester. Therefore, any future work would look at using a different acid protecting group, e.g. a *tert*-butyl (tBu) protected acid (**234**).

Deprotection of a tBu-ester is achieved by addition of TFA- something we have already seen the MIDA boronate is largely stable to. The tBu-ester analogue may also change properties of the peptoid monomer, such as solubility, making it easier to handle and purification more efficient. If this is the case, the yield from the reductive amination step may be inherently higher and optimisation of the reaction may be unnecessary.

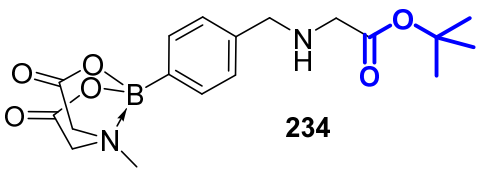

234

Chapter 2 also detailed our work on the synthesis of biaryl-linked cyclic peptoids. A library of biaryl-linked cyclic peptoids (**104**, **110**, **119** – **124**) was made via on-resin Suzuki-Miyaura cross-coupling in yields of 3 – 23%. The primary aim of this work was to synthesise novel peptoid scaffolds as proof of concept which can now be applied to other peptoid-based structures.

Optimisation of the reaction conditions is the obvious next stage in this work as this would enable the isolation of greater quantities of cyclic peptoid. Some of the byproducts of the Suzuki-Miyaura cross-coupling reaction arose from hydrodehalogenation of the iodine. This is a commonly observed side-reaction in cross-coupling reactions.[1-3] This competing reaction can be influenced by identity of the catalyst, strength and number of equivalents of base, solvent used and reaction temperature.[1,3] Thus, optimisation would involve screening for metal source, ligand, base, solvent and reaction temperature. This would allow better NMR spectra to be obtained, including NOE experiments. Data from NMR experiments can provide insights into the structure of these novel scaffolds.

Work in the group is currently underway to obtain crystal structures of these compounds in order to gain insight into how the biaryl group influences secondary structure. Crystal structures may also provide information that would be useful for optimisation of reaction conditions.

The peptoid library could be expanded to include chiral side-chains (example structure, **235**). The inclusion of a chiral side-chain would enable the use of circular dichroism experiments in order to gain insight into the structure of this class of cyclic peptoid. Furthermore, Suzuki-Miyaura cross-coupling is orthogonal to other methods of peptoid cyclisation (as discussed in **Chapter 1**), and therefore could provide a route to bicyclic peptoid scaffolds, for example by using carrying out Suzuki-Miyaura cross-coupling followed by CuAAC to generate a scaffold similar to bicyclic peptoid **236**.

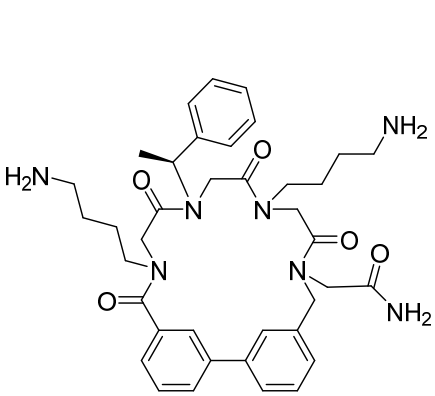

235

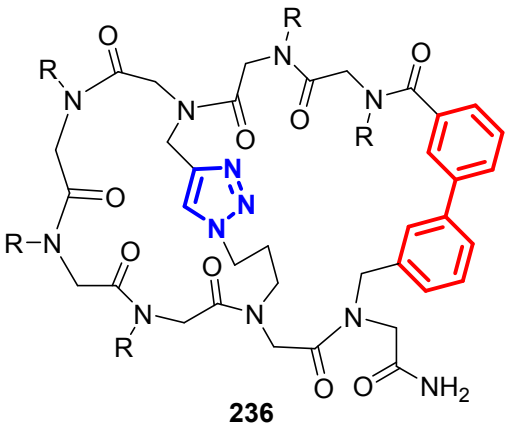

236

Further work would also investigate the biological activity of these compounds. Unfortunately, none of the peptoids tested (linear biaryl-containing peptoid **106** and cyclic biaryl-containing peptoids **104**, **110**, **119** and **120**) showed antibacterial activity against either *E. coli* or *S. aureus* at the concentrations tested. However, alteration of the peptoid side chains, for example by changing the length of *N*Lys side-chains, or replacement of a positively charged side-chain with a hydrophobic group may result in some antibacterial activity. In addition to antibacterial screening, the group has a particular interest in anti-leishmanials, so biaryl-linked cyclic peptoids could also be screened for activity against *L. mexicana.* Any screening for antimicrobial and antiparasitic activity should also be carried out alongside cell toxicity and haemolysis studies.

5.2 Nucleophosmin-targeting peptide (p15) and analogues

In **Chapter 3** we successfully synthesised the active domain of the nucleophosmin (NPM1)-targeting anticancer peptide, p15 (**126**, best isolated yield 19%) along with three stapled analogues: F-p15, (**127**, best isolated yield 32%), C=C p15 (**128**, best isolated yield 11%) and C-C p15 (**129**, best isolated yield from C=C-p15 50%). BLI binding assays were carried out by the Law lab at The Hong Kong Polytechnic University and preliminary results showed that p15 (**126**) and C-C p15 (**129**) bound to NPM1 more strongly than F-p15 (**127**) and C=C p15 (**128**)

The isolated yields of all the peptides synthesised were low, and little time was spent optimising conditions. This is an obvious area for further work. Loading of the 2-chlorotrityl chloride resin was not very efficient, as demonstrated by the lower than expected masses obtained from cleavage of the crude linear peptides. This could be a

result of the high water and acid sensitivity of 2-chlorotrityl chloride resin. As the resin ages and is exposed to atmospheric water, the loading sites will start to become 'capped' meaning fewer available loading sites and a lower resin loading. Alternatively, the resin-bound peptide could be partially cleaved during the course of the synthesis, as happened in the course of our initial attempts to form the disulphide bridge of p15 (**126**). A solution to this would be to use Rink Amide resin which is less water and acid sensitive. However, using Rink Amide results in an amide at the C-terminus rather than an acid, and this could affect the peptide's affinity for the target protein. That said, it should be noted that p15 needs to be attached to a cell-penetrating moiety to show activity in a cellular environment. Therefore, the functional group at the C-terminus may be irrelevant, particularly if attached to a cell-penetrating peptide or peptoid from this end.

Formation of the disulphide bond in p15 (**127**) was carried out via simultaneous deprotection of the Acm group on the cysteine and oxidation using iodine. This is an inherently inefficient method since prolonged reaction times result in undesired side-reactions, but limiting reaction times leads to only partial removal of the Acm groups from the cysteine residues and thus limits cyclisation.[4-6] An alternative method is solution-phase air oxidation of the deprotected peptide in a buffer solution at pH 7.5 – 8. For the p15 peptide, this is time consuming as the use of additives such as H_2O_2 to speed up the reaction is precluded by the presence of methionine which can also be oxidised. However, the final achievable yield of the desired peptide is higher than for the iodine oxidation method, and this is the method usually seen in the literature syntheses of p15.[7]

F-p15 (**128**) was synthesised via a solution-phase stapling reaction between the fully deprotected linear p15 peptide (**147**) and hexafluorobenzene (**145**). Following the reaction, the mono-substitued, uncyclised peptide (**148** and/or **149**), as well as the uncyclised parent peptide (**147**) could be seen in the LCMS. Increasing the concentration of the reaction mixture may speed up the reaction and push it to completion, but care must be taken not to increase concentration too much or the di-substituted, linear peptide may be seen. If increasing the concentration results in the appearance of the di-substituted linear peptide, increasing the reaction time, or heating the reaction mixture may be a better alternative route to improving the yield.

We also synthesised C=C p15 (**128**) via Grubbs' RCM on the resin-bound linear peptide where the cysteine residues had been replaced with allylglycine residues (**150**). Initial attempts at Grubbs' RCM resulted in only the uncyclised peptide (**151**) so different conditions were screened (**Table 3.1**). After each Grubbs' RCM, uncyclised

peptide could be seen in the LCMS, and this is likely to account for the poor yield. Longer reaction times and further additions of catalyst solution could improve this. Alternatively, the more reactive Grubbs' first and second generation catalysts could be used; whilst some of the conditions screened used the first generation catalyst, the reactions were only carried out at room temperature. Using the first and second generation catalysts at reaction temperatures similar to those used with the Hoveyda-Grubbs' second generation catalyst may result in faster reaction times.

The major problem with hydrogenation of C=C-p15 (**128**) to C-C-p15 (**129**) is that only a small quantity of C=C-p15 (**128**) was taken forward into the reaction. This means that small losses of peptide, for example in the course of removal from the palladium catalyst, translate into a large impact on the yield. Improvement of the RCM reaction to obtain more C=C-p15 (**128**) will enable the reaction to be carried out on a larger scale.

Optimising reaction conditions for the synthesis of all peptides enables the isolation of more pure peptide. This means that a wider range of crystallisation conditions can be screened. Obtaining crystal structures of the peptides, both individually and co-crystallised with NPM1, may offer insight into the binding of p15 and its analogues to NPM1 and enable further structural modifications to improve binding affinity and hence effectiveness in the treatment of cancers.

Should further results from binding assays confirm that C-C p15 (**129**) has comparative affinity to NPM1 when compared the original p15 (**126**), the next step will be to build p15 (**126**) and C-C p15 (**129**) onto cell-penetrating peptoids (CPPos), with a view to using the CPPos as more stable alternatives to the cell-penetrating TAT sequence used in CIGB-300 (**125**). Working to optimise the cyclisations is therefore worthwhile as this will allow more efficient synthesis of the chimeric peptides, allowing us to investigate their therapeutic effectiveness. Preliminary efforts in these investigations are described in **Chapter 4**.

5.3 Peptoid-p15 hybrids

In **Chapter 4** we described the synthesis of a series of six cell-penetrating peptoids (CPPos, **187** – **192**) that were first reported in 2012 by Kölmel *et al*.[8] Onto each of these CPPos was built the KLA peptide (**186**); a known anticancer peptide of sequence D-$(KLAKKLAK)_2$ to give six KLA-CPPos (**193** – **198**). The KLA peptide interacts with mitochondrial membranes, triggering permeation and mitochondrial swelling which induces apoptosis.[9, 10] Some of the CPPos synthesised by Kölmel *et al*. were shown to

localise in the mitochondria, and so cell viability assays were carried out on each of the KLA-CPPos (**Figures 4.12** and **4.13**) to investigate whether the CPPos improved the activity of KLA. Cell viability assays were also carried out on D-KLA amide (**199**, **Figure 4.11**) as a comparison to the KLA-CPPos (**193** – **198**). The KLA-CPPo conjugate with the best activity was KLA-CPPo6 (**198**) had an IC_{50} of ~8μM: more than 60 times lower than that of D-KLA amide. This was as expected: in the original work by Kölmel *et al*., the corresponding CPPo showed the best mitochondrial localisation. Mitochondrial localisation of KLA-CPPo6 was confirmed by flow cytometry and confocal microscopy experiments on the Rhodamine B tagged conjugate Rhod-KLA-CPPo6 (**201**, **Figures 4.15** and **4.16**). Further work could include the incorporation of a targeting moiety that improves selectivity for cancerous cells over healthy cells, and the corresponding *in vivo* experiments.

Having shown the ability of CPPos to transport a biologically active peptide into cells and improve activity over the free peptide, we then conjugated the p15 peptide (**126**) onto each CPPo. The p15 peptide (**126**) is the active domain of the anticancer peptide CIGB-300 (**125**) which was first discussed in **Chapter 3**. The p15 peptide triggers apoptosis by interacting with NPM1 which is localised in the nucleolus.[11] The CPPos reported by Kölmel *et al*. showed nuclear localisation to varying extents, although specific nucleolar localisation was not investigated. We therefore wanted to investigate whether the CPPos could act as a proteolytically stable alternative to the TAT peptide which is the cell-penetrating peptide used to transport p15 as CIGB-300. Six p15-CPPos were synthesised and on the end of each was attached 5-hexynoic acid to provide an alkyne as a reactive handle for the conjugation of an imaging probe *via* copper-catalysed azide-alkyne cycloaddition (CuAAC). The resin-bound Hyx-p15-CPPos (**228** – **233**) were sent to the Law lab at The Hong Kong Baptist University where the imaging component will be attached and anticancer activity evaluated.

Should any of our p15-CPPo conjugates show anticancer activity, we can then progress this work by synthesising the stapled C-C p15 analogue (**129**) onto the CPPos. These C-Cp15-CPPo hybrids would be expected to be more proteolytically stable than CIGB-300, and their respective anticancer properties could be compared.

5.4 Final Comments

In summary, we have successfully synthesised a library of biaryl-linked cyclic peptoids. Whilst these did not show any activity against *E. coli* or *S. aureus*, these compounds represent novel peptoid scaffolds which contain a ‘privileged structure.’

We have also successfully synthesised the active domain of the anticancer peptide CIGB-300 (p15) and three stapled analogues. BLI binding assays were carried out by the Law lab at The Hong Kong Polytechnic University and preliminary results showed that p15 (**126**) and C-C p15 (**129**) bound to NPM1 more strongly than F-p15 (**127**) and C=C p15 (**128**). However, work is ongoing to confirm these results and to obtain quantitative information on the binding affinity of these peptides to NPM1.

Continuing our work on making stabilised bioactive peptides, we synthesised a series of peptide-CPPo hybrids. The first set of peptide-peptoid hybrids were KLA-CPPos. We demonstrated that the conjugation of D-KLA to a CPPo which localised in the mitochondria significantly improved KLA activity compared to the free D-KLA amide. We then used the same CPPos and conjugated the p15 peptide to them, thus replacing the cell-penetrating TAT sequence of CIGB-300 with a more proteolytically stable alternative. We are awaiting the results of investigations into the anticancer activities of the p15-CPPos.

5.5 References

1. Z. Ahmadi and J. S. McIndoe, *Chem. Commun.*, 2013, **49**, 11488-11490.
2. G. P. McGlacken and I. J. S. Fairlamb, *Eur. J. Org. Chem.,*2009, 4011-4029.
3. L. Jedinák, R. Zátopková, H. Zemánková, A. Šustková and P. Cankař, *J. Org. Chem.,* 2017, **82**, 157-169.
4. P. Sieber, B. Kamber, B. Riniker and W. Rittel, *Helv. Chim. Acta*, 1980, **63**, 2358-2363.
5. H. Lamthanh, C. Roumestand, C. Deprun and A. MÉNez, *Int. J. Pept. Protein. Res.*, 1993, **41**, 85-95.
6. D. G. Simonsen, *J. Biol. Chem.*, 1933, **101**, 35-42.
7. S. E. Perea, O. Reyes, Y. Puchades, O. Mendoza, N. S. Vispo, I. Torrens, A. Santos, R. Silva, B. Acevedo, E. López, V. Falcón and D. F. Alonso, *Cancer Res.*, 2004, **64**, 7127-7129.
8. D. K. Kolmel, D. Furniss, S. Susanto, A. Lauer, C. Grabher, S. Brase and U. Schepers, *Pharmaceuticals*, 2012, **5**, 1265-1281.
9. H. M. Ellerby, W. Arap, L. M. Ellerby, R. Kain, R. Andrusiak, G. D. Rio, S. Krajewski, C. R. Lombardo, R. Rao, E. Ruoslahti, D. E. Bredesen and R. Pasqualini, *Nat. Med.*, 1999, **5**, 1032.
10. J. C. Mai, Z. Mi, S.-H. Kim, B. Ng and P. D. Robbins, *Cancer Res.*, 2001, **61**, 7709-7712.
11. Y. Perera, H. G. Farina, J. Gil, A. Rodriguez, F. Benavent, L. Castellanos, R. E. Gómez, B. E. Acevedo, D. F. Alonso and S. E. Perea, *Mol. Cancer Ther.*, 2009, **8**, 1189-1196.

Chapter 6

Experimental

6.1 Materials and equipment

All the chemical reagents and solvents from commercial sources were used without further purification. *N*-(*tert*-Butoxycarbonyl)-1,4-diaminobutane was purchased from TCI (Tokyo, Japan). 3-Iodobenzylamine was purchased from Acros Organics (Geel, Belgium). PyBOP was purchased from Apollo Scientific (Stockport, UK). All resins and amino acids were purchased from Novabiochem by Merck (Darmstadt, Germany). All other reagents and solvents were purchased from Sigma-Aldrich (St. Louis, MO, USA). NMR solvents were purchased from Goss Scientific (Crewe, UK). Solid phase peptoid and peptide synthesis was performed in Bond Elut solid phase extraction (SPE) cartridges with two polypropylene frits (20 mL) from Crawford Scientific (Lanarkshire, Scotland). Peptoid and peptide syntheses were performed manually in the Bond Elut cartridges. A Radleys Discovery Technology shaker was also used to mix solutions where indicated and aqueous solutions were lyophilised using a Christ Alpha 1-2 LD Plus freeze-drier. Solvents were removed under reduced pressure using a Büchi Rotavapor R11.

6.2 Characterisation

6.2.1 Liquid chromatography electrospray ionisation mass spectrometry

Analytical LC-MS data were obtained using a triple quadrupole mass spectrometer equipped with an Acquity UPLC (Waters Ltd, UK) and a photodiode array detector. Samples were injected onto the Acquity UPLC BEH C18 column (1.7 μm, 2.1 mm × 50 mm) with a flow rate of 0.6 mL min-1 and a linear gradient of 5–95 % of solvent B over 3.8 min (A = 0.1 % formic acid in H_2O, B = 0.1 % formic acid in acetonitrile). The flow was introduced into the electrospray ion source of the Aquity TQD mass spectrometer.

6.2.2 Quadrupole time-of-flight mass spectrometry

Measurements were performed using a QToF Premier mass spectrometer with an Acquity ultra-performance liquid chromatography system (Waters Ltd, UK). Samples were injected to the Acquity UPLC BEH C18 column (1.7 μm, 2.1 mm x 100 mm) with a flow rate of 0.6 mL min-1 and a linear gradient of 0–99 % of solvent B over 6 min (A = 0.1 % formic acid in H_2O, B = 0.1 % formic acid in acetonitrile). The solvent flow from the UPLC was injected into a 0.2 mL/min flow of acetonitrile which was introduced into the electrospray ion source.

6.2.3 Matrix-assisted laser desorption/ionisation mass spectrometry

MALDI-ToF analysis was obtained using an Autoflex II ToF/ToF mass spectrometer (Bruker Daltonik GmBH) equipped with a 337 nm nitrogen laser. The sample solution (ideally at 1 mg mL-1) was mixed with matrix solution, typically α-cyano-4-hydroxycinnamic acid (~ 50 mg mL-1) in the ratio 9:1 matrix to sample. 1 μL of the matrix/sample solution was spotted to the MALDI target and allowed to evaporate prior to analysis, where the metal target is placed into the MALDI ion source. The samples were analysed in positive detection mode with reflectron enhanced mass resolution for *m*/*z* between 500 and 5000. Internal mass calibration with known standards was used to established the mass accuracy. Variable laser intensities were used to ensure the most representative mass spectra for samples were produced. MALDI MS/MS was performed using LIFT technology (MALDI LIFT-ToF-ToF) which enables detection of product ions that result from elevated laser power.

6.2.4 Nuclear magnetic resonance spectroscopy

^{1}H, ^{13}C, ^{19}F NMR and ^{11}B spectra were obtained on the following machines; Varian Mercury-400 MHz, Varian VNMRS-600 MHz and Bruker Avance-400 MHz spectrometers. Chemical shifts are reported in parts per million (δ ppm) and relative to residual solvent peaks. J couplings are reported in megahertz (MHz). Multiplicities: s = singlet, d = doublet, t = triplet.

6.3 Chemical Synthesis

6.3.1 Mono-MIDA boronate (74)

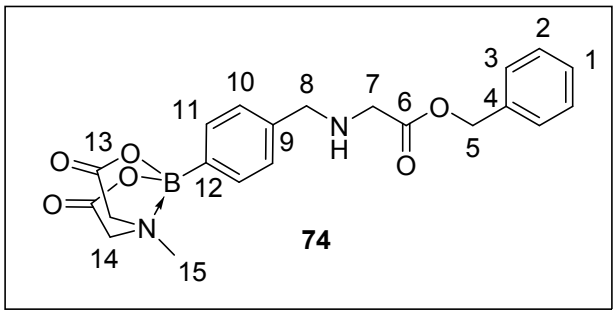

Sodium triacetoxyborohydride (365 mg, 1.72 mmol) was added to a stirred suspension of 4-formylphenylboronic acid MIDA ester (**69**, 300 mg, 1.15 mmol) and glycine benzyl ester (**73**, 348 mg, 1.72 mmol) in dry acetonitrile (10 mL) under nitrogen and the reaction mixture left to stir at room temperature for 48 hours. The mixture was quenched with saturated aqueous sodium bicarbonate and the acetonitrile removed *in vacuo*. The mixture was resuspended in water (20 mL) and washed with ethyl acetate (3 x 50 mL), then the organic layers were collected, dried over magnesium sulphate and the solvent removed in vacuo to yield the crude product as a sticky yellow solid (358 mg) which was further purified by column chromatography (ether:acetonitrile 9:1 ~ 1:1 gradient) to give MIDA boronate (**74**) as a colourless solid (160 mg, 34%). δ_B (128 MHz CD_3CN) 11.80; δ_H (700 MHz CD_3CN) 2.48 (3 H, s, H-15), 3.40 (2 H, s, H-7), 3.86 (2 H, s, H-8), 3.85 – 4.07 (4 H, m, H-14), 5.14 (2H, s, H-5), 7.31 – 7.45 (9 H, m, H1-3 and H10-11); δ_C (176 MHz CD_3CN)* 48.4, 50.7, 53.4, 62.7, 66.9, 128.7, 129.1, 129.1, 129.5, 133.5, 137.4, 142.2, 169.5, 173.1; HRMS (ESI^+) $C_{21}H_{24}{}^{10}BN_2O_6^+$ ($[M+H]^+$) requires 410.1764; found 410.1759.

*Missing peak corresponding to 1 x quaternary carbon

Spectra can be found in **Appendix A**.

6.3.2 Di-MIDA boronate (75)

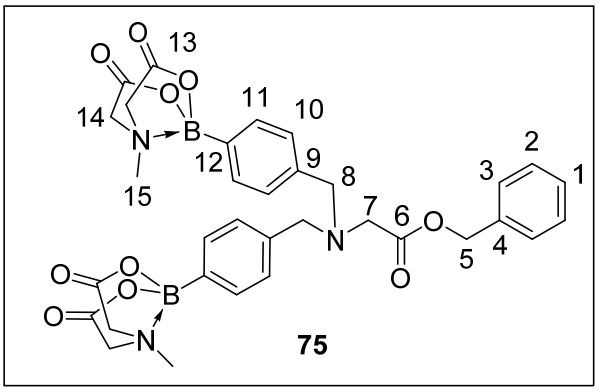

4-formylphenylboronic acid MIDA ester (**69**, 100 mg, 0.38 mmol) was added to a stirred suspension of glycine benzyl ester (**73**, 83 mg, 0.41 mmol) in acetonitrile (2 mL) and stirred at room temperature for 1 hour. Sodium cyanoborohydride (52 mg, 0.82 mmol) was added to the reaction mixture and left to stir at room temperature overnight. The solvent was removed *in vacuo* and the crude mixture redissolved in ethyl acetate (20 mL) and washed twice with saturated aqueous sodium bicarbonate (2 x 10 mL), then once with water (10 mL). The organic layers were combined, dried over magnesium sulphate and the solvent removed *in vacuo* to yield the crude product as a yellow oil which was further purified by column chromatography to give MIDA boronate (**75**) as a colourless solid (20 mg, 8%). δ_B (128 MHz CD_3CN) 11.70; δ_H (700 MHz CD_3CN) 2.46 (6 H, s, H-15), 3.30 (2 H, s, H-7), 3.78 (4 H, s, H-8), 3.97 (8 H, m, H-14), 5.11 (2H, s, H-5), 7.38 (13 H, m, H1-3 and H10-11); δ_C (176 MHz CD_3CN)* 48.4, 54.5, 58.5, 62.7, 66.7, 129.1, 129.1, 129.4, 129.5, 133.4, 137.4, 141.3, 169.5, 171.9; HRMS (ESI$^+$) $C_{33}H_{36}{}^{10}B_2N_3O_{10}^+$ ([M+H]$^+$) requires 654.2659; found 654.2662.

*Missing peak corresponding to 1 x quaternary carbon

Spectra can be found in **Appendix A**.

6.4 Peptoid Synthesis

Solid phase sub-monomer synthesis of peptoids is detailed here.[1] Amines used for peptoid synthesis were *N*-(*tert*-Butoxycarbonyl)-1,4-diaminobutane for *N*lys side-chains, benzylamine for *N*phe side-chains, 4-chlorobenzylamine for *N*pcb side-chains, 4-methoxybenzylamine for *N*pmb side-chains, 3-iodobenzylamine and 4-iodoaniline.

6.4.1 Rink Amide resin:

Fmoc-protected Rink Amide resin (normally 100–300 mg, 0.1–0.2 mmol, typical loading between 0.6 – 0.8 mmol g^{-1}) was swollen in DMF (at least 1 hour, overnight preferred, at room temperature) in a 20 mL polypropylene syringe fitted with two polyethylene

frits. The resin was deprotected with piperidine (20 % in DMF *v*/*v*, 2 x 20 min) and washed with DMF (5 x 2 mL). The resin was treated with bromoacetic acid (2 mL, 0.6 M in DMF) and DIC (0.20 mL, 50 % *v*/*v* in DMF) for 20 minutes at room temperature at 400 rpm. The resin was washed with DMF (5 x 2 mL), before the desired amine sub-monomer was added (2 mL, 0.8–2.0 M in DMF) and allowed to react for 60 minutes at room temperature on the shaker. The resin was again washed with DMF (5 x 2 mL) and the bromoacetylation and amine displacement steps were repeated until the final submonomer had been added and the desired peptoid sequence had been obtained. The resin was shrunk in diethyl ether to remove DMF in preparation for cleavage, as described in **Section 6.7.1** and purified using RP-HPLC as described in **Section 6.7.1**. If further modification of the peptoid was required, the resin was covered with DMF until required. If the peptoid was to be left for more than a day, the resin was washed with diethyl ether (5 x 2 mL) and stored in the fridge.

6.4.2 2-Chlorotrityl chloride resin:

2-Chlorotrityl chloride resin (normally 100–250 mg, 0.1–0.2 mmol, typical loading 1.22 mmol g^{-1}) was swollen in dry DCM (45 minutes at room temperature) in a 20 mL polypropylene syringe fitted with two polyethylene frits. The resin was washed with dry DCM (3 x 2 mL) and loaded with bromoacetic acid (2 mL, 0.6 M in DMF) and neat DIPEA (16 eq. with respect to the resin) for 30 minutes at RT on a shaker at 400 rpm. The resin was washed with DMF (5 x 2 mL), before the desired amine sub-monomer was added (2 mL, 1.5 M in DMF) and allowed to react for 60 minutes at RT on the shaker. The resin was again washed with DMF (5 x 2 mL) and the resin was treated with bromoacetic acid (2 mL, 0.6 M in DMF) and DIC (0.2 mL, 50 % *v*/*v* in DMF) for 20 minutes at RT on the shaker. The resin was washed again with DMF (3 x 2 mL) and amine displacement and bromoacetylation steps repeated until the final sub-monomer had been added and the desired linear peptoid had been obtained. The resin was shrunk in diethyl ether to remove DMF in preparation for cleavage, as described in **Section 6.7**. If further modification of the peptoid was required, the resin was covered with DCM until required. If the peptoid was to be left for more than a day, the resin was washed with diethyl ether (5 x 2 mL) and stored in the fridge.

6.4.3 Addition of 3- or 4- carboxyphenylboronic acid MIDA ester

The resin-bound peptoid was treated with a solution of 3- or 4- carboxyphenyl boronic acid MIDA ester (8 eq. with respect to the resin, in DMF) and DIC (0.4 mL, 50 % v/v in

DMF) and left for 1 hour at RT on the shaker. Following this, the resin was washed with DMF (5 x 2 mL) and then left suspended in DMF until ready for attempted cyclisation.

6.4.4 Addition of glycine residue or glycine-glycine spacer to N terminus of peptoids

The linear peptoid was synthesised via manual SPPS, as in **Sections 6.4.1** or **Section 6.4.2** and the glycine spacer added as follows. Peptoids on resin were swollen in DMF in a polypropylene syringe fitted with a polyethylene frit (at least 1 hour, overnight preferred, at RT). DIPEA (5 equivalents with respect to the resin) was added to a solution Fmoc-protected glycine (5 equivalents with respect to the resin, dissolved in the miniumum amount of DMF) and PyBOP (5 equivalents with respect to the resin in DMF). The DIPEA/PyBOP/glycine solution (2.0 mL) was then added to the resin bound peptoid and left for 1 hour at 25 ˚C on a shaker at 400 rpm. The resin was washed with DMF (5 x 2 mL) and treated with piperidine (20 % in DMF v/v, 2 x 20 minutes) and then washed with DMF (5 x 2 mL). Where the aim was addition of a glycine-glycine spacer, the procedure was repeated. Otherwise the peptoid was suspended in DMF in preparation for the addition of 3- or 4- carboxyphenyl boronic acid MIDA ester.

6.4.5 On-resin Suzuki-Miyaura cross-coupling

6.4.5.1 Intermolecular cross-coupling: synthesis of linear peptoid 106

Following removal of DMF, the resin-bound peptoid **105** (0.1 mmol) was treated with a mixture of tetrakis palladium (6 mg, 5.0 mol %), potassium carbonate (138 mg, 1.0 mmol), SPhos (4 mg, 0.01 mmol) in DMF (2 mL) and iodobenzene (0.11 mL, 1.0 mmol) and heated at 80 ˚C on the shaker at 400 rpm for 8 hours. The solution phase was removed by filtration and the resin washed with DMF (5 x 2 mL), DCM (5 x 2 mL), methanol (5 x 2 mL), water (5 x 2 mL), methanol 5 x 2 mL), DCM (5 x 2 mL) and diethyl ether (5 x 2 mL). Following cleavage from the resin and lyophilisation as described in **Section 6.7.1**, the crude peptoid was purified by RP-HPLC as described in **Section 6.8.1** to give the linear peptoid (**106**) as a white solid. Characterisation data can be found in **Section 6.10**, **Table 6.1** and **Appendix B**.

6.4.5.2 Intramolecular cross-coupling: synthesis of cyclic peptoids

Following removal of DMF, the resin-bound peptoid (0.1 mmol) was treated with a mixture of tetrakis palladium (6 mg, 5.0 mol %), potassium carbonate (138 mg, 1.0 mmol) and SPhos (4 mg, 0.01 mmol) in DMF (2 mL) and heated at 80 ˚C on the shaker

at 400 rpm for 8 hours. The solution phase was removed by filtration and the resin washed with DMF (5 x 2 mL), DCM (5 x 2 mL), methanol (5 x 2 mL), water (5 x 2 mL), methanol (5 x 2 mL), DCM (5 x 2 mL) and diethyl ether (5 x 2 mL). Following cleavage from the resin and lyophilisation as described in **Section 6.7.1**), the crude peptoid was purified by RP-HPLC as described in **Section 6.8.1** to give the cyclic peptoid as a white solid. Characterisation data can be found in **Section 6.10**, **Table 6.1** and **Appendix B**.

6.5 Solid Phase Peptide Synthesis

Fmoc SPPS procedures are detailed in the following sections. Amino acid side chain functionality was protected as follows: Fmoc-D-Ala-OH, Fmoc-allylglycine-OH Fmoc-Arg(Pbf)-OH, Fmoc-Cys(Acm)-OH, Fmoc-Cys(Trt)-OH, Fmoc-Gly-OH, Fmoc-His(Trt)-OH, Fmoc-Leu-OH, Fmoc-D-Leu-OH, Fmoc-D-Lys(Boc)-OH, Fmoc-Met-OH, Fmoc-Pro-OH, Fmoc-Ser(tBu)-OH, Fmoc-Thr(tBu)-OH, Fmoc-Trp(Boc)-OH,. Fmoc deprotections were carried out using a 20 % (*v*/*v*) solution of piperidine in DMF.

6.5.1 Loading procedures

Rink Amide Resin

Fmoc-protected Rink Amide resin (normally 100–300 mg, 0.1–0.2 mmol, typical loading between 0.6 – 0.8 mmol g^{-1}) was swollen in DMF (at least 1 hour, overnight preferred, at room temperature) in a 20 mL polypropylene syringe fitted with two polyethylene frits. The resin was deprotected with piperidine (20 % in DMF *v*/*v*, 2 x 20 min) and washed with DMF (5 x 2 mL). DIPEA (5 equivalents with respect to the resin) was added to a solution. Fmoc-protected allylglycine (5 equivalents with respect to the resin, dissolved in the miniumum amount of DMF) and PyBOP (5 equivalents with respect to the resin in DMF). The DIPEA/PyBOP/glycine solution (2.0 mL) was then added to the resin bound peptoid and left for 1 hour at RT on a shaker at 400 rpm. The resin was washed with DMF (5 x 2 mL) and treated with piperidine (20 % in DMF v/v, 2 x 20 minutes) and then washed with DMF (5 x 2 mL). Peptide synthesis then proceeded as detailed in **Section 6.5.2**.

2-Chlorotrityl Chloride Resin

2-Chlorotrityl chloride resin (normally 100–250 mg, 0.1–0.2 mmol, typical loading 1.22 mmol g^{-1}) was swollen in dry DCM (45 minutes at room temperature) in a 20 mL polypropylene syringe fitted with two polyethylene frits. The resin was washed with dry

DCM (3 x 2 mL) and loaded with Fmoc-Cys(Acm)-OH or Fmoc-Cys(Trt)-OH (2.5 equivalents with respect to the resin, dissolved in the minimum amount of DCM) and neat DIPEA (2.5 eq. with respect to the resin) for 30 minutes at RT on a shaker at 400 rpm. The resin was then washed with DMF (5 x 2 mL) and treated with a 2:1 solution of DCM:MeOH with DIPEA (2.5 equivalents with respect to the resin) for 10 minutes on the shaker. Peptide synthesis then proceeded as detailed in Section 6.5.2.

6.5.2 Peptide Synthesis

Peptide synthesis was either carried out directly onto the resin (see **Section 6.5.1** for loading procedures) or onto a linear peptoid sequence with a terminal glycine-glycine spacer (see **Sections 6.4.2 and 6.4.4**). If not already swollen, the sequence on resin was swollen in DMF if on Rink Amide resin, DCM if on 2-chlorotrityl chloride resin, in a polypropylene syringe fitted with a polyethylene frit (at least 1 hour, overnight preferred, at RT). The resin was washed with DMF x 5. DIPEA (5 equivalents with respect to the resin) was added to a solution of Fmoc-protected amino acid (5 equivalents with respect to the resin) and PyBOP (5 equivalents with respect to the resin) in the minimum amount of DMF. The DIPEA/PyBOP/amino acid solution (2.0 mL) was immediately added to the resin bound peptoid and left for 1 hour at RT on a shaker at 400 rpm. The resin was washed with DMF (5 x 2 mL) and treated with piperidine (20 % in DMF v/v, 2 x 20 minutes) and then washed with DMF (5 x 2 mL). Further amino acid couplings and Fmoc-deprotection steps were made as necessary. The resin was washed with DMF (5 x 2 mL) and diethyl ether (5 x 2 mL) prior to cleavage from the resin as described in **Section 6.7** and purification by RP-HPLC as described in **Section 6.8.1**. If further modification of the peptoid was required, the resin was covered with DMF (for Rink Amide resin) or DCM (for 2-chlorotrityl chloride resin) until required. If the peptoid was to be left for more than a day, the resin was washed with diethyl ether (5 x 2 mL) and stored in the fridge.

6.5.3 Addition of 5-Hexynoic Acid Monomers

The linear peptide was synthesised via manual SPPS, as in **Section 6.5.2** and 5-hexynoic acid added as follows. Peptides on resin were swollen in DCM in a polypropylene syringe fitted with a polyethylene frit (at least 1 hour, overnight preferred, at RT). The resin was washed with DMF x 5 and DIPEA (5 equivalents with respect to the resin) was added to a solution 5-hexynoic acid (5 equivalents with respect to the resin) and PyBOP (5 equivalents with respect to the resin) in the minimum amount of DMF. The DIPEA/PyBOP/5-hexynoic acid solution (2.0 mL) was immediately added to

the resin bound peptide and left for 1 hour at 25 ˚C on a shaker at 400 rpm. The resin was washed with DMF (5 x 2 mL) and another addition of DIPEA/PyBOP/5-hexynoic acid solution (2.0 mL) was carried out. After washing with DMF (5 x 2 mL), the resin was washed with diethyl ether (5 x 2 mL) and a portion cleaved from the resin as described in **Section 6.7.1**.

6.5.4 Synthesis of linear p15 peptide with Acm-protected cysteine (136)

The peptide was synthesised on 2-chlorotrityl chloride resin and loaded with Fmoc-Cys(Acm)-OH as described in **Section 6.5.1** on an 0.2 mmol scale with respect to the resin. The Fmoc group was deprotected by addition of piperidine (20 % in DMF *v*/*v*, 2 x 20 minutes) and the resin washed with DMF x 5. DIPEA (5 equivalents with respect to the resin) was added to a solution of Fmoc-Thr(tBu)-OH (5 equivalents with respect to the resin) and PyBOP (5 equivalents with respect to the resin) in the minimum amount of DMF. The DIPEA/PyBOP/amino acid solution (2.0 mL) was immediately added to the resin bound peptoid and left for 1 hour at RT on a shaker at 400 rpm. The resin was washed with DMF (5 x 2 mL) and treated with piperidine (20 % in DMF v/v, 2 x 20 minutes) and then washed with DMF (5 x 2 mL). Further amino acid couplings and Fmoc-deprotection steps were made as necessary. Fmoc-Ser(tBu) and Fmoc-Cys(Acm)-OH underwent double coupling. The resin was washed with DMF (5 x 2 mL). The peptide was then cyclised according to **Section 6.6.1**. A portion of the resin was washed with diethyl ether (5 x 2 mL) prior to test cleavage from the resin as described in **Section 6.7**).

6.5.5 Synthesis of linear p15 peptide with Trt-protected cysteine (147)

The peptide was synthesised on 2-chlorotrityl chloride resin and loaded with Fmoc-Cys(Trt)-OH as described in **Section 6.5.1** on an 0.2 mmol scale with respect to the resin. The Fmoc group was deprotected by addition of piperidine (20 % in DMF *v*/*v*, 2 x 20 minutes) and the resin washed with DMF x 5. DIPEA (5 equivalents with respect to the resin) was added to a solution of Fmoc-Thr(tBu)-OH (5 equivalents with respect to the resin) and PyBOP (5 equivalents with respect to the resin) in the minimum amount of DMF. The DIPEA/PyBOP/amino acid solution (2.0 mL) was immediately added to the resin bound peptoid and left for 1 hour at RT on a shaker at 400 rpm. The resin was washed with DMF (5 x 2 mL) and treated with piperidine (20 % in DMF v/v, 2 x 20 minutes) and then washed with DMF (5 x 2 mL). Further amino acid couplings and Fmoc-deprotection steps were made as necessary. Fmoc-Ser(tBu) and Fmoc-Cys(Trt)-OH underwent double coupling. The resin was washed with DMF (5 x 2 mL). The resin

was washed with diethyl ether (5 x 2 mL) prior to cleavage from the resin as described in **Section 6.7.1** and hexafluorobenzene stapling as described in **Section 6.6.2**.

6.5.6 Synthesis of linear allylglycine p15 peptide analogue (150)

The peptide was synthesised on Rink Amide resin and loaded with Fmoc-allylglycine-OH as described in **Section 6.5.1** on an 0.2 mmol scale with respect to the resin. The initial allylglycine coupling step was repeated and the resin washed with DMF x 5. The Fmoc group was deprotected by addition of piperidine (20 % in DMF *v*/*v*, 2 x 20 minutes) and the resin washed with DMF x 5. DIPEA (5 equivalents with respect to the resin) was added to a solution of Fmoc-Thr(tBu)-OH (5 equivalents with respect to the resin) and PyBOP (5 equivalents with respect to the resin) in the minimum amount of DMF. The DIPEA/PyBOP/amino acid solution (2.0 mL) was immediately added to the resin bound peptoid and left for 1 hour at RT on a shaker at 400 rpm. The resin was washed with DMF (5 x 2 mL) and treated with piperidine (20 % in DMF v/v, 2 x 20 minutes) and then washed with DMF (5 x 2 mL). Further amino acid couplings and Fmoc-deprotection steps were made as necessary. Fmoc-Ser(tBu) and Fmoc-allylglycine-OH underwent double coupling. The resin was washed with DMF (5 x 2 mL). The peptide was then cyclised according to **Section 6.6.3**. A portion of the resin was washed with diethyl ether (5 x 2 mL) prior to test cleavage from the resin as described in **Section 6.7.1**.

6.5.7 Synthesis of KLA-peptoid hybrids

(Note: Peptide synthesis and purification was carried out by Jingyi Zong at Durham University).

Peptoids were synthesised on Rink Amide resin as described in **Section 6.4.1** on an 0.1 mmol scale. Following addition of two glycine residues as described in **Section 6.4.4**, the peptide sequence was synthesised as described in **Section 6.5.2**. Peptide-peptoids were cleaved from the resin as described in Section 6.7.1 and purified by RP-HPLC as described in **Section 6.8.1**. LCMS and MALDI data can be found in **Section 6.10**, **Table 6.3** and **Appendix D**.

6.5.8 Synthesis of Rhod-KLA-CPPo6

(Note: Procedure carried out by Jingyi Zong at Durham University).

CPPo6 was synthesised on Rink Amide resin as described in **Section 6.4.1** on a 0.03 mmol scale. Following addition of two glycine residues as described in **Section 6.4.4**,

the peptide sequence was synthesised as described in **Section 6.5.2**. The Rhodamine (59.6 mg, 0.125 mmol, 5.0 equiv) was coupled by addition of DIC (31.9µL, 0.125 mmol, 5.0 equiv) and HOBt (16.9 mg, 0.125 mmol, 5.0 equiv) in DMF and incubated for 1 hour at RT. Rhodamine coupling was repeated to ensure the completion of the reaction. The final product was cleaved by addition of trifluoroacetic acid (95% in CH_2Cl_2) and incubated for 2.5 hours. The cleavage solution was filtered and the resin was thoroughly washed with MeOH. This procedure of adding cleavage solution and rinsing with methanol was repeated until the cleavage solution was colourless. The cleavage solution was diluted with water and lyophilised to give the crude product. HRMS and MALDI data can be found in **Section 6.10**, **Table 6.3**, and in **Appendix D**.

6.5.9 Synthesis of p15-peptoid hybrids

Peptoids were synthesised on 2-chlorotrityl resin as described in **Section 6.4.2**. A portion of the resin was washed with diethyl ether x 5 prior to cleavage as described in **Section 6.7.3**. Following addition of two glycine residues as described in **Section 6.4.4**, the peptide sequence was synthesised as described in **Section 6.5.2**. Addition of 5-hexynoic acid was carried out as described in **Section 6.5.3**. The resin was washed with diethyl ether x 5, a portion set aside for test cleavage as described in **Section 6.6** and the remainder sent to Hong Kong Polytechnic University. MALDI data can be found in **Section 6.10**, **Table 6.4** and in **Appendix E**.

6.6 Peptide post-translational modifications

6.6.1 Disulphide bridge formation

The linear peptide was synthesised on 2-chlorotrityl chloride and loaded with Fmoc-Cys(Acm)-OH as described in **Section 6.5.4**. A solution of iodine (127 mg, 1.0 mmol) in DCM (1 mL) and DIPEA (0.18 mL, 1.0 mmol) was added to the resin-bound peptide (0.1 mmol) and left on the shaker at 400 rpm for 90 minutes. The peptide was washed with DCM x 5, DMF x 5 and diethyl ether x5 prior to cleavage from the resin as described in **Section 6.7.1** and purification as described in **Section 6.8.1**. Cyclised p15 (**126**) was obtained as a white powder in 19% yield. Characterisation data can be found in **Section 6.10**, **Table 6.2** and in **Appendix C**.

6.6.2 Hexafluorobenzene stapling

The linear peptide was synthesised on 2-chlorotrityl chloride and loaded with Fmoc-Cys(Trt)-OH as described in **Section 6.5.5**. The cleaved, fully deprotected, crude peptide (12 mg, 0.01 mmol) was dissolved in 1 mL of DIPEA (50 mM) in DMF and

hexafluorobenzene (0.006 mL, 0.05 mmol) was added and the reaction mixture left on the shaker at 400rpm for 4 hours at room temperature. The DMF was removed *in vacuo* and the crude peptide was purified by HPLC, as described in **Section 6.8.1** to give F-p15 (**127**) as a white powder in 32% yield. Characterisation data can be found in **Section 6.10**, **Table 6.2** and in **Appendix C**.

6.6.3 Grubbs Ring-Closing Metathesis of peptides

The linear peptide was synthesised on Rink Amide resin as described in **Section 6.5.6**. The linear peptide was washed with DCM (3 x 2 mL) and DCE (3 x 2 mL). The Hoveyda-Grubbs 2nd generation catalyst (20 mol%) was dissolved in 2 mL of a solution of DCE containing 10% LiCl (0.4M) in DMF. This catalyst solution was added to the resin-bound linear peptide and the mixture stirred at 80 °C for 48 hours. The peptide was washed with DCE (5 x 2 mL), DCM (5 x 2mL), MeOH (5 x 2mL), water (5 x 2 mL), MeOH (5 x 2 mL), DCM (5 x 2 mL), DMF (5 x 2 mL) and diethyl ether (5 x 2 mL) before being cleaved from the resin as described in **Section 6.7.2** and purified by HPLC as described in **Section 6.8.1** to give C=C p15 (**128**) as a white powder in 11% yield. Characterisation data can be found in Section 6.**10**, **Table 6.2** and in **Appendix C**.

6.6.4 Hydrogenation of C=C stapled peptides

C=C p15 (**129**) was synthesised as described in **Sections 6.5.6** and **6.6.2**. Hydrogen was passed over a stirred mixture of the cleaved, purified peptide and palladium on carbon in ethanol for 2 hours at room temperature and the progress of the reaction monitored by LCMS. On completion of the reaction, the reaction mixture was centrifuged at 13400 rpm for 5 minutes, the supernatant transferred to a round-bottomed flask and ethanol removed *in vacuo* to afford the pure C-C stapled peptide (**129**) as a white powder in 50% yield with respect to the starting C=C p15 peptide (**128**). Characterisation data can be found in **Section 6.10**, **Table 6.2** and in **Appendix C**.

6.7 Cleavage from acid-labile resins

6.7.1 Rink Amide Resin or 2-Chlorotrityl chloride resin when simultaneous deprotection of side-chains is desired

Final cleavage from resin was achieved using TFA (95 %), H_2O (5 %) and TIPS (5 %). For test cleaves approximately 1 mL of the cleavage cocktail was used and for cleavage from 100 mg resin, approximately 4 mL of the cleavage cocktail was added. The resin was then placed on the shaker at 400 rpm for 2 hours for peptoids and 4 hours for peptides and the resin removed by filtration. The cleavage cocktail was removed *in vacuo*, the crude product precipitated in diethyl ether (45 mL) and the precipitate retrieved by trituration. The crude product was dissolved in a mixture of acidified H_2O and MeCN and lyophilised.

6.7.2 Rink Amide resin or 2-Chlorotrityl chloride resin when simultaneous deprotection of side-chains is desired and avoidance of methionine oxidation is necessary

Final cleavage from resin was achieved using TFA (94 %), EDT (2.5 %), H_2O (2.5 %) and TIPS (1 %). For test cleaves approximately 1 mL of the cleavage cocktail was used and for cleavage from 100 mg resin, approximately 4 mL of the cleavage cocktail was added. The resin was then placed on the shaker at 400 rpm for 4 hours and the resin removed by filtration. The cleavage cocktail was removed *in vacuo*, the crude product precipitated in diethyl ether (45 mL) and the precipitate retrieved by trituration. The crude product was dissolved in a mixture of acidified H_2O and MeCN and lyophilised.

6.7.3 2-Chlorotrityl Chloride Resin leaving acid labile side-chain protecting groups intact

Final cleavage from resin was achieved using hexafluoroisopropanol in DCM (20 % *v*/*v*). For test cleaves approximately 1 mL of the cleavage cocktail was used and for cleavage from 100 mg resin, approximately 4 mL of the cleavage cocktail was added. The resin was then placed on the shaker at 400 rpm for 30 minutes and the resin removed by filtration. The cleavage cocktail was removed *in vacuo*, the crude product dissolved in a mixture of H_2O and MeCN and lyophilised.

6.8 Purification Procedures

6.8.1 Preparative high performance liquid chromatography

Preparative RP-HPLC was performed with a semi-preparative Perkin Elmer Series 200 LC pump fitted with a 785A UV/Vis detector using a SB-Analytical ODH-S optimal column (250 × 10 mm, 5 Cm); flow rate 2 ml min^{-1}; linear gradient elution 0-50% of solvent B over 60 min, then 50-100% of solvent B over 30 min (*A* = 0.1% TFA in 95% H_2O and 5% MeCN, *B* = 0.1% TFA in 5% H_2O and 95% MeCN) with detection at 280 nm. Relevant fractions were collected, lyophilised and analysed by LC-MS.

6.8.2 Analytical high performance liquid chromatography

Samples were dissolved in 100 µL acidified water and the purity of products was estimated by an injection of 50 µL to analytical RP-HPLC using a Perkin Elmer 200 Series LC pump with a Perkin-Elmer 785A UV-vis detector on an SB Analytical column (ODS-H Optimal), 4.6 x 100mm , 3.5 µm; flow rate = 1 mL min-1; loop size = 20 µL; λ = 280 nm; gradient: 0–100 % solvent B over 30 min (solvent A: 95 % H2O, 5 % MeCN, 0.05 % TFA; solvent B: 95 % MeCN, 5 % H2O, 0.03 % TFA).

6.9 Biological Experiments

6.9.1 Antibacterial Testing against *S. aureus* and *E. coli*

6.9.1.1 Bacterial culture preparation

Escherichia coli K-12 wild-type strain (W3110 / ATCC27325, F-, λ-, *rpoS(Am)*, *rph-1*,*Inv*(*rrnD-rrnE*)), *Staphylococcus aureus* (3R7089 strain Oxford / ATCC9144) were selected for bacteriological studies as representative Gram-negative (*E. coli*) and Gram-positive (*S. aureus*)species. Bacterial cultures were prepared by streaking bacterial strains onto LB agar plates with an inoculation loop and incubated overnight at 37°C. A single colony was selected and placed in 5 mL of Iso-sensitest broth (Oxoid, ThermoScientific) and incubated with shaking for 16–18 h at 37 °C to provide liquid cultures for testing.

6.9.1.2 Antibacterial plate preparation

Plates were prepared according to the previously described protocol for MIC determination.[2] Testing was conducted in 96-well plates (Sarsted, Fisher Scientific). Bacteria were grown from overnight cultures in Iso-sensitest broth to an A650nm of 0.07 equivalent to a 0.5 MacFarland standard (240 µM BaCl2 in 0.18 M H2SO4). This

culture was diluted ten-fold with Iso-sensitest broth before use. Peptoids were initially dissolved in water (300 µL) and diluted further in Iso-sensitest broth (150 µL) to achieve maximum concentrations to test the available peptoids in triplicate at a single concentration each (**Table 2.2**). 50 µL of inoculum and 50 µL of peptoid solution were added to each test well. Experiments were performed in triplicate. A positive control for bacterial growth contained only the inoculum and Isosensitest broth. A sterile control contained only isosensitest broth (100 µL). The plates were incubated at 37 °C for 16 h with shaking. Quantitative data was attained from absorbance values using a Biotek Synergy H4 plate reader.

6.9.2 Bio-layer interferometry (BLI) binding assays

(Note: BLI assays were carried out by the Law group at The Hong Kong Polytechnic University).

The binding kinetics of B23-peptides to recombinant human B23 protein was determined using BLI on Octet RED (FortéBio, Shanghai, China) following manufacturer protocol. All the interaction analyses were performed at 30°C in PBS 0.2% DMSO buffer. Loading of Nickel-charged Tris-NTA (Ni-NTA) biosensors (FortéBio) was conducted by exposing His-tagged B23 containing 0.1mg/mL to biosensor tips for two hours. The 96-well microplates used in the Octet were filled with 200µl of sample or buffer per well and agitated at 1000 rpm. The loaded biosensors were washed in buffer for 600 seconds and transferred to the wells containing 30µg B23 peptides in buffer, respectively. The association and dissociation was observed for 100 seconds for each sample.

6.9.3 Cell culture

Human cervical carcinoma HeLa cells were purchased from the American type Culture Collection (ATCC) (#CCL-185, ATCC, Manassas, VA, USA). The HeLa cells were grown in Dulbecco's Modified Eagle Medium (DMEM) supplemented with 10% fetal bovine serum (FBS), 1% penicillin and streptomycin at 37°C and 5% CO2.

6.9.4 MTT assay

(*Note: MTT experiments were carried out by Lijun Jiang at Hong Kong Baptist University*).

Cells (105per sample) were incubated in a 96 well-plate overnight. Afterwards, HeLa or MRC-5 cells treated with the peptide or peptoidfor 24 hours were further incubated in dark for 24h. Cell viability was determined by the 3-(4,5-Dimethyl-2-thiazolyl)-2,5-diphenyl-2-H-tetrazolium bromide (MTT) reduction assay. The cell monolayers were rinsed with PBS and then incubated with 0.5 mg/ml MTT solution for 3h (5% CO2,

37°C). The formazan crystal formed was dissolved in DMSO and the absorbance of dissolved formazan crystal at 540 and 690 nm was measured using a 96 -well plate reader (ELx800 Absorbance Microplate Reader).

6.9.5 Flow cytometry analysis on cellular uptake

(Note: Flow cytometry was carried out by the Wong group at Hong Kong Baptist University).

Cells (105 per sample) were seeded to 35 mm Petri dish for overnight and then the cells were incubated with Rhod-KLA-CPPo6. Afterwards cells were trypsinized and washed twice with phosphate -buffered saline (PBS). The Rhod-KLA-CPP06's uptake by cells was analysed by flow cytometry. The cells were excited with 488 nm argon laser and emission was collected with FL - 3 (equipped with 650 nm long pass filter) and 10000 events were analysed.

6.9.6 Confocal microscopic imaging

(Note: Confocal microscopy was carried out by the Wong group at Hong Kong Baptist University).

Cells were seeded onto coverslip in 35 mm culture dishes overnight. The cells were initially incubated with Rhod-KLA-CPPo6 for 30 min in the dark. The emitted fluorescent signals were examined using a Leica SP5 (upright configuration) confocal microscope equipped with argon laser, HeCd laser and a femtosecond - pulsed Ti: Sapphire laser (Libra II, Coherent) inside the tissue culture chamber (5% CO2, 37 °C). A 40*oil immersion objective and a pinhole size of 110 μm was used for image capturing.

6.10 Characterisation of Peptides and Peptoids: Tables

Table 6.1 Biaryl-containing peptoids

Compound number	Accurate Mass	
	Calculated $[M+H]^+$	Observed $[M+H]^+$
106	454.2818	454.2819
104	651.3982	651.4004
110	580.2347	580.3238
119	651.3982	651.3933
120	580.2347	580.3260
121	779.4932	779.4903
122	708.4197	708.4199
123	779.4932	779.4959
124	708.4197	708.4185

Table 6.2 p15 peptides and analogues

Compound number	Accurate Mass	
	Calculated $[M+H]^+$	Observed $[M+H]^+$
126	1288.5389	1288.5404
127	1436.5326	1436.5377
128	1249.6265	1249.6272
129	1251.6421	1251.6460

Table 6.3 KLA-CPPo hybrids

Name	Accurate Mass		MALDI-ToF
	Calculated	Observed	
D-KLA (**199**)	1523.0889 = $[M+H]^+$	1523.0907	1545.9 = $[M+Na]^+$
KLA-CPPo1 (**193**)	735.1549 = $[M+3H]^{3+}$	735.1545	2203.5 = $[M+H]^+$
KLA-CPPo2 (**194**)	1085.2479 = $[M+2H]^{2+}$	1085.2368	2191.5 = $[M +Na]^+$
KLA-CPPo3 (**195**)	1109.7399 = $[M+2H]^{2+}$	1109.7328	2240.5 = $[M + Na]^+$
KLA-CPPo4 (**196**)	1126.7205 = $[M+2H]^{2+}$	1126.7159	2252.9 = $[M + H]^+$
KLA-CPPo5 (**197**)	1111.7152 = $[M+2H]^{2+}$	1111.7184	2244.4 = $[M + H]^+$
KLA-CPPo6 (**198**)	1136.2072 = $[M+2H]^{2+}$	1136.2086	2293.2 = $[M + Na]^+$
Rhod-KLA-CPPo6 (**201**)	540.3324 = $[M+5H]^{5+}$	540.3219	2696.5 = $[M+H]^+$

Table 6.4 p15-CPPo hybrids (crude)

Name	MALDI-ToF
Hyx-p15-CPPo7 (**222**)	2208.5 = $[M+H]^+$
Hyx-p15-CPPo8 (**223**)	2173.4 = $[M +H]^+$
Hyx-p15-CPPo9 (**224**)	2222.7 = $[M + H]^+$
Hyx-p15-CPPo9 (**225**)	2257.3 = $[M + H]^+$
Hyx-p15-CPPo10 (**226**)	2227.1 = $[M + H]^+$
Hyx-p15-CPPo11 (**227**)	2276.1 = $[M + H]^+$

6.11 References

1. R. N. Zuckermann, J. M. Kerr, S. B. H. Kent and W. H. Moos, *J. Am. Chem. Soc.*, 1992, **114**, 10646-10647.
2. J. M. Andrews, *J. Antimicrob. Chemother.*, 2001, **48 Suppl 1**, 5-16.

Appendices

Spectra of Compounds

Appendix A

Spectra of MIDA boronate peptoid monomers

1. Spectra of Mono-MIDA boronate (74)

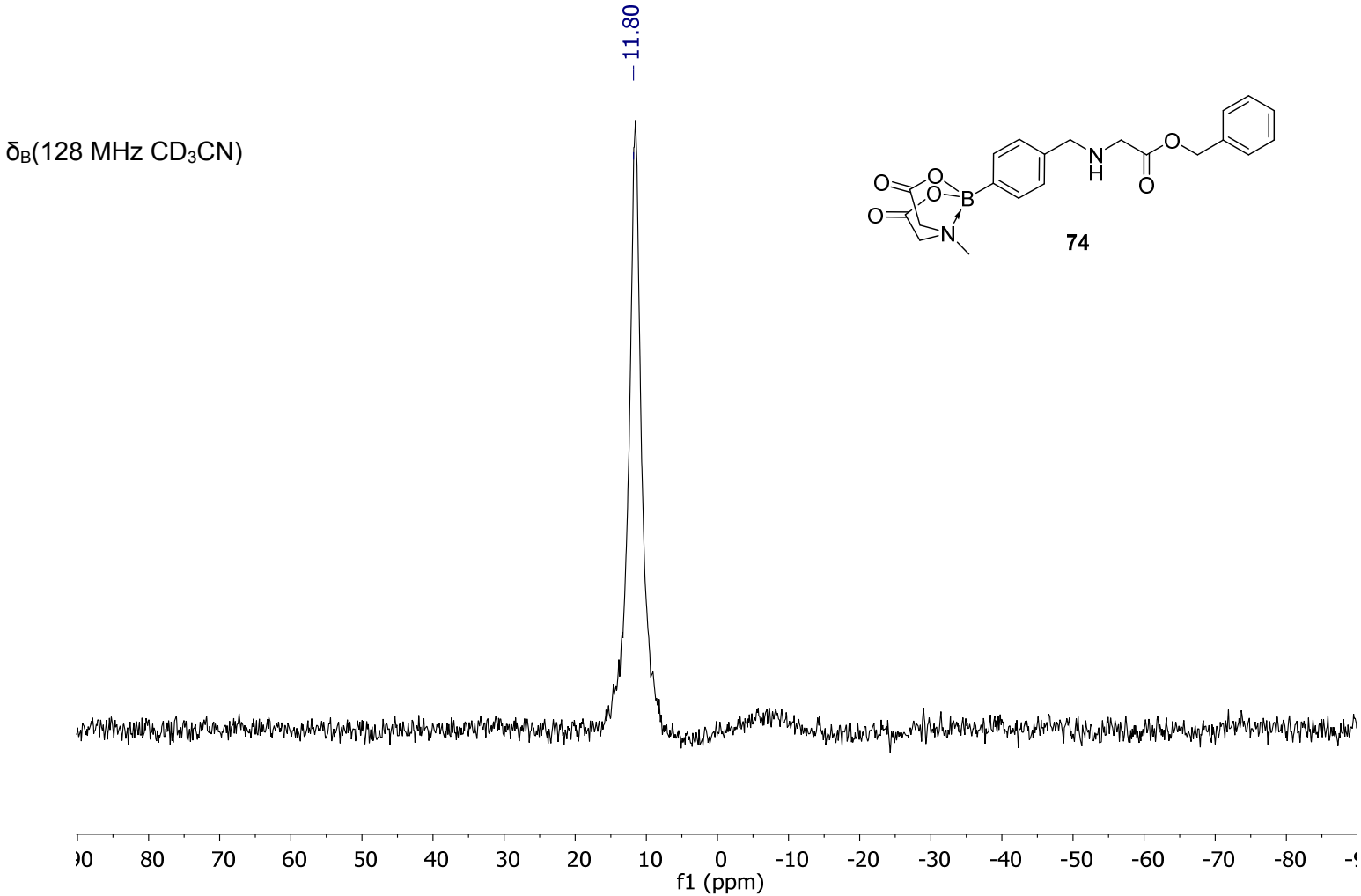

Figure A1 ^{11}B NMR of mono-MIDA ester **74**.

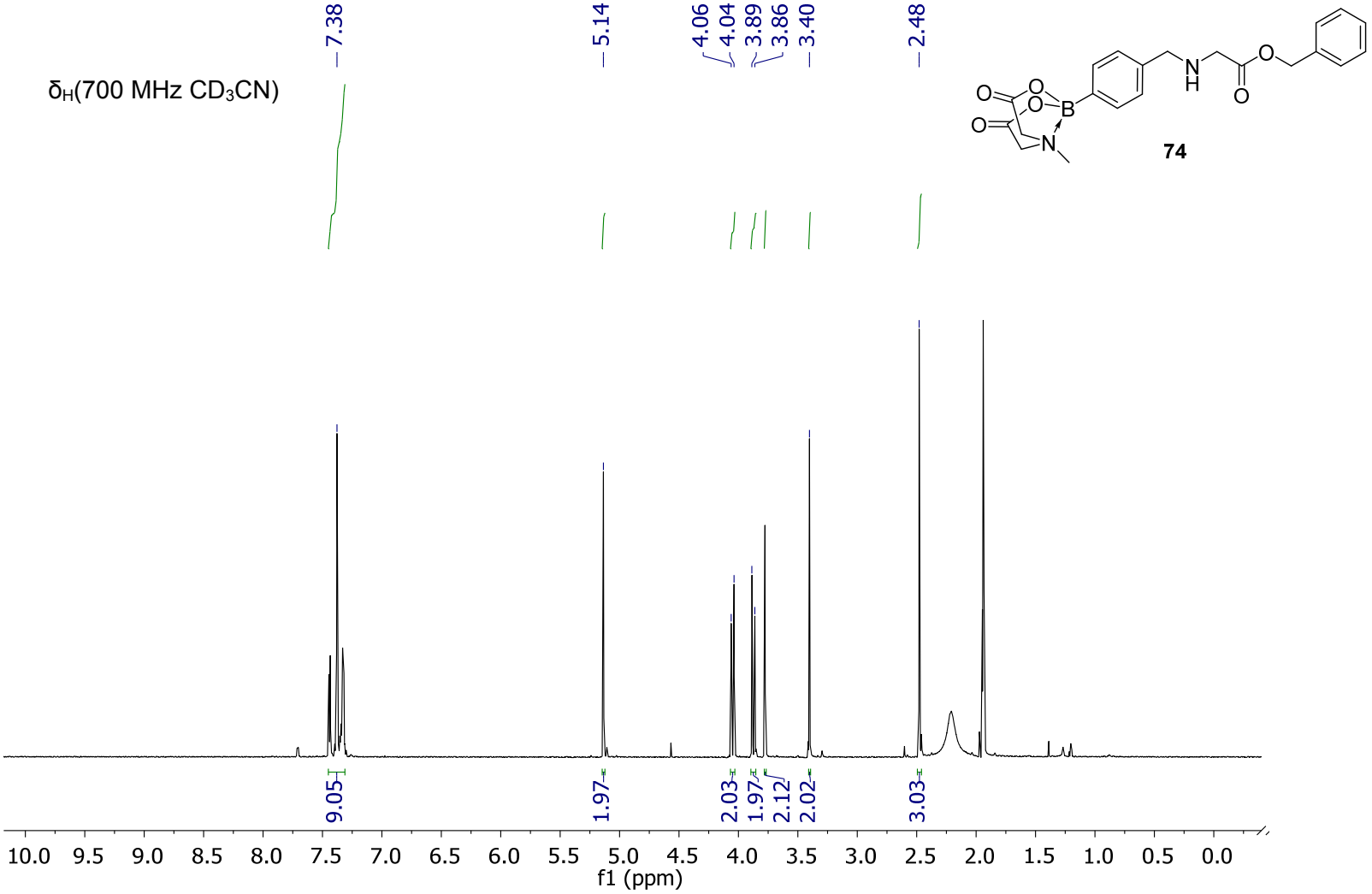

Figure A2 ^{1}H NMR of mono-MIDA ester **74**.

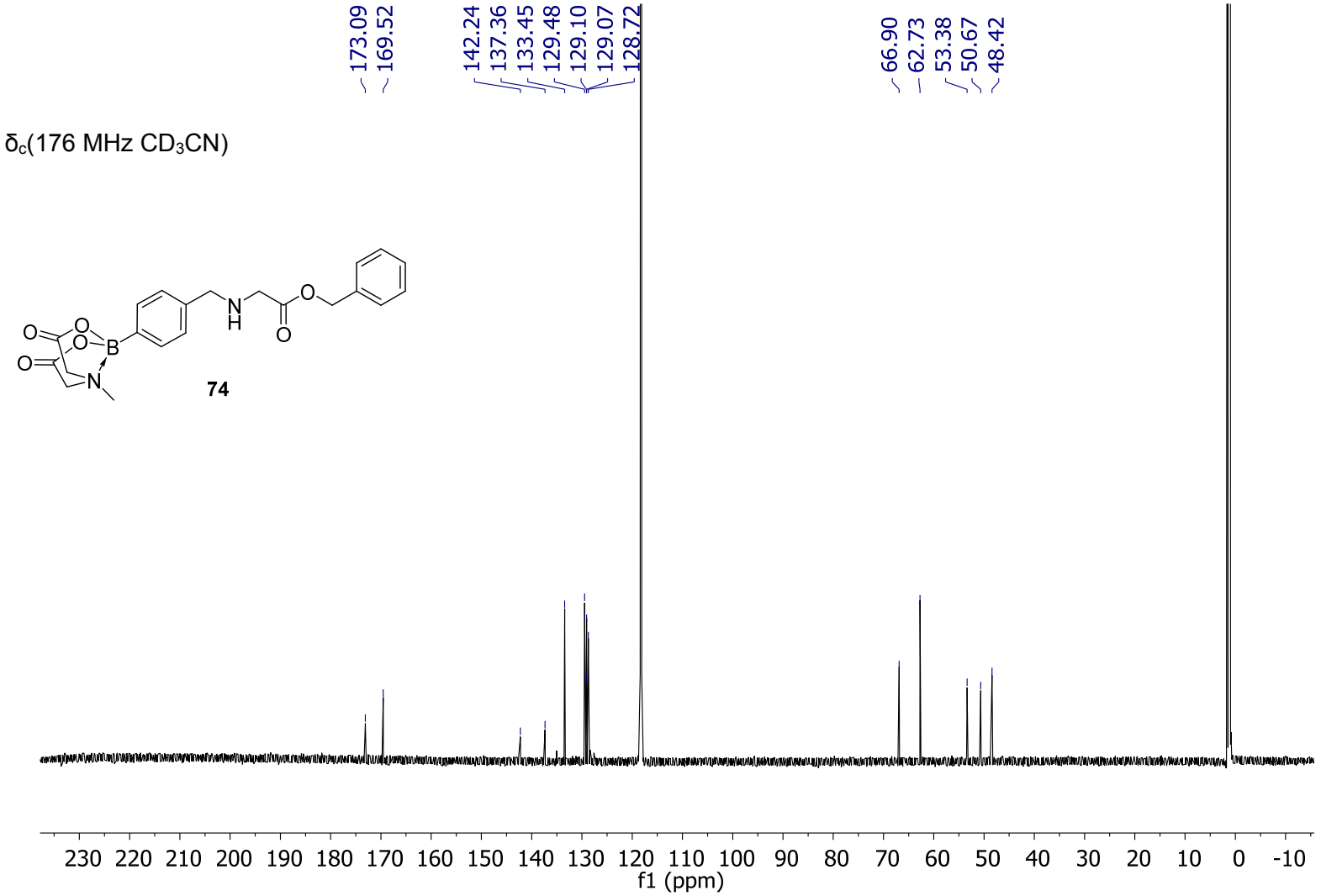

Figure A3 ^{13}C NMR of mono-MIDA ester **74**.

Elemental Composition Report

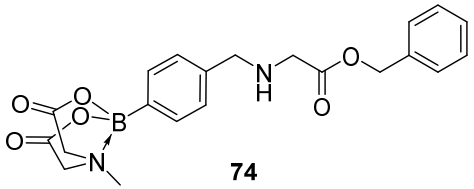

74

Single Mass Analysis

Tolerance = 2.5 PPM / DBE: min = -1.5, max = 50.0
Element prediction: Off
Number of isotope peaks used for i-FIT = 3

Monoisotopic Mass, Even Electron Ions
24397 formula(e) evaluated with 29 results within limits (all results (up to 1000) for each mass)
Elements Used:
C: 0-50 H: 0-90 10B: 0-1 N: 0-7 O: 0-20 28Si: 0-1 P: 0-3 S: 0-3

Alexandra Webster
AMW-02-032-F19-20 261 (2.170) Cm (261:279)

1: TOF MS ES+
3.31e+005

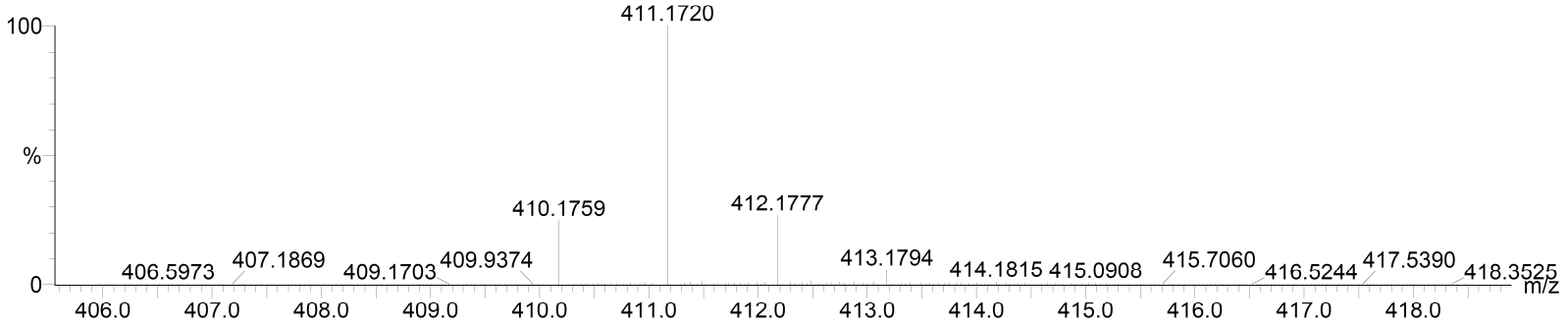

Figure A4 HRMS of mono-MIDA ester (**74**), $C_{21}H_{24}{}^{10}BN_2O_6$, calculated $[M+H]^+$ = 410.1764, observed $[M+H]^+$ = 410.1759.

2. Spectra of Di-MIDA boronate (75)

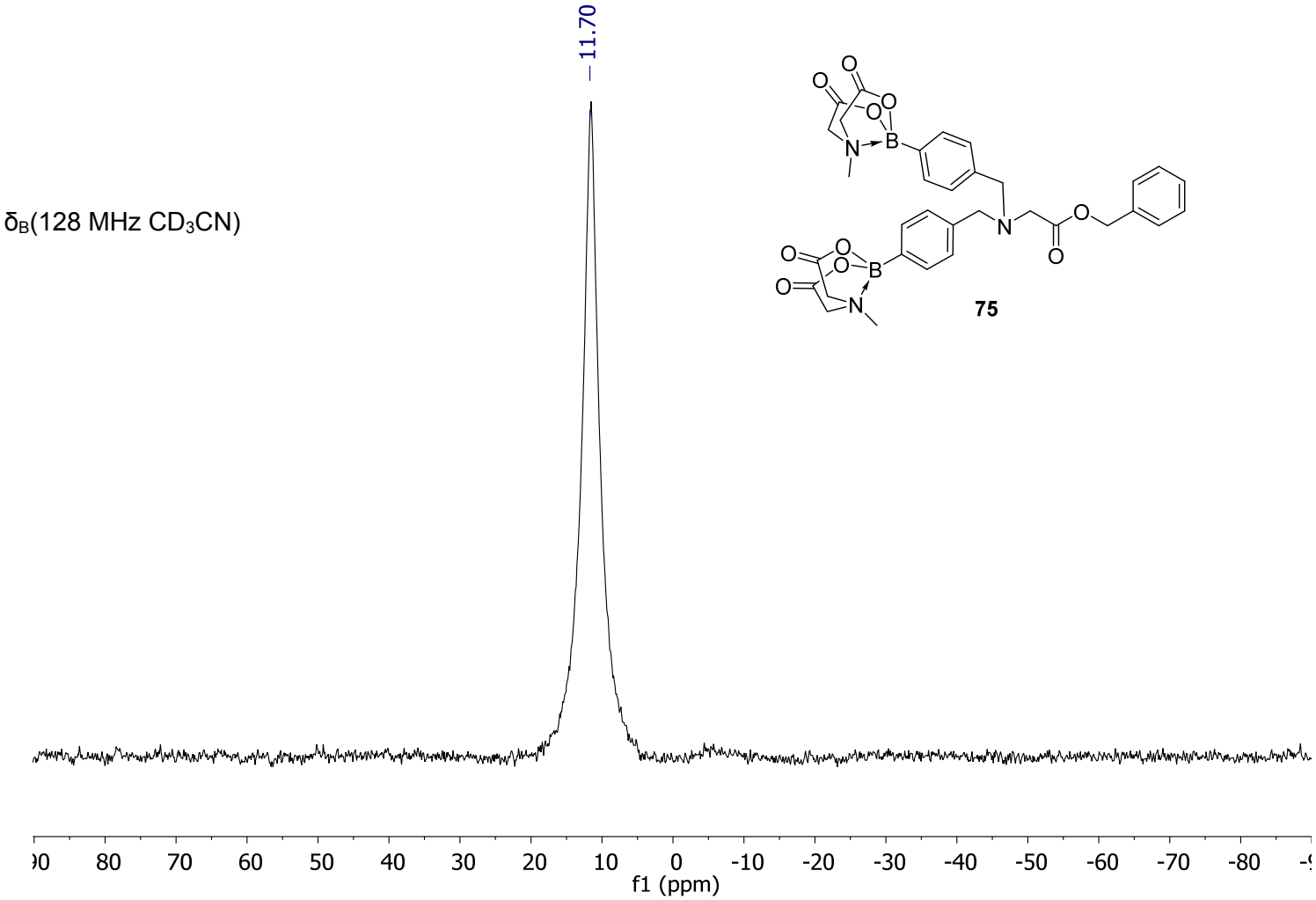

Figure A5 ^{11}B NMR of di-MIDA ester **75**.

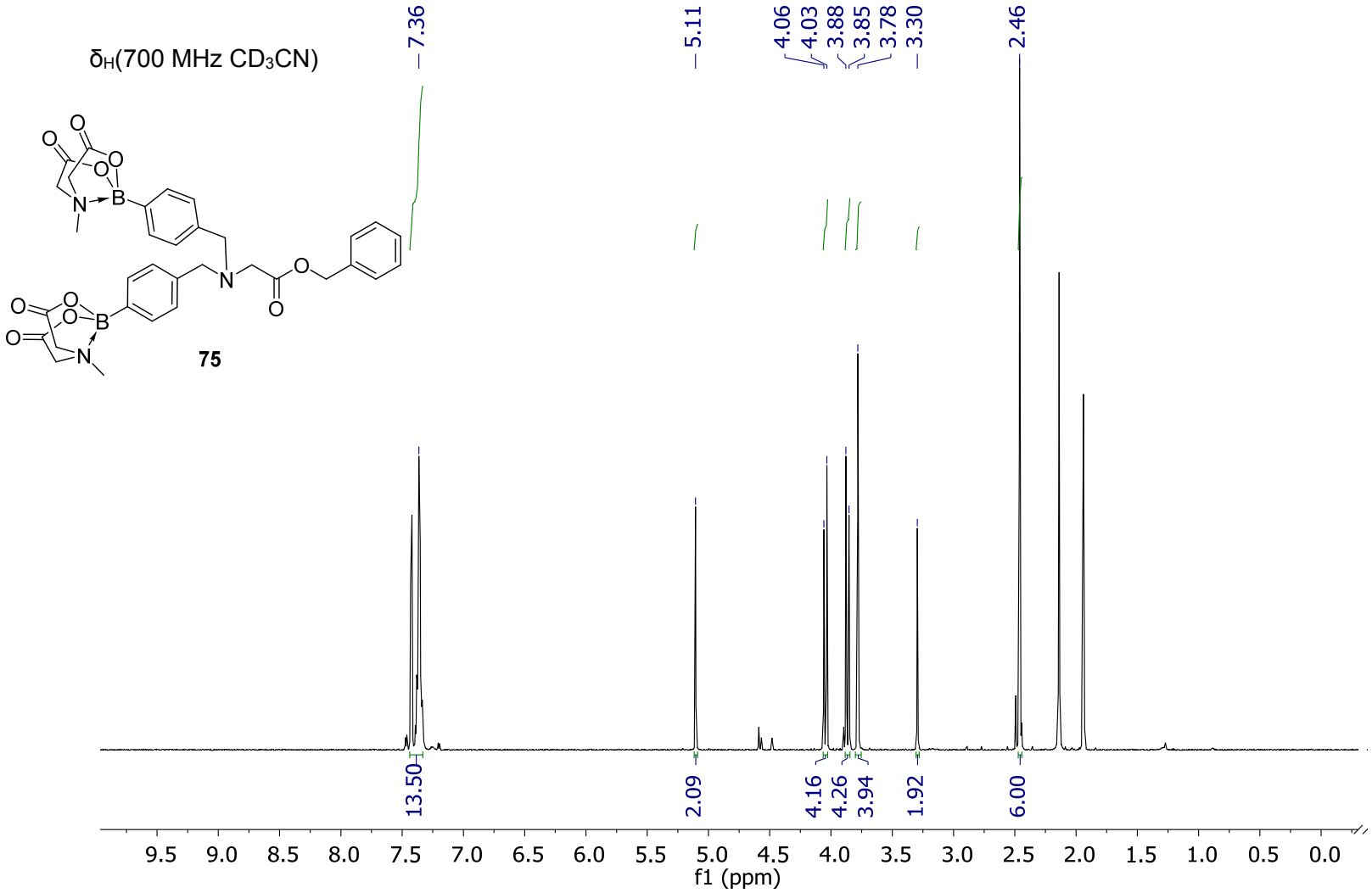

Figure A6 ^{1}H NMR of di-MIDA ester **75**.

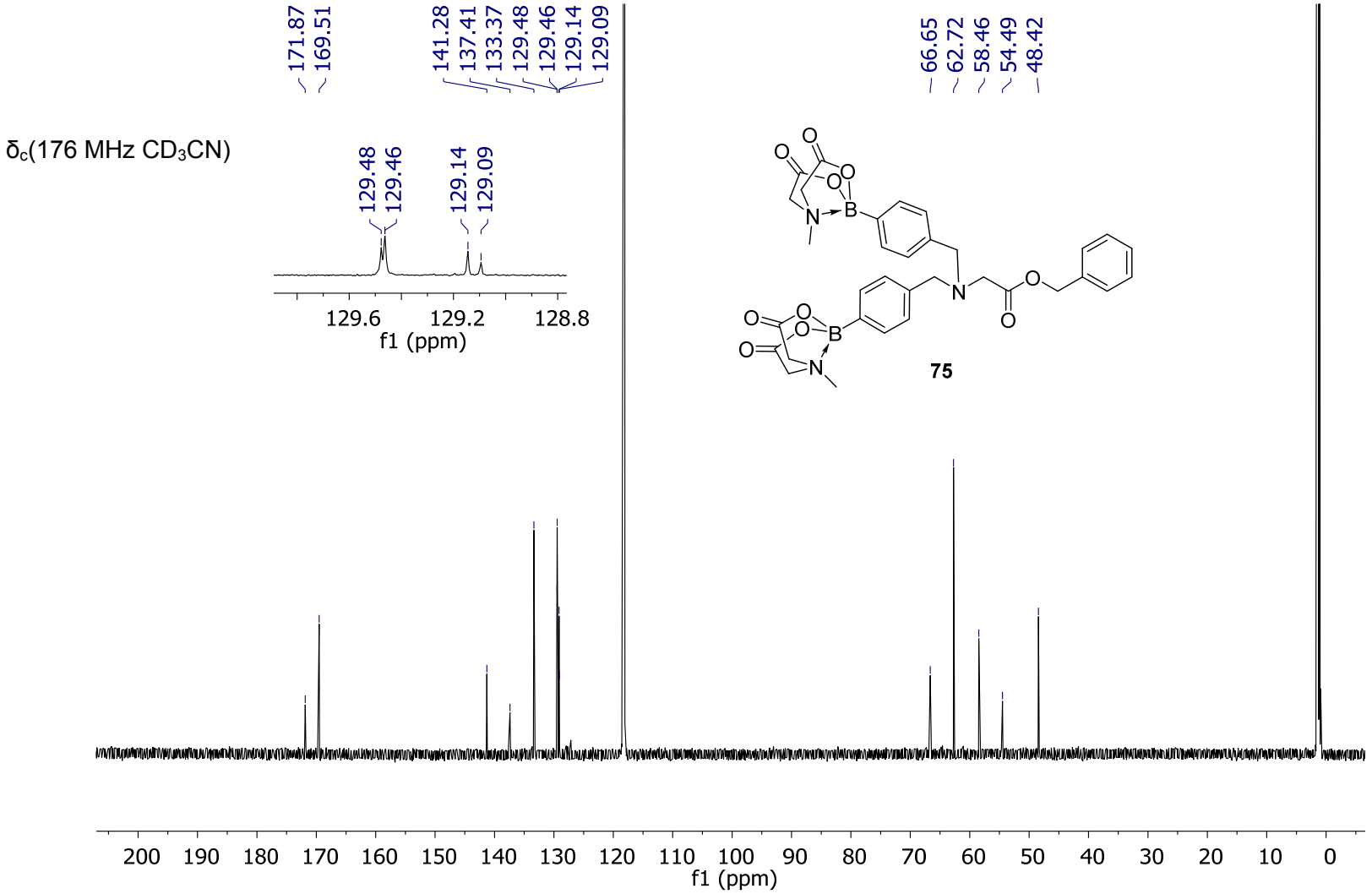

Figure A7 ^{13}C NMR of di-MIDA ester **75**.

Elemental Composition Report

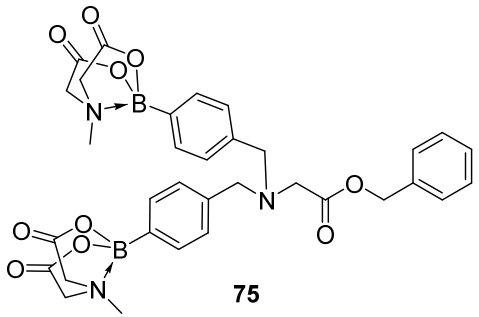

Single Mass Analysis

Tolerance = 5.0 PPM / DBE: min = -1.5, max = 50.0
Element prediction: Off
Number of isotope peaks used for i-FIT = 3

Monoisotopic Mass, Even Electron Ions
948 formula(e) evaluated with 5 results within limits (all results (up to 1000) for each mass)
Elements Used:
C: 0-50 H: 0-90 10B: 0-2 N: 0-3 O: 0-10

Alexandra Webster
AMW-02-032-F17-18 395 (3.250) Cm (395:403)

1: TOF MS ES+
6.97e+004

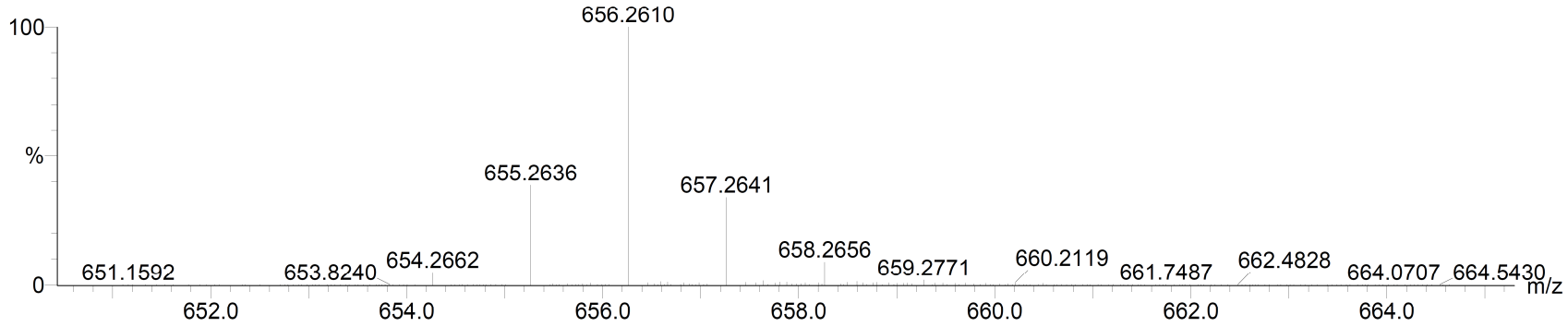

Figure A8 HRMS of di-MIDA ester (**75**), $C_{33}H_{35}{}^{10}B_2N_3O_{10}$, calculated $[M+H]^+$ = 654.2659, observed $[M+H]^+$ = 654.2662.

Appendix B

Spectra of Biaryl-Containing Peptoids

1. Linear Biaryl-Containing Peptoid 106

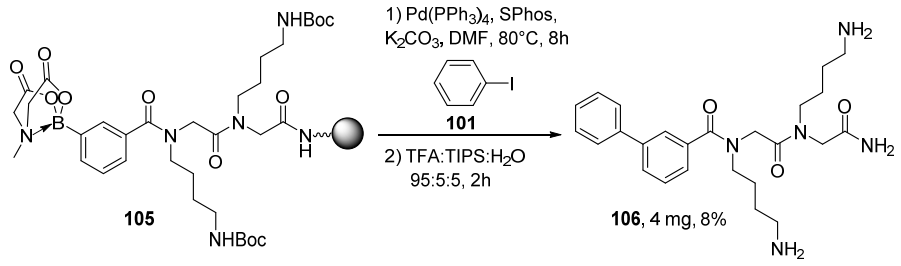

Figure B1 Synthesis of linear biaryl-containing peptoid **106**. Synthesis was carried out on Rink Amide resin on a 0.2 mmol scale. Linear peptoid synthesis was carried out according to procedures **6.4.1** and **6.4.3**. Suzuki-Miyaura cross-coupling was carried out on a 0.1 mmol scale according to procedure and **6.4.5.1**. Cleavage and purification was carried out according to procedures **6.7.1** and **6.8.1**.

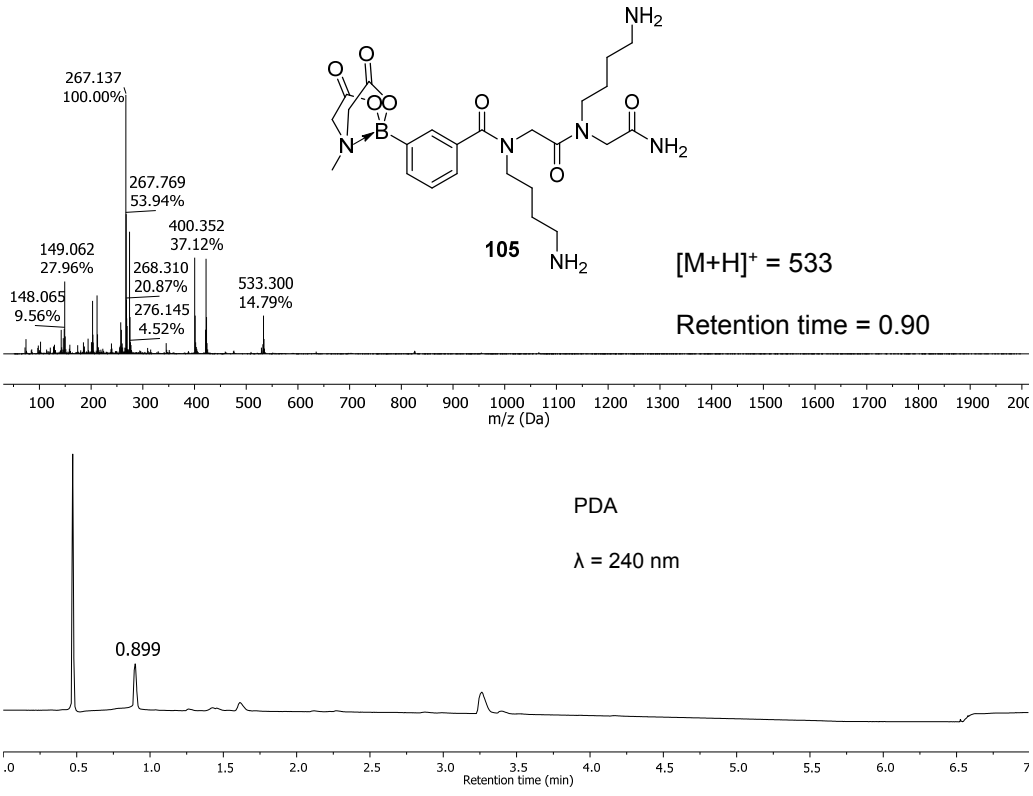

Figure B2 LCMS of crude linear peptoid **105**.

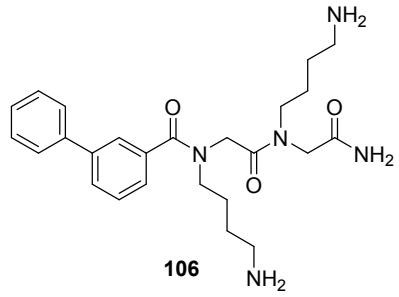

Elemental Composition Report **Page 1**

Single Mass Analysis
Tolerance = 3.0 mDa / DBE: min = -1.5, max = 50.0
Element prediction: Off
Number of isotope peaks used for i-FIT = 3

Monoisotopic Mass, Even Electron Ions
5691 formula(e) evaluated with 19 results within limits (up to 500 closest results for each mass)
Elements Used:
C: 0-60 H: 0-90 N: 0-10 O: 0-7 Cl: 0-1 Br: 0-1 F: 0-3

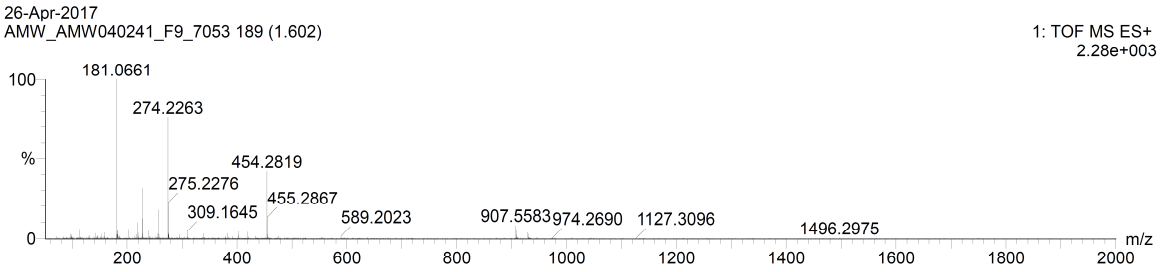

Figure B3 HRMS of linear biaryl peptoid **106**, $C_{25}H_{35}N_5O_3$, calculated $[M+H]^+$ = 454.2818, observed $[M+H]^+$ = 454.2819.

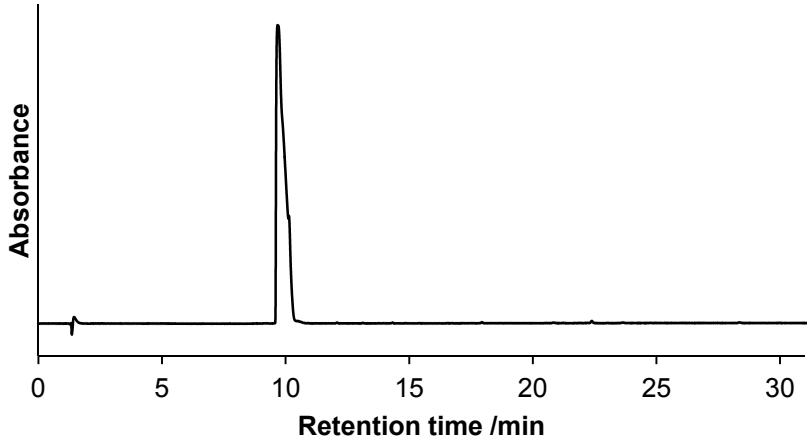

Figure B4 Analytical HPLC trace of cyclic peptoid **106**. Detection at 280 nm.

2. Biaryl-Containing Cyclic Peptoid 104

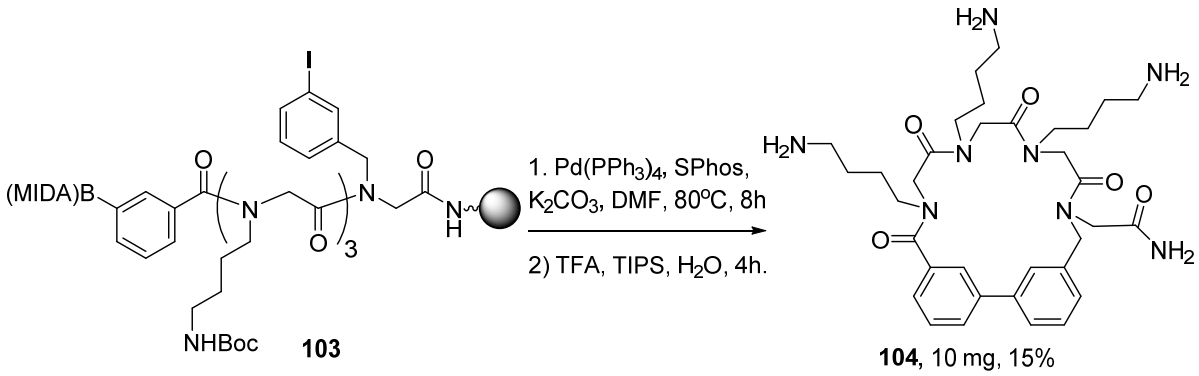

Figure B5 Synthesis of cyclic peptoid **104**. Synthesis of the linear peptoid was carried out on Rink Amide resin on a 0.2 mmol scale. Linear peptoid synthesis was carried out according to procedures **6.4.1** and **6.4.3**. Cyclisation *via* Suzuki-Miyaura cross-coupling was carried out on a 0.1 mmol scale according to procedure **6.4.5.2**. Cleavage and purification was carried out according to procedures **6.7.1** and **6.8.1**.

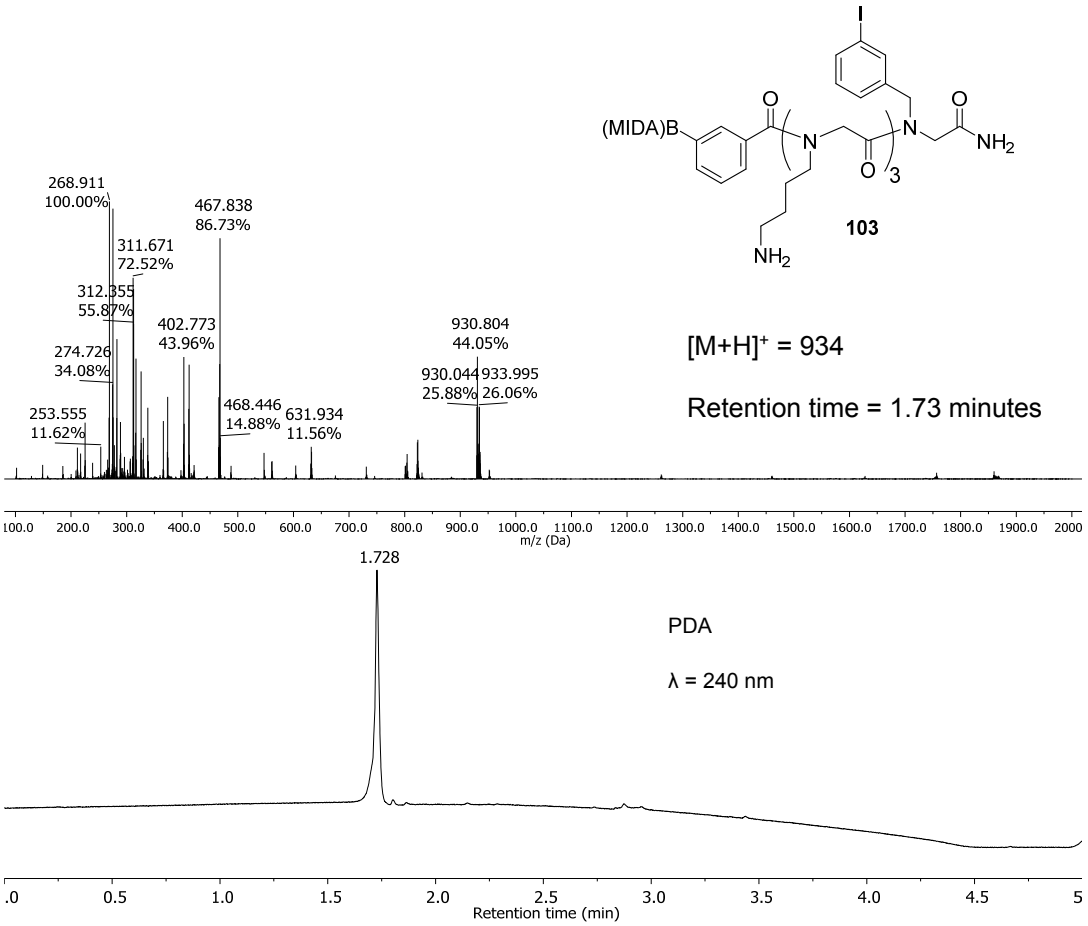

Figure B6 LCMS of crude linear peptoid **103**.

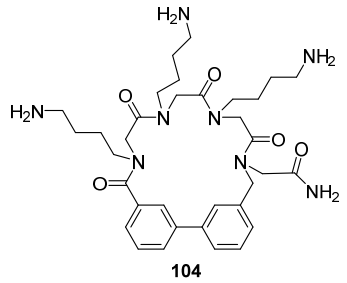

Elemental Composition Report **Page 1**

Single Mass Analysis
Tolerance = 3.0 mDa / DBE: min = -1.5, max = 50.0
Element prediction: Off
Number of isotope peaks used for i-FIT = 3

Monoisotopic Mass, Even Electron Ions
412 formula(e) evaluated with 3 results within limits (up to 500 best isotopic matches for each mass)
Elements Used:
C: 0-70 H: 0-90 N: 0-8 O: 0-5
Alexandra Webster
AMW-03-023 F3 122 (1.015) Cm (122:128)

1: TOF MS ES+
6.47e+003

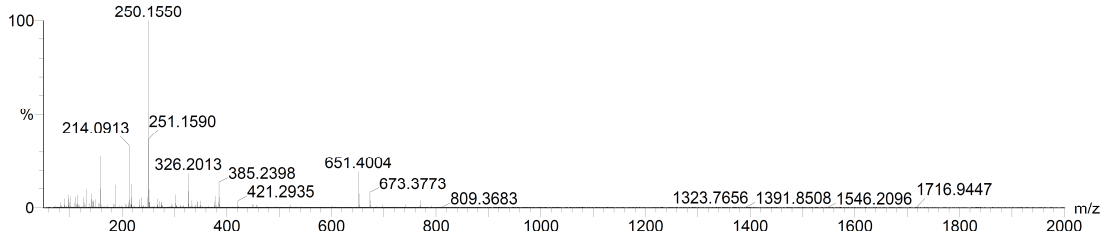

Figure B7 HRMS of biaryl-containing cyclic peptoid **104**, $C_{34}H_{50}N_8O_5$, calculated $[M+H]^+$ = 651.3982, observed $[M+H]^+$ = 651.4004.

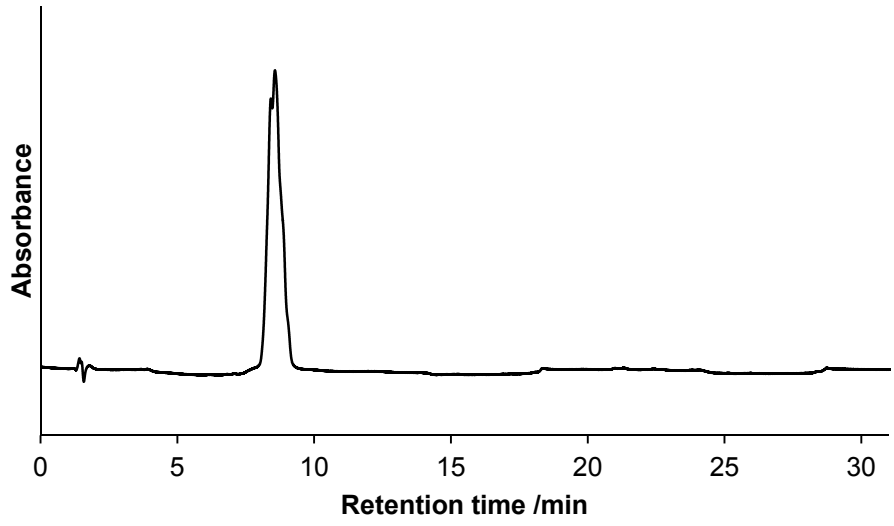

Figure B8 Analytical HPLC trace of cyclic peptoid **104**. Detection at 280 nm.

3. Biaryl-Containing Cyclic Peptoid 110

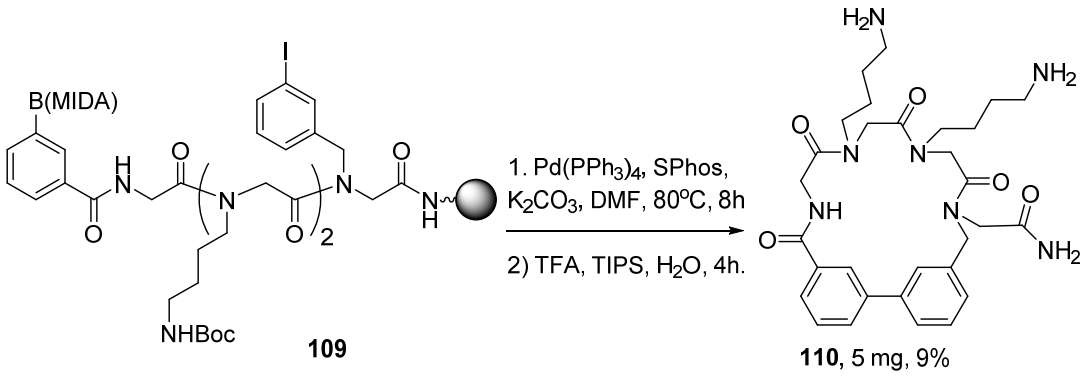

Figure B9 Synthesis of cyclic peptoid **110**. Synthesis of the linear peptoid was carried out on Rink Amide resin on a 0.2 mmol scale. Linear peptoid synthesis was carried out according to procedures **6.4.1**, **6.4.3** and **6.4.4**. Cyclisation *via* Suzuki-Miyaura cross-coupling was carried out on a 0.1 mmol scale according to procedure **6.4.5.2**. Cleavage and purification was carried out according to procedures **6.7.1** and **6.8.1**.

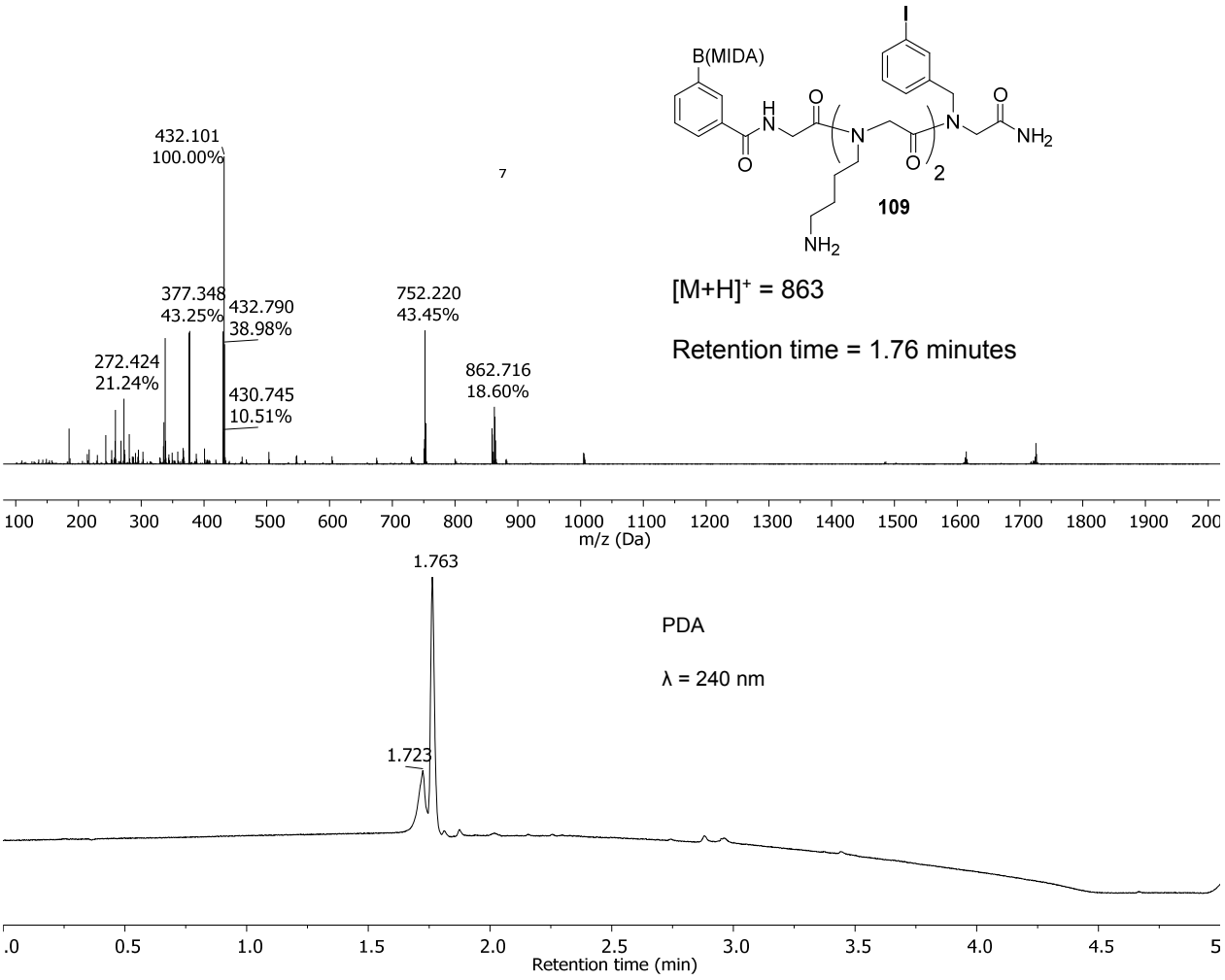

Figure B10 LCMS of crude linear peptoid **109**.

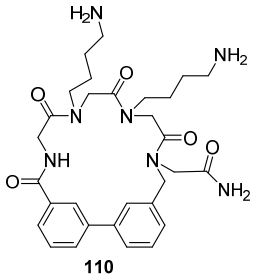

110

Elemental Composition Report **Page 1**

Single Mass Analysis
Tolerance = 3.0 mDa / DBE: min = -1.5, max = 50.0
Element prediction: Off
Number of isotope peaks used for i-FIT = 3

Monoisotopic Mass, Even Electron Ions
340 formula(e) evaluated with 2 results within limits (up to 500 best isotopic matches for each mass)
Elements Used:
C: 0-70 H: 0-90 N: 0-7 O: 0-5
Alexandra Webster
AMW-03-011 F18 171 (1.415) Cm (169:172)

1: TOF MS ES+
5.89e+004

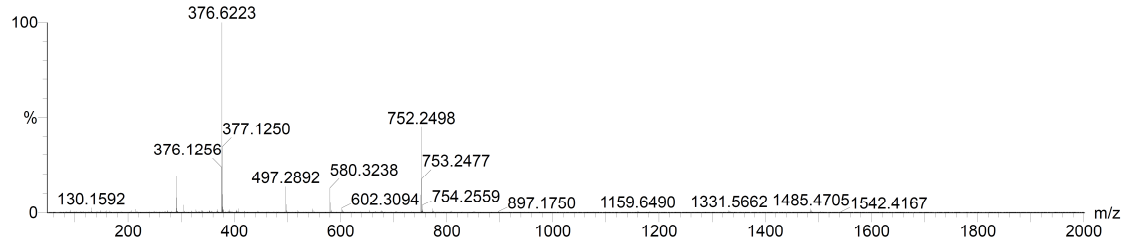

Figure B11 HRMS of biaryl-containing cyclic peptoid **110**, $C_{30}H_{41}N_7O_5$, calculated $[M+H]^+$ = 580.2347, observed $[M+H]^+$ = 580.3238.

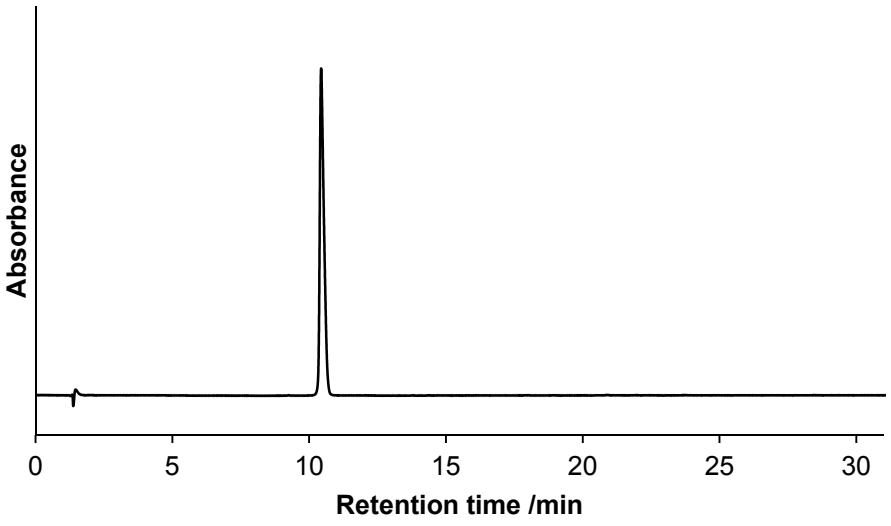

Figure B12 Analytical HPLC trace of cyclic peptoid **110**. Detection at 280 nm.

4. Biaryl-Containing Cyclic Peptoid 119

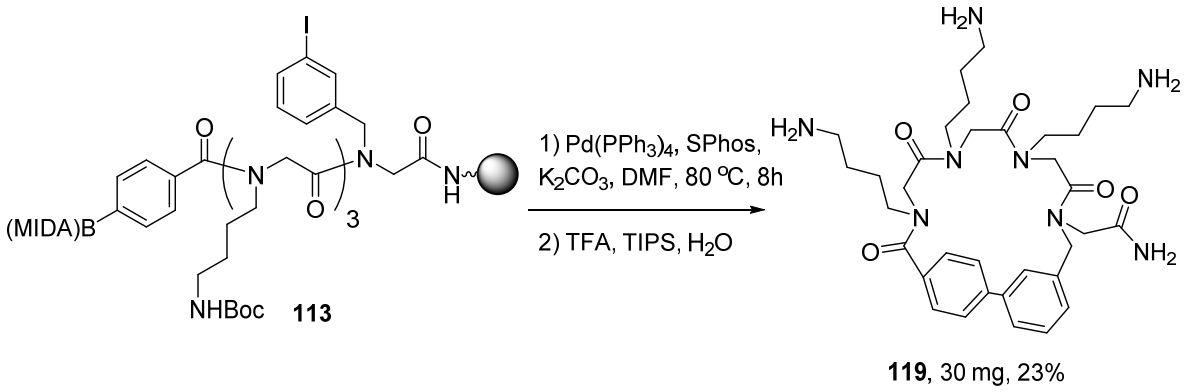

Figure B13: Synthesis of cyclic peptoid **119**. Synthesis of the linear peptoid was carried out on Rink Amide resin on a 0.2 mmol scale. Linear peptoid synthesis was carried out according to procedures **6.4.1** and **6.4.3**. Cyclisation *via* Suzuki-Miyaura cross-coupling was carried out on a 0.1 mmol scale according to procedure **6.4.5.2**. Cleavage and purification was carried out according to procedures **6.7.1** and **6.8.1**.

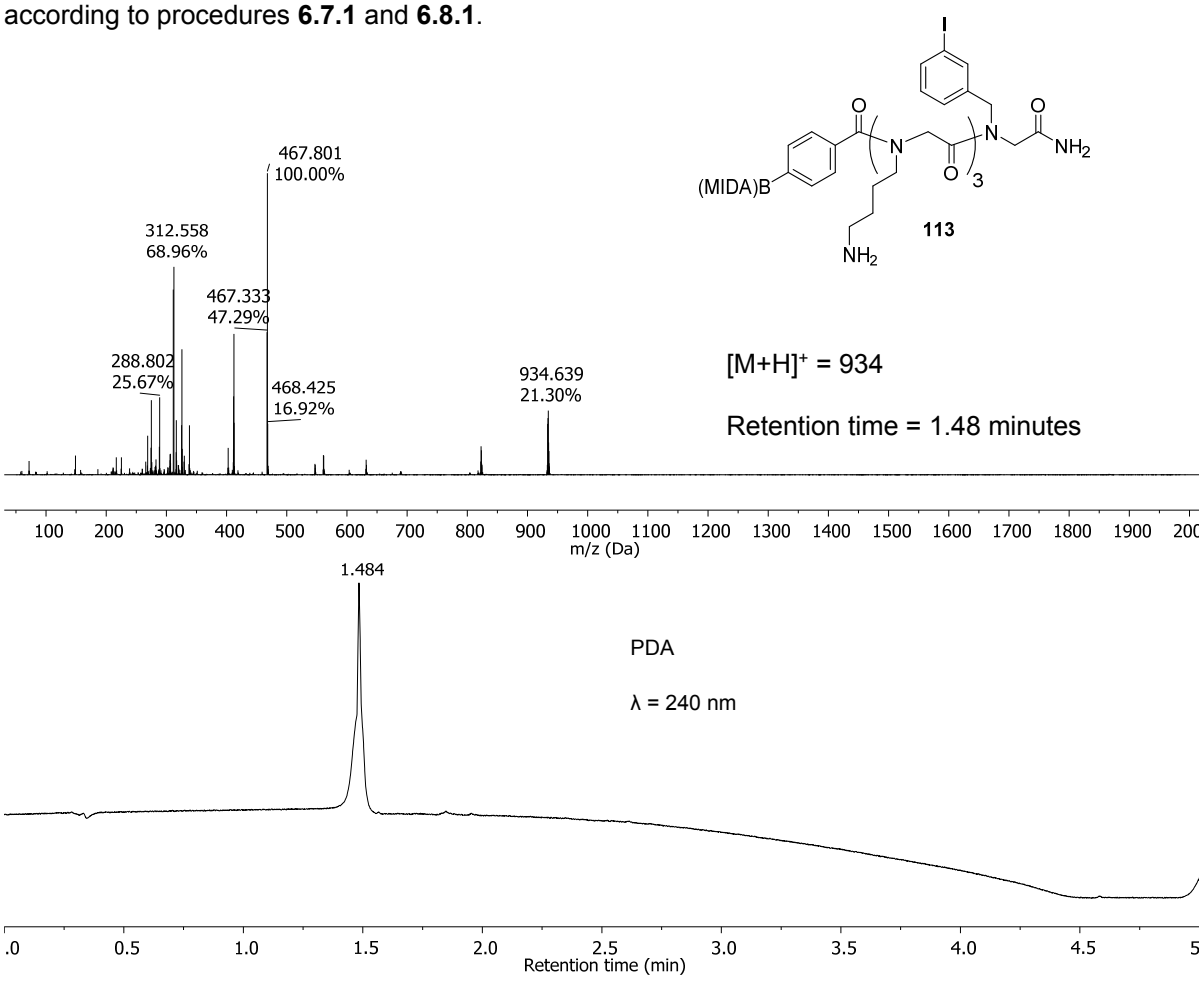

Figure B14 LCMS of crude linear peptoid **113**.

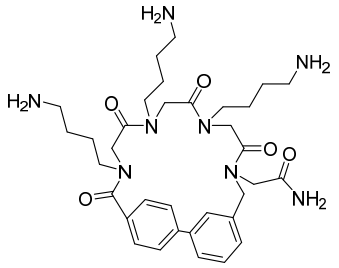

119

Elemental Composition Report **Page 1**

Single Mass Analysis
Tolerance = 3.0 mDa / DBE: min = -1.5, max = 50.0
Element prediction: Off
Number of isotope peaks used for i-FIT = 3

Monoisotopic Mass, Even Electron Ions
1767 formula(e) evaluated with 12 results within limits (up to 500 best isotopic matches for each mass)
Elements Used:
C: 0-40 H: 0-75 N: 0-10 O: 0-10 S: 0-2
Alexandra Webster

20-May-2016
AMW-03-042(2) F3 138 (0.929) Cm (138:146)

1: TOF MS ES+
1.72e+004

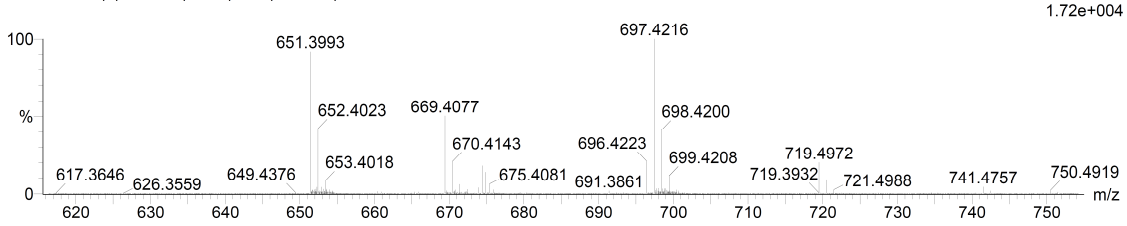

Figure B15 HRMS of biaryl-containing cyclic peptoid **119**, $C_{34}H_{50}N_8O_5$, calculated $[M+H]^+$ = 651.3982, observed $[M+H]^+$ = 651.3933.

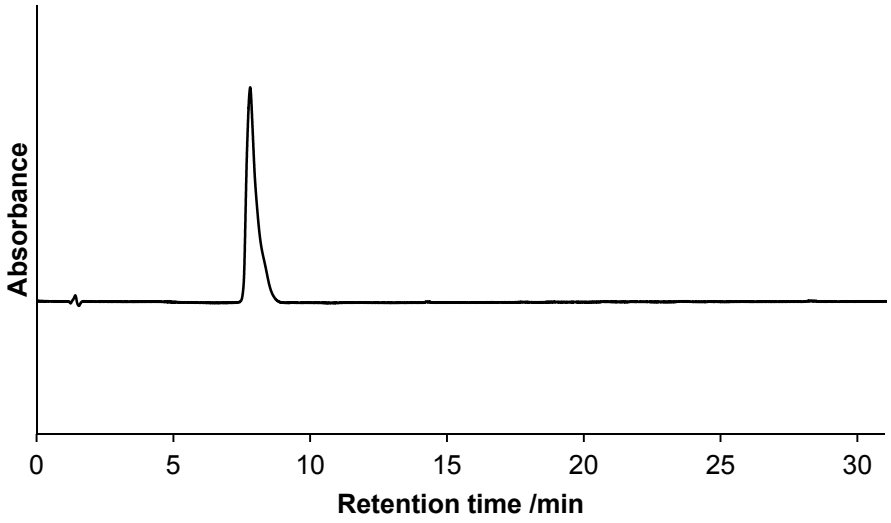

Figure B16 Analytical HPLC trace of cyclic peptoid **119**. Detection at 280 nm.

5. Biaryl-Containing Cyclic Peptoid 120

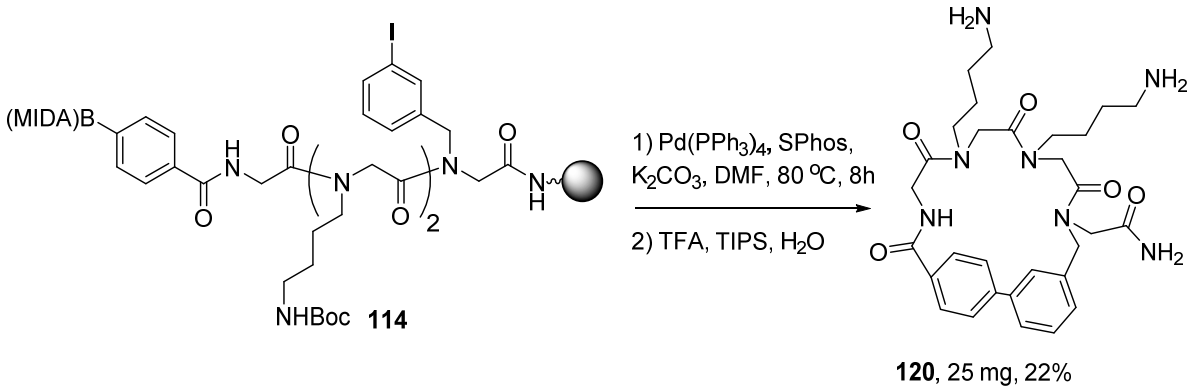

Figure B17 Synthesis of cyclic peptoid **120**. Synthesis of the linear peptoid was carried out on Rink Amide resin on a 0.2 mmol scale. Linear peptoid synthesis was carried out according to procedures **6.4.1**, **6.4.3** and **6.4.4**. Cyclisation *via* Suzuki-Miyaura cross-coupling was carried out on a 0.1 mmol scale according to procedure **6.4.5.2**. Cleavage and purification was carried out according to procedures **6.7.1** and **6.8.1**.

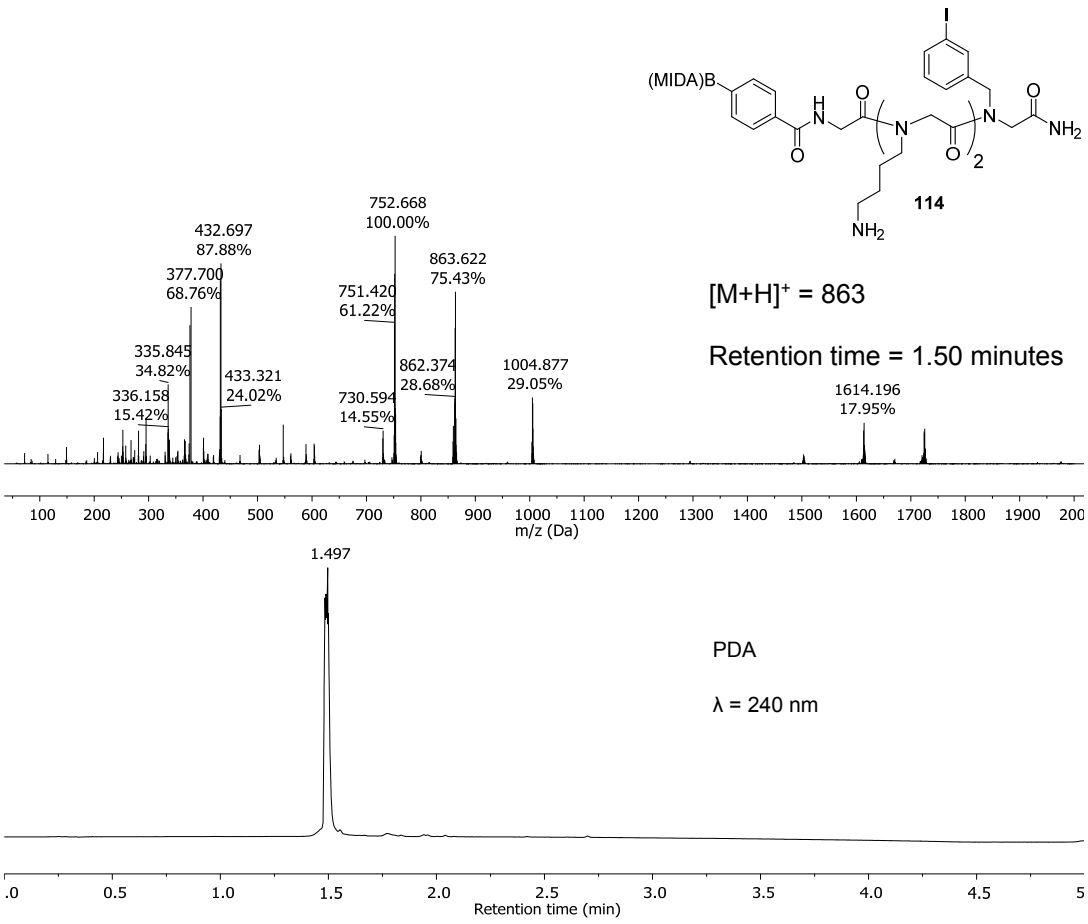

Figure B18 LCMS of crude linear peptoid **114**.

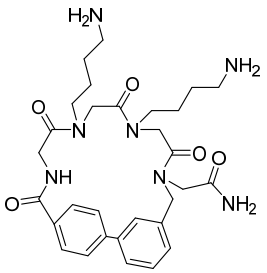

120

Elemental Composition Report **Page 1**

Single Mass Analysis
Tolerance = 3.0 mDa / DBE: min = -1.5, max = 50.0
Element prediction: Off
Number of isotope peaks used for i-FIT = 3

Monoisotopic Mass, Even Electron Ions
151 formula(e) evaluated with 1 results within limits (up to 500 best isotopic matches for each mass)
Elements Used:
C: 0-30 H: 0-50 N: 0-7 O: 0-5 96Ru: 0-1

<sample_description>

05-May-2016
AMW_AMW030413_F2_4822 136 (1.129) Cm (133:138)

1: TOF MS ES+
1.17e+005

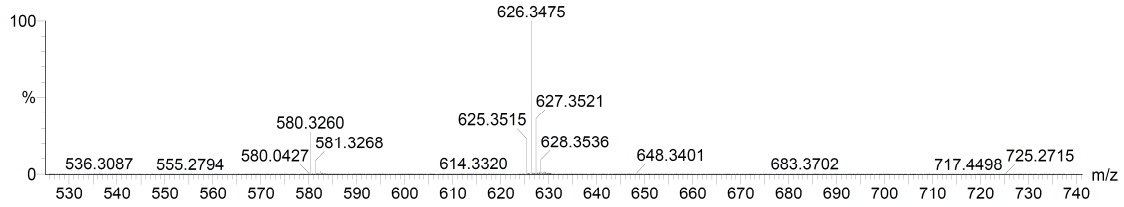

Figure B19 HRMS of biaryl-containing cyclic peptoid **120**, $C_{30}H_{41}N_7O_5$, calculated $[M+H]^+$ = 580.2347, observed $[M+H]^+$ = 580.3260.

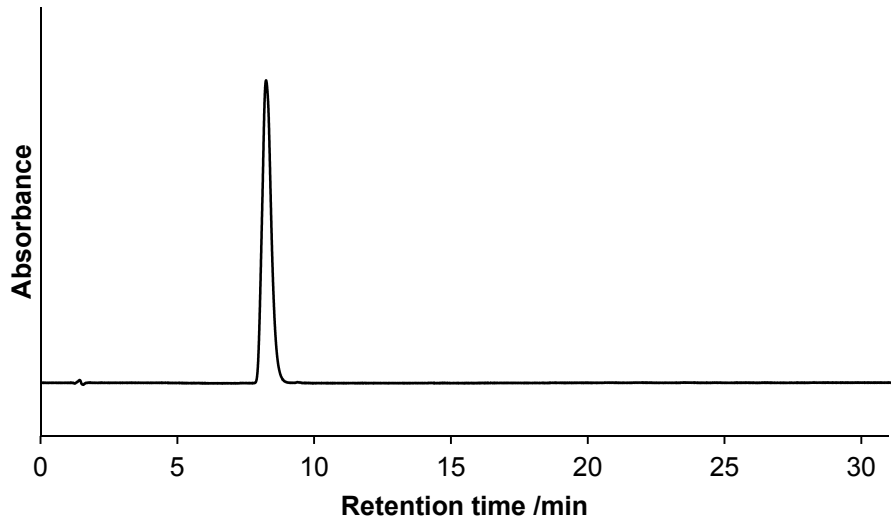

Figure B20 Analytical HPLC trace of cyclic peptoid **120**. Detection at 280 nm.

6. Biaryl-Containing Cyclic Peptoid 121

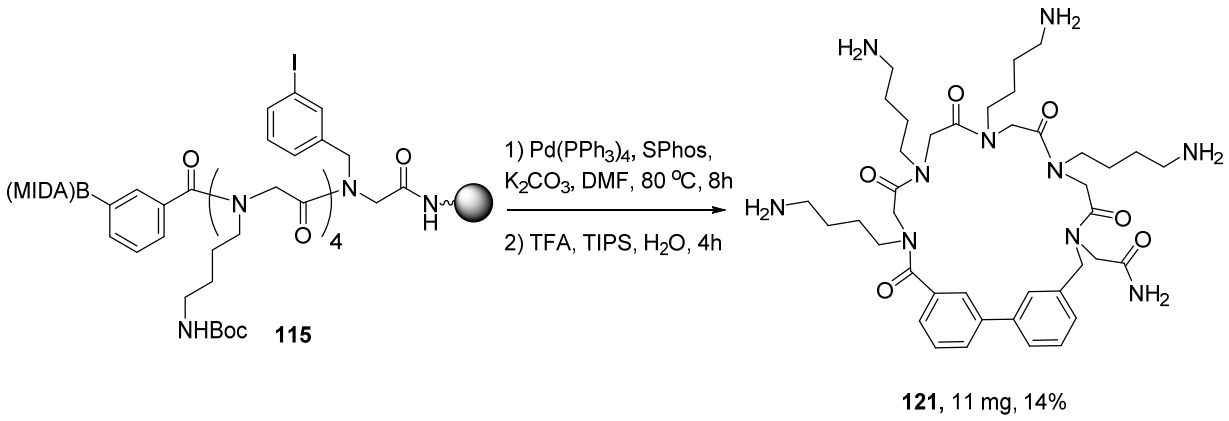

Figure B21 Synthesis of cyclic peptoid **121**. Synthesis of the linear peptoid was carried out on Rink Amide resin on a 0.2 mmol scale. Linear peptoid synthesis was carried out according to procedures **6.4.1** and **6.4.3**. Cyclisation *via* Suzuki-Miyaura cross-coupling was carried out on a 0.1 mmol scale according to procedure **6.4.5.2**. Cleavage and purification was carried out according to procedures **6.7.1** and **6.8.1**.

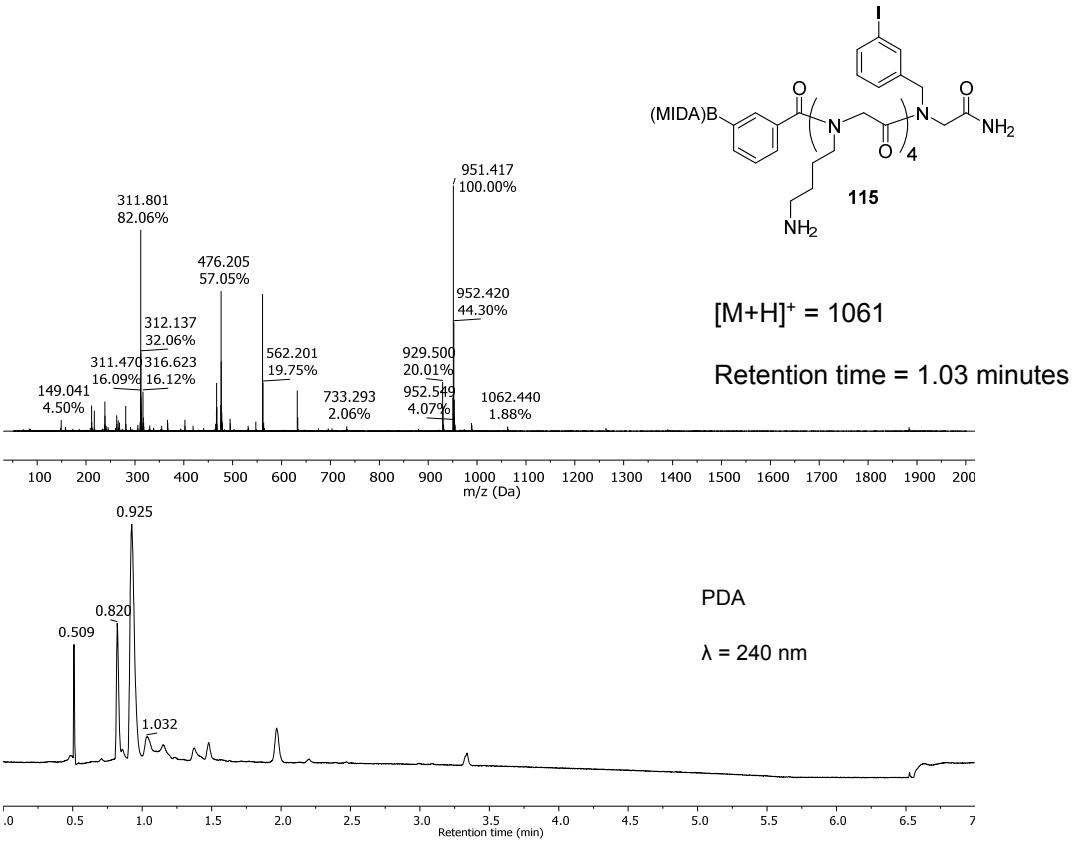

Figure B22 LCMS of crude linear peptoid **115**. Peak at 0.925 minutes corresponds to the free boronic acid $[M+H]^+$ = 950.

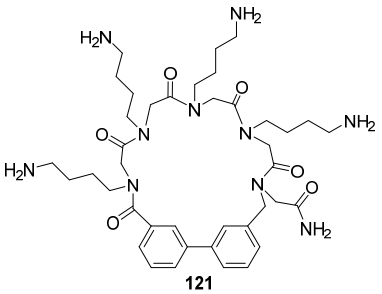

Elemental Composition Report **Page 1**

Single Mass Analysis
Tolerance = 5.0 PPM / DBE: min = -1.5, max = 50.0
Element prediction: Off
Number of isotope peaks used for i-FIT = 3

Monoisotopic Mass, Even Electron Ions
186 formula(e) evaluated with 1 results within limits (up to 500 best isotopic matches for each mass)
Elements Used:
C: 0-45 H: 0-70 N: 0-10 O: 0-9
<sample_description>

30-Jun-2016
AMW_AMW040122_F4_5255 121 (1.026) Cm (121)

1: TOF MS ES+
1.16e+002

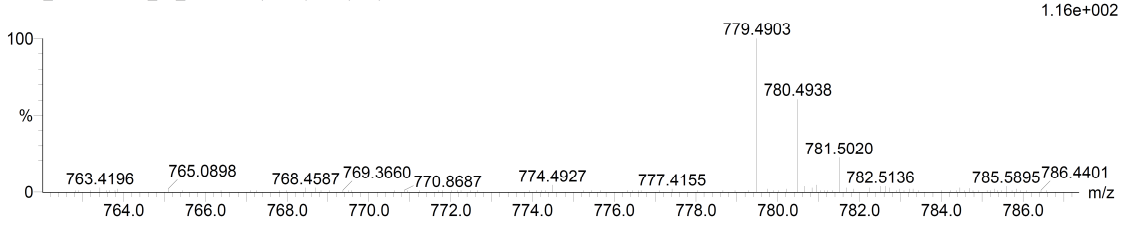

Figure B23 HRMS of biaryl-containing cyclic peptoid **121**, $C_{40}H_{62}N_{10}O_6$, calculated $[M+H]^+$ = 779.4932, observed $[M+H]^+$ = 779.4903.

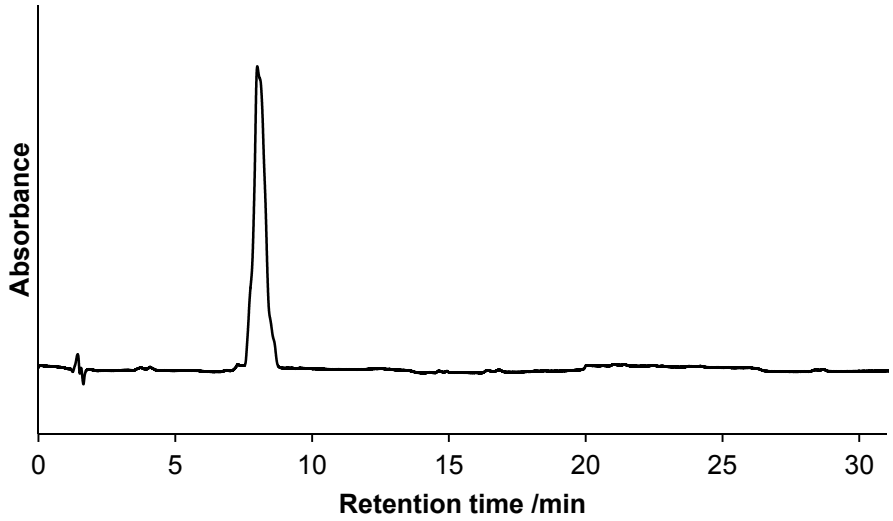

Figure B24 Analytical HPLC trace of cyclic peptoid **121**. Dection at 280 nm.

7. Biaryl-Containing Cyclic Peptoid 122

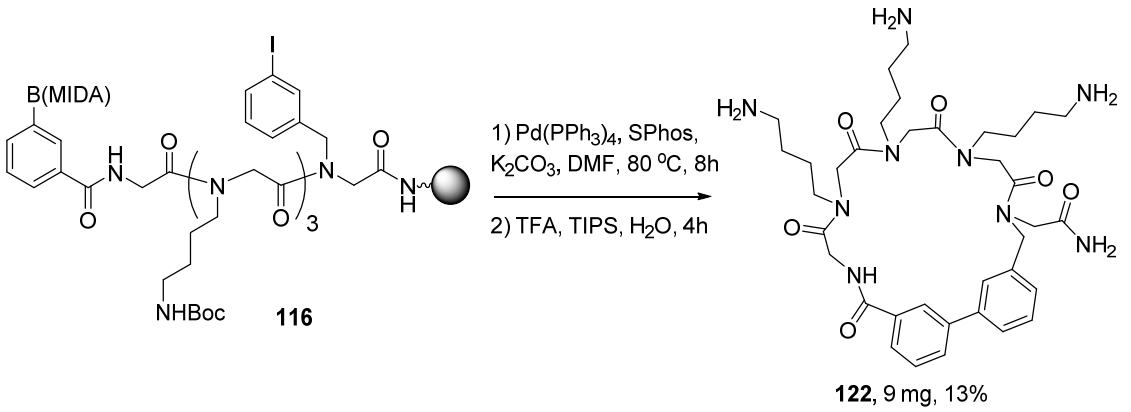

Figure B25 Synthesis of cyclic peptoid **122**. Synthesis of the linear peptoid was carried out on Rink Amide resin on a 0.2 mmol scale. Linear peptoid synthesis was carried out according to procedures **6.4.1**, **6.4.3** and **6.4.4**. Cyclisation *via* Suzuki-Miyaura cross-coupling was carried out on a 0.1 mmol scale according to procedure **6.4.5.2**. Cleavage and purification was carried out according to procedures **6.7.1** and **6.8.1**.

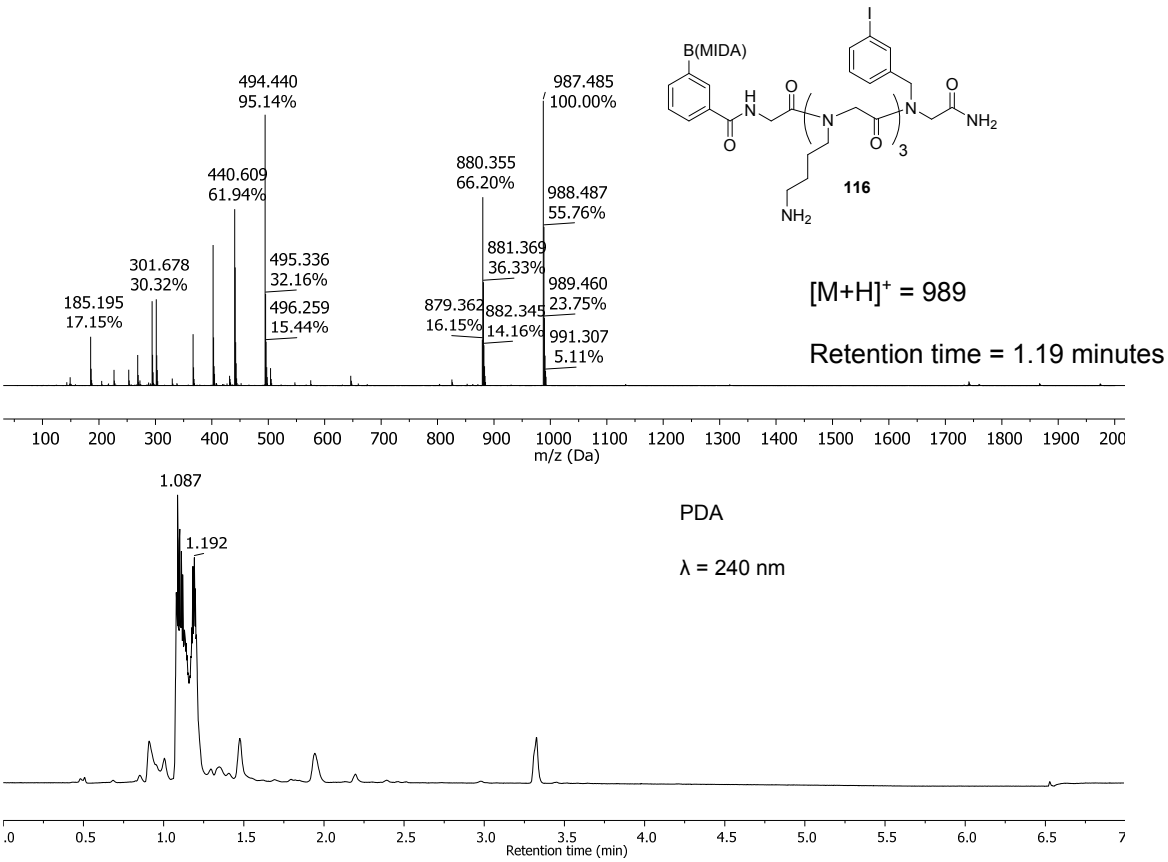

Figure B26 LCMS of crude linear peptoid **116**.

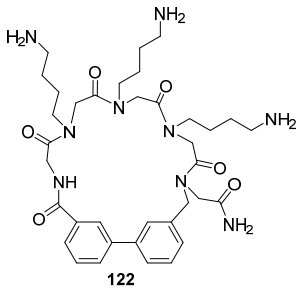

122

Elemental Composition Report **Page 1**

Single Mass Analysis
Tolerance = 3.0 mDa / DBE: min = -1.5, max = 50.0
Element prediction: Off
Number of isotope peaks used for i-FIT = 3

Monoisotopic Mass, Even Electron Ions
884 formula(e) evaluated with 4 results within limits (up to 500 best isotopic matches for each mass)
Elements Used:
C: 0-50 H: 0-75 N: 0-10 O: 0-6 127I: 0-1

<sample_description>

26-May-2016
AMW_AMW040012_F3_5068 134 (1.114) Cm (134:139)

1: TOF MS ES+
2.24e+003

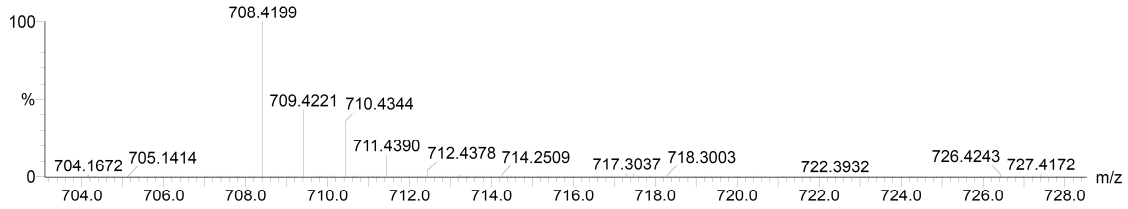

Figure B27 HRMS of biaryl-containing cyclic peptoid **122**, $C_{36}H_{53}N_9O_6$, calculated $[M+H]^+$ = 708.4197, observed $[M+H]^+$ = 708.4199.

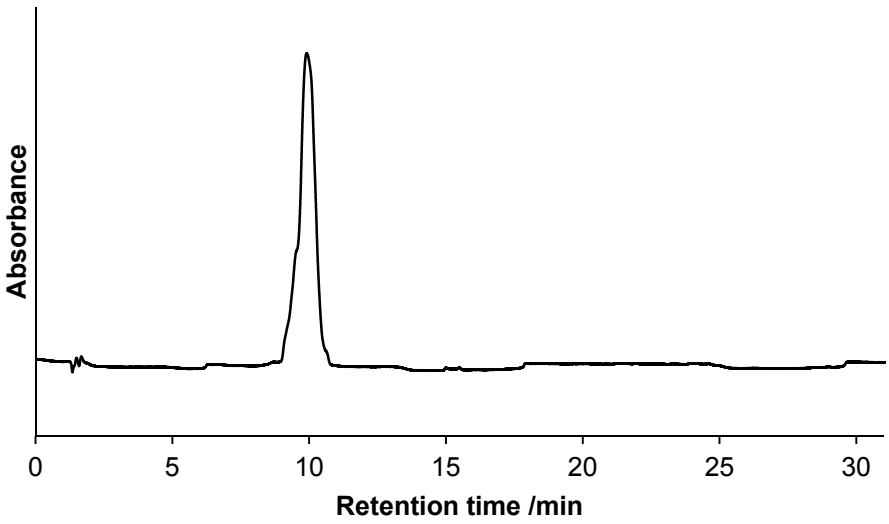

Figure B28 Analytical HPLC trace of cyclic peptoid **122**. Detection at 280 nm.

8. Biaryl-Containing Cyclic Peptoid 123

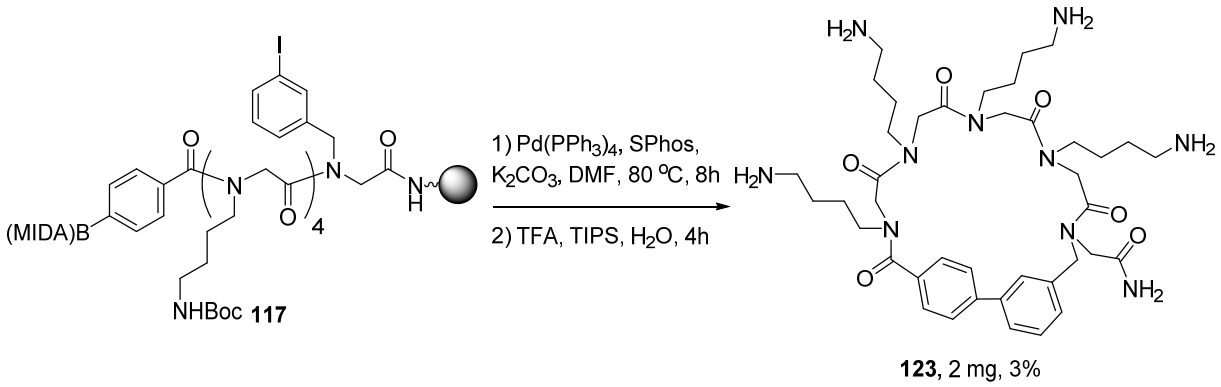

Figure B29 Synthesis of cyclic peptoid **123**. Synthesis of the linear peptoid was carried out on Rink Amide resin on a 0.2 mmol scale. Linear peptoid synthesis was carried out according to procedures **6.4.1** and **6.4.3**. Cyclisation *via* Suzuki-Miyaura cross-coupling was carried out on a 0.1 mmol scale according to procedure **6.4.5.2**. Cleavage and purification was carried out according to procedures **6.7.1** and **6.8.1**.

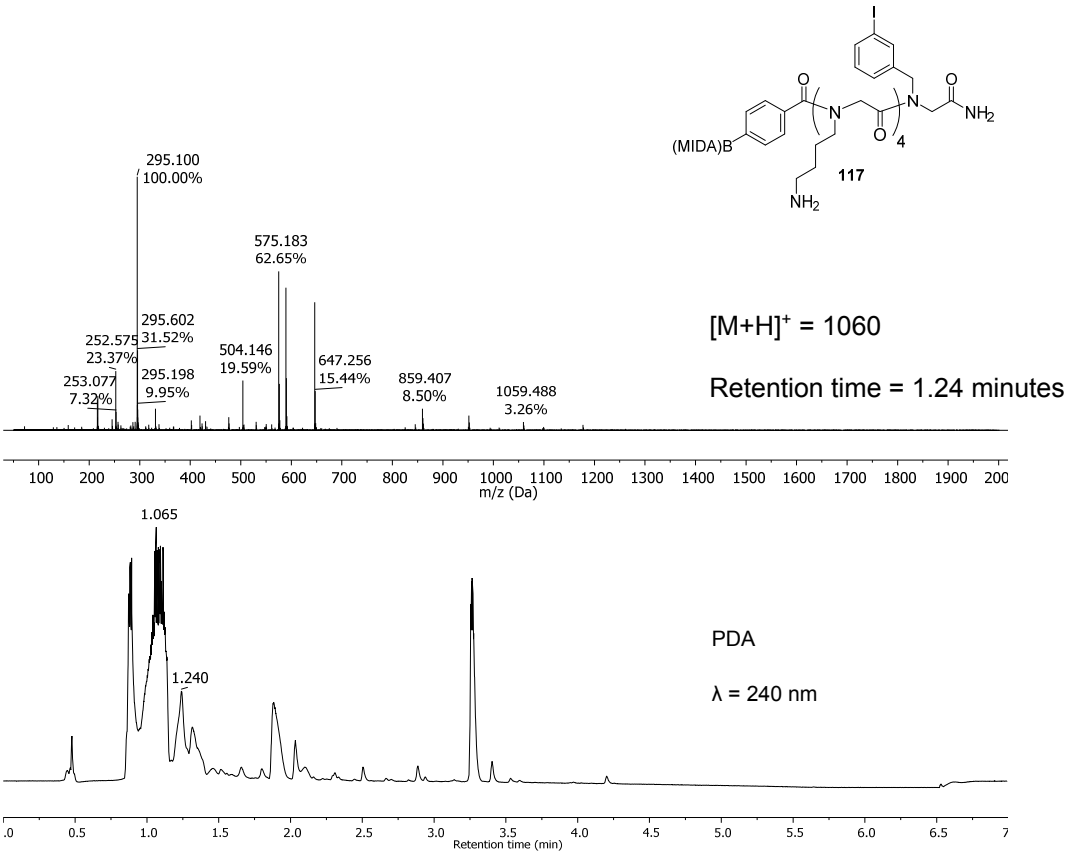

Figure B30 LCMS of crude linear peptoid **117**. Peak at 1.08 minutes corresponds to the free boronic acid $[M+H]^+ = 951$.

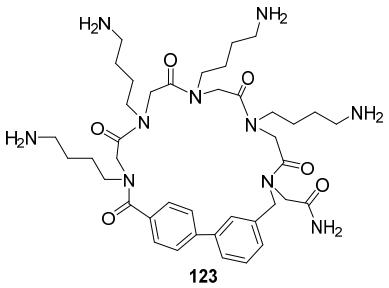

Elemental Composition Report **Page 1**

Single Mass Analysis
Tolerance = 3.0 mDa / DBE: min = -1.5, max = 50.0
Element prediction: Off
Number of isotope peaks used for i-FIT = 3

Monoisotopic Mass, Even Electron Ions
694 formula(e) evaluated with 2 results within limits (up to 500 best isotopic matches for each mass)
Elements Used:
C: 0-50 H: 0-75 N: 0-10 O: 0-6 127I: 0-1

<sample_description>

26-May-2016
AMW_AMW040041_F8_5081 62 (0.520) Cm (60:64)

1: TOF MS ES+
4.62e+002

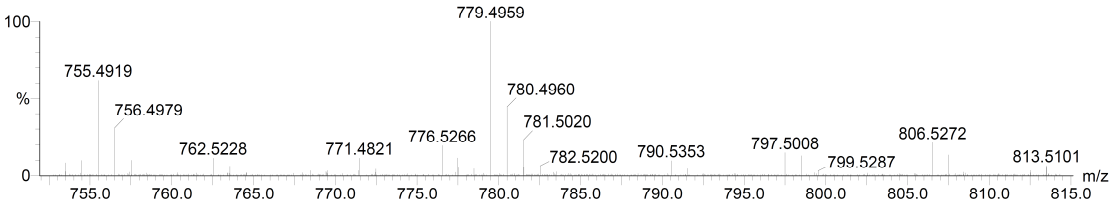

Figure B31 HRMS of biaryl-containing cyclic peptoid **123**, $C_{40}H_{62}N_{10}O_6$, calculated $[M+H]^+$ = 779.4932, observed $[M+H]^+$ = 779.4959.

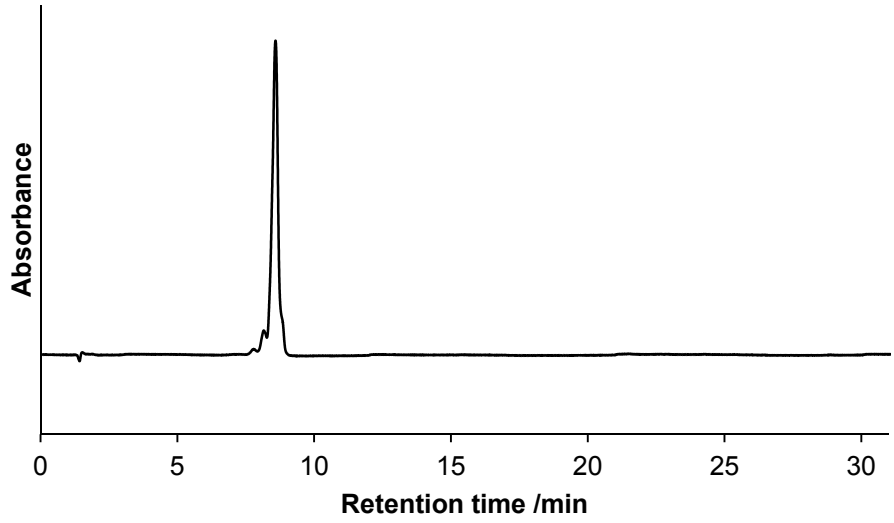

Figure B32 Analytical HPLC trace of cyclic peptoid **123**. Detection at 280 nm.

9. Biaryl-Containing Cyclic Peptoid 124

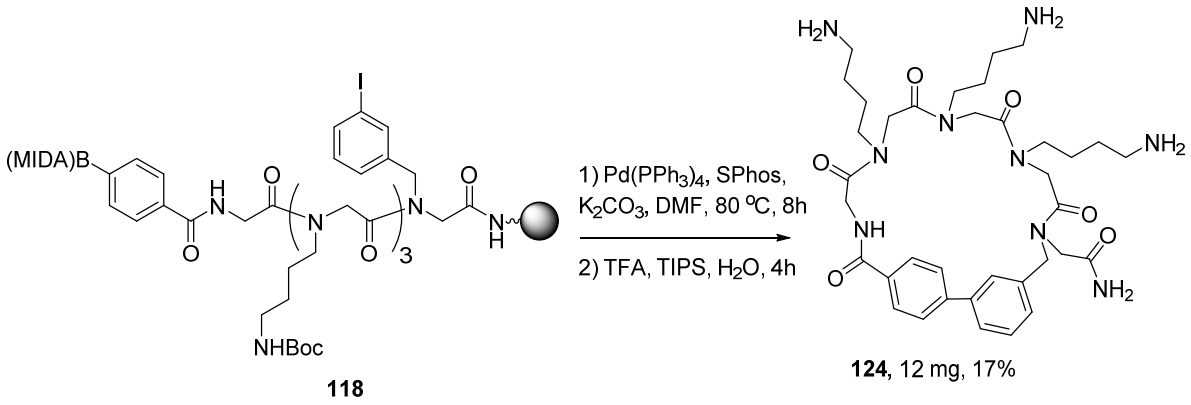

Figure B33 Synthesis of cyclic peptoid **124**. Synthesis of the linear peptoid was carried out on Rink Amide resin on a 0.2 mmol scale. Linear peptoid synthesis was carried out according to procedures **6.4.1**, **6.4.3** and **6.4.4**. Cyclisation *via* Suzuki-Miyaura cross-coupling was carried out on a 0.1 mmol scale according to procedure **6.4.5.2**. Cleavage and purification was carried out according to procedures **6.7.1** and **6.8.1**.

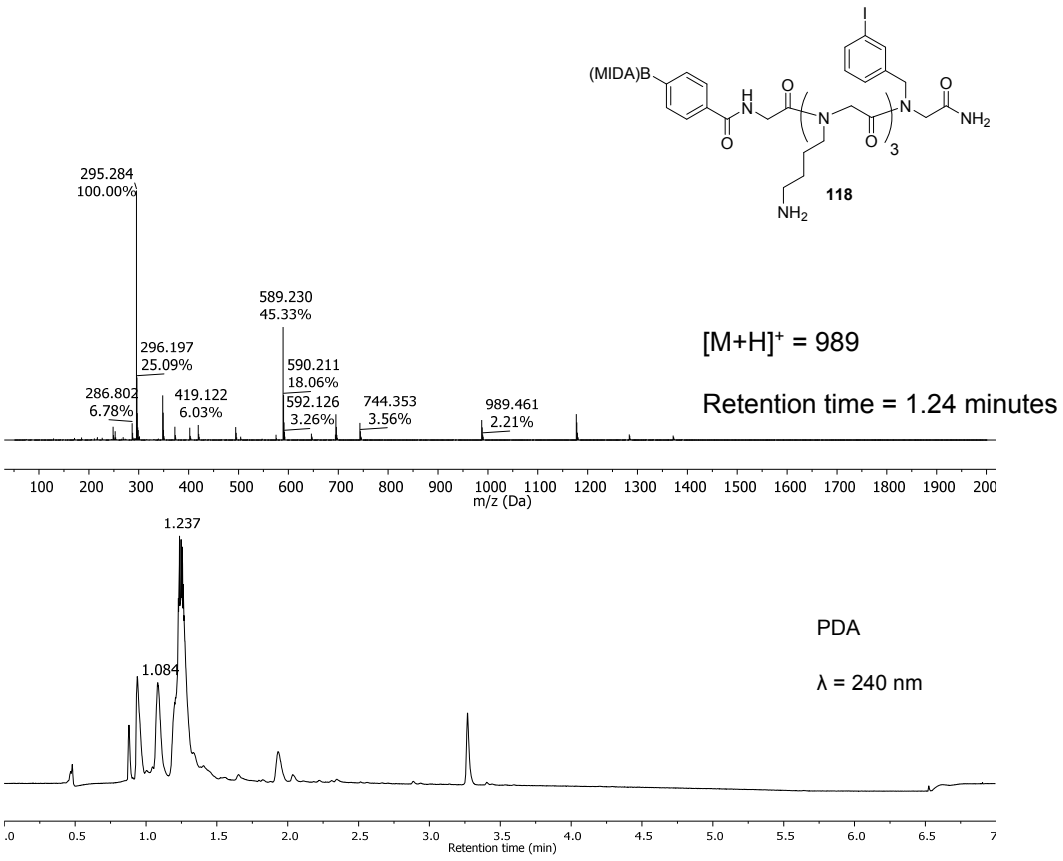

Figure B34 LCMS of crude linear peptoid **118**. Peak at 1.08 minutes corresponds to the free boronic acid $[M+H]^+$ = 880.

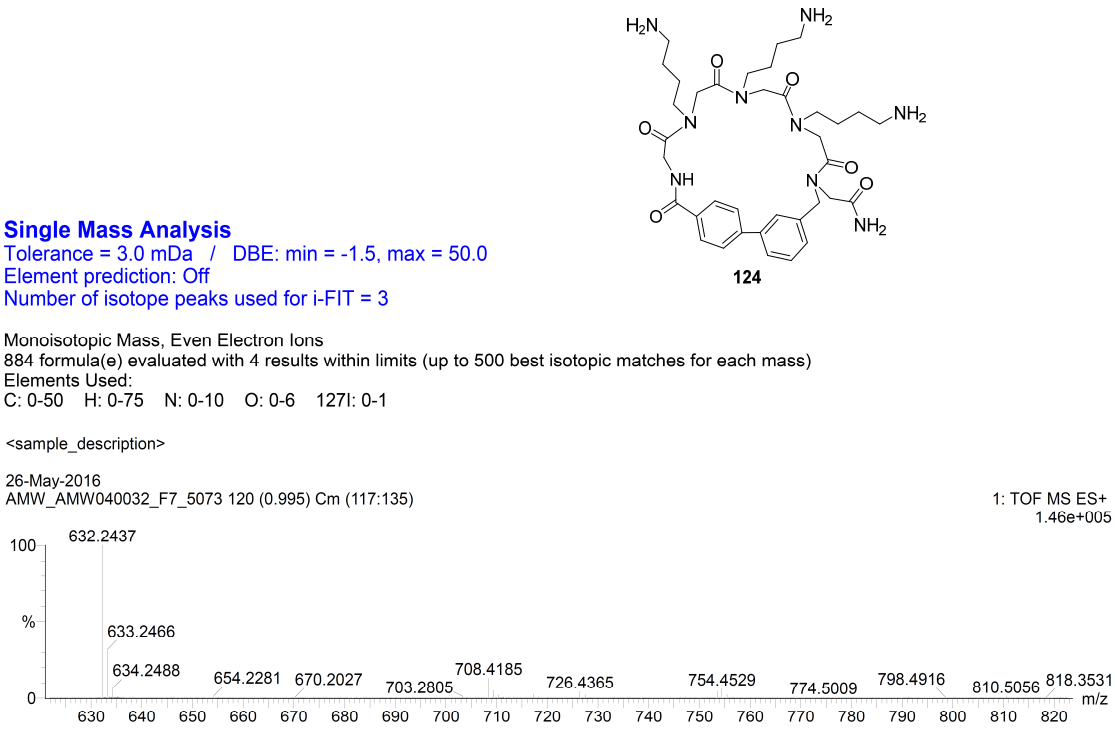

Figure B31 HRMS of biaryl-containing cyclic peptoid **124**, $C_{36}H_{53}N_9O_6$, calculated $[M+H]^+$ = 708.4197, observed $[M+H]^+$ = 708.4185.

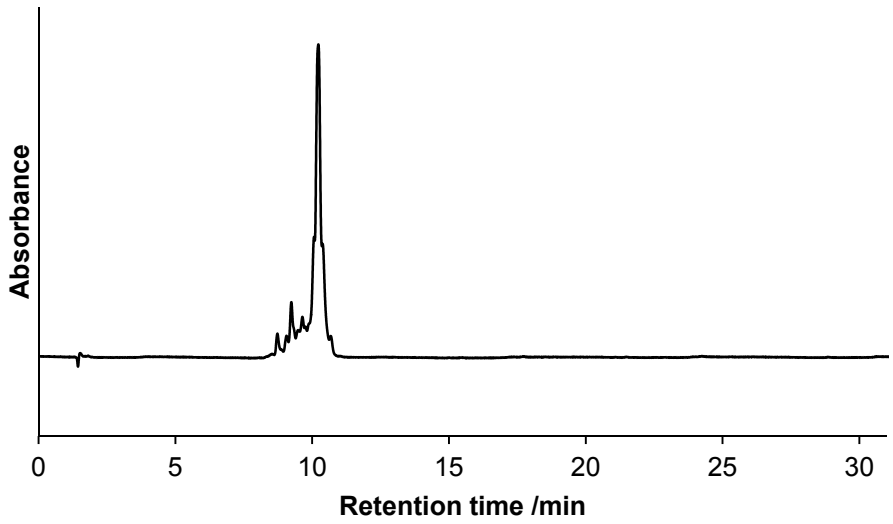

Figure B36 Analytical HPLC trace of cyclic peptoid **124**.Dection at 280 nm.

Appendix C

Spectra of p15 Peptide and Analogues

1. Disulphide-Bridged p15 peptide 126

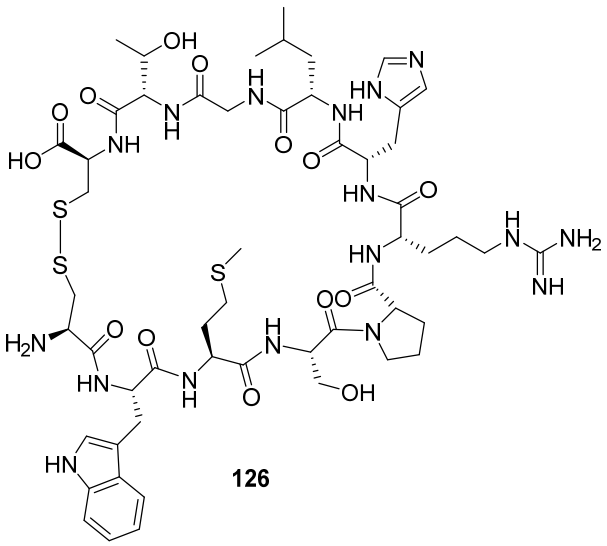

Figure C1 Disulphide-bridged p15 peptide. Synthesis of the linear peptide was carried out on 2-chlorotrityl chloride resin on a 0.2 mmol scale. Linear peptide synthesis was carried out according to procedure **6.5.4**. Cyclisation *via* disulphide bridge formation was carried out on a 0.1 mmol scale according to procedure **6.6.1**. Cleavage and purification was carried out according to procedures **6.7.2** and **6.8.1**.

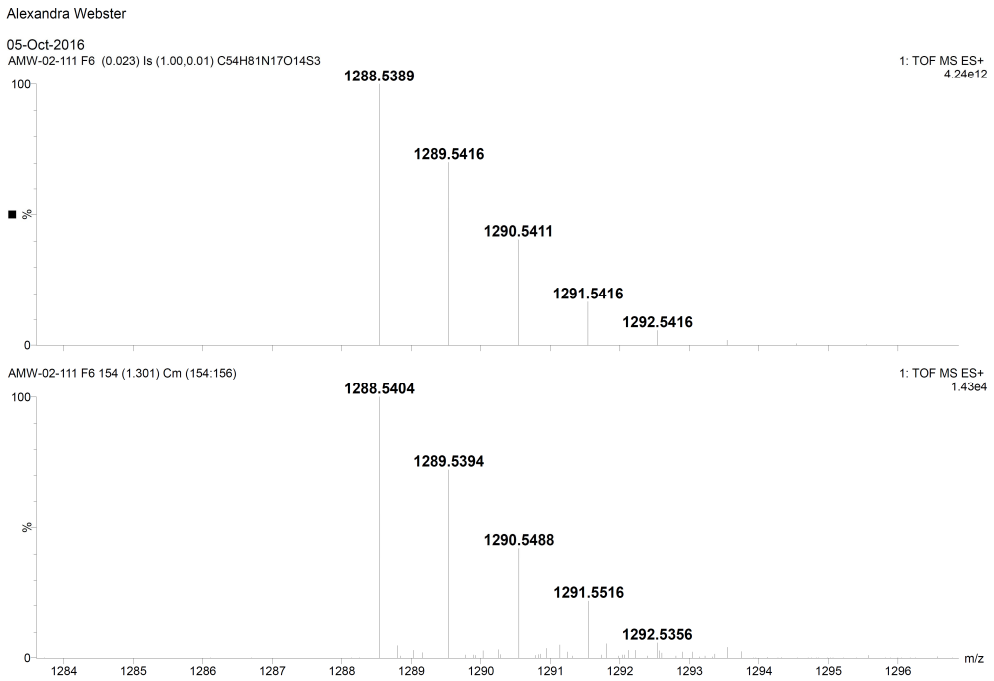

Figure C2 HRMS of disulphide-bridged p15 peptide **126**, $C_{54}H_{81}N_{17}O_{14}S_3$, calculated $[M+H]^+$ = 1288.5389, observed $[M+H]^+$ = 1288.5404.

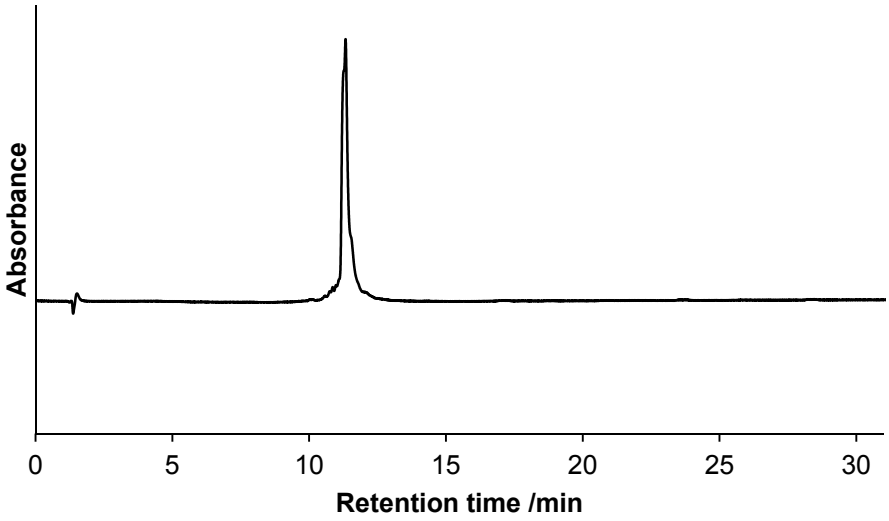

Figure C3 Analytical HPLC trace of p15, **126**, detection at 280 nm.

2. F-p15 peptide 127

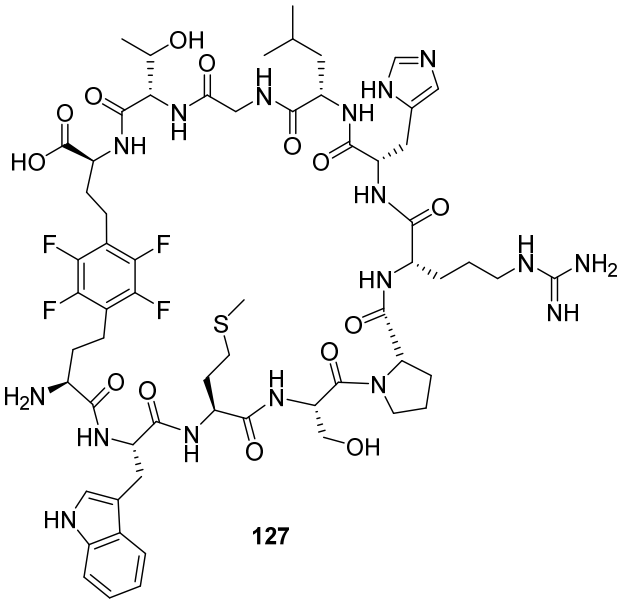

127

Figure C4 F-p15 peptide. Synthesis of the linear peptide was carried out on 2-chlorotrityl chloride resin on a 0.2 mmol scale. Linear peptide synthesis was carried out according to procedure **6.5.5** and cleaved from the resin according to procedure **6.7.1**. Cyclisation *via* hexafluorobenzene stapling was carried out on a 0.1 mmol scale according to procedure **6.6.2**. Purification was carried out according to procedure **6.8.1**.

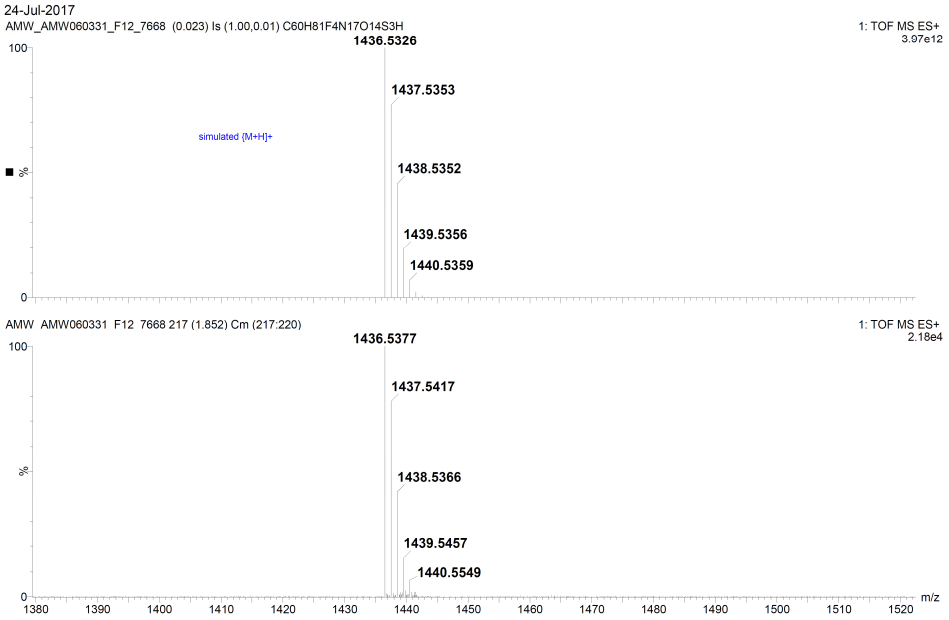

Figure C5 HRMS of F-p15 peptide **127**, $C_{60}H_{81}F_4N_{17}O_{14}S_3$, calculated $[M+H]^+$ = 1436.5326, observed $[M+H]^+$ = 1436.5377.

.

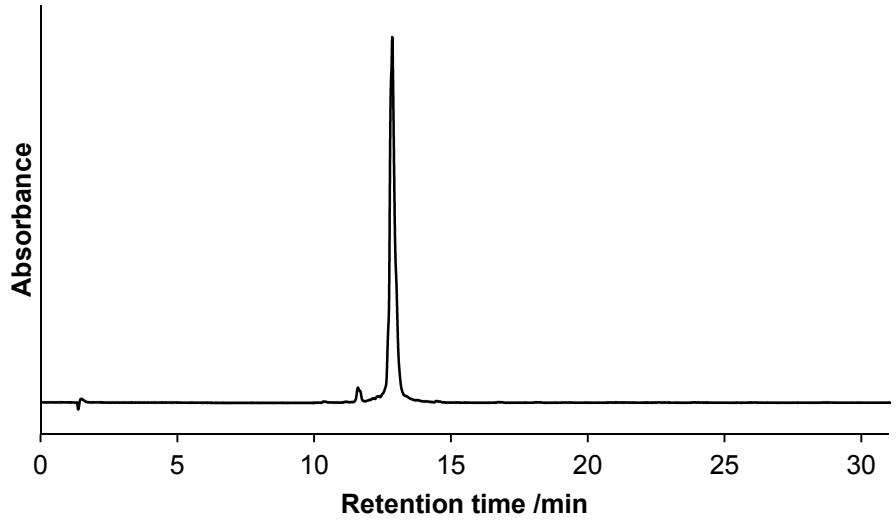

Figure C6 Analytical HPLC trace of F-p15, **127**. Detection at 280 nm.

δ_F(376 MHz, D_2O) 4F, -133.36 - -134.27 (m)

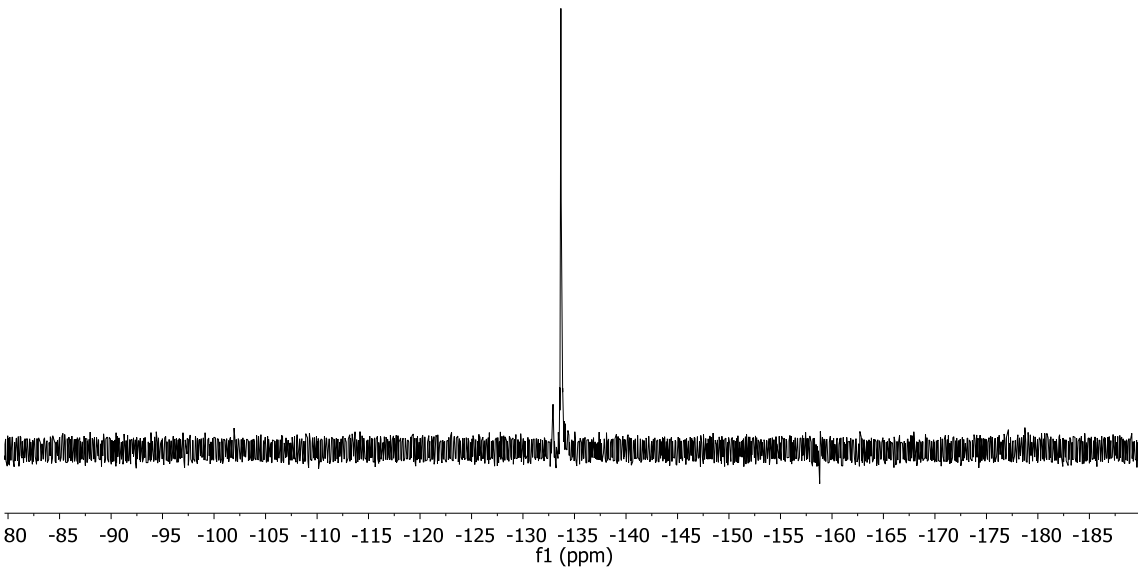

Figure C7 19F NMR spectrum of F-p15, **127**. Peak at -76.55 ppm arises from TFA.

3. C=C p15 peptide 128

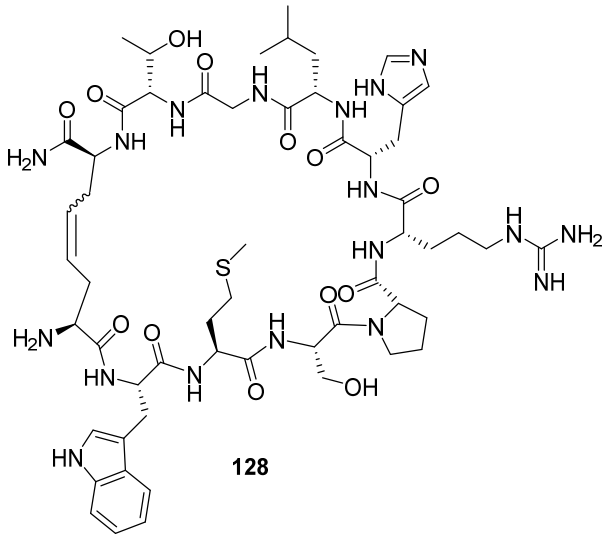

Figure C8 C=C p15 peptide. Synthesis of the linear peptide was carried out on 2-chlorotrityl chloride resin on a 0.2 mmol scale. Linear peptide synthesis was carried out according to procedure **6.5.6**. Cyclisation *via* Grubbs' RCM was carried out on a 0.05 mmol scale according to procedure **6.6.3**. Cleavage and purification was carried out according to procedures **6.7.2** and **6.8.1**.

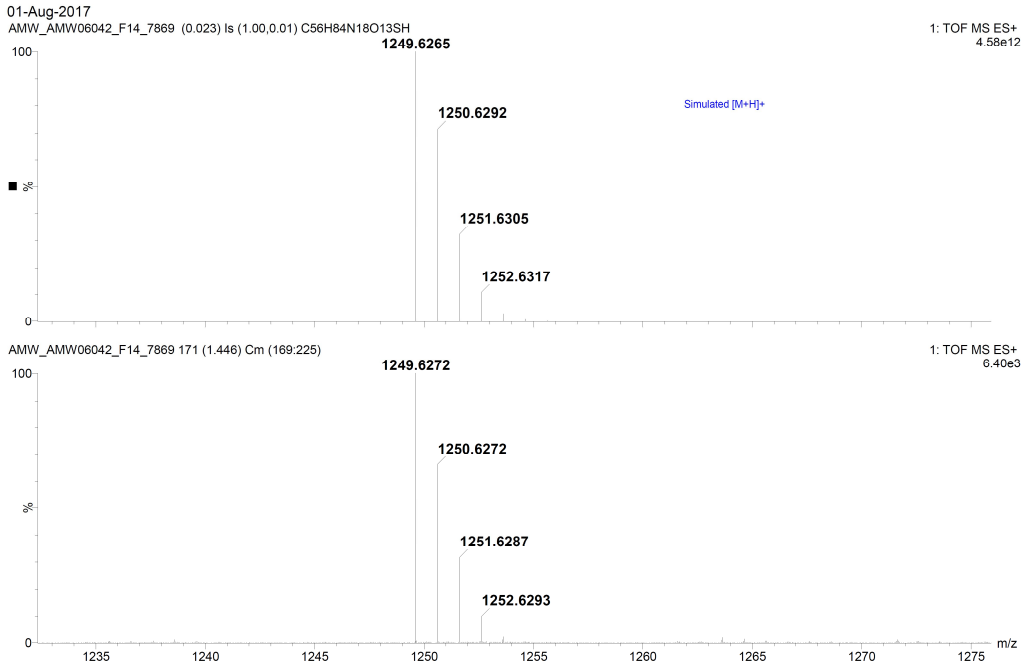

Figure C9 HRMS of C=C p15 peptide **128**, $C_{56}H_{84}N_{18}O_{13}S$, calculated $[M+H]^+$ = 1249.6265, observed $[M+H]^+$ = 1249.6272.

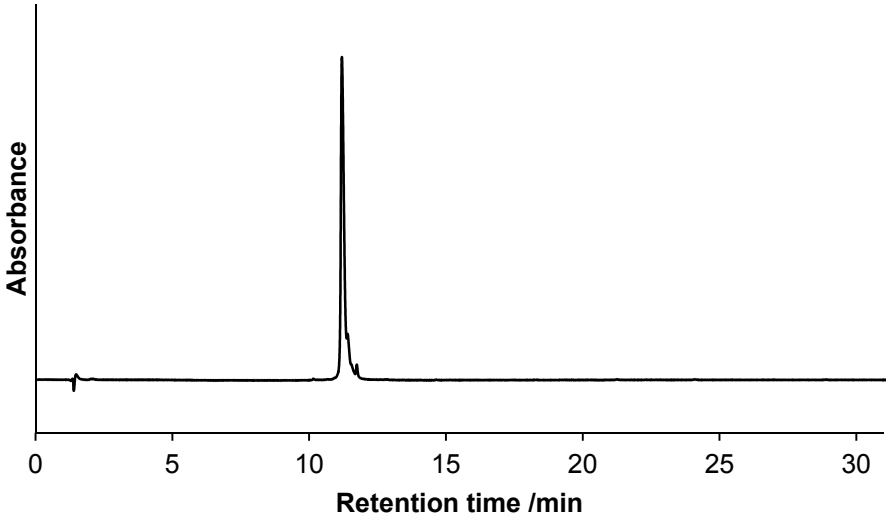

Figure C10 Analytical HPLC trace of C=C p15, **128**. Detection at 280 nm.

4. C-C p15 peptide 129

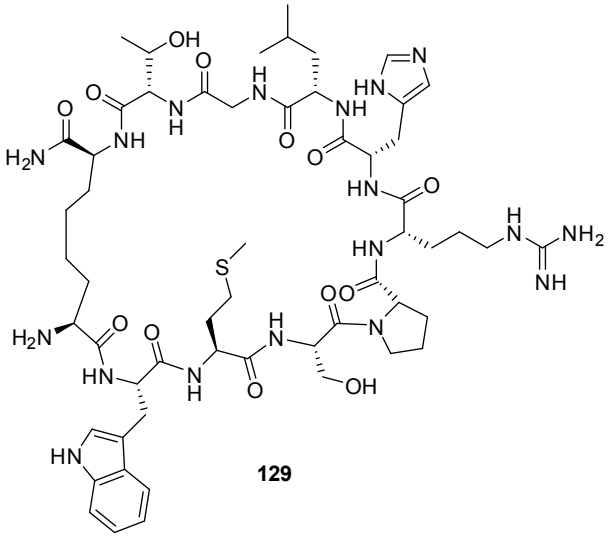

129

Figure C11 C-C p15 peptide. Peptide **129** was synthesised from C=C p15, **128**. Hydrogenation of C=C p15 was carried out according to procedure **6.6.4**.

Elemental Composition Report **Page 1**

Single Mass Analysis
Tolerance = 5.0 PPM / DBE: min = -1.5, max = 50.0
Element prediction: Off
Number of isotope peaks used for i-FIT = 3

Monoisotopic Mass, Even Electron Ions
1525 formula(e) evaluated with 11 results within limits (up to 500 closest results for each mass)
Elements Used:
C: 0-70 H: 0-90 N: 0-18 O: 0-13 S: 0-2

24-Aug-2017
AMW-07-001 187 (1.580) Cm (178:197)

1: TOF MS ES+
3.25e+003

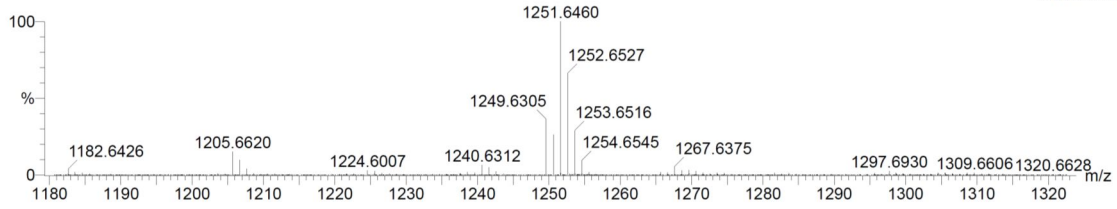

Figure C12 HRMS of C-C p15 peptide **129**, $C_{56}H_{86}N_{18}O_{13}S$, calculated $[M+H]^+$ = 1251.6421, observed $[M+H]^+$ = 1251.6460.

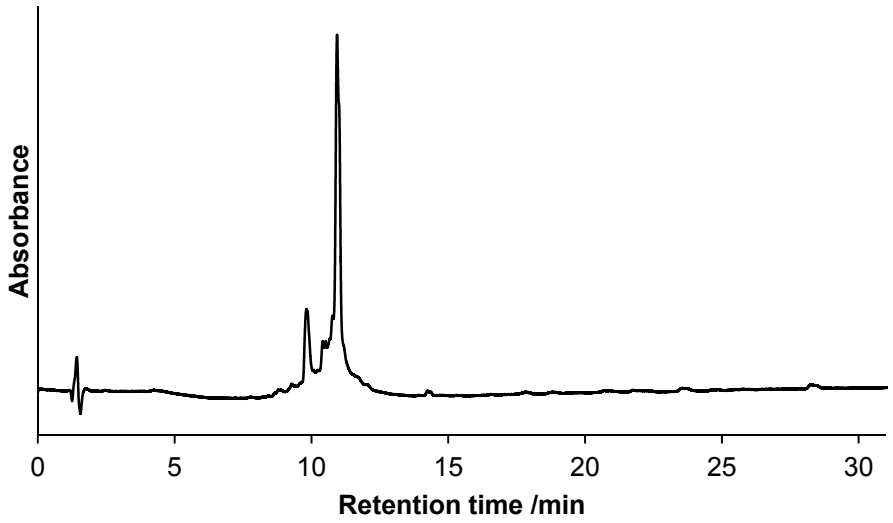

Figure C13 Analytical HPLC trace of p15-C-C, **129**. Detection at 280 nm.

Appendix D

Spectra of KLA-CPPos

1. D-KLA amide 199

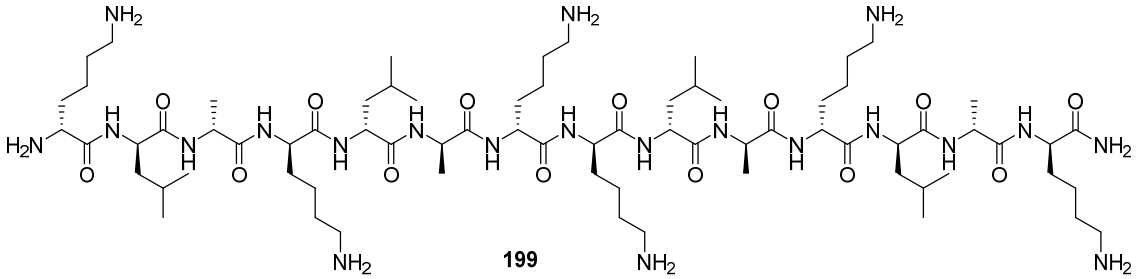

H-klakklakklakklak-NH_2

Figure D1 D-KLA amide. Synthesis of the linear peptide was carried out on Rink amide resin. Linear peptide synthesis was carried out according to procedure **6.5.1** and **6.5.2**. Cleavage and purification was carried out according to procedures **6.7.1** and **6.8.1**.

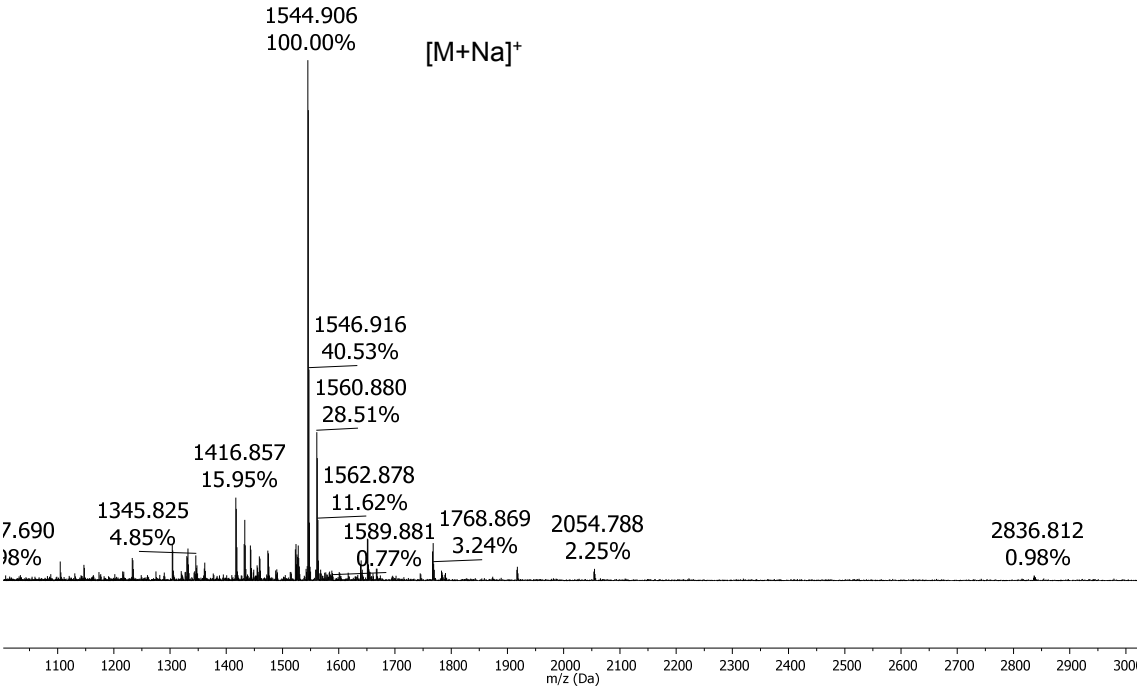

Figure D2 MALDI-ToF of D-KLA, **199**, $C_{72}H_{139}N_{21}O_{14}$, [M] = 1523.0.

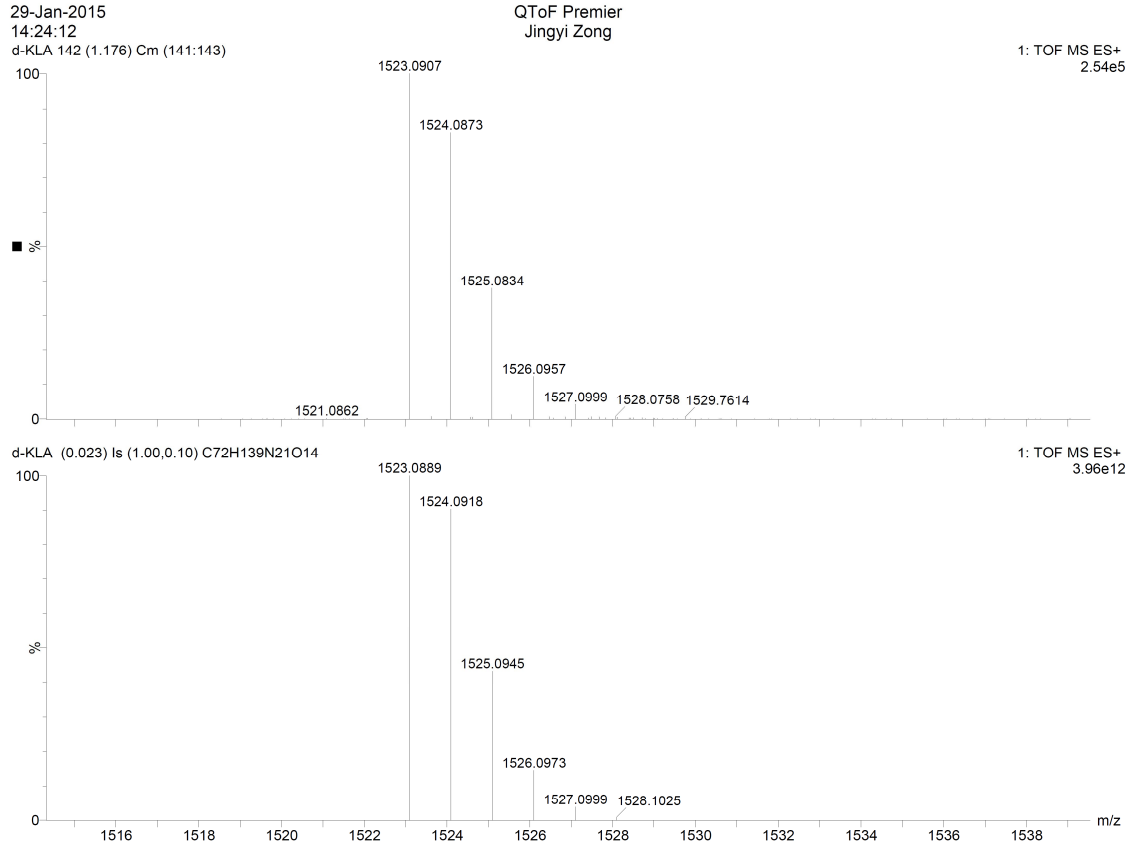

Figure D3 HRMS of D-KLA, **199**, $C_{72}H_{138}N_{21}O_{14}$, calculated $[M+H]^+$ = 1523.0889, observed $[M+H]^+$ = 1523.0907.

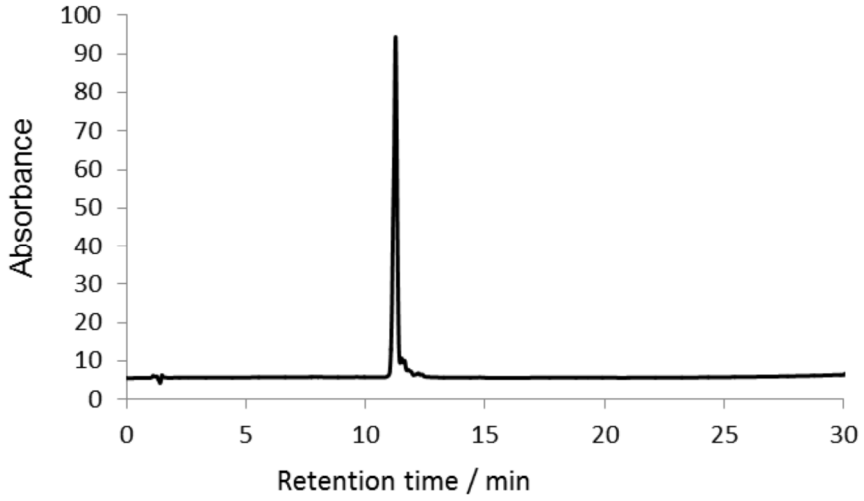

Figure D4 Analytical HPLC trace of D-KLA, **199**.

2. KLA-CPPo1 193

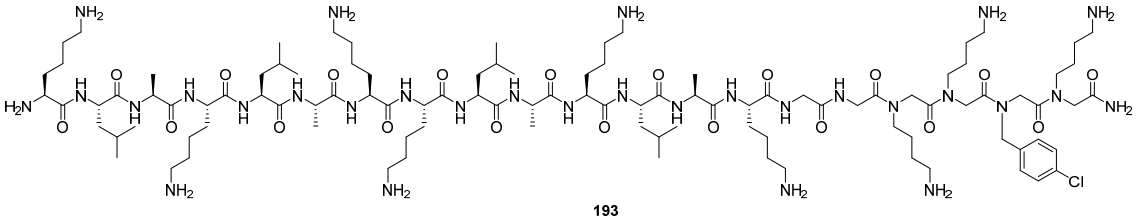

193

H-klakklakklakklak-GG-*N*lys-*N*lys-*N*pcb-*N*lys-NH_2

Figure D5 KLA-CPPo1. Synthesis of the peptide-peptoid was carried out on Rink amide resin. Peptoid synthesis was first carried out according to procedure **6.4.1** and **6.4.4**. Peptide synthesis was then carried out according to procedure **6.5.2**. Cleavage and purification was carried out according to procedures **6.7.1** and **6.8.1**.

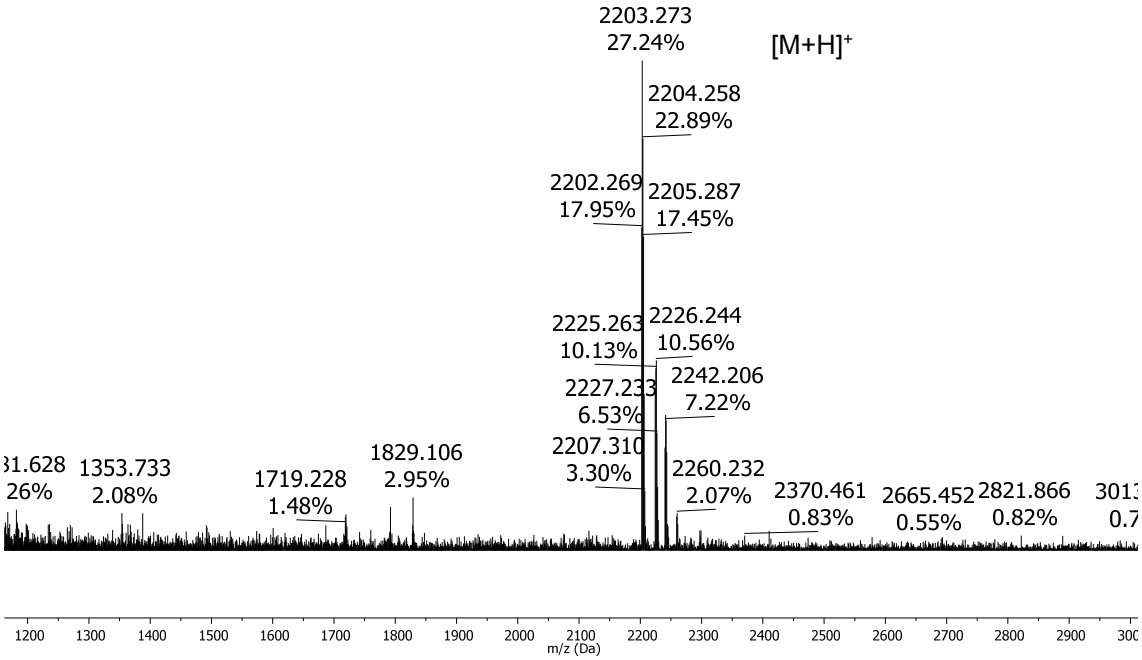

Figure D6 MALDI-ToF of KLA-CPPo1, **193**, $C_{103}H_{189}ClN_{30}O_{20}$, [M] = 2203.3.

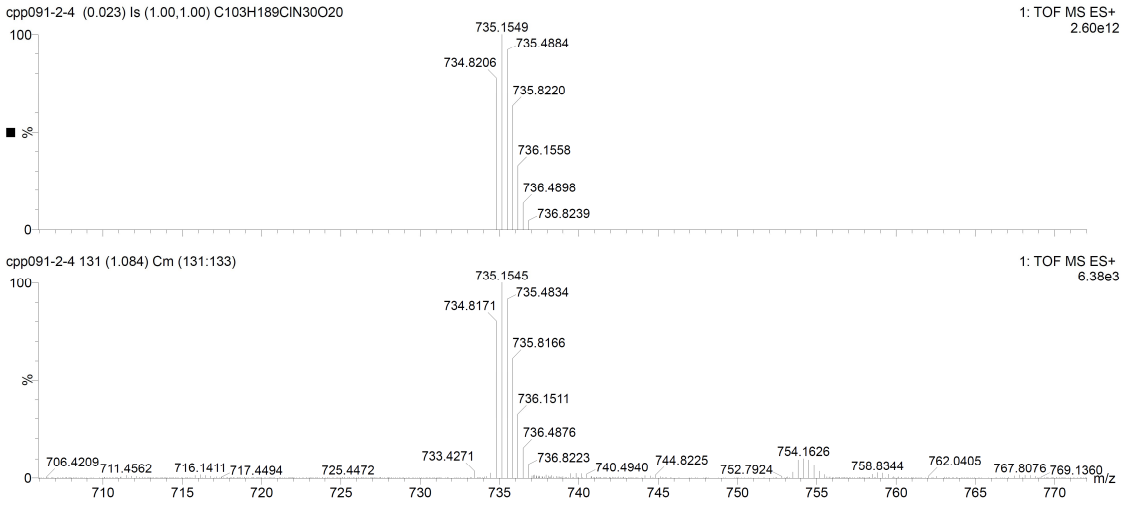

Figure D7 HRMS of KLA-CPPo1, **193**, $C_{103}H_{189}ClN_{30}O_{20}$, calculated $[M+3H]^{3+}$ = 735.1549, observed $[M+3H]^{3+}$ = 735.1545.

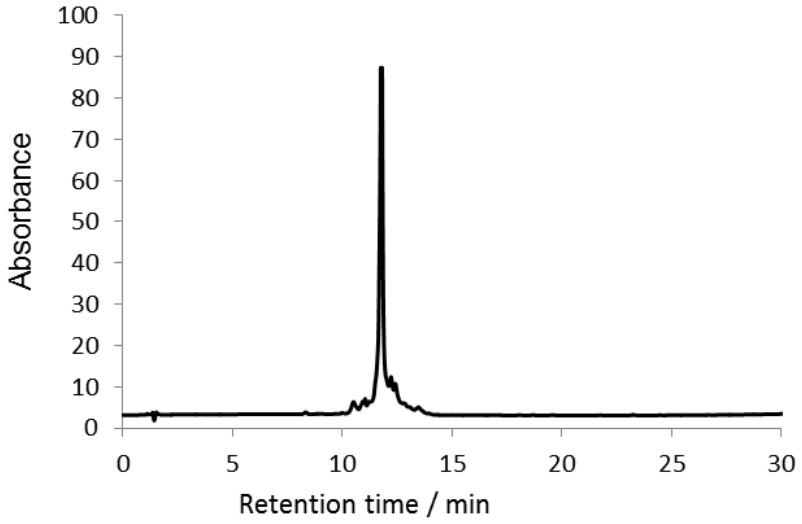

Figure D8 Analytical HPLC trace of KLA-CPPo1, **193**.

3. KLA-CPPo2 194

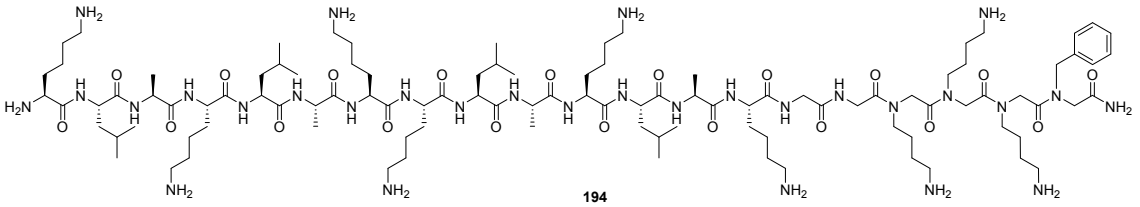

H-klakklakklakklak-GG-*N*lys-*N*lys-*N*lys-*N*phe-NH_2

Figure D9 KLA-CPPo2. Synthesis of the peptide-peptoid was carried out on Rink amide resin. Peptoid synthesis was first carried out according to procedure **6.4.1** and **6.4.4**. Peptide synthesis was then carried out according to procedure **6.5.2**. Cleavage and purification was carried out according to procedures **6.7.1** and **6.8.1**.

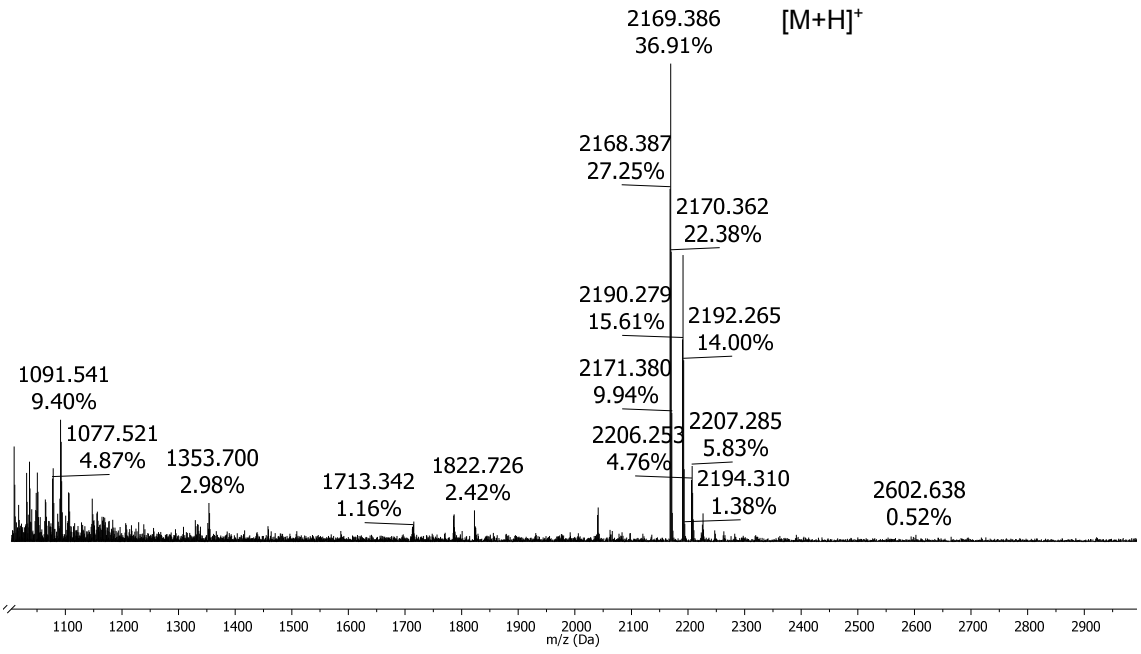

Figure D10 MALDI-ToF of KLA-CPPo2, **194**, $C_{103}H_{190}N_{30}O_{20}$, [M] = 2168.8.

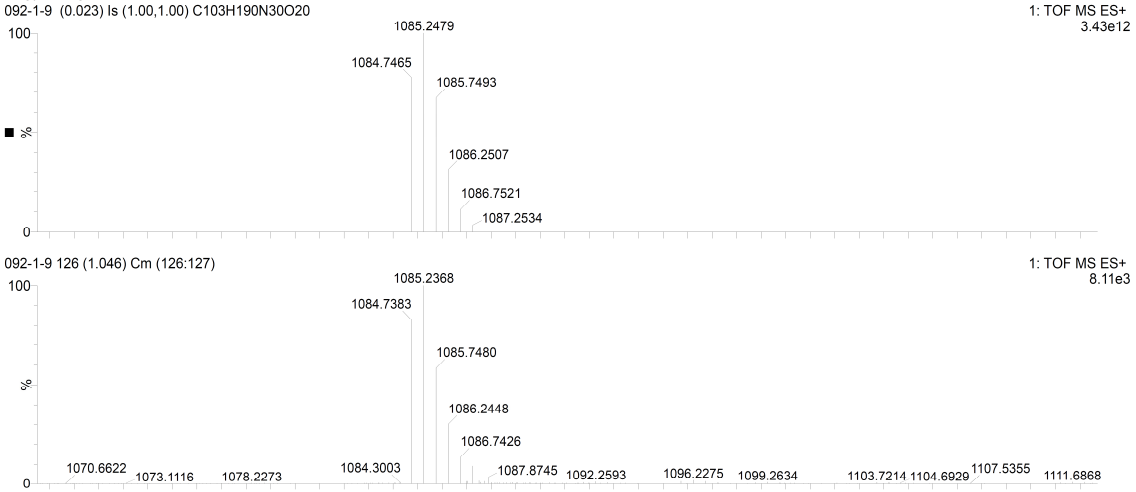

Figure D11 HRMS of KLA-CPPo2, **194**, $C_{103}H_{190}N_{30}O_{20}$, calculated $[M+2H]^{2+}$ = 1085.2479, observed $[M+2H]^{2+}$ = 1085.2368.

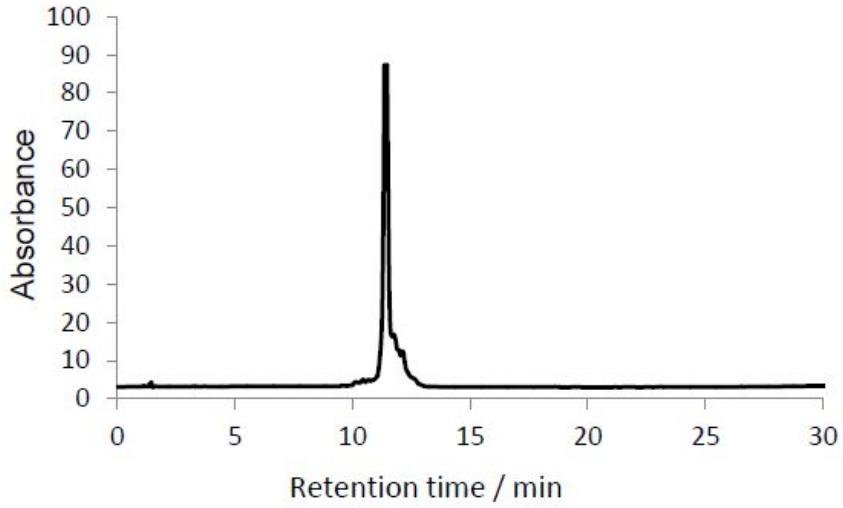

Figure D12 Analytical HPLC trace of KLA-CPPo2, **194**.

4. KLA-CPPo3 195

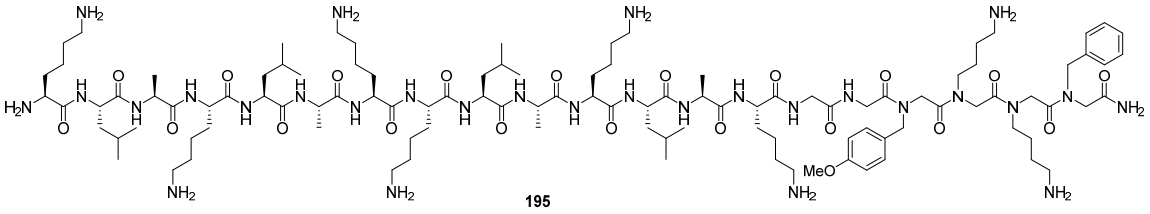

H-klakklakklakklak-GG-*N*pmb-*Nlys*-*N*lys-*N*phe-NH_2

Figure D13 KLA-CPPo3. Synthesis of the peptide-peptoid was carried out on Rink amide resin. Peptoid synthesis was first carried out according to procedure **6.4.1** and **6.4.4**. Peptide synthesis was then carried out according to procedure **6.5.2**. Cleavage and purification was carried out according to procedures **6.7.1** and **6.8.1**.

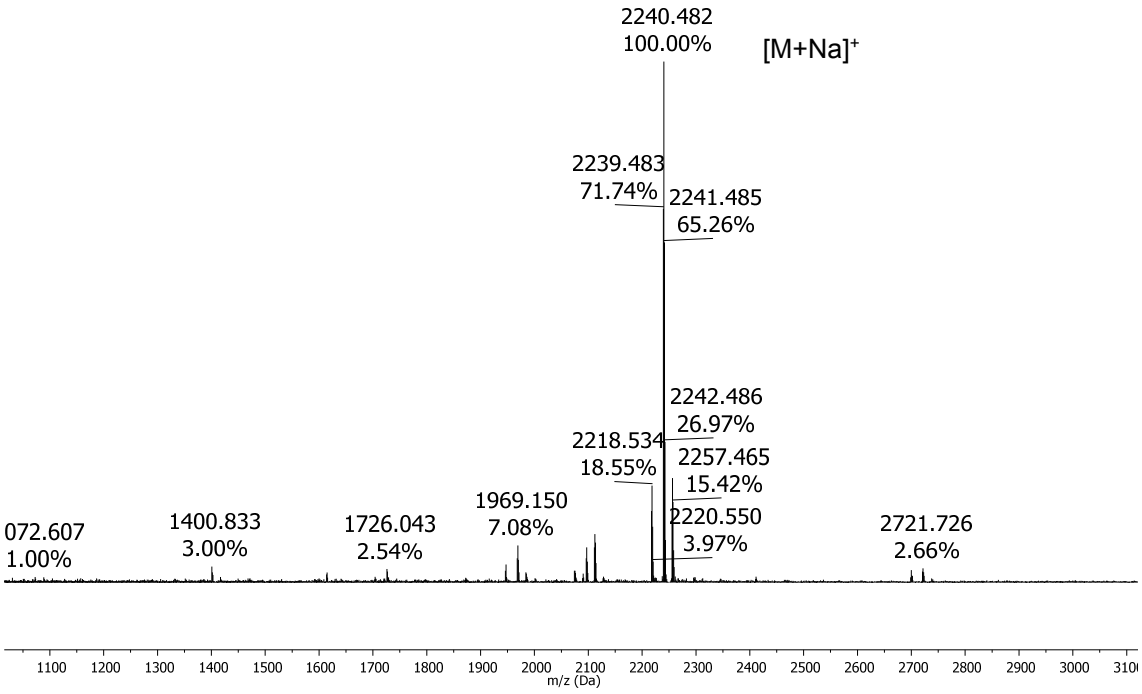

Figure D14 MALDI-ToF of KLA-CPPo3, **195**, $C_{107}H_{189}N_{29}O_{21}$, [M] = 2217.8.

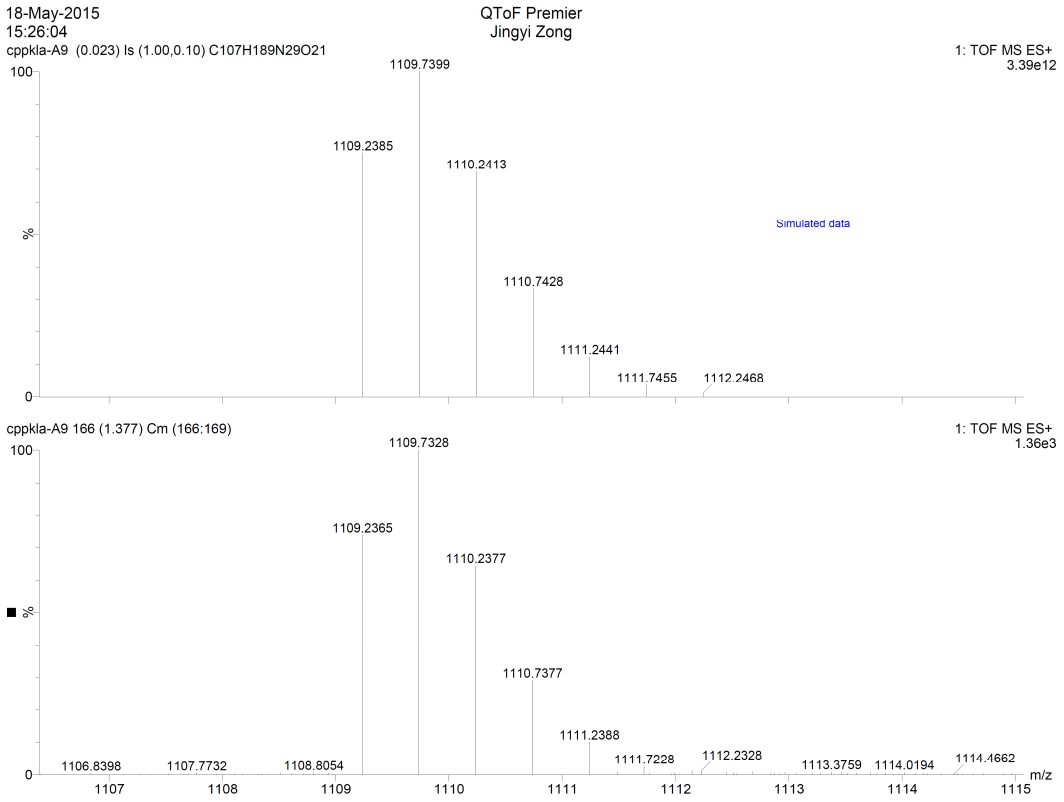

Figure D15 HRMS of KLA-CPPo3, **195**, $C_{107}H_{189}N_{29}O_{21}$, calculated $[M+2H]^{2+}$ = 1109.7399, observed $[M+2H]^{2+}$ = 1109.7328.

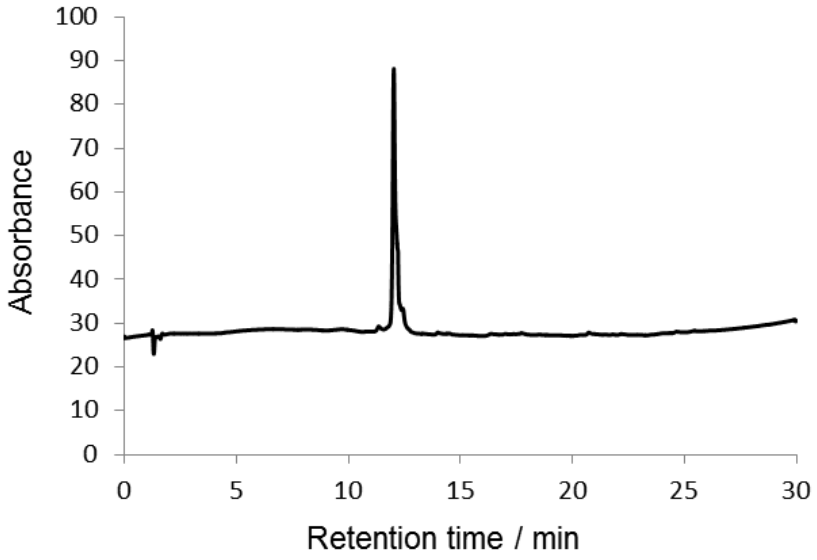

Figure D16 Analytical HPLC trace of KLA-CPPo3, **195**.

5. KLA-CPPo4 196

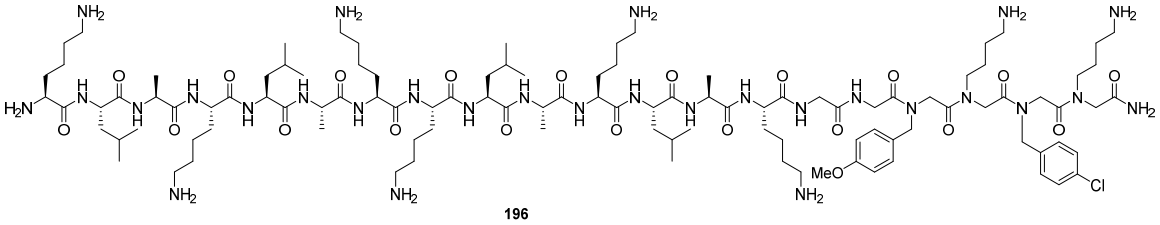

196

H-klakklakklakklak-GG-*N*pmb-*Nlys*-*N*pcb-*N*lys-NH_2

Figure D17 KLA-CPPo4. Synthesis of the peptide-peptoid was carried out on Rink amide resin. Peptoid synthesis was first carried out according to procedure **6.4.1** and **6.4.4**. Peptide synthesis was then carried out according to procedure **6.5.2**. Cleavage and purification was carried out according to procedures **6.7.1** and **6.8.1**.

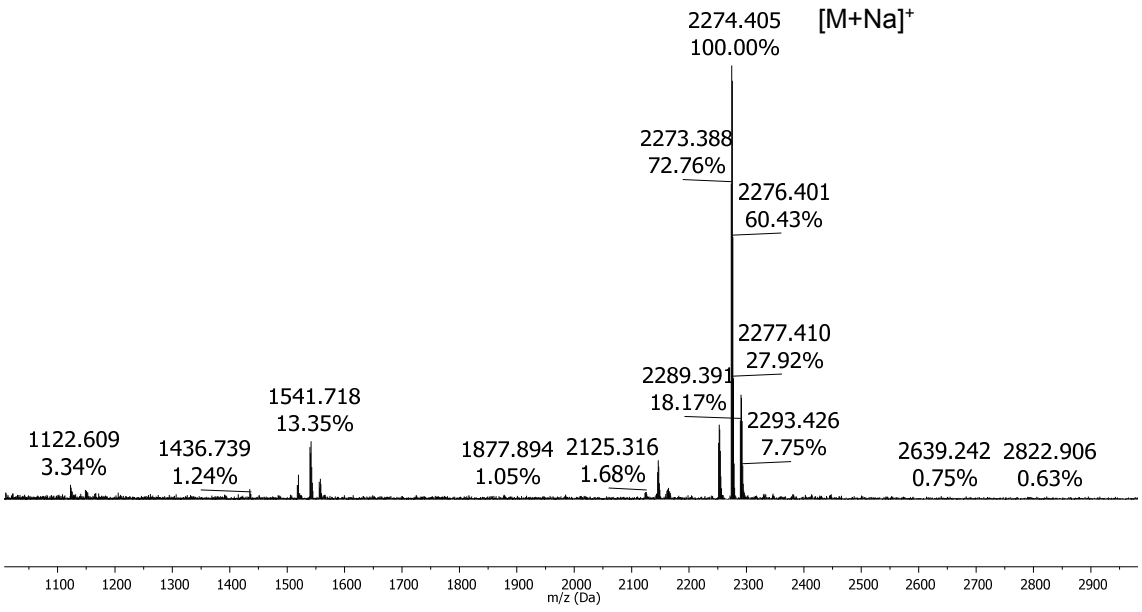

Figure D18 MALDI-ToF of KLA-CPPo4, **196**, $C_{107}H_{188}ClN_{29}O_{21}$, [M] = 2252.31.

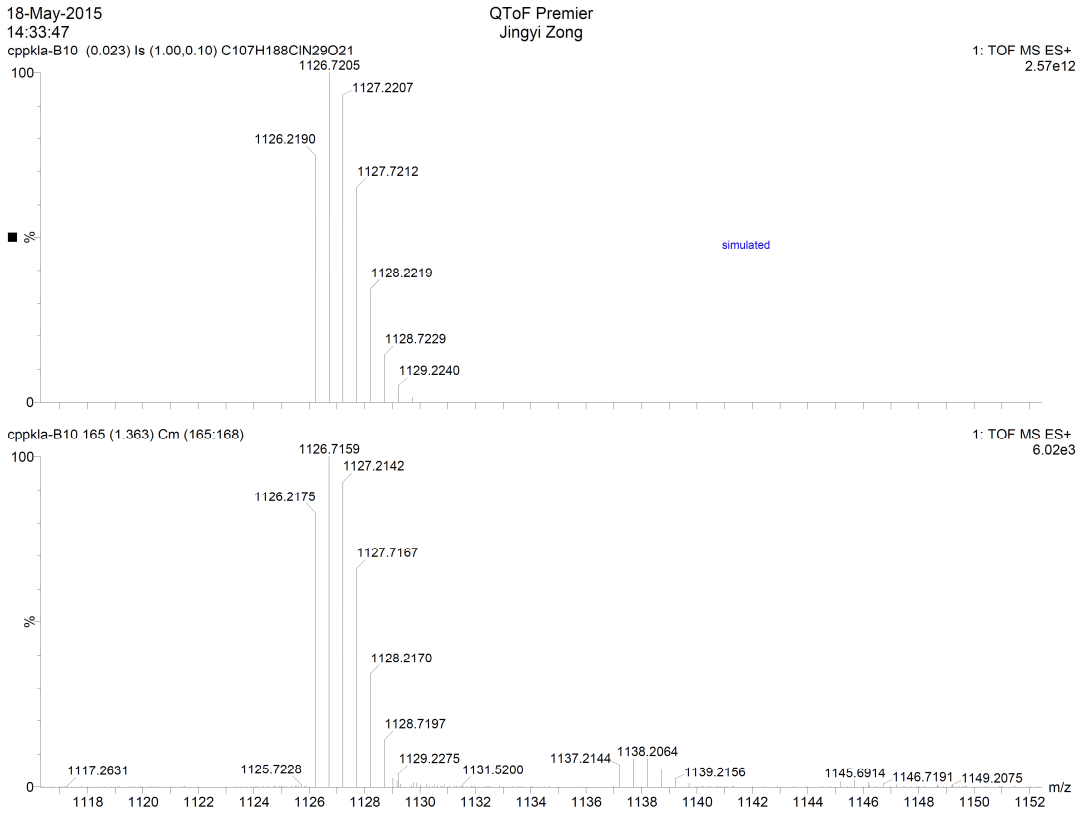

Figure D19 HRMS of KLA-CPPo4, **196**, $C_{107}H_{188}ClN_{29}O_{21}$, calculated $[M+2H]^{2+}$ = 1126.7205, observed $[M+2H]^{2+}$ = 1126.7159.

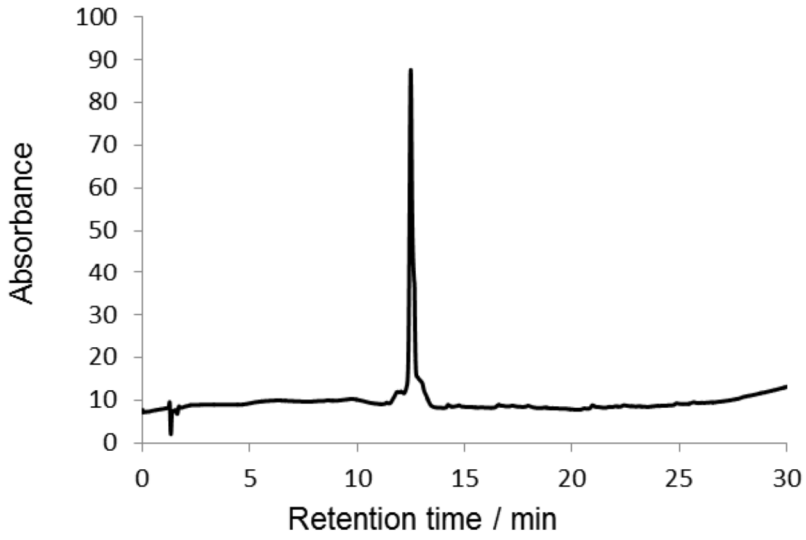

Figure D20 Analytical HPLC trace of KLA-CPPo4, **196**.

6. KLA-CPPo5 197

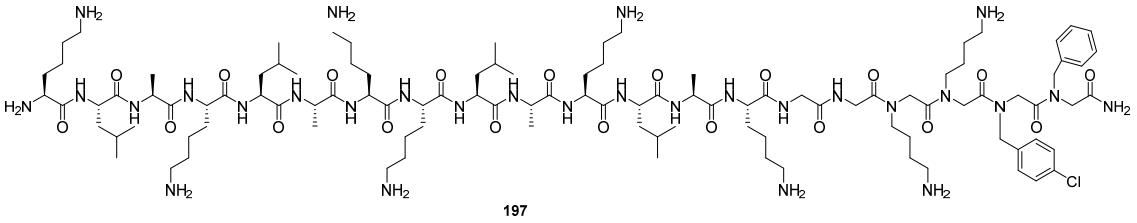

197

H-klakklakklakklak-GG-*N*lys-*N*lys-*N*pcb-*N*phe-NH_2

Figure D21 KLA-CPPo5. Synthesis of the peptide-peptoid was carried out on Rink amide resin. Peptoid synthesis was first carried out according to procedure **6.4.1** and **6.4.4**. Peptide synthesis was then carried out according to procedure **6.5.2**. Cleavage and purification was carried out according to procedures **6.7.1** and **6.8.1**.

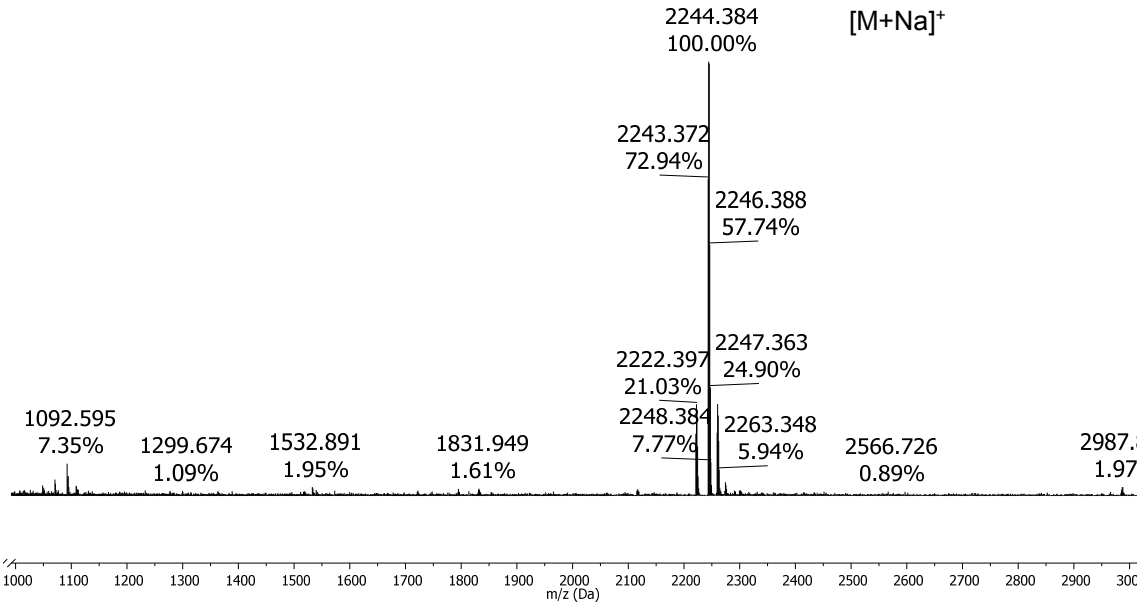

Figure D22 MALDI-ToF of KLA-CPPo5, **197**, $C_{106}H_{186}ClN_{29}O_{20}$, [M] = 2222.3

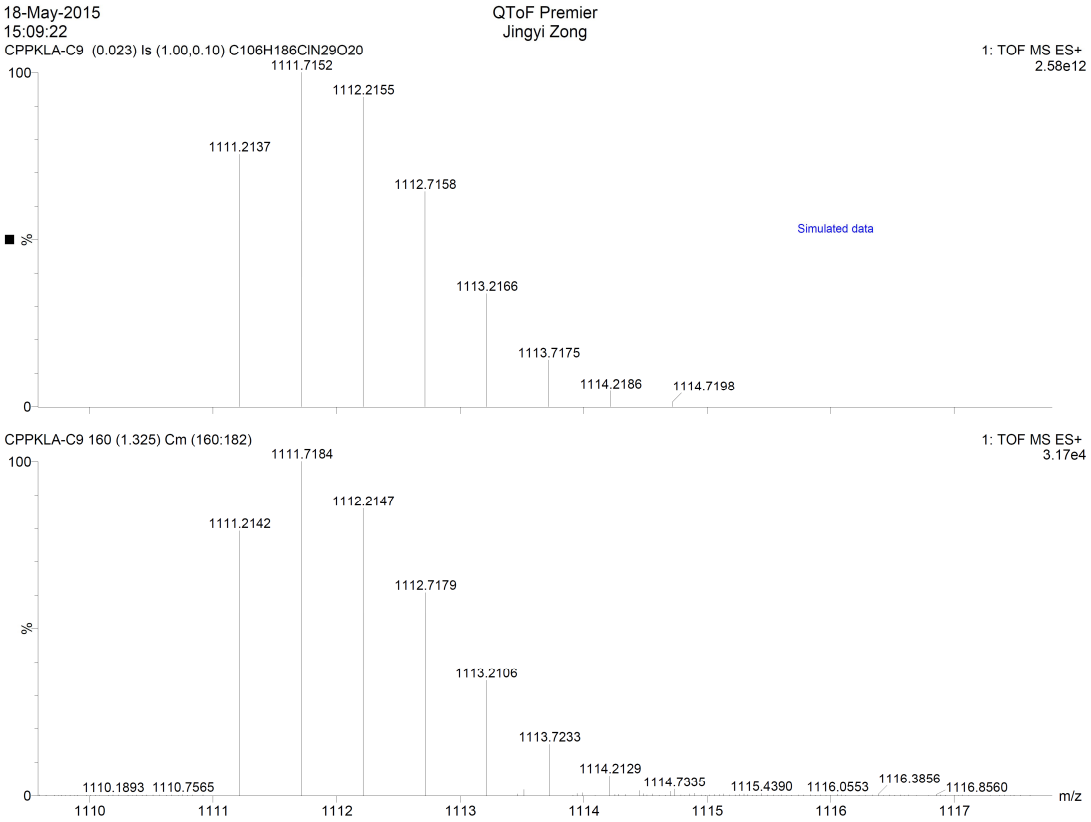

Figure D23 HRMS of KLA-CPPo5, **197**, $C_{106}H_{186}ClN_{29}O_{20}$, calculated $[M+2H]^{2+}$ = 1111.7152, observed $[M+2H]^{2+}$ = 1111.7184.

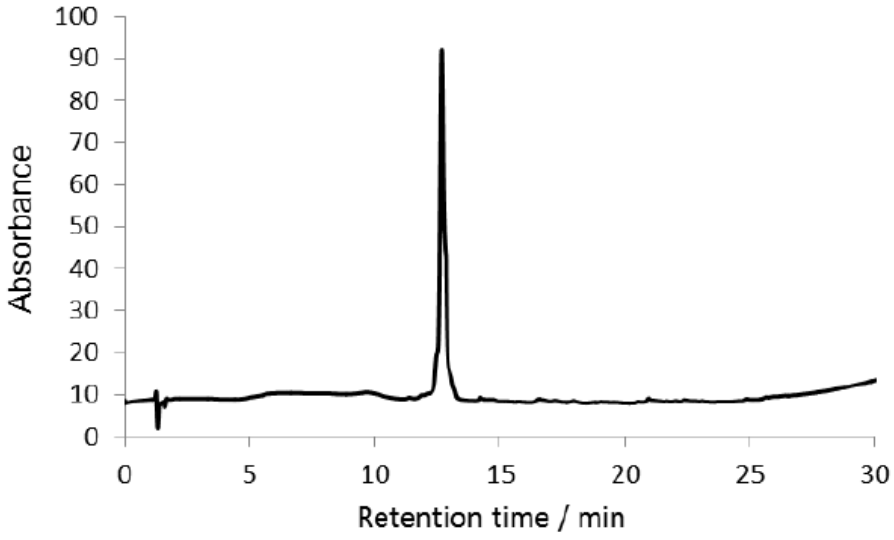

Figure D24 Analytical HPLC trace of KLA-CPPo5, **197**.

7. KLA-CPPo6 198

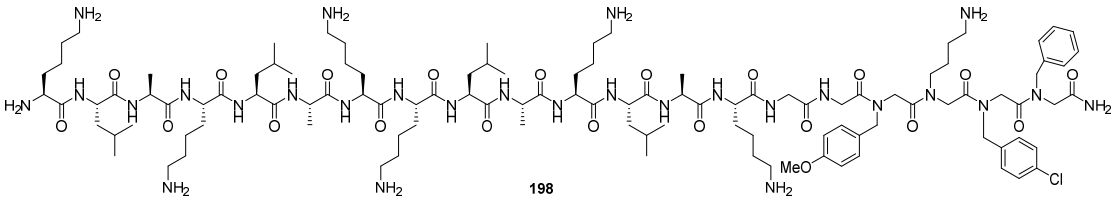

H-klakklakklakklak-GG-*N*pmb-*N*lys-*N*pcb-*N*phe-NH_2

Figure D25 KLA-CPPo6. Synthesis of the peptide-peptoid was carried out on Rink amide resin. Peptoid synthesis was first carried out according to procedure **6.4.1** and **6.4.4**. Peptide synthesis was then carried out according to procedure **6.5.2**. Cleavage and purification was carried out according to procedures **6.7.1** and **6.8.1**.

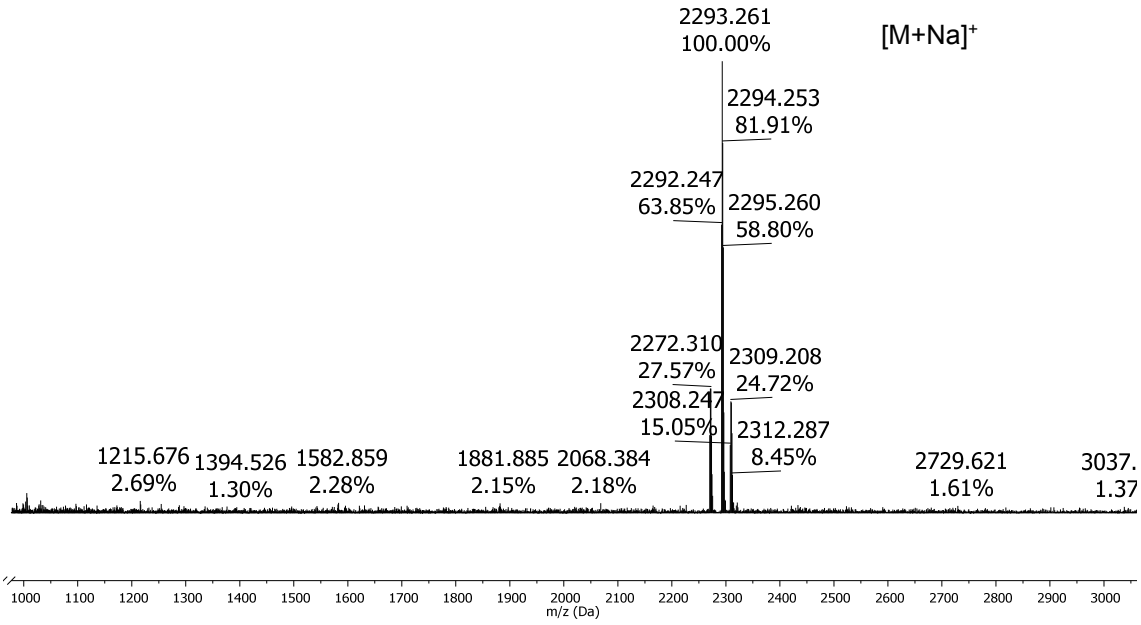

Figure D26 MALDI-ToF of KLA-CPPo6, **198**, $C_{110}H_{185}ClN_{28}O_{21}$, [M] = 2271.3.

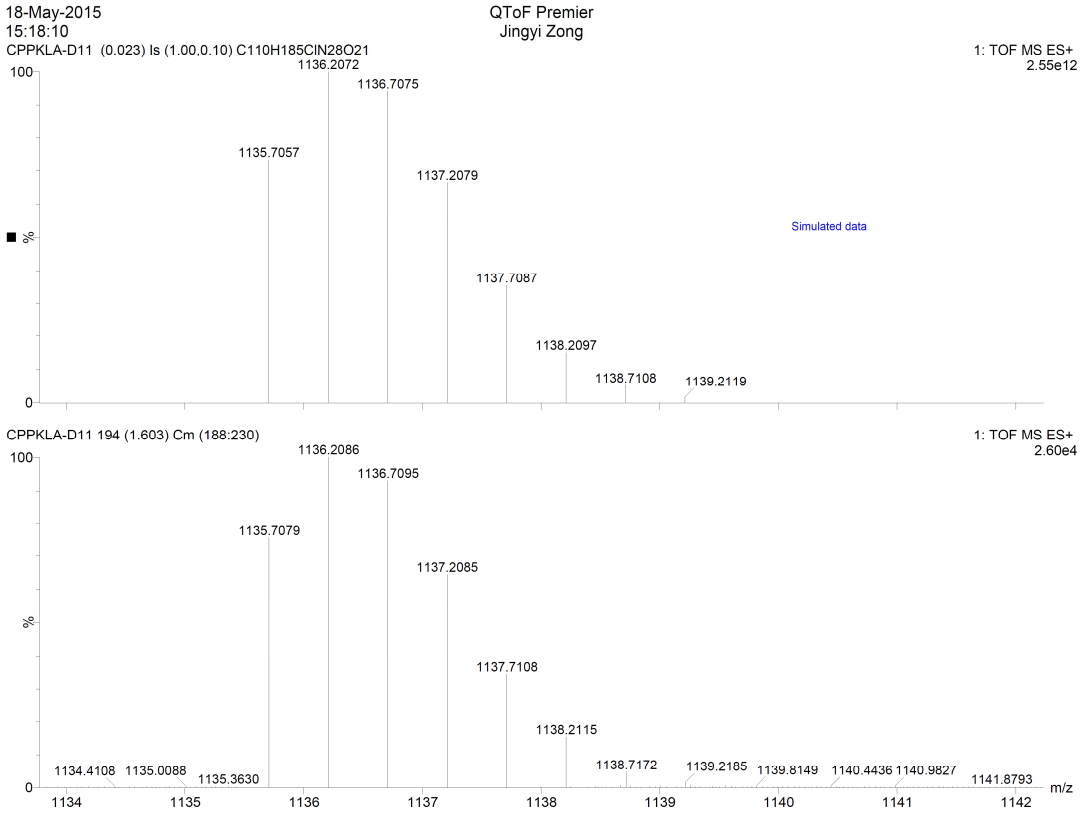

Figure D27 HRMS of KLA-CPPo6, **198**, $C_{110}H_{185}ClN_{28}O_{21}$, calculated $[M+2H]^{2+}$ = 1136.2072, observed $[M+2H]^{2+}$ = 1136.2086.

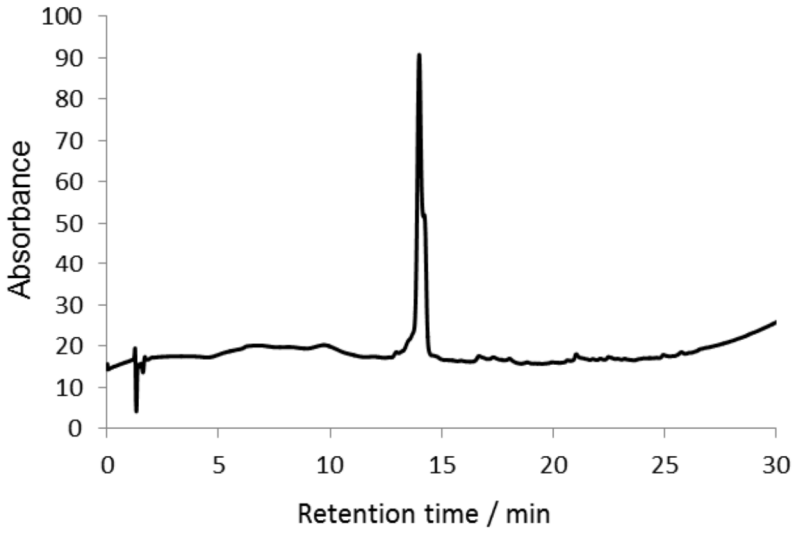

Figure D28 Analytical HPLC trace of KLA-CPPo6, **198**.

8. Rhod-KLA-CPPo6 201

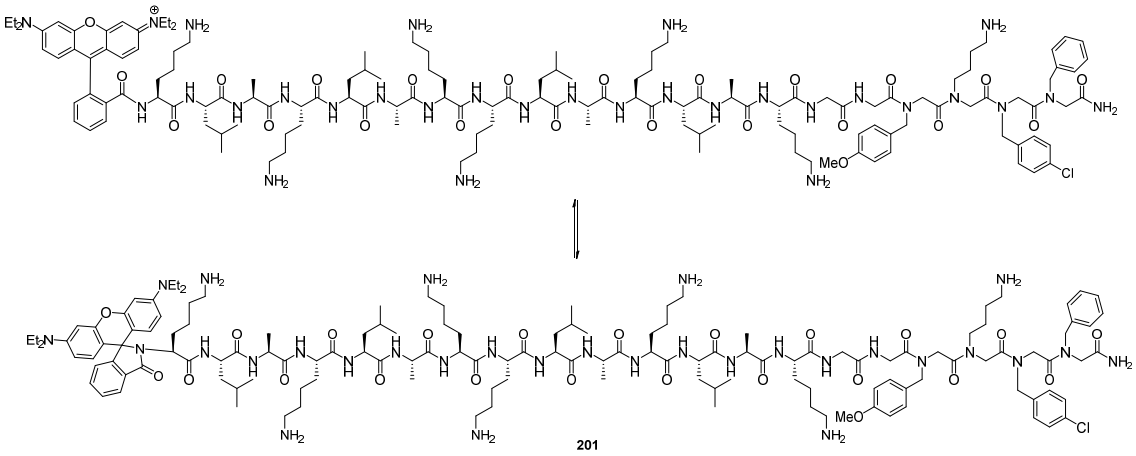

Rhod-klakklakklakklak-GG-*N*pmb-*Nlys*-*N*pcb-*N*phe-NH_2

Figure D29 Rhod-KLA-CPPo6. Synthesis of the peptide-peptoid was carried out on Rink amide resin. Peptoid synthesis was first carried out according to procedure **6.4.1** and **6.4.4**. Peptide synthesis was then carried out according to procedure **6.5.2**. Rhodamine was coupled to the peptide-peptoid according to procedure **6.5.8**. Cleavage and purification was carried out according to procedures **6.7.1** and **6.8.1**.

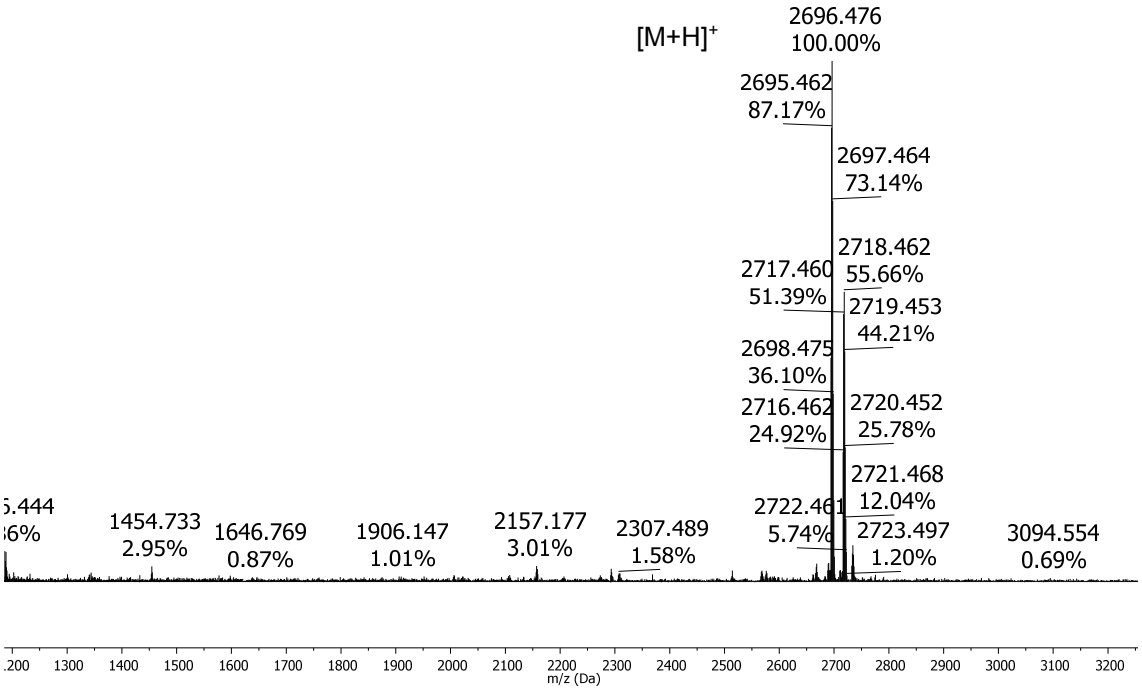

Figure D30 MALDI-ToF of Rhod-KLA-CPPo6, **201**, $C_{128}H_{214}N_{30}O_{23}Cl$, [M] = 2695.9.

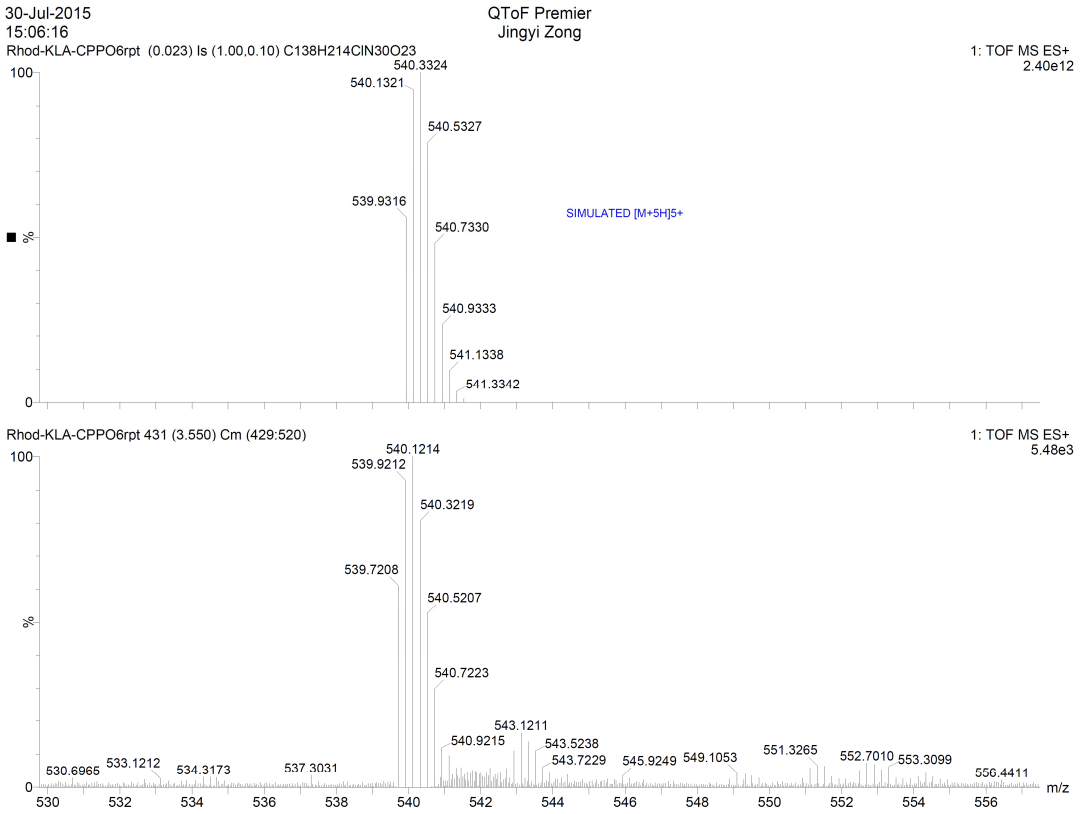

Figure D31 HRMS of Rhod-KLA-CPPo6, **201**, $C_{138}H_{213}ClN_{30}O_{23}$, calculated $[M+5H]^{5+}$ = 540.3324, observed $[M+5H]^{5+}$ = 540.3219.

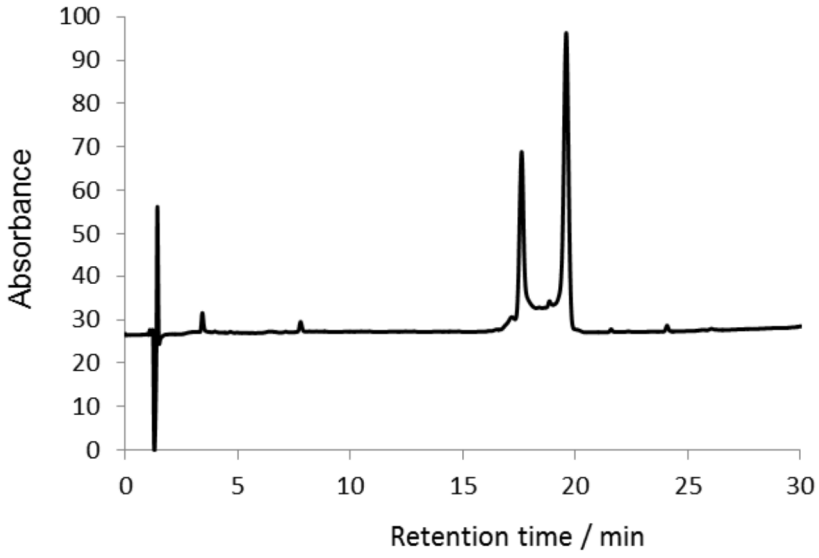

Figure D32 Analytical HPLC trace of Rhod-KLA-CPPo6, **201**

Appendix E

Spectra of p15-CPPos

1. Hyx-p15-CPPo7 222 (crude)

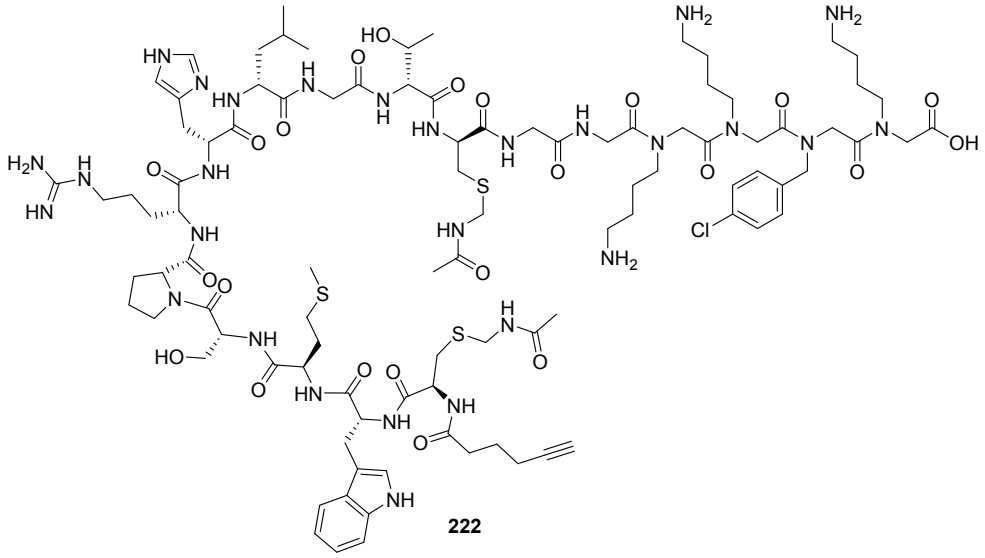

Hyx-CWMSPRHLGTC-GG-*N*lys-*N*lys-*N*pcb-*N*lys-NH_2

Figure E1 Hyx-p15-CPPo7. Synthesis of the peptide-peptoid was carried out on 2-chlorotrityl chloride resin on a 0.2 mmol scale. Peptoid synthesis was first carried out according to procedure **6.4.2** and **6.4.4**. Peptide synthesis was then carried out according to procedure **6.5.2**. Addition of 5-hexynoic acid was carried out according to procedure **6.5.3**. Test cleavages were carried out according to procedures **6.7.1** or **6.7.3**.

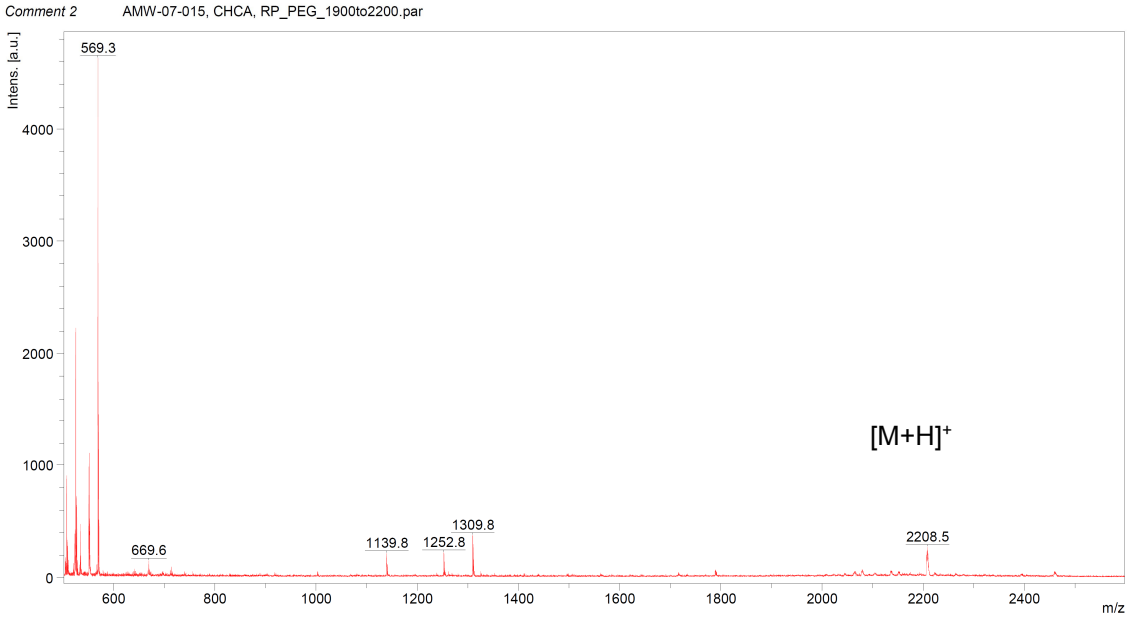

Figure E2 MALDI-ToF of crude Hyx-p15-CPPo7, **222**, $C_{97}H_{149}ClN_{28}O_{23}S_3$, [M] = 2207.1.

2. Hyx-p15-CPPo8 223 (crude)

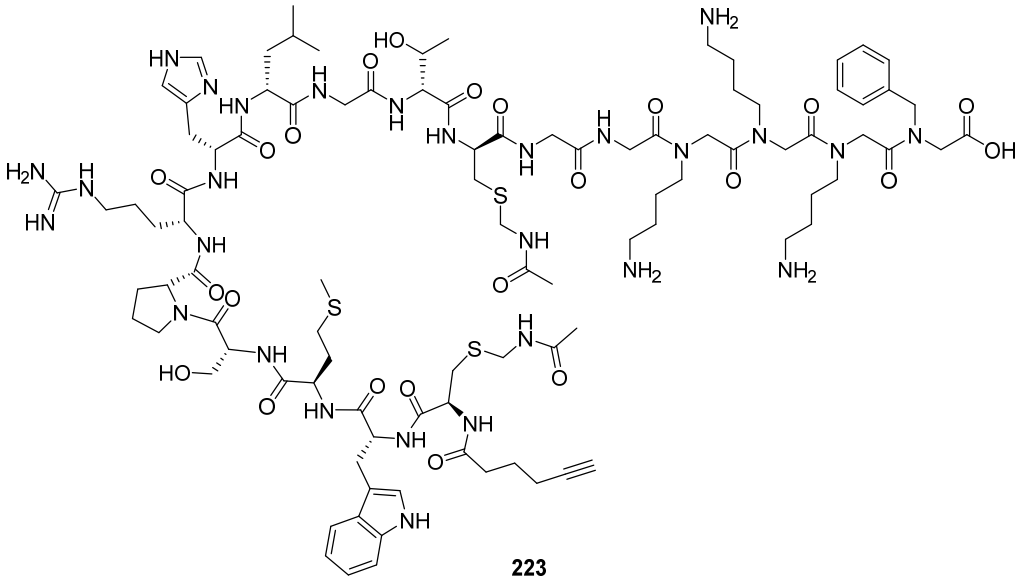

223

Hyx-CWMSPRHLGTC-GG-*N*lys-*N*lys-*N*lys-*N*phe-NH_2

Figure E3 Hyx-p15-CPPo8. Synthesis of the peptide-peptoid was carried out on 2-chlorotrityl chloride resin on a 0.2 mmol scale. Peptoid synthesis was first carried out according to procedure **6.4.2** and **6.4.4**. Peptide synthesis was then carried out according to procedure **6.5.2**. Addition of 5-hexynoic acid was carried out according to procedure **6.5.3**. Test cleavages were carried out according to procedures **6.7.1** or **6.7.3**.

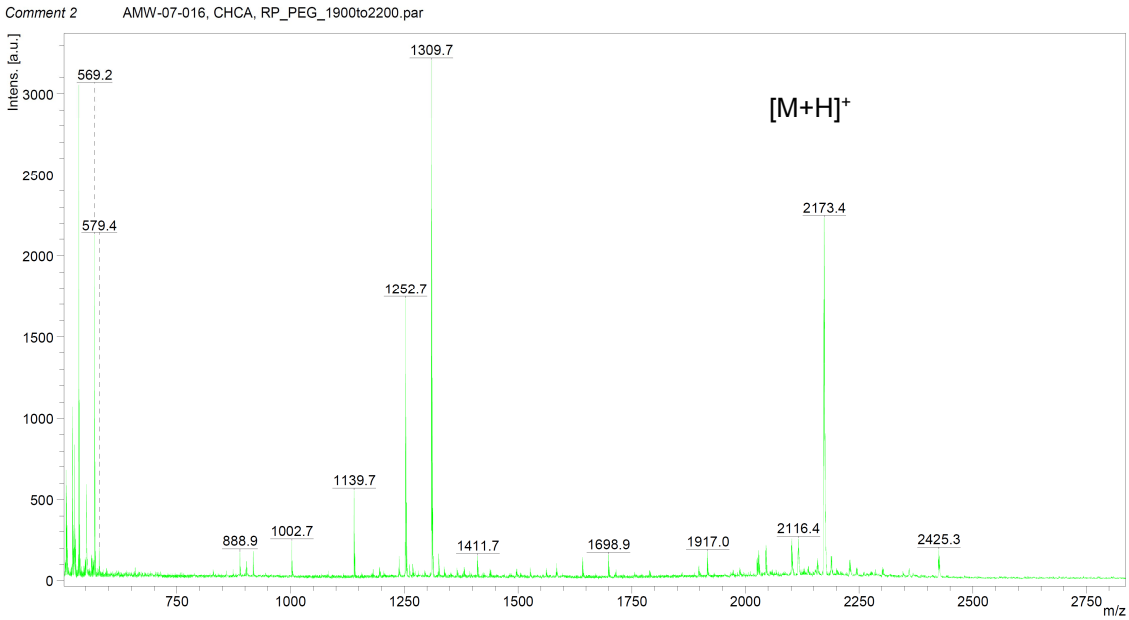

Figure E4 MALDI-ToF of crude Hyx-p15-CPPo8, **223**, $C_{97}H_{150}N_{28}O_{23}S_3$, [M] = 2172.6.

3. Hyx-p15-CPPo9 224 (crude)

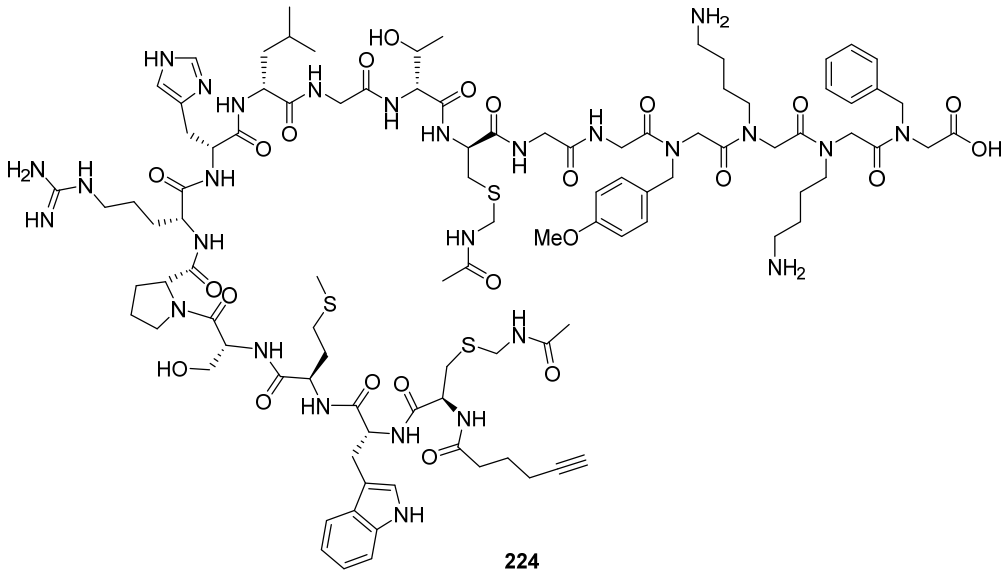

224

Hyx-CWMSPRHLGTC-GG-*N*pmb-*N*lys-*N*lys-*N*phe-NH_2

Figure E5 Hyx-p15-CPPo7. Synthesis of the peptide-peptoid was carried out on 2-chlorotrityl chloride resin on a 0.2 mmol scale. Peptoid synthesis was first carried out according to procedure **6.4.2** and **6.4.4**. Peptide synthesis was then carried out according to procedure **6.5.2**. Addition of 5-hexynoic acid was carried out according to procedure **6.5.3**. Test cleavages were carried out according to procedures **6.7.1** or **6.7.3**.

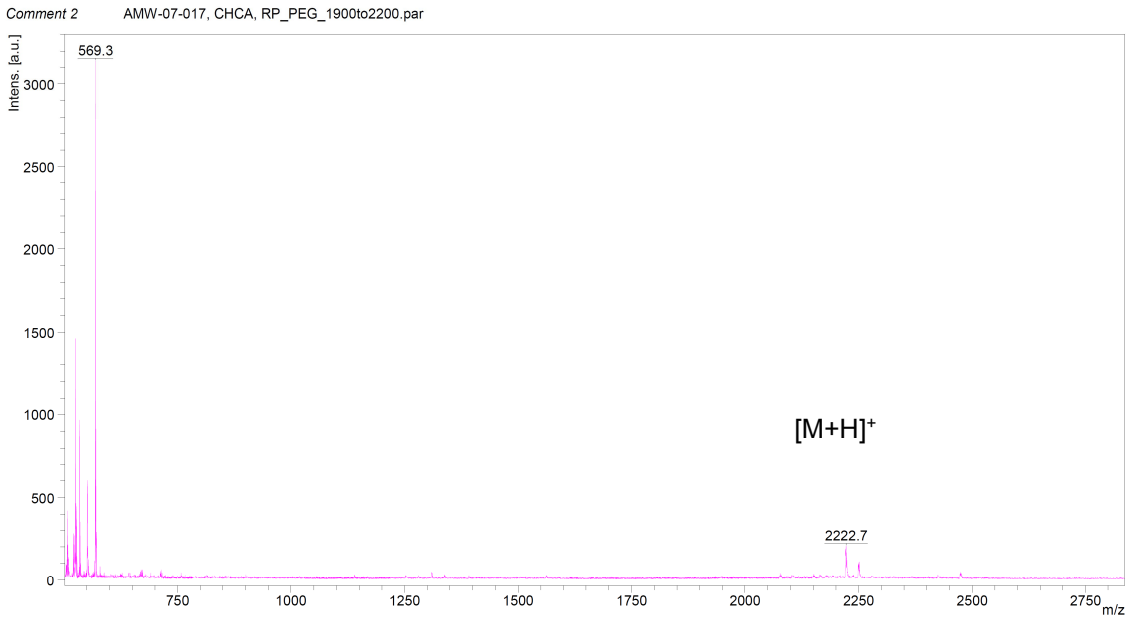

Figure E6 MALDI-ToF of crude Hyx-p15-CPPo9, **224**, $C_{101}H_{149}N_{27}O_{24}S_3$, [M] = 2221.7.

4. Hyx-p15-CPPo10 225 (crude)

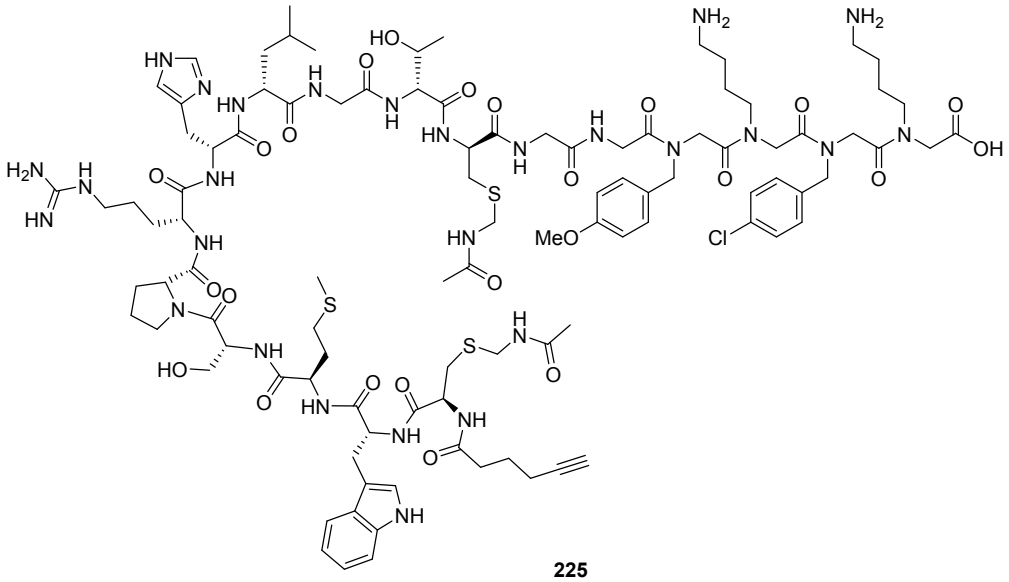

225

Hyx-CWMSPRHLGTC-GG-*N*pmb-*N*lys-*N*pcb-*N*lys-NH_2

Figure E7 Hyx-p15-CPPo10. Synthesis of the peptide-peptoid was carried out on 2-chlorotrityl chloride resin on a 0.2 mmol scale. Peptoid synthesis was first carried out according to procedure **6.4.2** and **6.4.4**. Peptide synthesis was then carried out according to procedure **6.5.2**. Addition of 5-hexynoic acid was carried out according to procedure **6.5.3**. Test cleavages were carried out according to procedures **6.7.1** or **6.7.3**.

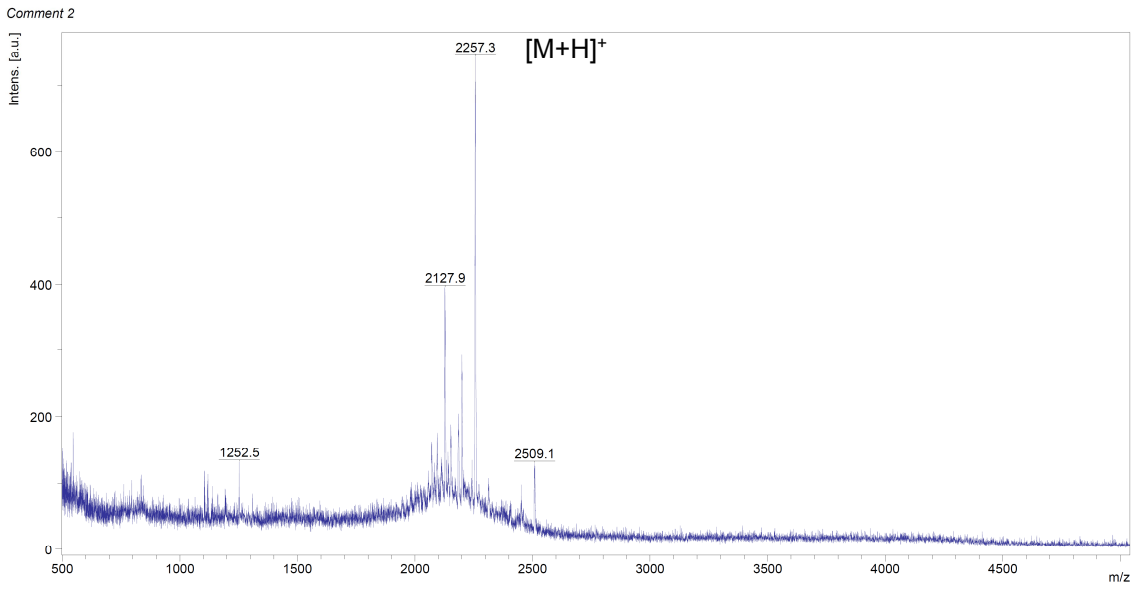

Figure E8 MALDI-ToF of crude Hyx-p15-CPPo10, **225**, $C_{101}H_{148}ClN_{27}O_{24}S_3$, [M] = 2256.1.

5. Hyx-p15-CPPo11 226 (crude)

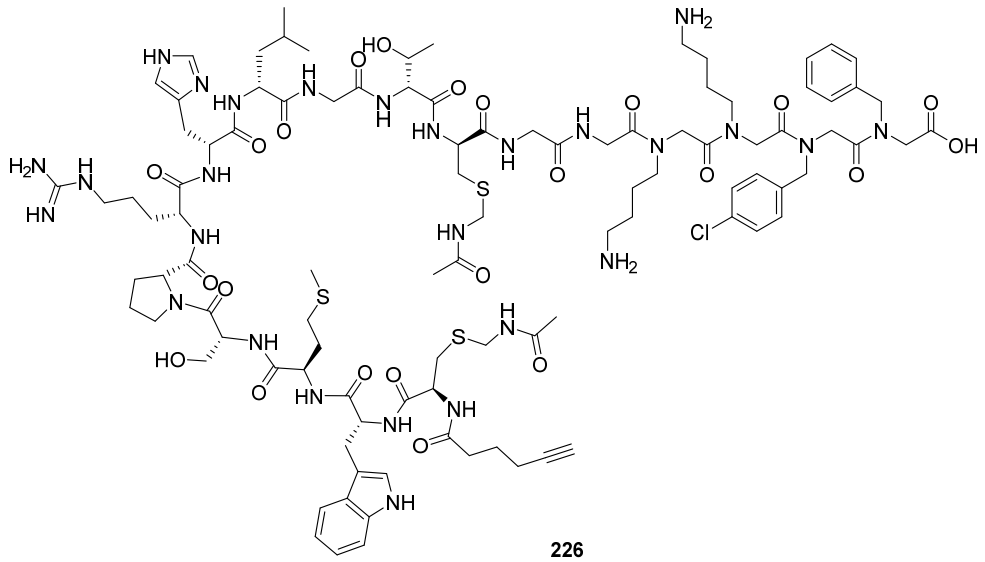

226

Hyx-CWMSPRHLGTC-GG-*N*lys-*N*lys-*N*pcb-*N*phe-NH_2

Figure E9 Hyx-p15-CPPo7. Synthesis of the peptide-peptoid was carried out on 2-chlorotrityl chloride resin on a 0.2 mmol scale. Peptoid synthesis was first carried out according to procedure **6.4.2** and **6.4.4**. Peptide synthesis was then carried out according to procedure **6.5.2**. Addition of 5-hexynoic acid was carried out according to procedure **6.5.3**. Test cleavages were carried out according to procedures **6.7.1** or **6.7.3**.

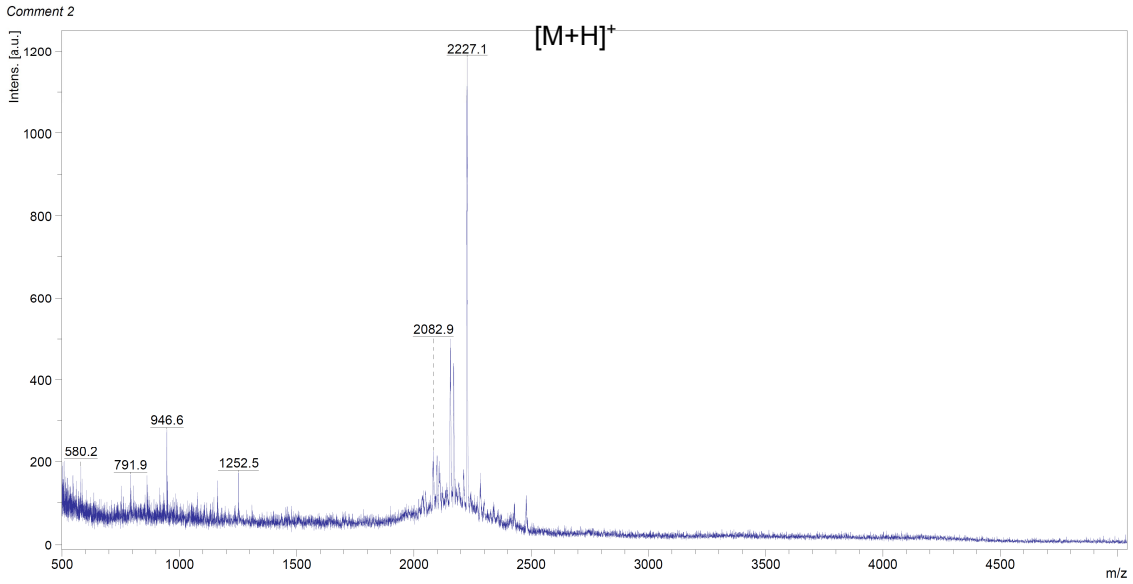

Figure E10 MALDI-ToF of crude Hyx-p15-CPPo11, **226**, $C_{100}H_{146}ClN_{27}O_{23}S_3$, [M] = 2226.1.

6. Hyx-p15-CPPo12 227 (crude)

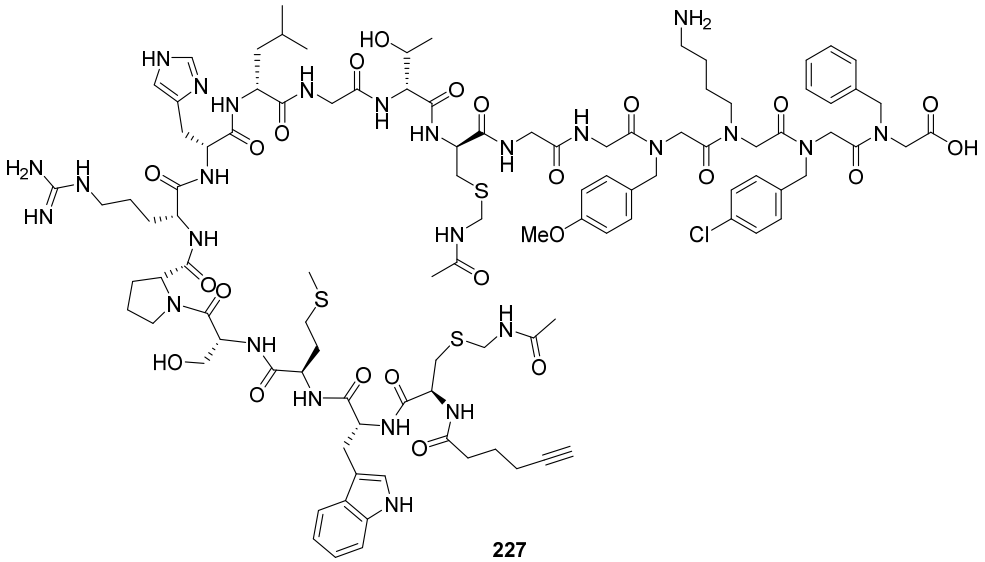

227

Hyx-CWMSPRHLGTC-GG-*N*pmb-*N*lys-*N*pcb-*N*phe-NH_2

Figure E11 Hyx-p15-CPPo7. Synthesis of the peptide-peptoid was carried out on 2-chlorotrityl chloride resin on a 0.2 mmol scale. Peptoid synthesis was first carried out according to procedure **6.4.2** and **6.4.4**. Peptide synthesis was then carried out according to procedure **6.5.2**. Addition of 5-hexynoic acid was carried out according to procedure **6.5.3**. Test cleavages were carried out according to procedures **6.7.1** or **6.7.3**.

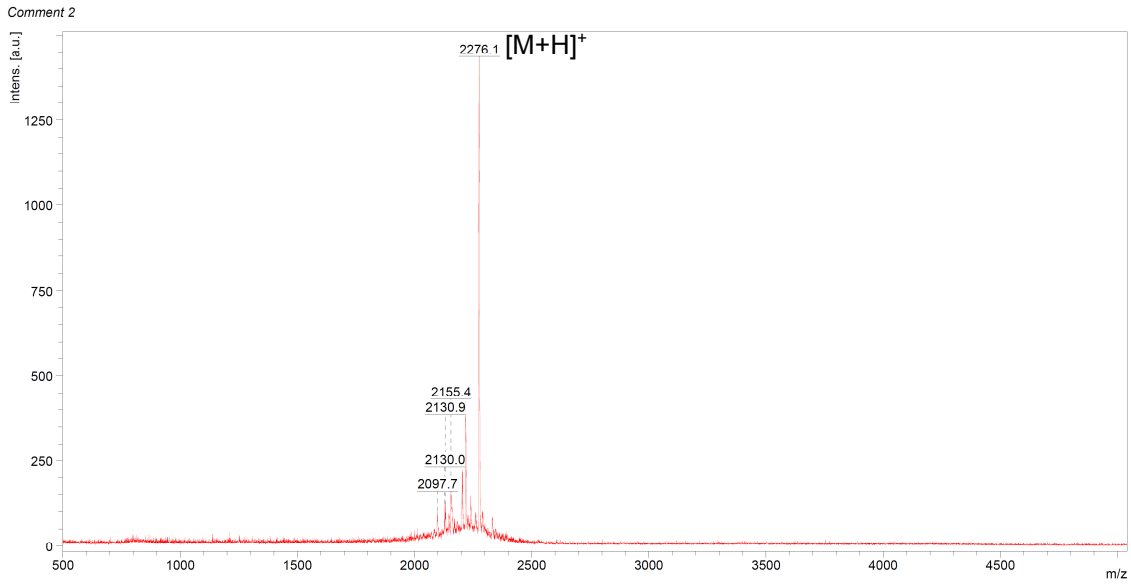

Figure E12 MALDI-ToF of crude Hyx-p15-CPPo12, **227**, $C_{104}H_{145}ClN_{26}O_{24}S_3$, [M] = 2275.1.